AFAL-TR-66-57

6633-1-F

6633-1-F = RL-2142

Air Force Avionics Laboratory
Research and Technology Division
Air Force Systems Command
Wright-Patterson Air Force Base, Ohio

Derivation of Aerospace Antenna Coupling-Factor Interference Prediction Techniques

by
J. A. M. LYON, R. M. KALAFUS, Y- K. KWON, C. J. DIGENIS,
M. A. H. IBRAHIM and C-C CHEN

Technical Report AFAL-TR-66-57

April 1966

Contract AF 33(615)-1761, Project 4357, Task 435709

THE UNIVERSITY OF MICHIGAN
COLLEGE OF ENGINEERING
DEPARTMENT OF ELECTRICAL ENGINEERING
Radiation Laboratory

Administered through:
OFFICE OF RESEARCH ADMINISTRATION • ANN ARBOR

THE UNIVERSITY OF MICHIGAN

6633-1-F

Derivation of Aerospace Antenna Coupling-Factor Interference Prediction Techniques

Final Report
June 1964 through September 1965

by

J.A.M. Lyon, R.M. Kalafus, Y-K Kwon,
C.J. Digenis, M.A.H. Ibrahim and C-C Chen.

April 1966

Contract AF 33(615)-1761
Proj. 4357, Task 435705

Air Force Avionics Laboratory, AVWC
Research and Technology Division, AFSC
Wright-Patterson Air Force Base, Ohio 45433

When Government drawings, specifications, or other data are used for any purpose other than in connection with a definitely related Government procurement operation, the United States Government thereby incurs no responsibility nor any obligation whatsoever; and the fact that the Government may have formulated, furnished, or in any way supplied the said drawings, specifications, or other data, is not to be regarded by implication or otherwise as in any manner licensing the holder or any other person or corporation, or conveying any rights or permission to manufacture, use, or sell any patented invention that may in any way be related thereto.

Qualified requestors may obtain copies of this report from the Defense Documentation Center (DDC), Cameron Station, Alexandria Va. 22314.

Copies of this report should not be returned to the Air Force Avionics Laboratory unless return is required by security regulations, contractual obligations, or notice on a specific document.

FOREWORD

This report Nr 6633-1-F was prepared by the University of Michigan, Ann Arbor, Michigan, under the direction of Mr. Ralph Hiatt and Professor J. A. M. Lyon and on Air Force Contract AF 33(615)-1761 under Task Nr 435709 of Project 4357 "(U) Electromagnetic Compatibility Control Techniques". The work was administered under the direction of the Air Force Avionics Laboratory, Electronic Warfare Division, Research and Technology Division, Wright-Patterson Air Force Base Ohio. The Task Engineer was Mr. Olin E. Horton; the Project Engineer, Mr. Herbert Bartman.

The studies presented herein began 1 Feb 1962 under Contract AF 33 (657)-8178 and were concluded 15 Nov 1965.

This report was submitted 3 January 1966.

This technical report has been reviewed and is approved.

JOSEPH A. DOMBROWSKI
Lt Colonel, USAF
Chief, Electronic Warfare Division

TABLE OF CONTENTS

TABLE OF CONTENTS
(continued)

ABSTRACT

This report emphasizes procedures to determine the power interference coupling from one antenna to another. The two antennas need not be similar. Simplified methods including graphs showing the variation of coupling vs angular orientation, frequency or distance are presented for a number of antenna types. Nomographs have been designed to make possible the rapid calculation of the coupling between two antennas. The last chapter of the report (VIII) shows by example the manner of calculation using the nomographs. In the main body of the report, details are given concerning the methods of obtaining the coupling between two antennas by analysis and also by measurements in the laboratory. Some of the more mathematical aspects of the analysis have been introduced as appendices to the report. For a reader interested primarily in the system interference problem, Chapters I and VIII will be helpful. The simplified formulas for coupling in the far region will prove interesting and the numerous experimental data graphs will be helpful for the various types of antennas represented. The presence of a third antenna or scattering object may occasionally influence substantially the coupling between two antennas, especially in the case of very weak coupling. Some discussion of the influence of scattering objects is given.

NOMENCLATURE

This list applies to symbols used in the main body of this report. Symbols encountered in the appendices are defined therein.

a	Slot dimension in H-plane; radius of curvature of cylindrical or spherical ground surface.
A	Effective aperture.
b	Slot dimension in E-plane.
c	Aperture radius of conical horn; speed of light.
C	Coupling.
C_o	Coupling between two parallel isotropic antennas.
C_s	Coupling due to scatterer.
d	Diameter of cylindrical waveguide.
D	Directivity.
E	Electric field intensity.
f	Frequency.
J	Bessel function of the first kind.
$\hat{h}_i$	Unit vector perpendicular to $\hat{q}_i$ and parallel to the ground plane.
$\hat{h}_s$	Unit vector perpendicular to $\hat{q}_s$ and parallel to the ground plane.
H	Magnetic field intensity.
I	Current.
k	Wave number.
$(K_{11}c)$	First root of J_1.
$(K_{11}'c)$	First root of J_1'.
L	Greatest linear dimension of the largest slot; height of conical horn.
p	Polarization mismatch factor.
$P(\phi)$	Power density in the ϕ direction.
q	Impedance mismatch factor.
$\hat{q}_i$	Unit vector directed from transmitter to scattering center.

$\hat{q}_s$	Unit vector directed along the line between scattering center and receiving antenna.
r	Distance of field point from source point.
r	As a subscript; refers to the receiver.
R	First spherical coordinate (field point); with subscript it indicates resistance.
R_o	Center-to-center spacing of two antennas.
s	As subscript refers to the scatterer.
S	Standing wave ratio.
$\bar{\bar{S}}$	Scattering dyadic.
SWR	Standing Wave ratio.
t	As a subscript; refers to the transmitter.
$\hat{v}_i$	Unit vector perpendicular to $\hat{q}_i$ and $\hat{h}_i$.
V	Voltage.
W	Power.
Y	Admittance.
β	Inclination of the major axis of an elliptically polarized antenna with respect to some fixed axis.
γ	Second spherical coordinate (aperture point).
ϵ	Dielectric constant.
ζ	Third cartesian coordinate (source point).
η	Second cartesian coordinate (source point).
θ	Second spherical coordinate (field point).
θ_a	Flare angle of a rectangular horn (H-plane).
θ_b	Flare angle of a rectangular horn (E-plane).
θ_c	Flare angle of a conical horn.
λ	Wavelength.
μ	Permeability.
ν_c	Angle between two planes containing the cylinder axis and the two antennas.

ν_s	Angle between two antennas on a plane containing the center of the sphere and the two antennas.
ξ	First cartesian coordinate (source point).
$\bar{\pi}^*$	Hertzian magnetic fector.
ρ	First cylindrical coordinate (source point).
τ	Second cylindrical coordinate (source point).
ϕ	Third spherical coordinate (field point).
ψ	Third spherical coordinate (aperture point).
ω	Angular frequency.

I

INTRODUCTION

This report presents detailed information on a wide variety of coupling situations involving two antennas. Concentration of effort has been made upon flush-mounted antennas. This has been due to the often specified requirement of flush-mounting for antennas utilized in airborne and aerospace vehicles. Some of the most common types of antennas useful for flush-mounting have been covered. The antennas which have been used in these coupling studies are: a) rectangular slots; b) E-sectoral rectangular horns; c) H-sectoral rectangular horns; d) pyramidal rectangular horns; e) conical horns; f) circular Archimedian spirals; g) square Archimedian spirals. In addition, a monopole antenna, erected perpendicular to the conducting metal plane used as a ground plane often has been used as a probe of the fields of other antennas. Also a Yagi array of monopoles has been used in a brief study of coupling involving this antenna.

For those most interested in system interference problems, section VIII illustrates by simple example the use of data from nomographs. These examples show how to compute coupling from one antenna to another like antenna. Also there are examples for the coupling from one antenna to an unlike antenna such as from a circular Archimedian spiral to a rectangular slot antenna. The manner of compensating for curvature of the metal mounting surface is also shown in section VI.

For the most part, low- and medium- gain antennas have been used in these coupling studies; all antennas have a directivity of less than 20 db. It is believed that the coupling of antennas having directivities in this designated range presents a relatively severe problem. Antennas with higher directivities can be handled by the same methods. It is necessary to extend the usual definition of directivity

since in general the main beams of the antennas are not collinear. The directivity function as used in this report is defined as a function of the angles designating direction. In the consideration of antennas of high directivity with main lobe pointed along the metal mounting surface, the directivity function along the radius vector designated could approach the maximum directivity as specified for the main lobe. Such cases are within the scope of this report.

The power coupling factor has been studied on the basis of matched antennas. This corresponds to a maximum of power transfer from one antenna to another. All analysis and measurements have been made upon the basis of cw or continuous wave propagation. Modulation of signals can well represent an important factor in the determination of tolerable level of power coupling in the overall interference problem of one system to another. Modulation of signals can be considered as an additional factor which can be dealt with separately since the power coupling based upon the cw assumption applies to most cases of modulated signals. Effects of mismatch, filtering techniques, and connected circuitry beyond the terminal reference planes of antennas are ignored. Such effects can also be accounted for by appropriate additional factors introduced into the interference problem. Similarly, non-linear effects are ignored; these could be introduced although with somewhat greater difficulty into system interference studies.

No attempt has been made in these studies to account for the effect on power coupling interference of either mechanical or electronic scanning since this can be treated as a type of modulation. Peak and average power values as well as the details of time sequence in the scanning pattern should be considered ultimately. If the mode of scanning changes under certain operational conditions then it is likely that the interference problem must be solved on a statistical basis. Even with all these possibilities, it is believed that the cw coupling studies contained in this report represent the most basic approach necessary for use in the power coupling interference problem.

The coupling problems associated with an antenna having a highly asymmetric pattern such as one with the main beam directed along the metal mounting surface can be treated utilizing information in this report. In such a case, the appropriate directivity corresponding to an angle very nearly 90^{o} giving a ray along the surface is necessary. Also, in the consideration of such antennas, it is important to have in mind the boundary condition which indicates that the tangential electric field must be zero just off the metal mounting surface. Such antennas with asymmetric patterns will be more highly coupled to another antenna if both of the antennas involved have main beams along the metal surface with the electric field normal to the metal surface. A vertically polarized surface-wave line or area source mounted in a conducting ground plane would be a general class of antennas where coupling could be predicted by the general ideas in this report. Such asymmetric antennas should be considered with pattern compensation made for the location of the antenna within and also flush to the metal surface. The effect of the curvature of the conducting metal surface would be substantial on this type of antenna. The modifications indicated in section VI for curvature of the ground surface would not fully account for the situation involving the vertically polarized surface wave antenna mounted flush on the ground surface, since the surface curvature within the Fresnel zone could be appreciable.

These coupling studies have been made with the recognition of dependency upon frequency, spacing, orientation, polarization and scattering objects. In the case of transmitting and receiving antennas mounted in the same surface, the analysis can frequently be made from available coupling formulas of two antennas in free-space. For example, two parallel monopoles operating over a conducting ground surface, have the same coupling as two dipoles having the same spacing and operating in free-space. Likewise, two rectangular slots in a common ground plane show a coupling corresponding to two magnetic dipoles in free-space with recognition that all energy is confined to half-space.

In the investigation of the effect of surface curvature it was found that if the radius of curvature is greater than twice the free-space wavelength, its effect can be obtained by the analysis included in this report. In fact, the formulas give reasonably accurate results down to a radius of curvature equal to the free-space wavelength. For frequencies in L-band and higher, such formulas appear to be adequate. For surfaces having a radius of curvature less than one half the free-space wavelength, the surface must be considered an integral part of the radiator, and the problem is more complicated.

The low-gain antennas used in these studies were monopoles, rectangular slots, spirals, and, in general, antennas having a lineal dimension less than 1.5 wavelengths. The medium-gain antennas used are characterized by having beams perpendicular to the conducting metal mounting surface.

The report includes extended calculations on the effects of scattering from objects other than the two antennas between which coupling is observed. These studies are applicable to a metal edge such as is present on various airfoils and other scatterers.

In the presentation of data numerous graphs, charts and nomographs have been utilized. The data considered to be most important or most useful is in the main body of the report. In Appendix A an analysis of the coupling between planar apertures is given. In Appendix B the more detailed information on coupling due to other scatterers is given. Additional experimental data on coupling between rectangular horns is presented in Appendix C.

II

FAR FIELD COUPLING FORMULAS

2.1 Antennas in Free Space

In most textbooks the terms gain, aperture, and directivity are used in claculating the power transferred from one antenna to another. These terms are usually attributed to the antenna itself; for example, it is frequently stated that a horn has a gain of 15 db above isotropic. In order to consider variations with angle, these terms must be generalized.

The coupling between two antennas at a given frequency is defined as the ratio of the power received to the power transmitted, or

$$C = \frac{W_r}{W_t} \tag{2.1}$$

The general form of the expression for free space coupling is

$$C = C_o(R_o)\, D_t^f(\theta_t, \phi_t)\, D_r^f(\theta_r, \phi_r)\, P\, q_r\, q_t \tag{2.2}$$

where $C_o(R_o)$ is the coupling between two "parallel" isotropic antennas a distance R_o apart, given by: (see Fig. 2-1)

$$C_o(R_o) = \left(\frac{\lambda}{4\pi R_o}\right)^2 . \tag{2.3}$$

$D^f(\theta, \phi)$ is the free space directivity function, defined by:

$$D^f(\theta, \phi) = \frac{4\pi \left|\overline{E}(\theta, \phi)\right|^2}{\int_0^{2\pi}\int_0^{\pi} \left|\overline{E}(\theta, \phi)\right|^2 \sin\theta \, d\theta \, d\phi} \tag{2.4}$$

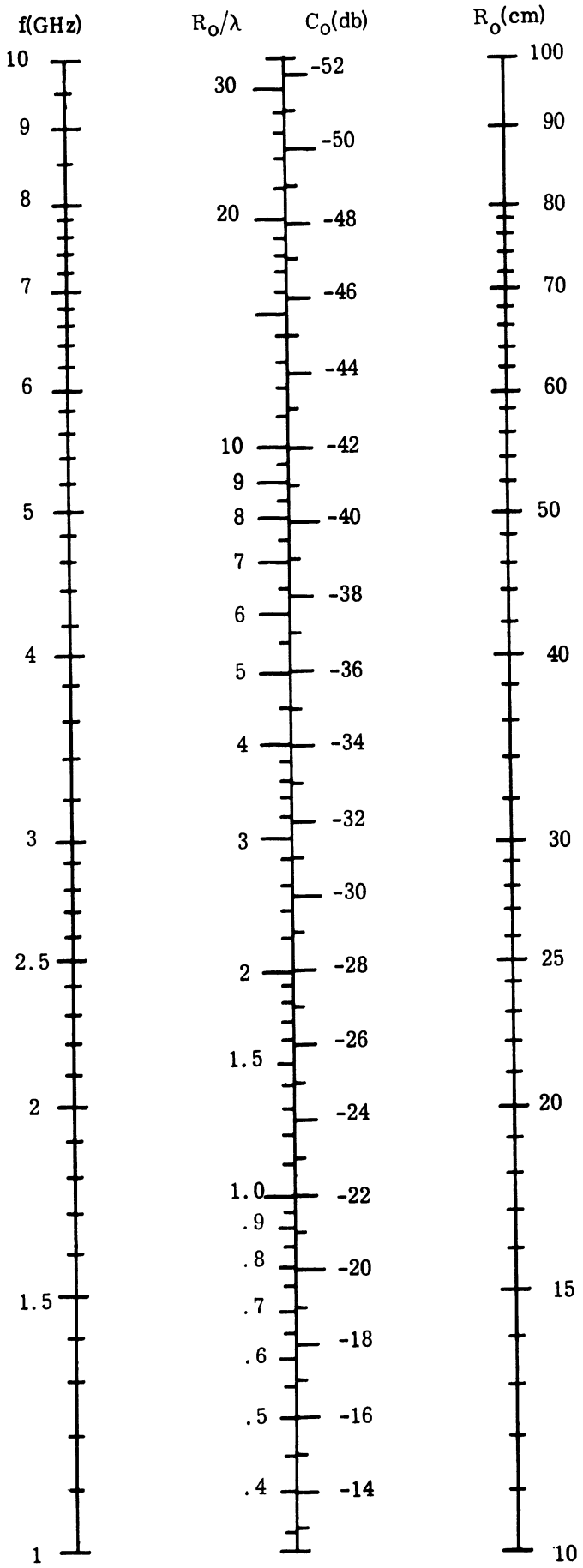

FIG. 2-1: $C_o(R_o)$ VS R_o/λ

This gives the ratio of the power density in a given direction (θ, ϕ) to the average power density. The subscripts t and r refer to transmitter and receiver, respectively. The maximum value of $D^f(\theta, \phi)$ is called the "directivity" of the antenna (Fig. 2-2). The symbol p is the polarization mismatch, equal to one for a perfect match (Section 2.5), and q is the impedance mismatch, which accounts for reflection and losses in the antenna (Section 2.4). For two lossless, perfectly matched antennas whose polarizations are matched (e.g., two parallel, linear dipoles), $p = 1$ and $q_t = q_r = 1$.

The advantage of this formulation is that the spacing dependence and angular dependence of each antenna are separated, since for the far-field case $D(\theta, \phi)$ is independent of R_o. Here the coupling between two antennas is compared with that between two isotropic antennas at the same spacing. Thus if C_o = -60 db, and neither antenna lies on the main beam of the other, the coupling will be less than -60 db (assuming no reflections from surrounding objects).

2.2 Antennas on a Common Surface

The major emphasis of this report is on pairs of antennas mounted in a common conducting surface, as the skin of an airplane or missile, or a mounting plate. In this case the tangential electric field is zero (or very small for a good conductor), and the polarization is vertical. Thus the polarizations of the transmitting and receiving antennas are parallel, and $p = 1$, identically.

Furthermore, the coupling between two vertical dipoles in free space is identical with that of two corresponding monopoles in a ground plane at the same spacing. Defining a "semi-isotropic" antenna as one which has a constant pattern factor above the ground plane and zero below, the coupling between two semi-isotropic antennas on the same ground plane is the same as the coupling between two isotropic antennas.

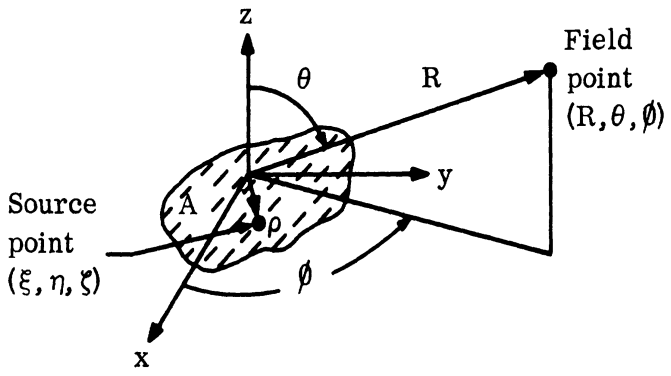

FIG. 2-2a: GEOMETRY OF GENERAL GROUND PLANE APERTURE

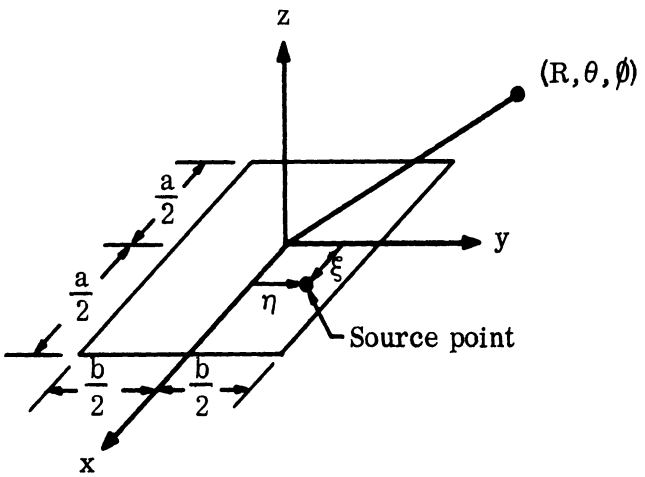

FIG. 2-2b: GEOMETRY OF RECTANGULAR APERTURE

For two antennas in the same flat conducting surface, $\theta = 90^{o}$, and the expression for the coupling becomes:

$$C = C_o (R_o)\, D_t (\phi_t)\, D_r (\phi_r)\, q_t\, q_r \tag{2.5}$$

where

$$D(\phi) = \frac{2\pi \left| \bar{E} (\pi/2, \phi) \right|^2}{\int_0^{2\pi} \int_0^{\pi/2} \left| \bar{E} (\theta, \phi) \right|^2 \sin\theta \, d\theta \, d\phi} = D(\pi/2, \phi) \tag{2.6}$$

and as before (see Fig. 2-1)

$$C_o (R_o) = \left(\frac{\lambda}{4\pi R_o}\right)^2 . \tag{2.3}$$

2.3 Relation of $D(\theta, \phi)$ to the Usual Definitions of Gain, Directivity, Aperture, and Mutual Impedance

As stated above, the "directivity" of an antenna is the maximum value of $D(\theta, \phi)$.

"Gain" usually given in decibels, is equal to the directivity diminished by losses.

"Aperture" has usually been associated with the directivity of an antenna, but recently this has been generalized to account for angular variations (Tai, 1961), so that several apertures are defined (for free space):

(a) Effective aperture:

$$A = \frac{\lambda^2}{4\pi} D^f(\theta, \phi)\, pq$$

(b) Effective aperture, polarization matched:

$$A_m = \frac{\lambda^2}{4\pi} D^f(\theta, \phi)\, q$$

(c) Effective aperture, impedance matched:

$$A_n = \frac{\lambda^2}{4\pi} D^f(\theta, \phi)\, p$$

(d) Optimum effective aperture:

$$A_{op} = \frac{\lambda^2}{4\pi} D^f_{max} \,. \tag{2.7}$$

where D^f_{max} is the maximum value of $D^f(\theta, \phi)$. The latter definition is one usually used for effective aperture, or maximum effective aperture.

If both antennas are on the same ground plane, then the apertures must be half those above, e.g.

$$A = \frac{\lambda^2}{8\pi} D^f(\theta, \phi)\, pq \tag{2.8}$$

The directivity function $D(\theta, \phi)$ of Section 2.2 will be used throughout this report.

"Mutual impedance" is a term often used in connection with interference studies. Coupling actually carries less information, unless a phase measurement is also taken. Coupling is related to mutual impedance by:

$$C = \frac{|Z_{12}|^2}{4 R_t R_r} q_t q_r \qquad (2.9)$$

where Z_{12} is the mutual impedance, and $Z_{12} << R_t$ or R_r.

R_t is the input resistance of the transmitter

R_r is the input resistance of the receiver

$q = \frac{4S}{(1+S)^2}$

S is the standing wave ratio (SWR).

2.4 Effects of Impedance Mismatch and Losses

Frequently coupling takes place between antennas which operate at different frequencies. Here it is necessary to consider the filtering action of the receiving antenna. The SWR of an antenna at a given frequency is a measure of its rejection of an incident signal. The coupling calculated in the report gives a measure of the power received under matched conditions. Thus from Fig. 2-3 if the SWR of the receiving antenna is 5, the actual coupling will be 2.5 db below the calculated level. In using the figure, a horizontal line is drawn from one vertical line to the other.

Losses are not considered in any detail in this report. Generally they do not affect the shape of the patterns appreciably. Typical results can be taken from the experimental data. These data were obtained by comparing the power

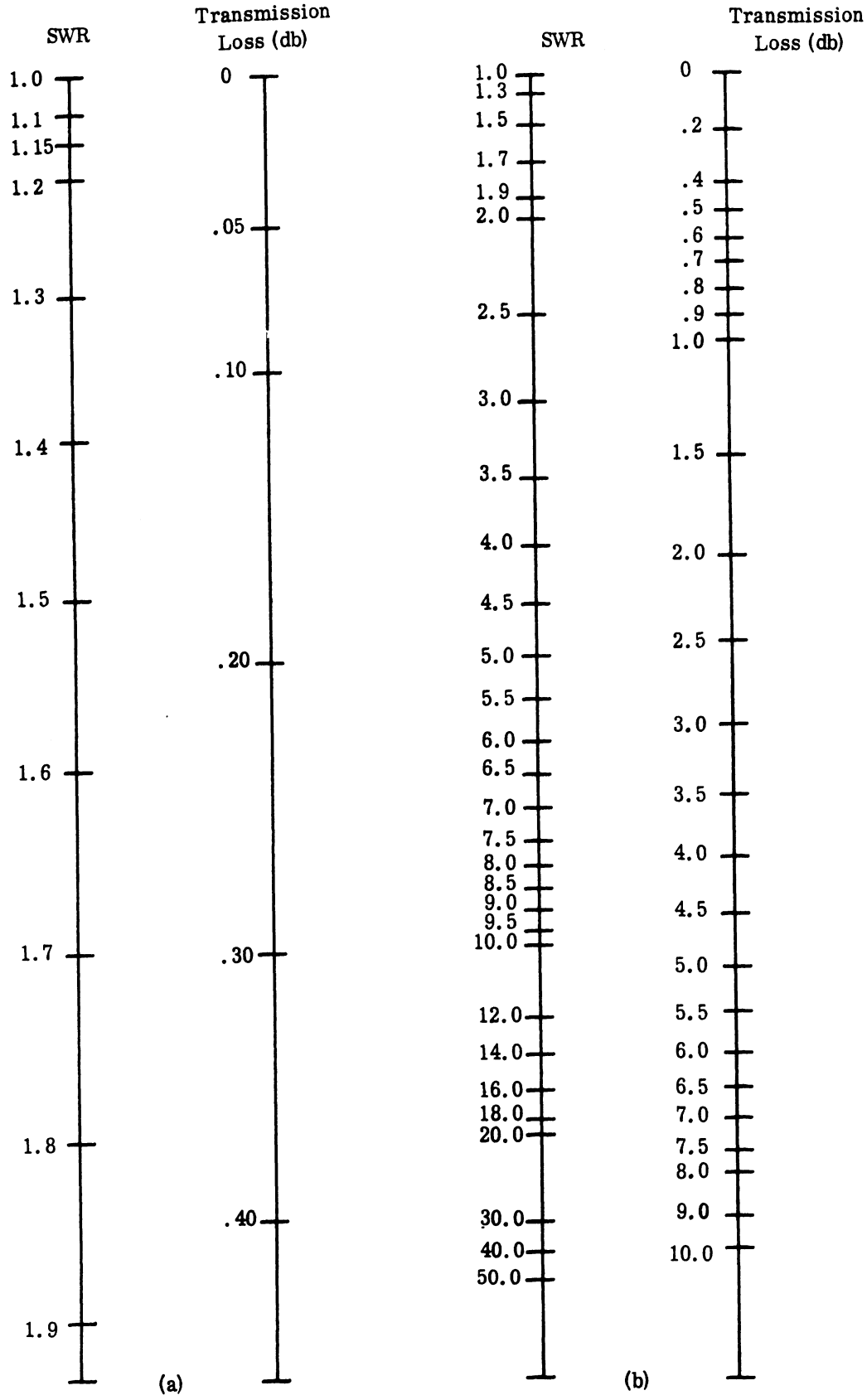

FIG. 2-3: NOMOGRAPH RELATING SWR AND TRANSMISSION LOSS

delivered to a receiver load to that delivered to the transmitting antenna; thus the measurement contains the losses in both the transmitting and receiving antennas. In the case of slots, comparison of theoretical and experimental data indicate about 1 db per antenna; for the horns, from 1 to 3 db per antenna. It should be noted that for convenience brass was used extensively in the experiments whereas better conducting material may be used in practice.

2.5 Effects of Polarization Mismatch for Antennas in Free Space

For the sake of completeness, a brief discussion of the power transfer between elliptically polarized antennas is included here. It should be pointed out that this discussion does not bear on most of the items in this report, due to the presence of the ground plane, which dictates a vertically polarized wave, and matched polarization conditions.

The polarization mismatch is expressed by

$$p = \frac{1+s_r^2 s_t^2 + 2 s_r s_t \cos(\alpha_r + \alpha_t)}{(1+s_r^2)(1+s_t^2)} \qquad (2.10)$$

where s and α are defined below.

Usually if antennas are elliptically polarized, this ellipticity is expressed by the shape, and the inclination of the major axis; i.e. r_e and β_e are specified, where

r_e is called the axial ratio, given by

$$r_e = \frac{\text{minor axis}}{\text{major axis}} .$$

β is the inclination of the major axis with respect to some fixed axis and the ellipse describes the locus of the electric field vector. The quantity r_e ranges from -1 to +1, and referring to Fig. 2-4, the following convention is taken with respect to the sign of r_e:

+: transmits or receives a right-handed, or clockwise wave

-: transmits or receives a left-handed, or counter-clockwise wave.

Note that an antenna transmitting a right-hand wave will receive a left-handed wave, and vice versa.

The quantities s and α are related to r_e and β by:

$$s = \sqrt{\frac{r_e^2 + \tan^2 \beta}{1 + r_e^2 \tan^2 \beta}} \tag{2.11}$$

$$\tan \alpha = \frac{2 r_e}{(1 - r_e^2) \sin^2 \beta} \cdot \tag{2.12}$$

Examples: (a) two dipoles - linear polarization: $r_e = 0$ for bothe transmitter and receiver:

$$s_r = \tan \beta_r, \quad s_t = \tan \beta_t, \quad \alpha_r = \alpha_t = 0, \quad \text{and } p = \cos^2 (\beta_t - \beta_r).$$

Then p = 1 if the dipoles are parallel ($\beta_t = \beta_r$), and p = 0 if the dipoles are perpendicular ($\beta_t = \beta_r \pm 90^o$).

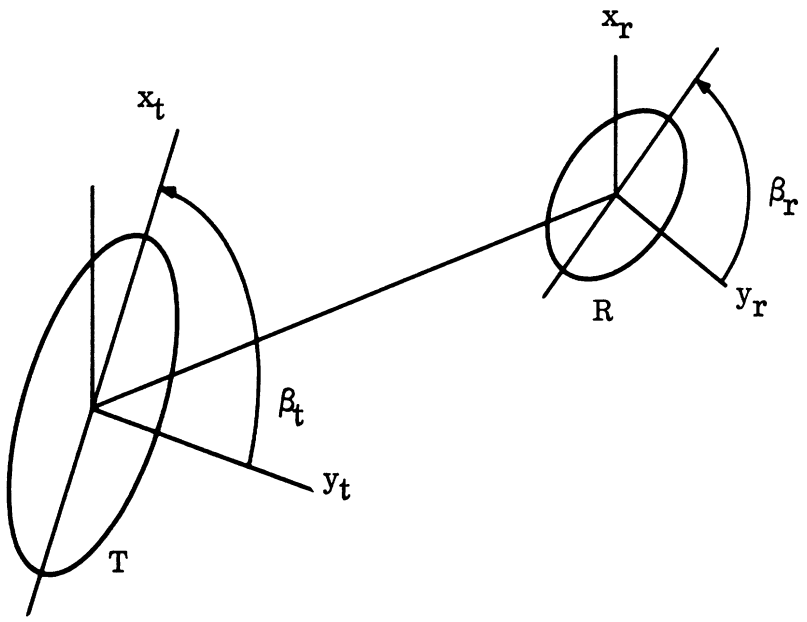

FIG. 2-4: GEOMETRY FOR ELLIPTICALLY POLARIZED ANTENNAS

(b) Circularly polarized antennas:

$r_e = +1$ for both transmitter and receiver:

$$s_r = s_t = 1$$

$$\alpha_r = \pm 90^o, \quad \alpha_t = \pm 90^o$$

then

$$p = \frac{1 + \cos(\alpha_r + \alpha_t)}{2}. \tag{2.13}$$

If both antennas transmit a right-hand wave, then $\alpha_t = 90^o$, $\alpha_r = -90^o$, and $p = 1$. If one of the polarizations is reversed, $p = 0$.

For more detail, one should consult Section 5.2, Tai (1961), Deschamps (1951), and Rumsey (1961).

III

FIRST ORDER APPROACHES TO ESTIMATING COUPLING WITH NOMOGRAPHS

The knowledge of the coupling between two simple antennas, such as two monopoles, may be used to estimate the coupling level between two arbitrary antennas. In this section simple antennas are first considered and then attention is given to successively more complicated antennas, providing estimates of the way they differ from the corresponding simpler cases. All antennas considered are flush-mounted, so that the coupling formulas from Section 2.2 are used:

$$C = C_o(R_o)\, D_t(\phi_t)\, D_r(\phi_r)\, q_t\, q_r . \tag{3.1}$$

This formula holds for spacings greater than L^2/λ i.e. $R_o > L^2/\lambda$, where L is the greatest linear dimension of the largest antenna. The expression may also require modification for angles where $D(\phi)$ becomes very small, i.e. on a null. These cases will be discussed further in Chapter IV.

3.1 Thin Monopoles

If two monopoles are mounted perpendicular to the ground plane, the directivity function $D(\phi)$ is independent of angle.

For short monopoles, i.e., having lengths less than $\lambda/10$,

$$D(\phi) = D_{max} = 1.5, \text{ or } 1.76 \text{ db}. \tag{3.2}$$

For resonant quarter - wave monopoles

$$D(\phi) = D_{max} = 1.64, \text{ or } 2.15 \text{ db}. \tag{3.3}$$

Thus the coupling between two quarter-wave monopoles, each perfectly matched and lossless, is 4.3 db above $C_o(R_o)$. This case is important enough to deserve a separate nomograph (Fig. 3-1).

3.2 Slots

The directivity function for a short, thin slot is given by

$$D(\phi) = 1.5 \cos^2 \phi \qquad (3.4)$$

except at $\phi = 90^o$ (see Fig. 3-2). Near $\phi = 90^o$, the coupling may be near-field coupling, which cannot be expressed in the far-field coupling form. This is discussed further in Section 4.2.3. By short and thin is meant: for this expression to be accurate within $5^o/_o$, $b < 0.2\lambda$ and $a < 0.35\lambda$.

For a thin slot a half-wavelength long,

$$D(\phi) = 1.64 \cos^2 (\frac{\pi}{2} \sin \phi) \qquad (3.5)$$

Note that the maximum values of $D(\phi)$ for the two cases above are the same as for the monopoles of equal length.

The general slot case is discussed in detail in Section 4.2 along with nomographs for calculations. The values of $D(\phi)$ above are limiting cases.

3.3 Approximate Horn Coupling

The antennas considered thus far have been low-gain, broad beam radiators. The aperture fields of the slots are known with some precision, and the resulting field patterns are relatively unaffected by the inaccuracies. As the aperture is increased in size, this is no longer true. First of all, the aperture fields are more sensitive to small disturbances. Second, the resulting fields are more

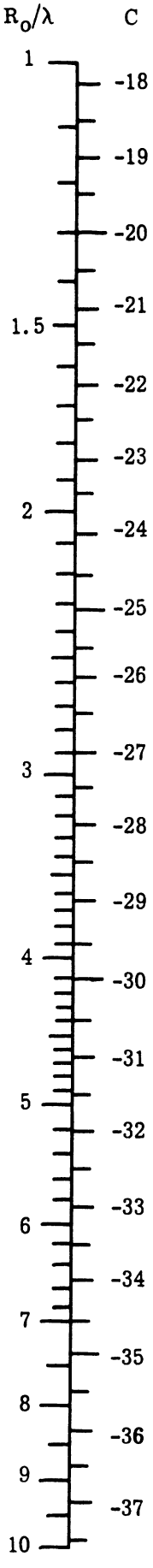

FIG. 3-1: NOMOGRAPH FOR CALCULATING COUPLING BETWEEN TWO QUARTER WAVE MONOPOLES

sensitive to small changes in the aperture fields, although on the main beam it remains relatively insensitive. Third, conventional configurations (such as horns) do not give plane waves at the aperture, but rather curved wave fronts. For a common type of horn, as well as many practical antennas, the main beam is perpendicular to the surface, and coupling takes place through the side lobes.

A very rough estimate of the coupling between two horns, accurate to about $\pm$ 10 db, (except at a null), can be obtained without knowledge of the flare angles; in this estimate the following expression is used:

$$D(\phi) = \frac{16}{\pi}\left(\frac{a}{\lambda}\right)\left(\frac{b}{\lambda}\right)\frac{\cos^2\phi}{\sqrt{1-\left(\frac{\lambda}{2a}\right)^2}} f_1(v)\, f_2(u) \tag{3.6}$$

where the geometry is that of Fig. 3-2, and

$$f_1(v) = \left\{ \begin{array}{ll} \dfrac{\sin v}{v}, & v < \pi/2 \\ \\ \dfrac{1}{v}, & v > \pi/2 \end{array} \right\}$$

$$f_2(u) = \left\{ \begin{array}{ll} \dfrac{\cos u}{1-\dfrac{4u^2}{\pi^2}}, & u < \pi \\ \\ \dfrac{1}{1-\dfrac{4u^2}{\pi^2}}, & u > \pi \end{array} \right\} \tag{3.7}$$

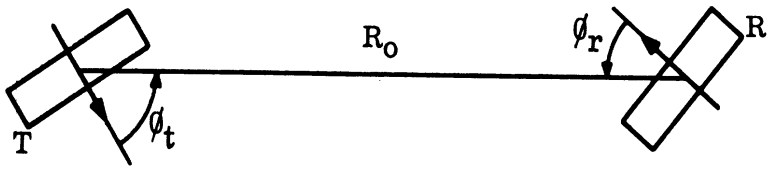

FIG. 3-2: SLOT GEOMETRY

$$u = \pi \left(\frac{a}{\lambda}\right) \sin \phi$$

$$v = \pi \left(\frac{b}{\lambda}\right) \cos \phi$$

A set of nomographs for finding $D(\phi)$ by this formula is given in Fig. 3-3. The use of these nomographs is explained in Section 8.2.3 where an example is given. This expression may be used for obtaining "ball park" coupling levels for aperture type antennas where the axis of the main beam is normal to the surface on which the antennas are mounted. More accurate expressions for the standard horn are given in Section 4.4.2. The curves of Figs. C-1-a through C-2-m demonstrate the comparative coupling levels of the above expression (3.6) and the more detailed and accurate ones.

3.4 Approximate Spiral Coupling

The spiral is a low gain radiator which differs from the antennas discussed before in that it is not linearly polarized. Along the beam axis a well designed spiral is very nearly circularly polarized.

Due to the presence of the conducting ground plane, the electric field along the ground plane is vertically polarized. Thus the coupling between two spirals is dependent only on $D_t(\phi_t)$ and $D_r(\phi_r)$, and does not depend on the sense of polarization of each antenna. For example, if two spirals having opposite senses of polarization have the same pattern factor, their couplings with a third antenna will be identical (same spacing, orientation assumed).

To a first approximation spirals are omni-directional with a progressive phase shift as the angle ϕ is changed. From the experimental data the circular spiral has an average pattern factor given by

$$D(\phi) = -8 \text{ db (axial, or } 1\lambda \text{ mode)} \qquad (3.8)$$

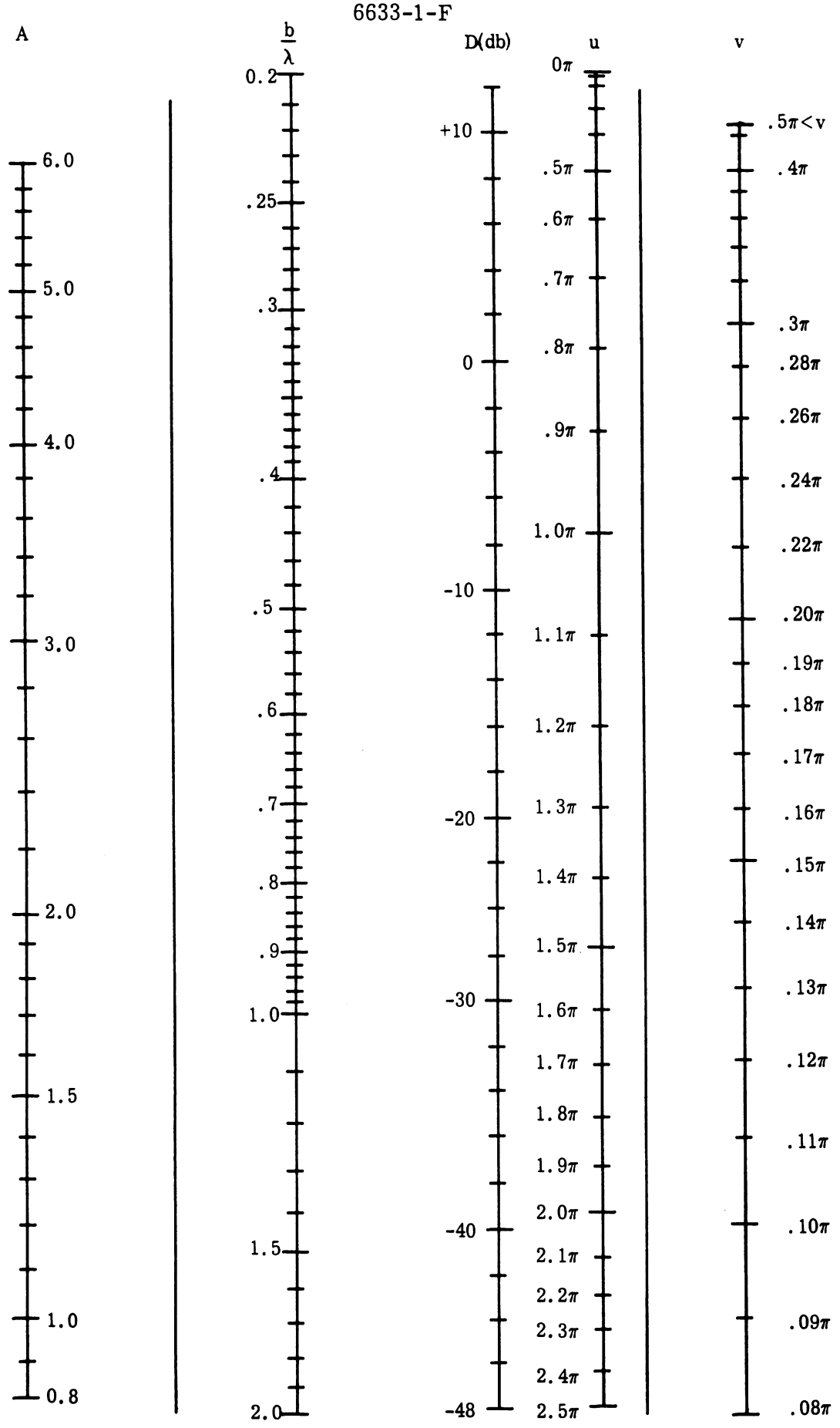

FIG. 3-3: NOMOGRAPH FOR CALCULATING THE DIRECTIVITY FUNCTION OF A RECTANGULAR HORN

The square spiral has a slightly higher value since it has slightly broader beam:

$$D(\phi) = -7 \text{ db} \tag{3.9}$$

These are average values taken over the design band. At a particular frequency and angle, the pattern factor may vary significantly from this value, but over a band of frequencies this expression is adequate. Spirals are discussed in more detail in Section 4.3.

3.5 Fresnel Zone Modifications

The far field coupling formulas are usually considered to be valid for the condition:

$$R_o > \frac{2L^2}{\lambda} \tag{3.10}$$

where L is the largest linear dimension of the larger antenna. This criterion was derived by considering a phase difference of $22\ ^1/_2{}^o$ between a plane wave and a spherical wave incident on a flat plate. This apparently has little to do with the criterion desired for coupling, i.e., the spacing at which the coupling deviates from its far field expression by, for example, 1 db.

A study by Jacobs (1960) indicates that for the maximum coupling case, i.e. two horns "looking at" each other, a variation of 1 db is encountered at about $R_o = L^2/\lambda$ for several aperture field distributions. For the experimental data taken here, the coupling patterns inside this region change somewhat in shape, particularly at the pattern minima, but the change in level is close to the 6 db per spacing octave which is the fall-off characteristic of the far field. This is discussed further in Section 4.5.

IV

DETAILED CONSIDERATIONS OF COUPLING

In this chapter more accurate calculations and expressions are given for the antennas described in Chapter III, with other related antennas as well. The theoretical results are compared with experiment. Fabrication problems, design criteria, and antenna details are discussed as well as the limitations on the theoretical models. Fresnel zone and near field effects are described and harmonic frequency effects and higher order modes are considered.

4.1 Monopoles

The emphasis in this report is on coupling levels rather than phase information. For monopoles a quarter wavelength long, or less, the directivity function $D(\phi)$ does not change significantly as the shape of the radiator is changed. An estimate of these changes can be obtained from the slot data of Section 4.2 . The coupling of dipoles and monopoles has received much attention in the literature (King, 1946, Blasi, 1954). There the concern has been to obtain high accuracy in calculating phase in applications to arrays. Here, the directivity functions of Section 3.1 are sufficient.

4.2 Slots and Open-ended Waveguides

The general problem of coupling of two rectangular apertures was treated in this study. In particular, solutions were found to the following cases (see Fig. 4-22).

1) Directivity functions of an open-ended waveguide for arbitrary size: TE_{10} mode, far field.
2) E-plane coupling: TE_{10} mode, near and far field.
3) H-plane coupling: TE_{10} mode, near field only.

An outline of the derivation of the solutions is given in Appendix A. Only results and curves are presented here, including a nomograph for calculating the coupling between two slots.

4.2.1 Pattern Factor for Small Slots and Open-ended Waveguides

From Appendix A (Sect. A.2), the normalized pattern factor $D(\phi)$ for an arbitrary rectangular aperture, assuming a constant phase front at the aperture, is

$$D(\phi) = \frac{3}{2F}\cos^2\phi\left(\frac{\sin v}{v}\right)^2\left(\frac{\cos u}{1-\frac{4u^2}{\pi^2}}\right)^2 \tag{4.1}$$

where

$$u = \pi\left(\frac{a}{\lambda}\right)\sin\phi$$
$$v = \pi\left(\frac{b}{\lambda}\right)\cos\phi \tag{4.2}$$

and F is a modification factor having the following properties:

$$F \doteq 1, \qquad \text{for } a/\lambda \text{ and } b/\lambda \text{ small,}$$
$$F \doteq \frac{3\pi}{32}\,\frac{\sqrt{1-\left(\frac{\lambda}{2a}\right)^2}}{\left(\frac{a}{\lambda}\right)\left(\frac{b}{\lambda}\right)}, \quad a/\lambda \text{ and } b/\lambda \text{ large} \tag{4.3}$$

Fig. 4-1 shows F as a function of a/λ, with α as a parameter, where $\alpha = b/a$. For $\alpha < 0.5$, which is the case for slots, and $a/\lambda < 0.8$, F is given approximately by:

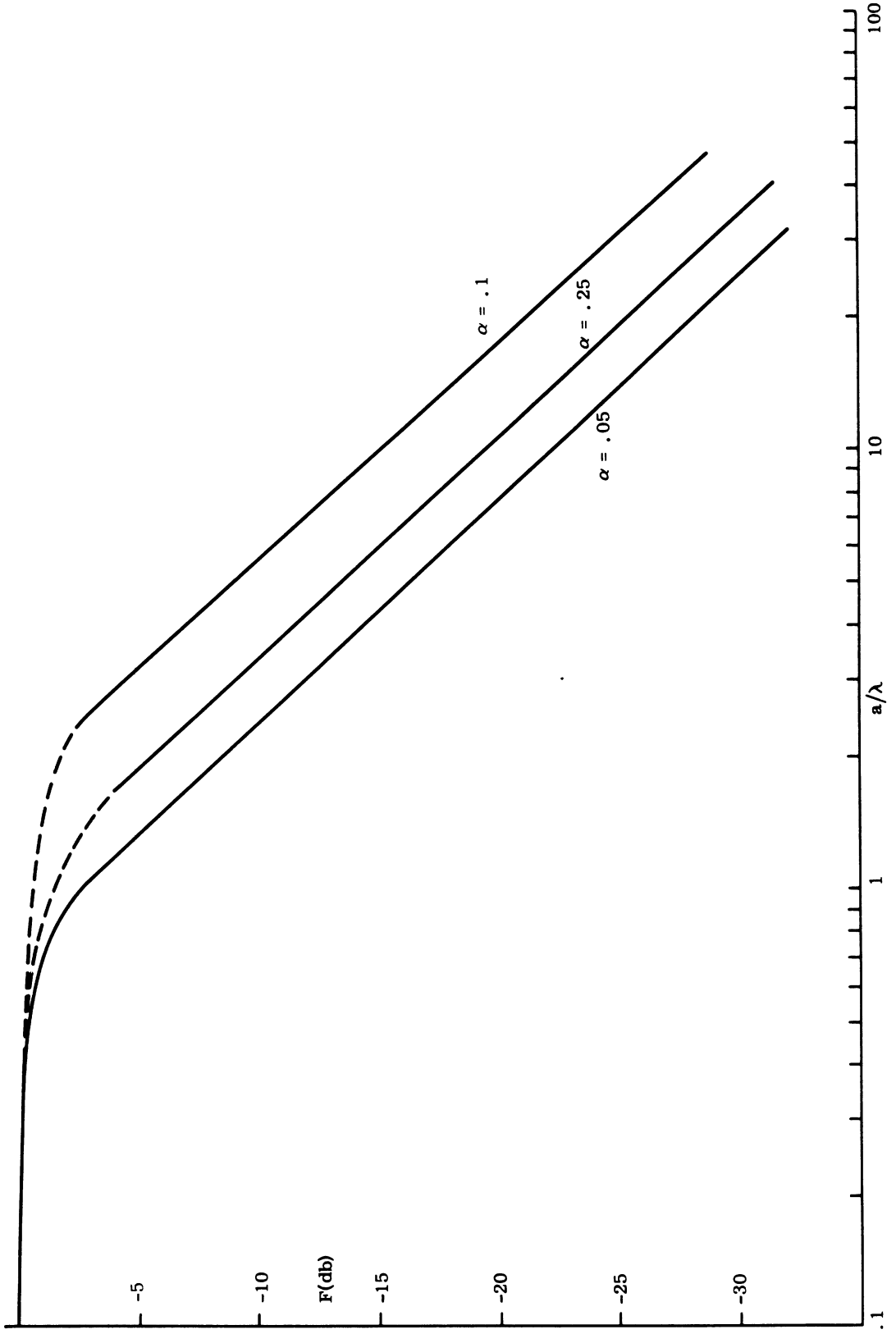

FIG. 4-1: MODIFICATION FACTOR "F" VS a/λ

$$F = 1 - \left(\frac{a}{\lambda}\right)^2 (.374 + 1.360\alpha^2) + \left(\frac{a}{\lambda}\right)^4 (.130 + .365\alpha^2 + .556\alpha^4)$$

$$- \left(\frac{a}{\lambda}\right)^6 (.154 + .218\alpha^2) \qquad (4.4)$$

Figure 4-2 is a nomograph for calculating the directivity function $D(\phi)$. For convenience the nomograph in Fig. 4-3 is included. It facilitates the calculation of the coupling between a pair of slots or open-ended waveguides. Instructions for using the nomographs, including worked examples, are given in Chapter VIII.

There are two assumptions involved in the use of the formulas and nomographs:

a) Each slot is in the far field of the other; this is not much of a restriction, since the slots must be practically touching before any significant discrepancy occurs. This is discussed in Section 4.2.2.

b) Neither ϕ_t nor ϕ_r are 90^o. When this happens, the far field term approaches zero, and the near field dominates. This is shown in Section 4.2.3.

4.2.2 Broadside Coupling of Open-ended Waveguides

When two open-ended waveguides are in the broadside, or E-plane configuration, where $\phi_r = \phi_t = 0^o$ or 180^o, the problem can be solved for any spacing, including the near field. The problem of two open-ended waveguides having the same dimensions is treated in detail in Appendix A. In order to consider near-field effects it is no longer possible to treat each antenna separately; they must be considered as a pair.

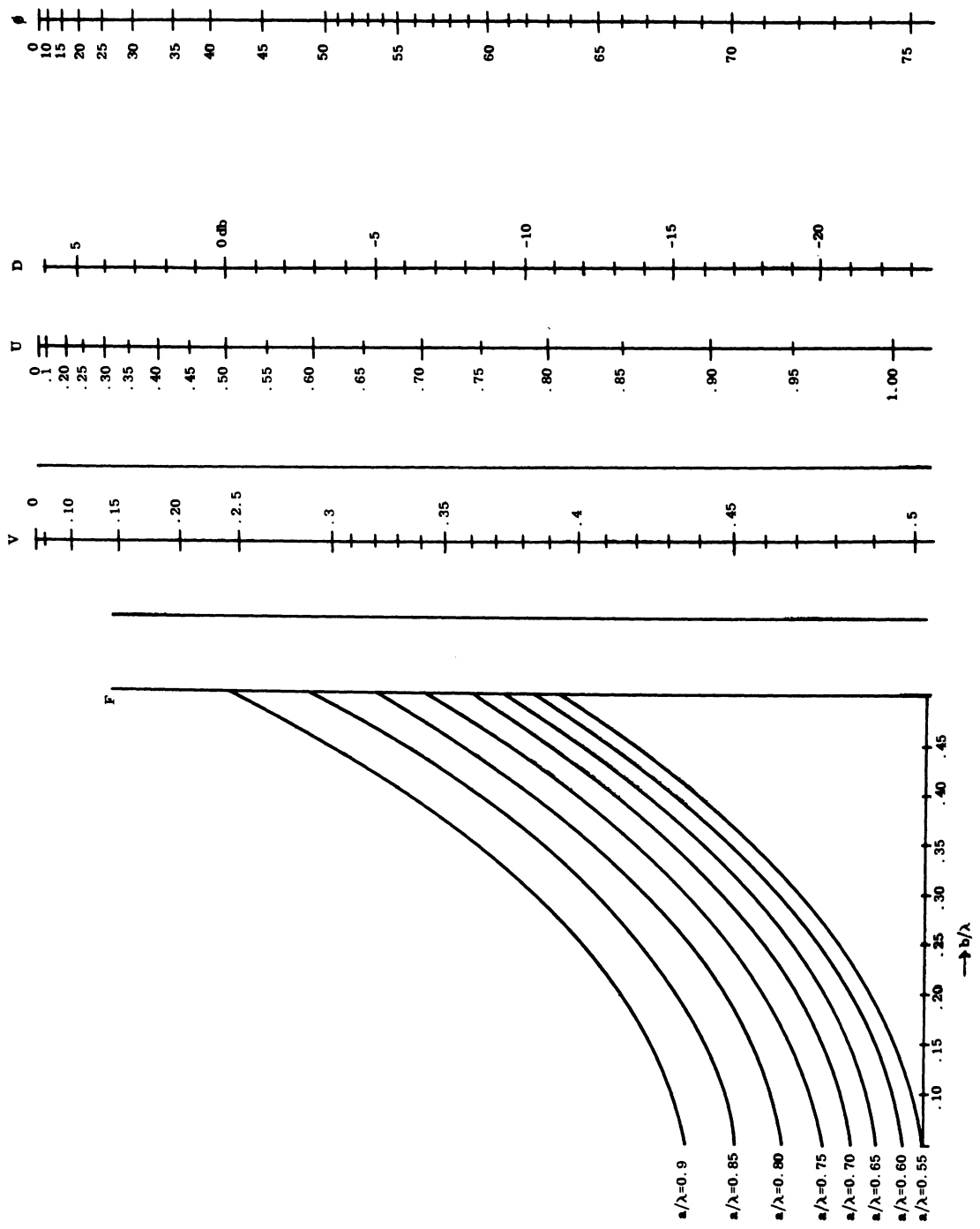

FIG. 4-2: NOMOGRAPH FOR CALCULATING DIRECTIVITY FUNCTION D(φ)

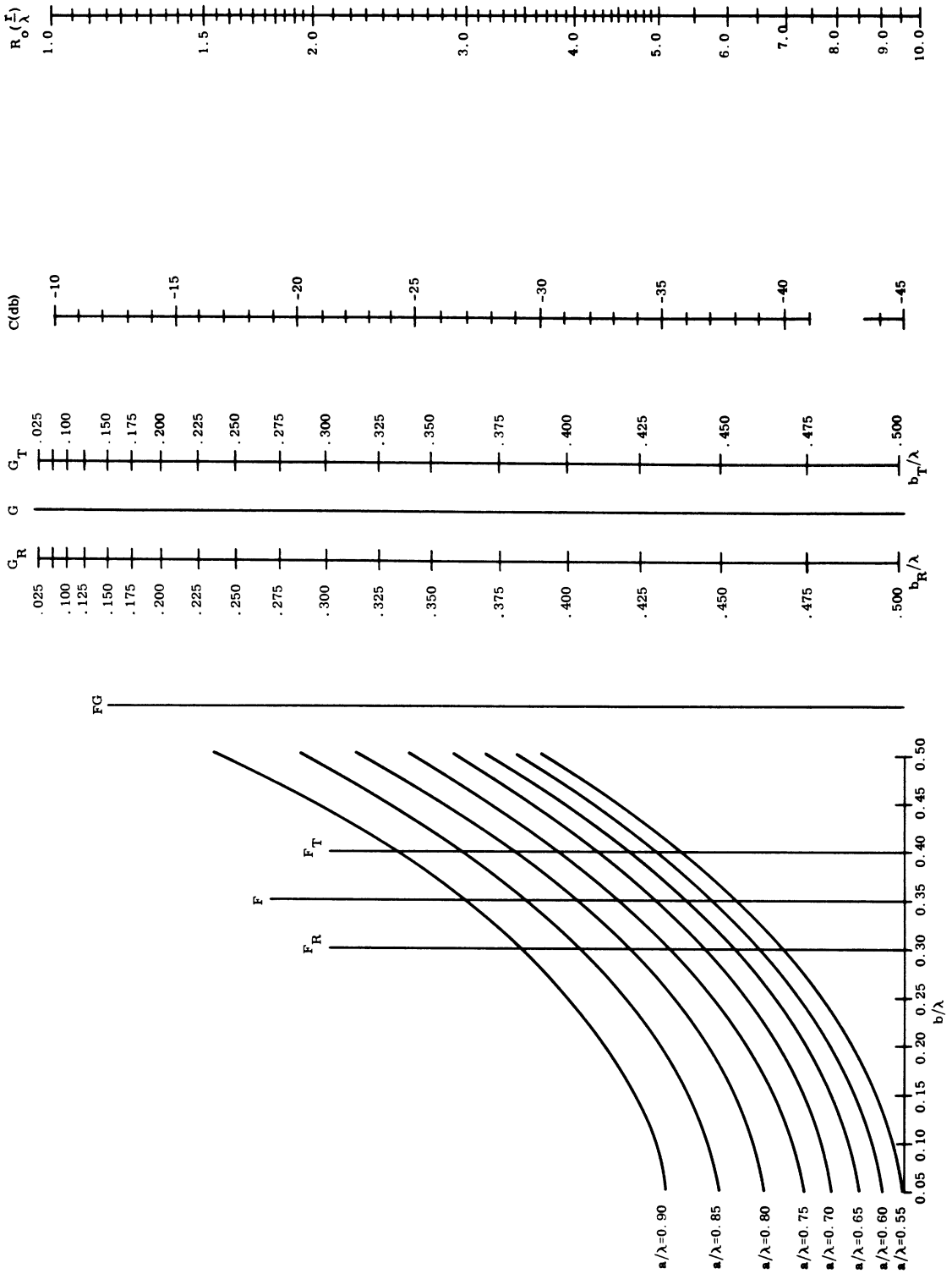

FIG. 4-3: COUPLING BETWEEN TWO SLOTS IN ANY DIRECTION

The coupling must be modified by the factor N:

$$C = C_o (R_o)\, D_t(\phi_t)\, D_r(\phi_r)\, N\, q_t\, q_r \tag{4.5}$$

where

$$N = \frac{|K_1|^2}{16\pi^2 \left(\frac{b^4}{R_o^2 a^2}\right) \left(\frac{\sin v}{v}\right)^4} \tag{4.6}$$

and

$$K_1 = \frac{\pi^4}{a^4} \left\{ \int_{R_o-b}^{R_o+b} dy\, (b - |R_o - y|) \cdot\cdot \int_o^a \left\{ \left(1 - \frac{\lambda^2}{4a^2}\right)(a - \xi) \cos\frac{\pi\xi}{a} + \left(1 + \frac{\lambda^2}{4a^2}\right) \sin\frac{\pi\xi}{a} \right\} \cdot\cdot \frac{e^{-jk\sqrt{y^2+\xi^2}}}{\sqrt{y^2+\xi^2}}\, d\xi \right\} . \tag{4.7}$$

Experimental data were obtained for broadside open-ended waveguides for several spacings, as shown in Fig. 4-4. The straight line represents the 6 db per octave decrease in coupling associated with the far-field formula. The calculated coupling level checks within 0.5 db of the observed level, which is closer than the expected accuracy of the measuring system. It should be noted that for the extreme left experimental point the waveguides are as close as it is physically possible to place them. Thus for practical purposes, the far-field coupling of Section 4.2.1 may be used.

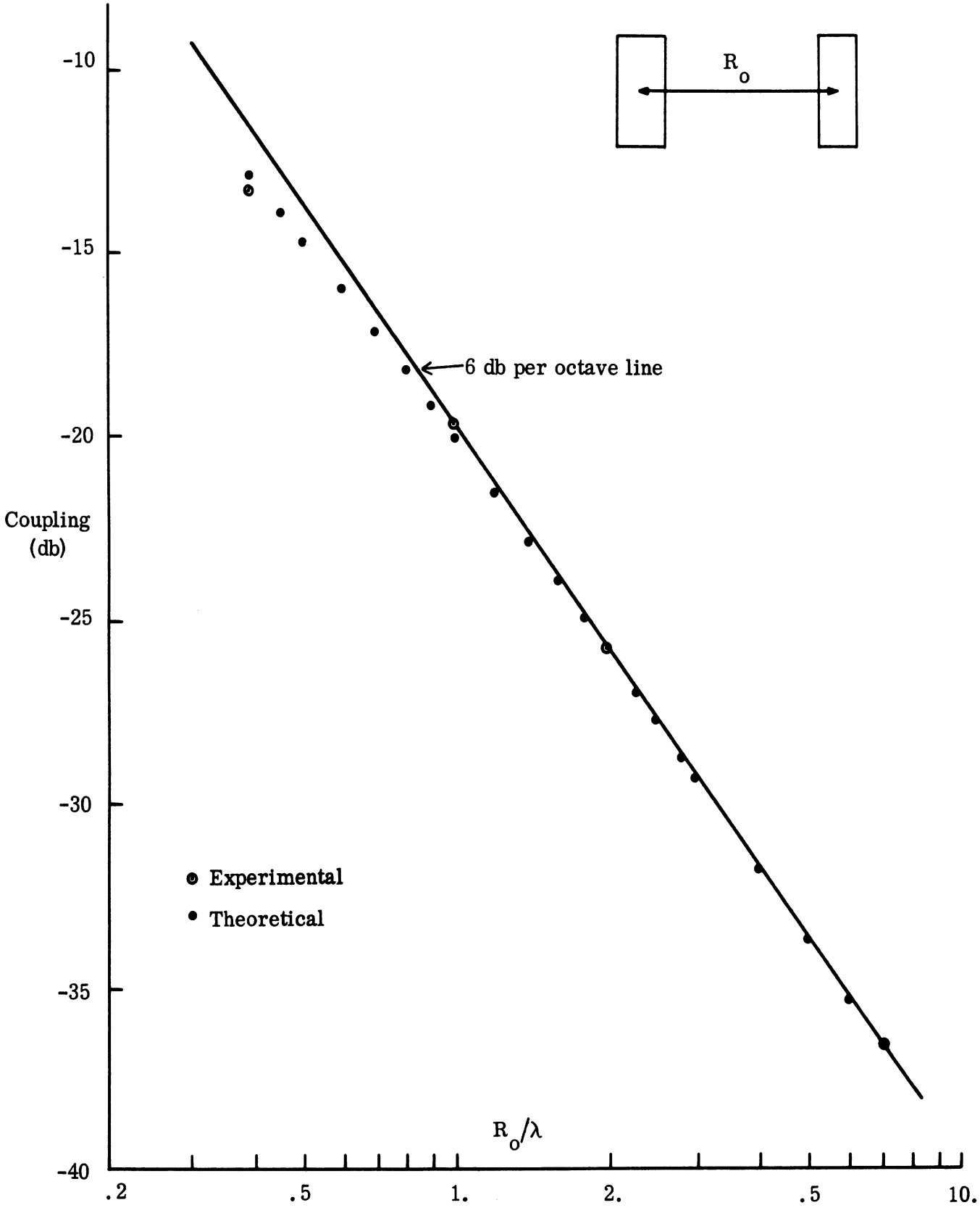

FIG. 4-4: BROADSIDE COUPLING OF OPEN-END WAVEGUIDES VS CENTER TO CENTER SPACING

4.2.3 Generalized Formulas for Slot Coupling

When the two open-end waveguides are positioned so that their narrow sides are facing each other (H-plane configuration) the formulas developed in the preceding sections have to be modified. The general formula for coupling can only be obtained through the solution of boundary value problems comprising the whole transmitting and receiving structures. An approach to the problem is outlined in the Appendix A and the complete details were given by Kwon (1965). In the present section, the construction of the general formula will be attempted from the simplified engineering point of view. If the size of the two waveguides is such that the fundamental mode is the only propagating mode, one can view the coupling as a two-port network problem where subscripts "1" and "2" designate the transmitting and receiving port respectively. Since no generators are in the receiving guide and the wave transmitted into the receiving guide from the half-space does not reflect back (matched conditions), one can set

$$Y^{(R)} = Y^{(R)}_{10} = \frac{\sqrt{k^2 - (\frac{\pi}{a_r})^2}}{\omega\mu} \tag{4.8}$$

(the subscript 10 refers to dominant mode).

Then, the derivation of the following algebraic formula is a purely algebraic matter.

$$R_e\left[V_2 I_2\right] = \frac{I}{Y^{(R)}_{10}} \frac{\left|I_2\right|^2}{\left|V_1\right|^2} R_e\left[\frac{V_1 I_1^*}{Y^{(T)*}}\right] = \frac{1}{Y^{(R)}_{10}} \frac{\left|Y_{12}\right|^2}{\left|1+\frac{Y_{22}}{Y^{(R)}_{10}}\right|^2} R_e\left[\frac{V_1 I_1^*}{Y^{(T)*}}\right] \tag{4.9}$$

where * designates complex conjugate and

$$Y^{(T)} = G^{(T)} + j\,B^{(T)} \tag{4.10}$$

The meaning of $G^{(T)}$ and $B^{(T)}$ is obvious. If $G^{(T)} >> B^{(T)}$, then

$$C = \frac{W_R}{W_T} = \frac{R_e\left[V_2\, I_2^*\right]}{R_e\left[V_1\, I_1^*\right]} = \frac{\left|Y_{12}\right|^2}{Y_0^{(R)}\, G^{(T)} \left|1 + \dfrac{Y_{22}}{Y_0^{(R)}}\right|^2} \tag{4.11}$$

Since $Y_{21} = Y_{12} << Y_{11}$ or Y_{22}, one can have

$$G^{(T)} \approx Y^{(T)} = Y_{11} - \frac{Y_{12}\, Y_{21}}{Y_{22} + Y_0^{(R)}} \approx Y_{11} \approx G_{11} \tag{4.12}$$

and

$$Y_0^{(R)} = Y^{(R)} \approx Y_{22} \approx G_{22} \tag{4.13}$$

then

$$C = \frac{\left|Y_{21}\right|^2}{4\, G_{11}\, G_{22}}\,, \text{ (true for no admittance mismatch)} \tag{4.14}$$

which is equivalent to (2.9). It will be shortly shown that (4.14) reduces to the far-field coupling formula. Equation (4.14) is a generally acceptable formula

even for the near field case, if the circuit parameters satisfy the assumptions leading to (4.14)

Another coupling formula equivalent to (4.14) is

$$C = \frac{W_R}{W_T} = \frac{\left(\frac{I_2}{Y_0^{(R)}}\right)^2}{G^{(T)}|V_1|^2} = \frac{1}{Y_0^{(R)} G^{(T)}} \left(\frac{I_2}{V_1}\right)^2 = \frac{|I_2|^2}{2\, Y_{10}^{(R)} W_T} \tag{4.15}$$

where no approximation is used.

The circuit parameters in (4.14) are given by: (Kwon, 1965)

$$G_{11} = \frac{2}{\pi^3} \sqrt{\frac{\epsilon}{\mu}} \left(\frac{a_t}{b_t}\right) \delta_t, \quad G_{22} = \frac{2}{\pi^3} \sqrt{\frac{2}{\mu}} \left(\frac{a_r}{b_r}\right) \delta_r \tag{4.16}$$

$\delta_i = R_{11}^{(1)}(a_i, b_i)$ [see (A.41c) of Appendix A]

$$\doteqdot \frac{4}{3} \pi (k b_i) \left(\frac{b_i}{a_i}\right) F_i \quad [F_i \text{ is given by (4.4)}] \tag{4.17}$$

$$Y_{12} = -\frac{1}{\pi j \omega \mu} \frac{1}{\sqrt{(a_t b_t)(a_r b_r)}} J_{10,\,10}. \tag{4.18}$$

For $\phi_t \neq \frac{\pi}{2}$ ($\phi_t = \frac{\pi}{2} - \alpha$, $\phi_r = \frac{\pi}{2} - (\alpha - \beta)$, (see Fig. A-2, Appendix A),

$$J_{10,\,10} = \frac{16}{R_o}\left(\frac{a_t}{\pi}\right)\left(\frac{a_r}{\pi}\right) e^{-jkR_o} \cdot \sin\left(\frac{kb_t}{2}\cos\phi_t\right) \cdot C\left(\frac{ka_t}{\pi}\sin\phi_t\right)$$

$$\cdot \sin\left(\frac{kb_r}{2}\cos\phi_r\right) \cdot C\left(\frac{ka_r}{\pi}\sin\phi_r\right) \qquad (4.19)$$

where

$$C\left(\frac{ka}{\pi}\sin\phi\right) = \frac{\cos\left(\frac{ka}{2}\sin\phi\right)}{1 - \left(\frac{ka}{\pi}\right)^2 \sin^2\phi} \cdot \qquad (4.20)$$

For $\phi_t = \frac{\pi}{2}$

$$J_{10,\,10} = -j\frac{4}{R_0^2}\left(\frac{a_t}{\pi}\right)\left(\frac{a_r}{\pi}\right) e^{-jkR_o} \cdot b_t \cdot \frac{\cos\left(\frac{ka_t}{2}\right)}{\left(1 - \frac{k^2 a_t^2}{\pi^2}\right)} O_1, \qquad (4.21)$$

where

$$O_1 = \left\{ 6\,\frac{\sin\left(\frac{kb_r}{2}\cos\phi_r\right)}{\cos\phi_r} - (kb_r)\cos\left(\frac{kb_r}{2}\cos\phi_r\right)\right\} \sin\phi_r\, C\left(\frac{ka_r}{\pi}\sin\phi_r\right)$$

(see equations A.36d) and (A.36e) of Appendix A).

Substituting (4.16) - (4.19) into (4.14), one obtains the following expressions for coupling:

For $\phi_t \neq \frac{\pi}{2}$,

$$C = \left[\frac{3}{(kR_o)(kb_t)(kb_r)}\right]^2 \frac{1}{F_t F_R} \left[\sin\left(\frac{kb_t}{2}\cos\phi_t\right) C\left(\frac{ka_t}{\pi}\sin\phi_t\right)\right]^2$$

$$\cdot \left[\sin\left(\frac{kb_r}{2}\cos\phi_r\right) \cdot C\left(\frac{ka_r}{\pi}\sin\phi_r\right)\right]^2 \qquad (4.22)$$

and for $\phi_t = \frac{\pi}{2}$,

$$C = \left[\frac{3}{(kR_o)(kb_t)(kb_r)}\right]^2 \left[\frac{b_t}{4R_o}\right]^2 \frac{1}{F_t F_R} \left[\frac{\cos\left(\frac{ka_t}{2}\right)}{1 - \left(\frac{ka_t}{\pi}\right)^2}\right]^2 O_1^2 . \qquad (4.23)$$

It is easy to show that (4.22) is identical with the far-field coupling formula obtained by using directivity concept.

If one uses (4.15) and the expressions for I_2 obtained in the Appendix A, one obtains the other coupling formulas, which are not bound by the assumptions leading to (4.14). The final results for the coupling are:

for $\phi_t \neq \frac{\pi}{2}$

$$C = \frac{32}{\pi^2} \frac{1}{(kb_r)\sqrt{1 - \left(\frac{\pi}{ka_r}\right)^2}} \left(\frac{a_t}{a_r}\right) \frac{1}{(kR_o)^2} \frac{1}{\delta_t} \cdot \left[\sin\left(\frac{kb_t}{\pi}\cos\phi_t\right) C\left(\frac{ka_t}{\pi}\sin\phi_t\right)\right]^2$$

$$\cdot \left[\sin\left(\frac{kb_r}{2}\cos\phi_r\right) C\left(\frac{ka_r}{\pi}\sin\phi_r\right)\right]^2 . \qquad (4.24)$$

For $\phi_t = \frac{\pi}{2}$,

$$C = \frac{2}{\pi^2} \frac{1}{(kR_o)\sqrt{1-(\frac{\pi}{ka_r})^2}} \frac{1}{(kR_o)^2} \frac{b_t}{R_o} \cdot \frac{1}{\delta_t} \left[\frac{\cos(\frac{ka_t}{2})}{1 - \frac{k^2 a_t^2}{\pi^2}} \right]^2 O_1^2 . \qquad (4.25)$$

The above coupling formulas for the slots, (4.22) through (4.25) give excellent agreement with experiment for $b < a\lambda$ and $R_o > \lambda$ as shown in the accompanying figures. The derivation of the coupling formula for $R_o < \lambda$ is difficult. However, for $a_t = a_r = a$, $b_t = b_r = b$ and $\phi_t = \phi_r = \phi$, the exact formula for coupling is given by:

$$C = \frac{1}{32} \frac{1}{\pi^2} \frac{1}{(kb)\sqrt{1-(\frac{\pi}{ka})^2}} (\frac{ka}{\pi})^2 \frac{|K|^2}{\delta} , \qquad (4.26)$$

where

$$K = \int_{-\frac{b}{a}\pi}^{\frac{b}{a}\pi} (\frac{b}{a}\pi - \sigma)\, d\sigma \int_0^{\pi} \left[(1 - \frac{\pi^2}{k^2 a^2})(\pi - \lambda)\cos\lambda \right.$$

$$\left. + (1 + \frac{\pi^2}{k^2 a^2}) \sin\lambda \right] \left[g(\frac{R_o}{a}\pi \sin\phi + \lambda, \frac{R_o}{a}\pi\cos\phi + \sigma) \right.$$

$$\left. + g(\frac{R_o}{a}\pi \sin\phi - \lambda, \frac{R_o}{a}\pi\cos\phi + \sigma) \right] \qquad (4.27)$$

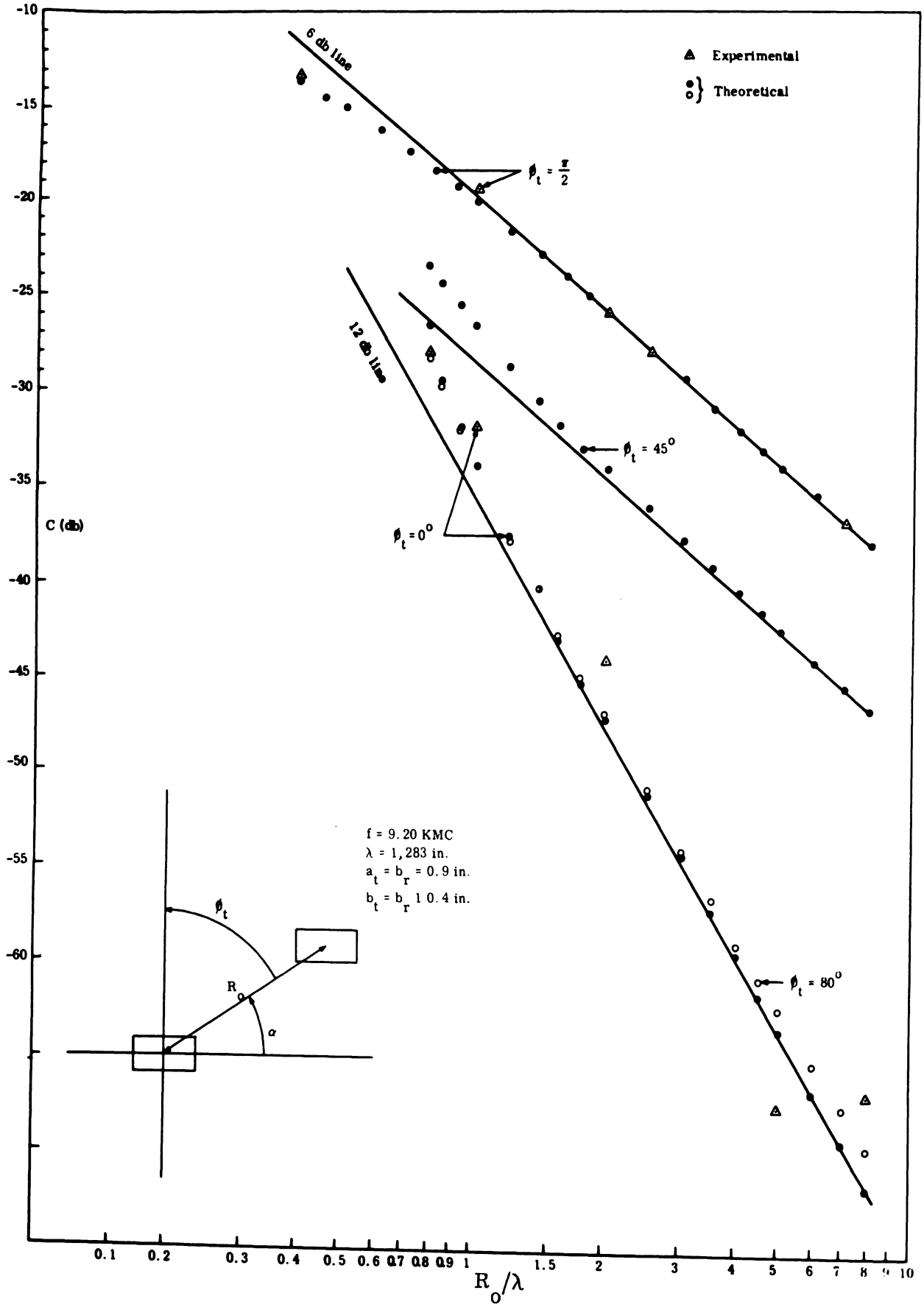

FIG. 4-5: COMPARISON BETWEEN EXPERIMENTAL AND THEORETIC RESULTS

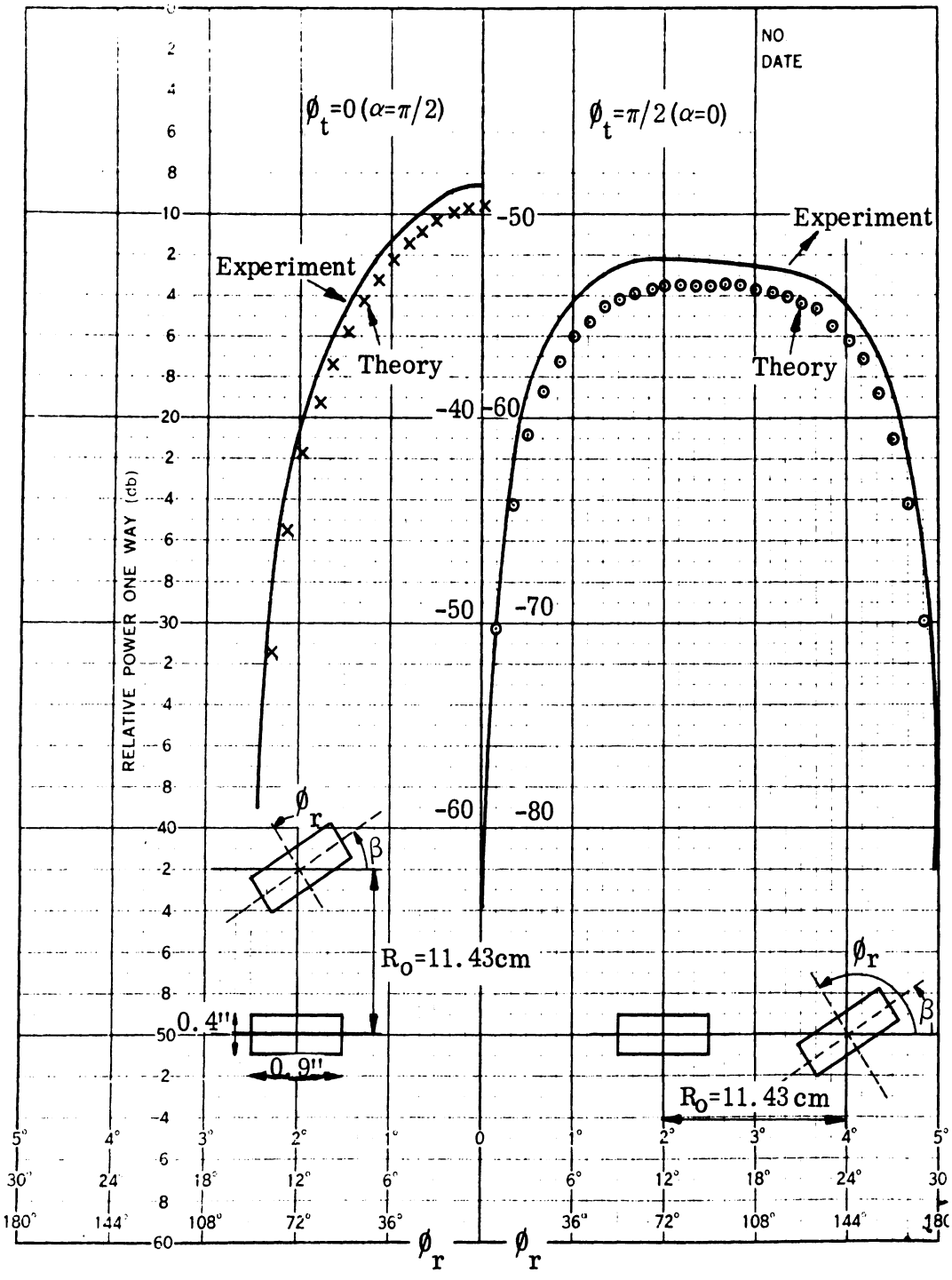

FIG. 4-6a: COMPARISON BETWEEN EXPERIMENT AND EQS (4-24) AND (4-25) f=8.03 GHz.

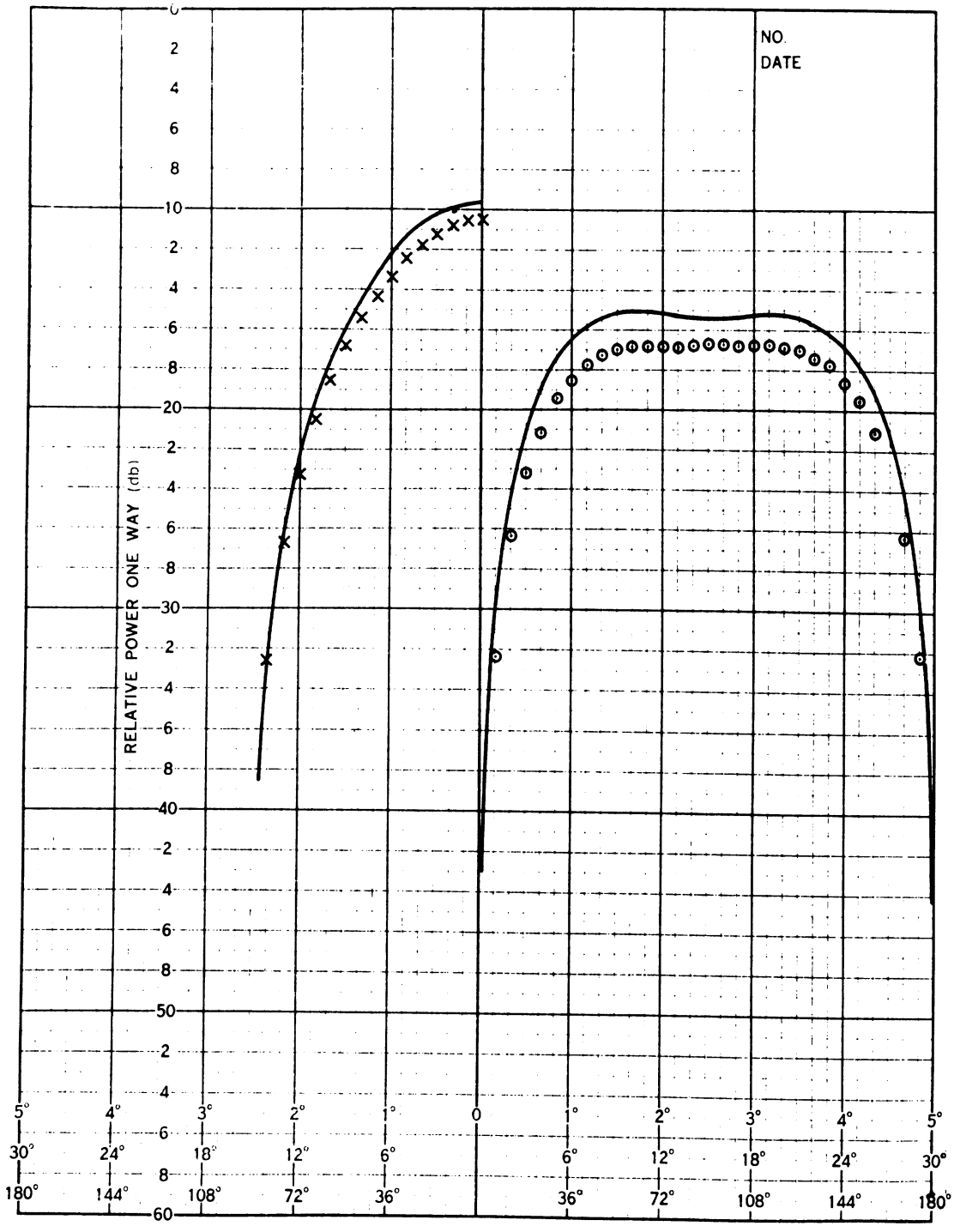

FIG. 4-6b: COMPARISON BETWEEN EXPERIMENT AND EQS (4-24) AND (4-25) f=9.03 GHz.

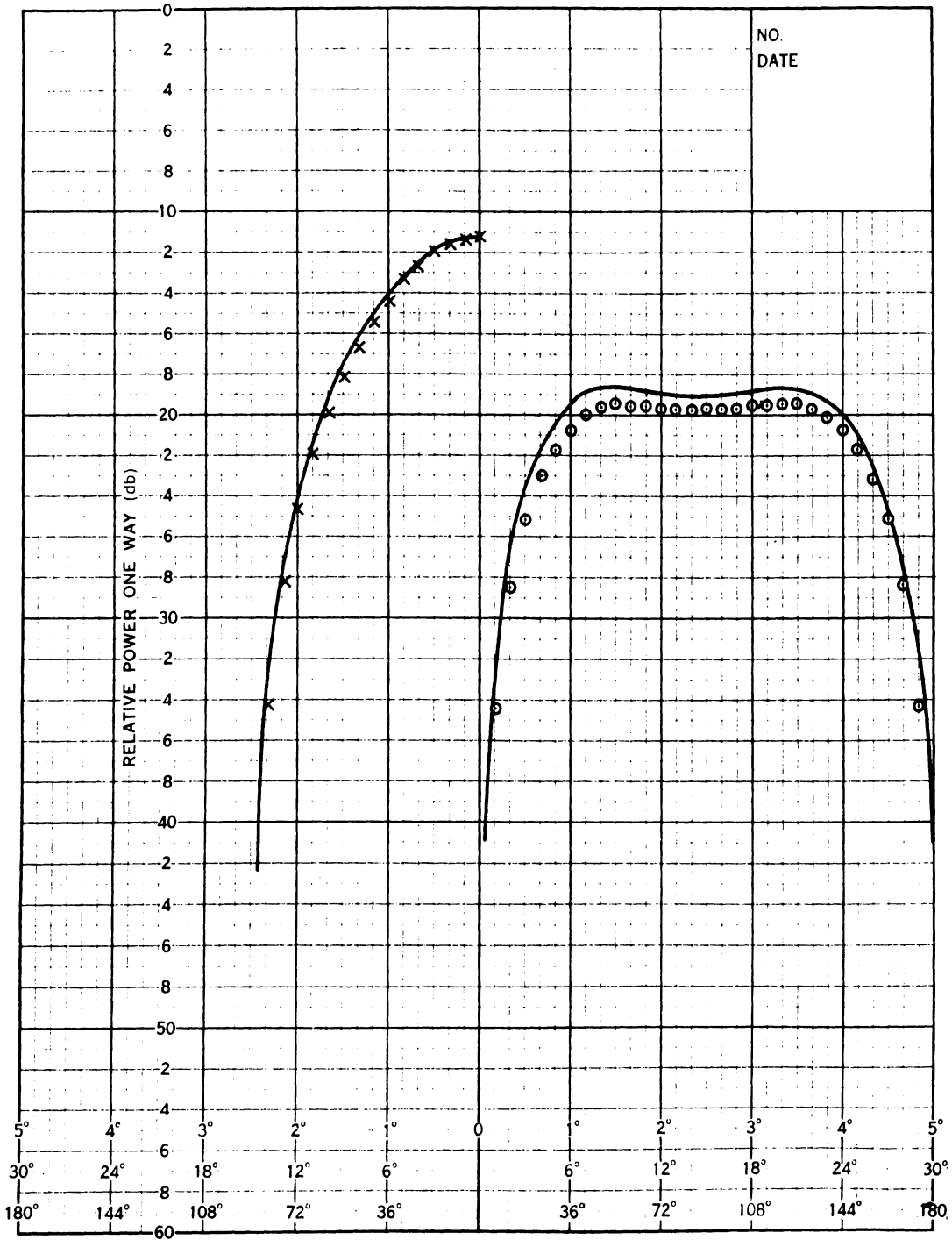

FIG. 4-6c: COMPARISON BETWEEN EXPERIMENT AND EQS (4-24) AND (4-25) f=10.03 GHz.

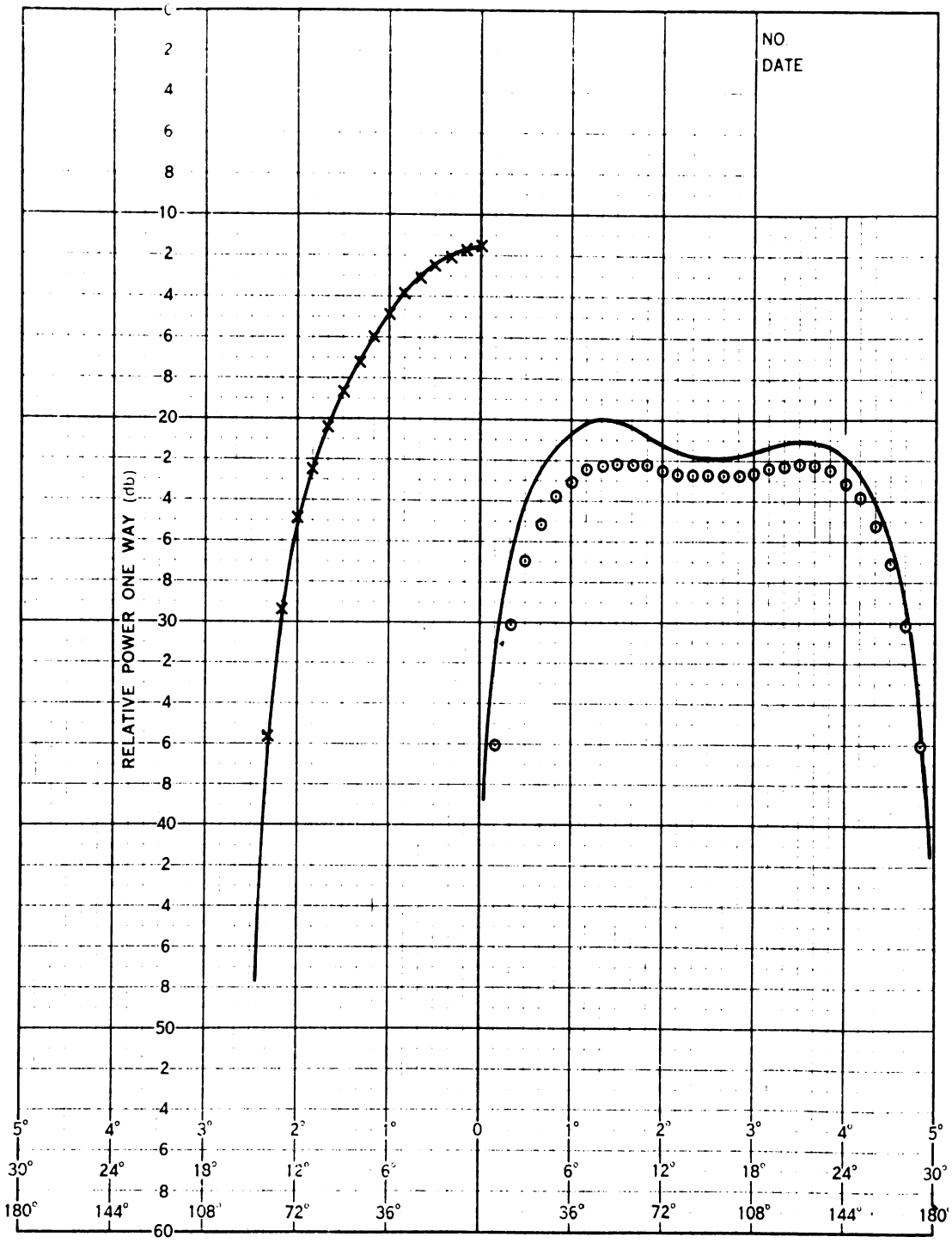

FIG. 4-6d: COMPARISON BETWEEN EXPERIMENT AND EQS (4-24) AND (4-25) f=11.03 GHz.

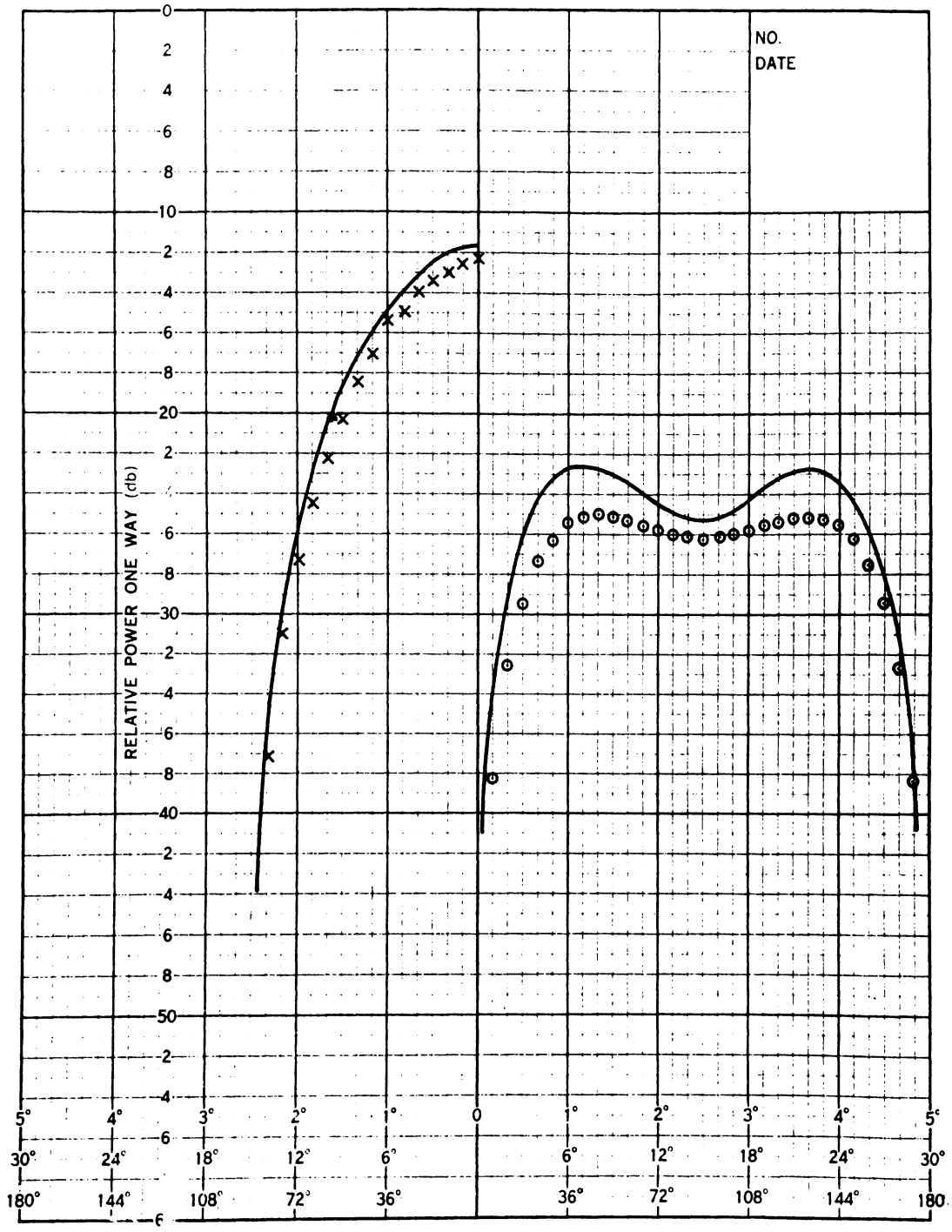

FIG. 4-6e: COMPARISON BETWEEN EXPERIMENT AND EQS (4-24) AND (4-25) f=12.03 GHz.

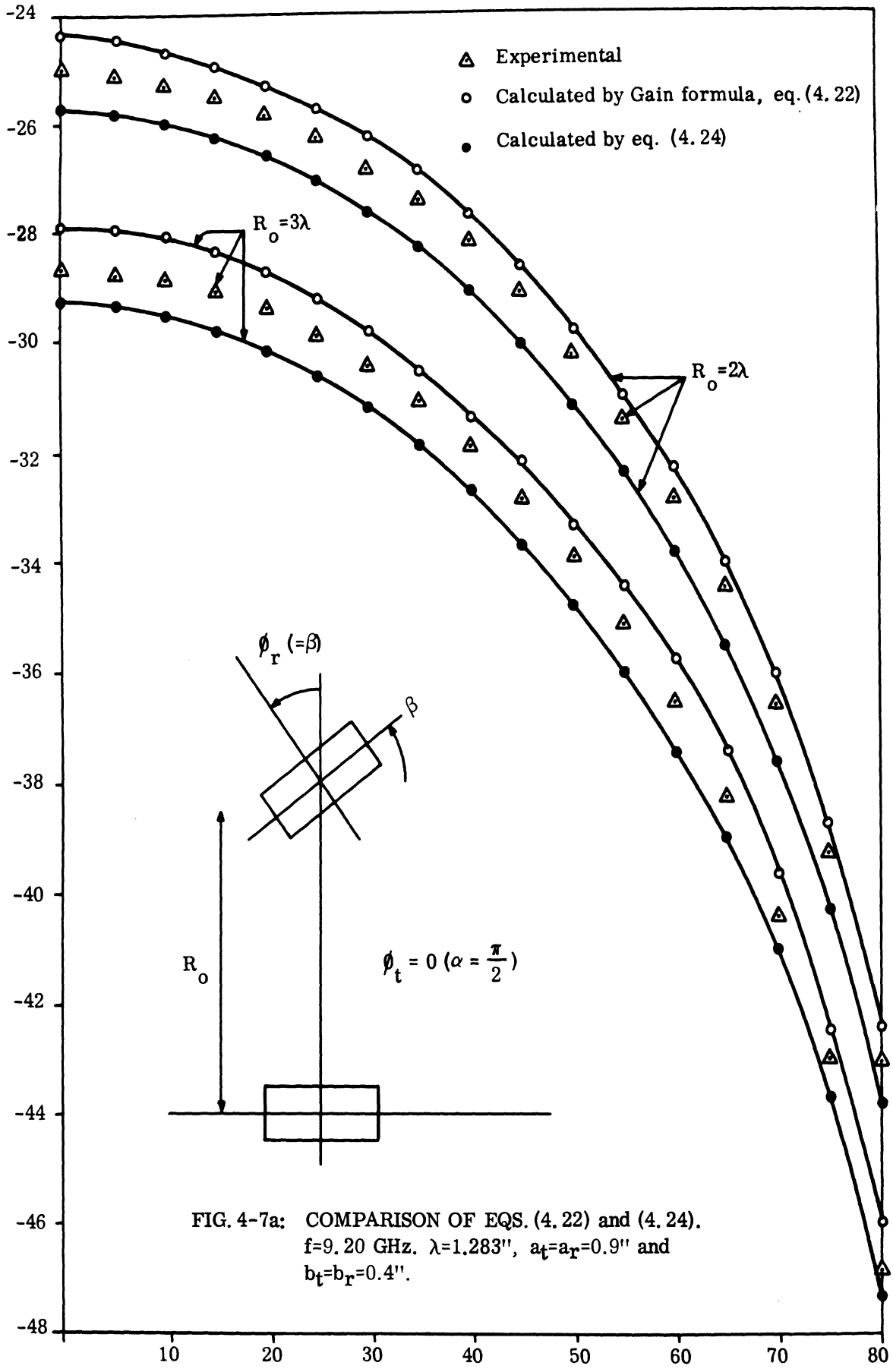

FIG. 4-7a: COMPARISON OF EQS. (4.22) and (4.24). f=9.20 GHz. λ=1.283", $a_t=a_r$=0.9" and $b_t=b_r$=0.4".

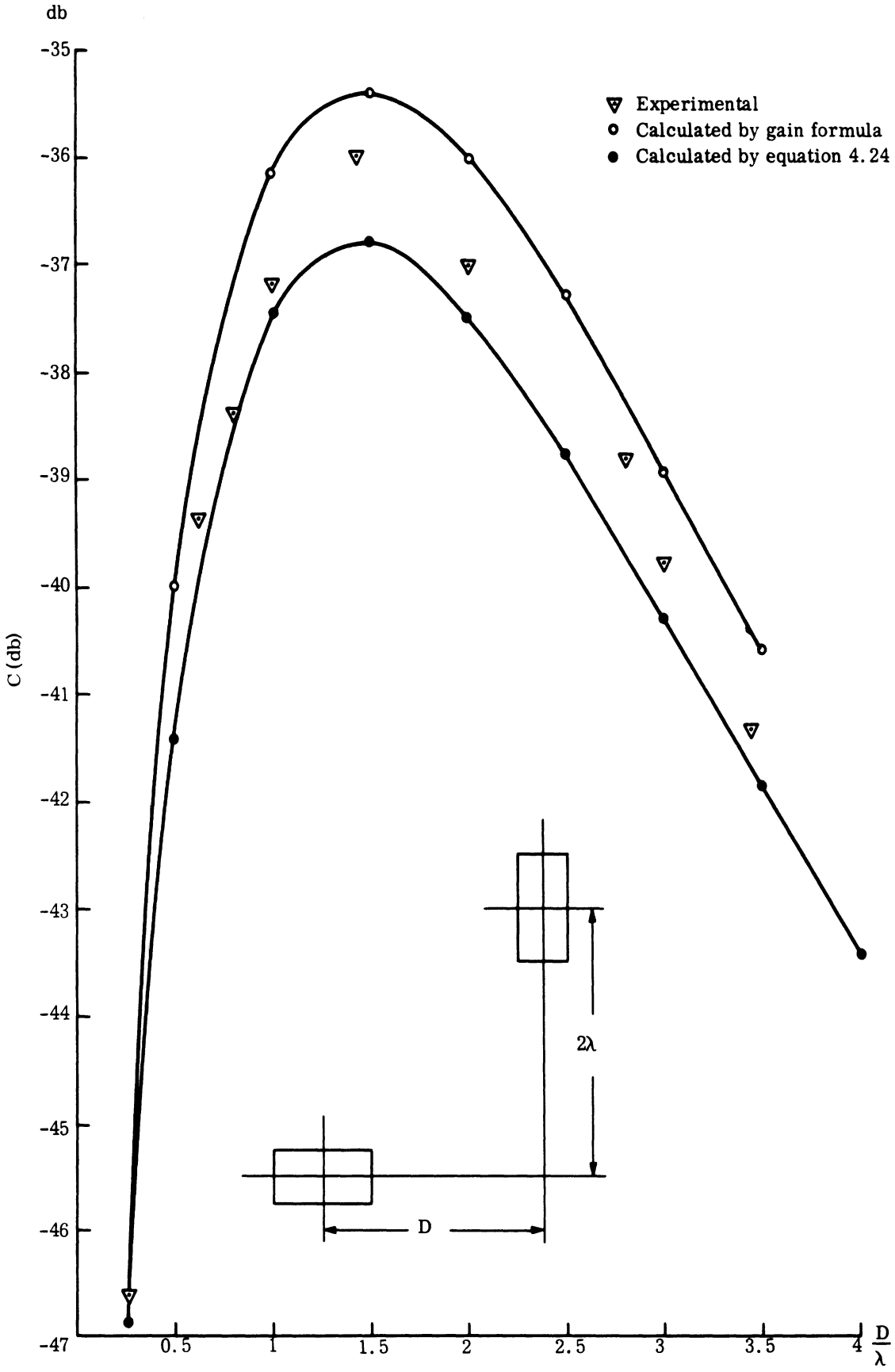

FIG. 4-7b: COMPARISON OF EQS. (4.22) AND (4.24)

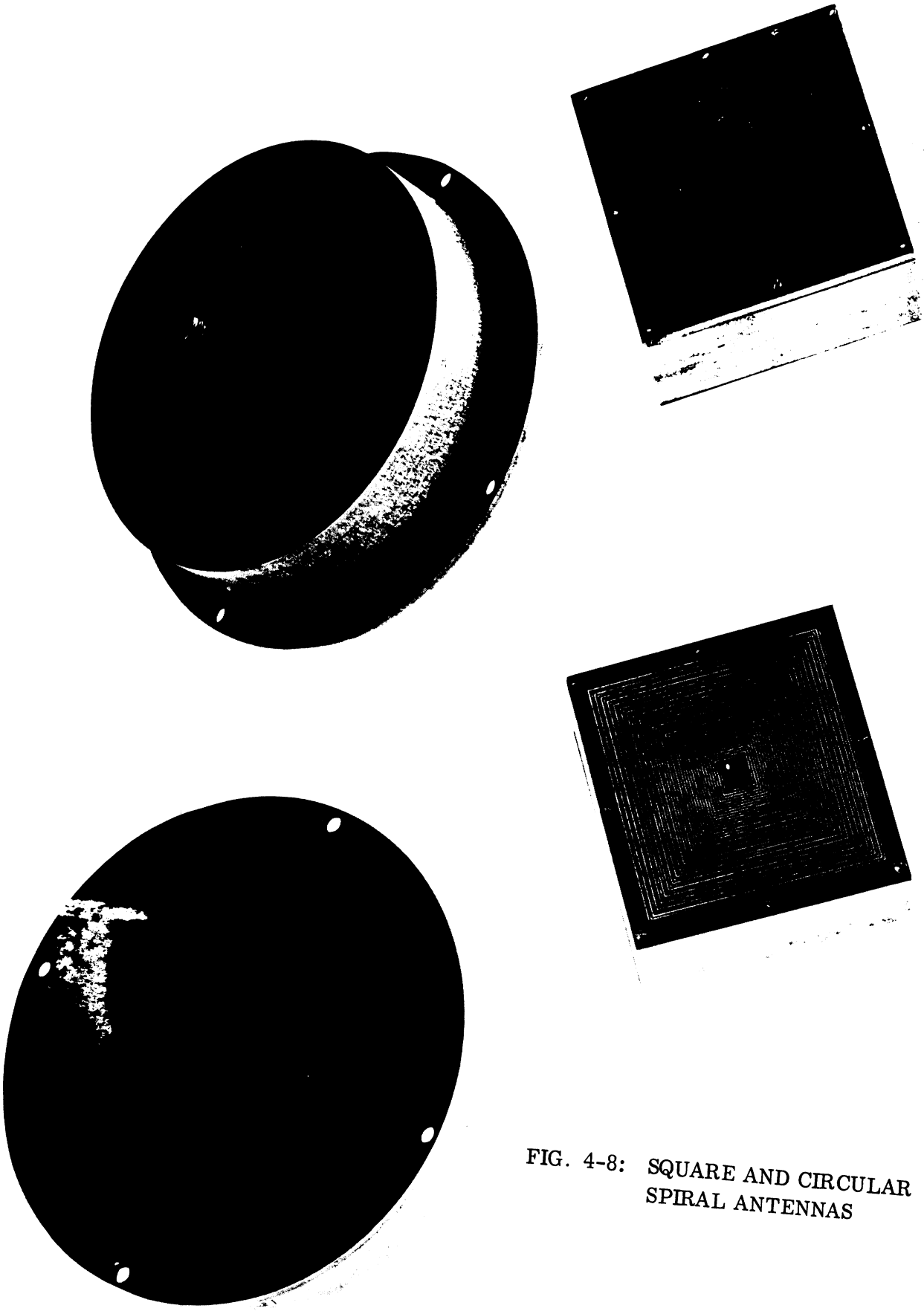

FIG. 4-8: SQUARE AND CIRCULAR SPIRAL ANTENNAS

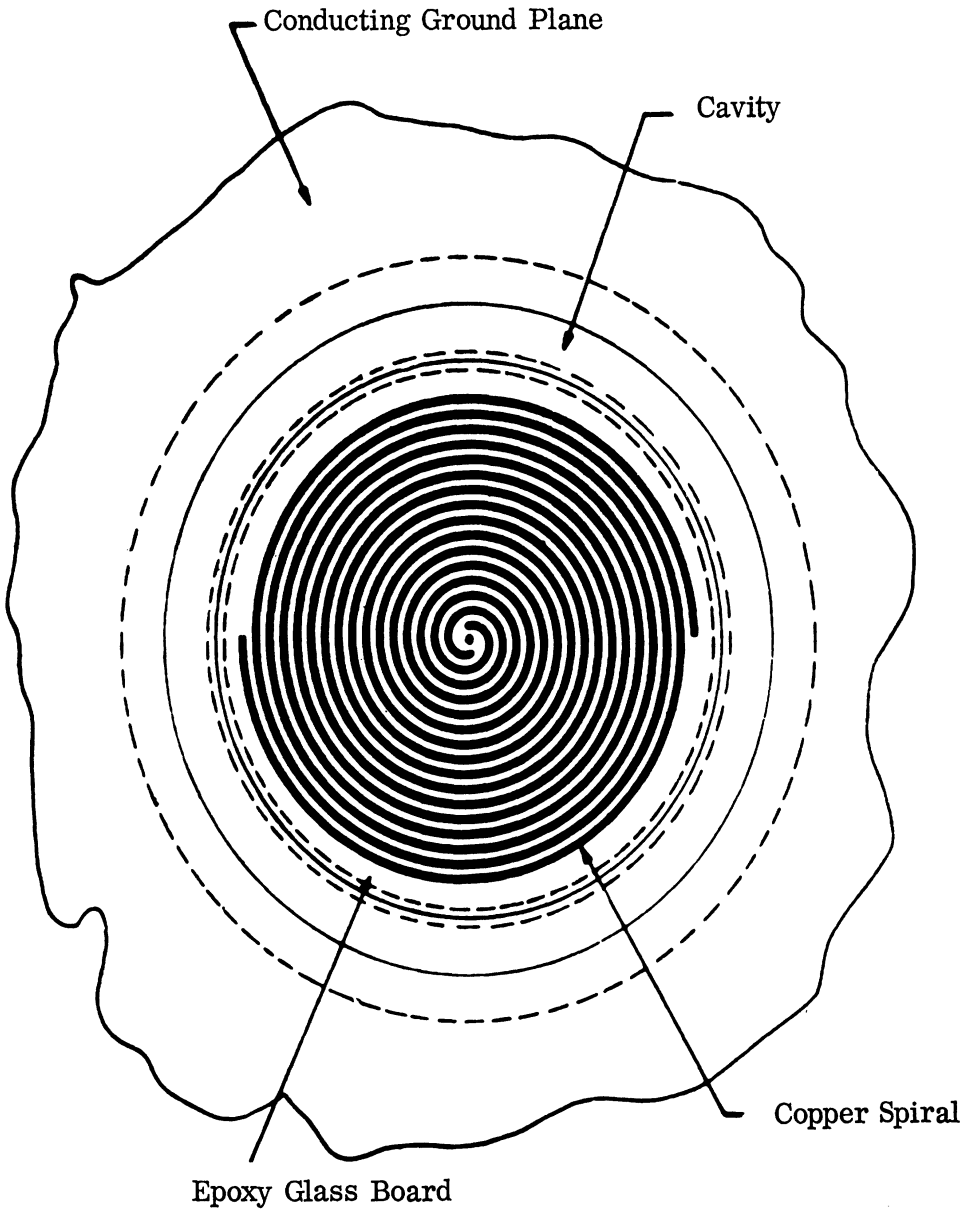

FIG. 4-9: CIRCULAR ARCHIMEDEAN SPIRAL FACE CONFIGURATION

and

$$g(u, v) = \frac{e^{-j\frac{ka}{\pi}\sqrt{u^2+v^2}}}{\sqrt{u^2+v^2}} \tag{4.28}$$

For $\phi = \frac{\pi}{2}$ and $\phi = 0$, C of (4.26) is compared with experimental results in Fig. 4-5, where C for $\alpha = 45^o$ and $\alpha = 80^o$ is also plotted.

Before closing the present section, some comments are necessary about the differences between (4.22) and (4.24) or (4.23) and (4.25). The lack of symmetry in (4.24) and (4.25) is due mainly to the fact that the assumption of (4.13) was not used in their derivation.* Therefore, as long as the assumption of (4.13) is valid, the coupling expressed by two set of formulae gives similar answers as illustrated in Figs. 4-6 and 4-7.

4.3 Spiral Antennas

4.3.1 Introduction and Summary of Spiral Properties

The widespread use of flush broadband antennas on aircraft and missiles, both singly and in arrays, has motivated a detailed study of coupling patterns. The Archimedean spiral is representative of this class and was thus chosen for further study. It provides a practical way of producing circularly polarized radiation over a wide band of frequencies. It is usually mounted in a conducting ground plane and backed by a cavity.

The square and circular spiral configurations are the most common types; samples are shown in Fig. 4-8. These spirals may be wound either clockwise or counterclockwise depending on the sense of circular polarization desired. Spiral antennas are usually fed out of phase in order to effect maximum radiation in the

* Equation (4.23) preserves symmetry when $\phi_r = \pi/2$.

axial direction (axial, or 1λ mode). A balun is used to provide a balanced feed.

The operation of the spiral antennas has been explained qualitatively in a number of papers and a summary of the operation is given here. As shown in Fig. 4-9, the antenna can be thought of as a two-wire transmission line which has been wrapped around the origin in such a way as to form a spiral. It is obvious that at any position along this line, the wire lengths differ. Furthermore, this difference in lengths steadily increases for points further removed from the origin. If two out-of-phase waves of current start at the center terminals and travel out along the transmission line, they will eventually become in phase when the difference in the lengths of the line wires becomes $\lambda/2$. It may be shown that the distance from the origin at which this in-phase condition occurs is given approximately by $r = \lambda/2\pi = .159\lambda$. This value is the radius of a ring one wavelength in circumference.

From considerations of this kind, it is generally assumed that most of the radiation from the spiral originates in a region near the one wavelength ring where neighboring current elements have small phase differences. For other regions of the antenna the fields tend to cancel. It is also reasonable to assume that the currents are attenuated in the region of the radiation ring due to radiation. If the ring is not too near the outer extremities of the antenna, the current magnitude may be reduced by radiation enough so that the reflections from the ends of the spiral arms can be neglected.

In a rough way, one can approximate a spiral at one frequency by a similarly shaped loop which carries a traveling wave. Thus, for a circular spiral, consider a circular loop with a circumference of one wavelength. The separation of parallel elements is the diameter $d = \lambda/\pi = .318\lambda$. For a square spiral, this distance is $d = \lambda/4 = .25\lambda$.

If dielectric is used extensively near the spiral (e.g. in the cavity), the radiating region will be reduced in size. The effective dielectric constant is not significantly altered until a substantial amount of dielectric is used, in terms of wavelengths. When this occurs, the effective spacing d decreases, which broadens the beam.

Thus the gain of a spiral antenna depends mainly on two factors; 1) the shape of the spiral, and 2) the effective dielectric constant surrounding the elements.

A square spiral will have a broader beam than a circular spiral, and thus less gain. Similarly, the effective dielectric constant varies directly with the width of the beam. Thus for maximum gain, a circular spiral should be utilized, using an air-filled cavity, as thin a printed circuit board as possible, and as low a dielectric constant as possible. The above conclusions are born out by the experimental data and a consideration of the resonant circumference condition.

Interest to date has centered largely around the near-axis, far-field properties, which can be obtained with rather crude approximations to current distribution. However, the interference effects between antennas in a common ground plane depend upon ground plane patterns which require a more detailed knowledge of current distribution.

An interesting factor of spiral ground plane patterns (Fig. 4-10) is their lack of omnidirectionality. However, ϕ-variations are not due to imperfections in spiral construction. These patterns were taken from a circular spiral to a $\lambda/4$ monopole. Even with a perfectly balanced feed (necessary for the axial mode), and with perfect mechanical symmetry, a coupling variation of several db will occur as the spiral is rotated in the ground plane. With the commercial spirals tested, other effects add to the basic ϕ-variations. These variations

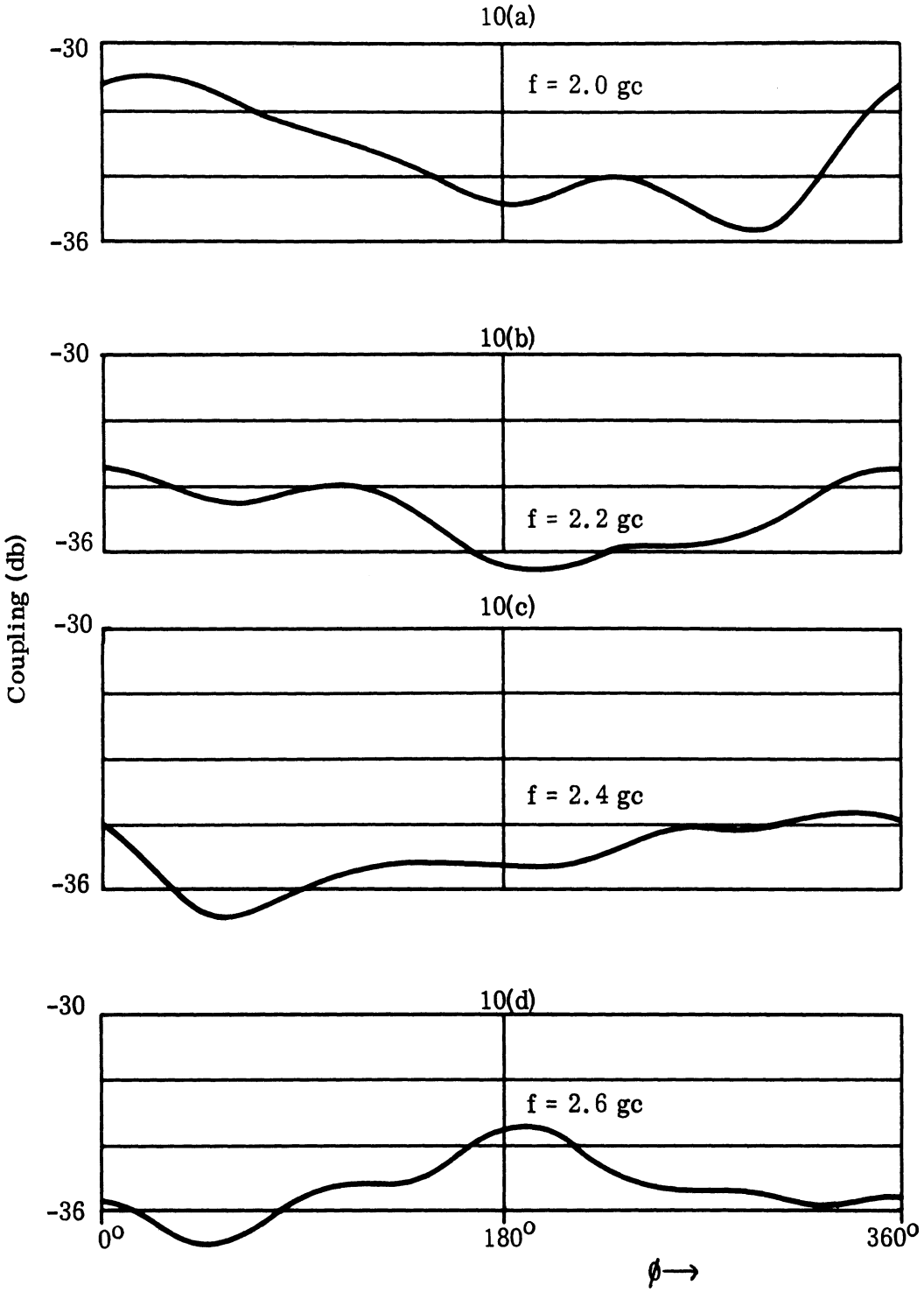

FIG. 4-10: COUPLING PATTERNS FOR CIRCULAR SPIRAL "A"

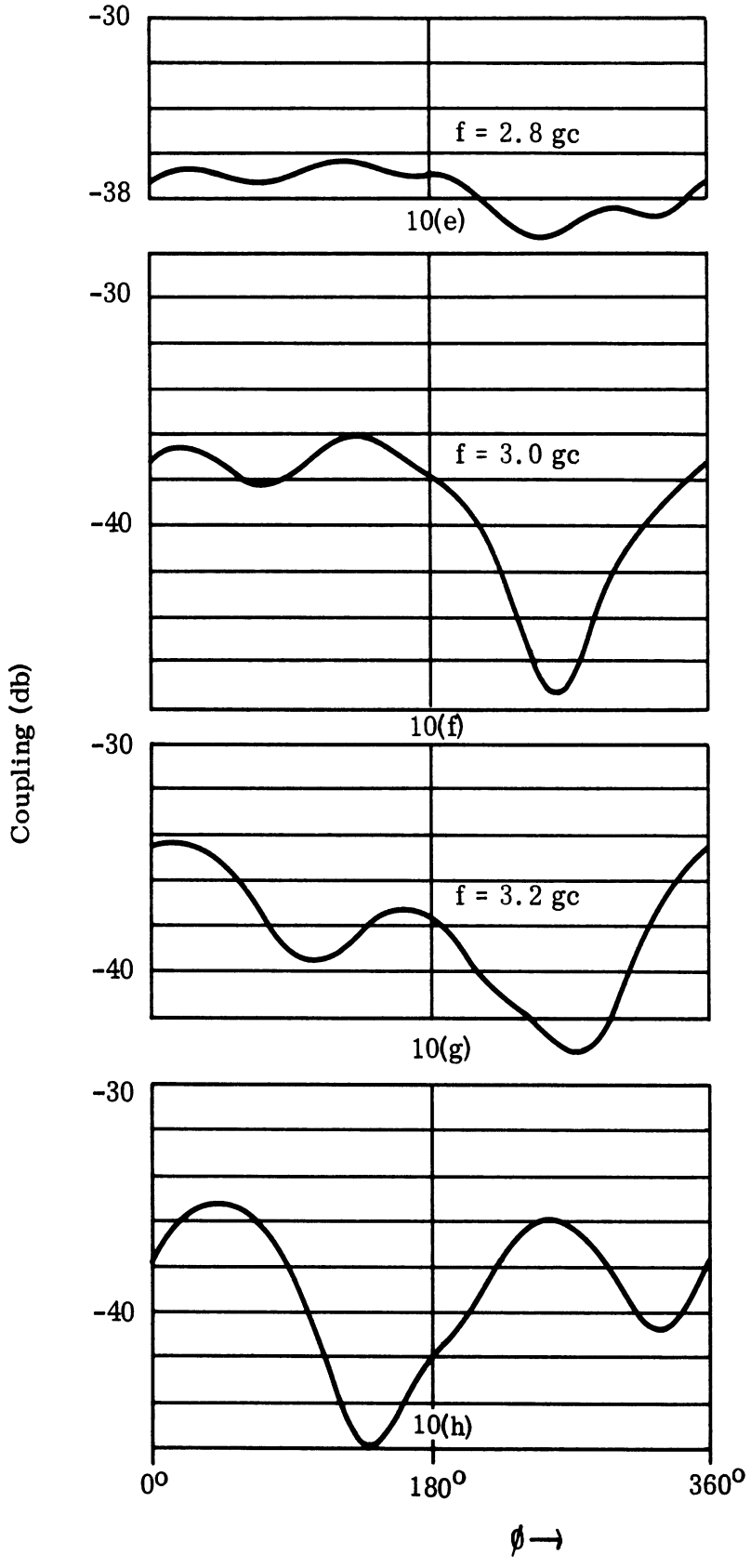

FIG. 4-10(Cont.). COUPLING PATTERNS FOR CIRCULAR SPIRAL "A"

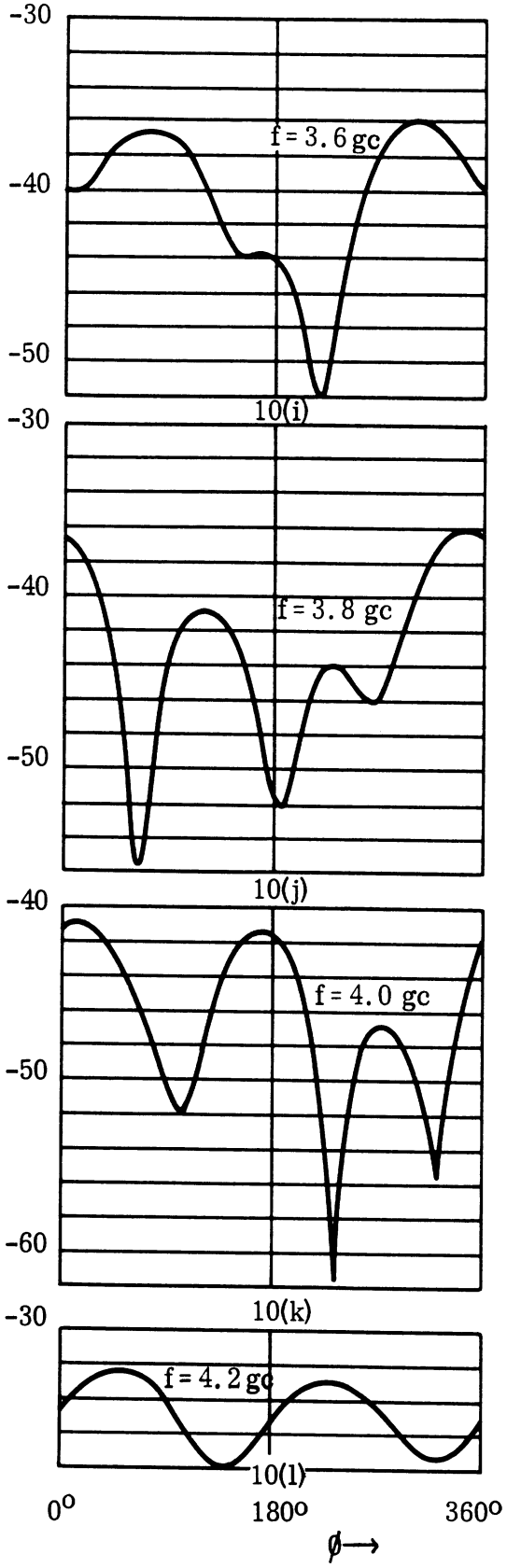

FIG. 4-10:(cont.). COUPLING PATTERNS FOR CIRCULAR SPIRAL "A"

stem from the following secondary causes and apply to all antennas in this class.

1) In-phase feed currents and the subsequent redistribution of current on the spiral.
2) Reflections from the ends of the spiral elements
3) Reflections from the cavity
4) Distributed, induced reflection by neighboring elements
5) Direct radiation from the feed and balun

The effects noted above are more critical in coupling properties than in near-axis properties. While it is difficult to isolate the effects of the several secondary causes, additional information thereon would help in the future design of flush antennas.

Variations in the ground plane coupling pattern are not completely undesirable for they may make possible appreciable decoupling by proper orientation. However, the observed ϕ-variations change rapidly with frequency, so the coupling reduction which results from optimum orientation will exist over a narrow frequency band only. For array purposes, it would often be better to have frequency independent ϕ-variations over the band, even at the expense of higher coupling levels.

4.3.2 Circular Archimedean Spiral

Two similar circular archimedean spirals obtained from AeroGeoAstro Corporation were tested singly and together. Pertinent information is given below.

Frequency range	2 - 4 GHz
Number of turns	13
Width of conductor	1.5 cm
Width of spacing	1.5 cm
Balun type	Roberts, strip-line
Diameter of cavity	10 cm.

In order to test each antenna singly, a quarter-wave monopole probe was used as a transmitter and located 11.3" from the spiral center. A 4' x 4' ground plane surrounded by absorbing material yielded results which agreed to within 0.5 db at large couplings (-35 db or higher) and to within 2 db at lower levels (-50 db) or the values obtained using a 12' x 12' plane in the anechoic chamber.

The general problem of coupling between flush antennas in a ground plane is greatly simplified by the fact that the incident field is linearly polarized, since the tangential E-field must be zero at the conductor. This, plus the fact that in the far field the fields look like an ordinary plane wave, means the great majority of problems can be solved merely knowing the coupling patterns. The implication that the winding sense of the spiral is irrelevant breaks down in the near field case because the receiving spiral in a spiral-to-spiral configuration subtends a large enough angle of the other so that the phase distribution of the incident field over the receiving area is no longer that of a constant-phase plane wave. This effect can be noted experimentally by comparing the couplings at large and small spacings.

Figure 4-10 shows typical coupling patterns between the spiral antenna and a tuned monopole probe. These exhibit sharp nulls near the upper end of the design band for both A and B antennas, due to cavity, balun radiation and second-mode effects. (The second mode is excited by in-phase currents at the feed, and has a null on the axis.) Figure 4-11 shows coupling patterns taken at three spacings for two similar circular spirals A and B at one frequency. At other frequencies the behavior was similar. (These data were taken before the experimental setup allowed continuous coupling patterns.) The patterns are fairly consistent as the spiral-to-monopole spacing is varied even at the extremely close spacings where the probe is 1.5" from the periphery. Even more consistent

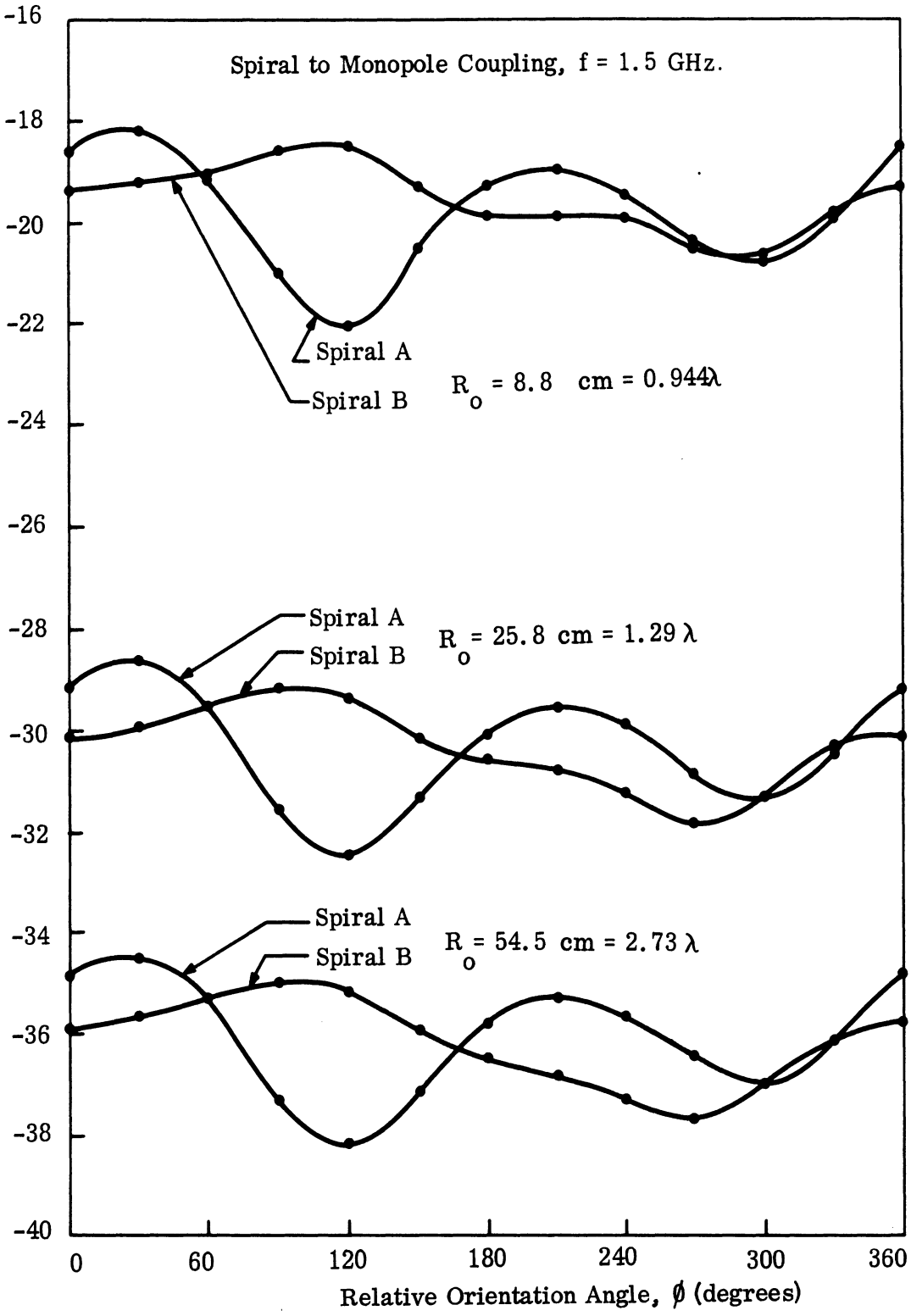

FIG. 4-11: COUPLING PATTERNS AT SEVERAL SPACINGS, CENTER-TO-CENTER

is the coupling level, which at the pattern maxima follows within 0.5 db of the ordinary 6 db per (distance) octave variation at distances of 1 wavelength or more. At closer spacings, the level tends to rise somewhat above the 6 db line by up to 1.5 db at 1/2 wavelength (Fig. 4-10).

Extensive tests were taken on the coupling patterns from 1.7 - 4.2 GHz in 50 MHz increments on spirals A and B. Rather than present all the curves involved, typical patterns are given in Fig. 4-10.

Using data from Fig. 4-10 and the expression

$$C = C_o \left(\frac{R_o}{\lambda}\right) D_t (\phi_t, f) D_r$$

where $R_o = \lambda$ and $C_o \left(\frac{R_o}{\lambda}\right)$ = constant

$D_t (\phi_t, f)$ = Circular Spiral Directivity Function, and

D_r = Monopole Directivity Function (independent of ϕ_r, f),

the maximum and minimum values of $D_t (\phi_t)$ for a particular frequency were calculated. These values are plotted as a function of the frequency in Fig. 4-12.

The coupling decreases noticeably near 3.8 GHz, where simultaneously the radiation pattern is becoming narrower. This increase in gain means more power is radiated along the axis, and thus less along the ground plane. The variations are small at lower frequencies and increase to extreme values at the higher frequencies, where sharp nulls occur. Just above the rated frequency band, the coupling increases sharply with small variations. The reason for this is that the second mode, which has a null on the axis of the spiral, becomes predominant. This mode occurs when the feed currents differ appreciably from the out-of-phase condition. There is a large in-phase component when the balun is

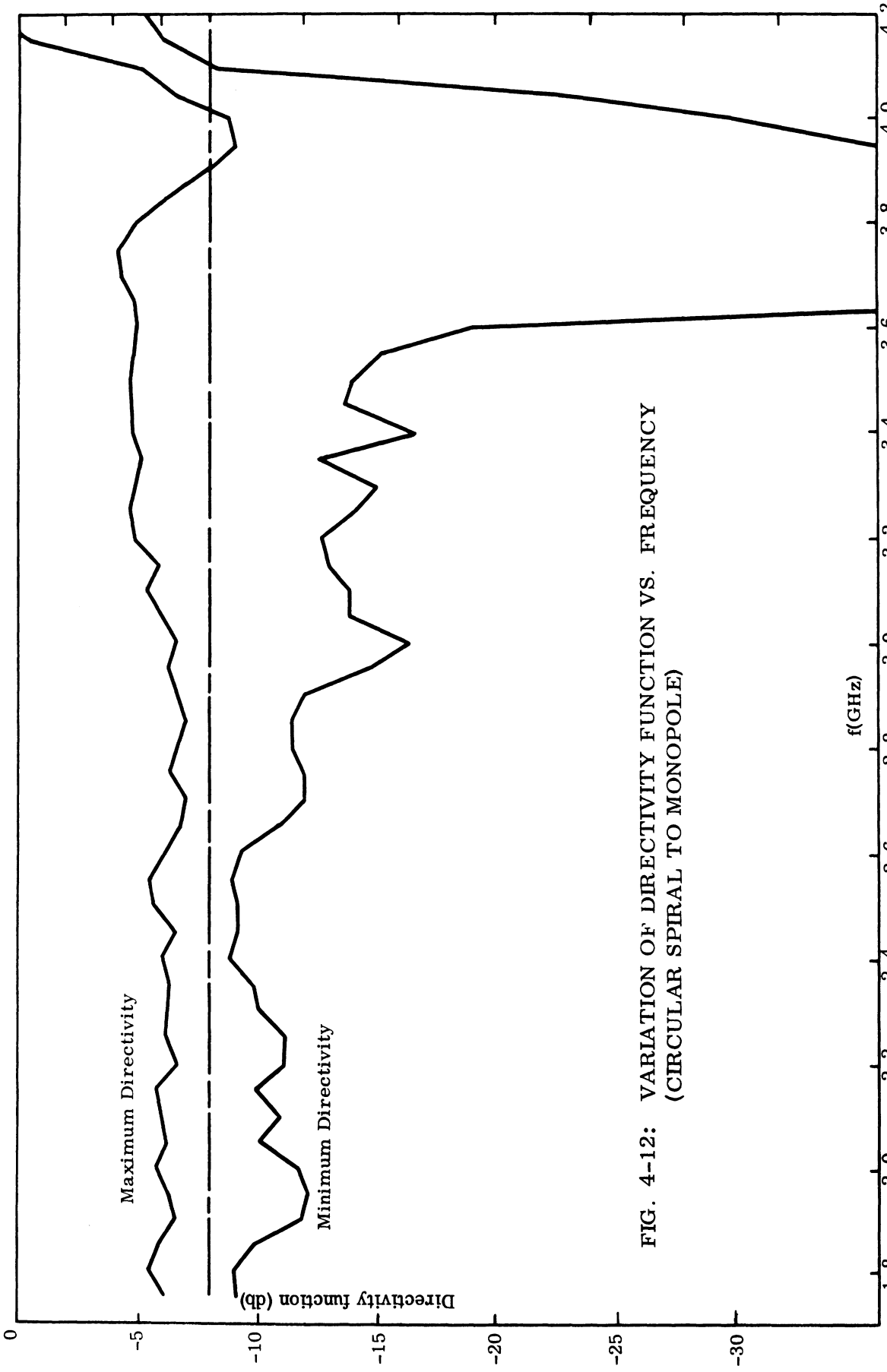

FIG. 4-12: VARIATION OF DIRECTIVITY FUNCTION VS. FREQUENCY (CIRCULAR SPIRAL TO MONOPOLE)

operated outside its designed band. Furthermore, the second mode has more energy concentrated along the ground plane, which accounts for the rise in the coupling level.

Figure 4-13 shows the angular position of the maxima as a function of frequency. An expanded angular scale is used for clarity; one should remember that $\phi = \phi + 2n\pi$ in the figures. At the lower end of the band, the maxima and minima shift quite rapidly. This is due to standing waves arising from reflections at the ends of the spiral elements. These standing waves are more predominant at lower frequencies because the current traveling wave is not sufficiently attenuated by radiation damping. The curves of Fig. 4-13 demonstrate that nulls of the pattern, which move in much the same manner as the maxima, can only be used for decoupling over a narrow frequency band.

4.3.3 Square Archimedean Spiral

Right-hand and left-hand wound square spirals were experimentally tested on the 12' x 12' ground plane in the anechoic chamber. Pertinent information is given below.

Type	Cavity-backed, two-arm, 20 turns
Frequency range	2 - 4 GHz
Balun type	Strip-line, Roberts, located in cavity
Manufacturer	Advanced Development Laboratories
Model No.	1L (left-hand wound) 3R (right-hand wound)
Overall Dimensions (antenna and cavity)	5 cm x 5 cm x 2.5 cm

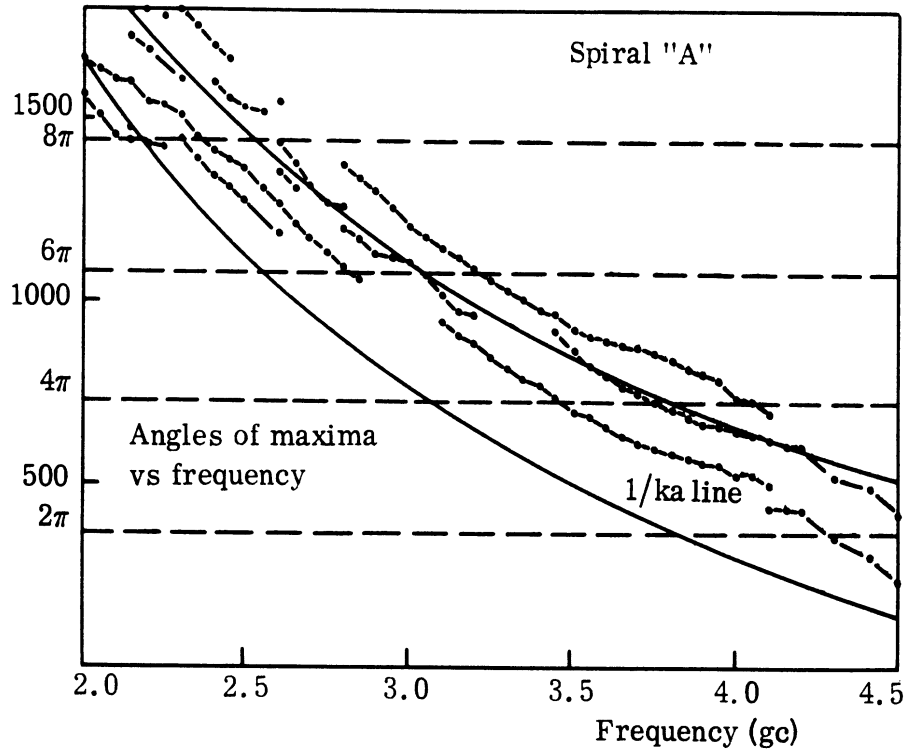

4-13a

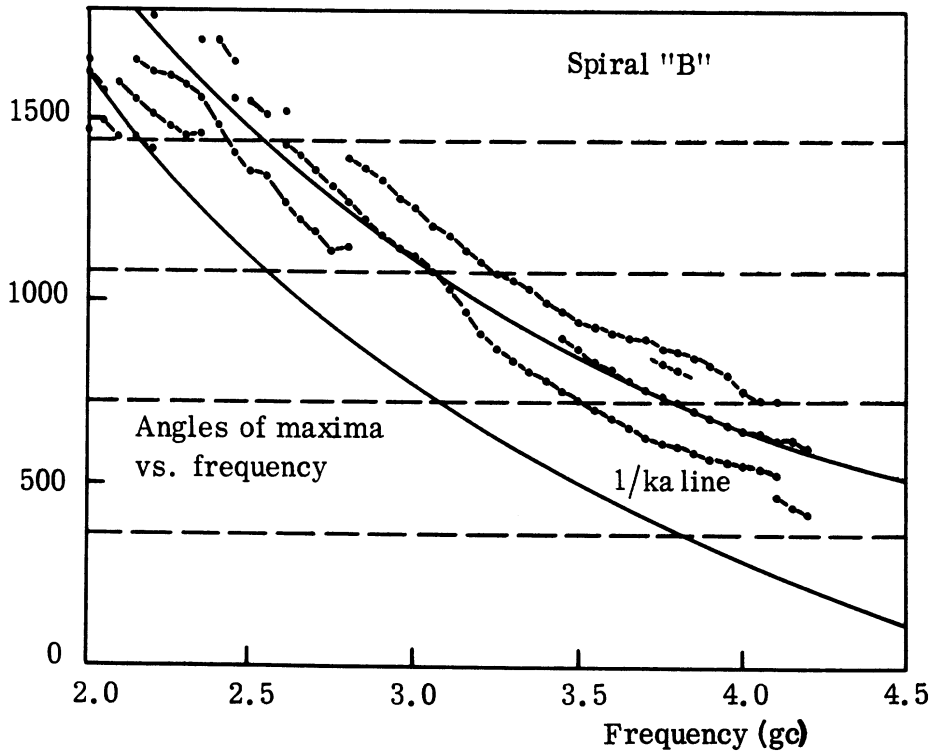

4-13b

FIG. 4-13: ANGLES OF MAXIMA OF COUPLING VS. FREQUENCY, SQUARE SPIRAL "IL" (a) FOR CIRCULAR SPIRAL "A" (b) FOR CIRCULAR SPIRAL "B"

Coupling measurements were taken between the square spiral antenna and a quarter-wave monopole. The monopole was perpendicular to the ground plane, and located 11.3" from the center of the square spiral antenna. Coupling patterns were recorded for frequencies from 2 - 4 GHz at 100 MHz intervals. Typical curves for spiral 1L are shown in Fig. 4-14.

Further study of these coupling patterns reveals a preponderance of maxima at locations radially out from the antenna corners ($\phi = 0^o$, 90^o, 180^o and 270^o).

Figure 4-15 indicates the maximum and minimum of the directivity function of the spiral antenna calculated in the same manner as for the circular spiral. Due to the relationship between coupling and directivity function (see Eq. 4.29), these curves indicate:

a) a relatively small variation in coupling as a function of frequency,

b) a relatively constant difference between maximum and minimum levels over the frequency range,

and c) a trend toward increased average coupling as the frequency is increased.

Comparison with the circular spiral indicates

a) a greater beamwidth than that observed for the circular spiral,

and b) a relatively constant gain over the frequency range of the antenna.

A number of measurements of coupling between the two square spirals 1L and 3R, were made for center-to-center spacing at a minimum. One side or face of the square housing of one spiral was placed in contact with a similar side of the second spiral. Over a frequency range of 2.4 - 4.0 GHz the coupling was approximately -33 db. The observed variation of coupling over this frequency range was 1 db.

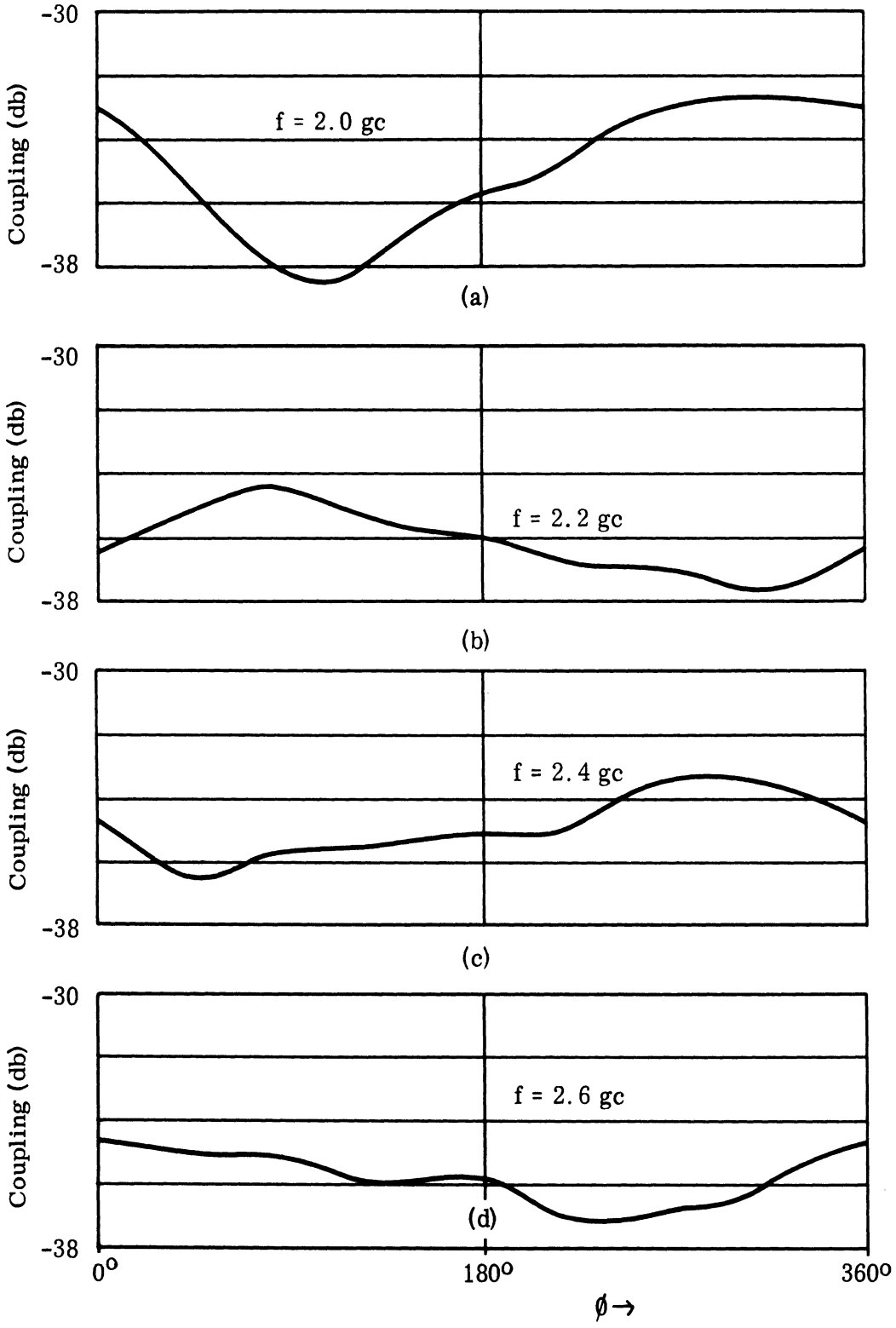

FIG. 4-14: COUPLING PATTERNS FOR SQUARE SPIRAL "1L"

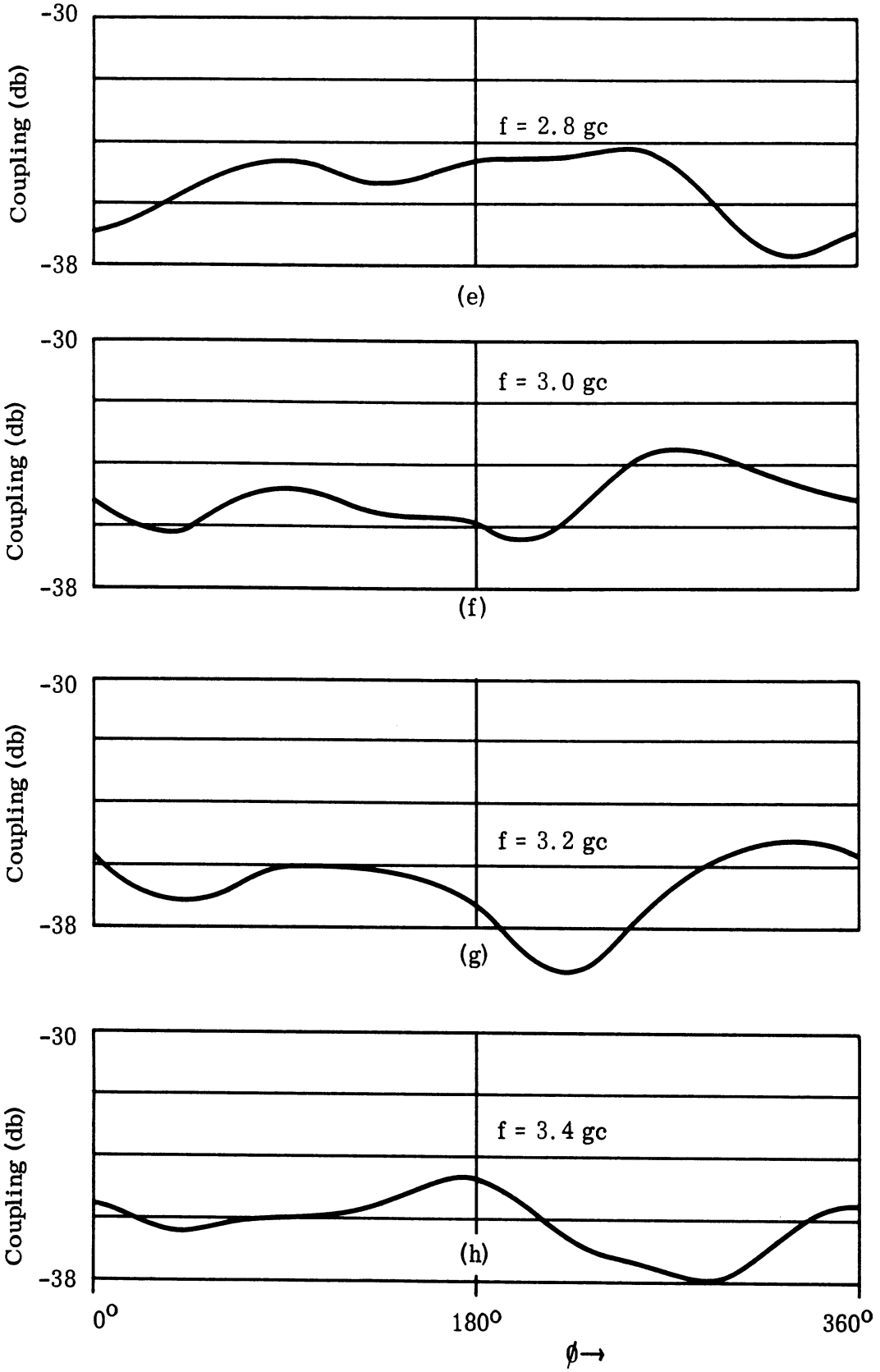

FIG. 4-14: (Cont.) COUPLING PATTERNS FOR SQUARE SPIRAL "1L"

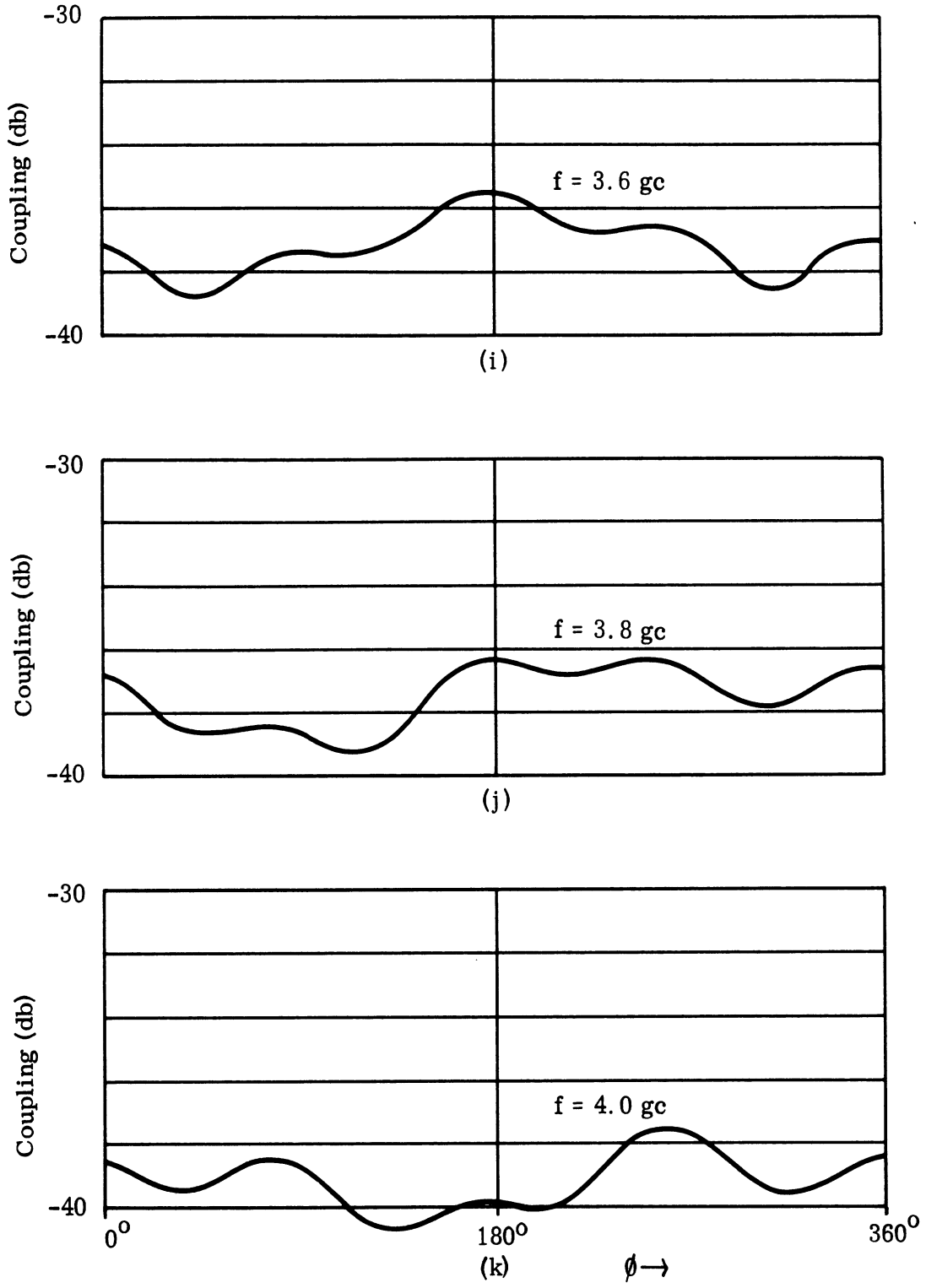

FIG. 4-14: (cont.) COUPLING PATTERNS FOR SQUARE SPIRAL "1L"

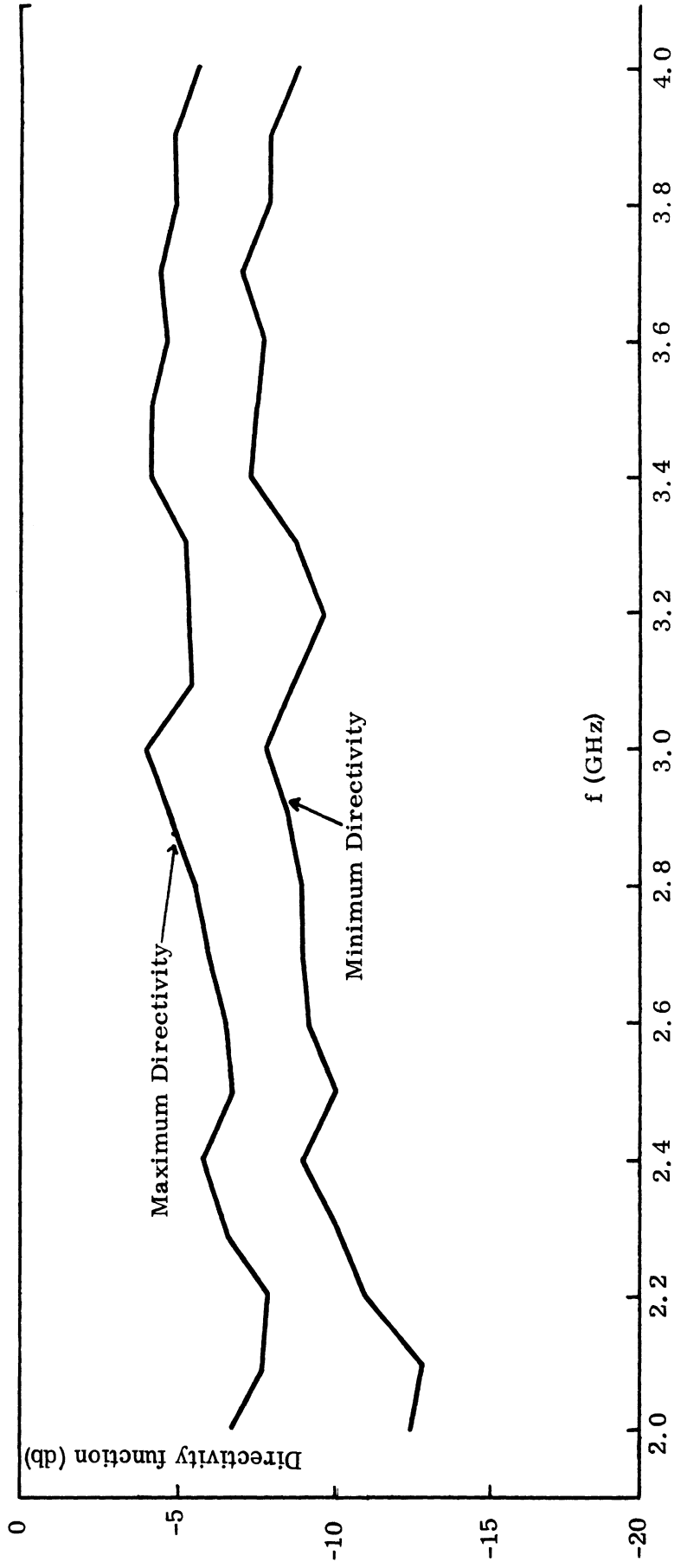

FIG. 4-15: VARIATION OF DIRECTIVITY FUNCTION VS FREQUENCY (SQUARE SPIRAL TO MONOPOLE)

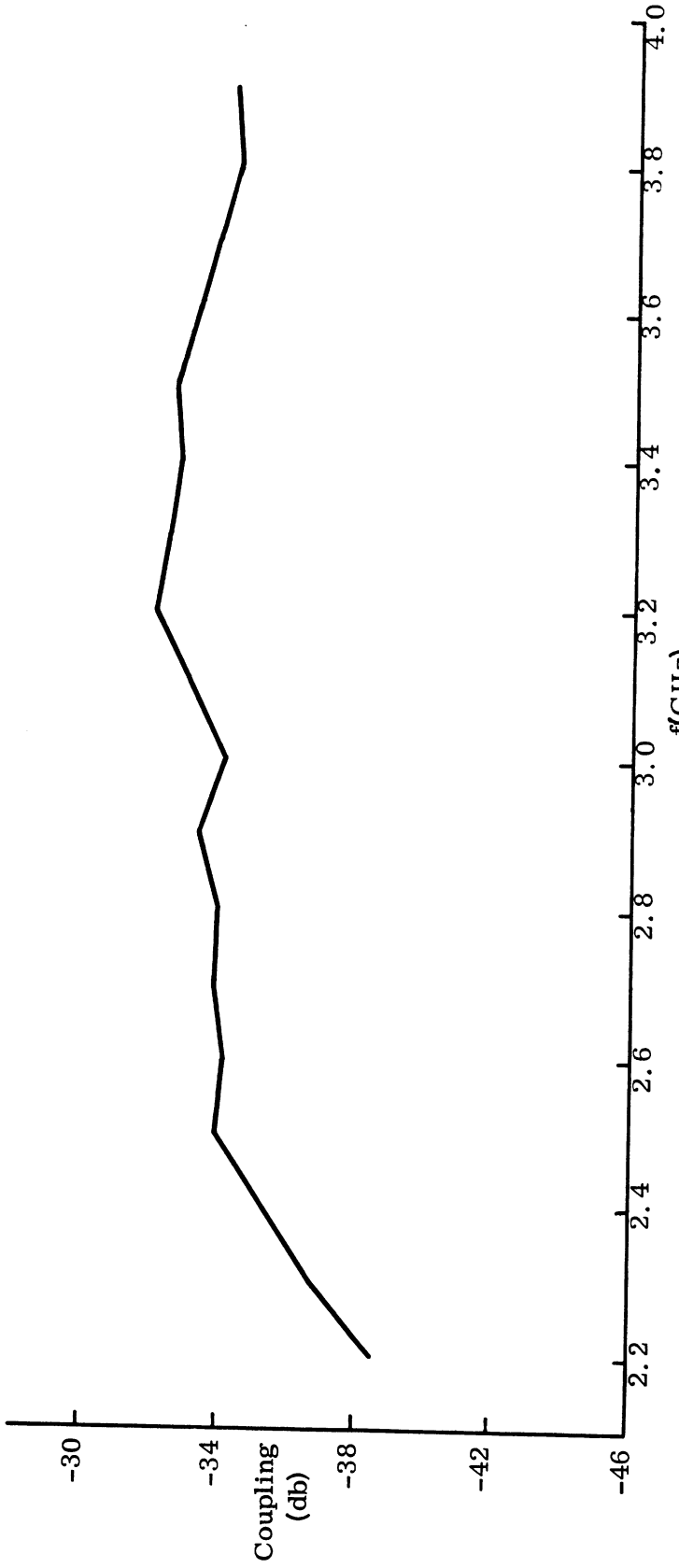

FIG. 4-16: NEAR FIELD COUPLING OF SQUARE SPIRAL TO SQUARE SPIRAL NORMALIZED TO ONE WAVELENGTH SPACING

4.4 Conical Horns

4.4.1 Theoretical Derivation

A theoretical derivation of the far field coupling for the conical horn can be made. By the postulate of a tangential E-field, E_ρ and E_ϕ in the aperture of the conical horn the Hertzian magnetic vector can be derived as

$$\bar{\pi}^*(\bar{R}) = \frac{1}{2\pi j\omega\mu} \iint \left[\bar{E}(\bar{\rho}) \times \hat{n}\right] \frac{e^{-jk\left|\bar{R}-\bar{\rho}\right|}}{\left|\bar{R}-\bar{\rho}\right|} \, dS \qquad (4.29)$$

The factor in front of the integral already includes the imaging effect of the ground plane. $\bar{E} \times \hat{n}$, the tangential E-field, vanishes in the ground plane. Therefore, the only contribution to the integral comes from the horn aperture.

From the Hertzian magnetic vector, the fields can be obtained as

$$\bar{E} = -j\omega\mu \nabla \times \bar{\pi}^* \qquad (4.30)$$

$$\bar{H} = \nabla(\nabla \cdot \bar{\pi}^*) + k^2 \bar{\pi}^* \qquad (4.31)$$

Using a spherical coordinate system as indicated in Fig. 4-17, only E_θ is non-vanishing in the ground plane ($\theta = \pi/2$). The field component E_θ is given by (Silver, 1949)

$$\left[E_\theta\right]_{\theta=\pi/2} = \frac{jke^{-jkR}}{2\pi R} (N_x \cos\phi + N_y \sin\phi) \qquad (4.32)$$

where N_x and N_y represent the integrals in $\bar{\pi}_x^*$ and $\bar{\pi}_y^*$, and

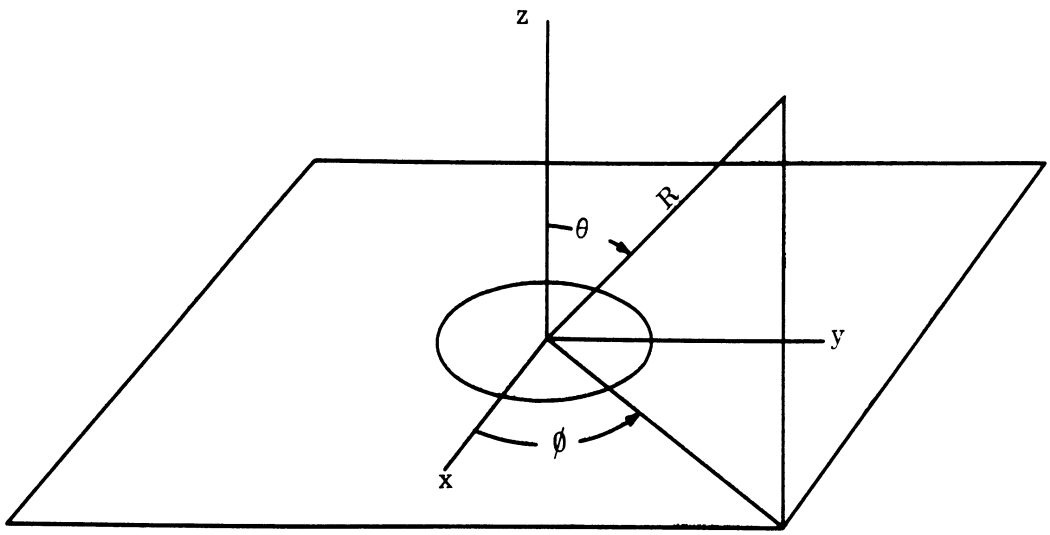

FIG. 4-17: COORDINATE SYSTEM FOR CONICAL HORN

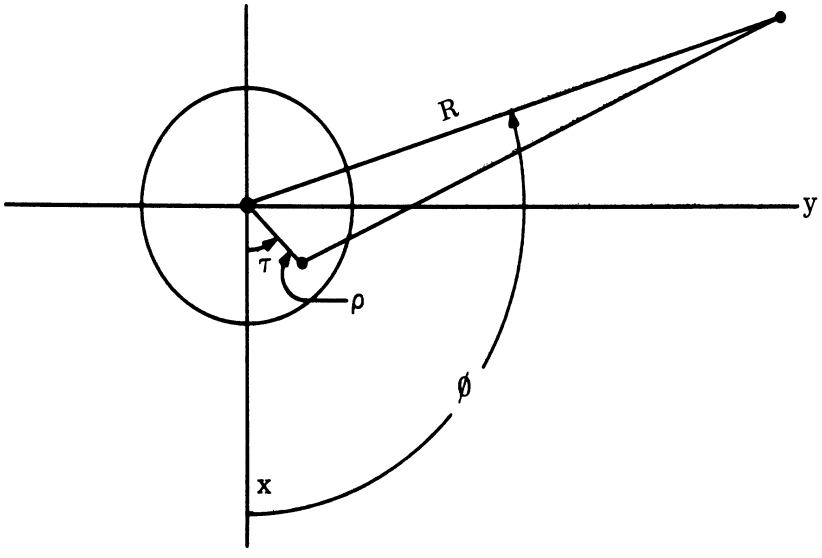

FIG. 4-18: COORDINATE SYSTEM IN GROUND PLANE FOR CONICAL HORNS

$$N_x = \iint (E_t)_x \, e^{jk(\xi \cos\phi + \eta \sin\phi)} dS \tag{4.33}$$

and

$$N_y = \iint (E_t)_y \, e^{jk(\xi \cos\phi + \eta \sin\phi)} dS \, . \tag{4.34}$$

Using the relations $\xi = \rho \cos\tau$, $\eta = \rho \sin\tau$ (see Fig. 4-18), one gets

$$N_x = \iint (E_t)_x \, e^{jk\rho \cos(\phi - \tau)} \rho d\rho d\tau \tag{4.35}$$

and

$$N_y = \iint (E_t)_y \, e^{jk\rho \cos(\phi - \tau)} \rho d\rho d\tau \, . \tag{4.36}$$

In order to evaluate the far field pattern, the tangential aperture field $\overline{E}_t$ has to be derived or postulated. For the present case, it was assumed that in the aperture the tangential E-field could be represented as a combination of circular waveguide modes TE_{11} and TM_{11}, both of them having their phase centers at the point where the extended walls of the conical horn would intersect (Fig. 4-19). There is experimental evidence available (Potter, 1963) that a mixture of these two modes actually exists in the aperture of even moderate flare angle conical horns.

The aperture fields assumed to exist are given by:

$\underline{TE_{11}}$

$$E_\rho = \frac{j\omega\mu \, F \sin\tau \, J_1(K'_{11} \rho)}{\rho} \tag{4.37}$$

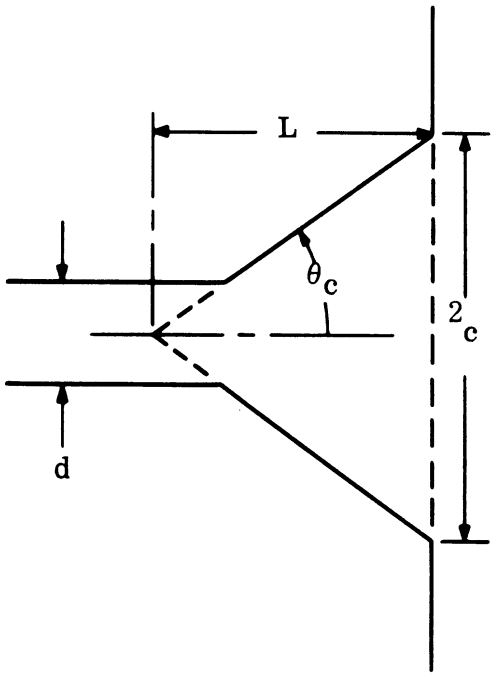

FIG. 4-19: CROSS SECTIONAL VIEW OF CONICAL HORN
c=4.6cm, d=2.54cm, L=26.4cm, θ_c=9.9°.

$$E_\tau = -j\omega\mu K_{11}' F \cos\tau J_1'(K_{11}'\rho) \tag{4.38}$$

where

$$F = \exp\left[-j\frac{2\pi}{\lambda}\sqrt{L^2+\rho^2}\right], \tag{4.39}$$

(for the definition of L, see Fig. 4-19) and where $(K_{11}'c)$ is the first root of J_1';

$$J_1'(K_{11}'c) = 0. \tag{4.40}$$

$\underline{TM_{11}}$

$$E_\rho = 2j\omega\mu K_{11}' F \sin\tau J_1(K_{11}\rho) \tag{4.41}$$

$$E_\tau = \frac{2j\omega\mu K_{11}' F \cos\tau J_1(K_{11}\rho)}{K_{11}\rho} \tag{4.42}$$

where $(K_{11}c)$ is defined as the first zero of J_1;

$$J_1(K_{11}c) = 0 \tag{4.43}$$

and F is defined above. In order to evaluate N_x and N_y (4.35) and (4.36), it is convenient to decompose the aperture fields into rectangular components, giving:

$\underline{TE_{11}}$

$$E_\xi = \frac{1}{2} j\omega\mu K_{11}' F\left[J_2(K_{11}'\rho)\sin 2\tau\right] \tag{4.44}$$

$$E_\eta = 2j\omega\mu K'_{11} F\left[J_o(K'_{11}\rho) - J_2(K'_{11}\rho)\cos 2\tau\right] \tag{4.45}$$

$\underline{TM_{11}}$

$$E_\xi = -j\omega\mu K_{11} F J_2(K_{11}\rho)\sin 2\tau \tag{4.46}$$

$$E_\eta = j\omega\mu K_{11} F\left[J_o(K_{11}\rho) + J_2(K_{11}\rho)\cos 2\tau\right] \tag{4.47}$$

For the TE_{11} mode there results

$$N_x = A\iint F \sin\tau\, e^{jk\rho\cos(\phi-\tau)} J_2(K'_{11}\rho)\,\rho d\rho d\tau \tag{4.48}$$

and

$$N_y = A\iint F\left[J_o(K'_{11}\rho) - J_2(K'_{11}\rho)\cos 2\tau\right] e^{jk\rho\cos(\phi-\tau)}\rho d\rho d\tau \tag{4.49}$$

where

$$A = \frac{1}{2} j\omega\mu K'_{11}.$$

Using the expansion

$$e^{jx\cos y} = J_o(x) + \sum_{n=1}^{\infty} 2j^n J_n(x)\cos ny, \tag{4.50}$$

these become

$$N_x = -2\pi A \sin 2\phi\, \Gamma_2(K'_{11}) \tag{4.51}$$

and

$$N_y = 2\pi A\left[\Gamma_0(K'_{11}) + \Gamma_2(K'_{11})\cos 2\phi\right] \tag{4.52}$$

where

$$\Gamma_0(\gamma) = \int_0^a F \rho \, J_o(\gamma\rho) \, J_o(k\rho) \, d\rho \tag{4.53}$$

and $$\Gamma_2(\gamma) = \int_0^a F\rho \, J_2(\gamma\rho) \, J_2(k\rho) \, d\rho \, . \tag{4.54}$$

For the TM_{11} mode one obtains:

$$N_x = -2A \iint F \sin 2\tau \, e^{ik\rho \cos(\phi - \tau)} \, J_2(K_{11}\rho) \, \rho d\rho d\tau \tag{4.55}$$

and $$N_y = 2A \iint F \left[J_o(K_{11}\rho) + J_2(K_{11}\rho) \cos 2\tau \right] e^{jk\rho \cos(\phi - \tau)} \rho d\rho d\tau \tag{4.56}$$

which become

$$N_x = 4\pi A \sin 2\phi \, \Gamma_2(K_{11}) \tag{4.57}$$

and $$N_y = 4\pi A \left[\Gamma_0(K_{11}) - \Gamma_2(K_{11}) \cos 2\phi \right] . \tag{4.58}$$

Combining the contributions due to the x and y polarizations according to (4.32), one gets:

$$E_\theta = \frac{jkA}{R} \left[\Gamma_0(K'_{11}) - \Gamma_2(K'_{11}) \right] \sin \phi \qquad \text{for } TE_{11} \text{ mode} \tag{4.59}$$

and $$E_\theta = \frac{2jkA}{R} \left[\Gamma_0(K_{11}) + \Gamma_2(K_{11}) \right] \sin \phi \qquad \text{for } TM_{11} \text{ mode} \tag{4.60}$$

or equivalently,

$$E_\theta = \frac{\omega\mu K'_{11} k}{2R}\left[\Gamma_0(K'_{11}) - \Gamma_2(K'_{11})\right]\sin\phi \qquad \text{for } TE_{11} \text{ mode} \quad (4.61)$$

and

$$E_\theta = \frac{\omega\mu K'_{11} k}{R}\left[\Gamma_0(K_{11}) + \Gamma_2(K_{11})\right]\sin\phi \qquad \text{for } TM_{11} \text{ mode.} \quad (4.62)$$

The integrals Γ_0 and Γ_2 (4.53 and 4.54) cannot be evaluated in closed form because of the factor F. However, in the limiting case of an aperture fed by a circular waveguide of the same size, this factor becomes equal to one. In this case Γ_0 and Γ_2 can be evaluated exactly using the relationship (Silver, 1949);

$$\int_0^c y J_n(\alpha y) J_n(\beta y)\, dy = \frac{c}{\alpha^2 - \beta^2}\left[J_n(\alpha c)\beta J'_n(\beta c) - J_n(\beta c)\alpha J'_1(\alpha c)\right]. \quad (4.63)$$

Now by definition $J'_1(K'_{11}c) = 0$ for the TE_{11} mode, and $J_1(K_{11}c) = 0$ for the TM_{11} mode, and the following evaluations can be made:

$$\Gamma_0(K'_{11}) = \frac{c}{K'^2_{11} - k^2} J_o(K'_{11}c)\left[K'^2_{11}\, cJ_o(kc) - kJ_1(kc)\right], \quad (4.64)$$

$$\Gamma_2(K'_{11}) = \frac{c}{K'^2_{11} - k^2} J_o(K'_{11}c)\left[kJ_1(kc) - K'^2_{11}\, cJ_2(kc)\right], \quad (4.65)$$

$$\Gamma_0(K_{11}) = \frac{-kc}{K'^2_{11} - k^2} J_o(K_{11}c)\, J_1(kc), \quad (4.66)$$

and $$\Gamma_2'(K_{11}) = -\frac{kc}{K_{11}'^2 - k^2} J_o(K_{11} c)\, J_1(kc) \tag{4.67}$$

Therefore, the particular combinations needed for deriving the normal E-field equations (4.61) and (4.62) are:

$$\Gamma_0'(K_{11}') - \Gamma_2'(K_{11}') = \frac{2c}{k} J_o(K_{11}' c)\, J_1(kc)\,, \tag{4.68}$$

and $$\Gamma_0'(K_{11}) + \Gamma_2'(K_{11}) = -\frac{2kc}{K_{11}^2 - k^2} J_o(K_{11} c)\, J_1(kc)\,. \tag{4.69}$$

$$E_\theta = \frac{\omega\mu K_{11}' c}{R} J_o(K_{11}' c)\, J_1(kc) \sin\phi, \qquad \text{for } TE_{11} \text{ mode} \tag{4.70}$$

and $$E_\theta = \frac{2\omega\mu K_{11}' k}{(K_{11}^2 - k^2)R} J_o(K_{11} c)\, J_1(kc) \sin\phi \qquad \text{for } TM_{11} \text{ mode.} \tag{4.71}$$

The directivity of the antenna is given as

$$D(\phi) = \frac{P(\phi) 2\pi R^2}{W}\,, \tag{4.72}$$

where $P(\phi)$ is the power density in the ϕ-direction and W is the total radiated power by the transmitting antenna. Then,

$$D = \frac{\frac{1}{2}\sqrt{\frac{\epsilon}{\mu}}\left|E_\theta\right|^2 2\pi R^2}{W}\,. \tag{4.73}$$

To calculate W, evaluate $\frac{1}{2}\,\mathrm{Re}(E_t \times H_t^*)$ over the aperture, giving:

$$W = \frac{k}{2\omega\mu}\int_0^{2\pi}\int_0^{c}\left(\left|E_x\right|^2+\left|E_y\right|^2\right)\rho\,d\rho\,d\tau\,. \tag{4.74}$$

There results for the TE_{11} and TM_{11} modes, respectively

$$W_E = \frac{\pi\beta_{11}'K_{11}'^2\omega\mu}{4}\int_0^{c}\left[J_o^2(K_{11}'\rho)+J_2^2(K_{11}'\rho)\right]\rho\,d\rho = \frac{\pi\beta_{11}'\omega\mu}{4}(K_{11}'^2c^2-1)\,J_1^2(K_{11}'c)$$

for the TE_{11} mode (4.75)

where

$$\beta_{11}' = \sqrt{k^2-K_{11}'^2} \tag{4.76}$$

and $$W_M = 16\pi\omega\mu\,\frac{k^2K_{11}^2}{\beta_{11}'\beta_{11}}\,J_o^2(K_{11}c) \qquad \text{for the } TM_{11} \text{ mode} \tag{4.77}$$

where

$$\beta_{11} = \sqrt{k^2-K_{11}^2}\,. \tag{4.78}$$

The total radiated power by the conical horn will then be the sum of that contained in the TE_{11} and TM_{11} modes, i.e.

$$W_{total} = R_1^2W_E+R_2^2W_M\,, \tag{4.79}$$

where R_1 and R_2 are the amplitudes with which the TE_{11} and TM_{11} modes are excited, respectively.

Using the directivity of the conical horn one can derive the coupling by the formula:

$$C = D_t(\phi_t)D_r(\phi_r)C_o(R_o) \tag{4.80}$$

where

D_t = directivity of the transmitting horn in the direction of the receiving horn

D_r = directivity of the receiving horn in the direction of the transmitting horn

$C_o = \lambda^2/4\pi R_o^2$

R_o = distance of separation of the conical horns from center to center measured in the common mounting plane.

Now, for identical transmitting and receiving horns each with circular polarization

$$D(\phi) = D_t(\phi_t) = D_r(\phi_r) \tag{4.81}$$

and the coupling becomes

$$D = D^2(\phi)C_o \tag{4.82}$$

While one can derive a closed form expression for F = 1 for Γ_0 and Γ_2 (equations (4.53) and (4.54)), these equations can be evaluated very easily numerically for any F. A computer program was written for this purpose, evaluating the integrals by using Simpson's formula. Figure 4-20 shows the theoretical maximum coupling value obtained as a function of frequency with a

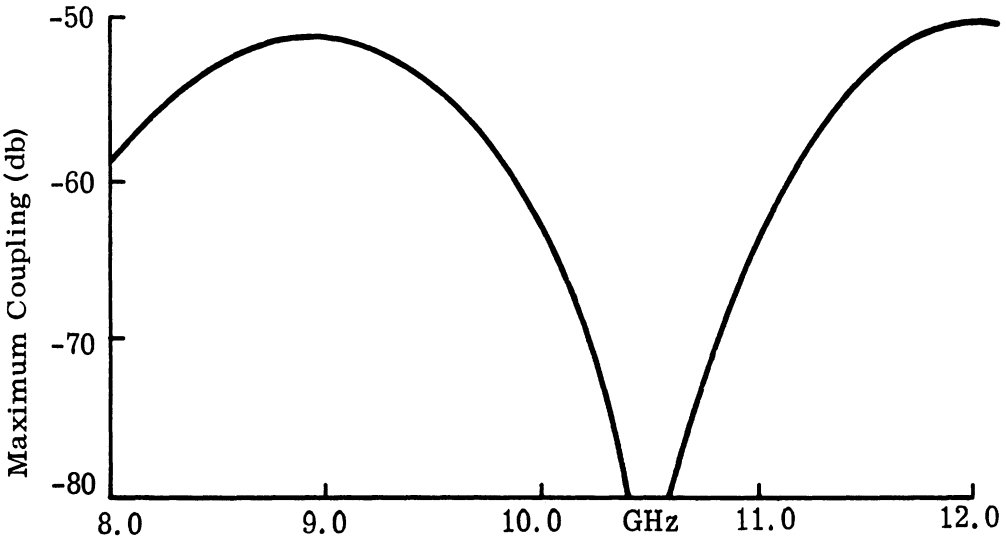

FIG. 4-20: COMPUTED COUPLING LEVELS FOR CONICAL HORNS AS A FUNCTION OF FREQUENCY. R_1=.9, R_2=.1, a=4.6cm, R_o= center-to-center spacing=36.6cm.

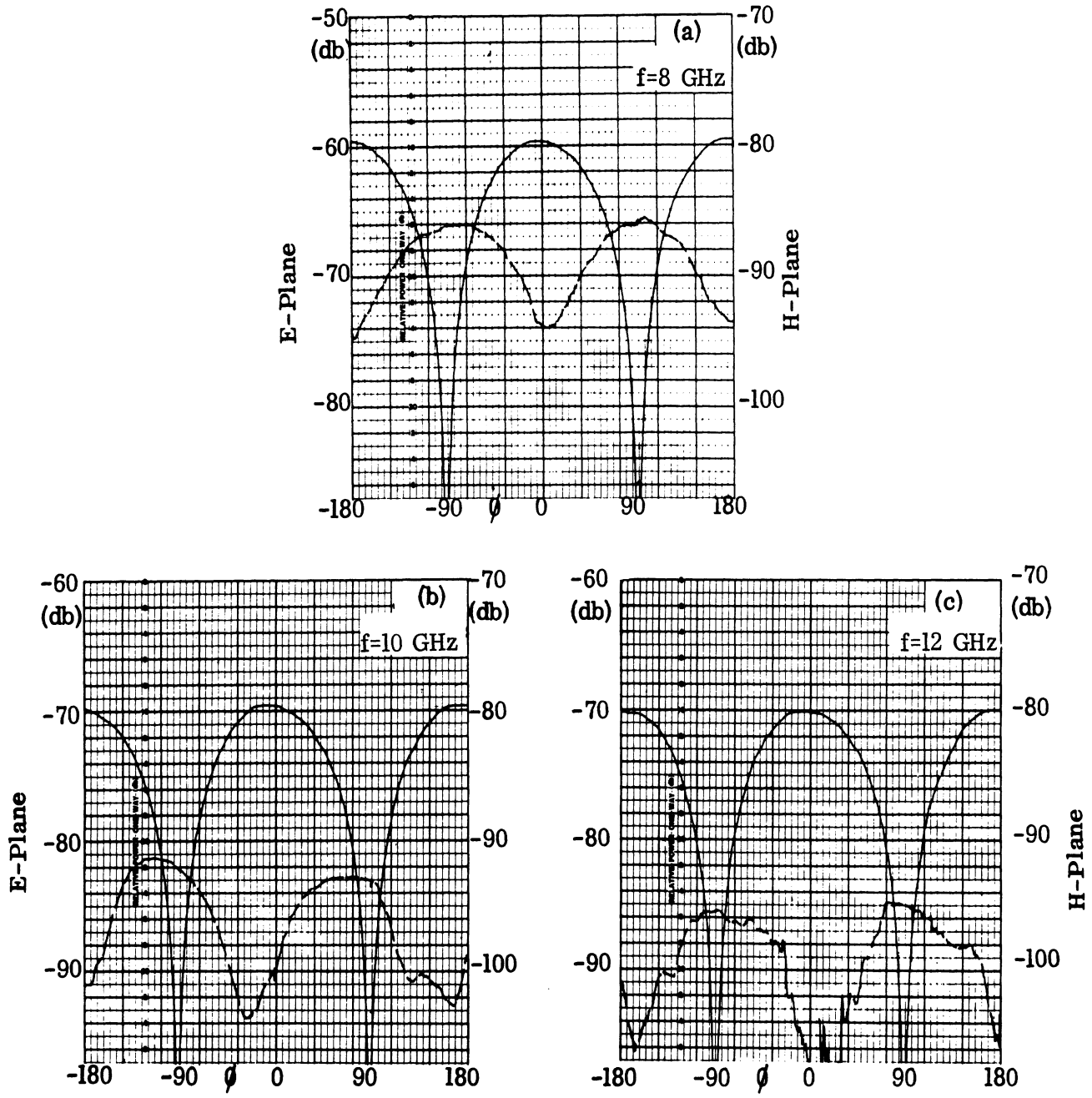

FIG. 4-21: CONICAL HORN COUPLING PATTERNS (LINEARLY POLARIZED)
(—) E-PLANE (--) H-PLANE.

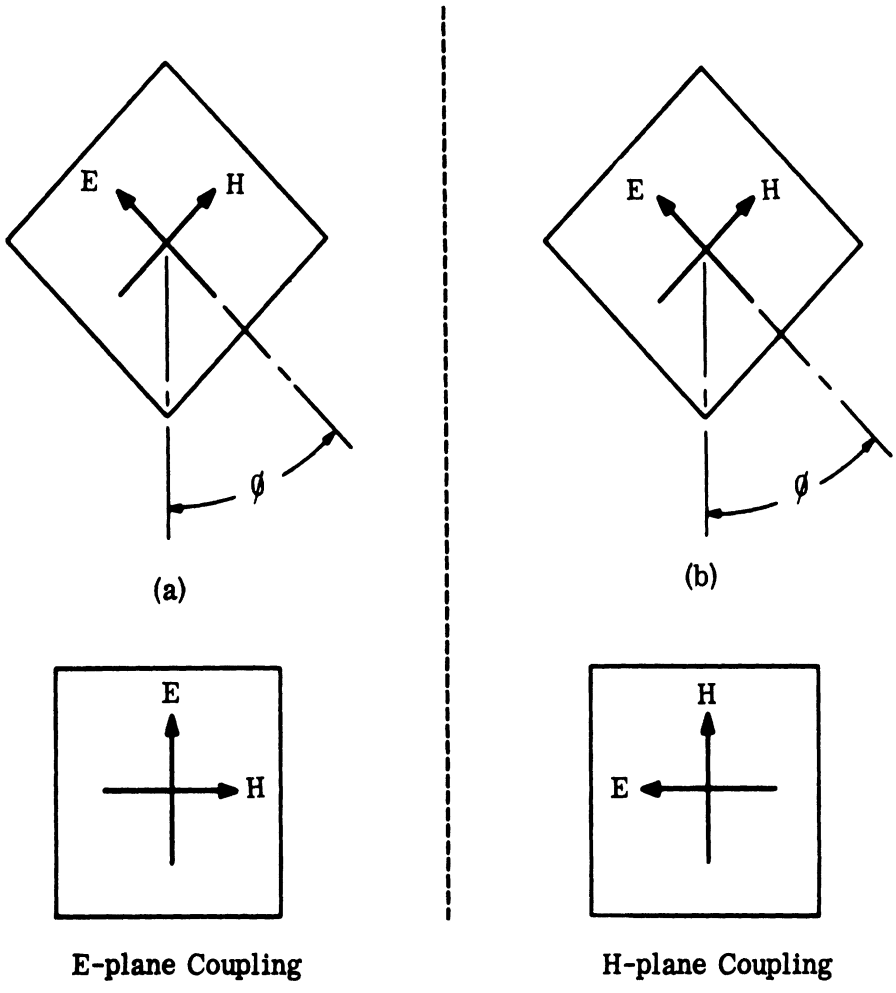

FIG. 4-22: DIFFERENTIATION BETWEEN E- AND H-PLANE COUPLING

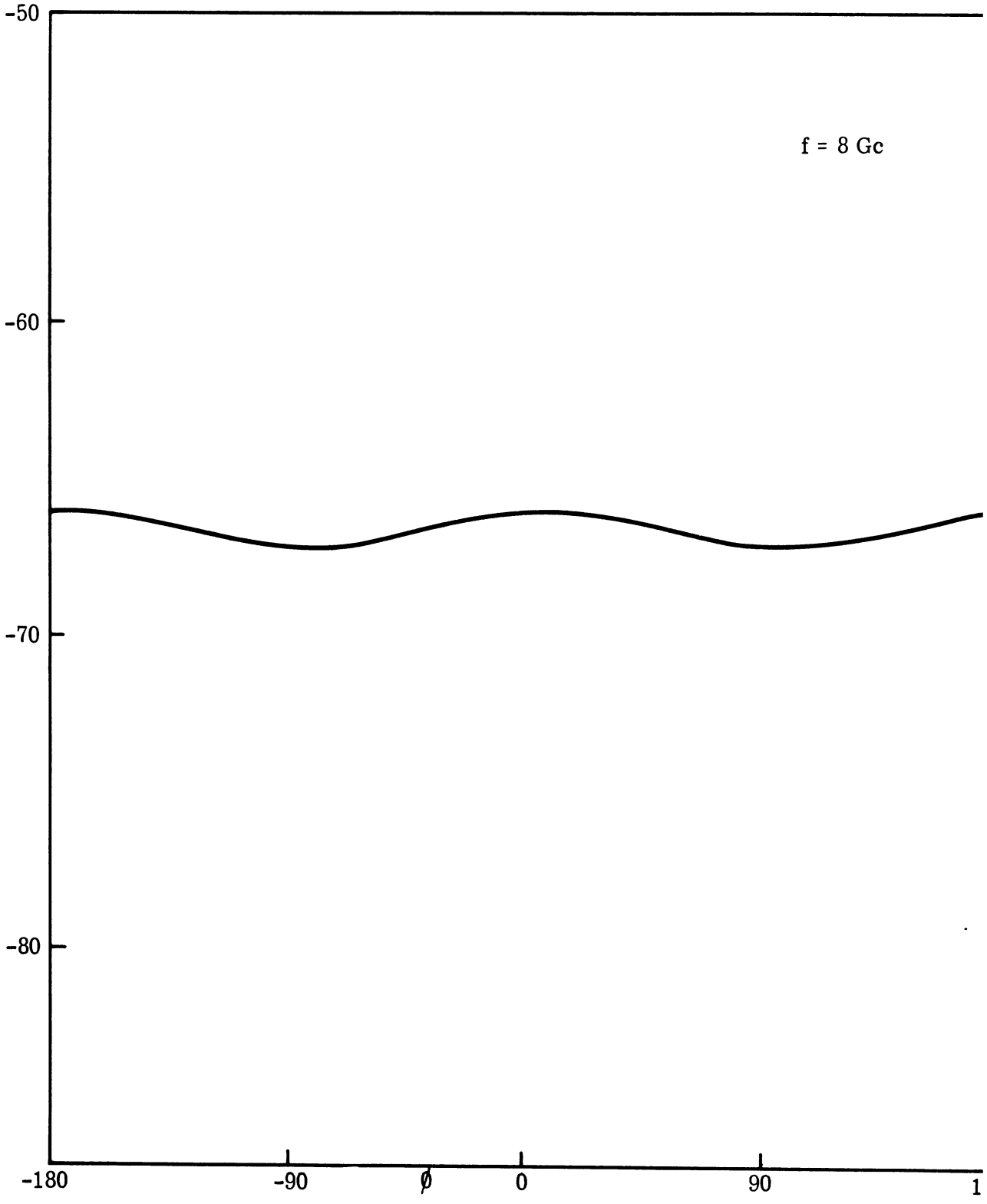

FIG. 4-23: CIRCULARLY POLARIZED CONICAL HORN COUPLING PATTERN

pair of horns of radius a = 4.6 cm, center to center spacing 36.6 cm and length L = 26.4 cm. $R_1 = .9$, $R_2 = .1$. Only a plot of the maximum coupling is needed in order to deduce the coupling for any orientation of the conical horns, since the directivity in the ground plane varies as sin ϕ.

4.4.2 Experimental Results

Experimental data were gathered for a pair of conical horns mounted in a ground plane with L = 26.4 cm, c = 4.6, $\theta_o = 9.9^o$ (Fig. 4-19). The gain of each of these horns is 18 db at 9 GHz. The data were taken for the linearly polarized case at 8, 10 and 12 GHz at a center to center spacing of 36.6 cm. The two curves shown in Figs. 4-21a to 4-21c, labelled E- and H-plane coupling, are described by the geometry of Fig. 4-22. It is seen from these curves that, indeed, as predicted by the analysis the coupling levels vary as sin ϕ. The maxima of the H-plane coupling are down 6 to 16 db from the maxima obtained for the E-plane coupling. At this spacing of 36.6 cm, the lowest coupling level obtainable for the linearly polarized pairs of conical horns is about -90 db. Figure 4-23 shows the E-plane coupling pattern as a function of rotation angle ϕ (of the receiving horn) at 8 GHz with both horns circularly polarized. Because of the phase quadrature relationship between the two orthogonal components existing in the horns, the nulls of the coupling patterns disappear. The slight variations in coupling are due to the aperture fields being somewhat elliptically polarized.

4.5 Rectangular Horns

To completely specify a two-horn coupling situation, it is necessary to know twelve parameters: the two dimensions of each horn aperture, the two flare angles of each, the spacing, the orientation angles and the frequency. For very crude approximations, one can reduce this to eight (see Section 3.3).

4.5.1 Directivity Function

To get an expression for far-field coupling, a knowledge of the aperture fields is necessary. The assumption is made here that the waveguide fields (TE_{10} mode) are reproduced over a curved phase front at the mouth of the horn. Thus higher order modes are ignored in representing the aperture field. This gives surprisingly accurate results, even for H-plane, or near field, coupling. This will be discussed later.

The electric field of an aperture-type antenna can be expressed in terms of an integral over the aperture: (see Fig. 2-2) :

$$\overline{E}(\overline{R}) = -\nabla \times \iint_{\text{aperture}} \frac{e^{-jkr}}{2\pi r} \overline{E}(\overline{\rho}) \times \hat{z}\, dS$$

(See for example, Harrington, 1961) where $r = \overline{R} - \overline{\rho}$.

Along the ground plane, the vertical component in the far field is:

$$E_\theta(R,\phi) = \frac{k}{2\pi j} \frac{e^{-jkR}}{R} E_o \cos\phi\, g_a(u)\, g_b(v)$$

where

$$g_a(u) = \frac{\pi}{2a} \int_{-a/2}^{a/2} f_a(\xi) \exp\left(\frac{jz\xi}{a} u\right) d\xi$$

$$g_b(v) = \frac{1}{b} \int_{-b/2}^{b/2} f_b(\eta) \exp\left(\frac{j2\eta}{b} v\right) d\eta$$

$$u = \pi\left(\frac{a}{\lambda}\right) \sin \phi$$

$$v = \pi\left(\frac{b}{\lambda}\right) \cos \phi$$

and the assumed aperture distributions are given by

$$f_a(\xi) = \cos \theta_\xi \cos\left(\frac{\pi\theta_\xi}{2\theta_a}\right) \exp\left(\frac{j\pi\xi}{\lambda} \csc \theta_\xi\right)$$

$$f_b(\eta) = \cos \theta_\eta \exp\left(\frac{j\pi\eta}{\lambda} \csc \theta_\eta\right)$$

$$\theta_\xi = \tan^{-1}\left(\frac{2\xi}{a} \tan \theta_a\right)$$

$$\theta_\eta = \tan^{-1}\left(\frac{2\eta}{b} \tan \theta_b\right) .$$

The "length" of the horn can be used as well, where

$$l_a = \frac{a}{2} \cot \theta_a$$

and $$l_b = \frac{b}{2} \cot \theta_b .$$

These quantities are shown in Fig. 4-24. Note that as θ_a and θ_b approach zero

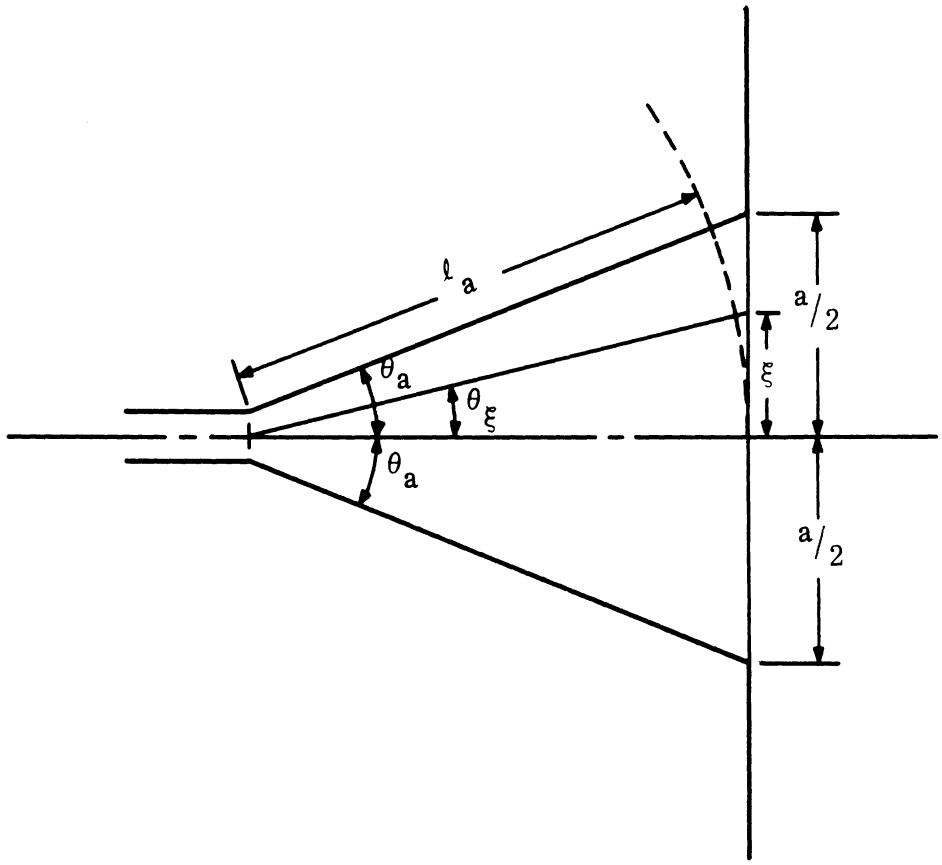

FIG. 4-24: RECTANGULAR HORN GEOMETRY. H-PLANE

$$f_a(\xi) \doteq \cos \frac{\pi \xi}{a}$$

$$f_b(\eta) \doteq 1$$

and

$$g_a(u) \doteq \frac{\cos u}{1 - \frac{4u^2}{\pi^2}}$$

$$g_b(v) \doteq \frac{\sin v}{v}$$

as in the case of open-ended waveguides.

The integrals for $g_a(u)$ and $g_b(v)$ cannot be evaluated for all angles by ordinary means. For this reason, discussion in the literature has been limited to small flare-angle approximations. Here the IBM-7090 computer was used to evaluate these integrals for flare half-angles up to 45^o. The results are tabulated in Table C-1. A set of design curves is also included in Figs. C-1a to C-1m.

The formulation here is for far-field only; section 4.5.2 which follows, considers near-field terms as well. The two formulations match in the far-field, and give results which match well with the experimental results. There are slight differences in the shapes of the coupling curves, in that the maxima and minima differ somewhat (on the order of 1 - 3 db), but the angular dependence is preserved very well. The levels of experimental and theoretical coupling generally match within 5 db. In most cases the theoretical coupling is above the experimental coupling; this is thought to be due to losses. The accuracy is

better than anticipated, considering that higher order modes were ignored, and noting that the sensitivity of coupling to changes in the aperture distribution is high.

4.5.2 E-Sectoral Horn Coupling

The coupling of the two E-sectoral horns is to be considered in this section. The transmitting horn is assumed to be excited by a waveguide supporting a TE_{10} mode and the receiving horn is also connected to a similar waveguide (which supports only TE_{10} mode), in which a measuring device is located. The details of derivation for coupling formulas are given in the Appendix A. The results are:

For $\phi_t \neq \frac{\pi}{2}$

$$C = 16\pi \left(\frac{a_r}{b_0}\right)\left(\frac{\gamma_1'}{k}\right)\left(\frac{\rho_2^{(t)}}{a_t}\right)\left(\gamma_1 \rho_2^{(t)}\right)\frac{1}{(\gamma_1 a_r)^2}\,\frac{1}{(\gamma_1 R_0)^2}\left(\frac{ka_r}{\pi}\right)^2\left(\frac{ka_t}{\pi}\right)^2\frac{1}{W'}$$

$$\cdot\,\frac{M_{01}(\gamma_1 b_0)}{\left|H_c(\gamma_1 b_r, 0)\right|^2}\left[C\left(\frac{ka_t}{\pi}\sin\phi_t\right)\right]^2\cos^2\phi_t\cos^2\phi_r\left|\nu_c(\gamma_1' b_t\cos\phi_t)\right|^2$$

$$\cdot\left|H^{cc}(\gamma_1 b_r\cos\phi_r, 0)\right|^2\left[C\left(\frac{ka_r}{\pi}\sin\phi_r\right)\right]^2 .$$

For $\phi_t = \frac{\pi}{2}$

$$C = -64\pi \left(\frac{a_r}{b_0}\right)\left(\frac{\gamma_1'}{k}\right)^2 \left(\frac{\rho_2^{(t)}}{a_t}\right)\left(\gamma_1 \rho_2^{(t)}\right) \frac{1}{(\gamma_1 a_r)^2} \frac{1}{(\gamma_1 R_0)^2} \frac{1}{(kR_o)^2} \left(\frac{ka_r}{\pi}\right)^2 \left(\frac{ka_t}{\pi}\right)^2$$

$$\cdot \frac{1}{W'} \frac{M_{01}(\gamma_1 b_0)}{\left[H_c(\gamma_1 b_r, 0)\right]^2} \frac{1}{W'} \left[C\left(\frac{ka_t}{\pi} \sin\phi_t\right)\right]^2_{\phi_t = \frac{\pi}{2}} \left|\nu(\gamma_1' b_t)\right|^2$$

$$\cdot \left[\left\{ J^{cc}(\gamma_1 b_r \cos\phi_r, 0)\, P_c(m=1) - \frac{1}{2}\frac{k}{\gamma_1} J^{tcs}(\gamma_1 b_r \cos\phi_r, 0) \cos\phi_r \sin\phi_r \right.\right.$$

$$\left. C\left(\frac{ka_r}{\pi} \sin\phi_r\right)\right\}^2$$

$$+ \left\{ Y^{cc}(\gamma_1 b_r \cos\phi_r, 0)\, P_c(m=1) - \frac{1}{2}\frac{k}{\gamma_1} Y^{tcs}(\gamma_1 b_r \cos\phi_r, 0) \cos\phi_r \sin\phi_r \right.$$

$$\left.\left. \cdot C\left(\frac{ka_r}{\pi} \sin\phi_r\right)\right\}^2 \right] .$$

For notations, refer to Appendix A.

Numerical examples are shown in Figs. 4-25 to 4-26, together with experiments results. See Fig. 5-1 for an explanation of ϕ_t and ϕ_r.

4.5.3 H-Sectoral Horn Coupling

The theory for the coupling of the two H-sectoral horns connected to waveguides supporting the TE_{10} mode is given in the last part of the Appendix A. The formulas for the coupling are very inconvenient for numerical calculations.

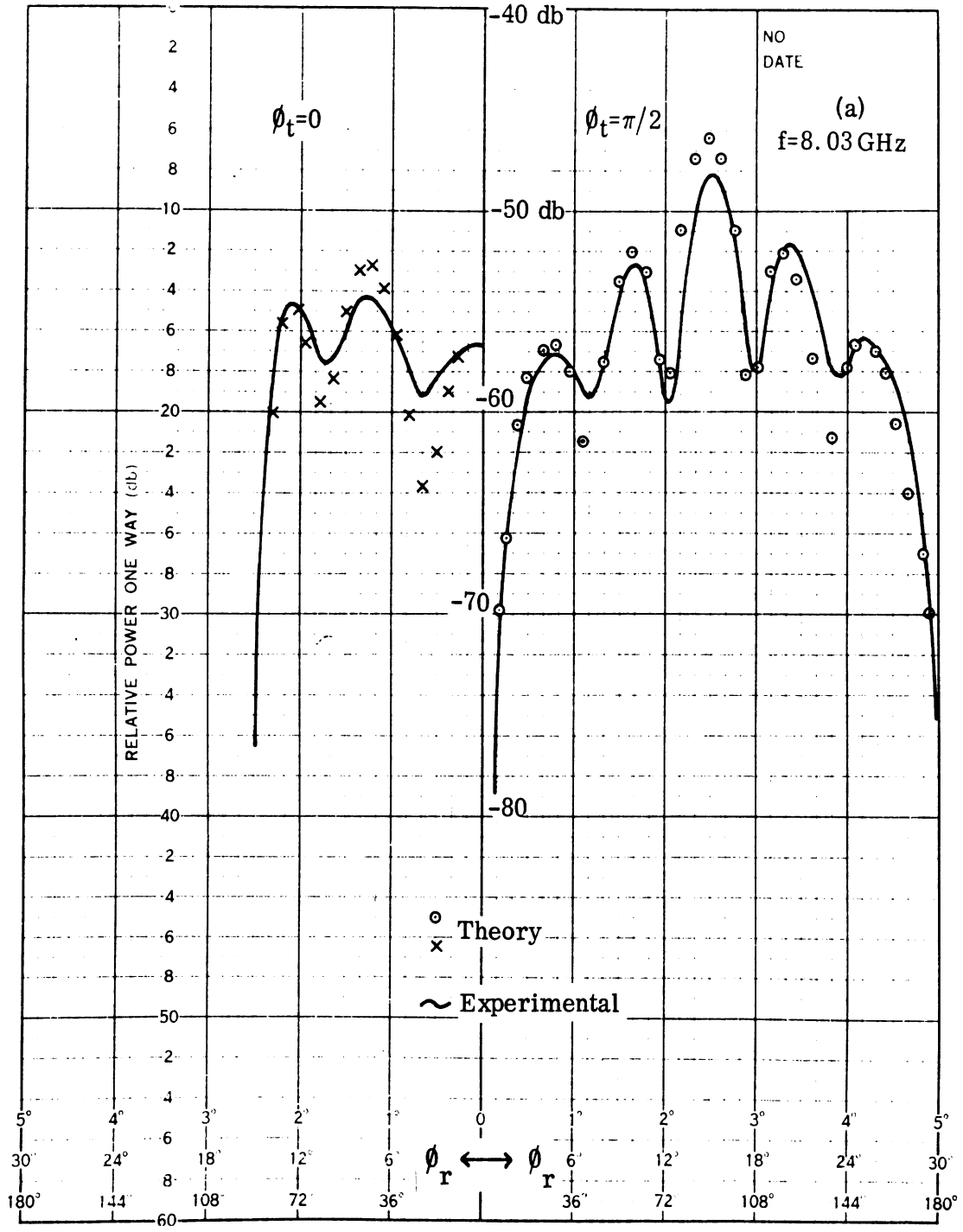

FIG. 4-25a: COMPARISON OF EXPERIMENT AND THEORY E-SECTORAL HORN. $R_o=22.86$ cm, $a_r=a_t=0.9''$, $b_r=b_t=3.22''$, $a_o=0.9''$, $b_o=0.4''$, $\rho(t)=\rho(r)=3.78''$.

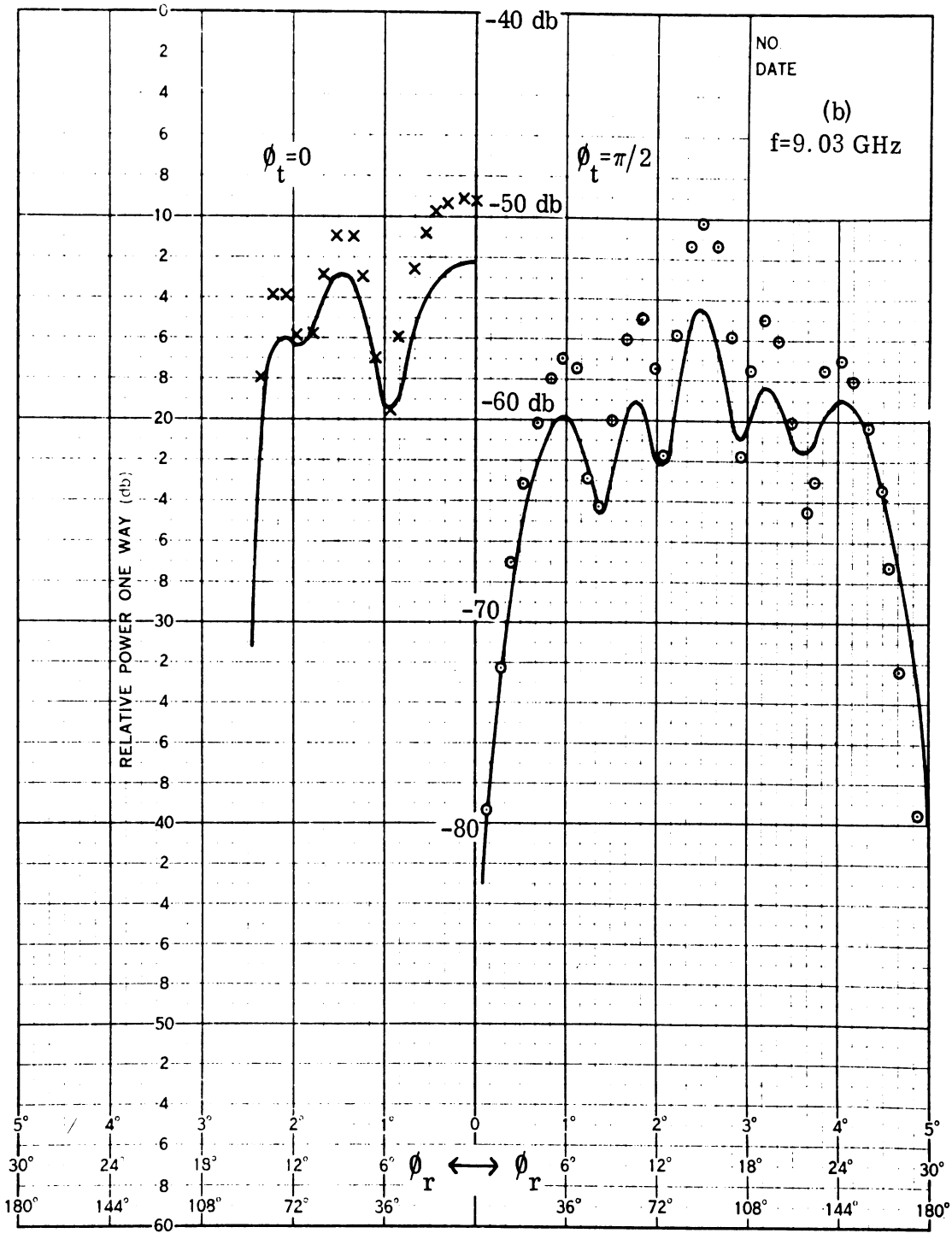

FIG. 4-25b: COMPARISON OF EXPERIMENT AND THEORY E-SECTORAL HORN. Horn data same as in Fig. 4-25a.

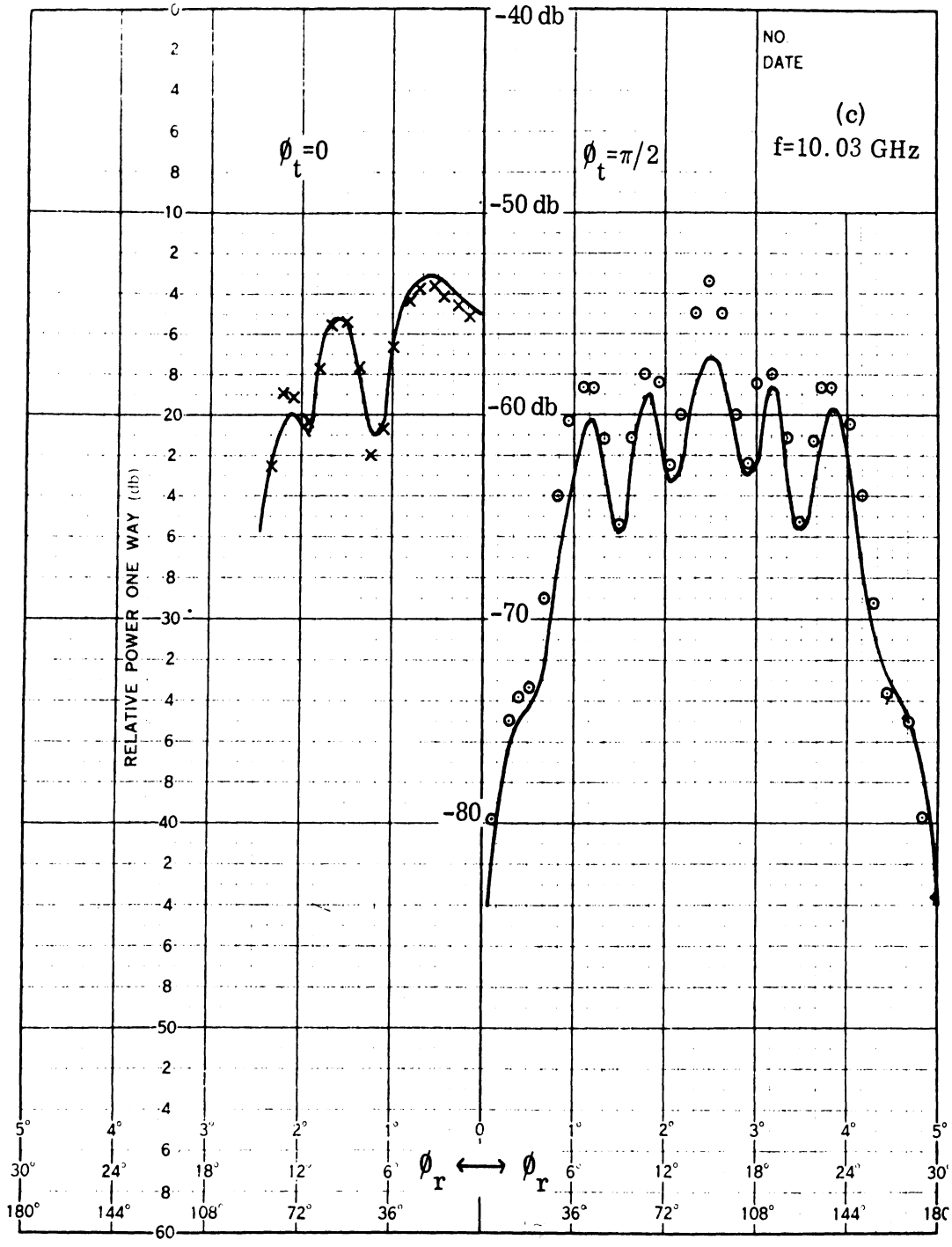

FIG. 4-25c: COMPARISON OF EXPERIMENT AND THEORY E-SECTORAL HORN
Horn data same as in Fig. 4-25a.

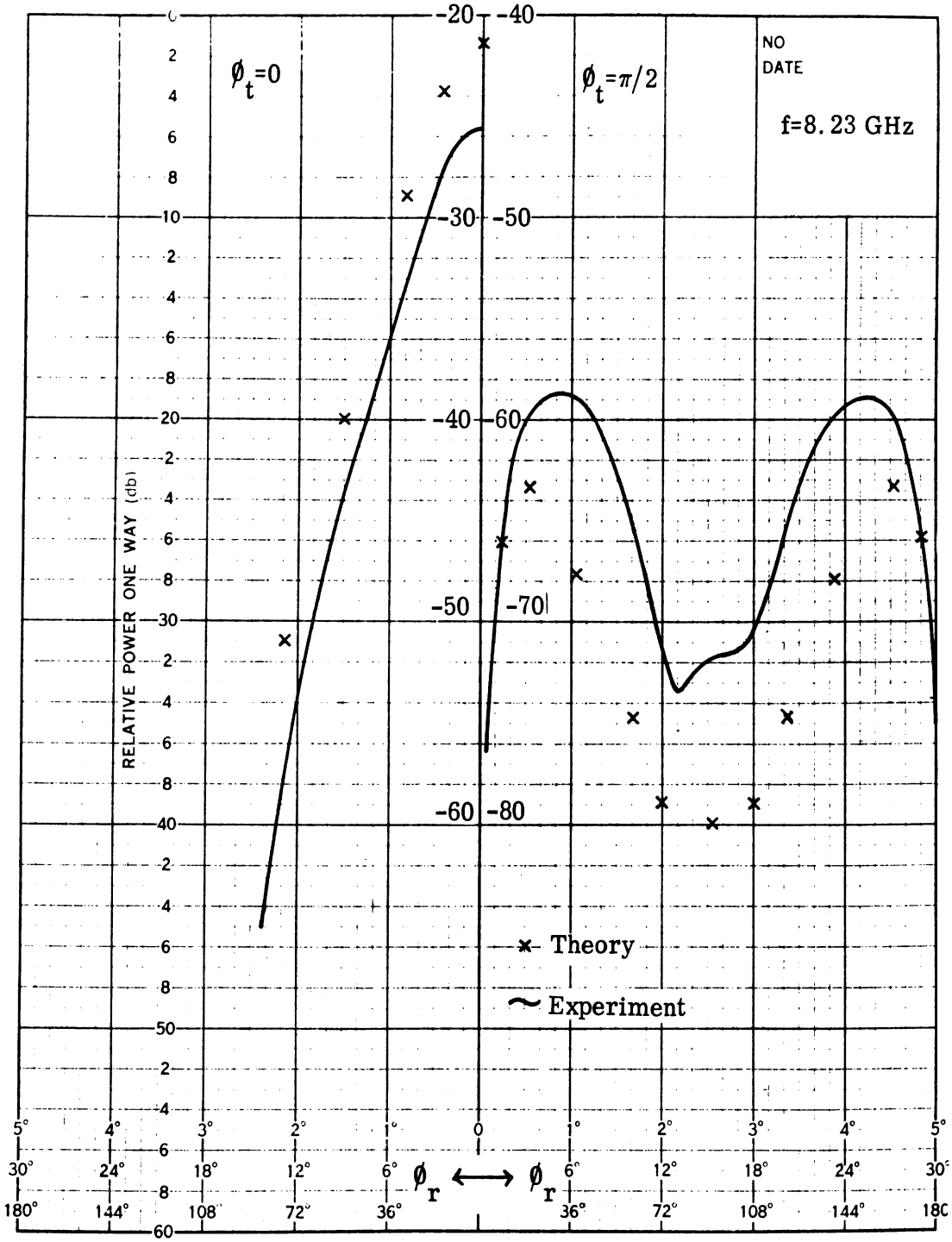

FIG. 4-26: COMPARISON OF THEORY AND EXPERIMENT.
H-SECTORAL HORN

It has been learned that, for the purpose of computation, further refinements, particularly with respect to the approximations used in the analysis, must be made. The formulas in the present form yields satisfactory results, if one picks two or three modes. Shown in the Fig. 4-26 is the comparison between experimental and theoretical result. The complete results of numerical calculations are contained in the separate memorandum by Kwon (1965).

4.5.4 Pyramidal Horn Coupling

A pair of pyramidal horns mounted in a ground plane was also tested at the same center-to-center spacing of 36.6 cm. There horns were fed from X-band waveguide (1.01 x 2.28 cm), which was flared out over a length of 10.1 cm to an opening of 4.77 x 6.04 cm. The horns have a gain of about 12 db at 9 GHz. Figure 4-27 shows both the E- and H-plane coupling curves. The coupling pattern for the E-plane case is more directional than for the conical horns because there is more tapering of the E-field in the pyramidal horn aperture. It is to be noted that this more selective coupling occurs even though the conical horns have a much larger aperture, and correspondingly, much higher gain. Due to the lower level of the sidelobes in the ground plane for the pyramidal horns, an antenna designer might want to consider using a pyramidal horn instead of conical to achieve lower coupling levels between adjacent horns. The general level of coupling observed for pyramidal horns is believed to be dependable. However, there was some scatter from the other objects in the anchoic chamber which entered into the observed coupling values, particularly as nulls were approached.

4.6 Yagi-Uda Monopole Array

The medium gain antennas discussed so far in this report have not had the main beam along the ground plane. The Yagi-Uda monopole array was chosen for study since it has its main beam along the ground plane, and polarization

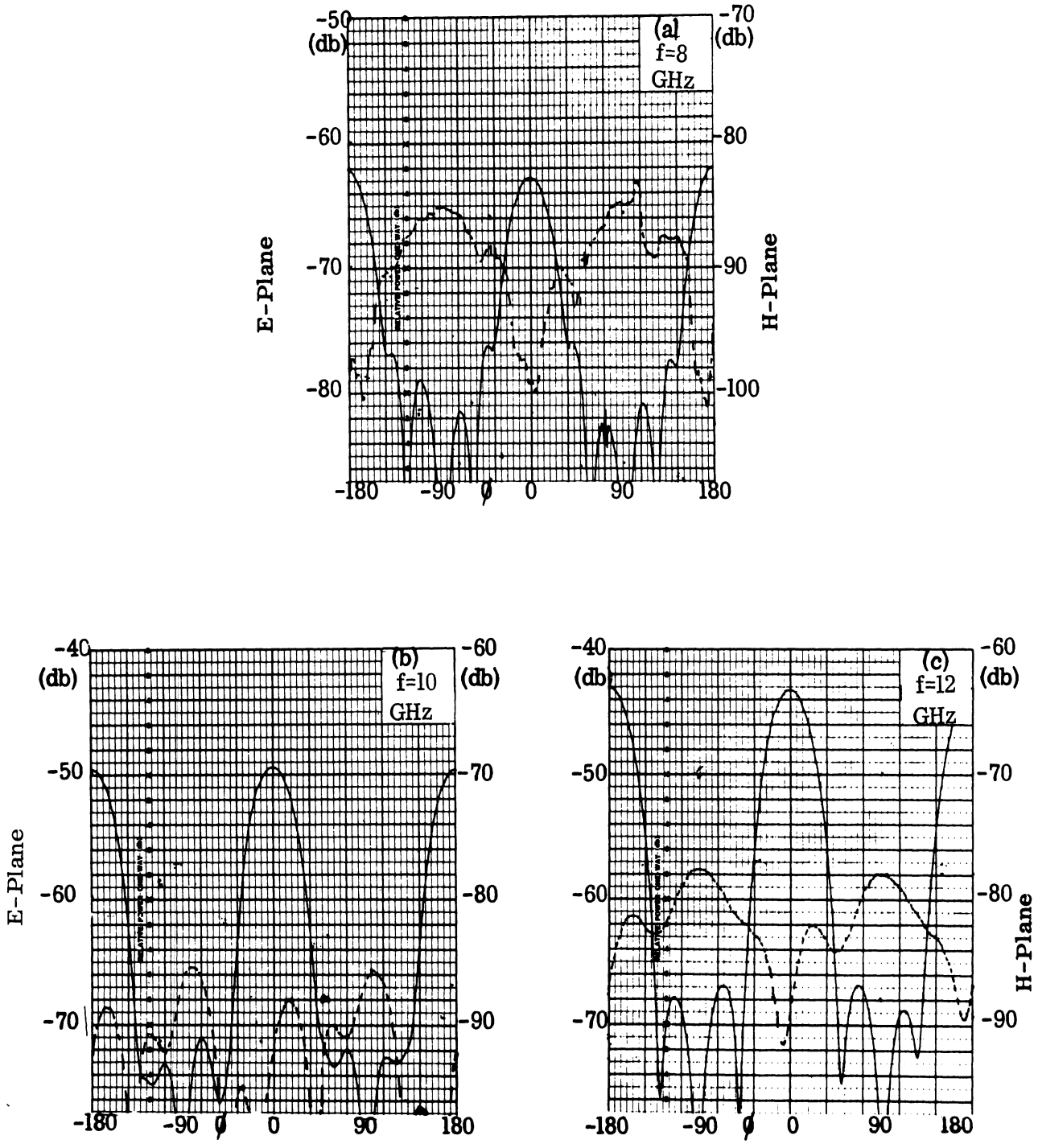

FIG. 4-27: PYRAMIDAL HORN COUPLING PATTERNS. (—)E-PLANE, (--) H-PLANE.

vertical to it. It also allows an investigation of the Fresnel zone region in the region of the main beam as well as the sidelobes.

An eight-element array was chosen, plus a taper section of two elements (Fig. 4-28). The reflector length was chosen to give maximum front-to-back ratio. The antenna was designed to give maximum gain in accordance with known design criteria (Jasik, 1961, Ehrenspeck and Poehler, 1958). Further adjustment of the element lengths gave little improvement, indicating the accuracy of the design procedures. A monopole probe was used as a receiving antenna with mounts as indicated in Fig. 4-28, allowing sampling of the field at a broad range of spacings at 30^{o} intervals. The measured gain of the yagi was 12 db with a front-to-back ratio of 19.5 db.

In Fig. 4-29, the results are plotted in actual distance, R_o, from the center of the circular plate housing the antenna. The center of the antenna was roughly at the third director from the feed. In particular, the curves for 0^{o} and 30^{o}, both of which are on the main beam, show very smooth behavior, and adhere to the 6 db/octave line, this indicates the phase center of the main beam is near the center of the antenna. It was anticipated that the main beam coupling would fall away from the 6 db/octave line at close spacings - an effect observed with large aperture antennas. Evidently this effect is not encountered to any significant degree with gains of 12 db or less.

In the sidelobes 60^{o} and 90^{o}, the coupling falls below the 6 db/octave line, and with the backlobes, rises well above. If a new phase center is defined for each angle of approach, the curves are more regular (Fig. 4-39). The phase center here is defined by taking the distance from the far hole to that point which gives coupling 12 db higher, as being 3/4 of the way to the phase center. This procedure may imply that the data is being forced to fit pre-conceived notions, but data, so presented, does appear to be more regular and reasonable.

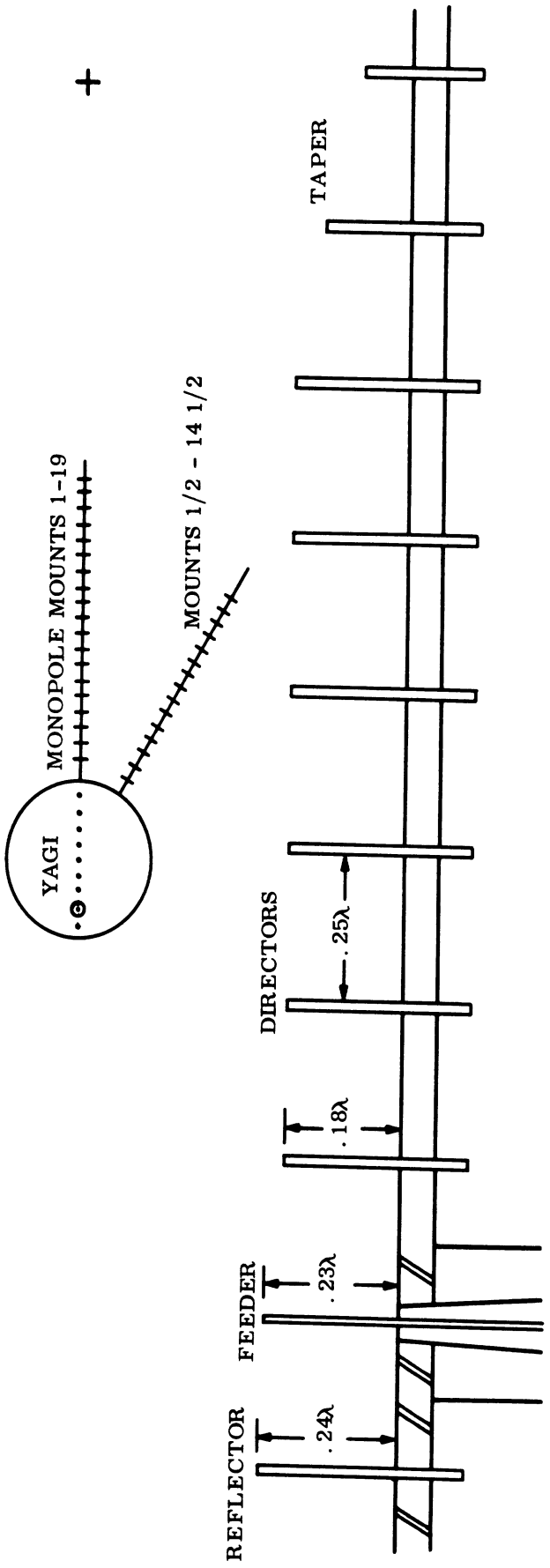

FIG. 4-28: YAGI-UDA MONOPOLE ARRAY

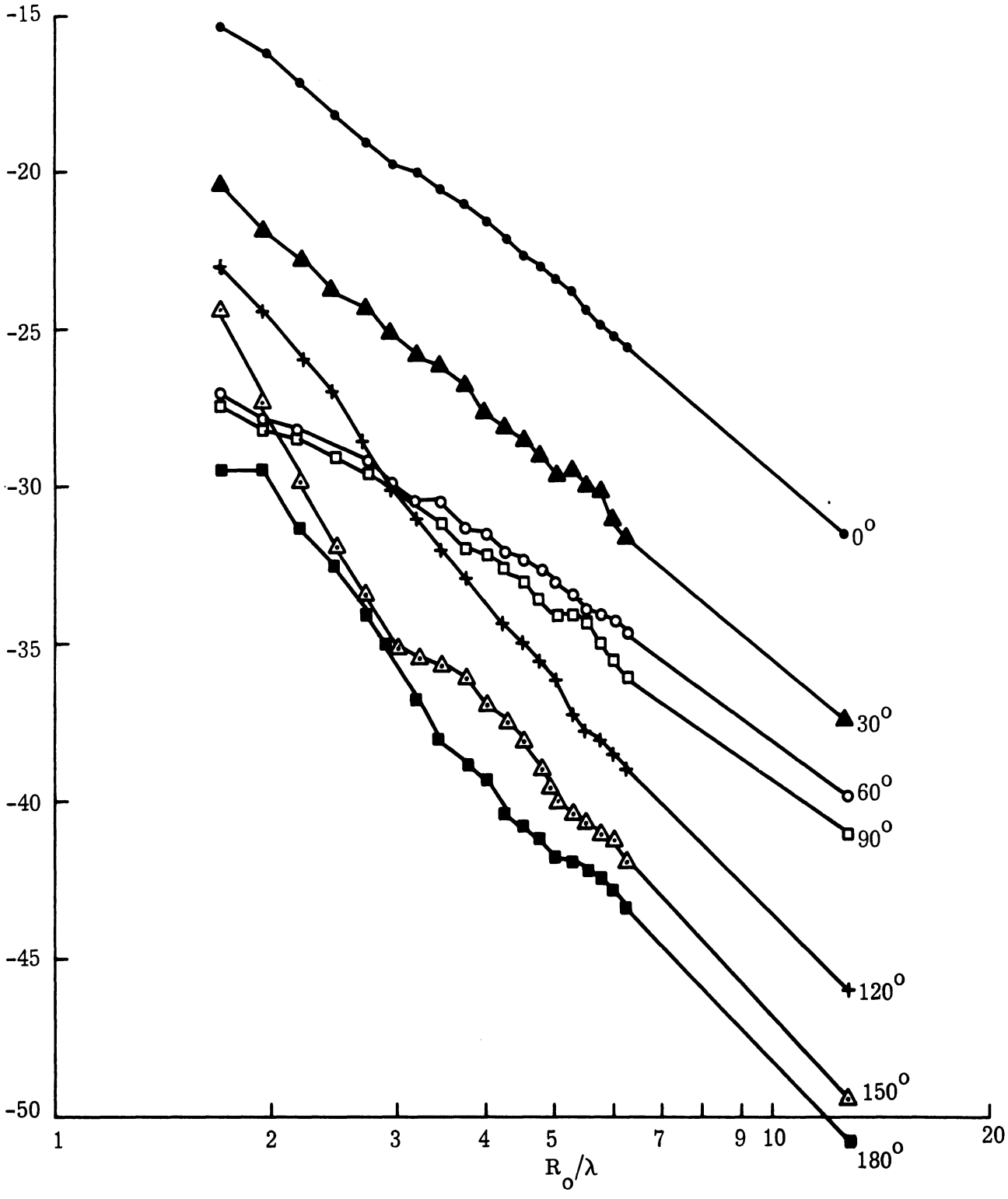

FIG. 4-29: COUPLING BETWEEN A YAGI-UDA ARRAY AND A MONOPOLE VS. SPACING FOR DIFFERENT ORIENTATIONS

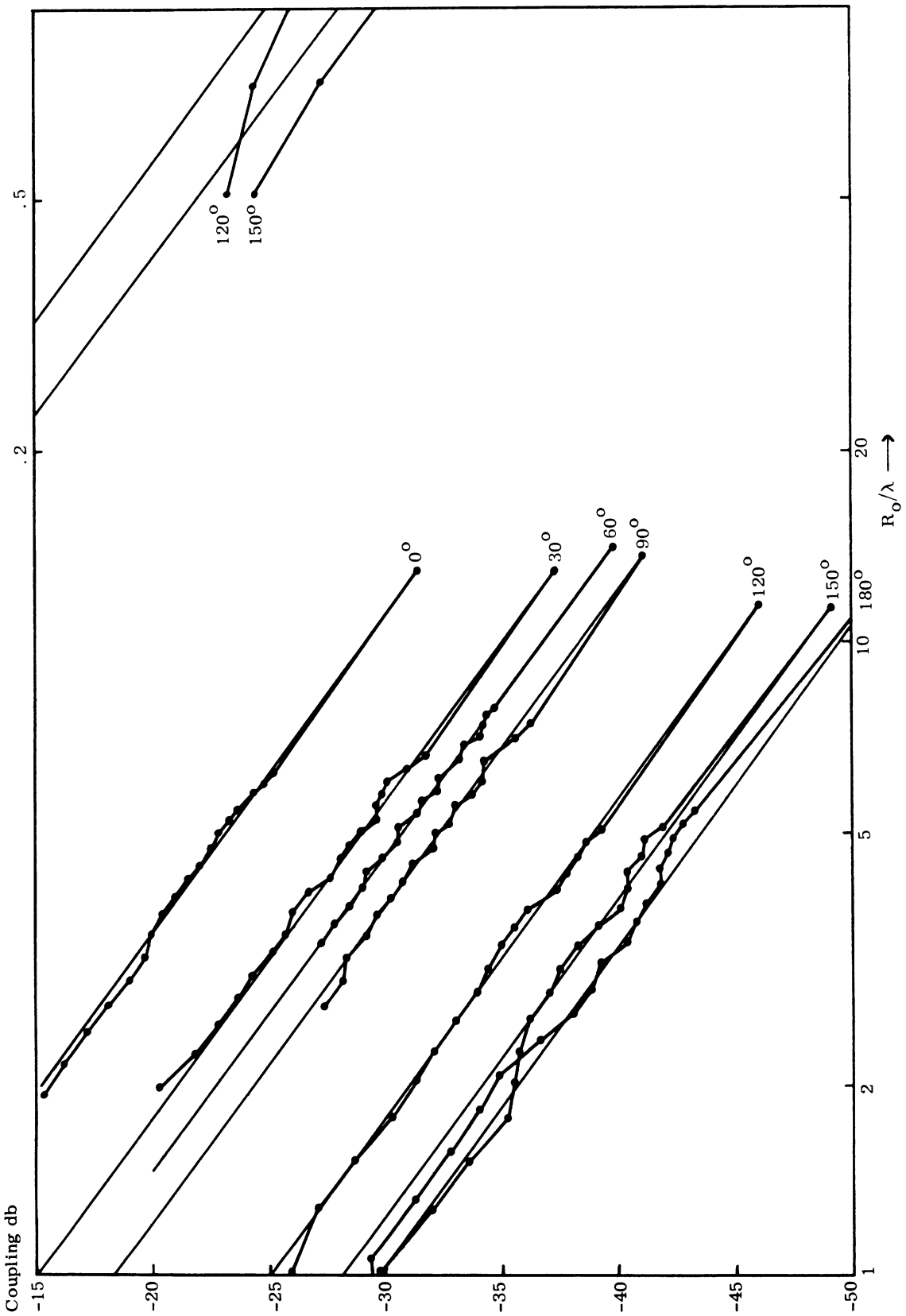

FIG. 4-30: COUPLING BETWEEN A YAGI-UDA ARRAY AND A MONOPOLE VS. SPACING FOR DIFFERENT ORIENTATIONS

Another representation which is meaningful is shown in Fig. 4-31. Here the lines of constant coupling amplitude are plotted. This shows the concentration of power along the elements, and the end-fire radiation. Some of the lesser deviations from regularity can be explained by reflections, but the gross effects are greater than experimental error. Repeatability was within 1/2 db, and few of the rapid deviations were greater than this.

4.7 Coupling of Slot and Horn Type Antennas to Higher Order Modes

A study of coupling, in which the individual modes present in the apertures are considered, complements other coupling studies discussed earlier in this report. In considering the influence of one system upon another it is possible that some of the modes actually produced through the incidence of a wave upon an antenna aperture are not present in the interior of the receiving system. These higher order modes can be excited at frequencies below the frequency level necessary for propagation in various elements of a system. Changing the frequency of operation can change the prevalence and strength of various modes. In waveguide systems some modes can be created that will not be transmitted if the operating frequency of the system is within the usual prescribed limits with respect to the cutoff frequency of the waveguide used. Usually the operating frequency is so chosen that only the principal or dominant mode, such as the TE_{10} mode in a rectangular waveguide, can exist. However, if a transmitting system is operating at frequencies well above the nominal frequency of a receiving system, which is subject to interference, signals of a higher order mode can be accepted. In discussing frequency and harmonic frequencies as related to systems which can interfere with each other it is appropriate also to consider the modal aspects of the interference. In analyzing and computing the level of modal coupling and later measuring modal coupling the values obtained may turn out to be astoundingly high. However, such modal coupling values must always be

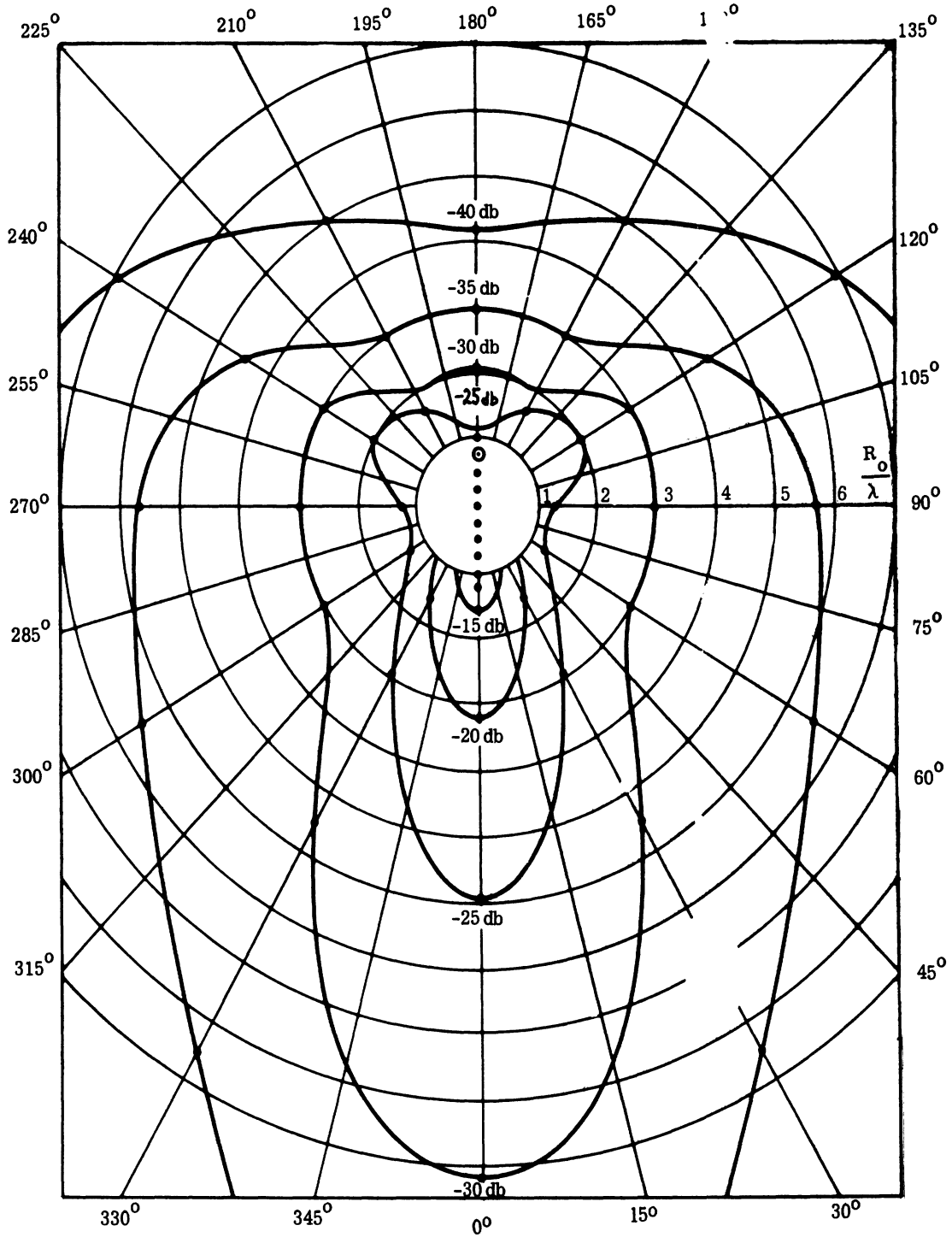

FIG. 4-31: COUPLING BETWEEN A YAGI-UDA ARRAY AND A MONOPOLE: CONSTANT COUPLING CONTOUR LINES

considered with the total filtering effects of each system brought to bear on the entire interference problem.

In considering the applicability of filtering to eliminate higher order modes it is therefore important to consider the design features of each system, particularly those of the receiving system. Interference caused by coupling determined on a modal basis can be very pronounced when the receiving system is designed to operate with more than one mode. Special attention must be given where one of the systems is of the dual or multi-mode variety. An example of higher order mode filtering is shown in Fig. 4-32; some of the modes whose cutoff frequency is influenced by the waveguide height may be eliminated through the reduction in height.

4.8 Effects of Harmonics on Coupling

4.8.1 Harmonic Content of Signal Sources

The harmonic content of signal sources is of great importance in the evaluation of interference caused by the coupling of one system to another. The presence of substantial harmonic content is a given transmitting system operating at a design frequency below that of a second system which is sufficiently coupled may result in a high interference level in the second system. The second system designed for a higher frequency than the fundamental frequency of the offending system does not have the advantage of frequency filtering under the critical condition where, say, the third harmonic of the offending system coincides with the fundamental of the receiving system. It is in such instances as this that the harmonic content of the signal source becomes a major factor in interference. An example would be the third harmonic of an S-band transmitting system interfering with an X-band receiving system.

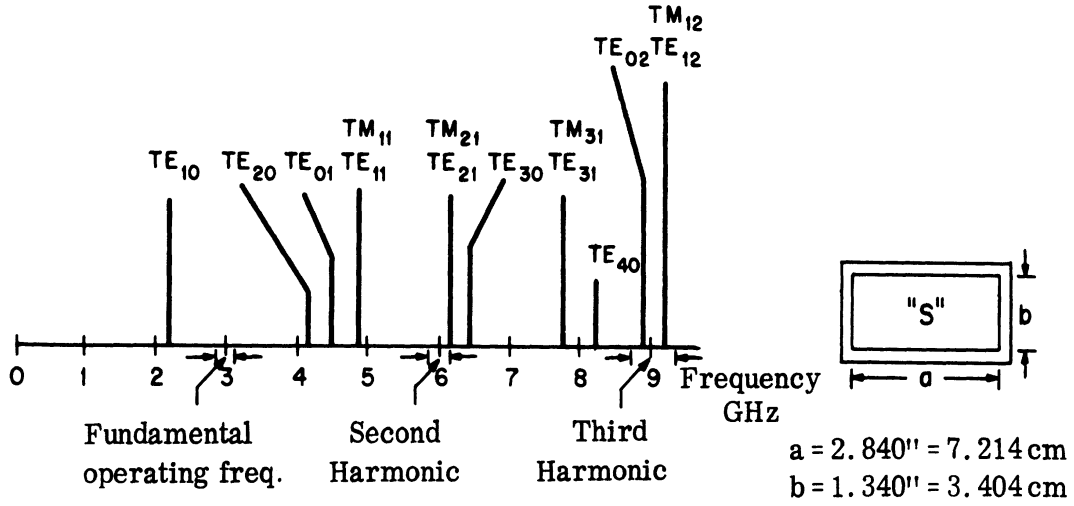

(a)

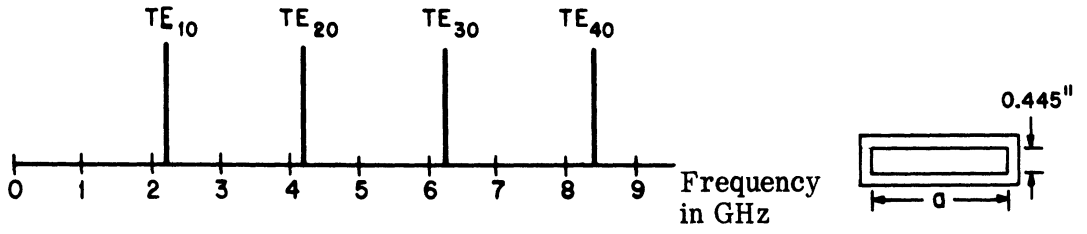

(b)

FIG. 4-32: THE EFFECT OF WAVE GUIDE SIZE ON MODE FILTERING. DATA BASED UPON MET (1959).

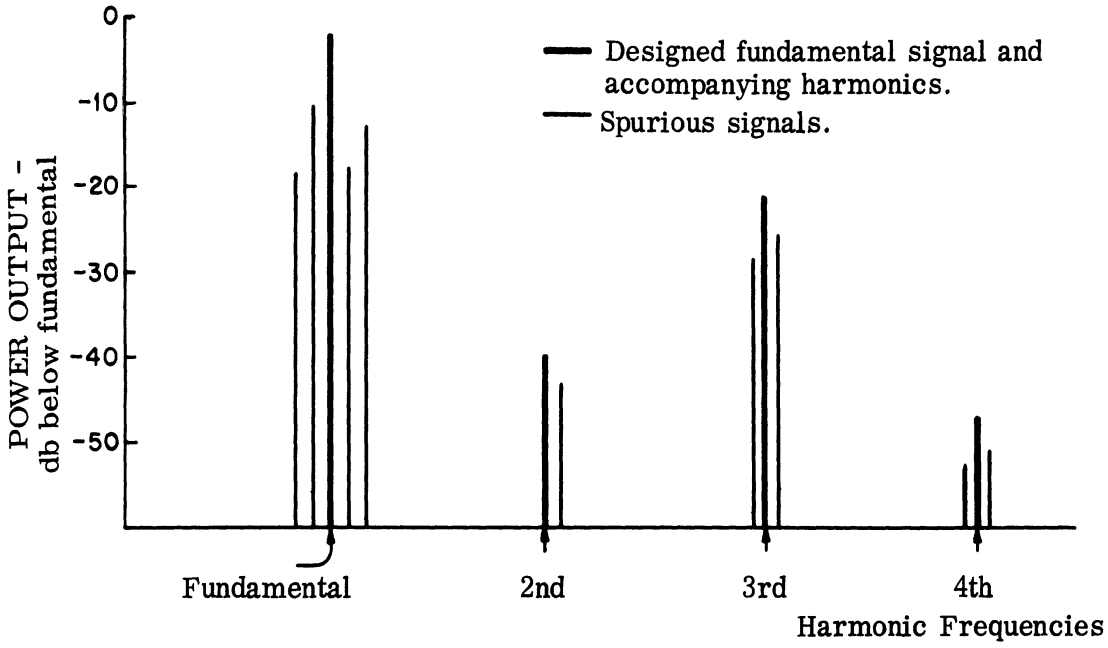

FIG. 4-33a: TYPICAL POWER - FREQUENCY OF MAGNETRON
Data based upon Matthaei (1964)

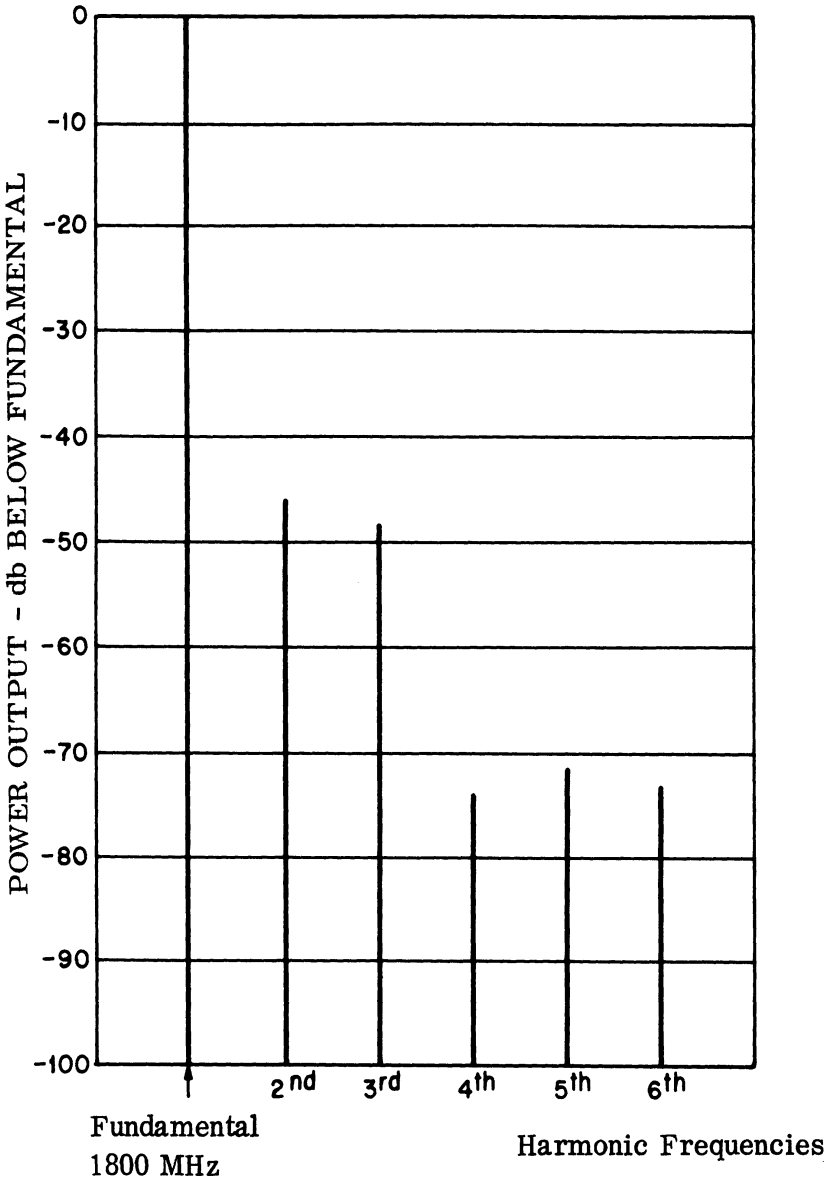

FIG. 4-33b: TYPICAL RELATIVE POWER - FREQUENCY SPECTRUM OF A KLYSTRON
Matthaei (1964)

The harmonic content of signal sources varies among the different types of signal sources. Figure 4-33 indicates the harmonic content of a number of frequently used signal sources. This information is submitted only as being reasonably typical. In this report, the ultimate influence of harmonic content is not incorporated in any interference problem. However, it is easy enough to use such information: it is convenient to speak of a given harmonic as being so many db below the power level of the central operating frequency of the source. Harmonic contents will then be considered at power levels which are from 10 - 20 db below the incident power levels at the central operation frequency.

4.8.2 Spiral Antenna Data Taken at Harmonic Frequencies

Data were taken on both square and circular spirals at harmonics of the normal operating frequencies. All the measurements were taken in an anechoic chamber with the spirals mounted in a 12' x 12' ground plane. Coupling patterns in the ground plane were taken for both the square spiral 1L and the circular spiral A, at frequencies between 8 - 10 GHz. These patterns are not included here but will be described briefly.

The coupling patterns for the circular spiral have 3– 5 irregularly spaced maxima. The ratio of absolute maximum to absolute minimum coupling varies from 15 - 25 db.

The coupling patterns for the square spiral have 5 - 7 irregularly spaced maxima. The ratio of absolute maximum to absolute minimum is greater than for the circular spiral since there are either one, or three, very deep nulls in many of the patterns.

4.9 Systems Aspects of Coupling

In considering the coupling effect due to higher order modes in the system interference problem, attention must be given ultimately to the filtering action of the detection system used. As an example of higher order mode coupling, consider an X-band system transmitting and an S-band system receiving. The presence of higher modes in the receiving system is not dependent on their existence in the transmitting system. Fortunately, in many cases a substantial amount of filtering is provided by the detection system. This means that a given receiving system may be much more sensitive to the desired mode, than to any of the higher order modes. The filtering action of the detection system can be of two kinds; 1) the associated frequency sensitive circuits of the detection system can afford frequency filtering, or 2) the placement of detection probes can result in modal filtering. The frequency filtering action of a detection system of a receiver would be a factor in the overall frequency filtering formula for the entire receiving system. If the receiving system had for example, 75 db filtering against an undesired signal at a specific frequency perhaps 10 db of this would be due to the frequency filtering action of the detection system. If the local oscillator of a receiver and its function is included is the ultimate detection process, then an additional factor which must be considered in the presence of harmonic content in the local oscillator signal. The presence of these harmonics which may mix with undesired harmonics from an offending transmitter may very well result in a substantial decrease in the frequency filtering action of a given receiving system. In the further consideration of filtering due to detection systems the sensitivity of the detection system to various types of modulation is important. The sensitivity of a detection system for one type of modulation as compared with another type of modulation represents a substantial item for study. The modulation aspects and the differences in filtering action due to sensitivity or lack of sensitivity to various types of offending modulation are not covered in this report.

The earlier discussion has shown that various higher order modes may exist somewhere between the radiator of a transmission system and the signal display or output of the receiving system. It is expected that quite often these modes will not exist at the output port of the receiving system. This may be due to the modal filtering which occurs due to the design of the receiving system elements including of course the cut off characteristic of any waveguide used. Detection systems and directional coupler devices are really modal filters and modal converters.

All of the energy occurring at harmonic frequencies should be eliminated or absorbed in some manner before it become part of the receiver output. Mode separating devices with absorbers for harmonic energy would then become justified. Studies of this type have not been undertaken in this project, but might very well be worthwhile in the overall interference problem.

The two port network representation for two systems where one interferes with another is a useful one to consider. Whether or not higher modes are available from the port which constitutes the output of the receiving system, depends upon the details of the receiving network. Somewhere in this network, perhaps in the design of directional couplers, detectors or modal fitters, provisions can be made so that an unwanted mode can be eliminated.

V

THE COUPLING BETWEEN TWO ANTENNAS DUE TO THE PRESENCE OF A SCATTERER

The concern herein will be with flush mounted antennas on a common ground plane, and the effect of a scattering object upon the coupling between the two antennas. When the two antennas are loosely coupled (i.e. the direct coupling is negligible) the presence of a scattering object may or may not produce significant coupling depending upon the parameters involved. It is the purpose of this section to determine the coupling due to the presence of a scatterer, with special emphasis on scatterers that would be of concern for aerospace vehicles.

5.1 Direct Coupling

First the expressions for the direct coupling (no scatterer present) between two flush mounted antennas on a common ground plane, will be briefly considered. The coupling is given by Eq. (2.5) for $q_t = q_r = 1$ by assumption:

$$C(R_o, \phi_t, \phi_r) = C_o(R_o)\, D_r(\phi_r)\, D_t(\phi_t) \tag{5.1}$$

where the directivity functions $D(\phi)$ are given by

$$D(\phi) = \frac{\left|\bar{E}\left(\frac{\pi}{2}, \phi\right)\right|^2}{\frac{1}{2\pi}\int_0^{2\pi}\int_0^{\pi/2} \left|\bar{E}(\theta, \phi)\right|^2 \sin\theta \, d\theta \, d\phi}$$

as in equation (2.6).

R_o represents the distance between the centers of the two antennas, and ϕ_t and ϕ_r denote the orientation of the antennas with respect to the line joining the centers of the two antennas. For convenience the angle ϕ will be the angle between the E plane of the antenna and the line joining the centers. (See Figure 5-1.)

5.2 Coupling Produced by a Scatterer in Space

Restrictions (some of which will be later removed) are now placed on the scatterer, transmitter and receiver geometry. Namely, the scatterer must be in the far field of both antennas, and in addition the receiving antenna must be in the far field of the scatterer (treated as a reradiating object). If R_r and R_t are the distances from the transmitting antenna and receiving antenna, respectively, to the center of the scatter, then not only must $R_r \gg \lambda$ and $R_t \gg \lambda$, but if L_r and L_t are the maximum cross sectional dimensions, respectively, of the aperture of the transmitting and receiving antennas, then

$$\frac{2L_t^2}{R_t\lambda} < 1 \text{ , and } \frac{2L_r^2}{R_r\lambda} < 1$$

must hold. This is the usual condition that the scattering object be in the far field (see Section 3.5). In addition if L_s is the maximum cross-sectional dimension of the scatterer as observed by the receiving antenna, then

$$\frac{2L_s^2}{R_r\lambda} < 1$$

should also hold. However, this latter condition limiting the size of the scattering object may be removed under certain conditions, and certain large scatterers may be treated when the receiving antenna is in the near field. If

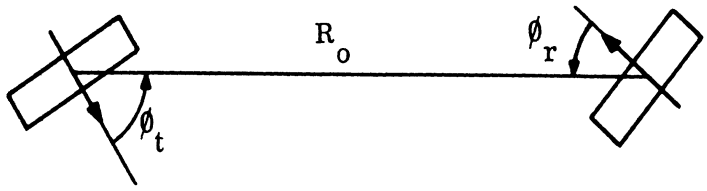

FIG. 5-1: SLOT GEOMETRY

the dominant scattered return from the large object comes from one or more finite scattering centers, then the scattered field can be treated as arising from these scattering centers. In this case R_r and R_t are the distances to the scattering center. As an example, the dominant return for high frequency scattering from a sphere (wavelength much less than the radius of the sphere) arises from a specular point (a single scattering center). Thus, the scattered field is treated as arising from a small region around the specular point, and the restriction that $2L_s^2/(R_r\lambda) < 1$, where L_s is the diameter of the sphere, is not required. On the other hand for a flat disc of diameter L_s this restriction is required for the case of specular return since the scattered field arises from the whole surface of the disc. However, when the scattered return from the disc is not specular, but arises from the neighborhood of two points, one on the near edge and the other from the far edge, there are two distinct scattering centers. The restriction $2L_s^2/(R_r\lambda) < 1$ may be removed, but the return must be treated as arising from two distinct scattering centers.

Summing up, when the whole scattering surface gives rise to a return at the receiving antenna the restriction $2L_s^2/(R_r\lambda) < 1$ must be used. When the scattered return arises from one or more finite scattering centers, then this restriction may be removed. Thus with this preamble one can employ the concepts of radar cross-section and scattering matrices to obtain the coupling.

Let the far field of the transmitting antenna be given by

$$\bar{E}_t = \frac{e^{-jkR_t}}{R_t}\,\bar{e}_t(\theta_t, \phi_t) \tag{5.3}$$

where (R_t, θ_t, ϕ_t) are spherical polar coordinates with the origin at the transmitting antenna. The azimuth angle ϕ_t is measured from the intersection of the

E field vector of the antenna with the ground plane. (See Figure 5-2). The directivity function is given by

$$\bar{D}_t(\theta_t, \phi_t) = \frac{\left|\bar{e}_t(\theta_t, \phi_t)\right|^2}{\frac{1}{2\pi}\int_0^{2\pi}\int_0^{\pi/2}\left|\bar{e}_t(\theta_t, \phi_t)\right|^2 \sin\theta_t \, d\theta_t \, d\phi_t} \tag{5.4}$$

and the power per unit area incident at a point S designated by (R_t, γ_t, ψ_t) is

$$P = \frac{W_t}{2\pi R_t^2} D_t(\gamma_t, \psi_t) \tag{5.5}$$

The vector $\bar{e}_t(\gamma_t, \psi_c)$ can be written in the form

$$\bar{e}_t(\gamma_t, \psi_t) = e_t(\gamma_t, \psi_t)\,\hat{p}_t \tag{5.6}$$

where $\hat{p}_t$ is a complex vector such that

$$(\hat{p}_t \cdot \hat{p}_t^{\,*}) = 1 \tag{5.7}$$

where $\hat{p}_t^{\,*}$ is the complex conjugate of $\hat{p}_t$. The vector $\hat{p}_t$ is a function of γ_t and ψ_t and has the form $\hat{p}_t = a_t\,\hat{\gamma}_t + b_t\,\hat{\psi}_t$ where $\hat{\gamma}_t$ and $\hat{\psi}_t$ are unit vectors in the spherical polar coordinates. From (5.7), we have

$$|a_t|^2 + |b_t|^2 = 1 \tag{5.8}$$

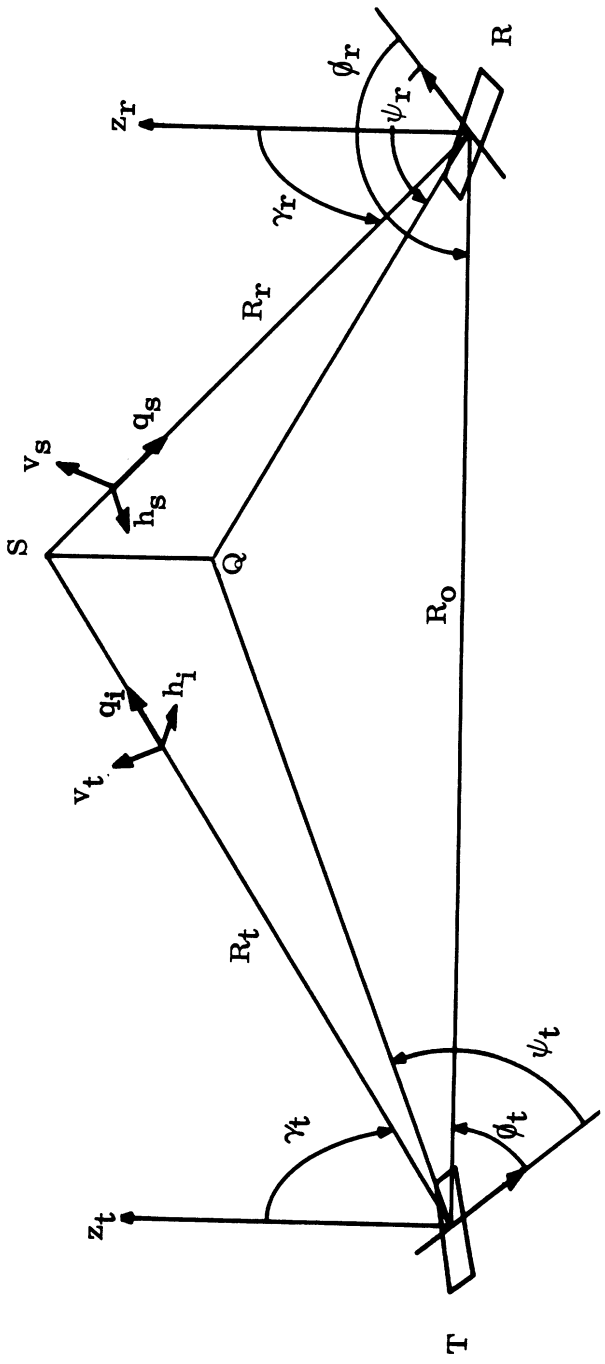

FIG. 5-2: TRANSMITTING AND RECEIVING ANTENNA CONFIGURATIONS

The vector $\hat{p}_t$ can be written in a more specific form, depending upon polarization as follows:

Linear polarization,

$$\hat{p}_t = \cos \beta_t \, \hat{\gamma}_t + \sin \beta_t \, \hat{\psi}_t \, . \tag{5.9}$$

Left-hand circular polarization,

$$\hat{p}_t = \frac{1}{\sqrt{2}} (\hat{\gamma}_t - j\hat{\psi}_t) \, . \tag{5.10}$$

Right-hand circular polarization,

$$p_t = \frac{1}{\sqrt{2}} (\hat{\gamma}_t + j\hat{\psi}_t) \, . \tag{5.11}$$

For the receiving antenna there are similar expressions. However, the coordinate system (R_r, γ_r, ψ_r) for the receiving antenna is centered at the receiving antenna and oriented with the E plane of the receiving antenna as is shown in Figure 5-2.

For convenience some auxiliary unit vectors are now introduced; they are indicated in Fig. 5-2. Define $\hat{q}_i$ to be the unit vector directed along the line from the transmitter to scattering center; $\hat{h}_i$ is defined as parallel to the ground plane and perpendicular to $\hat{q}_i$; $\hat{v}_i$ is taken to point away from the ground plane and be perpendicular to $\hat{q}_i$ and $\hat{h}_i$, so that the set $(\hat{q}_i, \hat{v}_i, \hat{h}_i)$ forms a right-handed triad. Let $\hat{q}_s$ be the unit vector directed along the line between scattering center and receiving antenna; $\hat{h}_s$ and $\hat{v}_s$ are defined as $\hat{h}_i$ and $\hat{v}_i$ above, so that $(\hat{q}_s, \hat{v}_s, \hat{h}_s)$ also forms a triad. Thus the following relations hold:

$$\hat{v}_i = -\hat{\gamma}_t,\ \hat{h}_i = -\hat{\psi}_t,\ \hat{v}_s = -\hat{\gamma}_r,\ \hat{h}_s = \hat{\psi}_r \tag{5.12}$$

and

$$\hat{p}_t = -a_t \hat{v}_i - b_t \hat{h}_i \tag{5.13}$$

With this, the concept of the scattering matrix, or dyadic, may be used. The scattered radiation in direction $\hat{q}_s$ produced by an incident field $\bar{E}_i(\hat{q}_i)$ (propagating in direction $\hat{q}_i$) is given by

$$\bar{E}_s(\hat{q}_s) = \bar{\bar{S}}(\hat{q}_s, \hat{q}_i) \cdot \bar{E}_i(\hat{q}_i) \tag{5.14}$$

where $\bar{\bar{S}}$ is the scattering dyadic, which can be written in the form

$$\bar{\bar{S}} = \begin{pmatrix} \hat{v}_s \hat{v}_i S_{vv} + \hat{v}_s \hat{h}_i S_{vh} \\ + \hat{h}_s \hat{v}_i S_{hv} + \hat{h}_s \hat{h}_i S_{hh} \end{pmatrix}. \tag{5.15}$$

Here it should be noted that $\bar{E}_i(\hat{q}_i)$ is the transmitted electric field to be evaluated at the scattering center; also, the dyadic $\bar{\bar{S}}$ is a function of the distance R_r from the scattering center to the receiver. The dyadic corresponds to the more common term "scattering matrix" in the obvious way, i.e. the corresponding matrix is

$$[S] = \begin{bmatrix} S_{vv} & S_{vh} \\ S_{hv} & S_{vv} \end{bmatrix} \tag{5.15a}$$

If the incident field is horizontally polarized, $\bar{E}_i(\hat{q}_i) = \hat{h}_i E_o$, then the scattered field is given by

$$\bar{E}_s(\hat{q}_s) = (S_{hh}\hat{h}_s + S_{vh}\hat{v}_s)E_o \tag{5.16}$$

and if the incident field is vertically polarized, $\bar{E}_i(\hat{q}_i) = \hat{v}_i E_o$, and

$$\bar{E}_s(\hat{q}_s) = (S_{hv}\hat{h}_s + S_{vv}\hat{v}_s)E_o . \tag{5.17}$$

The coefficients S_{vh} and S_{hv} of the scattering matrix represent cross-polarization effects. If the scatterer produces no cross-polarization then $S_{vh} = S_{hv} = 0$.

Following the treatment for the radiation patterns of the transmitting antenna, the radiation pattern of the receiving antenna viewed as a transmitter is represented in the form

$$\bar{E}_r = \frac{e^{-jkR_r}}{R_r} e_r(\gamma_r, \psi_r)\hat{p}_r \tag{5.18}$$

where

$$\hat{p}_r \cdot \hat{p}_r^* = 1.$$

From equations (5.3), (5.6) and (5.7) for the field incident on the receiving antenna, where $\bar{E}_i(\hat{q}_i) = \bar{E}_t(R_t)$, one obtains

$$\bar{E}_s(\hat{q}_s) = \frac{e^{-jkR_t}}{R_t} e_t(\gamma_t, \psi_t)\bar{\bar{S}}(\hat{q}_s, \hat{q}_i)\cdot\hat{p}_t . \tag{5.19}$$

The component of this which is coupled into the receiving antenna is $\bar{E}_s(\hat{q}_s)\cdot\hat{p}_r$; hence the effective power per unit area incident upon the receiving antenna is

$$\sqrt{\frac{\epsilon}{\mu}}\left|\hat{p}_r \cdot \bar{E}_s\right|^2 = \sqrt{\frac{\epsilon}{\mu}}\left|e_t(\gamma_t, \psi_t)\right|^2 \left|\hat{p}_r \cdot \bar{\bar{S}} \cdot \hat{p}_t\right|^2 . \tag{5.20}$$

The coupling due to the scatterer is thus given by the relation

$$C_s = C_o(R_t)\, D_t(\gamma_t, \psi_t)\, D_r(\gamma_r, \psi_r) \left|\hat{p}_r \cdot \bar{\bar{S}} \cdot \hat{p}_t\right|^2 . \tag{5.21}$$

The coupling is expressed in terms of the function of the two antennas, and the scattering matrix. Reduced expressions for $\left|\hat{p}_r \cdot \bar{\bar{S}}(\hat{q}_s, \hat{q}_i) \cdot \hat{p}_t\right|^2$ are derived below from the special cases of linear and circular polarization.

When the far field radiation pattern of the transmitting antenna is linearly polarized $\hat{p}_t$ is a real unit vector of the form

$$\hat{p}_t = \cos\beta_t \hat{\gamma}_t + \sin\beta_t \hat{\psi}_t \tag{5.22}$$

or

$$\hat{p}_t = -\cos\beta_t \hat{v}_i - \sin\beta_t \hat{h}_i . \tag{5.23}$$

Similarly when the receiving antenna pattern is linearly polarized, the following relation holds

$$\hat{p}_r = \cos\beta_r \hat{\gamma}_r + \sin\beta_r \hat{\psi}_r \tag{5.24}$$

or

$$\hat{p}_r = -\cos\beta_r \hat{v}_s + \sin\beta_r \hat{h}_s . \tag{5.25}$$

This gives, on using relation (5.15, or (5.16) and (5.17), the following expression:

$$\left|\hat{p}_r \cdot \bar{\bar{S}}(\hat{q}_s, \hat{q}_i) \cdot \hat{p}_t\right|^2 = \left|\cos\beta_r (\cos\beta_t S_{vv} - \sin\beta_t S_{hv})\right.$$

$$\left. - \sin\beta_r (\sin\beta_t S_{hh} - \cos\beta_t S_{vh})\right|^2 . \qquad (5.26)$$

For circular polarization the far field of the transmitting antenna has the form

$$\bar{E}_t = \frac{e^{-jkR_t}}{R_t} e_t(\gamma_t, \psi_t) \hat{p}_t \qquad (5.27)$$

with

$$\hat{p}_t = \frac{1}{\sqrt{2}} (\hat{\gamma}_t \pm j\hat{\psi}_t) = -\frac{1}{\sqrt{2}} (\hat{v}_i \pm j\hat{h}_i) \qquad (5.28)$$

where the plus sign is for right-hand circular polarization and the negative sign for left-hand circular polarization. A similar relationship holds for a circularly polarized receiving antenna, viewed as a transmitting antenna.

$$\bar{E}_r = \frac{e^{-jkR_r}}{R_r} e_r(\gamma_r, \psi_r) \hat{p}_r \qquad (5.29)$$

with

$$\hat{p}_r = \frac{1}{\sqrt{2}} (\hat{\gamma}_r \pm j\hat{\psi}_r) = \frac{1}{\sqrt{2}} (-\hat{v}_s \pm j\hat{h}_s) \qquad (5.30)$$

When both antennas are polarized in the same sense as transmitters, then the following relation holds

$$\left|\hat{p}_r \cdot \bar{\bar{S}}(\hat{q}_s, \hat{q}_i) \cdot \hat{p}_t\right|^2 = \frac{1}{4}\left|(S_{vv} + S_{hh}) \pm j(S_{hv} - S_{vh})\right|^2 \qquad (5.31)$$

when the upper sign is for left-hand circular polarization, and the bottom sign is for right-hand polarization. When the antennas are polarized in the opposite sense

$$\left|\hat{p}_r \cdot \bar{\bar{S}}(\hat{q}_s, \hat{q}_i) \cdot \hat{p}_t\right|^2 = \frac{1}{4}\left|(S_{vv} + S_{hh}) \pm j(S_{vh} + S_{hv}\right|^2 \qquad (5.32)$$

where the upper sign is for the receiving antenna being left-hand polarized, and the lower sign for it being right-hand polarized.

The special case where $S_{vv} = -S_{hh}$ and $S_{vh} = S_{hv} = 0$ will now be investigated. Before considering the particular scattering objects which possess these properties, the effect on the coupling of these relationships between the scattering dyadic elements should be discussed. For linear polarization, from equation (5.26) one obtains

$$\left|\hat{p}_r \cdot \bar{\bar{S}}(\hat{q}_s, \hat{q}_i) \cdot \hat{p}_t\right|^2 = \left|S_{vv}\right|^2 \cos^2(\beta_r - \beta_t). \qquad (5.34)$$

When both antennas are circularly polarized in the same sense, it follows from equation (5.3) that

$$\left|\hat{p}_r \, \bar{\bar{S}}(\hat{q}_s, \hat{q}_i) \cdot \hat{p}_t\right|^2 = 0. \qquad (5.35)$$

In this case the coupling is zero.

The factor $\left|S_{vv}\right|^2 = \left|S_{hh}\right|^2$ can be related to the radar cross section of the scattering object. The bistatic radar cross section σ is given by Crispin, et al (1959, pg. 155):

$$\sigma = \lim_{R_r \to \infty} 4\pi R_r^2 \frac{\left|\bar{E}_s \cdot \hat{p}_r\right|^2}{\left|\bar{E}_i\right|^2} \tag{5.36}$$

where E_s is the scattered field produced by an incident field E. In the case where $S_{vv} = -S_{hh}$ and $S_{vh} = S_{hv} = 0$, expression (5.36) can be given by the relationship

$$\sigma = \lim_{R_r \to \infty} 4\pi R_r^2 \left|S_{vv}\right|^2 \tag{5.37}$$

The expression for the coupling due to the scattering object can be represented in the form

$$C_s = \frac{4\pi\sigma}{\lambda^2} C_o(R_r)\, C_o(R_t)\, D_t(\gamma_t, \psi_t)\, D_r(\gamma_r, \psi_r) \cos^2(\beta_r - \beta_t) \tag{5.38}$$

when both antennas are linearly polarized. When the scattering object is far enough into the far field so that the vectors $\hat{q}_i$ and $\hat{q}_s$ are anti-parallel, σ reduces to the monostatic, or backscattering, cross-section.

For back-scattering and nose-on incidence to bodies of revolution, the following relations hold among the cross-polarization terms:

$$S_{vv} = -S_{hh} \quad \text{and} \quad S_{vh} = S_{hv}$$

Explicitly, the direction of incidence $\hat{q}_i$ is parallel to the axis of revolution of the body. For back-scattering $\hat{q}_s$ is parallel to the same axis.

For large convex bodies where the radius of curvature everywhere is greater than the wavelength λ, the scattered field arises from two contributions, the specular field associated with the geometric optics approximation and the diffracted field. For very large radii of curvature the specular contribution dominates. In this case $\sigma = \pi R_1 R_2$ where R_1 and R_2 are radii of curvature of the scattering body at the specular point. For back-scattering the specular point is a point on the surface where $\hat{q}_i$ is normal to the surface.

For large flat plates with dimensions much greater than λ and the incidence vector $\hat{q}_i$ normal to the surface, the main contribution to the back-scattered field is from the specular reflection which arises from the whole surface (edge contributions are negligible).

The back-scattering cross section for a flat plate of area A is

$$\sigma = \pi \frac{A^2}{\lambda^2}$$

5.3 Scatterers on a Common Ground Plane

The problem is now restricted to the case when the scatterer is on the ground plane or else, if the object is large, to the case when a dominant scattering center lies on the ground plane. In this case $\gamma_t = \gamma_r = \pi/2$. Due to the presence of the perfectly conducting ground plane the field incident upon the scatterer has a vertical component only and the scattered field at a point on the ground plane has a vertical component only. This yields the relationship

$$\left| \hat{p}_r^* \cdot \bar{\bar{S}} (\hat{q}_s, \hat{q}_i) \cdot \hat{p}_t \right|^2 = \left| S_{vv} \right|^2 \qquad (5.39)$$

giving the expression for the coupling

$$C_s = C_o(R_t)\, D_t\left(\frac{\pi}{2}, \psi_t\right) D_r\left(\frac{\pi}{2}, \psi_r\right) \left|S_{vv}\right|^2 \tag{5.40}$$

The direct coupling between two antennas separated by a distance of R_o is given by

$$C(R_o, \phi_r, \phi_t) = C_o(R_o)\, D_t(\phi_t)\, D_r(\phi_r)\,. \tag{5.41}$$

Thus equation (5.40) can be expressed by

$$C_s = \frac{C_o(R_t)}{C_o(R_o)} \left|S_{vv}\right|^2 C(R_o, \psi_t, \psi_r) = \left(\frac{R_o}{R_t}\right)^2 C(R_o, \psi_t, \psi_r) \left|S_{vv}\right|^2 . \tag{5.42}$$

The importance of this result is that it has two separate factors, one depending upon the properties of the scattering object, and the other, on the direct coupling between the two antennas for specific orientation and distance apart. Thus previously known values of the direct coupling can be inserted.

As an example, suppose that the E-plane of the receiving antenna is directed toward the scatterer, and the E-plane of the transmitter is directed away from the scatterer in which case $\psi_r = 0$, $\psi_t = \pi$. If the antennas are H-sectoral horns, we have from Appendix C, that the coupling $C(R_o, 0, 0,)$ is 39.3 db down, when $R_o = 45.3$ cm and the frequency is 10 GHz.

For a scattering object on an infinite ground plane, $\left|S_{vv}\right|$ is the value associated with the free space scattering by the object and its image. For example, (S_{vv}) for a hemisphere on a ground plane is the value obtained from the free space scattering by a sphere. Values of $\left|S_{vv}\right|$ or the related bistatic cross section, (5.37), are given by Crispin, et al (1959) for many scattering shapes. In addition, techniques used to compute $\left|S_{vv}\right|$ are prescribed here.

A few results are quoted in the following table where reference is made to the equivalent scatterer (the object and its image). The dipole results are obtained from Harrington (1964).

Equivalent Scatterer	Bistatic Cross-Section σ
Sphere (radius a where $a>>\lambda$)	πa^2 (not valid in forward direction).
Small Resonant Dipole, (Reactive Loading, losses neglected).	$.716\lambda^2$
Active Loaded Dipole at Resonant Length: (Load Resistance/Dipole Resistance = R_ℓ/R_m)	
(a) $R_\ell/R_m = 0$	$.8\lambda^2$
(b) $R_\ell/R_m = -.4$	$2.5\lambda^2$
(c) $R_\ell/R_m = -.8$	$20\lambda^2$

VI

EFFECTS OF SURFACE CURVATURE ON COUPLING

6.1 Limitations and Applications

Under certain conditions which are met in a number of aerospace configurations, the effect of a curved conducting skin on the coupling between two antennas along the skin can be claculated knowing the flat-plane coupling between the same antennas and the geometry of the skin. These conditions are:

1) The diameter of the skin is greater than about two wavelengths.
2) The curvature in the region of the antenna is small.
3) The Fresnel boundary is smaller than the radius of curvature.

These restrictions can be relaxed somewhat and still yield good results.

The problem was formulated in cylindrical coordinates but is valid for spherical geometries, or any geometry where the radius of curvature along the ray path between the two antennas is constant. The chief reference on this work is by Hasserjian and Ishimaru (1962). Their approach can be extended to treat other than thin resonant slots.

6.2 Procedure for Calculating Curvature Effect

Under the conditions listed above, the coupling between antennas T and R on a cylinder of radius a (see Fig. 6-1) or a sphere of radius a can be calculated by multiplying the flat-plate coupling by a factor f(y), where

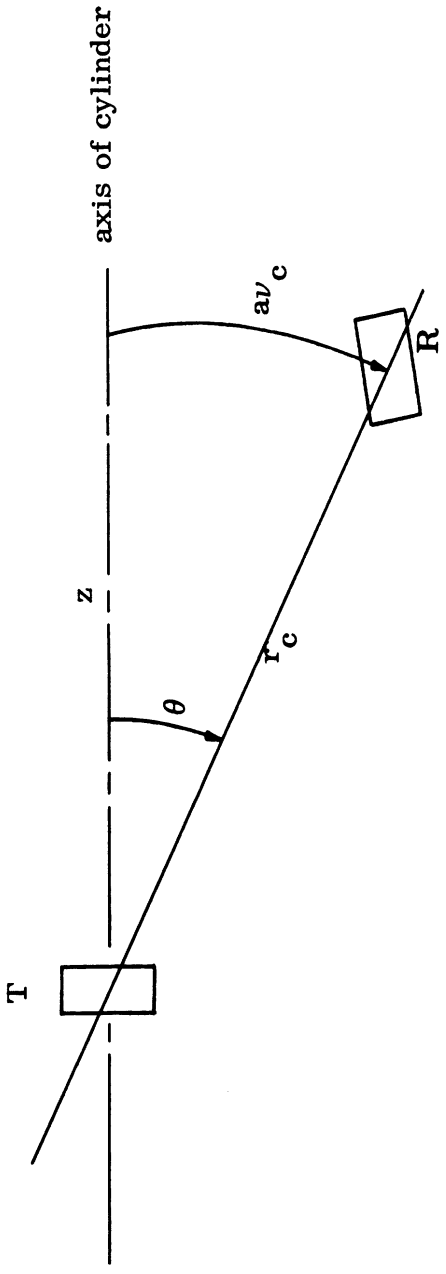

FIG. 6-1: GEOMETRY OF TWO SLOTS ON A CYLINDER

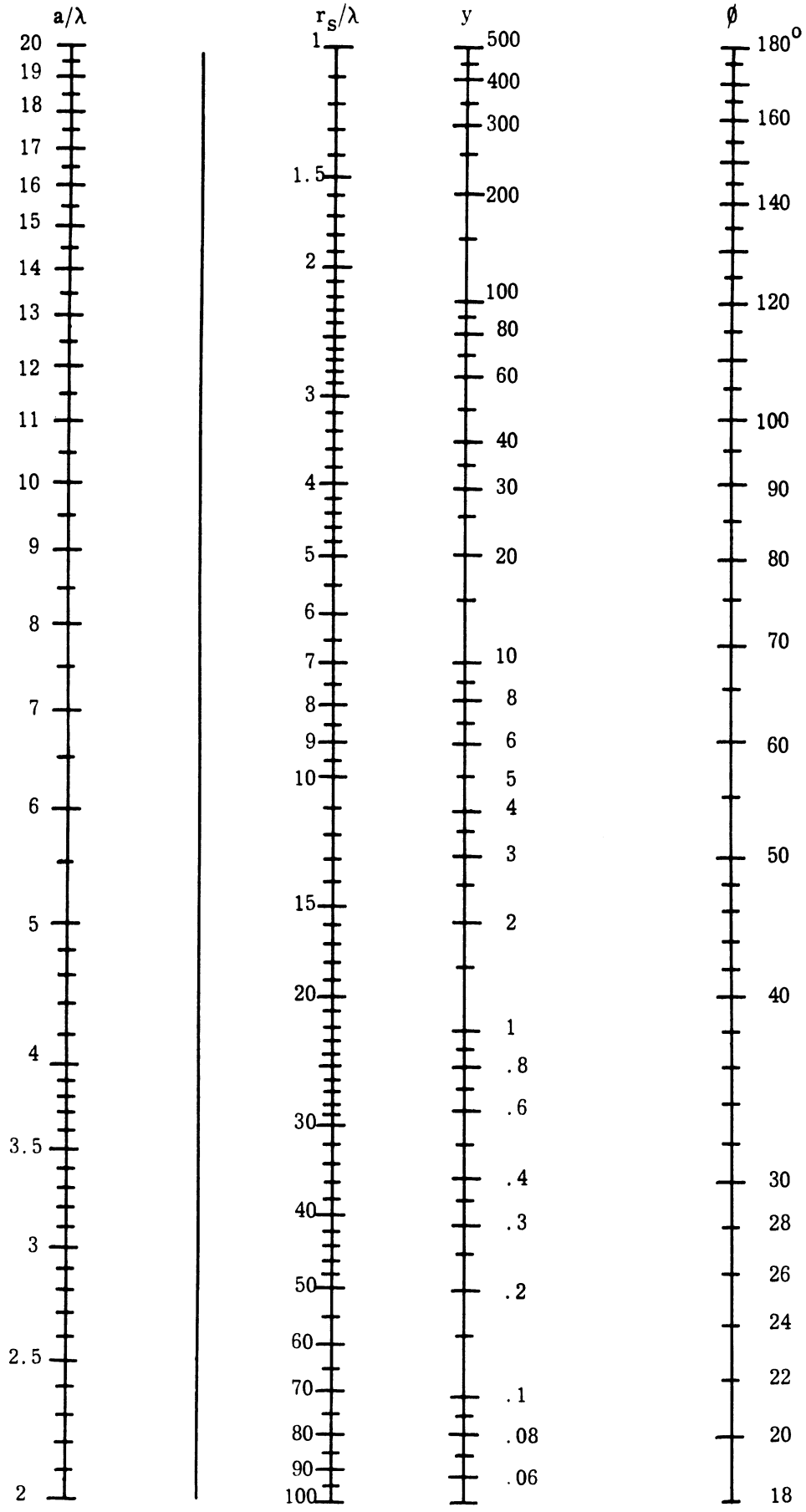

FIG. 6-2: Y FACTOR ON A CYLINDER

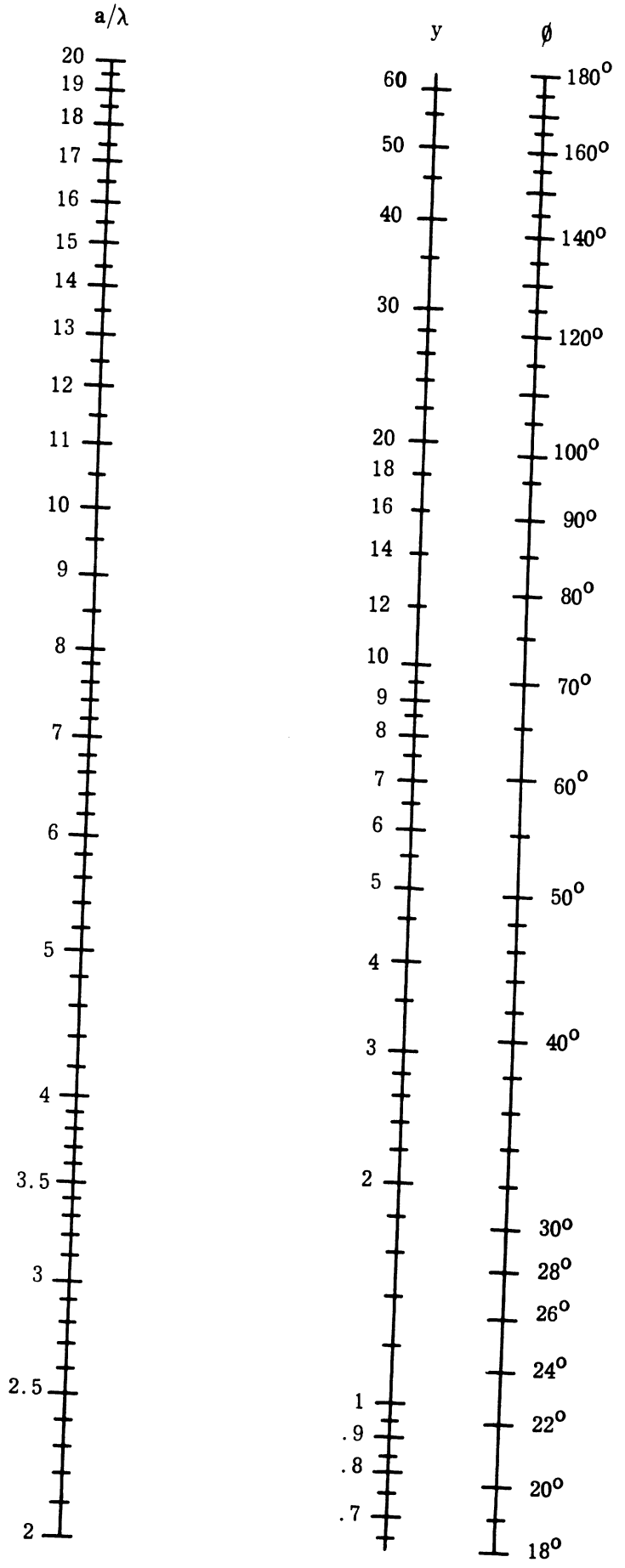

FIG. 6-3: Y FACTOR FOR SPHERE

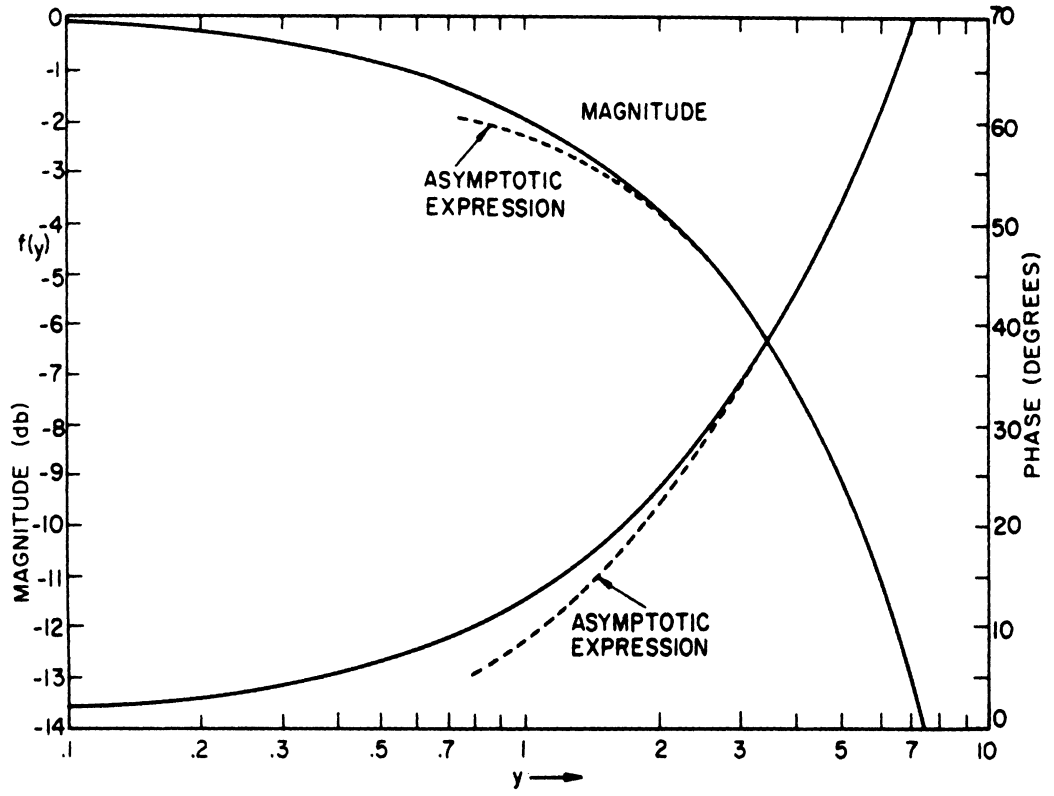

FIG. 6-4(a): CURVATURE FACTOR f(y) VS y (LOW RANGE)

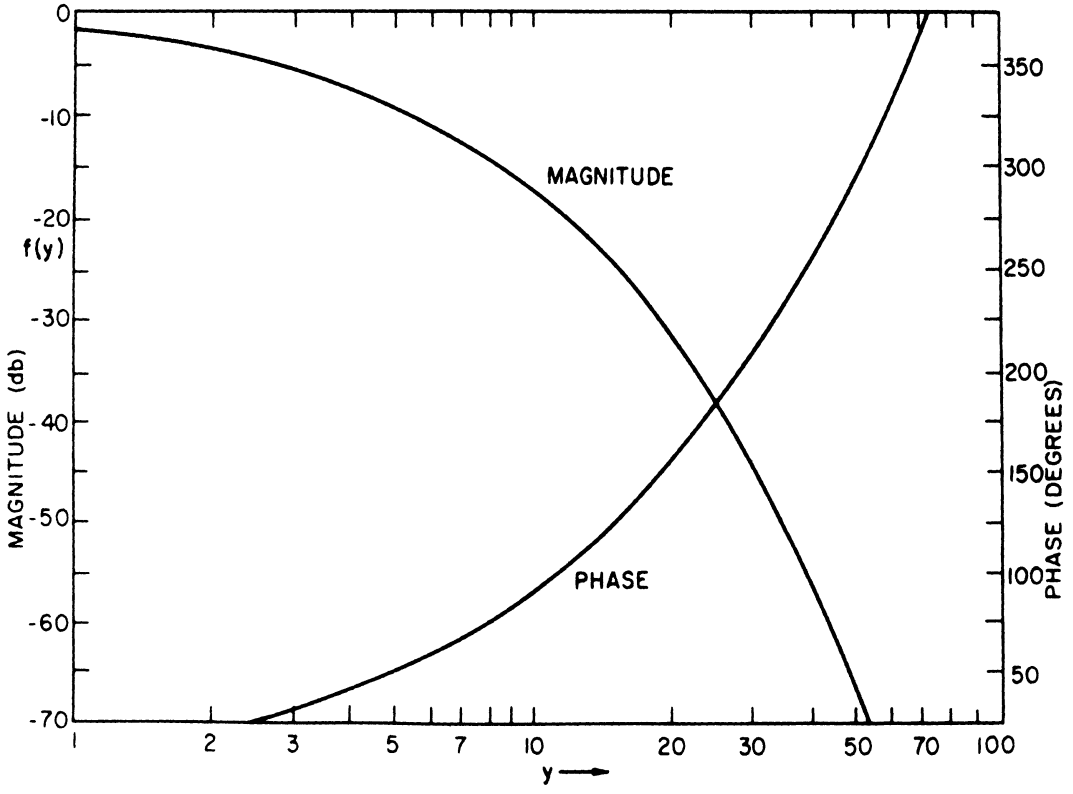

FIG. 6-4(b): CURVATURE FACTOR f(y) VS y (HIGH RANGE)

For a Cylinder:

$$y = \frac{ka\,\nu_c^2}{\sqrt{kr_c}} \ (\nu_c \text{ in radians}) = 7.64 \times 10^{-4} \frac{(a/\lambda)\,\nu_c^2}{\sqrt{\frac{r_c}{\lambda}}} \ (\nu_c \text{ in degrees})$$

$$r_c = \sqrt{z^2 + a^2 \nu_c^2} \ (\nu_c \text{ in radians}) = \sqrt{z^2 + \left(\frac{a\nu_c}{57.3}\right)^2} \ (\nu_c \text{ in degrees})$$

= distance from T to R along the surface.

ν_c is the angle between two planes containing the cylinder axis and the two antennas

For a Sphere:

$$y = \sqrt{ka}\,\nu_s^{3/2} \ (\nu_s \text{ in radians}) = 5.78 \times 10^{-3} \sqrt{\frac{a}{\lambda}}\,\nu_s^{3/2} \ (\nu_s \text{ in degrees}) .$$

ν_s is the angle between the antennas on a plane defined by the two antennas and the center of the sphere.

The flat surface coupling is the coupling of T and R separated by r_c or r_s, whichever is applicable, along a conducting plane. Nomographs to calculate y are given in Figs. 6-2 and 6-3. The function f(y) is given below, and in Figs. 6-4. Detailed instructions on the use of Figs. 5-2 through 6-4 are shown in Chapter VIII.

The analytical expression for f(y) is

$$f(y) = \begin{cases} 1 - e^{j\pi/4}\sqrt{\frac{\pi}{2}}\,\frac{y}{4} + \frac{7jy^2}{120}\sqrt{\frac{\pi}{2j}}\,e^{j\pi/4}\,\frac{y^3}{1024} \cdots, & \phi \text{ small} \\ e^{-j\pi/4}\sqrt{\pi}\left(\frac{y}{\sqrt{2}}\right)\sum_{m=1}^{\infty}\frac{\exp\left[-j\left(\frac{y}{\sqrt{2}}\right)^{2/3} t_m\right]}{t_m}, & \phi \text{ not small} \end{cases}$$

where

$$t_1 = 1.019^{-j\pi/3}$$

$$t_2 = 3.248\, e^{-j\pi/3}$$

$$t_3 = 4.820\, e^{-j\pi/3}$$

$$t_4 = 6.163\, e^{-j\pi/3}$$

$$t_5 = 7.372\, e^{-j\pi/3}$$

For large values of y, only the first term need be considered, and the asymptotic approximation holds:

$$\left|f(y)\right| \simeq 1.550\, y^{1/3}\, e^{-.7995\, h^{2/3}}$$

$$\left|f(y)\right|_{db} = 8.686\left[\frac{1}{3}\log_e y + .4380 - .7005\, y^{2/3}\right] db$$

$$= 20\left[\frac{1}{3}\log_{10} y + .1902 - .3042\, y^{2/3}\right] db$$

and the phase lag over the flat plate value is given by

$$\text{Phase}\left[f(y)\right] = .4045\, y^{2/3.} - .2818 \text{ radians}$$

$$= 23.18\, y^{2/3} - 15. \text{ degrees}.$$

The curves for f(y) are shown in Figs. 6-4(a) and 6-4(b).

The error introduced by using this expression is less than 0.5 percent in magnitude for $y \geq 2$, and in phase for $y \geq 4$. The latter terms of the series rapidly become more negligible as y increases.

To a first approximation, then, it is necessary to reduce the coupling found by "flattening" the cylinder into a plane by the curvature factor $\left|f(y)\right|$. As the curvature goes to zero, y approaches zero and $\left|f(y)\right|$ approaches unity.

Whenever more than one ray path may contribute significantly to the coupling, modification of the above procedure is necessary. While in theory there are an infinite number of paths corresponding to multiple encirclements of the cylinder, for the region of interest ($a \geq 2\lambda$) all except the two paths where $\phi > 360^{\circ}$ yield terms on the order of 70 db below the latter. Thus the modification need only be extended to treat two ray paths. The waves will interfere or reinforce according to the relative phase. In no case will the reinforcement be greater than 6 db over one path alone.

VII

EXPERIMENTAL FACILITIES

7.1 Description of Anechoic Chamber

The dimensions of the anechoic chamber are 50' x 30' x 15' , with a 12' square, 1/8" aluminum ground plane mounted in the center of one end wall (Fig. 7-1). The nine individual sections of the ground plane are joined by 2" aluminum tape to form an electrically continuous surface at microwave frequencies. The center section has a removable 2' x 3' section for the test antennas.

The ceiling and floor are covered with B. F. Goodrich HV-4 vinyl-covered, four-inch hairflex microwave absorber. The rear and wide walls are covered with VHP-18, 18" pyramidal absorber. The center of the rear wall is covered with VHP-26 absorber since it is normal to, and centered on, the mean axis of propagation for most measurements. The chamber is lined with interlocking aluminum foil sheets to provide a known uniform termination for the absorbing material and to shield the room from external signals. When the chamber is used for azimuth antenna patterns or radar scattering experiments, the ground plane is covered with HV-4 absorber.

All absorber used is in the form of 2 ft^2 sections, secured to the walls and ceiling by Velcro micro-hook fastener strips glued to the back of the absorbers, and velvet strips glued to the walls and ceiling. This allows rearrangement of the absorber to suit a particular measurement problem.

The frequency range of the chamber is 500 MHz - 50 GHz and has a nominal reflection coefficient, for normal incidence, of -50 db for X-band and above, tapering exponentially to -20 db for the lower frequencies. Typical return levels are much lower depending on the particular experiment, since normal incidence is usually avoided.

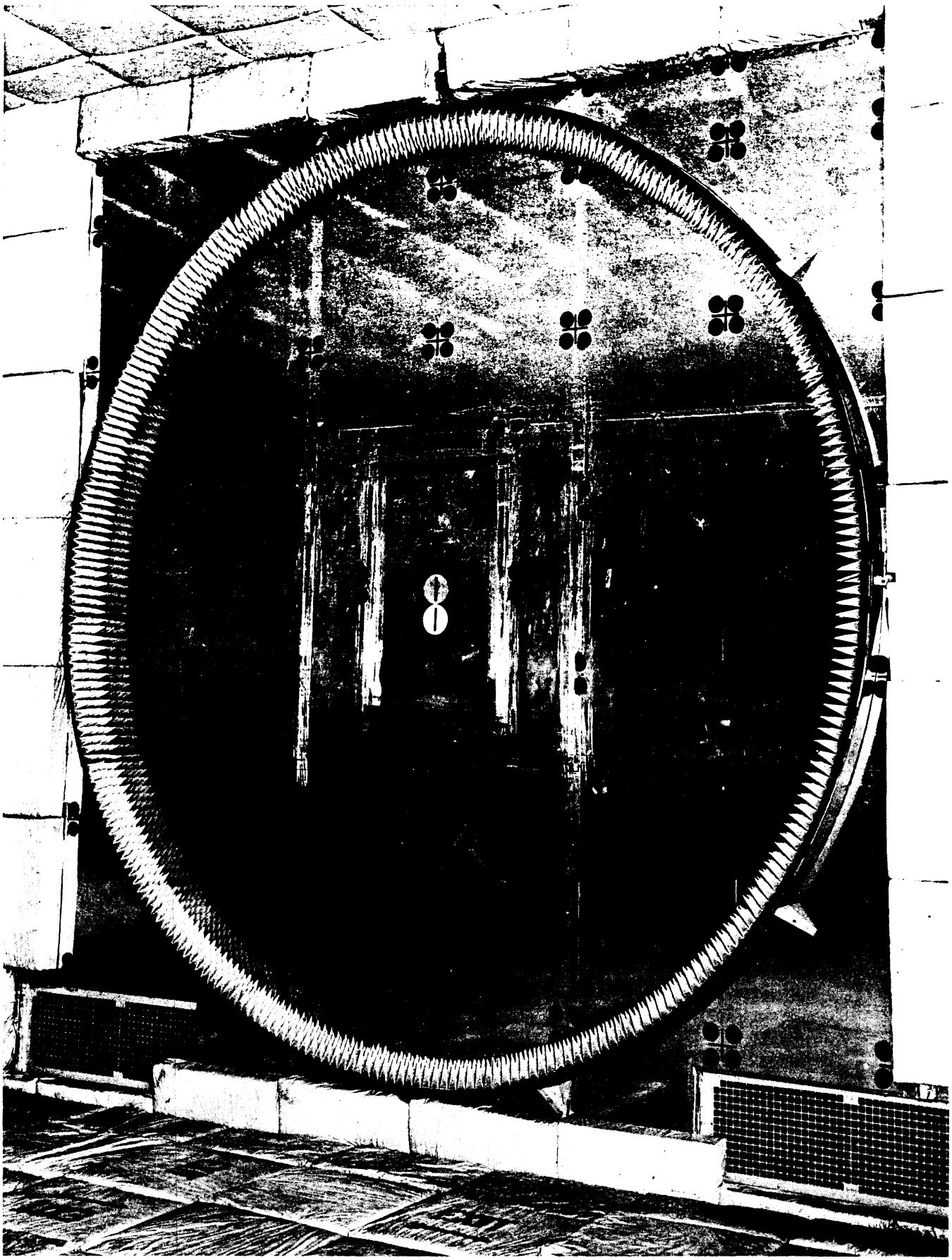

FIG. 7-1 ANECHOIC CHAMBER GROUND PLANE

7.2 Determination of Chamber Reflections by Swept Frequency Technique

In order to analyze the possibility of errors in the measured low-level coupling between widely separated conical horns (the repeatability of these data was very poor), it was decided that a swept frequency technique would be helpful.

The first results indicated that there was more than one path for the coupling energy between the horns, due to the presence of strong periodic perturbations of the coupling level as frequency was varied.

Figure 7-2 shows the situation which can lead to errors.

For maxima on the interference pattern,

$$2R - R_o = n\lambda_1 = (n+1)\lambda_2 = (n+2)\lambda_3 = \ldots = (n+m)\lambda_{m+1} \qquad (7.1)$$

For m cycles of interference, $\Delta f = f_{m+1} - f_1$

$$\lambda_1 = \frac{2R - R_o}{n} \quad \text{or} \quad f_1 = \frac{nc}{2R - R_o}$$

$$\lambda_{m+1} = \frac{2R - R_o}{n + m} \quad \text{or} \quad f_{m+1} = \frac{(n + m)c}{2R - R_o}$$

$$\Delta f = f_{m+1} - f_1 = \frac{mc}{2R - R_o}; \quad 2R - R_o = \frac{mc}{\Delta f} \qquad (7.2)$$

or

$$R = \frac{1}{2}\left[\frac{mc}{\Delta f} + R_o\right] \quad \text{for } R \gg R_o \qquad (7.3)$$

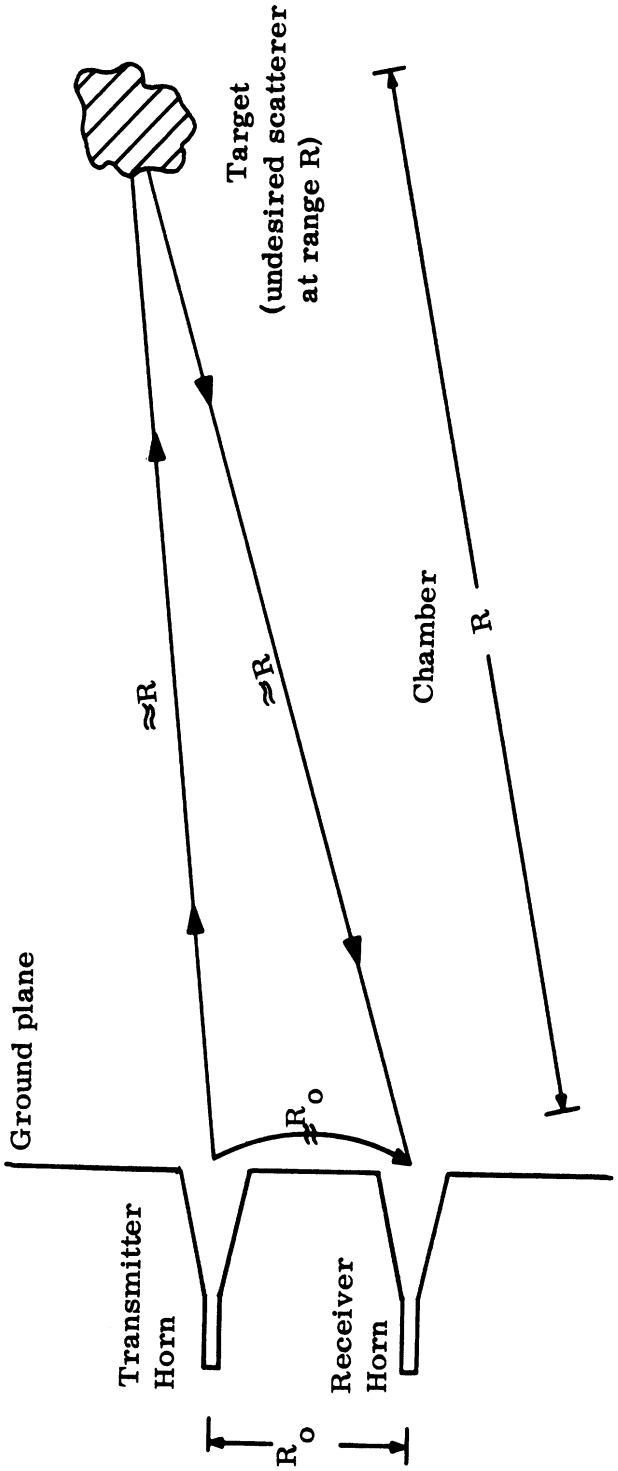

FIG. 7-2: GROUND PLANE AND SCATTERER GEOMETRY

where: R is the range of the interfering scatterer (target)

m is the number of interfering cycles

Δf is the range of frequency sweep

R_o is the distance between antennas

c is the speed of light

Equation (7.3) relates the periodicity of the perturbations of the differential path length between the direct and unwanted coupling paths. To prove the equation, a baffle of absorbing material, which provided a weak reflecting area and isolated many reflecting obstacles in the chamber, was placed normal to and six feet in front of the ground plane containing the conical horns. A swept-frequency coupling pattern was then recorded under these conditions. The measurement setup is shown in Fig. 7-3, and the expected result is obtained in the example below.

Example (Actual Results for Baffle at Six Feet):

For

$\Delta f = 5 \times 10^8$ Hz

$R_o = 36.6$ cm

$m = 5$

$c = 3 \times 10^{10}$ cm/sec

$$R = \frac{1}{2}\left[\frac{15 \times 10^{10}}{5 \times 10^{8}} + 36.6\right] = \frac{1}{2}(336.6) = 168.3 \text{ cm} = 5.5 \text{ ft.} \qquad (7.4)$$

In addition to the fundamental five-cycle interference pattern from the baffle, higher-order interference was present, indicating the presence of other reflecting objects. A systematic procedure was followed from this point on, whereby the unwanted reflections were eliminated, by recording swept

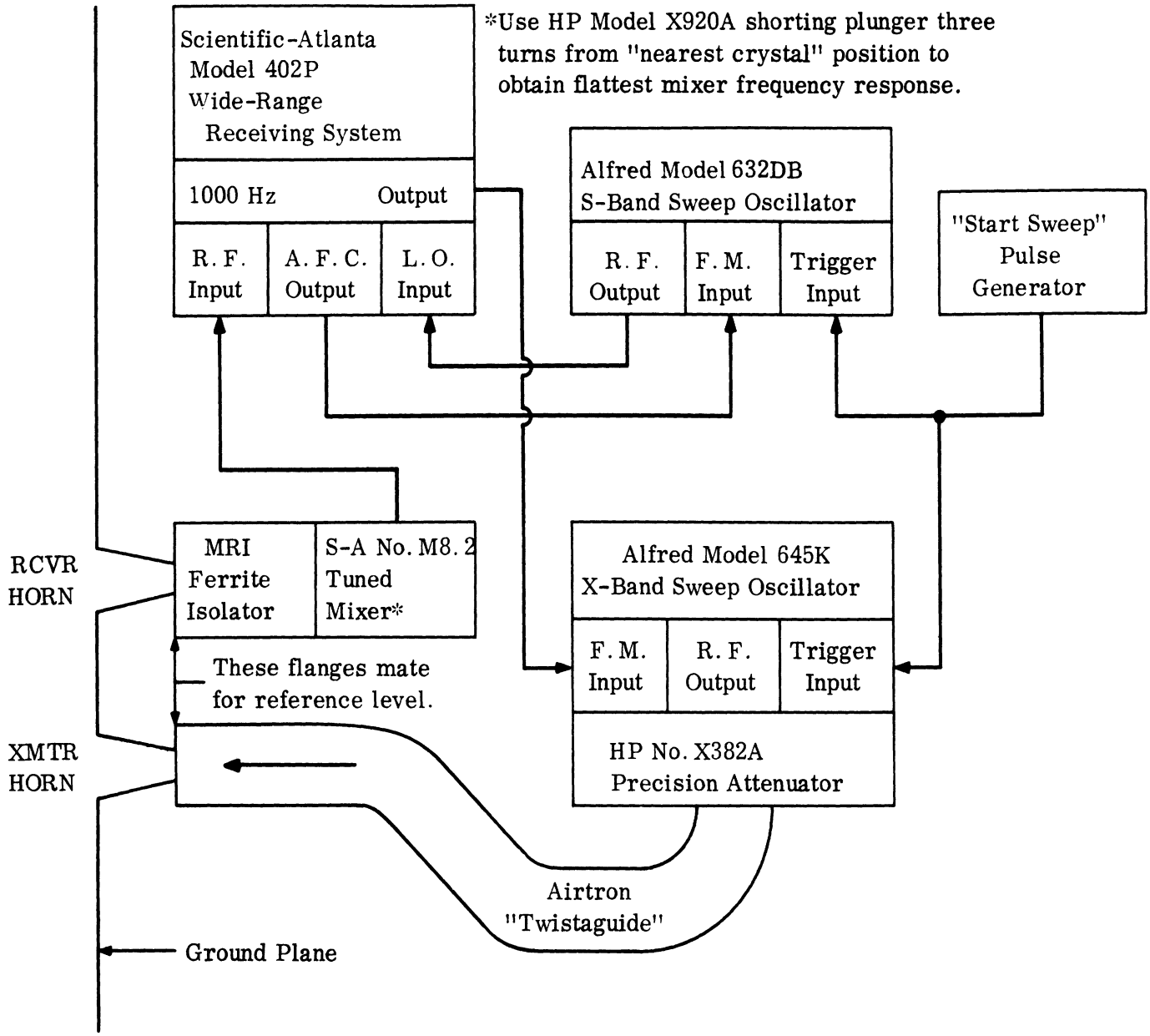

1. S-band oscillator unleveled at +10 dbm.
2. X-band oscillator unleveled at maximum output.
3. Adjust f_1 ("start" freq.) and f_2 ("stop" freq.) and "sweep speed" on each oscillator for near-constant 65 MHz i.f. for receiver; a.f.c. will correct minor tracking errors.
4. Set receiver sweep width (1000 Hz) to 3 MHz for best compromise between sensitivity and stability.

FIG. 7-3: CIRCUIT BLOCK DIAGRAM FOR SWEPT FREQUENCY MEASUREMENTS

frequency patterns with the baffle at increasing ranges to progressively expose more and more of the chamber. These data indicated that severe reflections from the VHP-18 pyramidal absorber on the floor and ceiling, and from over half the light fixtures in the ceiling (Fig. 7-4) were interfering with the coupling measurements. The pyramids were placed with HV-4 vinyl covered Hairflex and the problem lights were covered with the same. This reduced the reflections from the room from -70 db down to -90 db, thereby increasing measurement accuracy and repeatability of the low-level coupling between conical horns.

A similar problem reoccurred when it became necessary to measure the coupling between two H-Sectoral Horns. Because these antennas have fan-shaped beams in the E-plane, the E-plane coupling is very large (-30 db) and the H-plane coupling very small (-70 db). Since the antennas were located along a horizontal line on the ground plane, strong reflections resulted when they were oriented for H-plane coupling; this was due to the fan beams 'looking' at the floor and ceiling only seven feet away, and at the edges of the 4" Hairflex absorber and the top and bottom bearings for the swinging boom at the perimeter of the ground plane (Fig. (Fig. 7-5). These reflections caused the main beam coupling to dominate the direct H-plane coupling which was to be measured. To reduce the reflection from the boom bearings and the sides of the 4" Hairflex, a 12' diameter masonite ring, 6" wide, was mounted on the ground plane. The interior of this ring was covered with VHP-5 pyramidal absorber (-45 db reflection for normal incidence at X-band) facing the center of the ground plane (see Fig. 7-1). To reduce reflections from the floor and ceiling in the E-plane of the horns, the 2'x3' sub-ground plane was rotated 90^{o} so that the fan beams 'look' at the side walls which are 15' from the antennas. Then the swept frequency technique was applied to the problem. Measurements still indicated the presence of a strong scatterer at a range of 10'. This was traced to the portable baffle used in the previous measurements,

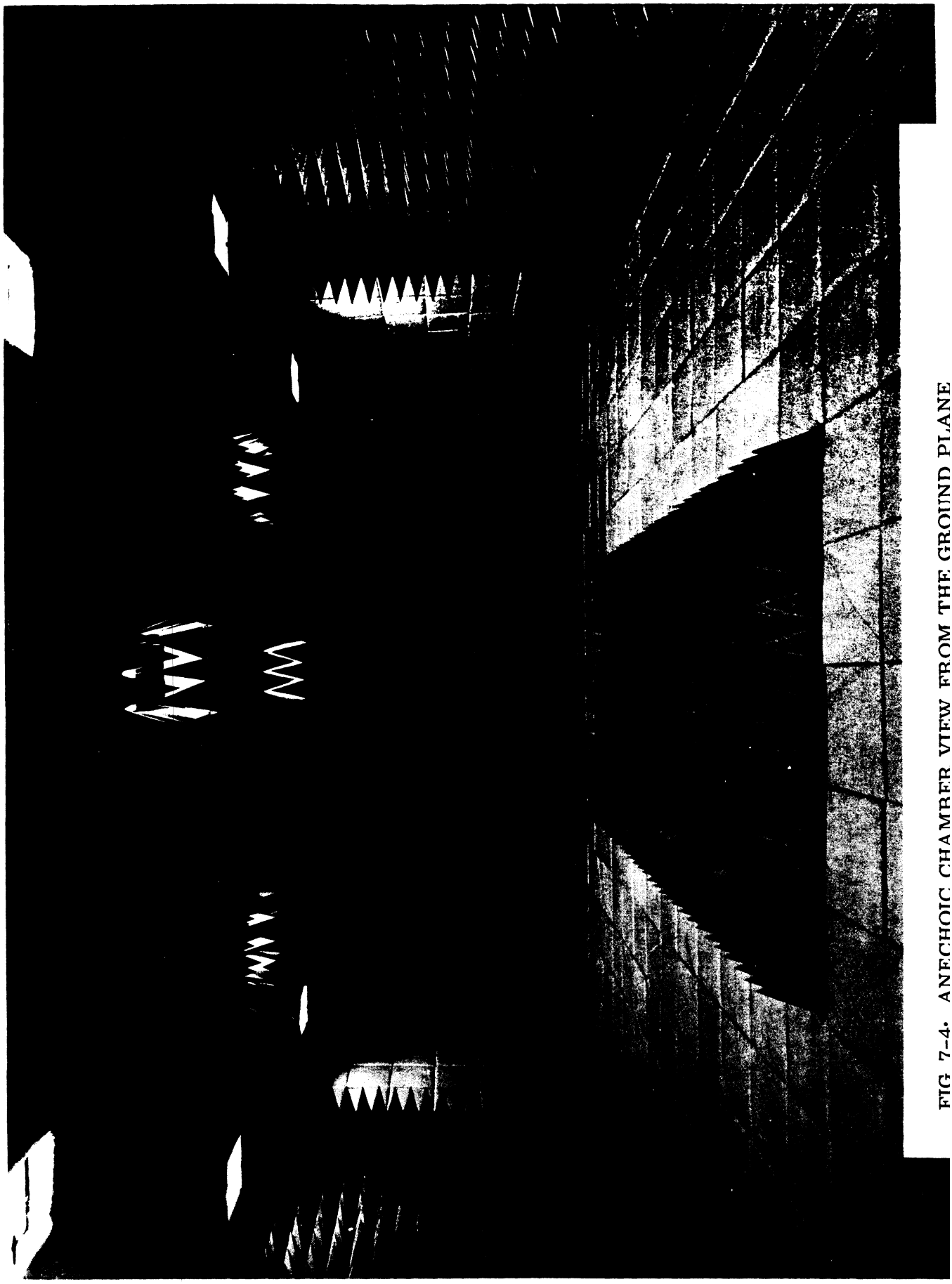

FIG 7-4. ANECHOIC CHAMBER VIEW FROM THE GROUND PLANE

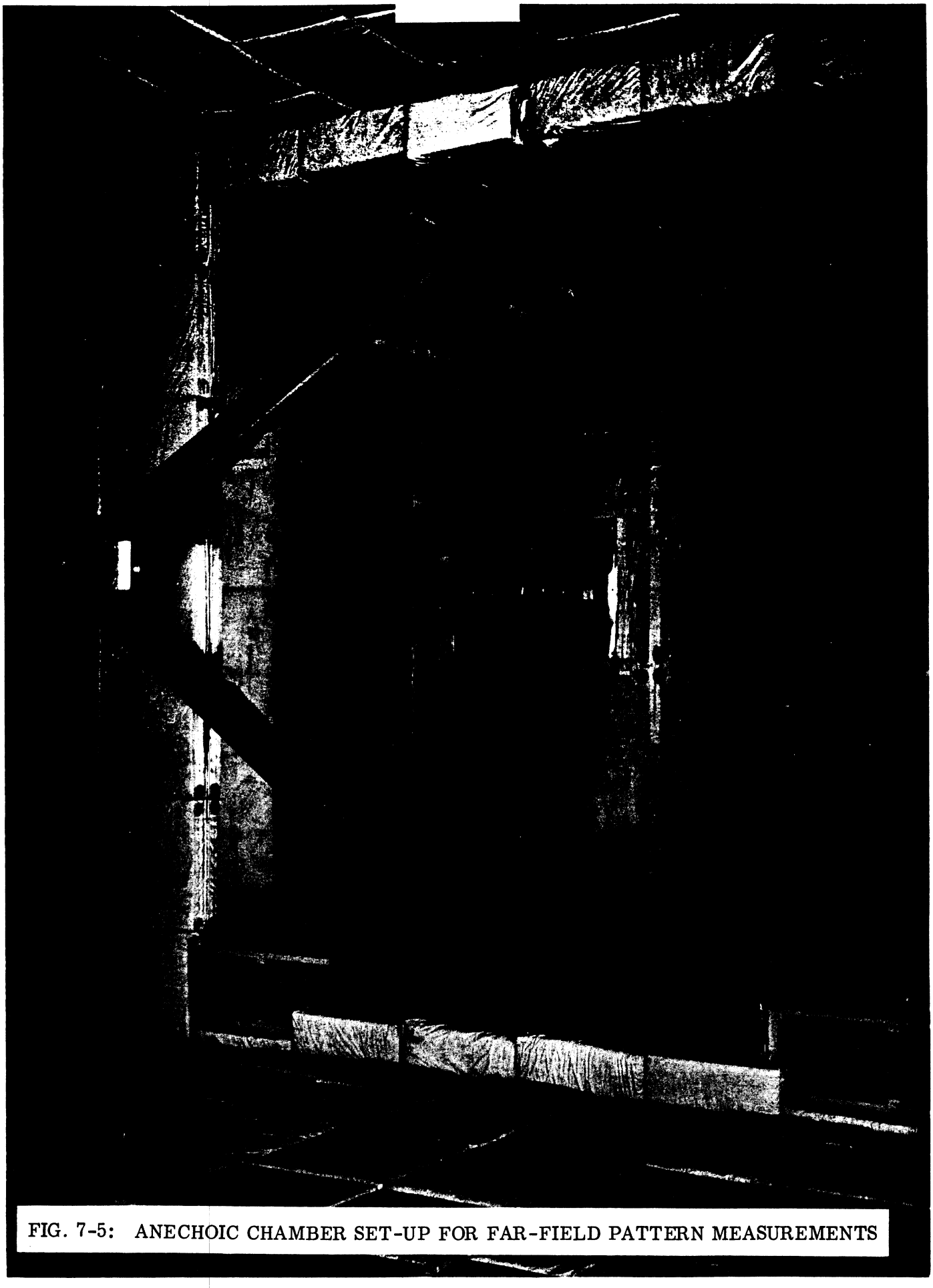

FIG. 7-5: ANECHOIC CHAMBER SET-UP FOR FAR-FIELD PATTERN MEASUREMENTS

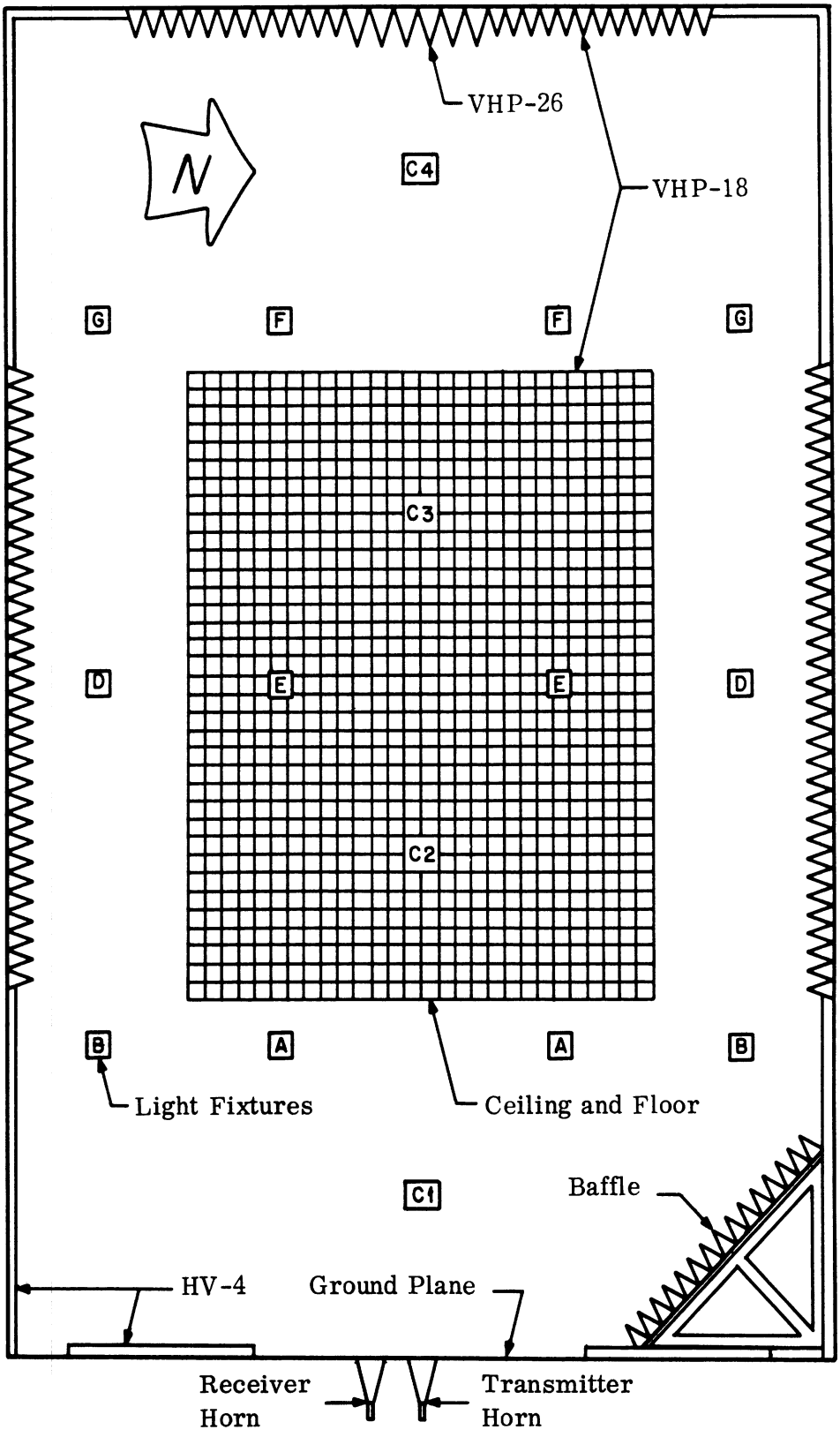

FIG. 7-6: CHAMBER BEFORE ABSORBER REARRANGEMENT

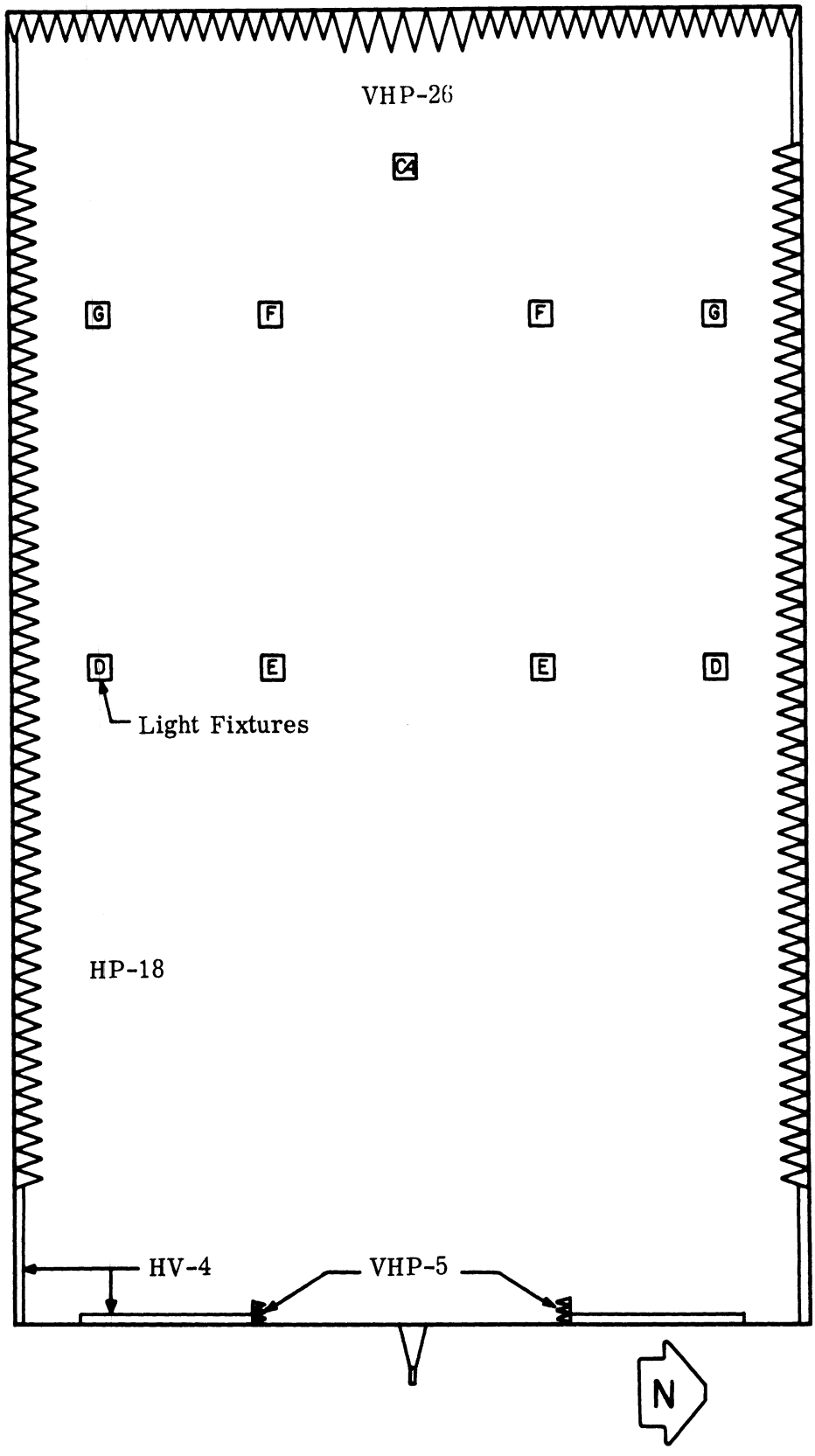

FIG. 7-7: CHAMBER AFTER ABSORBER REARRANGEMENT

which had been stored in a corner of the chamber at the junction of a side wall with the ground plane wall (Fig. 7-6). Again the problem was due to severe reflections from the sides of the VHP-18 pyramids mounted on the baffle. Removal of the baffle from the chamber reduced reflections to the point whereby a 15 db improvement resulted from these three corrections. For these H-sectoral horns, room return was then approximately -85 db, thus permitting accurate measurements of the coupling for any of the horn antennas. The final layout for the absorber is shown in Fig. 7-7.

7.3 Limitations on Coupling Accuracy

The measurement equipment is shown in Fig. 7-8. The limitations on coupling accuracy are described below.

1. Chamber reflections can cause a serious error in the measured value of antenna coupling, as shown in Fig. 7-9, e.g. a reflection 20 db below the coupling to be measured can cause an error of $\pm$ 1 db, depending on the relative phasing.

2. Minimum coupling level recordable with a tolerable noise is limited to approximately -90 db by a maximum receiver sensitivity of -85 dbm, by a maximum transmitter power of 20 dbm, and by losses (undesired losses plus deliberate padding) of 15 db.

3. Accuracy of coupling is limited by mechanical accuracy of the horns (and wedges), i.e., if a horn is mechanically (physically) asymmetrical, it cannot be expected to yield a symmetrical coupling pattern. The degree of flatness and continuity of the conducting ground plane also affects the accuracy of the coupling; the ground plane consists of nine pieces joined by metal tape and is flat to within one-eighth inch overall, and much less locally.

4. Coupling accuracy is also dependent on system linearity, which at best is approximately $\pm$ 0.25 db over a 60 db dynamic range.

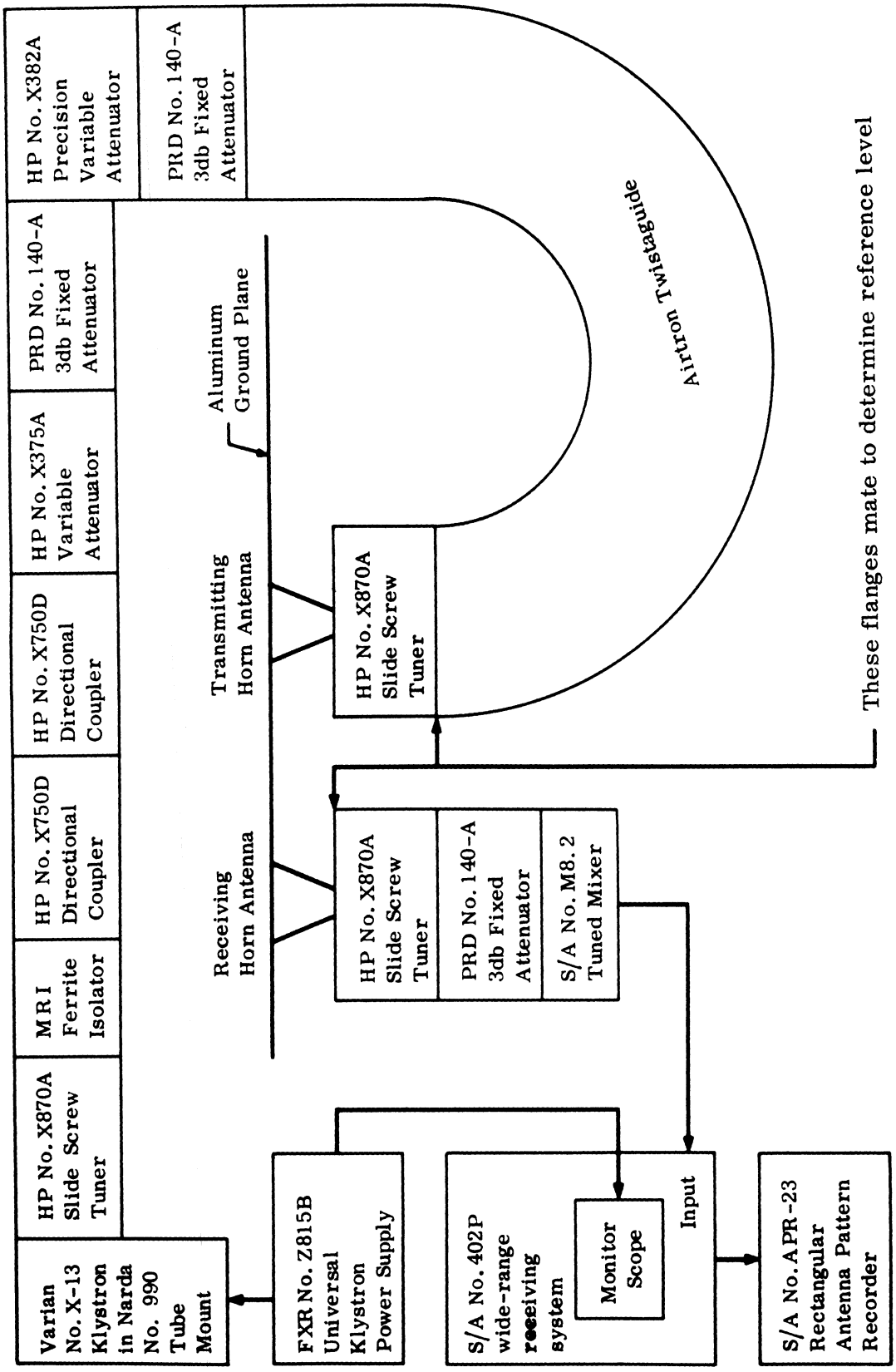

FIG. 7-8: ANTENNA COUPLING MEASUREMENT SYSTEM FOR X-BAND (FOR PATTERNS AT SINGLE FREQUENCIES).

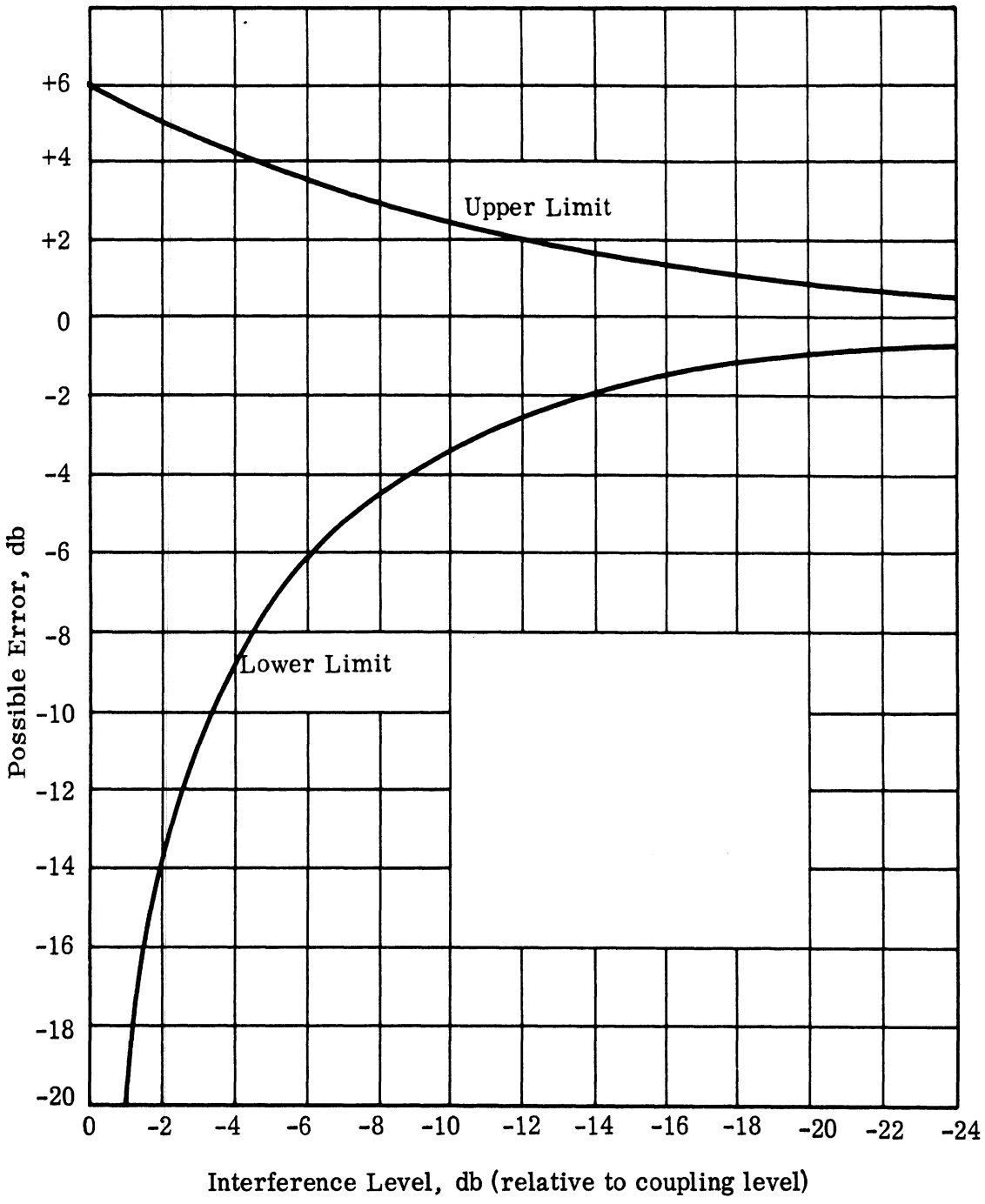

FIG. 7-9: RANGE OF POSSIBLE ERROR IN MEASURED COUPLING BETWEEN ANTENNAS DUE TO REFLECTIONS FROM UNDESIRED SCATTERING OBJECTS (FREQUENCY-COHERENT INTERFERENCE).

5. The precision attenuator used to establish a reference level coupling has an accuracy of ± 1 db at its 50 db setting although the probable error is less; this further limits measurement accuracy.

6. Another source of error is the drift of the klystron oscillator output power on the receiver gain, which may amount to ± 0.5 db over the time required to make a series of measurements before recalibrating the system.

7. At best, i.e., with no noise (moderate coupling level) with no interference due to chamber reflections, and with the system carefully calibrated, the maximum overall accuracy of a given measurement is estimated at ± 1 db. For low-level coupling (-75 db or less) where chamber reflections and/or noise can be present, the typical accuracy is probably ± 3 db.

8. The separation between centers of the two antennas is accurate to within ± 1 millimeter, an insignificant error.

9. The frequency accuracy is ± 0.01 per cent when the Dymec DY2650A Synchronizer is employed (e.g. 8.03 - 9.03 GHz) also an insignificant error.

10. The accuracy of orientation angles indicated is limited to ± 3^{o} because of the compact scale of the recording paper, but is typically within ± 1^{o}.

VIII

COUPLING COMPUTATIONS

8.1 Evaluation of Coupling by Nomograph Method

It is observed that all measured far field coupling falls off as 6db per spacing octave. Therefore, for estimating the coupling between any combination of flush-mounted antennas, it is only necessary to know the directivity of each antenna and the spacing between them. The far field coupling formula is given by

$$C = C_o(R)\, D_t(\phi)\, D_r(\phi) q \,. \tag{8.1}$$

8.2 Nomograph Procedure

The value of coupling C can be determined quickly by the nomograph method in the following three steps:

1. The dimensions and orientation of both transmitting and receiving antennas must be known or postulated. $D(\phi)$ can be obtained from the directivity nomographs in the previous sections of this report.

2. Enter (Fig. 8-1) the values of spacing R_o/λ. Look up $C_o(R)$ from the C_o scale.

3. The reduction of coupling due to mismatched impedance q factor can be found in Section 2.4 (Fig. 2-3) using VSWR. The coupling is given by

$$C(db) = C_o\, db + D_t\, db + D_r\, db + q\, db \tag{8.2}$$

The accuracy of the coupling obtained is within $\pm$ 2 db except for the horn antennas.

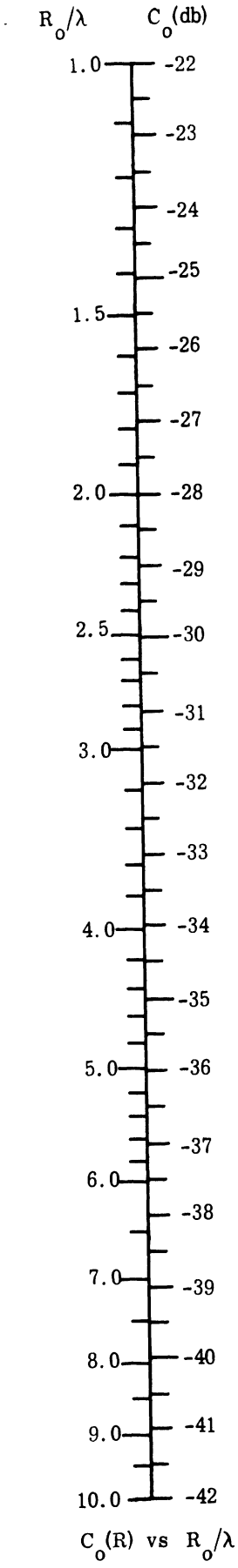

FIG. 8-1: COUPLING BETWEEN PARRALLEL ISOTROPIC ANTENNAS VS SEPARATION DISTANCE

Figure 8-2 shows the coupling between some simple antennas. The scales indicate the coupling between antennas of the same type. For a combination of different antennas, the coupling is the average of the two values read. The coupling between other antennas is illustrated in the following examples.

8.2.1 Example 1

Evaluate the coupling between a rectangluar slot antenna and a circular spiral antenna under the following conditions (see Fig. 8-3):

Slot dimensions, $a = 0.8\lambda$, $b = 0.4\lambda$

Orientation of the slot antenna with respect to the spiral antenna,

$$\phi = 45^{o}$$

Spacing between the slot and spiral,

$$R_{o} = 2\lambda$$

SWR of the transmitting antenna,

$$2 .$$

From the coupling formula (2.2),

$$u = \frac{a}{\lambda} \pi \sin \phi = 0.5656, \qquad v = \frac{b}{\lambda} \pi \cos \phi = 0.2828 .$$

Enter into Fig. 8-4 the values of a and b and obtain point (1). Draw a horizontal line from (1) to line F and obtain point (2). Locate points (3) and (5) with the values of v and u. Draw a straight line between (4) and (5) to obtain (6). Enter the value of ϕ at (7) and draw a straight line between (6) and (7) intersecting the D scale at point (8) which gives D = -2.9 db.

From Fig. 4-12 (Section 4.3), the average directivity of a circular Archimedean spiral is -8 db on a conducting plane surface.

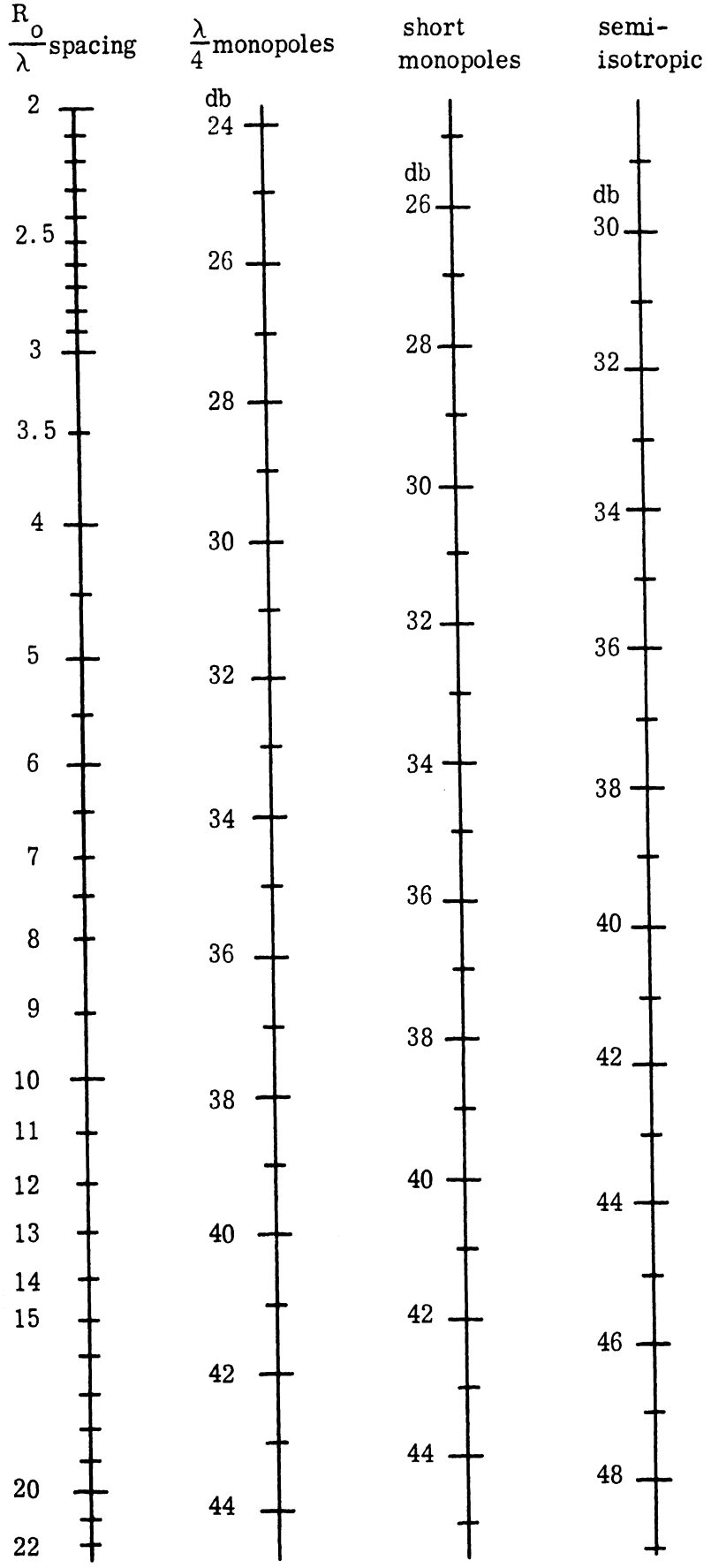

FIG. 8-2: COUPLING BETWEEN SIMPLE ANTENNAS

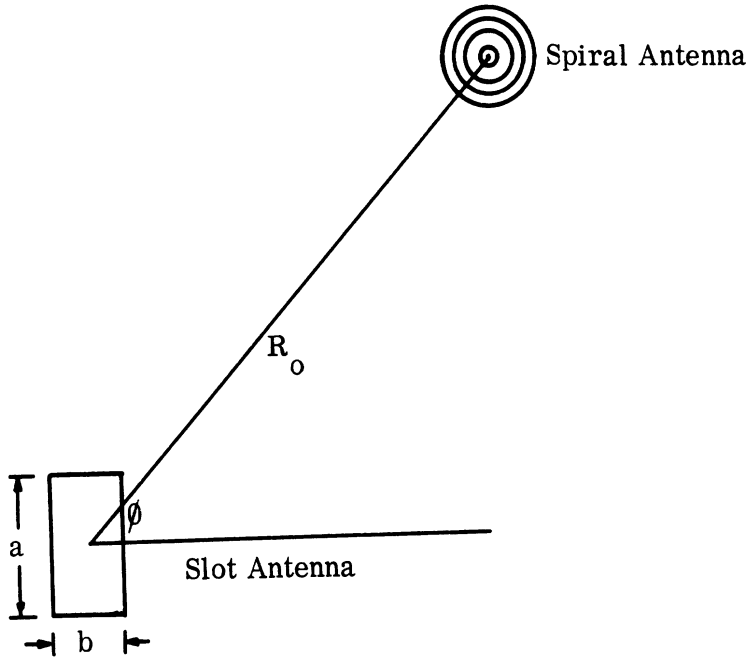

FIG. 8-3: COUPLING BETWEEN SLOT AND SPIRAL ANTENNA

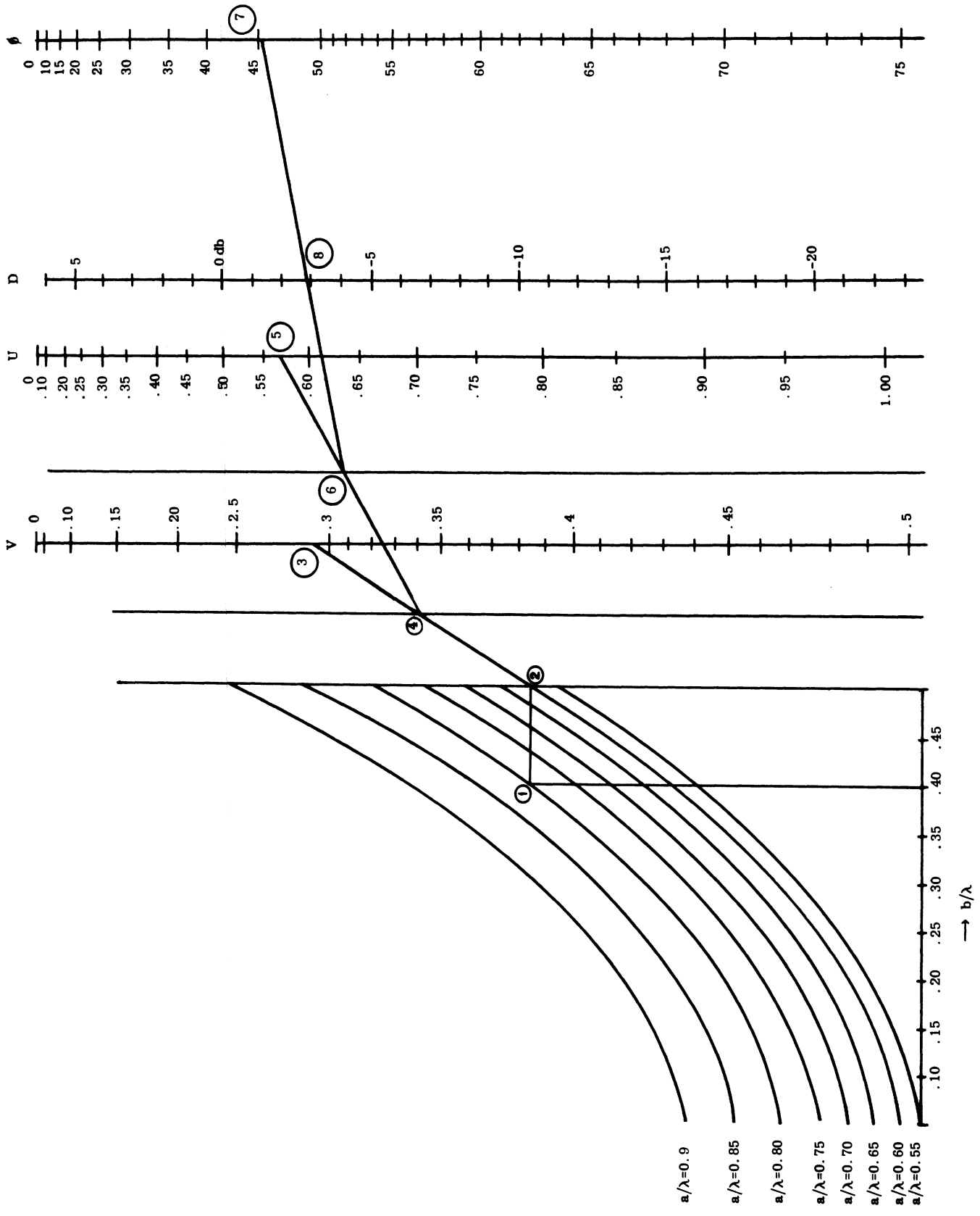

FIG. 8-4: NOMOGRAPH FOR CALCULATING DIRECTIVITY FUNCTION D(ϕ) FOR A SLOT ANTENNA

Enter Fig. 8-1 at $R_o/\lambda = 2$. Find C_o is -28 db.

From Fig. 2-3, q = -0.52 db for a 2:1 SWR. The result yields a coupling of

$$C(db) = -28 - 2.9 - 8 - 0.52 = -39.42 \text{ db.}$$

8.2.2 Example 2

If both antennas in Example 1 are mounted on a cylindrical surface with a radius equal to 4λ, and angle $\psi_c = 20^o$. Then the curvature effect factor, f(y), can be found by using Fig. 6-4 .

Enter Fig. 8-5 at $a_c/\lambda = 4$, $r_c/\lambda = 2$ and $\psi_c = 20^o$. Follow the progression of the circled numbers through the figure. There y = 0.86. From Fig. 6-4, f(y) = -1.7 db. Thus the coupling between these two antennas on a cylindrical surface is -39.42 -1.7 or - 41.1 db.

8.2.3 Example 3

Evaluate coupling between a E-sectoral horn antenna and a quarter wavelength monopole. Assume the following conditions.

Horn dimensions: $a = 0.8\lambda$, $b = 2.5\lambda$

Orientation of horn and monopole:

$$\phi = 20^o$$

Spacing between horn and monopole:

$$R_o = 10\lambda$$

SWR = 1.

Then

$$u = \frac{a}{\lambda}\pi \sin\phi = 0.274\,\pi, \qquad v = \frac{b}{\lambda}\pi\cos\phi = 2.35\,\pi.$$

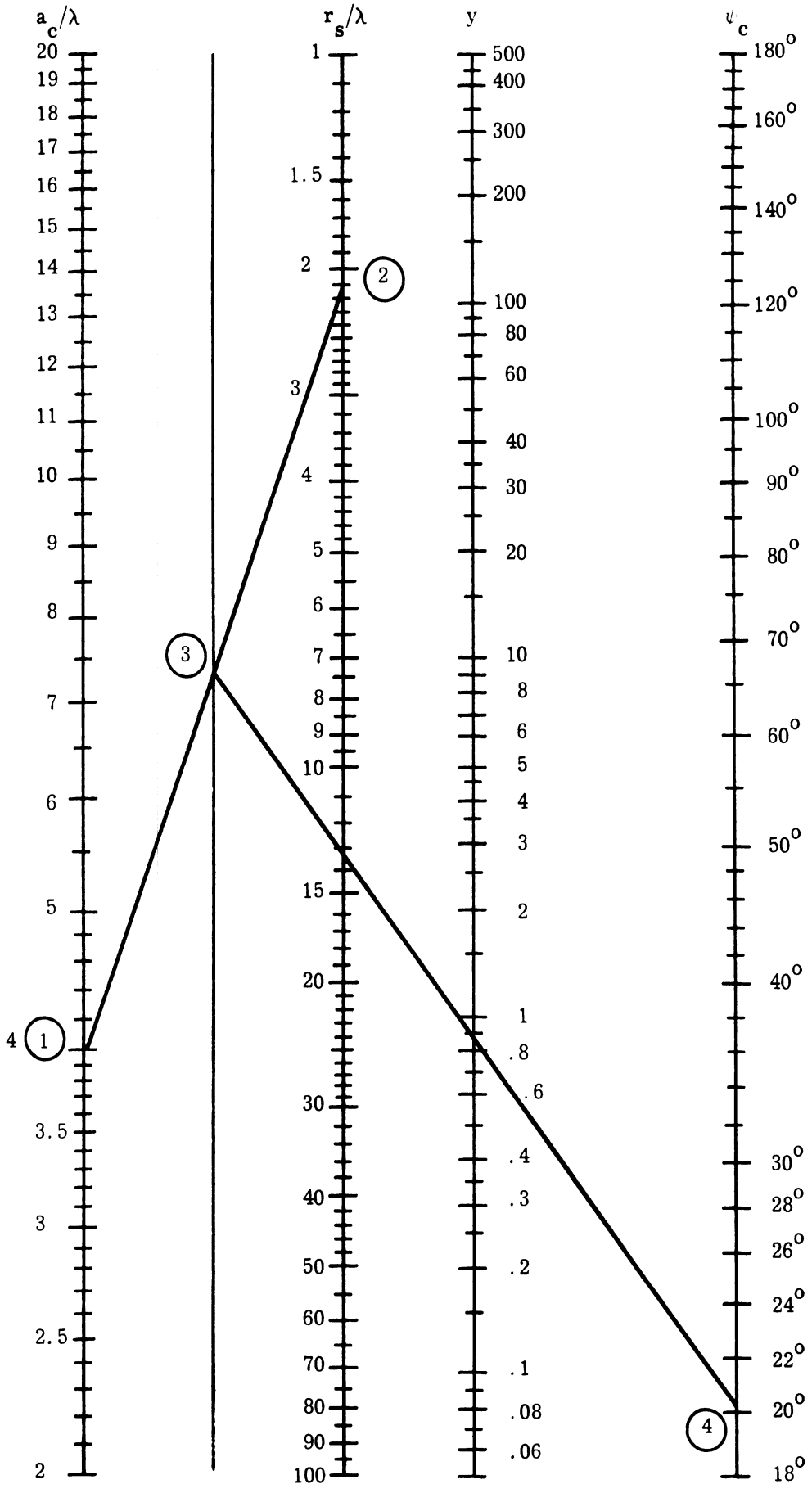

FIG. 8-5: Y FACTOR ON A CYLINDER

Enter Fig. 8-6 the directivity nomograph of a horn antenna with the values of a, b, u, v. Follow the order of progression as indicated by the circled numbers in the figure. On scale D, -7.3 db is found. The directivity of a quarter wave monopole perpendicular to a conducting surface is 2.15 db.

Enter Fig. 8-1 at $R_o/\lambda = 10$ and find that $C_o = -42$ db.

With the SWR = 1, q is 0 db.

The resulting coupling is

$$C(db) = -42 - 7.3 + 2 + 0 = -47.3 \text{ db}.$$

8.2.4 Example 4

Assume there is a quarter wave monopole located 4λ away from the center of the square archimedean spiral 1L at the frequency of 3.3 GHz.

From Fig. 4-15, Section 4.4, the directivities of the square spiral 1L at 3.3 GHz are:

$$D_{max} = -5.4 \text{ db}, \quad D_{avg} = -7.0 \text{ db}, \quad \text{and} \quad D_{min} = -9.0 \text{ db}$$

Enter Fig. 8-1 at $R_o/\lambda = 4$ and one finds that $C_o = -34$ db

The resulting couplings are:

$$C_{max}(db) = -34 - 5.4 + 2 = -37.4 \text{ db}$$

$$C_{avg}(db) = -34 - 7.0 + 2 = -39 \text{ db}$$

$$C_{min}(db) = -34 - 9.0 + 2 = -41 \text{ db}$$

8.2.5 Example 5

The problem is to evaluate the coupling between two parallel slots given the size of the slots, the distance between the slots and the frequency of operation. Assume the following conditions:

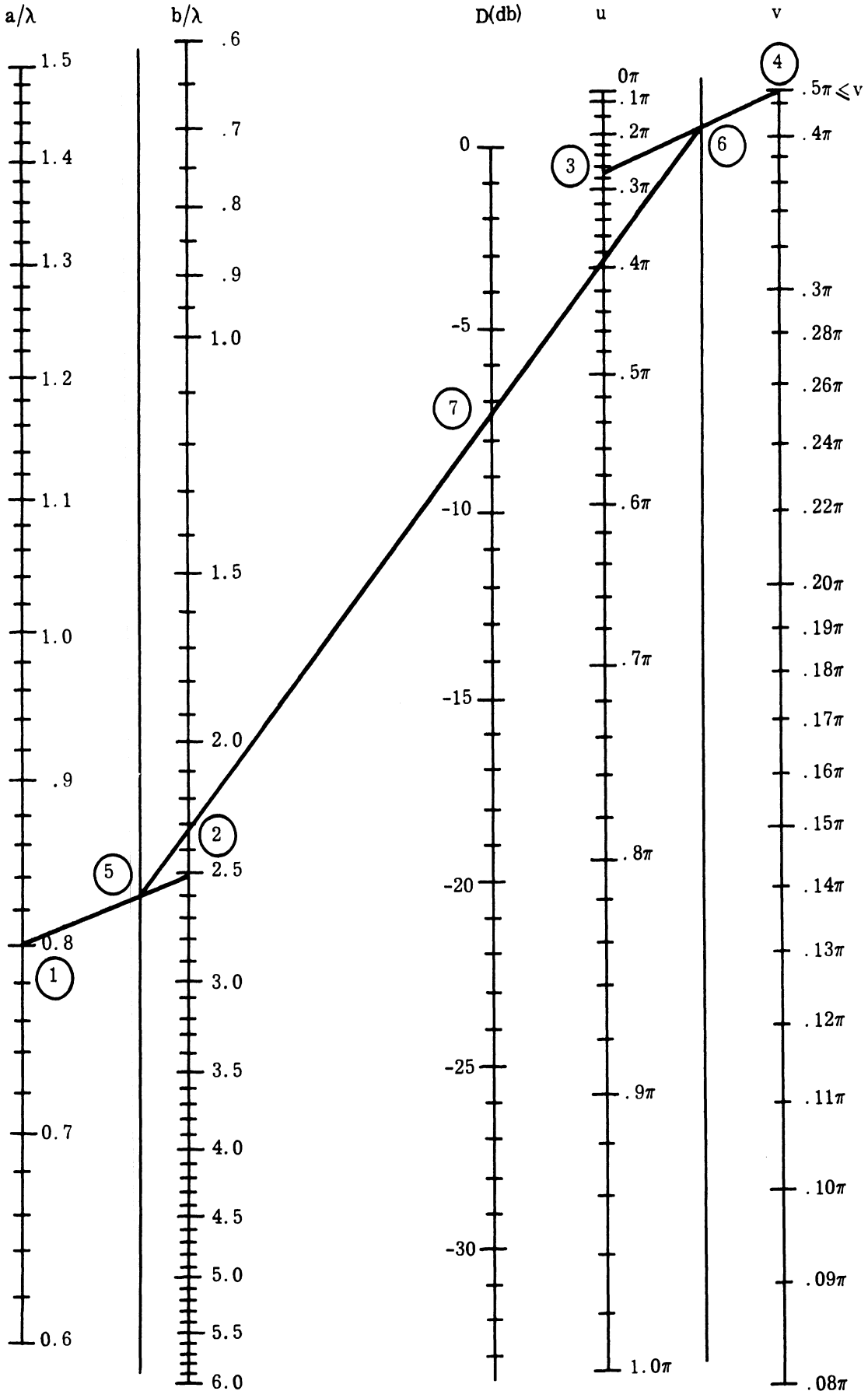

FIG. 8-6: NOMOGRAPH FOR CALCULATING DIRECTIVITY FUNCTION OF RECTANGULAR HORNS

f = 9.20 Kmc; λ = 3.26 cm = 1.283", R_o = 2.566" = 2λ

Transmitting antenna: a_t = 0.9" = 0.7λ b_t = 0.4" = 0.312λ

Receiving antenna: a_r = 0.77" = 0.6λ, b_r = 0.32" = 0.25λ

Enter Fig. 8-7 with the transmitter parameters a_t and b_t and obtain point (1). Draw a horizontal line from (1) to the line F_t, obtaining point (2). In a similar manner, use the receiver parameters a_r and b_r to obtain point (3) and (4) draw a straight line between (4) and (2) so that line F is intersected at (5). Enter the values of b_t and b_r on the D_t and D_r axes, respectively, and obtain points (6) and (7). Connect (6) and (7) with a straight line intersecting the D axis at point (8). A straight line between (8) and (5) gives (9) on the central axis. Enter the value of R_o on the R axis (10) and draw a straight line between (9) and (10) intersecting the C axis at (11). The coupling is given by the value at (11) on the C axis. In this case the coupling is -24.5 db.

If R_o exceeds 10λ the nomograph can still be used provided -20 db is added to the coupling obtained from the nomograph. Suppose R_o = 20λ. Enter the value of R_o on the R axis as 2λ which will give a coupling of -24.5 db as before; the total coupling will consequently be -24.5 -20.0 = -44.5 db.

In case the receiving antenna is rotated on an angle of $\phi_r = 60^o$ with respect to the axis between receiver and transmitter a modification is necessary. On the nomograph of Fig. 8-8 mark a point on the angle θ bar at the 60^o mark, call this point (M). Mark a point on the b/λ bar corresponding to the value 0.25 which is the b_t dimension. Call this point (N). Draw a line between (M) an (N) and let this line extend over to the bar marked G. Call this intersection point (P). Reading off this bar find a value 0.125 at (P). Returning to the main nomograph

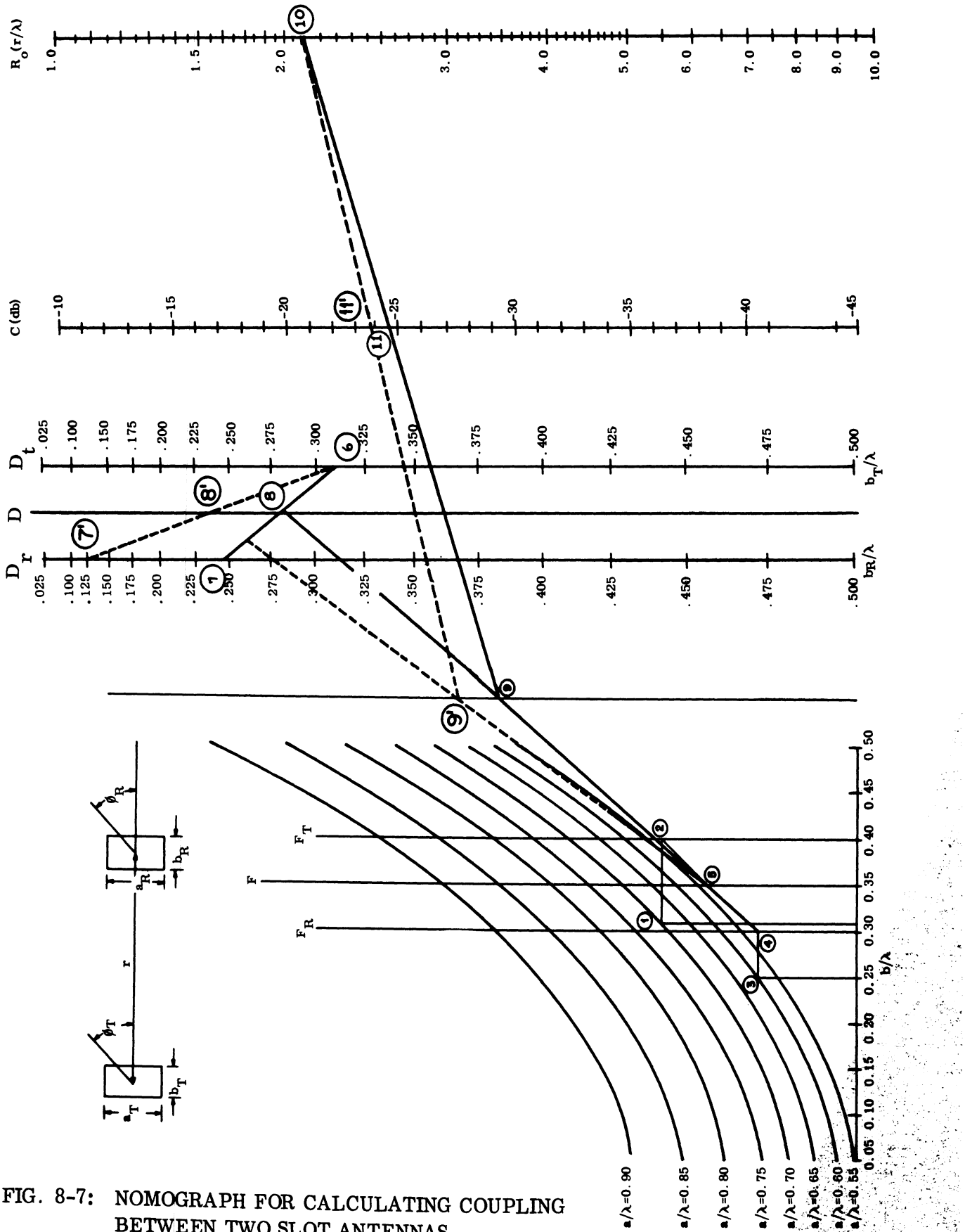

FIG. 8-7: NOMOGRAPH FOR CALCULATING COUPLING BETWEEN TWO SLOT ANTENNAS

of Fig. 8-7 and using the center stage of the nomograph enter the value of b_t (0.312λ) on bar D_t. Also enter the corrected D_r (0.125) obtained as point (P) on the nomograph of Fig. 8-8. This latter value of 0.125 is to be marked as point (7') on bar D_r in the center of the nomograph of Fig. 8-7. The value of b_t which has been entered on D_t is to be called (6). Draw a line from (6) to (7'). The intersection of this latter line with bar D is to be designated as (8'). Draw a line from the previously established point (5) to (8). The intersection of this line is to be designated as (9') on central bar. On the extreme right-hand bar of the nomograph of Fig. 8-8 indicate the spacing of two wavelengths at 2.0 and call this (10). Draw a line from (9') to (10). The intersection of this line with bar C is to be called (11'). Point (11') designates a value of coupling of 23.8 db. This value of coupling is not the true coupling for the sample problem but is an intermediate one which must be corrected in the manner described below.

On the nomograph of Fig. 8-9 enter the value of a_r (0.6) on the bottom horizontal bar. Call this (Q). Enter the angle 60^o on the slant bar toward the bottom of the nomograph of Fig. 8-9 and call this (S). Draw a line between (Q) and (S) letting it intersect the horizontal line immediately above and call this (U). Draw a vertical line from (U) upward to intersect the curve. Call this intersection (V). Draw a horizontal line from (V) to the right and let this line intersect the first vertical line. Call this intersection (W). On the extreme right hand bar of the nomograph of Fig. 8-9 put the value of 60^o and call this (X). Draw a line from (W) to (X) and designate the intersection of this line on bar K as (Y). The value at (Y) is -8.2 db, a coupling correction.

$$C_{tot} = C\,db + K\,db = -23.8\,db - 8.2\,db = -32\,db$$

where C_{tot} is the total resulting coupling. When both transmitting and receiving antennas are rotated, the same procedure on the supplementary nomographs

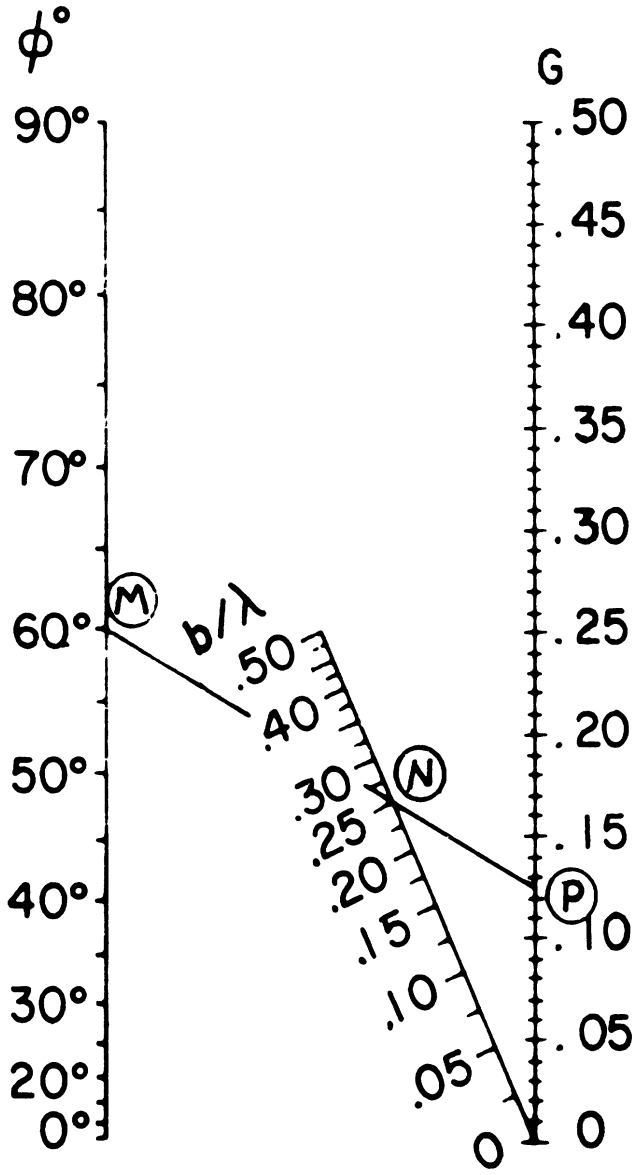

NOMOGRAPH (B)

FIG. 8-8: ANGULAR CORRECTION FOR WIDTH

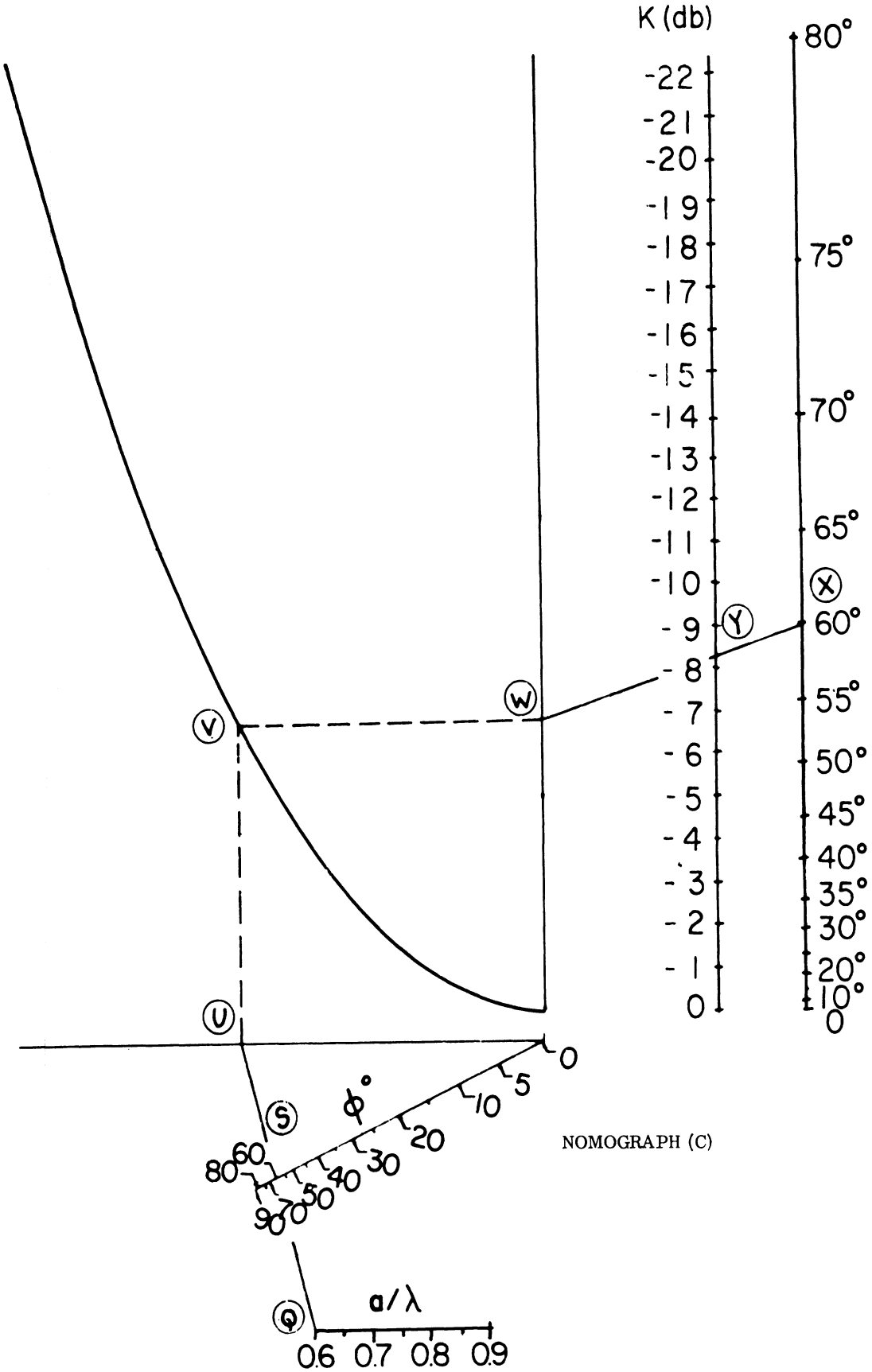

FIG. 8-9: ANGULAR CORRECTION FOR HEIGHTH

Figs. 8-8 and 8-9 must be made for each slot. The total coupling then would be;

$$C_{tot} = C\,db + K_r\,db + K_t\,db$$

K_t db and K_r db are obtained from Fig. 8-9.

8.2.6 Comparison of Calculations on Coupling

Some other typical combinations of coupling are listed in the following Table VIII-1 with spacing normalized to one wavelength and assuming a perfect impedance match.

	$\lambda/4$ monopole	Circular Spiral d = 10 cm	Rectangular Slot a=0.8λ, b=0.4λ	E-Sectoral a=0.75λ, b=2.5λ
$\lambda/4$ monopole	-17.7	-28	-17.8	-27
Circular Spiral	-28	-38	-28	-37
Rectangular Slot	-17.8	-28	-18	-27
E-Sectoral Horn	-27	-37	-27	-36

IX

REFERENCES

Blasi, E.A. (1954), "The Theory and Application of the Radiation Mutual-Coupling Factor," Proc. IRE, 42, No.7, pp. 1179-1183.

Crispin, J.W.Jr., R.F. Goodrich and K.M. Siegel (1959), "A Theoretical Method for the Calculation of the Radar Cross Sections of Aircraft and Missiles," The University of Michigan Radiation Laboratory Report No. 2591-1-H, AD 227 695 UNCLASSIFIED. 425 pgs.

Deschamps, J.G. (1951), "Geometrical Representation of the Polarization of a Plane Electromagnetic Wave," Proc. IRE, 39, pp. 540-544.

Ehrenspeck, H.W. and H. Poehler (1958), "A New Method for Obtaining Maximum Gain from Yagi Antennas," Air Force Cambridge Research Center Technical Report AFCRC-TR-58-355. UNCLASSIFIED:

Harrington, R.F. (1961), Time-Harmonic Electromagnetic Fields, McGraw-Hill p. 111.

Harrington, R.F. (1964), "Theory of Loaded Scatterers," Proc. IEE, (London) 111, No.4, pp. 617-623.

Hasserjian, G. and A. Ishimaru (1962), "Excitation of a Conducting Cylindrical Surface of Large Radius of Curvature," Trans. IRE, AP-10, No.3, pp.264-273.

Jacobs, E. (1960), "Maximum Power Transfer Between Large Aperture Antennas in the Fresnel Region," The University of Pennsylvania Report IS-60-UR-6, pp. 99-112.

Jasik, H. (1961), Antenna Engineering Handbook, McGraw-Hill, New York.

King, R.W.P. (1965), The Theory of Linear Antennas, Harvard University Press.

Marcuvitz, N. (1951) Waveguide Handbook, McGraw-Hill, New York.

Matthaei, G.L., L. Young and E.M.T. Jones (1964) Microwave Filter, Impedance-Matching Networks, McGraw-Hill, New York.

Met, V. (1959), "Absorptive Filters for Microwave Harmonic Power," Proc. IRE, 47, pp. 1862-1769.

Oberhettinger, F. (1954), "Diffraction of Waves by a Wedge," Comm. Pure and Appl. Math., 7, 551-563.

Rumsey, V.H. (1951), "Transmission Between Elliptically Polarized Antennas," Proc. IRE, 39, 535-540.

Kwon, Y.K. (1965), "Details of Mathematical Analysis of Rectangular Horn Apertures," The University of Michigan Radiation Laboratory Internal Memorandum.

Potter, P.D. (1963), "A New Horn Antenna with Suppressed Sidelobes and Equal Beamwidths," Microwave J., pp. 71-78. June.

Tai, C.T. (1961), "On the Definition of the Effective Aperture of Antennas," Trans. IRE, AP-9, No. 2, p. 224.

Vainshtein, L.A. (1959), "Waves of Current in a Thin Cylindrical Conductor-I, II" Sov. Phys. Tech. Phys., 4, pp. 601-626.

Vainshtein, L.A. (1961), "Current Waves in a Thin Cylindrical Conductor-III, IV" Sov. Phys. Tech. Phys., 6, pp. 19-38.

Silver, S. (1949). Microwave Antenna Theory and Design, McGraw-Hill, pp. 336-337.

X

ACKNOWLEDGEMENTS

Dr. Vaughan H. Weston and Dr. A.I. Simanyi of the Radiation Laboratory were major contributors of material in this report; Dr. Weston was responsible for the analysis of scattering as a factor in coupling as shown in Appendix B; Dr. Simanyi analyzed modal coupling and arranged the experiments on this subject; Mr. Richard B. Harris of The University of Michigan Institute of Science and Technology, was responsible for most of the experimental data included in this report.

APPENDIX A

ANALYSIS OF PLANAR APERTURE ANTENNA COUPLING

A.1 General

The present section is an excerpt from thesis work of Y-K Kwon to be published separately. Therefore frequent references are made to a complete internal memorandum (Kwon 1965). The purpose of the present study is the theoretical investigation of:

(i) Coupling of waveguide connected aperture antennas, and

(ii) Coupling of waveguide - horn connected aperture antennas.

To keep uniformity of the theory, (i) is treated as the degenerate case of (ii).

The two horn connected aperture antennas are shown in Fig. A-1 and Fig. A-2. The transmitting horn T_2 is excited by the waveguide T_1 and a measuring device is located in the waveguide R_1 connected to the receiving horn R_2. The coupling C between the two antennas is defined as the ratio of the power W_r received by the measuring device at R_1 to the power W_t transmitted from the aperture of transmitting antenna:

$$C = \frac{W_r}{W_t} \tag{1}$$

The calculation of W_r and W_t requires the correct knowledge of fields in R_1- and T_2- regions, which can only be evaluated through solving boundary value problems comprising the whole transmitting and receiving structures. This task is, no doubt, a staggering one, in view of the fact that the rigorous solution of a flush mounted antenna of the simplest geometry is yet to be obtained. However,

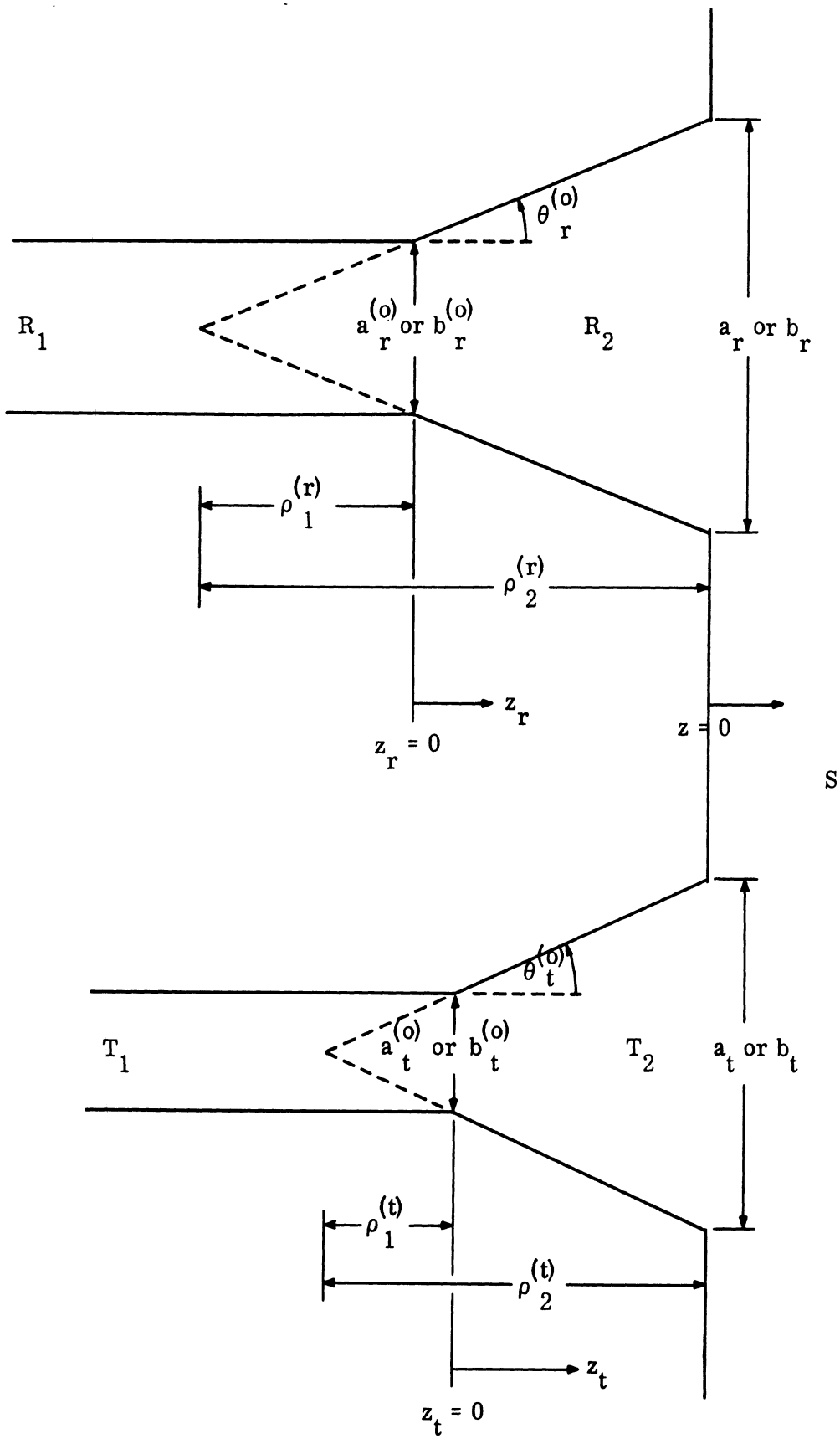

FIG. A-1: ANTENNA CONFIGURATION (SIDE VIEW)

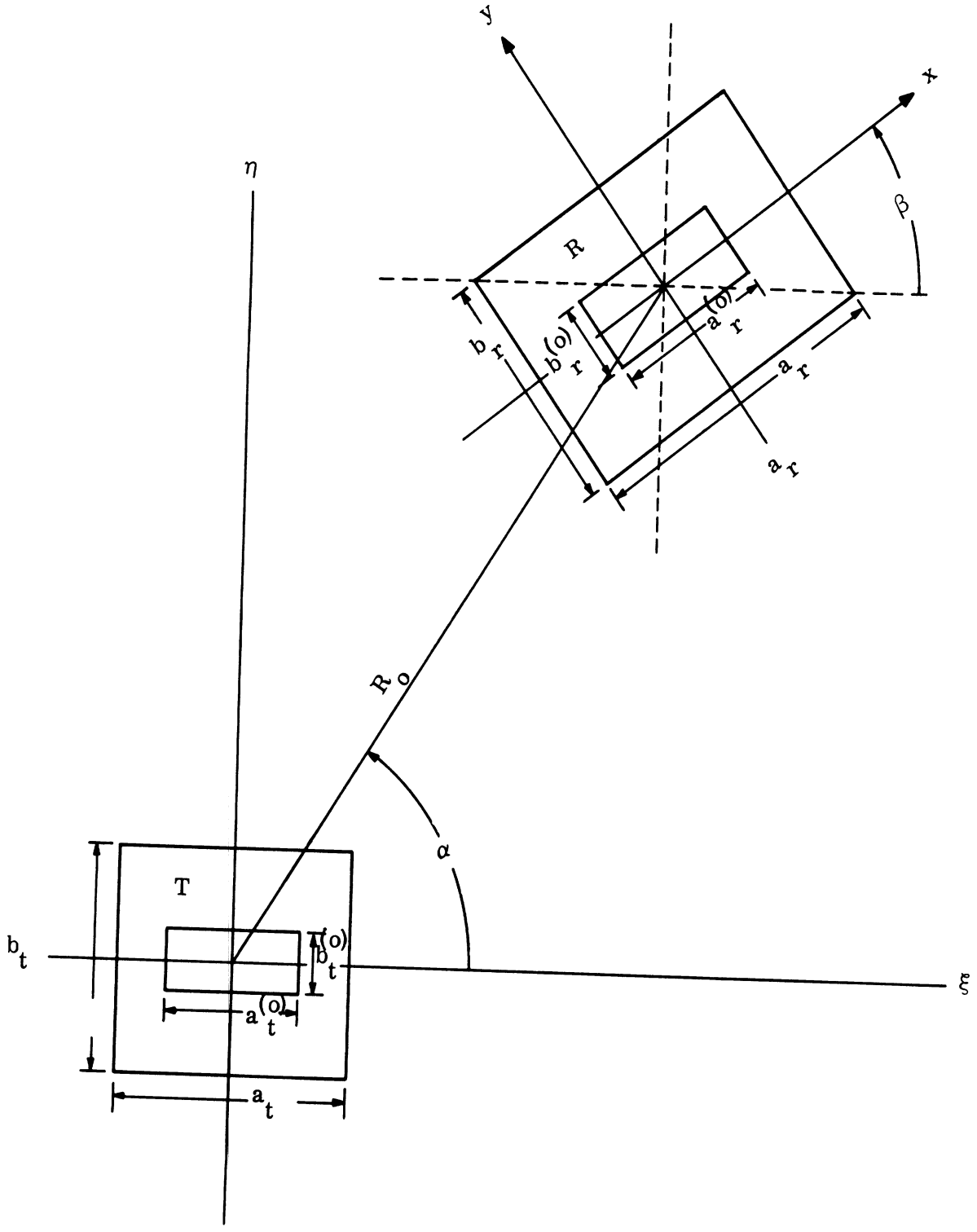

FIG. A-2: ANTENNA CONFIGURATION (FRONT VIEW)

under some reasonable assumptions, one can get formulas which predict experimental results with sufficient accuracy.

To determine the fields inside and outside of antenna systems, it is necessary and sufficient to specify the fields at the junctions, namely $z_t = 0$, $z_r = 0$ and $z = 0$. More specifically 1), the tangential components of Electrical fields at the apertures ($z = 0$) and junctions between waveguides and horns ($z_t = 0$ and $z_r = 0$) uniquely determine the fields everywhere. For regions T_1 and R_1, the tangential components of Electric field, $\bar{E}_t$, and tangential components of magnetic field $\bar{H}_t$ are given by:

$$\bar{E}_t(\bar{r}_{T_1}) = \sum_{i=1}^{\ell_t} V_i(z_t)\,\bar{e}_i(\bar{\rho}_t) + \sum_{j=\ell_t+1}^{\infty} V_j(z_t)\,\bar{e}_j(\bar{\rho}_t)$$

$$\bar{H}_t(\bar{r}_{T_1}) = \sum_{i=1}^{\ell_t} I_i(z_t)\,\bar{h}_i(\bar{\rho}_t) + \sum_{j=\ell_t+1}^{\infty} I_j(z_t)\,\bar{h}_j(\bar{\rho}_t) \qquad \text{(A.1)}$$

and

$$\bar{E}_t(\bar{r}_{R_1}) = \sum_{i=1}^{\ell_r} V_i(z_r)\,\bar{e}_i(\bar{\rho}_r) + \sum_{j=\ell_r+1}^{\infty} V_j(z_t)\,\bar{e}_j(\bar{\rho}_r)$$

$$\bar{H}_t(\bar{r}_{R_1}) = \sum_{i=1}^{\ell_r} I_i(z_r)\,\bar{h}_i(\bar{\rho}_r) + \sum_{j=\ell_r+1}^{\infty} I_j(z_t)\,\bar{h}_j(\bar{\rho}_r), \qquad \text{(A.2)}$$

In the above equations i and j are to be considered double summation indices and the first ℓ_t or ℓ_r modes are propagating ones and the remaining modes are decaying. The orthonormal transverse vector functions e_i and h_i are listed in Marcuvitz (1951). The amplitude factors V_i and I_i can be uniquely specified in terms of tangential electric fields at $z_t = 0$ or at $z_r = 0$ and the incident fields (Kwon 1965). The position vectors in the waveguides are decomposed into longitudinal components and transverse components:

$$\bar{r}_{T_1} = \bar{\rho}_t + \hat{z}\, z_t$$

$$\bar{r}_{R_1} = \bar{\rho}_r + \hat{z}\, z_r \qquad \hat{z}\text{: unit vector in z-direction} \tag{A.3}$$

For region S, the magnetic field is given by

$$\bar{H}(\bar{R}_s) = -\iint \bar{\bar{Y}}(\bar{R}_s : \bar{\rho}_t) \cdot \bar{M}_T(\bar{\rho}_t,\, z=0)\, dS_T - \iint \bar{\bar{Y}}(\bar{R}_s : \bar{\rho}_r)\, \bar{M}_R(\bar{\rho}_r,\, z=0)\, dS_R, \tag{A.4}$$

where the integrations are performed over the aperture S_T and S_B respectively, and

$$\bar{\bar{Y}}(\bar{R}_s : \bar{\rho}) = +\frac{i}{2\pi\omega\mu}\,(k^2 \bar{\bar{I}} + \nabla\nabla)\,\frac{e^{-ik\left|\bar{R}_s - \bar{\rho}\right|}}{\left|\bar{R}_s - \bar{\rho}\right|} \tag{A.5}$$

(∇ operates on $\bar{R}_s$)

$$\bar{M}_T = \bar{E}(\bar{\rho}_t,\, z=0) \times \hat{z} \tag{A.6a}$$

$$\overline{M}_R = \overline{E}(\overline{\rho}_r,\ z=0) \times \hat{z} \tag{A.6b}$$

$$\overline{\overline{I}} = \text{unit dyad} \tag{A.6c}$$

Next, the fields in the regions T_2 and R_2 should be specified. For an E-sectoral horn, the transverse components of the magnetic fields are given by (Kwon 1965 Section III):

$$H_x = \sum_{m=1}^{\infty}\sum_{p=0}^{\infty} \gamma_m^2 Z_{\frac{p\pi}{2\theta_o}}(\gamma_m\rho) \sin\frac{m\pi x_1}{a} \cos\frac{p\pi\phi}{2\theta_o} \tag{A.7a}$$

$$H_y = \sum_{m=1}^{\infty}\sum_{p=0}^{\infty} \left(\frac{m\pi}{a}\right)\left\{\frac{y}{\rho}\frac{d}{d\rho} Z_{\frac{p\pi}{2\theta_o}}(\gamma_m\rho) \cos\frac{p\pi\phi}{2\theta_o}\right.$$

$$\left. - \frac{u}{\rho}\left(\frac{p\pi}{2\theta_o}\right)\frac{1}{\rho} Z_{\frac{p\pi}{2\theta_o}}(\gamma_m\rho) \sin\frac{p\pi\phi}{2\theta_o}\right\}\cos\frac{m\pi x_1}{a}$$

$$+ j\omega\epsilon \sum_{n=0}^{\infty}\sum_{q=1}^{\infty}\left\{\frac{y}{\rho}\frac{1}{\rho} W_{\frac{q\pi}{2\theta_o}}(\gamma_n\rho) \cos\frac{p\pi\phi}{2\theta_o}\right.$$

$$\left. - \frac{u}{\rho}\frac{d}{d\rho} W_{\frac{q\pi}{2\theta_o}}(\gamma_n\rho) \sin\frac{p\pi\phi}{2\theta_o}\right\}\cos\frac{n\pi x_1}{a} \tag{A.7b}$$

where ρ, ρ_1, θ_o, a, etc., are pictorially shown in Fig. A.3 and

$$x_1 = x + \frac{a}{2} \qquad \rho = \sqrt{y^2 + u^2}$$

$$\phi = \theta + \theta_o \qquad u = \rho_1 + z_t \text{ (or } z_r)$$

$$\gamma_m^2 = k^2 - \frac{m^2\pi^2}{a^2} \tag{A.8}$$

$$Z_{\frac{p\pi}{2\theta_o}}(\gamma_m\rho) = A_{mp} H_{\frac{p\pi}{2\theta_o}}(\gamma_m\rho) + B_{mp} H^{(2)}_{\frac{p\pi}{2\theta_o}}(\gamma_m\rho) \tag{A.9a}$$

$$W_{\frac{q\pi}{2\theta_o}}(\gamma_n\rho) = C_{nq} H_{\frac{q\pi}{2\theta_o}}(\gamma_n\rho) + D_{nq} H_{\frac{q\pi}{2\theta_o}}(\gamma_n\rho) \tag{A.9b}$$

and A_{mp}, B_{mp}, C_{nq}, and D_{nq} are complex constants to be determined by boundary conditions.

As one can see from the above horn mode-functions the absence of orthogonality with respect to y-coordinate makes the determination of constants, A_{mp}, B_{mp}, C_{nq} and D_{nq} extremely difficult. Of course, with respect to a cylindrical coordinate system with x as the axial coordinate, one can construct orthonormal vector functions of the E-sectoral horn. Then one encounters ever more serious difficulties in the waveguide regions and half-space region. In other words, it is impossible to find one coordinate system which preserves orthogonality of vector

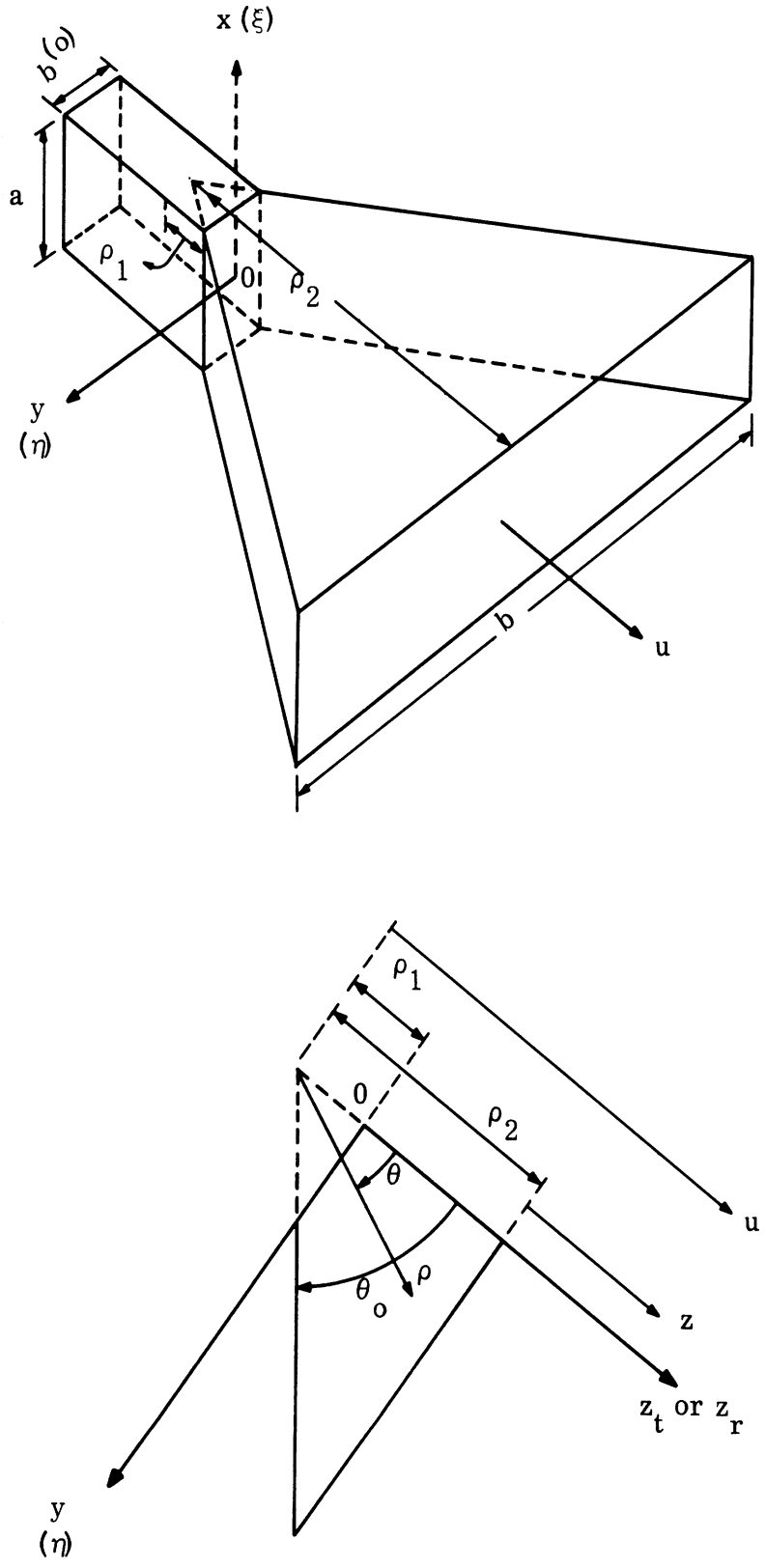

FIG. A-3: COORDINATE OF E-SECTORAL HORN

mode functions in all regions. For E-sectoral horn, this difficulty is less serious, because it still keeps the orthogonality in x-direction. This indicates that if one considers only TE_{mo} -modes in the E-sectoral horn, the preservation of orthogonality is achieved.

One of the major difficulties in the analysis of the present problem is the lack of orthogonality in the horn region with respect to a rectangular coordinate system in which the vector mode-functions of waveguide and the total field in the half-space beyond the metal plane are specified. To overcome this difficulty, a formalism to express the fields in the horn region in terms of uniform waveguide modes is developed (Kwon 1965). With this formalism, the tangential components of fields can be expressed in forms exactly the same as equation (A. 1) or equation (A. 2) with the same forms of transverse vector mode functions $\bar{e}_i$ and $\bar{h}_i$. The amplitudes of the modes V_i and I_i are determined by the differential equations:

$$\frac{dV_i'}{dz} + A_i' V_i' + j\omega\mu \frac{\gamma_i'^2}{k^2} I_i' = - \sum_{j(j\neq i)} E_{ij}' V_j' - \sum_p M_{ip} V_p'' \qquad \text{(A. 10a)}$$

$$\frac{dI_i'}{dz} - A_i' I_i' + j\omega \epsilon V_i' = - \sum_{j(j\neq i)} H_{ij}' I_j' - \sum_p N_{ip} I_p'', \qquad \text{(A. 10b)}$$

The summations over the double index j exclude $j=i$. These equations are for TM modes.

$$\frac{dI_q''}{dz} - A_q'' I_q'' + j\omega\epsilon \frac{\gamma_q''^2}{k^2} V_q'' = -\sum_j M_{qj}^{+} I_j' - \sum_{p(p\neq q)} H_{qp}'' I_p'' \qquad \text{(A.11a)}$$

$$\frac{dV_q''}{dz} + A_q'' V_q'' + j\omega\mu I_q'' = -\sum_j N_{qj}^{+} V_j' - \sum_{p(p\neq q)} E_{qp}'' V_p'' \qquad \text{(A.11b)}$$

The summation over the double index p excludes the case p = q. These equations for TE-modes. The coefficients are functions of z and are defined as

$$A_i' \equiv \frac{1}{2}\oint \tan\theta_o \left|\bar{e}_i'\right|^2 ds = \frac{1}{2}\oint \tan\theta_o \left|\bar{h}_i'\right|^2 ds \qquad \text{(A.12a)}$$

$$A_q'' \equiv \frac{1}{2}\oint \tan\theta_o \left|\bar{e}_q''\right|^2 ds = \frac{1}{2}\oint \tan\theta_o \left|\bar{h}_i''\right|^2 ds \qquad \text{(A.12b)}$$

$$E_{ij}' \equiv \iint \frac{d\bar{e}_i'}{dz}\cdot\bar{e}_j' \, dS = \iint \bar{h}_j'\cdot\frac{d\bar{h}_i'}{dz} \, dS \equiv H_{ji}' \qquad \text{(A.13a)}$$

$$H_{qp}'' \equiv \iint \bar{h}_q''\cdot\frac{d\bar{h}_p''}{dz} \, dS = \iint \frac{de_p''}{dz}\cdot\bar{e}_q'' \, dS \equiv E_{pq}'' \qquad \text{(A.13b)}$$

$$M_{ip} \equiv \iint \frac{d\bar{e}_i'}{dz} \, \bar{e}_p'' \, dS = \iint \bar{h}_p'' \, \frac{d\bar{h}_i'}{dz} \, dS \equiv M_{pi}^{\dagger} \qquad \text{(A.13c)}$$

$$N_{ip} \equiv \iint \bar{h}_i' \cdot \frac{d\bar{h}_p''}{dz}\, dS = \iint \frac{d\bar{e}_p''}{dz} \cdot \bar{e}_i'\, dS \equiv N_{pi}^{\dagger} \qquad \text{(A.13d)}$$

S is any transverse cross-section of the horn and s is the contour of S. $\theta^{(0)}$ is half of the flare angle. For rectangular horns, these coefficients are calculated and tabulated (Kwon 1965, Section V). When θ_o becomes zero, the A's, $\frac{d\bar{e}_i}{dz}$ and $\frac{d\bar{h}_i}{dz}$ go to zero, hence equations (A.11) are reduced to the ordinary waveguide transmission line equations.

A.2 The Coupling of Two Waveguide Connected Aperture Antennas

The present problem (Kwon 1965, Sections III and VII) is the degenerate case of the general situation in which the regions T_2 and R_2 are eliminated and the regions T_1 and R_1 are directly connected to the half-space S. Now, (A.1) and (A.4) are connected by invoking the continuity of tangential magnetic field on aperture T. Equating $\hat{z} \times \bar{H}$ on the aperture T, one obtains the following integral equation:

$$\sum_{i=1}^{\ell_t} I_i^{(T)}\, \hat{z} \times \bar{h}_i(\bar{\rho}_t) + \sum_{j=\ell_t+1}^{\infty} I_j^{(T)}\, \hat{z} \times \bar{h}_j(\bar{\rho}_t) = \hat{z} \times \iint \bar{\bar{Y}}(\bar{\rho}_t : \bar{\rho}_t')\, \hat{z} \times \bar{E}(\bar{\rho}_t')\, dS_T'$$

$$+ \hat{z} \times \iint \bar{\bar{Y}}(\bar{\rho}_t : \bar{\rho}_r) \cdot \left[\hat{z} \times \bar{E}(\bar{\rho}_r)\right] dS_r \qquad \text{(A.14a)}$$

The same operation on the aperture R yields:

$$\sum_{i=1}^{\ell_r} I_i^{(R)} \hat{z} \times \bar{h}_i(\bar{\rho}_r) + \sum_{j=\ell_r+1}^{\infty} I_j^{(R)} \hat{z} \times \bar{h}_j(\bar{\rho}_r) = \hat{z} \times \iint \bar{\bar{Y}}(\bar{\rho}_r : \bar{\rho}_t) \cdot \left[\hat{z} \times \bar{E}(\bar{\rho}_t)\right] dS_T$$

$$+ \hat{z} \times \iint \bar{\bar{Y}}(\bar{\rho}_r : \bar{\rho}_r') \cdot \left[\hat{z} \times \bar{E}(\bar{\rho}_r')\right] dS_R' \qquad \text{(A.14b)}$$

Since z_t and z_r in eqs. (A.1) and (A.2) are replaced by z throughout the present section, the subscripts "T" and "R" are used to indicate modal amplitudes of two waveguides.

An exact solution of the integral equations (A.14) is extremely difficult. Thus, it is desirable to employ some approximations. The usual approach to the approximation is setting up a variational formulation which is not sensitive to the exact nature of the aperture fields (Kwon 1965). The limited space for this section does not permit going into this formulation. As an alternate approach, eq. (A.14b) is multiplied in dot product fashion by $\hat{z} \times \bar{h}_i(\bar{\rho}_r)$ and the result is integrated over the aperture. Then, the following equations are obtained due to orthonormality of $\bar{h}_i$ (Marcuvitz 1951).

$$I_i^{(R)} = \iint dS_R \iint dS_T \, \bar{h}_i(\bar{\rho}_r) \cdot \bar{\bar{Y}}(\bar{\rho}_r : \bar{\rho}_t) \cdot \left[\hat{z}_o \times \bar{E}(\bar{\rho}_t)\right]$$

$$+ \iint dS_R \iint dS_R' \, \bar{h}_i(\bar{\rho}_r) \cdot \bar{\bar{Y}}(\bar{\rho}_r : \bar{\rho}_r') \cdot \left[\hat{z}_o \times \bar{E}(\bar{\rho}_r')\right] \qquad \text{(A.15)}$$

Similar expressions for $I_i^{(T)}$ can be obtained by interchanging $\bar{\rho}_r$ and $\bar{\rho}_t$ in the above equation. The accurate knowledge of the aperture fields $\bar{E}(\bar{\rho}_t)$ and $\bar{E}(\bar{\rho}_r)$ determines modal amplitudes in the guide regions, hence the fields. Since

the determination of $\overline{E}(\overline{\rho}_t)$ and $\overline{E}(\overline{\rho}_r)$ is difficult, one usually resorts to some assumptions compatible with boundary conditions and physical intuition. It is also to be noted that $\overline{E}(\overline{\rho}_t)$ on the transmitting aperture and $\overline{E}(\overline{\rho}_r)$ on the receiving aperture are mutually related. To clarify the inter-relation between $\overline{E}(\overline{\rho}_t)$ and $\overline{E}(\overline{\rho}_r)$ and introduce some assumptions, the following observations are made.

1. On the receiving aperture, the tangential magnetic fields satisfy:

$$\hat{z} \times \overline{H}_{in} = \hat{z} \times \overline{H}_s + \hat{z} \times \overline{H}_o \qquad \text{(A.16a)}$$

or

$$\hat{z} \times \left[\overline{H}_{in} - \overline{H}_s\right] = \hat{z} \times \overline{H}_o, \qquad \text{(A.16b)}$$

where $\overline{H}_o$ is field produced by the source (i.e., magnetic current in the transmitting aperture) when the receiving aperture is closed by perfect conductor. $\overline{H}_{in}$ and $\overline{H}_s$ are the scattered fields inside the guides and in the half-space when the conductor is removed.

2. Equation (A.16a) is exactly equivalent to eq. (A.14b). Since $\hat{z} \times \overline{H}_o$ never vanishes and both of the scattered fields $\overline{H}_{in}$ and $\overline{H}_s$ are smaller, in magnitude, than $\overline{H}_o$, then one can write:

$$\hat{z} \times \overline{H}_s = -c\, \hat{z} \times \overline{H}_{in}, \qquad \text{(A.17a)}$$

where c is complex number and,

$$\hat{z} \times \overline{H}_{in} = \frac{1}{1+c}\, \hat{z} \times \overline{H}_o \qquad \text{(A.17b)}$$

3. If the waveguide is removed, one has a symmetrically located groundplane with a hole in it. In this case, as in diffraction theory, C equals to 1 and

$$\hat{z} \times \bar{H}_{in} = \frac{1}{2} \hat{z} \times \bar{H}_{o} \tag{A.18}$$

4. Therefore, one can conclude that

$$\frac{1}{2} < \left| \frac{1}{1+c} \right| < 1 \tag{A.19}$$

In the subsequent analysis, c is assumed to be 1.

In view of the above approximation and (A.14b), eq. (A.15) becomes

$$I_i^{(R)} = \frac{1}{2} \iint dS_R \iint dS_T \, \bar{h}_i(\bar{\rho}_r) \cdot \bar{\bar{Y}}(\bar{\rho}_r : \bar{\rho}_t) \cdot \left[\hat{z}_o \times \bar{E}(\bar{\rho}_t) \right] \tag{A.20}$$

Next, (A.20) is used to compute the TE_{m0} mode coupling of two waveguide terminated antennas (Kwon, 1965). It is, now, assumed that the transmitting aperture field is a linear combination of TE_{m0} modes of transmitting guide, i.e.,

$$\bar{E}(\bar{\rho}_A) = \sum_{m'=1}^{\infty} V_{m'0}^{(T)} \, \bar{e}''_{m'0}(\bar{\rho}_t) \tag{A.21}$$

Substituting (A.21) into (A.20), one gets:

$$I_{mo}^{(R)} = \frac{1}{2} \sum_{m'=1}^{\infty} V_{m'0}^{(t)} \iint dS_R \iint dS_T \, \bar{h}''_{m0}(\bar{\rho}_r) \cdot \bar{\bar{Y}}(\bar{\rho}_r : \bar{\rho}_t) \cdot \bar{h}''_{m'0}(\bar{\rho}_t) , \tag{A.22}$$

where the relation $z \times \bar{e}''_{m'0} = \bar{h}''_{m'0}$ is used. Since only TE_{mo} modes are considered further, double primes are omitted henceforth. Now

$$\bar{h}_{m0} = \sqrt{\frac{2}{ab}} \sin \frac{m\pi x_1}{a}, \text{ where } x_1 = x + \frac{a}{2} \tag{A.23}$$

and using eq. (A.5), the eq. (A.22) becomes

$$I^{(R)}_{m0} = \frac{1}{2\pi j\omega\mu} \frac{1}{\sqrt{(a_t b_t)(a_r b_r)}} \sum_{m'=1}^{\infty} V^{(T)}_{m'0} \int_0^{a_t} d\xi_1 \int_0^{b_t} d\eta_1 \int_0^{a_r} dx_1 \int_0^{b_r} dy_1$$

$$\cdot \sin \frac{m'\pi\xi_1}{a_t} \sin \frac{m\pi x_1}{a_r} \hat{x} \cdot (k^2 \bar{\bar{I}} + \nabla\nabla) \cdot \hat{\xi}\, G(\xi, \eta : x, y), \tag{A.24}$$

where

$$G(\xi, \eta : x, y) = \frac{e^{-jk\sqrt{(x-\xi)^2 + (y-\eta)^2}}}{\sqrt{(x-\xi)^2 + (y-\eta)^2}} \tag{A.25}$$

For other notations, refer to Fig. (A-2). After some algebraic manipulations one gets:

$$I^{(R)}_{m0} = -\frac{1}{2\pi j\omega\mu} \frac{1}{\sqrt{(a_t b_t)(a_r b_r)}} \sum_{m'=1}^{\infty} J_{m0, m'0}\, V^{(T)}_{m'0} \tag{A.26}$$

where

$$J_{m0,m'0} = \int_0^{a_t} d\xi_1 \sin\frac{m'\pi\xi_1}{a_t} \Bigg\{ \cos\beta\left(k^2 - \frac{m^2\pi^2}{a_r^2}\right) \int_0^{b_t} d\eta_1 \int_0^{a_r} dx_1 \int_0^{b_r} dy_1 \sin\frac{m\pi x_1}{a_r} G(x,y:\xi,\eta)$$

$$- \cos\beta\left(\frac{m\pi}{a_r}\right) \int_0^{b_t} d\eta_1 \int_0^{b_r} dy_1 \left[(-1)^m G\left(x=\frac{a_r}{2}\right) - G\left(x=-\frac{a_r}{2}\right)\right]$$

$$+ \sin\beta\left(\frac{m\pi}{a_r}\right) \int_0^{b_t} d\eta_1 \int_0^{a_r} dx_1 \cos\frac{m\pi x_1}{a_r} \left[G\left(y=\frac{b_r}{2}\right) - G\left(y=-\frac{b_r}{2}\right)\right] \Bigg\} \qquad (A.27)$$

where

$$G\left(x=\frac{a_r}{2}\right) = G\left(x=\frac{a_r}{2}, y:\xi,\eta\right) \text{ etc.} \qquad (A.28)$$

The exact evaluation of $J_{m0,m'0}$ is extremely difficult. However, for special cases, $J_{m0,m'0}$ can be reduced to more manageable form. Before evaluating the integrals in (A.27) approximately, the special cases will be studied.

Case 1) $\beta = 0$, $a_t = a_r = a$, $b_t = b_r = b$. For this case (A.27) becomes:

$$J_{m0,m'0} = \frac{1}{2}\left(\frac{ka}{\pi}\right)^2 \left(\frac{a}{\pi}\right) \int_{-\frac{b}{a}\pi}^{\frac{b}{a}\pi} d\sigma \left(\frac{b}{a}\pi - |\sigma|\right) \int_0^{\pi} d\lambda$$

$$\cdot \left[\delta_{mm'} \left\{ \left(1 - \frac{m^2\pi^2}{k^2a^2}\right)(\pi - \lambda)\cos m\lambda + \frac{1}{m}\left(1 + \frac{m^2\pi^2}{k^2a^2}\right)\sin m\lambda \right\} \right.$$

$$-2(1-\delta_{mm'}) \left\{ \left(1 - \frac{m^2\pi^2}{k^2a^2}\right) \left[\frac{\cos\frac{(m+m')\lambda}{2}\sin\frac{(m-m')\lambda}{2}}{m-m'} \right.\right.$$

$$\left.\left. - \frac{\cos\frac{(m-m')\lambda}{2}\sin\frac{(m+m')\lambda}{2}}{m+m'} \right] - \left(\frac{m\pi}{ka}\right)^2 \frac{1}{m}\sin m'\lambda \right\} \Bigg] \cdot$$

$$\cdot \left[h\left(\frac{R_o}{a}\pi\cos\alpha + \lambda, \frac{R_o}{a}\pi\sin\alpha + \sigma\right) + h\left(\frac{R_o}{a}\pi\sin\alpha - \lambda, \frac{R_o}{a}\pi\sin\alpha + \sigma\right) \right]$$

(A.29a)

(m and m' are either both even or both odd)

where

$$h(t,s) = \frac{e^{-j\frac{ka}{\pi}\sqrt{t^2+s^2}}}{\sqrt{t^2+s^2}}$$

R_o is the center-to-center distance of two apertures.

$$J_{m0,m'0} = \left(\frac{ka}{\pi}\right)^2 \frac{a}{\pi} \int_{-\frac{b}{a}\pi}^{\frac{b}{a}\pi} d\sigma \left(\frac{b}{a}\pi - |\sigma|\right) \int_0^{\pi} d\lambda$$

$$\left\{\left(1 - \frac{m^2\pi^2}{k^2a^2}\right)\left[\frac{\sin\frac{(m-m')\lambda}{2}\cos\frac{(m+m')\lambda}{2}}{m+m'} - \frac{\sin\frac{(m+m')\lambda}{2}\cos\frac{(m-m')\lambda}{2}}{m-m'}\right]\right.$$

$$\left.\left\{h\left(\frac{R_o}{a}\pi\cos\alpha+\lambda, \frac{R_o}{a}\pi\sin\alpha+\sigma\right) - h\left(\frac{R_o}{a}\pi\cos\alpha-\lambda, \frac{R_o}{a}\pi\sin\alpha+\sigma\right)\right\}\right. \tag{A.29b}$$

(for m = odd, m' = even or m = even, m' = odd)

The following theorems can be obtained from eqs. (A.29a) and (A.29b).

Theorem 1: If $\frac{R_o}{a}\cos\alpha > 1$, $\sin\alpha \neq 0$, m = odd and m' = odd, $J_{m0,m'0}$ is of the order of $\frac{1}{R_o}$ as R_o becomes large. (Up to theorem 4, $\beta = 0$ is assumed).

Theorem 2: If $\frac{R_o}{a}\cos\alpha > 1$, $\sin\alpha \neq 0$, m = even and m' = even, $J_{m0,m'0}$ is, at most, of the order of $\frac{1}{R_o^2}$ as R_o becomes large.

Theorem 3: If $\frac{R_o}{a}\cos\alpha > 1$, $\sin\alpha \neq 0$ and (m = even, m' = odd) or (m = odd, m' = even), $J_{m0,m'0}$ becomes proportional to $\cos\alpha / R_o$ as R_o becomes large.

Theorem 4: If $\sin\alpha = 0$ and $\frac{R_o}{a} - 1 > \frac{b}{a}$, $J_{m0,m'0}$ is, at most, of the order of $\frac{1}{R_o^2}$.

Nomenclature of these theorems is indicated in the Fig. A-4(a) and A-4(b).

Before going into the next case, the exact coupling formula for m = 1 and m' = 1 is given for the purpose of comparison with experiment. The formula has the following expression

$$C = \frac{1}{32}\,\frac{1}{\pi^2}\,\frac{1}{(\gamma_1 b)}\,\left(\frac{ka}{\pi}\right)^2\,\frac{|K|^2}{R_{11}} \tag{A.30}$$

$$K = \int_{-\frac{b}{a}\pi}^{\frac{b}{a}\pi} \left(\frac{b}{a}\pi - |\sigma|\right) d\sigma \int_0^{\pi} d\lambda \left[\left(1 - \frac{\pi^2}{k^2 a^2}\right)(\pi - \lambda)\cos\lambda + \left(1 + \frac{\pi^2}{k^2 a^2}\right)\sin\lambda\right] \cdot$$

$$\cdot \left[h\left(\frac{R_o}{a}\,\pi\cos\alpha + \lambda,\ \frac{R_o}{a}\,\pi\sin\alpha + \sigma\right) + \left(\frac{R_o}{a}\,\pi\sin\alpha - \lambda,\ \frac{R_o}{a}\,\pi\sin\alpha + \sigma\right)\right] \tag{A.31}$$

$$\gamma_1 = k\sqrt{1 - \left(\frac{\pi}{ka}\right)^2}$$

$$\text{If} \begin{cases} \beta = 0 \\ \dfrac{R_o}{a}\cos\alpha > 1 \\ \sin\alpha \neq 0 \end{cases}$$

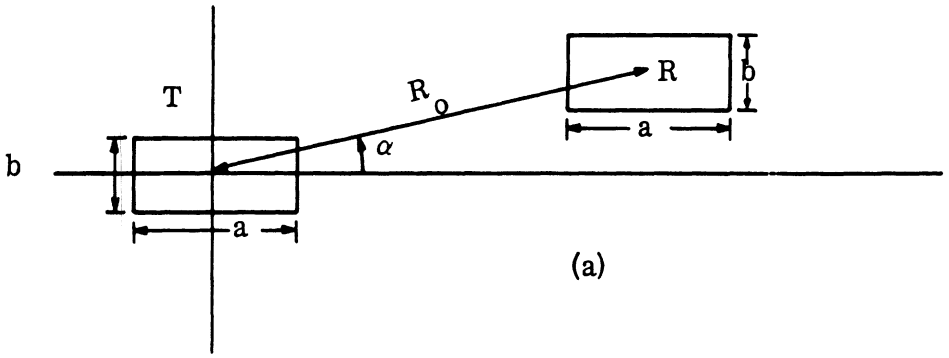

(a)

(1) $J_{m0,m'0} \sim \frac{1}{R_o}$ (far-field coupling) for m = odd, m' = odd

(2) $J_{m0,m'0} \lesssim \frac{1}{R_o^2}$ (near-field coupling) for m = even, m' = even

(3) $J_{m0,m'0} \sim \frac{\cos\alpha}{R_o}$ for m = odd, m' = even or m = even, m' = odd

If $\beta = 0$, $\frac{R_o}{a} > 1$, $\sin\alpha = 0$, $J_{m0,m'0} \frac{1}{R_o^2}$ (near-field coupling)

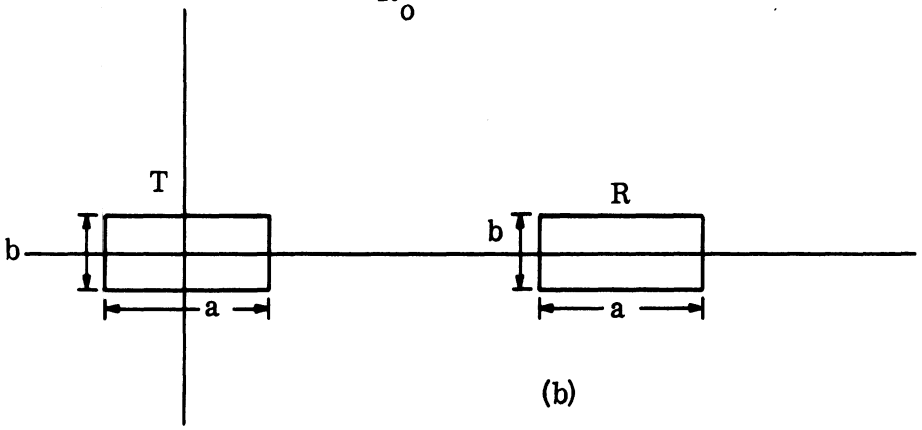

(b)

FIG. A-4: PICTORIAL ILLUSTRATION OF THEOREMS FOR $\beta = 0$

R_{11} is given by eq. (A.43).

C is plotted in the graph of Fig. A-5 for $\alpha = 0^o$, $\alpha = 10^o$, $\alpha = 45^o$ and $\alpha = 90^o$. For $\alpha = 0^o$ and $\alpha = 90^o$, the experimental values are also given. A computer program is available for similar cases as shown in the graph, but for any size slots the transmitting and receiving slots need not be the same size.

Case 2) $\beta = \frac{\pi}{2}$

For this case (A.27) becomes:

$$J_{m0,m'0} = \left(\frac{m\pi}{a_2}\right) \int_{-\frac{b_t}{2}}^{\frac{b_t}{2}} d\eta \int_{-\frac{a_t}{2}}^{\frac{a_t}{2}} d\xi \int_{-\frac{a_r}{2}}^{\frac{a_r}{2}} dx \Big[\left(\cos\frac{m\pi}{2}\right)\left(\cos\frac{m'\pi}{2}\right)\cos\frac{m\pi x}{a_r}\cos\frac{m'\pi\xi}{a_t}$$

$$-\left(\sin\frac{m\pi}{2}\right)\left(\sin\frac{m'\pi}{2}\right)\sin\frac{m\pi x}{a_r}\cos\frac{m'\pi\xi}{a_t} + \left(\cos\frac{m\pi}{2}\right)\left(\sin\frac{m'\pi}{2}\right)\cos\frac{m\pi x}{a_r}\cos\frac{m'\pi\xi}{a_t}$$

$$-\left(\sin\frac{m\pi}{2}\right)\left(\cos\frac{m'\pi}{2}\right)\sin\frac{m\pi x}{a_r}\sin\frac{m'\pi\xi}{a_t}\Big] \cdot \Big[g\left(R_o\cos\alpha - \frac{b_r}{2} - \xi,\ R_o\sin\alpha + x - \eta\right)$$

$$- g\left(R_o\cos\alpha + \frac{b_r}{2} - \xi,\ R_o\sin\alpha + x - \eta\right)\Big] \qquad \text{(A.32)}$$

where

$$g(u, v) = \frac{e^{-jk\sqrt{u^2+v^2}}}{\sqrt{u^2+v^2}}$$

Further reduction of the above triple integral seems to be impossible unless $a_r = b_t$. Some physical significance is extracted from (A.32) when put in the form of theorems.

Theorem 1: If $\alpha = \frac{\pi}{2}$, the odd modes of the transmitting aperture field do not contribute to the coupling, i.e.,

$$J_{m0,m'0} = 0, \text{ if } m' = 0.$$

Theorem 2: If $\alpha = 0$, no odd modes are generated in the receiving guide, i.e.,

$$J_{m0,m'0} = 0, \text{ if } m = \text{odd}$$

Theorem 3: If $\alpha = \frac{\pi}{2}$, m' = even, and

$$R_o - \frac{(b_t + a_r)}{2} > \frac{a_t + b_t}{2}, \text{ then}$$

$J_{m0,m'0}$ is, at most, of the order of $\frac{1}{R_o^2}$ as R_o becomes large.

Theorem 4: If $\alpha = 0$, m = even and

$$R_o - \frac{(a_t + b_r)}{2} > \frac{a_t + b_t}{2},$$

$J_{m0,m'0}$ is, at most, of the order of $\frac{1}{R_o^2}$ as R_o becomes large. The above four theorems are summarized in Fig. A-5.

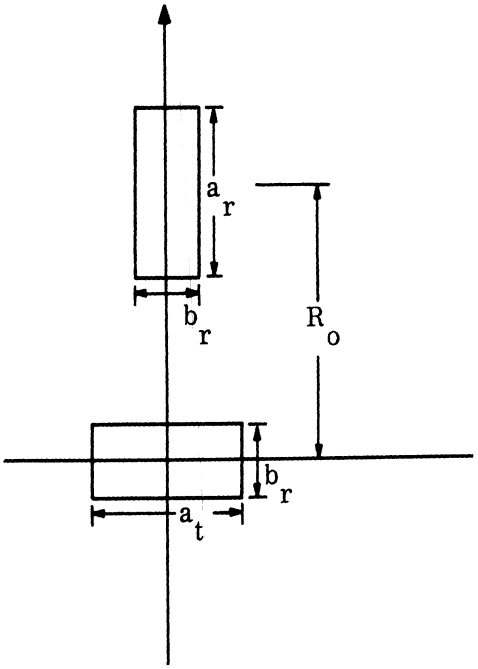

If $\begin{cases} \beta = \frac{\pi}{2} \left(\text{or } \frac{3\pi}{2}\right) \\ \sin\alpha = 1 \end{cases}$

(1) $J_{m0,m'0} = 0$ for m' = odd

(no coupling)

(2) $J_{m0,m'0} \sim \frac{1}{R_o^2}$ for m' = even

(near-field coupling)

(a)

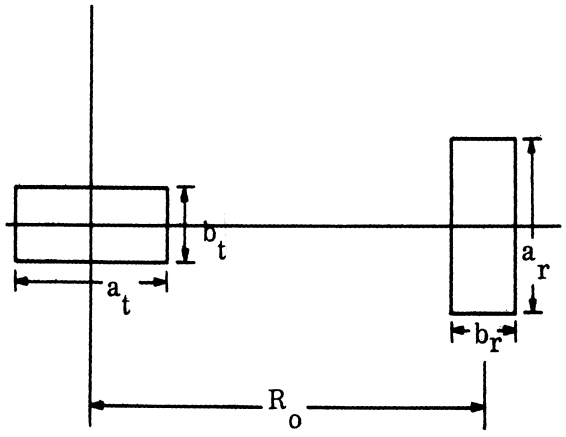

If $\begin{cases} \beta = \frac{\pi}{2} \left(\text{or } \frac{3\pi}{2}\right) \\ \sin\alpha = 1 \end{cases}$

(1) $J_{m0,m'0} = 0$ for m = odd

(2) $J_{m0,m'0} \lesssim \frac{1}{R_o^2}$ for m = even

(near field coupling)

(b)

FIG. A-5: PICTORIAL ILLUSTRATION OF THEOREMS FOR $\beta = \frac{\pi}{2}$

To evaluate the integral in (A.27) for general use, the following approximation is made:

$$G(x,y:\xi\mu) \doteq \frac{e^{-jkR_o}}{R_o}\left[1 - \frac{x}{R_o}\cos(\alpha-\beta) - \frac{y}{R_o}\sin(\alpha-\beta) + \frac{\xi}{R_o}\cos\alpha + \frac{\eta}{R_o}\sin\alpha - \left(\frac{jk}{2}\right)\frac{\left[x\sin(\alpha-\beta) - y\cos(\alpha-\beta) - \xi\sin\alpha + \eta\cos\alpha\right]^2}{R_o}\right]$$
$$e^{-jk\left[x\cos(\alpha-\beta) + y\sin(\alpha-\beta) - \xi\cos\alpha - \eta\sin\alpha\right]} + 0\left(\frac{1}{R_o^3}\right). \quad \text{(A.33)}$$

Substitution of (A.33) into (A.27) leads, after tedious algebra, to the following results:

For $a \neq 0$,

$$J_{m0,m'0} = \frac{16}{R_o}\left(\frac{a_t}{m'\pi}\right)\left(\frac{a_r}{m'\pi}\right)e^{-jkR_o}\sin\left(\frac{kb_t}{2}\sin\alpha\right)L(m'\cos\alpha)$$
$$\cdot\sin\left(\frac{kb_r}{2}\sin(\alpha-\beta)\right)\cdot\begin{cases} C\,\dfrac{ka_r}{m\pi}\cos(\alpha-\beta) \quad (m = \text{odd}) & \text{(A.34a)} \\ jS\,\dfrac{ka_r}{m\pi}\cos(\alpha-\beta) \quad (m = \text{even}) & \text{(A.34b)} \end{cases}$$

For $\alpha = 0$

$$J_{m0,m'0} = -\frac{4}{R_o^2}\left(\frac{a_t}{m'\pi}\right)\left(\frac{a_r}{m\pi}\right)b_t\,e^{-jkR_o}\,\frac{1}{\left[1 - \dfrac{k^2a_t^2}{m'^2\pi}\right]}$$

$$\begin{cases} j\, O_m \cos\left(\frac{ka_t}{2}\right) \quad (m = \text{odd},\ m' = \text{odd}) & \text{(A.35a)} \\ O_m \sin\left(\frac{ka_t}{2}\right) \quad (m = \text{even},\ m' = \text{even}) & \text{(A.35b)} \\ E_m \cos\left(\frac{ka_t}{2}\right) \quad (m = \text{even},\ m' = \text{odd}) & \text{(A.35c)} \\ -j\, E_m \sin\left(\frac{ka_t}{2}\right) \quad (m = \text{even},\ m' = \text{even}) , & \text{(A.35d)} \end{cases}$$

where

$$L(m' \cos\alpha) = \left(\sin\frac{m'\pi}{2}\right)^2 C\left(\frac{ka_t}{m'\pi}\cos\alpha\right) - j\left(\cos\frac{m'\pi}{2}\right)^2 S\left(\frac{ka_t}{m'\pi}\cos\alpha\right) \qquad \text{(A.36a)}$$

$$C\,\frac{ka_r}{m\pi}\cos(\alpha-\beta) = \frac{\cos\left(\frac{ka_r}{2}\cos(\alpha-\beta)\right)}{1-\frac{k^2a_r^2}{m^2\pi^2}\cos^2(\alpha-\beta)} \qquad \text{(A.36b)}$$

$$S\,\frac{ka_r}{m\pi}\cos(\alpha-\beta) = \frac{\sin\left(\frac{ka_r}{2}\cos(\alpha-\beta)\right)}{1-\frac{k^2a_r^2}{m^2\pi^2}\cos^2(\alpha-\beta)} \qquad \text{(A.36c)}$$

$$O_m = \left\{ 6 \frac{\sin\left(\frac{kb_r}{2}\sin\beta\right)}{\sin\beta} - (kb_r)\cos\left(\frac{kb_r}{2}\sin\beta\right) \right\} \cos\beta\, C\left(\frac{ka_r}{m\pi}\cos\beta\right)$$

$$+ \sin\left(\frac{kb_r}{2}\sin\beta\right) \cdot \sin\beta \left\{ \frac{4\left(\frac{ka_r}{m\pi}\right)^2 \cos\beta\, C\left(\frac{ka_r}{m\pi}\cos\beta\right) - ka_r \sin\left(\frac{ka_r}{2}\cos\beta\right)}{1 - \frac{k^2 a_r^2}{m^2\pi^2}\cos^2\beta} \right\}$$

(A. 36d)*

$$E_m = \left\{ 2 \frac{\sin\left(\frac{kb_r}{2}\sin\beta\right)}{\sin\beta} + (kb_r)\cos\left(\frac{kb_r}{2}\sin\beta\right) \right\} \cos\beta\, S\left(\frac{ka_r}{m\pi}\cos\beta\right)$$

$$- \sin\left(\frac{kb_r}{2}\sin\beta\right) \cdot \sin\beta \left\{ \frac{4\left(\frac{ka_r}{m\pi}\right)\cos\beta\, S\left(\frac{ka_r}{m\pi}\cos\beta\right) + ka_r \cos\left(\frac{ka_r}{2}\cos\beta\right)}{1 - \frac{k^2 a_r^2}{m^2\pi^2}\cos^2\beta} \right\}$$

(A. 36e)*

From eqs. (A. 26) and (A. 34) one determines $I_{m0}^{(R)}$ if $V_{m'0}^{(T)}$ is given. The mode amplitudes of transmitting aperture $V_{m'0}^{(T)}$ may be determined by using a variational procedure. However, it is usually satisfactory to use incident mode-amplitudes as $V_{m'0}^{(T)}$. For $\alpha = 0$ and $\sigma = \frac{\pi}{2}$, the expressions for $I_{m0}^{(R)}$ are as follows:

*) The last terms of (A. 36d) and (A. 36e) should be subject to more discussion (Kwon, 1965) and may be eliminated entirely.

For $\alpha = \frac{\pi}{2}$

$$I_{m0}^{(R)} = -\frac{8}{\pi^3 j\omega\mu}\left(\frac{a_t a_r}{b_t b_r}\right)^{\frac{1}{2}} \frac{1}{m}\frac{1}{R_o} e^{-jkR_o} \sin\left(\frac{kb_t}{2}\right) \sin\left(\frac{kb_r}{2}\cos\beta\right)$$

$$\begin{cases} C\left(\frac{ka_2}{m\pi}\sin\beta\right) \sum_{m'=odd} \frac{V_{m'o}^{(T)}}{m'} & (m = odd) \qquad \text{(A.37a)} \\ jS\left(\frac{ka_2}{m\pi}\sin\beta\right) \sum_{m'=odd} \frac{V_{m'}^{(T)}}{m'} & (m = even) \qquad \text{(A.37b)} \end{cases}$$

For $\alpha = 0$

$$I_{m0}^{(R)} = \frac{2}{\pi^3 j\omega\mu}\left(\frac{a_t a_r}{b_t b_r}\right)^{\frac{1}{2}} \frac{1}{m}\frac{b_1}{R_o^2} e^{-jkR_o} .$$

$$\begin{cases} O_m \left[j \sum_{m'=odd} \frac{V_{m'0}^{(T)}}{m'} \frac{\cos\left(\frac{ka_t}{2}\right)}{\left(1-\frac{k^2 a_t^2}{m'^2\pi^2}\right)} + \sum_{m'=even} \frac{V_{m'0}^{(T)}}{m'} \frac{\sin\left(\frac{ka_t}{2}\right)}{\left(1-\frac{k^2 a_t^2}{m'^2\pi^2}\right)} \right] & (m = odd) \qquad \text{(A.38a)} \\ E_m \left[\sum_{m'=odd} \frac{V_{m'o}^{(T)}}{m'} \frac{\cos\left(\frac{ka_t}{2}\right)}{\left(1-\frac{k^2 a_t^2}{m'^2\pi^2}\right)} - j \sum_{m'=even} \frac{V_{m'0}^{(T)}}{m'} \frac{\sin\left(\frac{ka_t}{2}\right)}{\left(1-\frac{k^2 a_t^2}{m'^2\pi^2}\right)} \right] & (m = even) \qquad \text{(A.38b)} \end{cases}$$

In terms of $I_{m0}^{(R)}$, the power received W_r is

$$W_r = \frac{1}{2} \sum_{m=1}^{\infty} \frac{\omega\mu}{\gamma_m} \left| I_{m0} \right|^2 \tag{A.39}$$

The remaining problem is the determination of W_t. The procedures for calculations are omitted and part of the results will be cited (Kwon 1965, Section IV).

$$W_t = \frac{1}{4\pi\omega\mu} \left[\delta_{mn} \sum_{m=1}^{\infty} \left| V_{m0}^{(T)} \right|^2 I_m (P_{mm}) \right.$$

$$\left. + (1 - \delta_{mn}) \sum_{m=1}^{\infty} \sum_{n=1}^{\infty} V_{m0}^{(T)} V_{n0}^{(T)} \, \mathrm{Im} (P_{mn}) \right] \tag{A.40}$$

where

$$P_{mm} = \left(\frac{4}{a_t b_t}\right) \left(\frac{a_t}{\pi}\right) \left(\frac{ka_t}{\pi}\right)^2 R_{mm}^{(1)} \tag{A.41a}$$

$$P_{mm} = 2 \left(\frac{4}{a_t b_t}\right) \left(\frac{a_t}{\pi}\right) \left(\frac{ka_t}{\pi}\right)^2 R_{mn}^{(2)} \tag{A.41b}$$

and

$$R_{mm}^{(1)} = \int_0^{\frac{b_t}{a_t}\pi} d\sigma \left(\frac{b_t}{a_t}\pi - \sigma\right) \int_0^{\pi} d\lambda \frac{e^{j\frac{ka_t}{\pi}\sqrt{\lambda^2+\sigma^2}}}{\sqrt{\lambda^2+\sigma^2}}$$

$$\left\{\left(1 - \frac{m^2\pi^2}{k^2 a_t^2}\right)(\pi - \lambda)\cos m\lambda + \left(1 + \frac{m^2\pi^2}{k^2 a_t^2}\right)\frac{1}{m}\sin m\lambda\right\} \qquad \text{(A.41c)}$$

(For $m = n$)

$$R_{mn}^{(2)} = \int_0^{\frac{b_t}{a_t}\pi} d\sigma \left(\frac{b_t}{a_t}\pi - \sigma\right) \int_0^{\pi} d\lambda \frac{e^{j\frac{ka_t}{\pi}\sqrt{\lambda^2+\sigma^2}}}{\sqrt{\lambda^2+\sigma^2}}$$

$$\cdot\left\{\left[1 - \left(\frac{m\pi}{ka_t}\right)\left(\frac{n\pi}{ka_t}\right)\right]\frac{\cos\frac{(m+n)}{2}\lambda \sin\frac{(m-n)}{2}\lambda}{m-n}\right.$$

$$\left. - \left[1 + \left(\frac{m\pi}{ka_t}\right)\left(\frac{n\pi}{ka_t}\right)\right]\frac{\cos\frac{(m-n)\lambda}{2}\sin\frac{(m+n)\lambda}{2}}{m+n}\right\} \qquad \text{(A.41d)}$$

($m \neq n$)

$I_m(P_{mn})$ = imaginary part of P_{mn}.

If the transmitting and the receiving guides are ordinary waveguides which accommodate only one propagating mode, one can set $m = m' = 1$ in eqs. (A.37), (A.38) and (A.39), and the summations become unnecessary. The expressions for W_t also become

$$W_t = \frac{1}{4\pi\omega\mu} \left|V_{10}^{(T)}\right|^2 I_m (P_{10})$$

$$= \frac{1}{4\pi\omega\mu} \left|V_{10}^{(T)}\right|^2 \left(\frac{4}{a_t b_t}\right) \left(\frac{a_t}{\pi}\right) \left(\frac{ka_t}{\pi}\right)^2 I_m (R_{11}^{(1)}) \qquad \text{(A. 42)}$$

If one further assumes $a_t = a_r$, $b_t = b_r$, the following formulas for coupling are obtained for $\alpha = \frac{\pi}{2}$, $\alpha = 0$, and $\beta = \frac{\pi}{2}$:

For $\alpha = \frac{\pi}{2}$:

$$C = \frac{32}{\pi^2} \frac{1}{\gamma_1 b} \frac{1}{k^2 R_o^2} \frac{1}{I_m (R_{11}^{(1)})} \sin^2 \left(\frac{kb}{2}\right) \sin^2 \left(\frac{kb}{2} \sin\beta\right) \left[C\left(\frac{ka}{\pi} \sin\beta\right)\right]^2$$

(A. 43)

for $\alpha = 0$:

$$C = \frac{2}{\pi^2} \frac{1}{(\gamma_1 R_o)} \frac{1}{(kR_o)^2} \frac{b}{R_o} \frac{1}{I_m (R_{11}^{(1)})} \left[\frac{\cos\left(\frac{ka}{2}\right)}{1 - \frac{k^2 a^2}{\pi^2}}\right]^2 O_1^2 \qquad \text{(A. 44)}$$

For $\beta = 0$

$$C = \frac{32}{\pi^2} \frac{1}{k^2 R_o^2} \frac{1}{I_m R_{11}^{(1)}} \sin^2 \left(\frac{kb}{2} \cos\alpha\right) \cdot \left[C\left(\frac{ka}{\pi} \cos\alpha\right)\right]^2 \cdot \frac{1}{\gamma_1 b}$$

$$\sin^2 \left(\frac{kb}{2} \sin\alpha\right) \cdot \left[C\left(\frac{ka}{\pi} \sin\alpha\right)\right]^2 \qquad \text{(A. 45)}$$

These couplings are plotted and compared with experimental results in the Figs. 4-6.

A.3 The Coupling of Two E-Sectoral Horn-Connected Aperture Antennas (Small Flare Angle Approximation)

If the flare angle $2\theta_o$ is much smaller than $\pi/2$ the following approximations are justified for equation (A.7).

$$\text{a)}\ \frac{y}{\rho} \doteqdot 0 \qquad \frac{p\pi\phi}{2\theta_o} \doteqdot \frac{py_1}{b} \qquad (y_1 = y + \frac{b}{2}) \qquad \frac{u}{\rho} \doteqdot 1 \tag{A.46}$$

b) The reflection can be ignored, that is, for the receiving horn (see eq. 9)

$$\frac{D_{nq}}{C_{nq}} \doteqdot 0 \doteqdot \frac{B_{mp}}{A_{mp}} \tag{A.47}$$

c) One can consider only those p's which satisfy:

$$\frac{p\pi}{2\theta_o} < \gamma_m \rho_1 \,. \quad \text{Henceforth let} \tag{A.48}$$

$$\psi_p = \frac{p\pi}{2\theta_o}$$

In other words those modes whose turning points are in the horn can be ignored, for they only contribute to the non-propagating wave in the receiving waveguide.

Imposing the condition of continuity of $\overline{E}_t$ and $\overline{H}_t$ at $z_r = 0$ (horn-guide junction) and z = 0 (aperture) of the receiving system, and using the approximations described above, one gets, from eqs. (A.2), (A.4) and (A.7),

$$\sum_{m=1}^{\infty}\sum_{p=0}^{\infty} V_{mp}^{''(R)}\,\bar{e}_{mp}^{''}(x,y) + \sum_{n=0}^{\infty}\sum_{q=1}^{\infty} V_{nq}^{'(R)}\,\bar{e}_{nq}^{'}(x,y)$$

$$= \hat{x}\sum_{n=0}^{\infty}\sum_{z=1}^{\infty} \gamma_n^2\, C_{nq}\, H_{\psi_q}^{(1)}\left(\gamma_n\sqrt{y^2+(\rho_1^{(r)})^2}\right)\cos\frac{n\pi x_1}{a_r}\sin\frac{q\pi y_1}{b_r}$$

$$+\hat{y}\left[j\omega\mu\sum_{m=1}^{\infty}\sum_{p=0}^{\infty}\gamma_m^2\, A_{mp}\, H_{\psi_p}^{(1)'}\left(\gamma_m\sqrt{y^2+(\rho_1^{(r)})^2}\right)\sin\frac{m\pi x_1}{a_r}\cos\frac{p\pi y_1}{b_r}\right.$$

$$\left.-\sum_{n=1}^{\infty}\sum_{q=1}^{\infty}\frac{1}{\rho_1^{(r)}}\left(\frac{n\pi}{a_r}\right)\left(\frac{q\pi}{2\theta_o}\right) C_{nq}\, H_{\psi_q}^{(1)}\left(\gamma_m\sqrt{y^2+(\rho_1^{(r)})^2}\right)\sin\frac{n\pi x_1}{a_r}\sin\frac{q\pi y_1}{b_r}\right]$$

(A.49a)

$$\sum_{m=1}^{\infty}\sum_{p=0}^{\infty} I_{m_p}^{(R)''}\,\bar{h}_{mp}'' + \sum_{n=0}^{\infty}\sum_{q=1}^{\infty} I_{nq}^{(R)'}\,\bar{h}_{nq}'$$

$$= \hat{x}\sum_{m=1}^{\infty}\sum_{p=0}^{\infty} \gamma_m^2\, A_{mp}\, H_{\psi_p}\left(\gamma_m\sqrt{y^2+(\rho_1^r)^2}\right)\sin\frac{n\pi x_1}{a_r}\cos\frac{p\pi y_1}{b_r}$$

$$-\hat{y}\left[\sum_{m=1}^{\infty}\sum_{p=0}^{\infty}\frac{1}{\rho_1^{(r)}}\left(\frac{m\pi}{a_r}\right)\left(\frac{p\pi}{2\theta_o}\right)A_{mp}\,H_{\psi_p}^{(1)'}\left(\gamma_m\sqrt{y^2+(\rho_1^r)^2}\right)\cos\frac{m\pi x_1}{a_r}\sin\frac{p\pi y_1}{b_r}\right.$$

$$\left.+\,j\omega\epsilon\sum_{n=0}^{\infty}\sum_{q=1}^{\infty}\gamma_n\, C_{nq}\, H_{\psi_q}^{(1)'}\;\gamma_n\sqrt{y^2+(\rho_1^{(r)})^2}\cos\frac{m\pi x_1}{a_r}\sin\frac{q\pi y_1}{b_r}\right]$$

(A.49b)

$$\hat{x}\sum_{m=1}^{\infty}\sum_{p=0}^{\infty}\gamma_m^2 A_{mp} H_{\psi_p}^{(1)}\left(\gamma_m\sqrt{y^2+(\rho_2^{(r)})^2}\right)\sin\frac{m\pi x_1}{a_r}\cos\frac{p\pi y_1}{b_r}$$

$$-\hat{y}\sum_{m=1}^{\infty}\sum_{p=0}^{\infty}\frac{1}{\rho_2^{(r)}}\left(\frac{m\pi}{a_r}\right)\left(\frac{p\pi}{2\theta_o}\right)A_{mp} H_{\psi_p}^{(1)'}\left(\gamma_m\sqrt{y^2+(\rho_2^{(r)})^2}\right)\cos\frac{m\pi x_1}{a_r}\sin\frac{p\pi y_1}{b_r}$$

$$+j\omega\epsilon\sum_{n=0}^{\infty}\sum_{q=1}^{\infty}\gamma_n C_{nq} H_{\psi_q}^{(1)'}\left(\gamma_n\sqrt{y^2+(\rho_1^{(r)})^2}\right)\cos\frac{m\pi x_1}{a_r}\sin\frac{q\pi y_1}{b_r}$$

$$=-\iint\bar{\bar{Y}}(\bar{\rho}_B:\bar{\rho}_A)\cdot\bar{M}_A^{(2)}(\bar{\rho}_A)\,dS_A-\iint\bar{\bar{Y}}(\bar{\rho}_B:\bar{\rho}_B')\cdot\bar{M}_B^{(2)}(\bar{\rho}_B')\,dS_B'$$

(A.50)

As mentioned previously lack of orthogonality of mode-functions with respect to y make it impossible to calculate the coefficients A_{mp} and C_{nq}. However, under the present small angle approximation, one may be justified to assume:

$$\sum_{q=0}^{\infty} \int_{o}^{b} f\left(\sqrt{y^2+\rho_{1,2}^2}\right) \begin{Bmatrix} \cos \frac{p\pi y_1}{b} \\ \sin \frac{p\pi y_1}{b} \end{Bmatrix} \begin{Bmatrix} \cos \frac{q\pi y_1}{b} \\ \sin \frac{q\pi y_1}{b} \end{Bmatrix} dy$$

$$\doteq \int_{o}^{b} f\left(\sqrt{y^2+\rho_{1,2}^2}\right) \begin{Bmatrix} \cos^2 \frac{p\pi y_1}{b} \\ \sin^2 \frac{p\pi y_1}{b} \end{Bmatrix} \qquad \text{(A.51)}$$

Now, multiplying $\hat{x}\, H_{\psi_p}^{(2)}\left(\sqrt{y^2+(\rho_2^{(r)})^2}\right) \sin \frac{m\pi x_1}{a_r} \cos \frac{p\pi y_p}{b_r}$ and

$y\, H_{\psi_p}^{(2)'}\left(\sqrt{y^2+(\rho_2^{(r)})^2}\right) \cos \frac{m\pi x_1}{a_r} \sin \frac{p\pi y_1}{b_r}$ on to (A.50) and subsequently integrating over the receiving aperture, one gets, in view of the approximation (A.51),

$$A_{mp} = \left(\frac{2}{\gamma_m^2 a_r}\right) \frac{J_{mp}^{(1)}}{H(m,p)}$$

and

$$C_{mp} = \frac{j2}{\omega \epsilon \gamma_m a_r}\left[\frac{J_{mp}^{(2)}}{H'(m,p)} + \left(\frac{m\pi}{a}\right)\left(\frac{p\pi}{2\theta_o}\right)\frac{1}{\gamma_m^2}\frac{1}{\rho_2^{(r)}}\frac{J_{mp}^{(1)}}{H(m,p)}\frac{M(m,p)}{H'(m,p)}\right]$$

(A.52)

where

$$J_{mp}^{(1)} = -\frac{1}{2}\int_{-\frac{b_r}{2}}^{\frac{b_r}{2}} dy\, H_{\psi_p}^{(2)}\left(\gamma_m\sqrt{y^2+(\rho_2^{(r)})^2}\right)\cos\frac{p\pi y_1}{b_r}\int_0^{a_r}\sin\frac{m\pi x_1}{a_r}\,dx_1$$

$$\cdot\iint \hat{x}\cdot\bar{\bar{Y}}\,(\bar{\rho}_B:\bar{\rho}_A)\;\bar{M}_A^{(2)}\,(\bar{\rho}_A)\,dS_A \qquad (A.53)$$

$$J_{mp}^{(2)} = -\frac{1}{2}\int_{-\frac{b_r}{2}}^{\frac{b_r}{2}} dy\, H_{\psi_p}^{(2)'}\left(\gamma_m\sqrt{y^2+(\rho_2^{(r)})^2}\right)\sin\frac{p\pi y_1}{b_r}\int_0^{a} dx_1\cos\frac{m\pi x_1}{a_r}$$

$$\cdot\iint \hat{y}\cdot\bar{\bar{Y}}\,(\bar{\rho}_B:\bar{\rho}_A)\;\bar{M}_A^{(2)}\,(\bar{\rho}_A)\,dS_A \qquad (A.54)$$

$$H(m,p) = \int_{-\frac{b_r}{2}}^{\frac{b_r}{a}} dy\left[\left\{J_{\psi_p}\left(\gamma_m\sqrt{y^2+(\rho_2^{(r)})^2}\right)\right\}^2\left\{Y_{\psi_p}\left(\gamma_m\sqrt{y^2+(\rho_2^{(r)})^2}\right)\right\}^2\right]\left\{\cos\frac{p\pi y_1}{b_2}\right\}^2$$

$$\doteqdot \frac{2}{\pi\gamma_m}\,\frac{1}{\rho_2^{(r)}}\left(1+\frac{1}{2}\,\frac{(\frac{p\pi}{2\theta_o})^2}{(\gamma_m\rho_2^{(r)})^2}\right)\cdot\frac{b_r}{2} \qquad (A.55)$$

$$H'(m,p) = \int_{-\frac{b_r}{2}}^{\frac{b_r}{2}} \left[\left\{ J'_{\psi_p} \gamma_m \sqrt{y^2 + (\rho_2^{(r)})^2} \right\}^2 + \left\{ Y'_{\psi_p} \gamma_m \sqrt{y^2 + (\rho_2^{(r)})^2} \right\} \right] \left(\sin \frac{p\pi y_1}{b_r}\right)^2 dy \qquad \text{(A.56)}$$

$$M(m,p) = \int_{-\frac{b_r}{2}}^{\frac{b_r}{2}} H^{(1)}_{\psi_p} \left(\gamma_m \sqrt{y^2 + (\rho_2^{(r)})^2}\right) H^{(2)'}_{\psi_p} \left(\gamma_m \sqrt{y^2 + (\rho_2^{(r)})^2}\right) \left(\sin \frac{p\pi y_1}{b_r}\right)^2 dy \qquad \text{(A.57)}$$

In the above calculations, the approximations given in eqs. (A.16) to (A.19) are used. Since A_{mp} and C_{nq} are known, the calculations of the amplitudes $V^{(R)}_{mp}$ and $I^{(R)}_{mp}$ from eqs. (A.49) are a matter of algebra. Assuming the field of transmitting aperture is given by:

$$\overline{E}_t(\overline{\rho}_t) = \hat{\eta} \cos\theta_t H_1^{(2)} \left(\gamma_1' \sqrt{\mu^2 + (\rho_2^{(t)})^2}\right) \sin \frac{\pi \xi_1}{a_t} \qquad \text{(A.58)}$$

One can obtain the following results for coupling (Kwon 1965 Section VIII).

i) $\alpha \neq 0$

a) Denoting $C^{(m,0)}$ as the parts of the coupling which excite TE_{m0} mode in the receiving waveguide, one has:

$$C^{(m0)} = -16\pi \left(\frac{a_r}{b_r^{(0)}}\right)\left(\frac{\gamma_1'}{k}\right)\left(\frac{\rho_2^{(t)}}{a_t}\right)\left(\gamma_m \rho_2^{(t)}\right)\frac{1}{(\gamma_m a_r)^2}\frac{1}{(\gamma_m R_o)^2}\left(\frac{ka_r}{m\pi}\right)^2\left(\frac{ka_t}{\pi}\right)^2$$

$$\frac{M_{01}(\gamma_m b_r^{(0)})}{\left|H_c(\gamma_m b_r, 0)\right|^2}\frac{1}{W'}\left[C\left(\frac{ka_t}{\pi}\cos\alpha\right)\right]^2 \sin^2\alpha \sin^2(\alpha-\beta)$$

$$\left|\nu_c(\gamma_1' b_t \sin\alpha)\right|^2 \left|H^{cc}(\gamma_m b_r \sin(\alpha-\beta), 0\right|^2$$

$$\begin{cases} \left[C\left(\frac{ka_r}{m\pi}\cos(\alpha-\beta)\right)\right]^2 & (m = \text{odd}) \qquad (A.59) \\ \left[S\left(\frac{ka_r}{m\pi}\cos(\alpha-\beta)\right)\right]^2 & (m = \text{even}) \qquad (A.60) \end{cases}$$

In the above superscript zero on the "b" dimension indicates the dimension is on the horn aperture to distinguish from the waveguide dimension.

b) The modal coupling $C^{(0,\,2n+1)}$ which excites only $TM_{0,\,2n+1}$ mode in the receiving guide is:

$$C^{(0,2n+1)} = 16\pi \left(\frac{a_r}{b_r^{(0)}}\right)\left(\frac{\gamma_1'}{k}\right)\left(\frac{\rho_2^{(t)}}{a_t}\right)\left(\frac{\rho_2^{(t)}}{a_r}\right)\frac{1}{(ka_r)}\,\frac{1}{(kR_o)^2}\left(\frac{ka_t}{\pi}\right)^2$$

$$\frac{M_{01}^{(c)}(kb_r^{(0)},\ 2\eta+1)}{H_c'(kb_r,\ 2\eta+1)^2}\,\frac{1}{W'}\left[C\left(\frac{ka_t}{\pi}\cos\alpha\right)\right]^2\sin^2\alpha$$

$$\left|\nu_c(\gamma_1' b_t \sin\alpha)\right|^2\left|H'^{cc}(kb_r\sin(\alpha-\beta),\ 2n+1)\right|^2\left[\sin\left(\frac{ka_2}{2}\cos(\alpha-\beta)\right)\right]^2$$

(A.61)

ii) $\alpha = 0$

$$C^{(m,0)} = 64\pi \left(\frac{a_r}{b_r^{(0)}}\right)\left(\frac{\gamma_1'}{k}\right)\left(\frac{\rho_2^{(t)}}{a_t}\right)(\gamma_m \rho_2^{(t)})\frac{1}{(\gamma_m a_r)^2}\frac{1}{(\gamma_m R_o)^2}\frac{1}{(kR_o)^2}\left(\frac{ka_r}{m\pi}\right)^2\left(\frac{ka_t}{\pi}\right)^2$$

$$\frac{M_{01}(\gamma_m b_r^{(0)})}{\left[H_c(\gamma_m b_r, 0)\right]^2}\frac{1}{W'}\left[C\left(\frac{ka_t}{\pi}\cos\alpha\right)\right]^2_{\alpha=0}\left|\nu(\beta_m, b_1)\right|^2$$

$$\cdot\left[\left\{J^{cc}(\gamma_m b_r \sin\beta, 0)P_c(m) - \frac{1}{2}\frac{k}{\gamma_m}J^{tcs}(\gamma_m b_r \sin\beta, 0)\sin\beta\cos\beta\, C\left(\frac{ka_r}{m\pi}\cos\beta\right)\right\}^2\right.$$

$$\left.+\left\{Y^{cc}(\gamma_m b_r \sin\beta, 0)P_c(m) - \frac{1}{2}\frac{k}{\gamma m}Y^{tcs}(\gamma_m b_r \sin\beta, 0)\sin\beta\cos\beta\, C\left(\frac{ka_r}{m\pi}\cos\beta\right)\right\}^2\right]$$

(m = odd)

$$\cdot\left[\left\{J^{cc}(\gamma_m b_r \sin\beta, 0)P_s(m) - \frac{1}{2}\frac{k}{\gamma m}J^{tcs}(\gamma_m b_2 \sin\beta, 0)\sin\beta\cos\beta\, S\left(\frac{ka_r}{m\pi}\cos\beta\right)\right\}^2\right.$$

$$\left.+\left\{Y^{cc}(\gamma_m b_r \sin\beta, 0)P_s(m) - \frac{1}{2}\frac{k}{\gamma_m}Y^{tcs}(\gamma_m b_2 \sin\beta, 0)\sin\beta\cos\beta\, S\left(\frac{ka_r}{m\pi}\cos\beta\right)\right\}^2\right]$$

(m = even)

(A.62)

$$C^{(0,2n+1)} = 64\pi \left(\frac{a_r}{b_r^{(0)}}\right)\left(\frac{\gamma_1'}{k}\right)^2 \left(\frac{\rho_2^{(t)}}{a_t}\right)\left(\frac{\rho_2^{(t)}}{a_r}\right)\frac{1}{(ka_r)}\frac{1}{(kR_o)^4}\left(\frac{ka_t}{\pi}\right)^2$$

$$\frac{M_{01}^{c}(kb_r^{(0)}, 2\eta+1)}{\left[H_c'(kb_r, 2\eta+1)\right]^2}\frac{1}{W'}\left[C\left(\frac{ka_t}{\pi}\cos\alpha\right)\right]^2_{\alpha=0}\left|\nu_c(\beta_{m'} b_t)\right|^2$$

$$\cdot\left[\left\{J^{'cc}(kb_r\sin\beta, 2\eta+1)\sin\beta\cdot q(\beta)+\frac{1}{2}J^{'\lambda cs}(kb_r\sin\beta, 2\eta+1)\cos\left(\frac{ka_r}{2}\cos\beta\right)\right\}^2\right.$$

$$\left.+\left\{Y^{'cc}(kb_r\sin\beta, 2\eta+1)\sin\beta\cdot q(\beta)+\frac{1}{2}Y^{'tcs}(kb_r\sin\beta, 2\eta+1)\cos\left(\frac{ka_r}{2}\cos\beta\right)\right\}^2\right] \qquad (A.63)$$

See eq. A.36 for definition $C\left(\frac{ka_t}{\pi}\cos\alpha\right)$, etc.

Several function forms which have been used are now defined as follows

$$M_{01}(\gamma_m b_r^{(0)}) = \int_0^{\frac{\gamma_m b_r^{(0)}}{2}} J_0(T)dt \int_0^{\frac{\gamma_m b_r^{(0)}}{2}} Y_1(T)dt - \int_0^{\frac{\gamma_m b_r^{(0)}}{2}} J_1(T)at \int_0^{\frac{\gamma_m b_r^{(0)}}{2}} Y_1(T)dt$$

(A.64)

where: $\left(T = \sqrt{t^2 + (\gamma_m \rho_1^{(r)})^2}\right)$

$$M_{01}(kb_r^{(0)}, 2n+1) = \int_0^{\frac{kb_r^{(0)}}{2}} J_{n'}'(T)\left(\cos\frac{(2n+1)\pi t}{kb_0^{(r)}}\right)^2 dt \int_0^{\frac{\gamma_m b_r^{(0)}}{2}} Y_{n'}(T)\left(\cos\frac{(2n+1)\pi t}{kb_0^{(r)}}\right)^2 dt$$

$$- \int_0^{\frac{kb_r^{(0)}}{2}} J_{n'}(T)\left(\cos\frac{(2n+1)\pi t}{kb_0^{(r)}}\right)^2 dt \int_0^{\frac{\gamma_m b_r^{(0)}}{2}} Y_{n'}'(T)\left(\cos\frac{(2n+1)\pi t}{kb_0^{(r)}}\right)^2 dt \qquad \text{(A.65)}$$

where: $n' = \dfrac{(2n+1)\pi t}{2\theta_r^{(0)}}$

$$H_c(\gamma_m b_r, 0) = \int_0^{\frac{\gamma_m b_r}{2}} \left\{\left[J_0(T)\right]^2 + \left[Y_0(T)\right]^2\right\} dt \qquad \text{(A.66)}$$

$$H_c'(kb_r, 2n+1) = \int_0^{\frac{kb_r}{2}} \left\{\left[J_{n'}'(T)\right]^2 + \left[Y_{n'}'(T)\right]^2\right\} \left(\cos\frac{(2n+1)\pi t}{kb_r}\right)^2 dt \qquad \text{(A.67)}$$

$$\nu_c(\gamma_1' b_t \sin\alpha) = \int_0^{\frac{\gamma_1' b_t}{2}} \frac{H_1^{(2)}(T)}{T} \cos\left(\frac{k}{\gamma_1'} t \sin\alpha\right) dt \qquad \text{(A.68)}$$

$$\nu(\gamma_1' b_t) = \int_0^{\frac{\gamma_1' b_t}{2}} \frac{H_1^{(2)}(T)}{T}\, dt \qquad \text{(A.69)}$$

$$H^{cc}(\gamma_m b_r \sin(\alpha-\beta),\ 0) = \int_0^{\frac{\gamma_m b_r}{2}} H_0^{(2)}(T) \cos\left(\frac{k}{\gamma_m} t \sin(\alpha-\beta)\right) dt \qquad \text{(A.70)}$$

$$H'^{cc}(kb_r \sin(\alpha-\beta),\ 2n+1) = \int_0^{\frac{kb_r}{2}} H_{n'}^{(2)}(T) \cos\frac{(2n+1)\pi t}{kb_r} \sin(t \sin(\alpha-\beta))\, dt \qquad \text{(A.71)}$$

$$J^{cc}(\gamma_m b_r \sin\beta, 0) = \mathrm{Re}\left[H^{cc}(\beta_m b_r \sin\beta)\right] \qquad \text{(A.72)}$$

(Re: Real part of)

(I_m: Imaginary part of)

$$Y^{cc}(\gamma_m b_r \sin\beta, 0) = I_m\left[H^{cc}(\beta_m b_r \sin\beta)\right] \qquad \text{(A.73)}$$

$$J^{tcs}(\gamma_m b_r \sin\beta, 0) = \int_0^{\frac{\gamma_m b_r}{2}} t J_o(T) \sin\left(\frac{k}{\gamma_m} t \sin\beta\right) dt \qquad \text{(A.74)}$$

$$Y^{tcs}(\gamma_m b_r \sin\beta, 0) = \int_0^{\frac{\gamma_m b_r}{2}} t\, Y_o(T) \sin\left(\frac{k}{\gamma_m} t \sin\beta\right) dt \qquad \text{(A.75)}$$

$$J^{'cc}(kb_r \sin\beta, 2n+1) = \mathrm{Re}\left[H^{'cc}(kb_r \sin\beta, 2n+1)\right] \qquad \text{(A.76)}$$

$$Y^{'cc}(kb_r \sin\beta, 2n+1) = \mathrm{Im}\left[H^{'cc}(kb_r \sin\beta, 2n+1)\right] \qquad \text{(A.77)}$$

$$J^{'tcs}(kb_r \sin\beta, 2n+1) = \int_0^{\frac{kb_r}{2}} t\, J_{n'}^{'}(T) \cos\frac{(2n+1)\pi t}{kb_r} \sin(t \sin\beta)\, dt \qquad \text{(A.78)}$$

$$Y^{'tcs}(kb_r \sin\beta, 2n+1) = \int_0^{\frac{kb_r}{2}} t\, Y_{n'}^{'}(T) \cos\frac{(2n+1)\pi t}{kb_r} \sin(t \sin\beta)\, dt \qquad \text{(A.79)}$$

$$P_c(m) = \cos\beta \cdot C\left(\frac{ka_r}{m\pi}\cos\beta\right) - \frac{1}{4}\sin^2\beta \, \frac{\left[4\left(\frac{ka_r}{m\pi}\right)^2 \cos\beta\, C\left(\frac{ka_r}{m\pi}\cos\beta\right) - ka_r \sin\left(\frac{ka_r}{2}\cos\beta\right)\right]}{1 - \frac{k^2 a_r^2}{m^2\pi^2}\cos^2\beta} \qquad \text{(A.80)}$$

$$P_c(m) = \cos\beta \cdot S\left(\frac{ka_r}{m\pi}\cos\beta\right)$$

$$-\frac{1}{4}\sin^2\beta \frac{\left[4\left(\frac{ka_r}{m\pi}\right)^2 \cos\beta\, S\left(\frac{ka_r}{m\pi}\cos\beta\right) + ka_r \cos\left(\frac{ka_r}{2}\cos\beta\right)\right]}{1 - \frac{k^2 a_r^2}{m^2\pi^2}\cos^2\beta}$$

(A.81)

$$q(\beta) = \left\{1 - \frac{1}{4}(1+\sin^2\beta)\right\} \frac{\sin\left(\frac{ka_r}{2}\cos\beta\right)}{\cos\beta} + \frac{(ka_r)}{4}\cos\left(\frac{ka_r}{2}\cos\beta\right)$$

(A.82)

$$W' = \int_0^{\frac{b_t}{a_t}\pi} d\sigma \frac{\left\{\sin\left(\frac{\gamma_1' a_t}{\pi}\right) \frac{a_t}{2\rho_2^{(t)}}\, \sigma\left(\frac{b_t}{a_t}\pi - \sigma\right)\right\}}{\sigma}$$

$$\int_0^{\pi} d\lambda \left\{\left[1 - \left(\frac{\pi}{ka_t}\right)^2\right](\pi - \lambda)\cos\lambda + \left[1 + \left(\frac{\pi}{ka_t}\right)^2\right]\sin\lambda\right\} \frac{\sin\left(\frac{ka_t}{\pi}\sqrt{\lambda^2+\sigma^2}\right)}{\sqrt{\lambda^2+\sigma^2}}$$

(A.83)

$C^{(1,0)}$ for the two identical horns are calculated and compared with experiments.

A.4 Coupling of H-Sectoral Horn

In the present section the following model is considered.

i) The incident field in the T_1-region consists only of the TE_{10}-mode.

ii) The flare-angles of horns of the transmitting and receiving structure are large.

iii) The distance R_o between two antennas is several times greater than the largest of any of the lined dimensions of the apertures.

iv) The excitation and coupling of other than TE_{m0}-modes are ignored. This is a reasonable assumption in view of the fact that the incident mode is a single TE_{10}-mode.

Due to the assumption iv) and the characteristics of the H-sectoral horn (i.e., b = constant), the only non-vanishing matrix components in eqs. (A.11) are E''_{qp} and H''_{qp}. Then, eq. (A.11) becomes: (omitting double prime on I and V).

$$\frac{dI_{mo}}{dz} + j\omega t \frac{\gamma_m}{k^2} V_{m0} = \sum_{m'(\neq m)} H''_{m0,m'0} I_{m'0} \qquad (A.84)$$

$$\frac{dV_{mo}}{dz} + j\omega\mu I_{m0} = - \sum_{m'(\neq m)} E''_{m0,m'0} V_{m'0} \qquad (A.85)$$

From the above 1st order differential equations, the following 2nd order differential equations are obtained:

$$\frac{d^2 V_{mo}}{dz^2} + (\gamma_m^2 - \sum_{m'(\neq m)} E''_{m0,m'0} E''_{m'0,m0}) V_{m0}$$

$$= \sum_{m'(\neq m)} \frac{dE_{m0,m'0}}{dz} V_{m'0}$$

$$+ \sum_{m'(\neq m)} \sum_{p(\neq m' \neq m)} E''_{m0,m'0} E''_{m'0,p0} V_{p0} \qquad \text{(A.86)}$$

$E''_{m0,m'0}$ and $H_{m0,m'0}$ are given by:

$$E''_{m0,m'0} = (-1)^{m+m'} \frac{2mm'}{m'^2 - m^2} \frac{a'}{a} \qquad \text{(A.87)}$$

$$H''_{m0,m'0} = -E_{m0,m'0} \qquad \text{(A.88)}$$

$$a' = \frac{da}{dz} .$$

By successive approximation the above eq. (A.86) can be solved up to the desired degree of accuracy (Kwon, 1965, Section IX). After calculating V_{mo} in the T_2- and R_2-region, one can proceed exactly the same as in the previous two cases. The final results for $\alpha = \frac{\pi}{2}$ and $\alpha = 0$ are given:

For $\alpha = \frac{\pi}{2}$

$$C = \frac{32}{\pi^2}\left(\frac{a_r}{b_r}\right)\frac{1}{(kR_o)^2}\frac{1}{(ka_t)}\sin^2\left(\frac{kb_t}{2}\right)\sin^2\left(\frac{kb_r}{2}\cos\beta\right)\frac{|\sigma|^2}{Q}$$

$$\cdot\Bigg[C\left(\frac{ka_r}{\pi}\sin\beta\right)\sum_{q=1}^{q=\text{odd}} g_q \frac{C\left(\frac{ka_r}{q\pi}\sin\beta\right)}{q}$$

$$+\sum_{q=1}^{\text{odd}}\sum_{m=3}^{\text{odd}} Z_{mq}^{oo}\frac{C\left(\frac{ka_r}{m\pi}\sin\beta\right)C\left(\frac{ka_r}{q\pi}\sin\beta\right)}{mq}$$

$$+\sum_{q=2}^{\text{even}}\sum_{m=2}^{\text{even}} Z_{mq}^{ee}\frac{S\left(\frac{ka_r}{m\pi}\sin\beta\right)S\left(\frac{ka_r}{q\pi}\sin\beta\right)}{mq}$$

$$+\sum_{q=1}^{\text{odd}}\sum_{m=2}^{\text{even}} Z_{mq}^{eo}\frac{S\left(\frac{ka_r}{m\pi}\sin\beta\right)S\left(\frac{ka_r}{q\pi}\sin\beta\right)}{mq}$$

$$+\sum_{q=2}^{\text{even}}\sum_{m=3}^{\text{odd}} Z_{mq}^{oe}\frac{C\left(\frac{ka_r}{m\pi}\sin\beta\right)S\left(\frac{ka_r}{q\pi}\sin\beta\right)}{mq}\Bigg] \qquad \text{(A. 89)}$$

For $\alpha = 0$

$$C = \frac{2}{\pi^2}\left(\frac{a_r}{b_r}\right)\frac{b_t^2}{R_o^2}\frac{1}{(kR_o)^2}\frac{1}{(ka_t)}\frac{1}{Q}\left[|\sigma_c|^2 + |\sigma_s|^2\right]$$

$$\cdot\left[O_1\sum_{q=1}^{\text{odd}} g_q O_q + \sum_{q=1}^{\text{odd}}\sum_{m=3}^{\text{odd}} Z_{mq}^{oo}\frac{O_m O_q}{mq}\right.$$

$$+\sum_{q=2}^{\text{even}}\sum_{m=2}^{\text{even}} Z_{mq}^{ee}\frac{E_m E_q}{mq} - \sum_{q=1}^{\text{odd}}\sum_{m=2}^{\text{even}} Z_{mq}^{eo}\frac{E_m O_q}{mq}$$

$$\left. - \sum_{q=2}^{\text{even}}\sum_{m=3}^{\text{odd}} Z_{mq}^{oe}\frac{O_m E_q}{mq}\right] \text{, for } O_m \text{ see equation (A.38a)}$$

(A.90)

where

$$Z_{mq}^{oo} = g_m g_q - 2\left\{L(\nu m)\frac{C_m g_q}{\nu_m^2 - \nu_1^2}\right.$$

$$\left. - \cos\Phi \cdot g_q \cdot T_m^{(3)}(t_2^{(0)})\frac{C_m}{2}\left[\frac{1}{\nu_m^2 - \nu_1^2} + \frac{m}{m^2 - 1}\right]\right\} \qquad \text{(A.91)}$$

$$Z_{mq}^{ee} = g_m g_q - 2\left\{ L(\nu m) \frac{C_m g_q}{\nu_m^2 - \nu_1^2} \right.$$

$$\left. - \cos\Phi\, g_q\, T_m^{(3)}(t_2^{(0)}) \left[\frac{C_m}{2} \frac{1}{\nu_m^2 - \nu_1^2} - \frac{m}{m^2 - 1} \right] \right\} \qquad \text{(A.92)}$$

$$Z_{mq}^{eo} = -2 \left\{ M(\nu_m) \frac{C_m g_q}{\nu_m^2 - \nu_1^2} + \sin\Phi \cdot g_q \cdot G_m^{(3)}(t_2^{(0)}) \left[\frac{C_m}{2} \frac{1}{\nu_m^2 - \nu_1^2} - \frac{m}{m^2 - 1} \right] \right.$$

$$\left. + (1 - \delta_{q1})\, C_m G_m^{(1)} \frac{2}{\nu_m^2 - \nu_1^2} \left[\frac{C_q G_q^{(2)}}{\nu_q^2 - \nu_1^2} + \frac{q G_q^{(3)}}{q^2 - 1} \right] \right\} \qquad \text{(A.93)}$$

$$Z_{mq}^{oe} = 2 \left\{ M(\nu m) \frac{C_m g_q}{\nu_m^2 - \nu_1^2} + \sin\Phi\, g_q G_m^{(3)} \left[\frac{C_m}{2} \frac{1}{\nu_m^2 - \nu_1^2} + \frac{m}{m^2 - 1} \right] \right.$$

$$\left. + C_m G_m^{(1)} \frac{2}{\nu_m^2 - \nu_1^2} \left[\frac{C_q G_q^{(2)}}{\nu_q^2 - \nu_1^2} - \frac{q G_q^{(3)}}{q^2 - 1} \right] \right\} \qquad \text{(A.94)}$$

$$\nu_m^2 = \left(\frac{m\pi}{a_r'}\right)^2 + \frac{1}{4} - 4m^2 \sum_{m'(\neq m)} \frac{m'^2}{(m'^2 - m^2)^2} \qquad \text{(A.95)}$$

$$C_m = (-1)^{m+1} m\left[\frac{1}{m^2-1} - 2\sum_{p(\neq m\neq 1)} \frac{p^2}{(p^2-1)(p^2-m^2)}\right] (m\neq 1)$$

(A.96)

$$\mu_{m'}^2 = \left(\frac{m'\pi}{a_t}\right)^2 + \frac{1}{4} - 4m^2 \sum_{m'(\neq m)} \frac{m'^2}{(m'^2-m^2)^2} \qquad \text{(A.97)}$$

$$G_m^{(1)}(t) = \frac{\sqrt{t}J_{\nu_m}(t_2)}{\frac{d}{dt}\left[\sqrt{t}J_{\nu_m}(t)\right]_{t=t_2^{(r)}}} \qquad \text{(A.98)}$$

$$G_m^{(2)}(t) = \frac{\frac{d}{dt}\left[\sqrt{t}J_{\nu_m}(t)\right]}{\frac{d}{dt}\left[\sqrt{t}J_{\nu_m}(t)\right]_{t=t_2^{(r)}}} \qquad \text{(A.99)}$$

$$G_m^{(3)}(t) = \frac{1}{\frac{d}{dt}\left[\sqrt{t}J_{\nu_m}(t)\right]_{t=t_2^{(r)}}} \frac{J_{\nu_m}(t)}{\sqrt{t}} \qquad \text{(A.100)}$$

$$g_1 = 1$$

$$g_m = (-1)^{m+2} \cdot 2 \left[\frac{m}{m^2-1} \left\{ \frac{1}{\nu_m^2 - \nu_1^2} + G_m^{(3)}(t_2^{(r)}) \right\} \right.$$

$$\left. + \sum_{p(\neq m \neq 1)} \frac{2p^2}{p^2-1} \cdot \frac{m}{m^2-p^2} \frac{1}{\nu_m^2 - \nu_1^2} \right] \qquad \text{(A.101)}$$

$$\Phi = (t_r - t_r^{(0)}) - \frac{\nu_1^2}{2} \left(\frac{1}{t_r^{(0)}} - \frac{1}{t_r} \right) \qquad \text{(A.102)}$$

$$\ell_1 = 1$$

$$\ell_{m'} = (-1)^{m'+1} \frac{2m'}{m'^2-1} \frac{1}{\mu_{m'}^2 - \mu_1^2} \cdot \qquad \text{(A.103)}$$

$$\sigma = \sum_{m'=\text{odd}} \frac{\ell_{m'}}{m'} \qquad \text{(A.104)}$$

$$\sigma_c = \sum_{m'=\text{odd}} \frac{\ell_{m'}}{m'} C\left(\frac{ka_t}{m'\pi}\right) \qquad \text{(A.105)}$$

$$\sigma_s = \sum_{m'-\text{even}(\neq 0)} \frac{\ell_{m'}}{m'} S\left(\frac{ka_t}{m'\pi}\right) \qquad \text{(A.106)}$$

$$L(\nu n) = \frac{\sin\bar{\Phi}\sqrt{t_r^{(0)}}\,J_{\nu_n}(t_r^{(0)}) - \cos\bar{\Phi}\sqrt{t_0}\,J'_{\nu_n}(t_r^{(0)})}{\frac{d}{dt}\left[\sqrt{t}\,J_{\nu_n}(t)\right]_{t=tr}} \qquad \text{(A.107)}$$

$$M(\nu n) = \frac{\cos\bar{\Phi}\sqrt{t_r^{(0)}}\,J_{\nu_n}(t) + \sin\bar{\Phi}\sqrt{t_r^{(0)}}\,J'_{\nu_n}(t_r^{(0)})}{\frac{d}{dt}\left[\sqrt{t}\,J_{\nu_n}(t)\right]_{t=t_r^{(0)}}} \qquad \text{(A.108)}$$

$$Q = R_{11}^{(1)} + \delta_{mn}\sum_{m=2}\frac{4m^2}{(m^2-1)^2(\mu_m^2-\mu_1^2)^2}R_{mm}^{(1)}$$

$$+2(1-\delta_{1m})\sum_{m=2}(-1)^{m+1}\frac{2^m}{m^2-1}\,\frac{1}{\mu_m^2-\mu_1^2}R_{1m}^{(2)}$$

$$+(1-\delta_{mn})\sum_{m=2}\sum_{n=2}(-1)^{m+n}\frac{4mn}{(m^2-1)(n^2-1)}\,\frac{}{(\mu_m^2-\mu_1^2)(\mu_n^2-\mu_1^2)}R_{mn}^{(2)}$$

A.5 Conclusions

The objective for the present analysis was to find relatively simple and manageable formulas having reasonable accuracy for the coupling between two planar aperture antennas spaced up to a few wave lengths apart. This objective has been accomplished for the case of waveguide terminated aperture antennas. Eqs. (A. 43) and (A. 44) predict experimental results up to a distance of one wavelength or slightly less. This indicates that the assumptions made in Eqs. (A. 16) through (A. 19) are justifiable for power calculations.

The significance of the formulas (A. 43) and (A. 44) is that expressions for the far-field ($\alpha = \frac{\pi}{2}$) and near-field ($\alpha = 0$) coupling are shown to be two special aspects of a unified general treatment, which cannot be accomplished through the use of the directivity concept. The near-field coupling formula for two ordinary waveguide terminated antennas (eq. (A. 44)) is as far as is known the first to be reported.

In the case of the E-Sectoral horn, some accuracy had to be sacrificed to keep the final results within the range of simple computer programming. However, eqs. (A. 59) through (A. 63) predict experimental results accurately in most significant aspects, e.g. power level and points of maxima and minima.

For H-Sectoral horns the analysis must be modified in order to adapt to a computer program; this remains to be done.

The present analysis can also be applied to higher mode coupling. There is some dependence of the modes of the aperture fields upon the relative location of two antennas. These relations are stated in the form of theorems.

APPENDIX B

COUPLING DUE TO SCATTERERS

B.1 Coupling Due to An Edge

Consider now the effect of a long edge upon the coupling between two antennas. Such an edge could be realized in practice by the intersection of a perfectly conducting ground plane and a flush-mounted radome, canopy or observation windown The length of the edge is assumed finite, but the antennas are close enough to the edge that the dominant return arises from specular scattering; thus the end effects are ignored. A condition upon the length of the edge will be given later. Since the main consideration is the return from the specular regions of the edge, there is essentially one scattering center, and the expression (5.42) can be used for the coupling. All that remains to do is to compute $\left|S_{vv}\right|^2$.

The first step is to compute the reflection coefficient for a plane wave travelling along a perfectly conducting semi-infinite face to an infinite wedge and incident obliquely toward the edge.

Consider a perfectly conducting wedge, the edge of which lies along the z axis of a cylindrical polar coordinate system (ρ, ϕ, z). The faces of the wedge will be given by $\phi = 0$ and $\phi = \phi_o$ (where ϕ_o is the exterior wedge angle). The incident radiation will be a plane wave travelling along the surface $\phi = 0$, obliquely toward the edge with the angle between the direction of propagation and z-axis being denoted by α. The incident electric intensity is given by

$$\overline{E}_i = \hat{y}\, e^{-jk\,(-x\sin\alpha + z\cos\alpha)} \qquad \text{(B.1)}$$

For the problem at hand, the electromagnetic field can be represented in terms of a two-dimensional scalar potential $V(\rho, \phi)$ by the relationships

$$\overline{E} = e^{-jkz \cos \alpha} \nabla x (\hat{z} V)$$

$$\overline{H} = j\sqrt{\frac{\epsilon}{\mu}}\, e^{-jkz \cos \alpha} \left[k V \sin^2 \hat{z} - j \nabla V \cos \alpha \right] \qquad (B.2)$$

where V is a solution of the scalar wave equation

$$\nabla^2 V + k'^2 V = 0 \qquad (B.3)$$

with

$$k' = k \sin \alpha . = \frac{2\pi}{\lambda} \sin \alpha \qquad (B.4)$$

The boundary condition that the tangential component of electric intensity vanishes on the faces of the wedge, gives the condition

$$\frac{\partial V}{\partial n} = 0, \text{ for } \phi = 0 \text{ and } \phi = \phi_o \qquad (B.5)$$

Where $\frac{\partial}{\partial n}$ represents the normal derivative. The incident field can be represented in terms of the potential V_i given by

$$V_i = E_o e^{+jk'x}, \quad E_o = +j/k' \qquad (B.6)$$

The problem reduces to finding the scattered scalar V_s such that $\frac{\partial (V_i + V_s)}{\partial n} = 0$ on the faces of the wedge, where in particular the scattered field on the back scattered direction (i.e. on the face $\phi = 0$) is required. Using the result of Oberhettinger (1954), (equation (29) therein) the appropriate Green's function is

$$G(\rho,\rho') = 2\left\{ H_o^{(2)}(k'\left|\rho-\rho'\right|) - \frac{\sin\frac{\pi^2}{\phi_o}}{\phi_o} \int_o^\infty \frac{H_o^{(2)}\left[k'(\rho^2+\rho'^2+2\rho\rho'\cosh x)^{1/2}\right]}{(\cosh\frac{\pi x}{\phi_o} - \cos\frac{\pi^2}{\phi_o}} dx \right\} \qquad \text{(B.7)}$$

which gives the total field at a point (ρ, $\phi = 0$) on the wedge due to a line source at (ρ, $\phi - 0$). To obtain the expression for a plane wave incident on the edge, multiply expression (B.7) by $\sqrt{\rho'}e^{jk'\rho'}$ and take the limit as $\rho' \longrightarrow \infty$. This yields the following expression

$$2A\left\{ e^{+jk'\rho} - \frac{\sin\frac{\pi^2}{\phi_o}}{\phi_o} \int_o^\infty \frac{\exp(-jk'\rho\cosh x)\,dx}{(\cosh\frac{\pi x}{\phi_o} - \cos\frac{\pi^2}{\phi_o})} \right\} \qquad \text{(B.8)}$$

For present purposes the factor A need not be specified. For an incident field of the form given by expression (B.6), the scattered field is given by the second term of expression (B.8) multiplied by $E_o/(2A)$, i.e.

$$V_s = \frac{E_o}{\phi_o} \sin\frac{\pi^2}{\phi_o} \int_o^\infty \frac{\exp(-jk'\rho\cosh x)}{\left(\cosh\frac{\pi x}{\phi_o} - \cos\frac{\pi^2}{\phi_o}\right)} dn \qquad \text{(B.9)}$$

At a sufficiently long distance away from the edge (i.e. $k'\rho \gg 1$), the integral expression (B.9) can be evaluated by the method of stationary phase, giving

$$V_s = -\frac{E_o}{\phi_o} \sin\frac{\pi^2}{\phi_o} \sqrt{\frac{\pi}{2k'\rho}} \frac{e^{-j(k'\rho+\pi/4)}}{\left(1-\cos\frac{\pi^2}{\phi_o}\right)} \tag{B.10}$$

Inserting this in the first equation of (B.2) gives the following expression for the back-scattered field

$$E_s = \hat{y} \frac{R}{\sqrt{k'\rho}} \exp\left[-jk'x - jkz\cos\alpha\right] \tag{B.11}$$

where

$$R = \frac{\sin\frac{\pi^2}{\phi_o}}{\phi_o} \frac{\sqrt{\pi/2}}{\left(1-\cos\frac{\pi^2}{\phi_o}\right)} e^{-j\pi/4} \tag{B.12}$$

For the particular case of a right-angled wedge ($\phi_o = 3\pi/2$,), the reflection factor R has the value

$$|R| = \frac{1}{3}\sqrt{\frac{2}{3\pi}} \tag{B.13}$$

Comparing the direction of propagation of the reflected wave to that of the incident wave, it is seen that the angles formed by the propagation vectors and the edge are the same. Hence, if a transmitter and receiver are a finite distance from the edge, the energy which is reflected from the edge to the receiver arises from a small scattering center on the edge. This scattering center is such that

the line form the transmitter to the scattering center, and the line from the receiver to the scattering center from the same angle with the edge, (see Fig. B-1). Thus the line TS and SR forms the ray path of the field directed from the transmitter to the receiver by way of the edge.

In order to compute the scattering matrix term S_{vv}, one must take into account the azimuthal curvature of the incident wave front arising from the transmitter. Consider the adjacent ray path going from transmitter to S' to receiver R' in Fig. B-1). Because of the curvature of the incident wave front, the energy incident on the segment of edge between S and S' will be spread out between the lines RS and R'S'. The ratio of the energy density between R and R' to the energy density between S and S' is $R_t/(R_t+R_r)$. Hence the electric intensity R must be multiplied by $\left[R_t/(R_t+R_r)\right]^{1/2}$ to take into account the curvature of the incident wave front. Thus S_{vv} is found by multiplying expression (B.11) by $\left[R_t/(R_t+R_r)\right]^{1/2}$ giving

$$\left|S_{vv}\right| = \frac{R}{\sqrt{k'\rho_r}} \sqrt{\frac{R_t}{R_t+R_r}} \qquad \text{(B.14)}$$

where $k' = k \sin\alpha$, and $\rho_r = R_r \sin\alpha$

For a right-angled wedge, the above reduces to

$$\left|S_{vv}\right|^2 = \frac{2}{27\pi} \left(\frac{R_t}{R_t+R_r}\right) \frac{1}{\sin^2\alpha} \qquad \text{(B.15)}$$

Hence from expression (5.42) the coupling due to a right-angled wedge is given by the relation

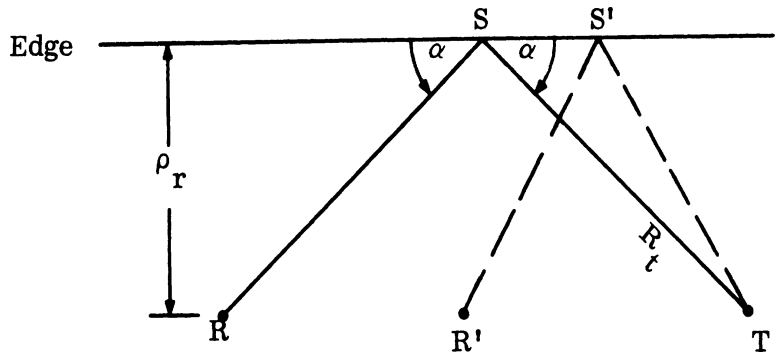

FIG. B-1: SCATTERING CENTER OF THE EDGE

$$C_s = \left(\frac{R_o}{R_t}\right)^2 \frac{2R_t}{27\pi(R_t+R_r)kR_r\sin^2\alpha} C(R_o, \psi_t, \psi_r) \qquad (B.16)$$

As an example, let the two antennas be the same distance ℓ from the edge, and a distance $2d_1$ apart. Then $\sin\alpha = \ell\,(\ell^2+d_1^2)^{-1/2}$, and $R_t = R_r = \sqrt{\ell^2+d_1^2}$. Further, let the antennas be mounted so that their E-planes are directed towards and away from, respectively, the scattering center of the edge: (See Fig. B-2)

$$C(R_o, \psi_t, \psi_r) = C(R_o, 0, 0) \qquad (B.17)$$

where $C(R_o, 0, 0)$ is the direct coupling between the two antenna a distance R_o apart, and oriented so that their E-planes lie along the line joining their centers. The coupling due to the edge is given by

$$C_s = \frac{1}{27\pi k\sqrt{\ell^2+d_1^2}} \left(\frac{R_o}{\ell}\right)^2 C(R_o, 0, 0) = \frac{1}{27\pi k\sqrt{\ell^2+d_1^2}} C(\ell, 0, 0)$$

$$= \frac{2}{27\pi}\left[C_o\left(\sqrt{\ell^2+d_1^2}\right)\right]^{1/2} \left(\frac{R_o}{\ell}\right)^2 C(R_o, 0, 0) \qquad (B.18)$$

The number $\left(\frac{2}{27\pi}\right)$ is (-16.3 db), so that C_s can be readily found from graphs available in this report. Note that the coupling is independent of R_o, which can be chosen for convenience.

As an example of this particular configuration, if the antennas are H-sectoral horns, the results of section 4.5.1 may be used. For a frequency of 10 GHz and a spacing R_o of 45.7 cm, the coupling for $\phi_r = \phi_r = 0$ is given in Fig. C-4c as -39.3 db. Several values of C_s are tabulated below:

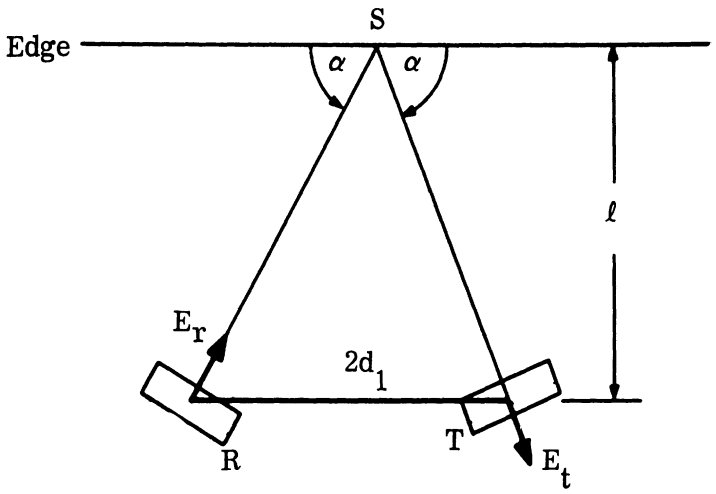

FIG. B-2: ORIENTATION OF ANTENNAS WITH RESPECT TO AN EDGE

$2d_1$	ℓ	C_s
45.7 cm	22.8 cm	-70.9 db
45.7 cm	11.4 cm	-63.7 db
22.8 cm	22.8 cm	-75.7 db
22.8 cm	11.4 cm	-67.9 db

Table B-1: Coupling level of two H-sectoral horns due to the presence of a right-angled wedge.

B.2 Coupling Due to the Leading Edge of a Wing

B.2.1 Part I: Geometric Optics Contribution for Antennas in Near Zone

The geometric optics scattering from the leading edge of a wing, taken to extend at right angles to the perfectly conducting common ground plane of two antennas, will now be considered. In the present analysis the termination of the wing will be neglected and taken to be infinite in extent; the contribution that arises from the scattering center at the base of the wing is desired. The leading edge of the wing will be taken to be a portion of a semi-infinite wedge. The associated geometry and orientations of the antennas with respect to the wedge on the ground plane is shown in Fig. B-3. The wing represented by the wedge extends out of the diagram. Since the scattered return from the wing arises from a small region around the base, there is esentally a local scattering center. Eq. (5.42) may be used, namely

$$C_s = \left(\frac{R_o}{R_t}\right)^2 \left|S_{vv}\right|^2 C(R_o, \phi_r, \phi_t) \qquad \text{(B.19)}$$

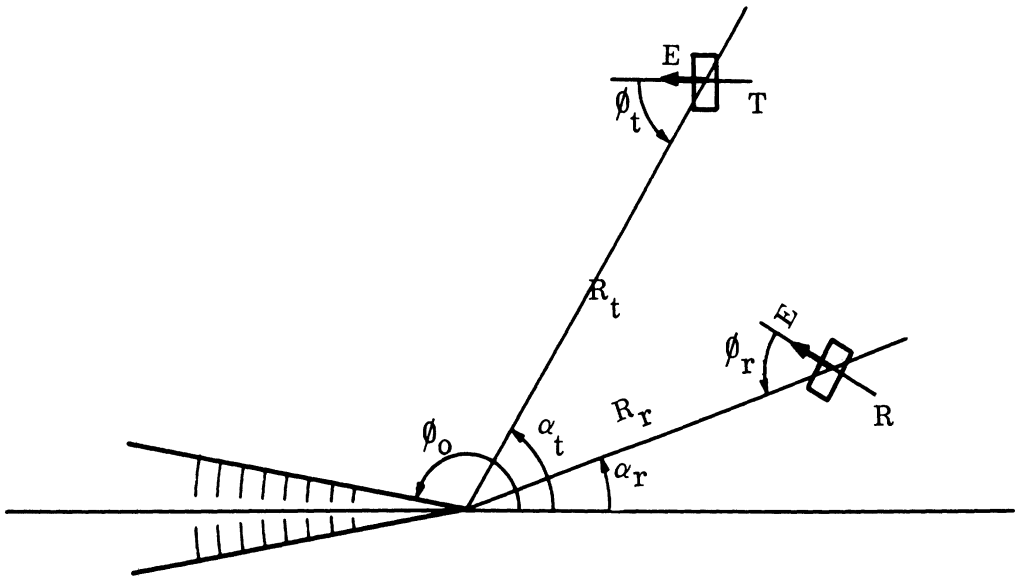

FIG. B-3: GEOMETRY AND ORIENTATIONS OF ANTENNAS WITH RESPECT TO WEDGE ON THE GROUND PLANE

where $C(R_o, \phi_r, \phi_t)$ is the direct coupling between the two antennas a distance R_o apart with orientation as indicated by Fig. 5-1. The basic problem is to obtain the scattering matrix term $\left|S_{vv}\right|$.

For a plane wave incident upon a wedge (exterior wedge half-angle ϕ_o) and polarized parallel to the edge, the scattered field at a sufficient number of wavelengths away from the edge, is given by Crispin, et al (1959):

$$E_s = -\frac{E_o}{4\phi_o} e^{-jkR_r} e^{-j\pi/4} \sqrt{\frac{2\pi}{kR_r}} \left(\frac{1}{A} + \frac{1}{B}\right) \sin^2 \frac{\pi}{2\phi_o} \qquad \text{(B.20)}$$

where

$$A = \cos\left[\frac{\pi}{2\phi_o}(\alpha_t + \alpha_r)\right] + \cos\frac{\pi^2}{2\phi_o} \qquad \text{(B.21)}$$

$$B = \left[\cos\frac{\pi}{2\phi_o}(\alpha_t - \alpha_r)\right] - \cos\frac{\pi^2}{2\phi_o} \qquad \text{(B.22)}$$

This results holds, provided that

$$2\phi_o > \pi + \left|\alpha_r + \alpha_t\right|$$

and

$$2\phi_o > \left|2\phi_1 - \pi\right| + \left|\alpha_r - \alpha_t\right|$$

Physically, this means that the position of receiver and transmitter is such that the scattered energy incident upon the receiver arises only from the edge, and not from specular scattering from either face of the wedge.

For a thin wedge $\phi_o \approx \pi$, in which case

$$A \approx \cos\left(\frac{\alpha_r + \alpha_t}{2}\right), \quad B \approx \cos\left(\frac{\alpha_r - \alpha_t}{2}\right) \tag{B.23}$$

However, in order to obtain the scattering matrix term (S_{vv}) one must take into account the effect of curvature of the incident wave front (in the vertical plane, i.e. perpendicular to ground plane). Expression (B.20) must be multiplied by a factor $\left[R_t/(R_t+R_r)\right]^{1/2}$. It follows that

$$\left|S_{vv}\right|^2 = \frac{2\pi}{kR_r}\left(\frac{R_t}{R_r+R_t}\right)\left[\frac{1}{4\phi_o}\left(\frac{1}{A}\right)\sin\frac{\pi^2}{2\phi_o}\right]^2 \tag{B.24}$$

which reduces to

$$\left|S_{vv}\right|^2 = \frac{R_t}{8\pi k R_r (R_r+R_t)}\left(\frac{1}{A}+\frac{1}{B}\right)^2 \tag{B.25}$$

for a thin wedge, $\phi_1 \approx \pi$.

The coupling is thus given by

$$C_s = \left(\frac{R_o^2}{R_r R_t}\right)\frac{1}{8\pi k(R_t+R_r)}\left(\frac{1}{A}+\frac{1}{B}\right)^2 C(R_o, \phi_r, \phi_t) \tag{B.26}$$

In order to illustrate the use of this result, consider two H-sectoral horns, both at the same distance from the wing (i.e. $R_r = R_t$). Consider a frequency of 10 GHz, and let R_o = 45.3 cm. The direct coupling term $C(R_o, \phi_r, \phi_t)$ can be obtained from known results. Let both antennas be oriented in the direction of the edge of the wing, i.e. such that $\phi_r = 0^o$, $\phi_t = 180^o$. Then suppose the direct coupling $C(R_o, 0, 0)$ has the value 2×10^{-4}, and

$$C_s = \left(\frac{R_o}{R_t}\right) \frac{1}{16\pi k R_t} \left(\frac{1}{A} + \frac{1}{B}\right)^2$$

Values of C_s are computed for various values of the parameters α_r, α_t, and R_t and are given in the table below

R_t	α_t	α_r	A	B	C_s
7.25"	60^o	0	.866	.866	57 db
7.25"	90^o	0	.707	.707	55 db
14.55"	60^o	0	.866	.866	66 db

Table B-2
Coupling Due to the Leading Edge of a Wing (Geometric Optics Cobtribution)

B.2.2 Part II: Contribution from the Traveling Wave Launched from the Wing Tip

In the previous section, the termination of the leading edge at the wing tip was neglected. Here consideration will be taken of this termination and the effect on the coupling.

The dominant currents producing the field scattered by the edge are edge currents. Besides those that are directly produced by the incident wave, there is a current that is alunched at the wing tip flowing along the edge inwards towards the fuselage (the ground plane of the antennas). This is reflected by the ground plane and a current flows outwards towards the tip. The total current (sum of the currents produced directly by the incident wave, and the traveling wave type currents flowing along the edge) is zero at the wing tip.

To obtain good estimates of the coupling, the leading edge will be modeled by a thin wire of finite length, for which theoretical results can be obtained. The main emphasis will be placed upon the current traveling from tip in toward the ground plane.

The first step will be to represent the far field pattern of the transmitting antenna given by expression (5.3) in terms of two Hertz vectors. The transmitting antenna coordinate system described in Fig. 5-2 will be used. The electric intensity can be expressed in terms of two potentials π and π^* by the relation.

$$E_t = \nabla\nabla\cdot(\pi\hat{z}) - \hat{z}\,\nabla^2\pi - j\omega\mu\nabla\times(\pi\hat{z}) \tag{B.27}$$

In particular, $E_{zt} = (k^2 + \frac{\partial^2}{\partial z})\pi$ (B.28)

For the far field one can set

$$\pi \sim \frac{e^{-jkr}}{r}\, g(\theta,\phi) \tag{B.29}$$

Thus on neglecting higher order terms in r, expression (B.28) becomes

$$E_{zt} \sim k^2 \frac{e^{-jkr}}{r} \sin^2\theta\, g(\theta,\phi) \tag{B.30}$$

Equating this to the z component of Eq. (5.3), one obtains

$$g(\theta,\phi) = \frac{-1}{k^2\sin\theta}\left[\hat{\theta}\cdot\bar{f}_t(\theta,\phi)\right] \tag{B.31}$$

Consider a vertical wire of length ℓ and radius a, extending out of the ground plane at the point $(p_t, \phi_t, z=0)$. The component of the incident field parallel to the wire (E_{zt}) is represented in terms of the scalar potential $\frac{e^{-jkr}}{r} g(\theta, \phi_t)$. From henceforth the variable ϕ_t will be dropped and the far field component $\hat{\theta} \cdot \bar{f}_t(\theta, \phi_t)$ will be written strictly as $f_t(\theta)$.

The next step will be to determine the current distribution produced on the wire by the incident wave. To simplify the analysis, the geometry of wire, ground plane, and transmitting antenna on the ground plane will be replaced by the equivalent geometry of the wire in free space extending a length ℓ above and below the $z=0$ plane, with the radiation field of the transmitting antenna being symmetrical with regards to the plane $z=0$. (i.e. $f_t(\theta) = f_t(\pi-\theta)$).

The problem of finding the current distribution on the wire can be treated in a similar manner as the analysis used by Vainshtein [1959] to obtain the current distribution on a wire of finite length with a plane wave incident. Let $\bar{J} = J\hat{z}$ be the current on the wire. Then the component of the electric intensity (at a point outside the wire) can be represented in the following form

$$E_z = + \frac{1}{jk} \left(k^2 + \frac{\partial^2}{\partial z^2}\right) A_z \qquad \text{(B.32)}$$

where

$$A_z = \frac{1}{4\pi} \sqrt{\frac{\mu_o}{\epsilon_o}} \int J \frac{e^{-jkR}}{R} \, ds \qquad \text{(B.33)}$$

The integral is over the surface of the wire, and R is the distance from a point of integration to the observation point. Set

$$2\pi a J = J_o \tag{B.34}$$

to be the total current per unit length of the wire. It is shown in Vainshtein (1959) that when the observation point approaches the surface of the wire, Eq. (B.33) can be approximated by

$$4\pi\sqrt{\frac{\epsilon_o}{\mu_o}}\, A_z = \int_{-\ell}^{\ell} \ln\left(\frac{2|z-\xi|}{a}\right) \operatorname{sgn}(z-\xi)\, \frac{d}{d\xi}\left(J_o(\xi)\, e^{-jk|z-\xi|}\right) d\xi \tag{B.35}$$

for a thin wire.

In addition, for a point on the wire

$$4\pi\sqrt{\frac{\epsilon_o}{\mu_o}}\, A_z = P_o\, e^{-jkz} + Q_o\, e^{\pm jkz} + S_o\, e^{-jkr_t(z)} \tag{B.36}$$

The current on the wire can be represented in the form

$$J_o(z) = P(z)e^{-jkz} + Q(z)e^{\pm jkz} + S(z)e^{-jkr_t(z)} \tag{B.37}$$

where P(z), Q(z) and S(z) are slowly varying functions.

The first two terms on the right-hand side of Eq. (B.37) represent the currents flowing along the wire and the third term is the current generated by the incident field. The current must vanish at the end points giving rise to the conditions

$$J_o(\ell) = J_o(-\ell) = 0 \tag{B.38}$$

Equations (B.35), (B.36) and (B.37) form an integral equation for the unknown factors P(z), Q(z), P_o and Q_o. Before investigating the solution, the appropriate

values of $S(z)$ and S_o must be obtained.

Physically the third terms on the right-hand side of equations (B.36) and (B.37) correspond to values that would be obtained for a wire of infinite length. It follows from Eq. (B.28), (B.29) and (B.30) that the potential A_i for the incident field has the form

$$A_{iz} \frac{-j\, f(\theta_t)}{kr_t \sin\theta_t} e^{-jkr_t}$$

Since the tangential components of the total electric field must vanish on the surface of the wire, we have

$$E_{iz} = -E_{sz} \quad \text{and} \quad A_{iz} = -A_{sz}$$

giving

$$A_{sz} = \frac{j\, e^{-jkr_t}}{kr_t \sin\theta_t} f(\theta_t) \tag{B.40}$$

Inserting this expression into the left-hand side of Eq. (B.29) for the infinite wire gives the relation

$$4\pi \sqrt{\frac{\epsilon_o}{\mu_o}} \left(\frac{+j}{k\rho_t}\right) e^{-jkr_t} f(\theta_t) = \int_{-\infty}^{\infty} \ln\left(\frac{2|z-\xi|}{a}\right) \operatorname{sgn}(z-\xi) \frac{d}{d\xi} \left(J_o(\xi)\, e^{-jk|z-\xi|}\right) d\xi \tag{B.41}$$

where $J(\xi) = S(\xi) \exp\left[-jkr_t(\xi)\right]$.

The relationship

$$\rho_t = r_t \sin\theta_t \tag{B.42}$$

is used, where ρ_t is the distance of the transmitting antenna from the base of the wire on the ground plane (see Fig. B-4). To obtain the asymptotic expression for $S(\xi)$, the integral in Eq. (B.41) is divided into two parts, the ranges of integration being from z to ∞, and $-\infty$ to z respectively. Because of symmetry one can take $z > 0$. The first integral has the form

$$-\int_z^{\infty} \ln\frac{2(\xi - z)}{a}\left\{S' - jkS\left(1 + \frac{\xi}{\sqrt{\rho_t^2+\xi^2}}\right)\right\}\exp\left(-jk(\xi - z) - jk\sqrt{\rho_t^2+\xi^2}\right)d\xi$$

$$+jk\,(1+\cos\theta_t)\,S(z)\,e^{-jkr_t}\int_0^{\infty}\ln\left(\frac{2t}{a}\right)e^{-ik(1+\cos\theta_t)t}\,dt, \tag{B.43}$$

which can be reduced to the following form

$$S(z)\,e^{-jkr_t}\,\ln\left[\frac{-2j}{\gamma ka\,(1+\cos\theta_t)}\right] \tag{B.44}$$

where $\gamma = 0.5772$ (B.45)

The second integral has the form

$$\int_{-\infty}^{z}\ln\frac{2(z-\xi)}{a}\left\{S' - jkS\left(-1 + \frac{\xi}{\sqrt{\xi^2+\rho_t^2}}\right)\right\}\exp -jk\left[(z-\xi) + \sqrt{\rho_t^2+\xi^2}\right]d\xi$$

(B.46)

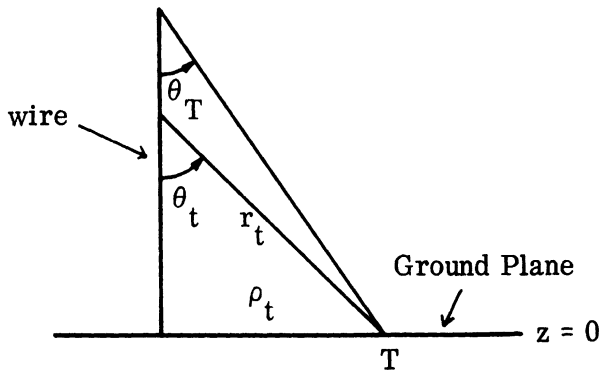

FIG. B-4: GEOMETRY OF WIRE PROTRUDING FROM THE GROUND PLANE

To obtain an asymptotic evaluation of the integral, let the value of z be in the range $|z| \leqslant \ell$. In addition it will be assumed that for the range $|z| < \ell$,

$$\left|\frac{S'(z)}{S(z)}\right| << k\left|1 - \frac{z}{\sqrt{\rho_t^2 + z^2}}\right| \tag{B.47}$$

This assumption will be examined further to determine the requirements that are necessary on the pattern of the transmitting antenna.

With assumption (B.47), expression (B.46) can be approximated by the relation

$$-jkS(z)\int_{-\infty}^{z} \ln\frac{2(z-\xi)}{a}\left[-1+\frac{\xi}{\sqrt{\rho_t^2+\xi^2}}\right]\exp\left[-jk\left(z-\xi+\sqrt{\rho_t^2+\xi^2}\right)\right] d\xi \tag{B.48}$$

Setting $\sigma = -\xi + \sqrt{\rho_t^2 + \xi^2}$,

and

$$\sigma_o = -z + \sqrt{\rho_t^2 + z^2}, \tag{B.50}$$

and employing the following relation

$$\ln\left(\frac{2(z-\xi)}{a}\right) = \ln\left(\frac{\sigma-\sigma_o}{a}\right) - \ln\left(\frac{\sigma}{a}\right) + \ln\left(\frac{\rho_t^2 + \sigma\sigma_o}{a\sigma_o}\right), \tag{B.51}$$

one obtains the following expression for relation (B.48)

$$jkS(z)\, e^{-jkz}\left\{ 2\, e^{-jk\sigma_o}\int_o^\infty \ln\frac{2s}{a}\, e^{-2jks}\, ds - 2\int_{\sigma_o/2}^\infty \ln\frac{2s}{a}\, e^{-2jks}\, ds \right.$$

$$\left. + \int_{\sigma_o}^\infty \ln\left(\frac{\rho_t^2 + \sigma\sigma_o}{\sigma\sigma_o}\right) e^{-jk\sigma}\, d\sigma \right\} \qquad \text{(B.52)}$$

Further reduction is achieved by employing the relation

$$2jk\int_o^\infty \ln\frac{2s}{a}\, e^{-2jks}\, ds = \ln\left(\frac{-j}{\gamma ka}\right) \qquad \text{(B.53)}$$

and integrating by parts the last two integrals in expression (B.52). This yields the following expression

$$S(z)e^{-jkr_t}\left\{ \ln\left(\frac{-j}{\gamma ka}\right) + \ln\left(\frac{\rho_t^2+\sigma_o^2}{\sigma_o^2}\right) - e^{jk\sigma_o}\int_{\sigma_o/2}^\infty \frac{e^{-2jk\sigma}}{\sigma}\, d\sigma \right.$$

$$\left. + e^{jk\sigma_o}\int_{\sigma_o}^\infty \frac{e^{-jk\sigma}\,\sigma_o\, d\sigma}{(\sigma\sigma_o+\rho_t^2)} \right\} \qquad \text{(B.54)}$$

last integral in the above expression is of the order of $(1/kr_t)$ and can be neglected In addition the following additional assumption will be made for the range $z \leqslant \ell$,

$$k\sigma_o >> 1 \text{ , or } k\left(-\ell + \sqrt{\ell^2+\rho_t^2}\right) >> 1 \qquad \text{(B.55)}$$

If $\rho_t << \ell$, then the requirement can be written in the following form

$$k\rho_t^2/\ell >> 1 \tag{B.56}$$

This inequality places a restriction upon the minimum distance between the transmitting antenna and the wire.

With the above restriction expression (B.54) can be approximated by the following

$$S(z)e^{-jkr_t} \ln\left[\frac{-j}{\gamma ka}\left(\frac{\rho_t^2+\sigma_o^2}{\sigma_o^2}\right)\right] \tag{B.57}$$

which reduces to the explicit form

$$S(z)e^{-jkr_t} \ln\left[\frac{-2j}{\gamma ka(1-\cos\theta_t)}\right] \tag{B.58}$$

where $\cos\theta_t = \dfrac{z}{\sqrt{\rho_t^2+z^2}}$ (B.59)

Combining expressions (B.41) and (B.58), and inserting the resulting sum for the right-hand side of equation (B.41), yields for S(z)

$$4\pi\sqrt{\frac{\epsilon_o}{\mu_o}}\left(\frac{j}{k\rho_t}\right) f(\theta_t) = 2S(z)\ln\left[\frac{-2j}{\gamma ka\sin\theta_t}\right], \tag{B.60}$$

giving

$$S(z) \sim \frac{j2\pi}{k\rho_t}\sqrt{\frac{\epsilon_o}{\mu_o}}\, f(\theta_t)\left[\ln\left(\frac{-2j}{\gamma ka\sin\theta_t}\right)\right]^{-1} \tag{B.61}$$

From (B. 36) and (B. 40) the following expression is derived for S_o

$$S_o(z) \sim \frac{j4\pi}{k\rho_t}\sqrt{\frac{\epsilon_o}{\mu_o}}\, f(\theta_t) \qquad \text{(B. 62)}$$

The remaining problem is to re-examine the inequality (B. 47). From expression (B. 61), this reduces to

$$\left|\frac{1}{f}\frac{\partial f}{\partial \theta_t} + \left[\ln\left(\frac{-2j}{\gamma ka \sin\theta_t}\right)\right]^{-1}\cot\theta_t\right| << \frac{k\rho_t}{1+\cos\theta_t} \qquad \text{(B. 63)}$$

The assumption that the antenna pattern is sufficiently slowly varying, or more explicitly, that $f(\theta_t)$ varies slowly over the distance of a wavelength on a circle of radius ρ_t centered at the transmitter, yields

$$\left|\frac{1}{f}\frac{\partial f}{6\theta_t}\right| << k\rho_t \qquad \text{(B. 64)}$$

The maximum value of the modulus of the second term on the left-hand side of (B. 63) for the range $0 < \cos\theta_t \leqslant \ell/\sqrt{\rho_t^2 + \ell^2}$ is the order of, or less than ℓ/ρ_t. Using the restriction given by inequality (B. 56) it follows that this term is small compared to the right-hand side of inequality (B. 63). Under the given restrictions inequality (B. 63) is satisfied.

The next step in the process is to obtain solutions for P(z) and Q(z). This involves obtaining solutions of the following equation.

$$\Lambda(J_o, z) = P_o e^{-jkz} + Q_o e^{jkz} + S_o e^{-jkr_t} \qquad \text{(B. 65)}$$

where for convenience the operator $\Lambda(J_o, z)$ is defined by the relation

$$\Lambda(J_o, z) = \int_{-\ell}^{\ell} \ln\left(\frac{2|z-\xi|}{a}\right) \operatorname{sgn}(z-\xi) \frac{d}{d\xi} \left(J_o(\xi)\, e^{-jk|z-\xi|}\right) d\xi \tag{B.66}$$

and the appropriate representation of $J_o(z)$ in terms of Q(z), P(z) etc. is given by relationship (B.37). From Vainshtein (1959), one can directly obtain the realtions

$$\Lambda(Pe^{jkz}, z) = g(0)\, P(z)e^{-jkz} - g(\ell - z)\, P(\ell)e^{-jk(2\ell - z)} + e^{-jkz}\int_{-\ell}^{z} \ln\frac{2(z-\xi)}{a}\, P'(\xi)d\xi \tag{B.67}$$

$$\Lambda(Qe^{-jkz}, z) = g(0)\, Q(z)e^{-jkz} - g(z+\ell)\, Q(-\ell)e^{-jk(z+2\ell)} - e^{-jkz}\int_{z}^{\ell} \ln\frac{2(\xi-z)}{a}\, Q'(\xi)\, d\xi \tag{B.68}$$

where

$$g(s) = \ln\frac{2s}{a} + e^{-2jks}\int_{s}^{\infty} \frac{e^{-2jk\sigma}}{\sigma}\, d\sigma \tag{B.69}$$

$$g(0) = \ln\frac{-j}{\gamma ka} \tag{B.70}$$

To obtain the complete expression for the right-hand side of equation (B.65) the term $\Lambda(e^{-jkr_t} S, z)$ has to be considered. From the symmetry relation $S(z) = S(-z)$, this term has the form:

$$\Lambda\left(e^{-jkr_t}s,\, z\right) = e^{-jkr_t} S_o + \int_{\ell}^{\infty} d\xi \left[S'(\xi) - jkS(\xi)\left(1 + \frac{\xi}{\sqrt{\rho_t^2 + \xi^2}}\right)\right] \cdot$$

$$\cdot e^{-jk\xi - jkr_t} \left[e^{jkz} \ln \frac{2(\xi - z)}{a} + e^{-jkz} \ln \frac{2(\xi + z)}{a} \right] \qquad \text{(B. 71)}$$

To reduce this expression $r_t(\xi)$ will be expanded about the point $\xi = \ell$, as follows

$$r_t = R_t + (\xi - \ell)\frac{\ell}{R_t} + \cdots$$

where $R_t = \sqrt{\rho_t^2 + \ell^2}$ (B. 72)

Then since the term $S'(\xi)$ is small compared to kS, the integral in expression (B. 71) can be approximated by

$$-j(k+w)\, S(\ell)\, e^{-jkR_t} \left\{ e^{jk(z-\ell)} \int_{\ell}^{\infty} e^{-j(k+w)(\xi-\ell)} \ln\left(2\frac{(\xi - z)}{a}\right) d\xi \right.$$

$$\left. + e^{-jk(z+\ell)} \int_{\ell}^{\infty} e^{-j(k+w)(\xi+\ell)} \ln \frac{2(\xi + z)}{a}\, d\xi \right\} \qquad \text{(B. 73)}$$

where $w = k\ell / R_t$. (B. 74)

Expression (B. 71) reduces to the form

$$\Lambda\left(e^{-jkr_t}S,\, z\right) = e^{-jkr_t}S_o - S(\ell)\, e^{-jkr_t}\left[e^{-jk(\ell - z)}\, g_+(\ell - z) + e^{-jk(\ell\, x\, z)}\, g_+(\ell + z)\right] \tag{B.75}$$

where

$$g_+(s) = j(k+w)\, e^{j(k+w)s}\int_s^\infty \ln\frac{2\sigma}{a}\, e^{-j(k+w)\,\sigma}\, d\sigma \tag{B.76}$$

Substitute the sum of expressions (B. 67) (B. 68) and (B. 75) for the right-hand side of equation (B. 65). Then equating terms which have the coefficient e^{jkt} and terms which have the coefficient e^{-jkz} one obtains, respectively, the relations

$$P_o = g(0)\, P(z) + \int_\ell^z \ln\frac{2}{a}(z-\xi)\, P'(\xi)\, d\xi - g(z+\ell)\, Q(-\ell)\, e^{-2jk\ell}$$

$$- S(\ell)\, e^{-jk\ell\ -jkr_t}\, g_+(z+\ell) \tag{B.77}$$

$$Q_o = g(0)\, Q(z) - \int_z^\ell \ln\frac{2}{a}(\xi - z)\, Q'(\xi)\, d\xi - g(\ell - z)\ P(\ell)\, e^{-2jk\ell}$$

$$- S(\ell)\, e^{-jk\ell\ -jkr_t}\, g_+(\ell - z) \tag{B.78}$$

The above two integral equations for P(z) and Q(z) can be further reduced. However, due to symmetry, P(z) = Q(-z), and only one equation need be considered. Considering equation (B.78), replace P(ℓ) by Q(-ℓ). Then set $z = \ell$, yielding an expression for Q_o in terms of Q(ℓ) and Q(-ℓ). Substituting this expression for Q_o back into the original relation, one obtains the following reduced equation for Q(z):

$$-\int_z^{\ell} \ln\left[\frac{-2j}{\gamma ka^2}(\xi - z)\right] Q'(\xi)\, d\xi = Q(-\ell)\, e^{-2jk\ell}\left[g(\ell - z) - g(0)\right]$$

$$+ S(\ell)\, e^{-jk\ell\ -jkR_t}\left[g_+(\ell - z) - g_+(0)\right] \qquad \text{(B.79)}$$

From Vainshtein (1959) the solution of this equation can be found, and is obtained in terms of two universal functions $\psi(z)$ and $\psi_+(z)$, by the following relation

$$Q(z) = -\psi_+(\ell - z)\, S(\ell)\, e^{-jk\ell\ -jkR_t} - Q(-\ell)\,\psi(\ell - z)\, e^{-2jk\ell} \qquad \text{(B.80)}$$

and inserting this expression for Q(-ℓ) into expression (B.80) giving

$$Q(z) = -S(\ell)\, e^{-jk\ell\ -jkR_t}\left[\psi_+(\ell - z) - \frac{\psi(\ell - z)\,\psi_+(2\ell)\, e^{-2jk\ell}}{1 + \psi(2\ell)\, e^{-2jk\ell}}\right] \qquad \text{(B.82)}$$

The appropriate expression for P(z) can be obtained on using the relationship P(z) = Q(-z). The current is now completely determined.

The universal functions $\psi(z)$ and $\psi_+(z)$ have the property that

$$\psi(0) = \psi_+(0) = 1 \tag{B.83}$$

Vainshtein (1959 and 1961) gives various approximate expressions for these functions, the accuracy of the approximation depending upon the smallness of the parameter ka. The particular approximate expression that will be used here is given by the following relations below, expressed in terms of a dimensionless variable x where

$$x = kz/q \tag{B.84}$$

$$\text{and } q = (ka)^2 \tag{B.85}$$

The expression for $\psi(z)$ is given by

$$\psi(z) = 2g(0)\left[I(x) - \theta(q)\, I(x,q)\right] \tag{B.86}$$

$$\text{where } g(0) = \ln \frac{-j}{\gamma ka} = \ln\left(\frac{-j}{\gamma\sqrt{q}}\right), \tag{B.87}$$

$$I(x) = \int_0^\infty \frac{e^{-xt}\,dt}{t\left[\pi^2 + (\ln \frac{\gamma^2 t}{2j})^2\right]} \tag{B.88}$$

$$I(x,q) = -e^{2jqx}\int_x^\infty e^{-2jq\xi}\, I'(\xi)\, d\xi, \tag{B.89}$$

and $$\theta(q) = \frac{1 - \frac{1}{2g(0)}}{\frac{1}{1+\gamma^2 q} - \frac{1}{2g(0)}} \qquad \text{(B.90)}$$

The expression for $\psi_+(z)$ is similar, given by

$$\psi_+(z) = 2g_+(0)\left[I(x) - \theta(q_+ I(x, q_+)\right] \qquad \text{(B.91)}$$

where the parameter q_+ in the expression $f_n\theta(q_+)$ and $I(x, q_+)$ is given by

$$q_+ = \frac{k(k+w)a^2}{2} \qquad \text{(B.92)}$$

The factor $g_+(0)$ associated with expression (133) and the corresponding expression for (B.90) is given by

$$g_+(0) = \ln\left[\frac{-j}{\gamma\sqrt{\frac{k(k+w)}{2}}\, a}\right] \qquad \text{(B.93)}$$

It is now possible to compute the scattered field produced by the wire. The scattered field produced by the currents on the wire ($0 \leqslant z \leqslant \ell$), will be computed first, with the effects of the ground plane (and the wire's image) ignored. The scattered field will then be decomposed into two main contributions, that arising from the currents at the base of the wire (near the ground plane) and that arising from the currents in the vicinity of the end of the wire. In the calculations of the coupling with an antenna on the common ground plane, the effects of the ground plane on the scattered field will then be taken into account.

With this in mind, the vector potential A associated with the currents on the wire ($0 \leqslant z \leqslant \ell$) will be first considered. From Eq. (B. 33) the vector potential is given by

$$\overline{A} = z \frac{1}{4\pi} \sqrt{\frac{\mu_o}{\epsilon_o}} \int_o^{\ell} \frac{e^{-jkR}}{R} \left[e^{-jk\xi} P(\xi) + e^{jk\xi} Q(\xi) + S(\xi)\, e^{-jkr_t(\xi)} \right] d\xi \tag{B.94}$$

where

$$R = \sqrt{x^2 + y^2 + (z-\xi)^2} \tag{B.95}$$

The electric intensity of the scattered field is expressed in terms of the potential $\overline{A} = A\hat{z}$ by the relation

$$jk\, \overline{E} = (\nabla\nabla \cdot A) - \nabla^2 \overline{A} \tag{B.96}$$

Employing cylindrical polar coordinates (ρ, ϕ, z) with the $z = 0$ plane being the ground plane, and the wire lying along the z-axis, the components of the electric field intensity are given by

$$jk\, E_z = \left(\frac{\partial^2}{\partial z^2} + k^2\right) A \tag{B.97}$$

$$jkE_\rho = \frac{\partial^2 A}{\partial z \partial \rho} \tag{B.98}$$

To obtain the values of E_z and E_ρ on the plane $z = 0$, the following relations are required

$$\left[\frac{\partial^2}{\partial \rho \partial z} \left(\frac{e^{-jkR}}{R} \right) \right]_{z=0} = \frac{e^{-jkr}}{R^3} k^2 \rho \xi \left[1 - \frac{j}{kR} - \frac{1}{(kR)^2} \right] \tag{B.99}$$

$$\left[\left(k^2+\frac{\partial^2}{z^2}\right)\left(\frac{e^{-jkR}}{R}\right)\right]_{z=0} = \frac{e^{-jkR}}{R^3}\rho^2k^2\left[1-\frac{j}{kR\rho^2}(\rho^2-2\xi^2)+\frac{2\xi^2-\rho^2}{k^2\rho^2R^2}\right]$$

(B. 100)

The analysis will be performed for the case $kR>>1$, with the following restriction placed upon the length ℓ,

$$k\rho^2\sqrt{\rho^2+\ell^2} >> \ell^2 \qquad \text{(B. 101)'}$$

which implies that if $\ell>\rho$, then $k\rho^2/\ell>>1$. Thus with the above consideration, terms of the order of $1/(kR)$ and $\xi^2/(\rho^2kR)$ can be neglected in expressions (B. 99) and (B. 100).

The electric intensity is given by the approximation

$$\overline{E} = -\frac{jk}{4\pi}\sqrt{\frac{\mu_o}{\epsilon_o}}\,\rho\int_o^\ell \frac{e^{-jkR}}{R^2}J_o(\xi)\left[\frac{\rho}{R}\hat{z}+\frac{\xi}{R}\hat{\rho}\right]d\xi \qquad \text{(B. 102)}$$

For a field point on the ground plane ($z=0$) at a distance ρ from the wire, using relationship (B. 37) for the current, it is seen that the evaluation of expression (B. 102) requires the computation of the following three integrals.

$$\int_o^\ell e^{-jk(R+\xi)}\frac{P(\xi)}{R^2}\left[\frac{\rho}{R}\hat{z}+\frac{\xi}{R}\hat{\rho}\right]d\xi\,, \qquad \text{(B. 103)}$$

$$\int_o^\ell e^{-jk(R-\xi)}\frac{Q(\xi)}{R^2}\left[\frac{\rho}{R}\hat{z}+\frac{\xi}{R}\hat{\rho}\right]d\xi \qquad \text{(B. 104)}$$

$$\int_0^{\ell} e^{-jk(R+r_t)} \frac{S(\xi)}{R^2}\left[\frac{\rho}{R}\hat{z}+\frac{\xi}{R}\hat{\rho}\right] d\xi \qquad \text{(B.105)}$$

All of these integrals are characterized by the integrand being composed of the product of a rapidly oscillating function times a slowly varying function. Hence, asymptotic techniques such as stationary phase techniques might be used. Integrals (B.103) and (B.104), however, have no stationary phase points in the range of integration and hence the dominant return arises from the end points. The third integral does possess a stationary point at $z=0$. The contribution arising from the stationary phase point will be evaluated first, since physically it corresponds to the geometric optics contribution.

The latter contribution at a distance ρ_r from the wire is given by

$$\overline{E} = \frac{-jk}{\rho_r 4\pi}\sqrt{\frac{\mu_o}{\epsilon_o}}\, z \int_0^{\infty} e^{-jk(R+r_t)} S(0)\, d\xi \qquad \text{(B.106)}$$

where

$$R = \sqrt{\rho_r^2 + \xi^2} \qquad \text{(B.107)}$$

$$r_t = \sqrt{\rho_t^2 + \xi^2} \qquad \text{(B.108)}$$

The integral can be evaluated by the stationary phase technique, yielding the expression

$$\overline{E} = \hat{z}\,\frac{k}{4\pi}\left[\frac{\mu_o\,\pi}{\epsilon_o\, 2k\left(\frac{1}{\rho_t}+\frac{1}{\rho_r}\right)}\right]^{1/2} \frac{S(0)}{\rho_r}\, e^{-jk(\rho_t+\rho_r)-3j\pi/4} \qquad \text{(B.109)}$$

which, on employing expression (B.64), becomes

$$\bar{E} = \hat{2}\frac{1}{2}\sqrt{\frac{\pi}{2}}\left[k\rho_t\rho_r(\rho_t+\rho_r)\right]^{-1/2} f_t(\tfrac{\pi}{2})\left[\ln\frac{-2j}{\gamma ka}\right]^{-1} e^{-jk(\rho_t+\rho_r)-j\pi/4} \tag{B.110}$$

However this result has to be corrected to take into account the effect of the ground plane. This implies multiplying the right-hand side of expression (B.110) by 2. Since the amplitude of the field incident at the base of the wire is $f_t(\pi/2)/\rho_t$, expression (B.110) can be normalized to correspond to an incident field of unit intensity. This yields the scattering matrix term

$$\left|S_{vv}\right|^2 = \frac{\pi}{4}\,\frac{\rho_t}{k\rho_r(\rho_t+\rho_r)}\,\left|\ln(\frac{-2j}{\gamma ka})\right|^{-2} \tag{B.111}$$

It is now possible to make a comparison between the two models of the wing edge. Eq. (B.25) gives the scattering matrix coefficient when the edge of the wing is modeled by a half-plane, and equation (B.111) when the leading edge is represented by a wire. The main difference is that the factor

$$4\pi^2\left|\ln(\frac{-2j}{\gamma ka})\right|^2 \tag{B.112}$$

in Eq. (B.111) corresponds to the factor

$$(\frac{1}{A}+\frac{1}{B})^2 \tag{B.113}$$

In Eq. (B.25) where A and B are given by relation (B.23). Typical values of A and B that were given were A=B=.866, implying that the factor (B.113) is the order of 5. For a wire radius such that $ka \sim 2\times10^{-1}$, factor (B.112) is approximately 8.

Hence, the modeling of the edge of the wing by a wire, as far as the geometric return from the edge is concerned, yields a good estimate. The main reason for modeling the leading edge of the wing by a wire is to deduce the effect of the ends of the wing upon the coupling. Thus, attention will be returned to considering expressions (B.103), (B.104) and the contribution of expression (B.105) arising from the vicinity of $\xi = \ell$. The evaluation of these integrals involves, mainly, the technique of integration by parts. Performing such a process, expression (B.103) becomes

$$\frac{P(\ell)\left[\sin\theta_r \hat{z} + \cos\theta_r \hat{\rho}\right]}{-jkR_r^2 (1+\cos\theta_r)} e^{-jkR_r - jk\ell} + \frac{P(0)}{jk\rho_r^2} e^{-jk\rho_r} \hat{z} \qquad \text{(B.114)}$$

The distance of the receiver (or observation point) from the end of the wing (or wire) is given by

$$R_r = \sqrt{\ell^2 + \rho_r^2} \qquad \text{(B.115)}$$

and the angle subtended at the end of the wire is

$$\sin\theta_r = \rho_r / R_r \qquad \text{(B.116)}$$

Expression (B.104) will be split up into two integrals, the ranges of integration being $\infty \leqslant z \leqslant \ell$ and $-\infty \leqslant z \leqslant 0$. The second integral will be evaluated by integration by parts. Thus yields the following approximation for expression (B.104).

$$\int_{-\infty}^{\ell} \frac{Q(\xi)}{R^2} e^{-jk(R-\xi)} \left\{ \frac{\rho}{R} \hat{z} + \frac{\xi}{R} \hat{\rho} \right\} d\xi - \frac{Q(0)}{jk\rho_r^2} e^{-jk\rho_r} \hat{z} \qquad \text{(B.117)}$$

The remaining contribution to consider is that arising from the end point $\xi = \ell$ of expression (B.105). This is given by

$$\frac{S(\ell)\left[\sin\theta_r \hat{z} + \cos\theta_r \hat{\rho}\right]}{-jkR_r^2 (\cos\theta_r + \cos\theta_T)} e^{-jk(R_t + R_r)} \qquad \text{(B.118)}$$

where R_t is the distance of the transmitter from the end of the wing, θ_T is the particular value of θ_t given by Eq. (B.59) with $z = \ell$, namely

$$\cos\theta_T = \ell / R_t \qquad \text{(B.119)}$$

The combination of Eqs. (B.114), (B.117) and (B.118) yields the contribution to the scattered field arising from the currents at the end of the wire, as follows

$$\overline{E} = \frac{-jk}{4\pi} \sqrt{\frac{\mu_o}{\epsilon_o}} \rho_r \left\{ \int_{\infty}^{\ell} \frac{Q(\xi)}{R^2} e^{-jk(R-\xi)} \left[\frac{P}{R} \hat{z} + \frac{\xi}{R} \hat{\rho} \right] d\xi \right.$$

$$\left. - \frac{(\sin\theta_r \hat{z} + \cos\theta_r \hat{\rho})}{jkR_r^2} e^{-jkR_r} \left[\frac{P(\ell) e^{-jk\ell}}{(1+\cos\theta_r)} + \frac{S(\ell) e^{-jkR_t}}{(\cos\theta_r + \cos\theta_T)} \right] \right\} \qquad \text{(B.120)}$$

In expression (B.120) the dominant part arises from the integral. Physically, this represents the contribution from a current launched at the tip of the wire and traveling towards the ground plane. Radiation from such a traveling

wave is endfire towards the ground plane. If the receiver is close enough to the wire it may pick up a significant amount of energy from this wave. The dominant contribution to this integral arises from the vicinity of the point $\xi = \ell$. With the restriction that $k\rho_r^2/\ell >> 1$, and expanding $R(\xi)$ as follows

$$R(\xi) \sim R_r + (\xi - \ell)\cos\theta_r +$$

The integral in expression (B. 120) can be approximated by

$$\frac{(1+\cos\theta_r)}{-jk\rho_r^2}(\sin\theta_r \hat{z} + \cos\theta_r \hat{\rho})\, e^{-jk(R_r - \ell)}\left\{-Q(\ell) - \int_0^\infty e^{-jk(1-\cos\theta_r)x} Q'(\ell - x)dx\right\} \tag{B.121}$$

As indicated by expression (B. 82) Q(z) is expressed as a linear combination of the universal functions $\psi_+(\ell - z)$ and $\psi(\ell - z)$, i.e.

$$Q(z) = -S(\ell)\, e^{-jk(\ell + R_t)}\left[\psi_+(\ell - z) - A\psi(\ell - z)\right], \tag{B.122}$$

$$A = \frac{\psi_+(2\ell)\, e^{-2jk\ell}}{1 + \psi(2\ell)\, e^{-2jk\ell}} \tag{B.123}$$

The evaluation of the expression

$$\int_0^\infty e^{-jk(1-\cos\theta_r)x} Q'(\ell - x)\, dx = -S(\ell)\, e^{-jk(\ell + R_t)}\left[I_2 - AI_1\right] \tag{B.124}$$

requires the computation of the two integrals

$$I_1 = \int_o^\infty \exp\left[-jk(1-\cos\theta_r)\,z\right]\,\psi'(z)\,dz \qquad \text{(B.125)}$$

$$I_2 = \int_o^\infty \exp\left[-jk(1-\cos\theta_r)\,z\right]\,\psi_+'(z)\,dz \qquad \text{(B.126)}$$

From relationships (B.84) and (B.86), the first integral I_1 takes the form

$$I_1 = 2g(o)\int_o^\infty e^{-2jq'x}\left\{ I'(x)\,(1-\theta) + 2jq\theta\, e^{+2jqx}\int_x^\infty e^{-2jq\xi}\, I'(\xi)\,d\xi \right\} dx, \qquad \text{(B.127)}$$

with $2q' = (1-\cos\theta_r)\,q$. (B.128)

Integrating by parts the second term in the integral yields the relation

$$I_1 = 2\,g(0)\left[\left(1-\frac{q'}{q'-q}\theta\right)\int_o^\infty e^{-2jq'\xi}\, I'(\xi)\,d\xi + \frac{q}{q'-q}\int_o^\infty e^{-2jq\xi}\, I'(\xi)\,d\xi\right] \qquad \text{(B.129)}$$

The above can be simply reduced using the following relation given by Vainshtein (1959)

$$\int_o^\infty e^{-2jq\xi}\, I'(\xi)\,d\xi = -\frac{1}{1+\gamma^2 q} + \frac{1}{\ln\left[-j/(\gamma\sqrt{q})\right]} \qquad \text{(B.130)}$$

Further simplification will be achieved, in assuming that the wire is sufficiently thin so that $\gamma^2 q = \gamma^2 (ka)^2 << 1$. With this approximation, expression (B.129(reduces to the form

$$I_1 \sim \frac{-2}{(1+\cos\theta_r)} \left[1 - \ln\left(\frac{-j}{\gamma ka}\right) \Big/ \ln\left(\frac{-j\sqrt{2}}{\gamma ka \sqrt{1-\cos\theta_r}}\right) \right] \qquad \text{(B.131)}$$

$$I_2 \sim - \frac{(1+\cos\theta_r)}{(\cos\theta_r + \cos\theta_T)} \left[1 - \ln\left(\frac{-j}{\gamma ka}\sqrt{\frac{2}{1+\cos\theta_T}}\right) \Big/ \ln\left(\frac{-j}{\gamma ka}\sqrt{\frac{2}{1-\cos\theta_r}}\right) \right]$$

(B.132)

From Eqns. (B.121), (B.122), (B.131) and (B.132) the appropriate expression for the integral in Eq. (B.120) is obtained. Combining all the results, one obtains the following form for the scattered electric field strength.

$$\overline{E} = \frac{1}{4\pi}\sqrt{\frac{\mu_o}{\epsilon_o}}\,\frac{S(\ell)}{k\rho_r}\, e^{-jk(R_t+R_r)} (\sin\theta_r \hat{z} + \cos\theta_r \hat{\rho})\, F\,, \qquad \text{(B.133)}$$

$$F = \frac{(1+\cos\theta_r)(1+\cos\theta_t)}{(\cos\theta_r + \cos\theta_T)}$$

$$\left[\ln\left(\frac{-j}{\gamma ka}\sqrt{\frac{2}{1+\cos\theta_t}}\right) + 2A \ln\left(\frac{-j}{\gamma ka}\right) \right] \Big/ \ln\left(\frac{-j}{\gamma ka}\sqrt{\frac{2}{1-\cos\theta_r}}\right)$$

(B.134)

Physically, expression (B.133) represents a spherical wave originating from the end of the wire, and polarized in a vertical plane (plane containing the wire). The coefficient A arises from the multiple reflections of the traveling waves at the ground plane and end of the wire. Without going into details, it can be shown that for a sufficiently long wire ($k\ell >> 1$) , A can be approximated by

$$A \doteq \left\{ \frac{2\ln(-j/(\gamma ka) - \ln(\frac{1+\cos\theta_T}{2})}{\ln\left[-j\,4\ell\,/\,(\gamma ka^2)\right]} \right\} e^{-2jk\ell}$$

Henceforth, the length of the wire will be taken to be sufficiently long so that the term with A as a coefficient, can be neglected.

The factor $S(\ell)$, given by expression (B.61), contains the amplitude and phase of the field incident at the end of the wire. The scattering matrix coefficient $\left|S_{vv}\right|$ is obtained by a process of normalization of the modules of expression (B.133), whereby the amplitude of the incident field is divided out. This yields

$$\left|S_{vv}\right| = \frac{R_t\,(1+\cos\theta_r)(1+\cos\theta_t)}{2k\rho_t\rho_r(\cos\theta_r+\cos\theta_T)} \left| \ln(\frac{-j}{\gamma ka}\sqrt{\frac{2}{1+\cos\theta_r}}) \right| \cdot$$

$$\cdot \left| \ln(\frac{-j}{\gamma ka}\sqrt{\frac{2}{1-\cos\theta_r}})\ln(\frac{-2j}{\gamma ka\sin\theta_T}) \right|^{-1} \qquad \text{(B.135)}$$

Unfortunately, because of the approximations made in the analysis, formula (B.335) is not symmetric with respect to the angles θ_r and θ_T.

Expression (B.135) can be represented in a symmetric form by making the following approximations

$$\ln\left(\frac{-j}{\gamma ka}\sqrt{\frac{2}{1+\cos\theta_r}}\right) \doteq \ln\left(\frac{-j}{\gamma ka}\right) \tag{B.136}$$

$$\ln\left(\frac{-j}{\gamma ka}\sqrt{\frac{2}{1-\cos\theta_r}}\right) \doteq \ln\left(\frac{-2j}{\gamma ka \sin\theta_r}\right) \tag{B.137}$$

The error will be small for values of θ_r and θ_T lying between 0^o and 45^o, and ka not too large. As an example, taking the value ka = 2×10^{-1}, we obtain

$$\ln\left(\frac{-j}{\gamma ka}\right) \doteq 1.04$$

$$\left|\ln\left(\frac{-j}{\gamma ka}\sqrt{\frac{2}{1+\cos\theta_r}}\right) - \ln\left(\frac{-j}{\gamma ka}\right)\right| < .08$$

for $0<\theta_r<\pi/4$. Thus the error is small.

The symmetric form of S_{vv} is given by

$$\left|S_{vv}\right| = \frac{R_t}{k\rho_t\rho_r} D(\theta_T, \theta_r) \tag{B.138}$$

$$K(\theta_T,\theta_r) = \frac{(1+\cos\theta_r)(1+\cos\theta_T)}{2(\cos\theta_T+\cos\theta_r)}\left|\ln\left(\frac{-j}{\gamma ka}\right)\right|\left|\ln\left(\frac{-2j}{\gamma ka\sin\theta_T}\right)\right|^{-1}\left|\ln\left(\frac{-2j}{\gamma ka\sin\theta_r}\right)\right|^{-1} \tag{B.139}$$

For θ_T and θ_r ranging in values between 10^o and 45^o, and ka = .2 (where a is the wire radius), K takes on values between .2 and .5. However the results were derived for a wire model of the leading edge of the wing. In the actual case where the scattering is due to currents originating from the tip of the wing, and traveling along the edge towards the ground plane, K would be different. However, taking the value of K associated with the thin wire problem would yield a good estimate. For the values of angles θ_r and θ_T under consideration, K can be taken to be of the order of 1/2. Recall that the results were derived under the assumptions that the quantities $k\ell$, $k\rho_r$, $k\rho_t$, $k\rho_t^2/\ell$, and $k\rho_r^2/\ell$ were much greater than unity. In addition ρ_r/ℓ and ρ_t/ℓ were taken to be less than or equal to unity. This restricts the values of θ_T and θ_r.

With these considerations, the coupling due to the currents launched at the tip of the wing, is given by

$$C_s = C_o(R_t)\, D_t(\theta_T, \phi_t)\, D_r(\theta_r, \phi_r) \left|S_{vv}\right|^2 \left|\hat{p}_r \cdot \hat{v}_s\right| \left|\hat{p}_t \cdot \hat{v}_i\right|$$

$$= 4K^2 C_o(\rho_t)\, C_o(\rho_r)\, D_t(\theta_t, \phi_t)\, D_r(\theta_r, \phi_r) \left|\hat{p}_r \cdot \hat{v}_s\right| \left|\hat{p}_t \cdot \hat{v}_i\right| \qquad \text{(B.140)}$$

where K is approximately the order of 1/2.

The important feature to notice about the coupling is that it depends predominantly upon the distances of the receiver and transmitter from the leading edge of the wing (and not the distances to the tip). If the wing was tilted and not perpendicular to the ground plane, then the distances ρ_t and ρ_r would be perpendicular distances from the transmitter and receiver to the leading edge. Tilting the wing away from the transmitter and receiver would decrease the values of θ_r, ρ_t, θ_T and ρ_r.

APPENDIX C

RECTANGULAR HORN DATA

C.1 Curves and Tables for Rectangular Horn Coupling Calculation

In Section 4.5.1 an expression is given for the directivity function of a rectangular horn in terms of a finite integral. This integral was evaluated for values of flare half-angle up to 45°, and dimensions up to ten wavelengths, using an IBM - 7090 computer. The results are indicated in Table C-1. Curves are plotted for a number of horns for dimensions up to five wavelengths in Figs. C-1a to C-1m, C-2a to C-2m. Also included are the simplified curves obtained from Section 3.3 for approximate answers. These are given in Table C-2 as well. It should be noted that the flare angle utilized is actually the flare half-angle of the horn, as in Fig. 4-24. Also, the calculations are far-field, and thus applications must satisfy the $\frac{L^2}{\lambda}$ spacing criterion of Section 3.5. This is discussed further in Sections C.2 and C.3.

Several points should be noted in using the tables:

(1) The angle referred to as "PHI" is related to ϕ of the formulas by PHI = $\phi + 90^{\circ}$. The function SINE-SQUARED PHI becomes $\cos^2\phi$. This discrepancy does not appear in the curves.

(2) The functions G_u and G_v as utilized are defined as follows:

$$G_u = \frac{\pi^2}{16\sqrt{1-(\frac{\lambda}{2a})^2}} (\frac{a}{\lambda}) \left| g_a(u) \right|^2$$

$$G_v = \frac{1}{4} (\frac{b}{\lambda}) \left| g_b(v) \right|^2$$

so that the directivity function $D(\phi)$ is given by

$$D(\phi) = \frac{\pi}{4} G_u G_v \cos^2 \phi$$

or

$$D(\phi)db = -1.04\,db + (G_u)db + (G_u)db + (\cos^2 \phi)db$$

The three functions G_u, G_v, and $\cos^2 \phi$ are obtained from table C-1.

In Figs. C-1 and C-2 to follow, the following points should be noted:

(1) The zero level of the chart paper corresponds to +10 db. Thus readings should be increased by 10 db.

(2) Flare half-angles of 0^o, 20^o, and 40^o are indicated on the left, while flare half-angles of 10^o and 30^o are indicated on the right, along with the approximating curve of Section 3.3.

(3) The following scheme is used for identifying the curves

On the left: 0^o - •; 20^o - x; 40^o - Δ

On the right: 10^o - •; 30^o - x; Gross - Δ

(4) The flare half-angle of Fig. C-1 is θ_a, while that of Fig. C-2 is θ_b.

(5) The curves plot the following functions in db:

$\frac{\pi}{2} G_u$ vs ϕ

and

$G_v \cos^2 \phi$ vs ϕ

so that $D(\phi)$ can be obtained from the charts by

$$D(\phi)_{db} = (\frac{\pi}{2} G_u)_{db} + (G_v \cos^2 \phi)_{db} - 3 \text{ db}.$$

(6) The extra curve on the right-hand side of the charts is the simplified function of Section 3.3. By comparing this with the other curves, representing various flare angles, its accuracy in a given situation can be estimated.

TABLE C-1: HORN COUPLING FUNCTIONS (VALUES IN DB)

G-SUB-U (A/L,FLARE ANGLE,PHI)

A/LAMBDA = 1.0

FLARE ANGLE	Ø=84°	12	18	24	30	36	PHI 42	48	54	60	66	72	78	84	Ø=0°
0.	-6.69	-6.32	-5.74	-4.98	-4.09	-3.12	-2.13	-1.14	-.22	.62	1.35	1.94	2.37	2.63	2.72
5	-6.67	-6.30	-5.72	-4.96	-4.08	-3.12	-2.13	-1.15	-.23	.61	1.33	1.92	2.35	2.61	2.70
10	-6.59	-6.23	-5.67	-4.93	-4.06	-3.11	-2.14	-1.17	-.26	.57	1.29	1.87	2.30	2.56	2.64
15	-6.47	-6.13	-5.58	-4.86	-4.02	-3.10	-2.15	-1.21	-.31	.51	1.21	1.78	2.20	2.46	2.55
20	-6.31	-5.99	-5.47	-4.79	-3.98	-3.09	-2.17	-1.26	-.39	.41	1.10	1.66	2.07	2.32	2.41
25	-6.13	-5.83	-5.34	-4.69	-3.93	-3.09	-2.21	-1.33	-.49	.28	.95	1.49	1.89	2.14	2.22
30	-5.94	-5.66	-5.20	-4.60	-3.89	-3.09	-2.26	-1.42	-.62	.11	.76	1.28	1.66	1.90	1.98
35	-5.74	-5.49	-5.07	-4.52	-3.85	-3.12	-2.34	-1.55	-.79	-.09	.52	1.02	1.39	1.61	1.69
40	-5.57	-5.33	-4.95	-4.45	-3.85	-3.17	-2.44	-1.71	-1.01	-.35	.22	.69	1.04	1.26	1.33
45	-5.42	-5.21	-4.87	-4.42	-3.87	-3.26	-2.60	-1.93	-1.28	-.67	-.14	.30	.63	.83	.90

A/LAMBDA = 1.4

FLARE ANGLE	6	12	18	24	30	36	PHI 42	48	54	60	66	72	78	84	90
0	-22.31	-20.38	-17.77	-14.89	-12.01	-9.24	-6.66	-4.31	-2.22	-.41	1.11	2.30	3.16	3.68	3.85
5	-21.15	-19.56	-17.26	-14.59	-11.84	-9.14	-6.61	-4.29	-2.21	-.41	1.09	2.28	3.14	3.66	3.83
10	-18.84	-17.75	-16.01	-13.80	-11.36	-8.87	-6.46	-4.21	-2.19	-.42	1.06	2.23	3.08	3.59	3.76
15	-16.58	-15.81	-14.52	-12.76	-10.68	-8.45	-6.22	-4.10	-2.16	-.45	.99	2.14	2.97	3.48	3.65
20	-14.65	-14.06	-13.05	-11.64	-9.90	-7.95	-5.93	-3.96	-2.12	-.49	.90	2.02	2.83	3.32	3.48
25	-13.02	-12.54	-11.72	-10.56	-9.09	-7.40	-5.60	-3.80	-2.09	-.54	.78	1.85	2.63	3.11	3.27
30	-11.65	-11.24	-10.55	-9.57	-8.32	-6.86	-5.26	-3.63	-2.06	-.62	.63	1.64	2.39	2.84	2.99
35	-10.48	-10.12	-9.53	-8.68	-7.61	-6.34	-4.94	-3.48	-2.06	-.73	.43	1.38	2.08	2.51	2.66
40	-9.49	-9.17	-8.64	-7.91	-6.98	-5.87	-4.65	-3.36	-2.08	-.88	.18	1.06	1.72	2.12	2.25
45	-8.64	-8.36	-7.90	-7.25	-6.44	-5.48	-4.42	-3.29	-2.16	-1.08	-.12	.68	1.27	1.64	1.77

A/LAMBDA = 1.8

FLARE ANGLE	6	12	18	24	30	36	PHI 42	48	54	60	66	72	78	84	90
0	-18.66	-19.04	-19.96	-22.18	-28.69	-29.91	-17.19	-10.73	-6.14	-2.61	.13	2.21	3.67	4.54	4.82
5	-18.41	-18.72	-19.48	-21.17	-24.52	-23.97	-16.38	-10.50	-6.06	-2.59	.13	2.19	3.64	4.51	4.80
10	-17.71	-17.87	-18.28	-19.06	-19.98	-18.89	-14.60	-9.87	-5.82	-2.51	.13	2.15	3.58	4.43	4.72

15	-16.74	-16.74	-16.80	-16.92	-16.82	-15.61	-12.71	-9.01	-5.46	-2.40	.12	2.07	3.47	4.30	4.58		
20	-15.63	-15.56	-15.31	-15.03	-14.47	-13.24	-11.01	-8.08	-5.03	-2.25	.11	1.97	3.31	4.11	4.38		
25	-14.50	-14.28	-13.92	-13.40	-12.63	-11.41	-9.56	-7.17	-4.58	-2.09	.07	1.82	3.10	3.87	4.13		
30	-13.40	-13.11	-12.65	-12.01	-11.14	-9.95	-8.34	-6.34	-4.13	-1.94	.02	1.64	2.83	3.56	3.81		
35	-12.34	-12.02	-11.51	-10.81	-9.90	-8.75	-7.32	-5.61	-3.72	-1.82	-.06	1.41	2.51	3.19	3.42		
40	-11.35	-11.02	-10.49	-9.76	-8.86	-7.77	-6.48	-5.00	-3.38	-1.73	-.19	1.12	2.12	2.74	2.95		
45	-10.43	-10.10	-9.57	-8.86	-7.99	-6.97	-5.80	-4.51	-3.12	-1.71	-.38	.77	1.65	2.21	2.40		

A/LAMBDA = 2.2

FLARE ANGLE	PHI																
	6	12	18	24	30	36	42	48	54	60	66	72	78	84	90		
0	-21.15	-20.26	-19.08	-17.97	-17.37	-17.97	-21.80	-33.20	-13.82	-6.48	-1.70	1.64	3.89	5.20	5.64		
5	-20.97	-20.10	-18.93	-17.81	-17.13	-17.51	-20.12	-22.54	-13.13	-6.33	-1.67	1.63	3.87	5.17	5.60		
10	-20.46	-19.62	-18.48	-17.32	-16.49	-16.36	-17.20	-16.85	-11.56	-5.91	-1.57	1.61	3.80	5.08	5.51		
15	-19.67	-18.89	-17.79	-16.59	-15.56	-14.93	-14.63	-13.45	-9.83	-5.32	-1.42	1.58	3.68	4.93	5.34		
20	-18.68	-17.96	-16.90	-15.68	-14.49	-13.48	-12.55	-11.06	-8.26	-4.65	-1.23	1.53	3.52	4.71	5.11		
25	-17.57	-16.90	-15.89	-14.66	-13.37	-12.12	-10.86	-9.26	-6.92	-3.98	-1.04	1.46	3.30	4.42	4.80		
30	-16.38	-15.77	-14.81	-13.60	-12.26	-10.88	-9.46	-7.84	-5.81	-3.37	-.86	1.35	3.03	4.07	4.42		
35	-15.17	-14.60	-13.70	-12.53	-11.19	-9.77	-8.30	-6.71	-4.90	-2.85	-.72	1.20	2.70	3.64	3.96		
40	-13.97	-13.44	-12.60	-11.49	-10.19	-8.79	-7.33	-5.80	-4.18	-2.43	-.65	.99	2.30	3.14	3.42		
45	-12.81	-12.32	-11.54	-10.53	-9.27	-7.93	-6.53	-5.10	-3.64	-2.14	-.65	.72	1.83	2.55	2.80		

A/LAMBDA = 2.6

FLARE ANGLE	PHI																
	6	12	18	24	30	36	42	48	54	60	66	72	78	84	90		
0	-33.37	-38.95	-42.43	-28.70	-22.42	-18.59	-16.75	-17.88	-33.14	-13.49	-4.63	.57	3.86	5.72	6.33		
5	-31.65	-34.27	-34.66	-27.71	-22.09	-18.35	-16.42	-17.00	-21.14	-12.51	-4.48	.59	3.84	5.69	6.29		
10	-28.59	-29.41	-29.08	-25.55	-21.16	-17.68	-15.56	-15.11	-15.38	-10.50	-4.06	.64	3.78	5.58	6.17		
15	-25.80	-25.97	-25.44	-23.19	-19.84	-16.69	-14.39	-13.10	-11.98	-8.48	-3.48	.72	3.67	5.40	5.97		
20	-23.41	-23.30	-22.67	-20.97	-18.32	-15.49	-13.10	-11.31	-9.61	-6.76	-2.84	.80	3.52	5.15	5.69		
25	-21.34	-21.07	-20.38	-18.94	-16.73	-14.19	-11.80	-9.77	-7.83	-5.36	-2.22	.88	3.31	4.82	5.33		
30	-19.49	-19.13	-18.39	-17.08	-15.17	-12.88	-10.57	-8.45	-6.45	-4.25	-1.67	.93	3.06	4.42	4.88		
35	-17.80	-17.39	-16.62	-15.39	-13.68	-11.60	-9.42	-7.33	-5.36	-3.37	-1.23	.92	2.74	3.94	4.35		
40	-16.24	-15.80	-15.02	-13.85	-12.29	-10.41	-8.38	-6.39	-4.51	-2.71	-.91	.85	2.36	3.37	3.73		
45	-14.79	-14.33	-13.55	-12.45	-11.01	-9.31	-7.46	-5.61	-3.87	-2.25	-.73	.70	1.90	2.73	3.02		

A/LAMBDA = 3.0

FLARE ANGLE	PHI																
	6	12	18	24	30	36	42	48	54	60	66	72	78	84	90		
0	-23.86	-23.74	-24.01	-25.60	-31.73	-33.00	-21.07	-16.66	-16.89	-155.59	-9.24	-1.04	3.60	6.12	6.93		
5	-23.73	-23.59	-23.81	-25.22	-29.92	-30.10	-20.66	-16.29	-15.90	-19.27	-8.62	-.96	3.58	6.08	6.88		
10	-23.35	-23.16	-23.24	-24.20	-26.72	-25.97	-19.53	-15.31	-13.82	-13.32	-7.21	-.74	3.54	5.96	6.74		
15	-22.73	-22.48	-22.38	-22.80	-23.77	-22.59	-17.96	-13.99	-11.70	-9.91	-5.64	-.43	3.46	5.75	6.50		
20	-21.92	-21.60	-21.28	-21.21	-21.21	-19.79	-16.20	-12.53	-9.84	-7.58	-4.22	-.07	3.35	5.46	6.17		
25	-20.94	-20.54	-20.05	-19.58	-18.97	-17.41	-14.42	-11.08	-8.27	-5.86	-3.05	.27	3.20	5.09	5.74		
30	-19.83	-19.37	-18.72	-17.96	-16.97	-15.32	-12.72	-9.71	-6.96	-4.55	-2.12	.55	2.99	4.64	5.22		
35	-18.63	-18.12	-17.35	-16.39	-15.18	-13.49	-11.16	-8.46	-5.86	-3.56	-1.41	.74	2.72	4.11	4.60		
40	-17.36	-16.82	-15.98	-14.89	-13.56	-11.87	-9.75	-7.34	-4.95	-2.81	-.92	.83	2.38	3.49	3.89		
45	-16.06	-15.51	-14.63	-13.48	-12.10	-10.45	-8.52	-6.37	-4.23	-2.30	-.64	.77	1.96	2.80	3.10		

A/LAMBDA = 3.4

FLARE ANGLE	PHI 6	12	18	24	30	36	42	48	54	60	66	72	78	84	90
0	-34.32	-30.92	-27.34	-24.53	-23.21	-24.85	-41.87	-22.18	-16.04	-17.62	-17.87	-3.32	3.11	6.42	7.46
5	-33.41	-30.45	-27.09	-24.35	-23.01	-24.37	-31.88	-21.51	-15.55	-15.68	-14.22	-3.09	3.11	6.37	7.40
10	-31.39	-29.22	-26.38	-23.83	-22.42	-23.11	-25.86	-19.82	-14.29	-12.52	-9.98	-2.49	3.11	6.23	7.23
15	-29.15	-27.61	-25.32	-23.01	-21.48	-21.40	-21.90	-17.66	-12.68	-9.87	-7.03	-1.70	3.11	6.00	6.95
20	-27.02	-25.88	-24.02	-21.93	-20.29	-19.53	-18.82	-15.42	-11.02	-7.80	-4.92	-.91	3.08	5.68	6.56
25	-25.04	-24.12	-22.56	-20.66	-18.92	-17.64	-16.26	-13.30	-9.43	-6.16	-3.38	-.21	3.02	5.27	6.06
30	-23.17	-22.38	-21.02	-19.26	-17.45	-15.82	-14.07	-11.38	-7.98	-4.86	-2.24	.34	2.90	4.77	5.45
35	-21.40	-20.68	-19.44	-17.78	-15.94	-14.11	-12.17	-9.69	-6.70	-3.83	-1.41	.73	2.71	4.19	4.74
40	-19.71	-19.02	-17.86	-16.28	-14.45	-12.54	-10.53	-8.22	-5.60	-3.04	-.86	.92	2.43	3.54	3.95
45	-18.07	-17.41	-16.30	-14.80	-13.02	-11.10	-9.11	-6.98	-4.69	-2.45	-.55	.93	2.05	2.81	3.09

A/LAMBDA = 3.8

FLARE ANGLE	PHI 6	12	18	24	30	36	42	48	54	60	66	72	78	84	90
0	-29.33	-30.76	-35.36	-46.50	-28.87	-23.62	-23.26	-37.44	-20.20	-15.07	-27.61	-6.53	2.39	6.62	7.93
5	-29.10	-30.41	-34.22	-38.89	-28.43	-23.38	-22.85	-30.07	-19.52	-14.24	-16.35	-5.88	2.42	6.57	7.87
10	-28.45	-29.44	-31.86	-33.28	-27.23	-22.70	-21.70	-24.26	-17.76	-12.39	-10.68	-4.42	2.51	6.42	7.67
15	-27.48	-28.10	-29.37	-29.55	-25.57	-21.63	-20.08	-20.22	-15.52	-10.36	-7.37	-2.85	2.64	6.17	7.34
20	-26.29	-26.58	-27.07	-26.65	-23.70	-20.25	-18.22	-17.04	-13.21	-8.50	-5.12	-1.50	2.76	5.82	6.88
25	-24.96	-24.98	-24.94	-24.17	-21.75	-18.66	-16.30	-14.40	-11.05	-6.87	-3.50	-.44	2.84	5.38	6.30
30	-23.55	-23.35	-22.95	-21.95	-19.80	-16.98	-14.44	-12.16	-9.14	-5.48	-2.31	.33	2.84	4.84	5.60
35	-22.08	-21.72	-21.07	-19.89	-17.89	-15.28	-12.68	-10.26	-7.49	-4.32	-1.45	.83	2.74	4.23	4.80
40	-20.57	-20.09	-19.27	-17.98	-16.05	-13.62	-11.08	-8.64	-6.11	-3.38	-.87	1.08	2.52	3.54	3.94
45	-19.04	-18.48	-17.54	-16.18	-14.33	-12.05	-9.64	-7.29	-4.99	-2.66	-.53	1.09	2.16	2.80	3.03

A/LAMBDA = 4.2

FLARE ANGLE	PHI 6	12	18	24	30	36	42	48	54	60	66	72	78	84	90
0	-29.80	-28.60	-27.60	-28.08	-33.51	-34.75	-23.87	-22.99	-39.17	-16.49	-16.51	-11.35	1.42	6.76	8.36
5	-29.63	-28.46	-27.45	-27.86	-32.51	-33.05	-23.56	-22.43	-28.68	-15.81	-13.92	-9.29	1.51	6.70	8.28
10	-29.14	-28.03	-27.02	-27.21	-30.28	-29.89	-22.68	-20.94	-22.36	-14.11	-10.26	-6.11	1.77	6.54	8.05
15	-28.36	-27.34	-26.33	-26.21	-27.80	-26.81	-21.31	-18.91	-18.07	-12.00	-7.45	-3.61	2.11	6.27	7.67
20	-27.35	-26.42	-25.39	-24.94	-25.40	-24.01	-19.60	-16.71	-14.72	-9.88	-5.34	-1.78	2.45	5.90	7.14
25	-26.16	-25.31	-24.25	-23.48	-23.11	-21.44	-17.70	-14.55	-11.99	-7.93	-3.74	-.48	2.72	5.43	6.47
30	-24.84	-24.03	-22.94	-21.90	-20.94	-19.05	-15.74	-12.52	-9.73	-6.23	-2.52	.41	2.86	4.87	5.68
35	-23.42	-22.64	-21.50	-20.24	-18.87	-16.85	-13.83	-10.69	-7.86	-4.80	-1.61	.96	2.84	4.24	4.80
40	-21.92	-21.15	-19.97	-18.55	-16.92	-14.81	-12.03	-9.06	-6.33	-3.64	-.96	1.21	2.65	3.54	3.87
45	-20.36	-19.59	-18.39	-16.86	-15.09	-12.96	-10.40	-7.66	-5.11	-2.77	-.57	1.20	2.29	2.80	2.94

A/LAMBDA = 4.6

FLARE ANGLE	PHI 6	12	18	24	30	36	42	48	54	60	66	72	78	84	90
0	-42.25	-85.01	-37.14	-29.99	-27.17	-29.82	-36.37	-22.85	-24.74	-21.95	-14.26	-20.49	.18	6.81	8.75
5	-40.22	-44.10	-36.25	-29.75	-26.98	-29.27	-33.60	-22.47	-23.46	-20.57	-12.93	-12.38	.39	6.76	8.66
10	-36.86	-37.94	-34.23	-29.07	-26.41	-27.84	-29.44	-21.40	-20.65	-17.54	-10.38	-7.05	.93	6.59	8.39
15	-33.91	-34.17	-31.95	-28.02	-25.50	-25.92	-25.84	-19.77	-17.57	-14.28	-7.94	-3.92	1.60	6.32	7.95
20	-31.41	-31.32	-29.74	-26.69	-24.28	-23.79	-22.70	-17.79	-14.71	-11.32	-5.89	-1.85	2.22	5.93	7.34

25	-29.21	-28.93	-27.63	-25.15	-22.81	-21.60	-19.86	-15.66	-12.17	-8.81	-4.22	-.45	2.68	5.45	6.58
30	-27.21	-26.80	-25.60	-23.46	-21.16	-19.42	-17.28	-13.54	-9.98	-6.73	-2.87	.48	2.94	4.89	5.70
35	-25.32	-24.80	-23.64	-21.69	-19.41	-17.31	-14.93	-11.55	-8.11	-5.05	-1.82	1.03	2.98	4.24	4.75
40	-23.50	-22.90	-21.72	-19.86	-17.60	-15.31	-12.82	-9.74	-6.55	-3.73	-1.06	1.28	2.79	3.54	3.78
45	-21.72	-21.05	-19.83	-18.03	-15.81	-13.45	-10.96	-8.15	-5.28	-2.77	-.58	1.25	2.38	2.80	2.86

A/LAMBDA = 5.0

FLARE ANGLE	PHI														
	6	12	18	24	30	36	42	48	54	60	66	72	78	84	90
0	-30.73	-30.93	-32.78	-42.71	-34.14	-27.16	-29.62	-30.34	-21.56	-153.23	-14.77	-26.53	-1.39	6.81	9.11
5	-30.62	-30.79	-32.50	-40.00	-33.50	-26.93	-28.94	-29.11	-21.02	-26.93	-13.75	-12.93	-.96	6.75	9.00
10	-30.24	-30.34	-31.69	-36.04	-31.91	-26.25	-27.19	-26.39	-19.54	-20.04	-11.48	-7.22	.04	6.59	8.70
15	-29.63	-29.62	-30.50	-32.76	-29.88	-25.16	-24.91	-23.31	-17.43	-15.46	-9.01	-4.00	1.15	6.32	8.19
20	-28.81	-28.67	-29.08	-30.01	-27.70	-23.71	-22.45	-20.27	-15.07	-11.95	-6.74	-1.90	2.08	5.94	7.50
25	-27.79	-27.52	-27.50	-27.56	-25.48	-21.99	-19.97	-17.39	-12.73	-9.15	-4.80	-.47	2.73	5.47	6.65
30	-26.62	-26.22	-25.83	-25.28	-23.26	-20.07	-17.56	-14.74	-10.55	-6.91	-3.22	.47	3.07	4.90	5.68
35	-25.30	-24.78	-24.10	-23.11	-21.07	-18.08	-15.29	-12.37	-8.61	-5.14	-1.98	1.04	3.12	4.26	4.67
40	-23.86	-23.24	-22.31	-21.01	-18.93	-16.07	-13.19	-10.28	-6.93	-3.77	-1.08	1.29	2.90	3.55	3.69
45	-22.32	-21.61	-20.51	-18.99	-16.86	-14.14	-11.29	-8.49	-5.54	-2.76	-.52	1.27	2.43	2.81	2.82

A/LAMBDA = 5.4

FLARE ANGLE	PHI														
	6	12	18	24	30	36	42	48	54	60	66	72	78	84	90
0	-39.76	-35.40	-31.75	-30.42	-34.86	-36.03	-26.60	-33.90	-23.81	-24.16	-17.57	-16.60	-3.35	6.74	9.44
5	-39.00	-35.09	-31.59	-30.26	-34.21	-34.91	-26.32	-31.69	-23.23	-22.37	-16.35	-11.80	-2.51	6.69	9.32
10	-37.20	-34.21	-31.10	-29.75	-32.59	-32.46	-25.48	-27.87	-21.60	-18.78	-13.54	-7.14	-.79	6.54	8.97
15	-35.12	-32.94	-30.30	-28.93	-30.54	-29.74	-24.14	-24.23	-19.26	-15.17	-10.43	-4.11	.83	6.29	8.40
20	-33.07	-31.46	-29.25	-27.82	-28.35	-27.05	-22.39	-20.92	-16.60	-11.99	-7.62	-2.04	2.05	5.93	7.62
25	-31.10	-29.86	-27.98	-26.48	-26.13	-24.44	-20.35	-17.89	-13.92	-9.31	-5.27	-.59	2.83	5.47	6.67
30	-29.22	-28.18	-26.53	-24.93	-23.91	-21.90	-18.16	-15.15	-11.42	-7.09	-3.42	.40	3.22	4.92	5.63
35	-27.38	-26.46	-24.93	-23.23	-21.70	-19.44	-15.94	-12.69	-9.20	-5.29	-2.01	1.02	3.24	4.28	4.58
40	-25.56	-24.68	-23.21	-21.41	-19.53	-17.10	-13.80	-10.53	-7.29	-3.88	-1.02	1.30	2.96	3.57	3.62
45	-23.74	-22.87	-21.41	-19.53	-17.42	-14.91	-11.81	-8.68	-5.73	-2.83	-.43	1.30	2.43	2.82	2.81

A/LAMBDA = 5.8

FLARE ANGLE	PHI														
	6	12	18	24	30	36	42	48	54	60	66	72	78	84	90
0	-35.20	-38.09	-57.78	-35.74	-30.26	-33.95	-32.56	-26.32	-34.41	-20.96	-24.16	-13.72	-5.86	6.61	9.75
5	-34.98	-37.60	-46.13	-35.32	-30.08	-33.30	-31.84	-25.89	-31.02	-20.14	-20.92	-11.01	-4.20	6.57	9.61
10	-34.32	-36.30	-40.17	-34.17	-29.52	-31.63	-30.00	-24.64	-26.18	-17.99	-15.88	-7.26	-1.48	6.45	9.22
15	-33.32	-34.63	-36.41	-32.58	-28.61	-29.47	-27.61	-22.76	-21.94	-15.20	-11.58	-4.42	.66	6.24	8.57
20	-32.09	-32.84	-33.51	-30.78	-27.37	-27.13	-24.99	-20.45	-18.20	-12.36	-8.16	-2.32	2.10	5.92	7.70
25	-30.72	-31.02	-31.04	-28.85	-25.84	-24.71	-22.29	-17.95	-14.89	-9.76	-5.50	-.79	2.96	5.49	6.66
30	-29.24	-29.20	-28.79	-26.85	-24.08	-22.27	-19.60	-15.45	-12.00	-7.48	-3.47	.30	3.34	4.95	5.56
35	-27.68	-27.39	-26.65	-24.80	-22.15	-19.86	-17.00	-13.07	-9.53	-5.58	-1.98	1.00	3.32	4.31	4.50
40	-26.04	-25.55	-24.57	-22.71	-20.11	-17.52	-14.57	-10.89	-7.47	-4.05	-.96	1.34	2.98	3.59	3.58
45	-24.34	-23.69	-22.51	-20.60	-18.03	-15.30	-12.35	-8.98	-5.80	-2.90	-.37	1.35	2.40	2.82	2.83

A/LAMBDA = 6.2

FLARE ANGLE	PHI 6	12	18	24	30	36	42	48	54	60	66	72	78	84	90
0	-34.78	-33.43	-33.23	-38.20	-39.10	-29.94	-38.03	-27.57	-31.47	-21.86	-41.02	-12.99	-9.22	6.42	10.03
5	-34.62	-33.30	-33.07	-37.56	-38.10	-29.71	-36.08	-27.15	-29.49	-21.13	-23.97	-11.05	-5.87	6.40	9.88
10	-34.14	-32.90	-32.59	-35.97	-35.88	-29.03	-32.60	-25.94	-25.74	-19.13	-16.79	-7.78	-1.96	6.33	9.44
15	-33.38	-32.24	-31.82	-33.98	-33.37	-27.93	-29.21	-24.06	-21.92	-16.36	-11.94	-4.95	.60	6.17	8.72
20	-32.40	-31.36	-30.79	-31.89	-30.89	-26.45	-26.05	-21.70	-18.33	-13.36	-8.32	-2.71	2.18	5.92	7.75
25	-31.22	-30.27	-29.54	-29.79	-28.45	-24.64	-23.05	-19.08	-15.08	-10.51	-5.57	-1.00	3.07	5.53	6.63
30	-29.89	-29.00	-28.11	-27.67	-26.04	-22.57	-20.18	-16.39	-12.19	-7.98	-3.49	.24	3.42	5.00	5.47
35	-28.43	-27.56	-26.51	-25.54	-23.64	-20.35	-17.46	-13.80	-9.69	-5.87	-1.97	1.03	3.36	4.34	4.43
40	-26.86	-25.98	-24.77	-23.38	-21.25	-18.07	-14.93	-11.42	-7.59	-4.17	-.94	1.42	2.97	3.59	3.58
45	-25.19	-24.28	-22.92	-21.22	-18.92	-15.83	-12.63	-9.32	-5.88	-2.91	-.35	1.42	2.37	2.80	2.89

A/LAMBDA = 6.6

FLARE ANGLE	PHI 6	12	18	24	30	36	42	48	54	60	66	72	78	84	90
0	-48.37	-51.24	-37.39	-32.92	-36.00	-37.07	-29.66	-39.12	-25.77	-26.88	-23.81	-13.64	-14.15	6.18	10.30
5	-45.82	-46.95	-37.07	-32.76	-35.53	-36.26	-29.34	-35.99	-25.18	-25.43	-20.95	-11.95	-7.20	6.18	10.14
10	-42.04	-42.22	-36.15	-32.28	-34.29	-34.32	-28.42	-31.46	-23.52	-22.11	-16.14	-8.72	-2.21	6.18	9.64
15	-38.92	-38.77	-34.84	-31.49	-32.57	-31.93	-26.95	-27.47	-21.08	-18.25	-11.87	-5.64	.60	6.11	8.84
20	-36.34	-36.03	-33.29	-30.42	-30.61	-29.41	-25.02	-23.84	-18.23	-14.51	-8.42	-3.10	2.25	5.93	7.78
25	-34.08	-33.67	-31.60	-29.08	-28.49	-26.82	-22.76	-20.44	-15.30	-11.17	-5.69	-1.15	3.14	5.58	6.58
30	-32.03	-31.52	-29.81	-27.52	-26.28	-24.20	-20.30	-17.27	-12.52	-8.33	-3.59	.24	3.47	5.05	5.39
35	-30.08	-29.49	-27.93	-25.75	-23.99	-21.57	-17.77	-14.36	-10.00	-6.01	-2.03	1.11	3.37	4.36	4.38
40	-28.17	-27.48	-25.97	-23.81	-21.66	-18.98	-15.29	-11.77	-7.83	-4.19	-.96	1.50	2.95	3.58	3.60
45	-26.27	-25.47	-23.95	-21.76	-19.33	-16.49	-12.97	-9.52	-6.04	-2.87	-.34	1.48	2.34	2.78	2.95

A/LAMBDA = 7.0

FLARE ANGLE	PHI 6	12	18	24	30	36	42	48	54	60	66	72	78	84	90
0	-35.20	-35.89	-40.83	-43.43	-32.89	-37.72	-31.92	-33.45	-26.49	-156.49	-20.42	-15.60	-24.00	5.87	10.56
5	-35.08	-35.72	-40.20	-42.13	-32.70	-36.87	-31.53	-32.39	-25.97	-31.61	-19.00	-13.73	-7.89	5.92	10.37
10	-34.70	-35.22	-38.66	-39.50	-32.12	-34.86	-30.42	-29.91	-24.44	-24.45	-15.69	-9.97	-2.30	6.01	9.82

15	-34.09	-34.43	-36.74	-36.81	-31.19	-32.43	-28.71	-26.89	-22.09	-19.31	-12.01	-6.33	.62	6.06	8.93
20	-33.26	-33.46	-34.74	-34.30	-29.92	-29.88	-26.55	-23.72	-19.22	-15.03	-6.72	-3.40	2.29	5.96	7.78
25	-32.24	-32.18	-32.75	-31.92	-28.34	-27.28	-24.06	-20.54	-16.15	-11.44	-5.97	-1.22	3.17	5.64	6.51
30	-31.05	-30.78	-30.75	-29.62	-26.50	-24.64	-21.38	-17.45	-13.18	-8.46	-3.78	.29	3.48	5.09	5.32
35	-29.69	-29.25	-28.75	-27.34	-24.43	-21.98	-18.63	-14.56	-10.46	-6.06	-2.13	1.20	3.36	4.37	4.37
40	-28.19	-27.58	-26.70	-25.04	-22.20	-19.36	-15.95	-11.95	-8.11	-4.20	-.98	1.57	2.94	3.55	3.65
45	-26.56	-25.79	-24.61	-22.72	-19.89	-16.83	-13.45	-9.67	-6.17	-2.85	-.30	1.50	2.33	2.75	3.00

A/LAMBDA = 7.4

FLARE ANGLE	PHI														
	6	12	18	24	30	36	42	48	54	60	66	72	78	84	90
0	-43.35	-38.28	-35.15	-37.12	-44.41	-32.27	-83.57	-29.04	-33.49	-28.42	-20.14	-19.32	-26.11	5.50	10.80
5	-42.39	-38.04	-35.01	-36.82	-42.60	-32.04	-43.13	-28.66	-31.85	-26.70	-19.04	-16.35	-7.95	5.61	10.59
10	-40.98	-37.36	-34.58	-35.96	-39.37	-31.36	-36.66	-27.53	-28.42	-23.00	-16.19	-11.23	-2.32	5.84	9.98
15	-39.04	-36.33	-33.88	-34.70	-36.30	-30.25	-32.38	-25.73	-24.61	-18.91	-12.67	-6.85	.61	6.02	9.01
20	-37.08	-35.04	-32.93	-33.15	-33.52	-28.74	-28.81	-23.38	-20.79	-15.01	-9.28	-3.56	2.29	6.00	7.77
25	-35.16	-33.61	-31.75	-31.41	-30.89	-26.86	-25.51	-20.66	-17.12	-11.54	-6.35	-1.20	3.18	5.71	6.44
30	-33.29	-32.04	-30.35	-29.51	-28.33	-24.68	-22.33	-17.78	-13.75	-8.58	-3.98	.37	3.49	5.13	5.26
35	-31.45	-30.36	-28.75	-27.48	-25.78	-22.28	-19.28	-14.94	-10.78	-6.16	-2.18	1.27	3.37	4.35	4.38
40	-29.59	-28.57	-26.98	-25.33	-23.21	-19.77	-16.40	-12.29	-8.25	-4.26	-.94	1.61	2.94	3.52	3.71
45	-27.70	-26.69	-25.04	-23.00	-20.65	-17.25	-13.74	-9.92	-6.21	-2.88	-.24	1.49	2.33	2.74	3.04

A/LAMBDA = 7.8

FLARE ANGLE	PHI														
	6	12	18	24	30	36	42	48	54	60	66	72	78	84	90
0	-39.37	-44.32	-47.68	-35.77	-37.02	-37.97	-33.38	-31.88	-38.95	-24.94	-22.19	-27.03	-17.10	5.08	11.03
5	-39.13	-43.56	-45.84	-35.59	-36.66	-37.36	-32.95	-31.35	-35.01	-24.13	-20.94	-19.20	-7.68	5.26	10.80
10	-38.42	-41.61	-42.64	-35.05	-35.66	-35.77	-31.74	-29.86	-29.83	-21.89	-17.72	-12.07	-2.36	5.67	10.13
15	-37.40	-39.45	-39.70	-34.17	-34.20	-33.66	-29.93	-27.64	-25.34	-18.72	-13.74	-7.11	.55	6.01	9.07
20	-36.13	-37.33	-37.12	-33.00	-32.42	-31.30	-27.67	-24.90	-21.22	-15.22	-9.93	-3.60	2.25	6.07	7.73
25	-34.72	-35.31	-34.79	-31.56	-30.43	-28.77	-25.09	-21.84	-17.41	-11.86	-6.68	-1.17	3.17	5.77	6.36
30	-33.20	-33.34	-32.58	-29.89	-28.25	-26.12	-22.30	-18.67	-13.95	-8.87	-4.09	.42	3.50	5.15	5.22
35	-31.60	-31.43	-30.42	-28.00	-25.92	-23.36	-19.44	-15.58	-10.91	-6.36	-2.17	1.31	3.39	4.33	4.41
40	-29.90	-29.44	-28.26	-25.92	-23.47	-20.58	-16.62	-12.70	-8.33	-4.36	-.88	1.62	2.95	3.48	3.76
45	-28.12	-27.44	-26.05	-23.70	-20.97	-17.84	-13.97	-10.16	-6.25	-2.90	-.18	1.48	2.33	2.74	3.05

A/LAMBDA = 8.2

FLARE ANGLE	PHI														
	6	12	18	24	30	36	42	48	54	60	66	72	78	84	90
0	-38.29	-36.94	-38.30	-66.77	-35.25	-41.39	-32.51	-57.98	-29.49	-25.61	-27.63	-36.06	-13.72	4.59	11.24
5	-38.14	-36.82	-38.08	-49.91	-35.05	-40.24	-32.21	-41.60	-28.81	-24.87	-24.90	-19.98	-7.42	4.88	10.99
10	-37.68	-36.43	-37.44	-43.74	-34.45	-37.74	-31.33	-35.05	-26.91	-22.75	-19.81	-12.26	-3.48	5.50	10.26
15	-36.94	-35.80	-36.45	-39.88	-33.47	-34.98	-29.90	-30.50	-24.15	-19.61	-14.77	-7.17	.42	6.01	9.11
20	-35.98	-34.93	-35.19	-36.86	-32.15	-32.22	-27.96	-26.55	-20.88	-16.01	-10.40	-3.62	2.18	6.14	7.69
25	-34.82	-33.86	-33.73	-34.24	-30.51	-29.46	-25.58	-22.84	-17.45	-12.45	-6.85	-1.17	3.16	5.83	6.29
30	-33.50	-32.59	-32.11	-31.78	-28.58	-26.66	-22.89	-19.29	-14.13	-9.24	-4.11	.42	3.53	5.15	5.21
35	-32.03	-31.14	-30.33	-29.37	-26.40	-23.81	-20.01	-15.96	-11.11	-6.55	-2.13	1.32	3.42	4.28	4.46
40	-30.43	-29.51	-28.41	-26.95	-24.01	-20.96	-17.12	-12.93	-8.49	-4.42	-.82	1.63	2.96	3.45	3.80
45	-28.71	-27.73	-26.35	-24.48	-21.50	-18.16	-14.35	-10.29	-6.35	-2.87	-.15	1.48	2.31	2.75	3.05

A/LAMBDA = 8.6

FLARE ANGLE	PHI 6	12	18	24	30	36	42	48	54	60	66	72	78	84	90
0	-53.46	-48.83	-38.51	-37.27	-51.17	-34.31	-42.23	-33.81	-28.78	-30.42	-65.91	-23.72	-12.06	4.03	11.45
5	-50.14	-47.28	-38.33	-37.08	-47.09	-34.09	-40.45	-33.15	-28.28	-28.94	-28.68	-18.54	-7.33	4.47	11.18
10	-45.86	-44.39	-37.76	-36.49	-42.34	-33.39	-37.11	-31.37	-26.80	-25.49	-20.93	-12.07	-2.70	5.36	10.38
15	-42.57	-41.63	-36.86	-35.55	-38.72	-32.26	-33.75	-28.86	-24.43	-21.29	-15.19	-7.21	.24	6.04	9.13
20	-39.91	-39.13	-35.70	-34.32	-35.70	-30.72	-30.50	-25.91	-21.39	-16.99	-10.56	-3.70	2.11	6.23	7.63
25	-37.62	-36.96	-34.32	-32.82	-32.94	-28.79	-27.28	-22.66	-18.01	-12.99	-6.91	-1.23	3.17	5.88	6.23
30	-35.54	-34.97	-32.74	-31.10	-30.28	-26.51	-24.03	-19.35	-14.62	-9.50	-4.12	.40	3.58	5.14	5.21
35	-33.55	-32.85	-30.99	-29.16	-27.61	-23.97	-20.78	-16.11	-11.46	-6.63	-2.11	1.32	3.45	4.24	4.51
40	-31.61	-30.82	-29.07	-27.03	-24.89	-21.25	-17.63	-13.09	-8.71	-4.41	-.80	1.64	2.95	3.44	3.83
45	-29.64	-28.76	-26.99	-24.73	-22.15	-18.49	-14.68	-10.42	-6.44	-2.83	-.14	1.49	2.28	2.78	3.02

A/LAMBDA = 9.0

FLARE ANGLE	PHI 6	12	18	24	30	36	42	48	54	60	66	72	78	84	90
0	-38.54	-39.92	-52.27	-39.26	-37.58	-38.78	-38.42	-31.54	-33.50	-152.66	-29.08	-20.11	-11.36	3.40	11.64
5	-38.42	-39.73	-49.25	-39.01	-37.69	-38.29	-37.62	-31.17	-32.48	-35.01	-25.82	-17.20	-7.49	4.04	11.35
10	-38.05	-39.15	-45.12	-38.26	-36.85	-36.96	-35.64	-30.08	-29.93	-27.74	-20.31	-11.96	-3.03	5.24	10.48
15	-37.43	-38.24	-41.83	-37.11	-35.58	-35.09	-33.10	-28.29	-26.57	-22.27	-15.09	-7.37	.03	6.09	9.14
20	-36.60	-37.16	-39.10	-35.67	-33.96	-32.88	-30.30	-25.87	-22.81	-17.46	-10.61	-3.86	2.05	6.31	7.57
25	-35.57	-35.76	-36.69	-33.99	-32.07	-30.43	-27.31	-22.96	-18.92	-13.21	-6.98	-1.32	3.21	5.91	6.18
30	-34.36	-34.27	-34.44	-32.12	-29.93	-27.76	-24.18	-19.76	-15.17	-9.60	-4.17	.38	3.64	5.11	5.23
35	-32.98	-32.65	-32.24	-30.05	-27.59	-24.92	-20.98	-16.51	-11.77	-6.66	-2.13	1.35	3.48	4.19	4.56
40	-31.45	-30.89	-30.02	-27.81	-25.06	-21.97	-17.83	-13.41	-8.84	-4.40	-.80	1.68	2.93	3.44	3.83
45	-29.76	-29.00	-27.75	-25.41	-22.40	-19.02	-14.85	-10.64	-6.47	-2.61	-.12	1.90	2.25	2.82	2.99

A/LAMBDA = 9.4

FLARE ANGLE	PHI 6	12	18	24	30	36	42	48	54	60	66	72	78	84	90
0	-45.78	-40.45	-38.38	-48.86	-37.47	-45.21	-33.93	-36.33	-51.86	-31.60	-24.76	-18.86	-11.34	2.69	11.83
5	-45.21	-43.27	-38.25	-47.06	-37.26	-43.52	-33.65	-35.55	-39.68	-29.92	-23.27	-16.72	-7.93	3.59	11.51
10	-43.75	-39.71	-37.80	-43.85	-36.60	-40.35	-32.80	-33.53	-33.00	-26.19	-19.55	-12.17	-3.46	5.14	10.57
15	-41.94	-38.84	-37.08	-40.87	-35.56	-37.21	-31.41	-30.79	-28.05	-21.81	-15.05	-7.70	-.17	6.16	9.14
20	-40.06	-37.72	-36.11	-38.21	-34.16	-34.25	-29.49	-27.63	-23.58	-17.39	-10.78	-4.10	2.02	6.39	7.51
25	-38.20	-36.40	-34.90	-35.75	-32.44	-31.35	-27.10	-24.17	-19.35	-13.28	-7.16	-1.42	3.27	5.93	6.15
30	-36.35	-34.92	-33.46	-33.37	-30.42	-28.43	-24.31	-20.58	-15.41	-9.70	-4.29	.38	3.70	5.06	5.27
35	-34.52	-33.29	-31.82	-30.98	-28.13	-25.42	-21.27	-17.05	-11.90	-6.74	-2.18	1.40	3.49	4.16	4.60
40	-32.65	-31.53	-29.97	-28.53	-25.61	-22.36	-18.16	-13.74	-8.90	-4.44	-.79	1.72	2.70	3.46	3.82
45	-30.73	-29.62	-27.93	-25.99	-22.91	-19.32	-15.14	-10.80	-6.48	-2.81	-.09	1.50	2.23	2.85	2.96

A/LAMBDA = 9.8

FLARE ANGLE	PHI 6	12	18	24	30	36	42	48	54	60	66	72	78	84	90
0	-42.66	-50.74	-44.20	-38.16	-64.94	-36.17	-38.47	-47.55	-33.11	-27.97	-23.91	-19.06	-11.91	1.89	12.01
5	-42.41	-49.11	-43.74	-38.01	-50.76	-35.94	-37.88	-42.37	-32.26	-27.17	-22.78	-17.17	-8.65	3.14	11.66
10	-41.67	-46.12	-42.49	-37.52	-44.60	-35.23	-36.28	-36.90	-30.00	-24.89	-19.67	-12.79	-3.94	5.08	10.65
15	-40.59	-43.31	-40.83	-36.72	-40.65	-34.07	-34.06	-32.57	-26.86	-21.49	-15.46	-8.18	-.35	6.23	9.12
20	-39.27	-40.84	-39.00	-35.62	-37.49	-32.48	-31.44	-28.63	-23.19	-17.51	-11.19	-4.34	2.03	6.45	7.45

25	-37.82	-38.61	-37.10	-34.25	-34.67	-30.50	-28.51	-24.78	-19.32	-13.53	-7.43	-1.49	3.34	5.93	6.13
30	-36.27	-36.52	-35.15	-32.61	-31.95	-28.14	-25.34	-20.97	-15.52	-9.92	-4.42	.42	3.74	5.02	5.32
35	-34.62	-34.49	-33.12	-30.71	-29.20	-25.47	-22.01	-17.29	-12.03	-6.88	-2.19	1.46	3.48	4.14	4.62
40	-32.89	-32.45	-30.99	-28.57	-26.37	-22.58	-18.67	-13.89	-9.00	-4.50	-.75	1.74	2.86	3.49	3.80
45	-31.06	-30.36	-28.75	-26.21	-23.48	-19.58	-15.47	-10.89	-6.54	-2.81	-.05	1.48	2.23	2.87	2.94

A/LAMBDA = 10.2

FLARE ANGLE	PHI 6	12	18	24	30	36	42	48	54	60	66	72	78	84	90
0	-40.99	-39.80	-43.88	-43.93	-38.91	-39.54	-47.07	-34.54	-30.90	-28.50	-25.42	-20.60	-13.05	1.00	12.19
5	-40.86	-39.70	-43.48	-43.43	-38.67	-39.14	-44.15	-34.06	-30.40	-27.75	-24.19	-18.53	-9.63	2.70	11.81
10	-40.42	-39.31	-42.38	-42.10	-37.94	-37.99	-39.86	-32.66	-28.91	-25.58	-20.84	-13.74	-4.43	5.04	10.72
15	-39.70	-38.67	-40.88	-40.34	-36.80	-36.30	-36.11	-30.50	-26.50	-22.22	-16.31	-8.69	-.47	6.31	9.10
20	-38.75	-37.80	-39.17	-38.38	-35.30	-34.24	-32.67	-27.74	-23.30	-18.17	-11.71	-4.54	2.07	6.51	7.39
25	-37.61	-36.72	-37.35	-36.32	-33.50	-31.86	-29.30	-24.51	-19.64	-14.02	-7.69	-1.50	3.41	5.91	6.13
30	-36.30	-35.44	-35.45	-34.17	-31.42	-29.20	-25.87	-21.00	-15.86	-10.22	-4.49	.48	3.77	4.97	5.36
35	-34.84	-33.97	-33.47	-31.90	-29.06	-26.30	-22.38	-17.44	-12.30	-7.02	-2.16	1.51	3.45	4.14	4.63
40	-33.23	-32.31	-31.37	-29.50	-26.47	-23.22	-18.93	-14.06	-9.17	-4.52	-.69	1.75	2.82	3.53	3.77
45	-31.48	-30.47	-29.14	-26.94	-23.68	-20.06	-15.65	-11.02	-6.61	-2.77	-.02	1.45	2.24	2.88	2.94

A/LAMBDA = 10.6

FLARE ANGLE	PHI 6	12	18	24	30	36	42	48	54	60	66	72	78	84	90
0	-58.20	-48.20	-40.08	-44.36	-39.63	-49.55	-36.16	-34.04	-33.91	-33.19	-30.01	-23.85	-14.87	.00	12.35
5	-53.70	-47.44	-39.96	-43.85	-39.40	-46.79	-35.84	-33.66	-33.17	-31.69	-27.66	-20.80	-10.83	2.27	11.95
10	-48.89	-45.62	-39.51	-42.50	-38.67	-42.69	-34.87	-32.52	-31.13	-28.17	-22.73	-14.81	-4.86	5.04	10.78
15	-45.44	-43.51	-38.78	-40.71	-37.52	-39.16	-33.33	-30.65	-28.13	-23.77	-17.25	-9.10	-.54	6.40	9.07
20	-42.72	-41.42	-37.79	-38.75	-36.01	-36.02	-31.25	-28.11	-24.47	-19.05	-12.13	-4.64	2.13	6.55	7.33
25	-40.40	-39.39	-36.56	-36.69	-34.19	-33.02	-28.70	-24.99	-20.43	-14.49	-7.83	-1.47	3.47	5.88	6.15
30	-38.29	-37.42	-35.11	-34.54	-32.08	-29.99	-25.74	-21.49	-16.37	-10.43	-4.50	.54	3.78	4.93	5.40
35	-36.29	-35.45	-33.44	-32.27	-29.69	-26.85	-22.49	-17.86	-12.59	-7.08	-2.12	1.54	3.42	4.16	4.63
40	-34.32	-33.44	-31.55	-29.86	-27.04	-23.62	-19.13	-14.36	-9.30	-4.50	-.65	1.74	2.81	3.56	3.74
45	-32.32	-31.35	-29.45	-27.29	-24.19	-20.36	-15.85	-11.20	-6.64	-2.73	-.01	1.42	2.26	2.87	2.94

A/LAMBDA = 11.0

FLARE ANGLE	PHI 6	12	18	24	30	36	42	48	54	60	66	72	78	84	90
0	-41.21	-43.52	-58.67	-39.68	-60.32	-37.91	-37.36	-41.59	-51.24	-157.10	-47.23	-30.72	-17.61	-1.13	12.51
5	-41.12	-43.30	-53.40	-39.54	-51.76	-37.67	-37.01	-40.13	-41.62	-37.69	-31.92	-23.52	-12.12	1.88	12.08
10	-40.74	-42.58	-48.30	-39.06	-45.96	-36.92	-35.97	-37.04	-35.11	-30.36	-24.04	-15.60	-5.19	5.05	10.83
15	-40.11	-41.51	-44.73	-38.26	-42.08	-35.72	-34.32	-33.58	-30.13	-24.69	-17.72	-9.33	-.56	6.47	9.03
20	-39.27	-40.20	-41.88	-37.17	-38.95	-34.08	-32.15	-29.96	-25.51	-19.47	-12.31	-4.67	2.18	6.57	7.29
25	-38.23	-38.73	-39.41	-35.79	-36.13	-32.04	-29.49	-26.16	-20.99	-14.68	-7.88	-1.44	3.51	5.85	6.17
30	-37.01	-37.13	-37.12	-34.14	-33.39	-29.61	-26.43	-22.22	-16.66	-10.51	-4.49	.57	3.78	4.91	5.44
35	-35.62	-35.41	-34.88	-32.22	-30.60	-26.83	-23.06	-18.30	-12.73	-7.09	-2.10	1.55	3.39	4.18	4.61
40	-34.00	-33.58	-32.61	-30.03	-27.69	-23.78	-19.57	-14.61	-9.35	-4.49	-.64	1.72	2.80	3.58	3.72
45	-32.34	-31.60	-30.24	-27.59	-24.66	-20.58	-16.15	-11.32	-6.64	-2.71	-.01	1.41	2.28	2.85	2.96

G-SUB-V (B/L,FLARE ANGLE,PHI)

B/LAMBDA = .4

FLARE ANGLE	PHI 6	12	18	24	30	36	42	48	54	60	66	72	78	84	90
0	2.02	1.94	1.82	1.66	1.46	1.24	.99	.74	.49	.25	.04	-.13	-.27	-.35	-.38
5	2.00	1.93	1.81	1.65	1.45	1.22	.98	.73	.48	.24	.03	-.14	-.28	-.36	-.39
10	1.97	1.89	1.77	1.61	1.42	1.19	.95	.70	.45	.21	.00	-.17	-.31	-.39	-.42
15	1.90	1.83	1.71	1.55	1.36	1.13	.89	.64	.39	.16	-.05	-.22	-.35	-.44	-.46
20	1.81	1.74	1.62	1.46	1.27	1.05	.81	.56	.32	.09	-.12	-.29	-.42	-.50	-.53
25	1.69	1.62	1.51	1.35	1.16	.94	.70	.46	.22	-.01	-.22	-.39	-.52	-.60	-.62
30	1.54	1.47	1.35	1.20	1.01	.80	.56	.32	.08	-.14	-.34	-.51	-.64	-.71	-.74
35	1.35	1.28	1.17	1.01	.83	.62	.39	.15	-.08	-.30	-.50	-.66	-.79	-.86	-.89
40	1.11	1.04	.93	.78	.60	.39	.17	-.06	-.29	-.50	-.69	-.85	-.97	-1.05	-1.07
45	.82	.75	.64	.50	.32	.12	-.10	-.32	-.54	-.75	-.94	-1.09	-1.21	-1.28	-1.30

B/LAMBDA = .8

FLARE ANGLE	PHI 6	12	18	24	30	36	42	48	54	60	66	72	78	84	90
0	4.95	4.65	4.16	3.48	2.63	1.62	.48	-.76	-2.08	-3.41	-4.68	-5.83	-6.76	-7.36	-7.57
5	4.93	4.64	4.14	3.47	2.62	1.61	.48	-.77	-2.07	-3.40	-4.67	-5.81	-6.72	-7.32	-7.52
10	4.89	4.59	4.10	3.43	2.58	1.58	.46	-.78	-2.07	-3.37	-4.62	-5.73	-6.62	-7.20	-7.40
15	4.81	4.51	4.03	3.36	2.52	1.53	.42	-.79	-2.06	-3.33	-4.54	-5.61	-6.46	-7.01	-7.20
20	4.69	4.40	3.92	3.26	2.44	1.46	.37	-.82	-2.05	-3.28	-4.44	-5.45	-6.25	-6.76	-6.93
25	4.54	4.25	3.78	3.13	2.32	1.37	.30	-.85	-2.04	-3.22	-4.31	-5.27	-6.00	-6.47	-6.63
30	4.35	4.07	3.60	2.96	2.17	1.24	.21	-.90	-2.04	-3.15	-4.18	-5.06	-5.73	-6.15	-6.30
35	4.11	3.83	3.38	2.76	1.99	1.09	.09	-.97	-2.05	-3.09	-4.04	-4.84	-5.45	-5.83	-5.96
40	3.81	3.54	3.10	2.50	1.76	.89	-.06	-1.06	-2.07	-3.04	-3.91	-4.63	-5.18	-5.51	-5.62
45	3.45	3.19	2.77	2.19	1.47	.65	-.25	-1.19	-2.13	-3.01	-3.80	-4.44	-4.92	-5.21	-5.31

B/LAMBDA = 1.2

FLARE ANGLE	PHI 6	12	18	24	30	36	42	48	54	60	66	72	78	84	90
0	6.59	5.90	4.75	3.09	.87	-2.05	-5.95	-11.67	-23.64	-21.67	-14.45	-11.62	-10.21	-9.53	-9.33
5	6.56	5.88	4.73	3.08	.87	-2.03	-5.87	-11.33	-20.07	-19.28	-13.95	-11.39	-10.06	-9.41	-9.22
10	6.50	5.82	4.68	3.04	.86	-1.96	-5.63	-10.44	-15.81	-15.74	-12.73	-10.76	-9.64	-9.07	-8.90
15	6.39	5.72	4.59	2.98	.85	-1.87	-5.26	-9.28	-12.74	-12.92	-11.27	-9.89	-9.02	-8.57	-8.42
20	6.24	5.58	4.47	2.89	.83	-1.74	-4.81	-8.09	-10.46	-10.73	-9.83	-8.92	-8.30	-7.95	-7.84
25	6.03	5.39	4.30	2.77	.80	-1.60	-4.32	-6.96	-8.68	-8.99	-8.52	-7.95	-7.53	-7.29	-7.21
30	5.77	5.14	4.09	2.62	.75	-1.45	-3.82	-5.94	-7.24	-7.57	-7.36	-7.03	-6.77	-6.62	-6.57
35	5.45	4.84	3.83	2.43	.69	-1.30	-3.33	-5.04	-6.06	-6.40	-6.35	-6.19	-6.05	-5.97	-5.94
40	5.06	4.48	3.51	2.20	.59	-1.18	-2.89	-4.26	-5.09	-5.42	-5.48	-5.44	-5.39	-5.36	-5.35
45	4.59	4.03	3.12	1.91	.46	-1.09	-2.51	-3.62	-4.29	-4.62	-4.74	-4.79	-4.80	-4.81	-4.81

B/LAMBDA = 1.6

FLARE ANGLE	PHI 6	12	18	24	30	36	42	48	54	60	66	72	78	84	90
0	7.66	6.42	4.23	.84	-4.56	-15.96	-15.62	-8.43	-6.07	-5.29	-5.24	-5.55	-5.95	-6.28	-6.40

5	7.63	6.39	4.22	.85	-4.43	-14.17	-14.09	-8.16	-5.97	-5.22	-5.20	-5.51	-5.92	-6.25	-6.37
10	7.54	6.32	4.17	.88	-4.06	-11.16	-11.35	-7.47	-5.66	-5.04	-5.07	-5.41	-5.83	-6.16	-6.29
15	7.40	6.19	4.09	.94	-3.52	-8.59	-8.89	-6.53	-5.20	-4.76	-4.87	-5.25	-5.69	-6.03	-6.15
20	7.19	6.01	3.97	1.00	-2.90	-6.54	-6.89	-5.52	-4.64	-4.41	-4.62	-5.04	-5.50	-5.84	-5.96
25	6.91	5.76	3.82	1.07	-2.26	-4.92	-5.29	-4.54	-4.04	-4.01	-4.31	-4.79	-5.26	-5.61	-5.74
30	6.56	5.46	3.62	1.13	-1.64	-3.61	-3.98	-3.64	-3.44	-3.58	-3.98	-4.50	-5.00	-5.35	-5.48
35	6.13	5.08	3.38	1.17	-1.09	-2.55	-2.92	-2.84	-2.87	-3.16	-3.64	-4.20	-4.71	-5.06	-5.19
40	5.60	4.63	3.08	1.17	-.62	-1.71	-2.06	-2.16	-2.36	-2.76	-3.30	-3.89	-4.40	-4.76	-4.88
45	4.97	4.08	2.72	1.13	-.25	-1.05	-1.38	-1.59	-1.91	-2.40	-2.98	-3.59	-4.11	-4.45	-4.58

B/LAMBDA = 2.0

FLARE ANGLE	PHI														
	6	12	18	24	30	36	42	48	54	60	66	72	78	84	90
0	8.40	6.40	2.66	-4.26	-137.42	-7.93	-4.62	-4.36	-5.70	-8.23	-11.88	-16.87	-24.01	-36.14	-141.67
5	8.36	6.37	2.66	-4.03	-16.09	-7.44	-4.47	-4.28	-5.64	-8.16	-11.75	-16.53	-22.53	-27.42	-28.09
10	8.24	6.28	2.68	-3.40	-10.13	-6.25	-4.06	-4.06	-5.48	-7.97	-11.40	-15.62	-19.79	-21.82	-22.03
15	8.05	6.14	2.70	-2.55	-6.71	-4.84	-3.47	-3.73	-5.21	-7.65	-10.85	-14.40	-17.22	-18.31	-18.44
20	7.77	5.93	2.72	-1.64	-4.36	-3.48	-2.79	-3.31	-4.86	-7.23	-10.15	-13.06	-15.05	-15.74	-15.84
25	7.40	5.65	2.73	-.78	-2.62	-2.27	-2.09	-2.84	-4.46	-6.74	-9.36	-11.73	-13.19	-13.70	-13.78
30	6.94	5.30	2.72	-.02	-1.29	-1.25	-1.43	-2.36	-4.01	-6.18	-8.51	-10.45	-11.57	-11.98	-12.06
35	6.37	4.88	2.67	.61	-.26	-.41	-.84	-1.90	-3.55	-5.59	-7.64	-9.25	-10.15	-10.50	-10.57
40	5.68	4.37	2.57	1.10	.51	.26	-.33	-1.48	-3.10	-4.99	-6.78	-8.12	-8.88	-9.19	-9.26
45	4.86	3.76	2.40	1.44	1.07	.75	.06	-1.11	-2.67	-4.39	-5.96	-7.09	-7.74	-8.02	-8.10

B/LAMBDA = 2.4

FLARE ANGLE	PHI														
	6	12	18	24	30	36	42	48	54	60	66	72	78	84	90
0	8.90	5.92	-.31	-22.43	-6.32	-3.45	-4.72	-9.17	-20.66	-18.72	-11.84	-9.49	-8.57	-8.24	-8.16
5	8.85	5.89	-.19	-13.16	-5.75	-3.29	-4.63	-9.04	-19.43	-17.97	-11.70	-9.42	-8.52	-8.20	-8.12
10	8.71	5.81	.16	-7.62	-4.42	-2.85	-4.36	-8.66	-16.96	-16.24	-11.28	-9.21	-8.37	-8.08	-8.01
15	8.46	5.67	.64	-4.32	-2.90	-2.22	-3.94	-8.07	-14.48	-14.26	-10.65	-8.88	-8.14	-7.88	-7.82
20	8.10	5.48	1.19	-2.06	-1.50	-1.51	-3.43	-7.32	-12.28	-12.35	-9.85	-8.43	-7.82	-7.61	-7.57
25	7.63	5.23	1.72	-.40	-.30	-.81	-2.87	-6.47	-10.35	-10.61	-8.95	-7.88	-7.42	-7.28	-7.25
30	7.04	4.90	2.18	.83	.67	-.16	-2.29	-5.58	-8.64	-9.03	-8.00	-7.26	-6.96	-6.88	-6.87
35	6.31	4.51	2.54	1.73	1.44	.41	-1.73	-4.67	-7.13	-7.60	-7.04	-6.60	-6.44	-6.43	-6.45
40	5.44	4.03	2.78	2.36	1.99	.86	-1.21	-3.80	-5.79	-6.32	-6.10	-5.91	-5.89	-5.95	-5.99
45	4.41	3.47	2.86	2.73	2.35	1.18	-.76	-3.00	-4.62	-5.17	-5.20	-5.22	-5.33	-5.45	-5.50

B/LAMBDA = 2.8

FLARE ANGLE	PHI														
	6	12	18	24	30	36	42	48	54	60	66	72	78	84	90
0	9.23	4.95	-5.92	-8.06	-2.81	-4.72	-13.15	-17.81	-9.16	-7.39	-7.75	-9.15	-10.92	-12.41	-13.01
5	9.17	4.95	-4.98	-6.67	-2.57	-4.59	-12.73	-16.84	-9.04	-7.33	-7.71	-9.10	-10.86	-12.34	-12.92
10	8.99	4.93	-3.03	-4.13	-1.93	-4.21	-11.63	-14.72	-8.68	-7.15	-7.58	-8.97	-10.69	-12.12	-12.68
15	8.68	4.89	-1.10	-1.85	-1.09	-3.65	-10.15	-12.41	-8.11	-6.87	-7.36	-8.75	-10.41	-11.76	-12.29
20	8.24	4.82	.50	-.05	-.21	-2.97	-8.54	-10.26	-7.37	-6.47	-7.06	-8.44	-10.04	-11.29	-11.77
25	7.65	4.71	1.75	1.32	.61	-2.25	-6.94	-8.32	-6.51	-5.98	-6.68	-8.06	-9.57	-10.72	-11.15
30	6.92	4.55	2.68	2.34	1.31	-1.52	-5.43	-6.59	-5.58	-5.41	-6.23	-7.60	-9.02	-10.07	-10.44
35	6.04	4.31	3.33	3.06	1.86	-.85	-4.06	-5.06	-4.63	-4.79	-5.72	-7.07	-8.41	-9.35	-9.68
40	4.98	3.98	3.71	3.51	2.25	-.24	-2.84	-3.72	-3.71	-4.14	-5.17	-6.50	-7.74	-8.59	-8.88
45	3.78	3.54	3.82	3.70	2.46	.26	-1.79	-2.57	-2.84	-3.49	-4.59	-5.88	-7.04	-7.80	-8.06

B/LAMBDA = 3.2

FLARE ANGLE	PHI 6	12	18	24	30	36	42	48	54	60	66	72	78	84	90
0	9.41	3.44	-27.88	-2.97	-3.39	-13.10	-12.83	-7.05	-7.47	-11.35	-20.63	-25.87	-16.79	-14.24	-13.59
5	9.34	3.51	-9.92	-2.46	-3.20	-12.50	-12.34	-6.95	-7.41	-11.26	-20.02	-24.19	-16.56	-14.11	-13.48
10	9.12	3.69	-4.09	-1.27	-2.69	-11.00	-11.07	-6.64	-7.22	-10.97	-18.53	-21.21	-15.92	-13.76	-13.18
15	8.75	3.94	-.82	.10	-1.97	-9.10	-9.40	-6.15	-6.90	-10.52	-16.73	-18.50	-15.00	-13.21	-12.71
20	8.22	4.20	1.33	1.34	-1.17	-7.16	-7.62	-5.50	-6.46	-9.90	-14.94	-16.21	-13.91	-12.51	-12.10
25	7.53	4.41	2.80	2.35	-.37	-5.32	-5.88	-4.72	-5.91	-9.16	-13.24	-14.24	-12.75	-11.70	-11.38
30	6.67	4.54	3.80	3.11	.36	-3.66	-4.28	-3.86	-5.27	-8.32	-11.64	-12.49	-11.57	-10.82	-10.58
35	5.65	4.53	4.41	3.62	.99	-2.20	-2.84	-2.98	-4.57	-7.40	-10.14	-10.92	-10.40	-9.90	-9.73
40	4.46	4.35	4.67	3.88	1.49	-.97	-1.60	-2.13	-3.83	-6.44	-8.73	-9.47	-9.24	-8.95	-8.85
45	3.17	3.98	4.61	3.87	1.84	.03	-.56	-1.35	-3.10	-5.47	-7.41	-8.13	-8.13	-8.00	-7.95

B/LAMBDA = 3.6

FLARE ANGLE	PHI 6	12	18	24	30	36	42	48	54	60	66	72	78	84	90
0	9.45	1.19	-8.50	-1.73	-8.08	-13.83	-6.36	-8.30	-18.96	-17.07	-10.77	-9.30	-9.31	-9.71	-9.92
5	9.37	1.48	-5.65	-1.40	-7.74	-12.96	-6.23	-8.20	-18.35	-16.71	-10.69	-9.25	-9.28	-9.68	-9.88
10	9.12	2.21	-1.90	-.58	-6.80	-10.95	-5.86	-7.92	-16.86	-15.74	-10.47	-9.13	-9.17	-9.58	-9.78
15	8.70	3.10	.80	.44	-5.48	-8.61	-5.26	-7.47	-15.02	-14.42	-10.10	-8.91	-8.99	-9.41	-9.61
20	8.10	3.92	2.67	1.43	-3.99	-6.35	-4.47	-6.84	-13.14	-12.93	-9.59	-8.61	-8.75	-9.17	-9.37
25	7.32	4.56	3.95	2.27	-2.51	-4.31	-3.55	-6.08	-11.31	-11.41	-8.96	-8.22	-8.43	-8.87	-9.07
30	6.36	4.96	4.77	2.91	-1.14	-2.53	-2.58	-5.22	-9.57	-9.89	-8.23	-7.74	-8.04	-8.49	-8.69
35	5.25	5.10	5.18	3.34	.06	-1.01	-1.61	-4.29	-7.92	-8.42	-7.41	-7.19	-7.58	-8.05	-8.25
40	4.02	4.94	5.23	3.54	1.05	.23	-.72	-3.35	-6.38	-7.01	-6.53	-6.57	-7.05	-7.54	-7.74
45	2.78	4.48	4.91	3.50	1.79	1.19	.05	-2.44	-4.97	-5.68	-5.62	-5.90	-6.46	-6.98	-7.18

B/LAMBDA = 4.0

FLARE ANGLE	PHI 6	12	18	24	30	36	42	48	54	60	66	72	78	84	90
0	9.38	-2.24	-3.15	-2.84	-134.30	-6.31	-7.86	-28.66	-11.51	-8.75	-10.22	-14.28	-21.08	-33.14	-138.67
5	9.29	-1.18	-2.00	-2.54	-18.93	-6.12	-7.74	-24.12	-11.37	-8.69	-10.16	-14.18	-20.65	-28.96	-31.10
10	9.01	.88	.18	-1.77	-12.49	-5.54	-7.38	-19.26	-10.95	-8.52	-10.01	-13.88	-19.55	-24.36	-25.02
15	8.55	2.77	2.15	-.77	-8.41	-4.64	-6.79	-15.72	-10.29	-8.24	-9.75	-13.40	-18.12	-21.07	-21.40
20	7.91	4.19	3.64	.28	-5.32	-3.50	-5.99	-12.91	-9.42	-7.84	-9.38	-12.77	-16.60	-18.54	-18.76
25	7.08	5.14	4.66	1.24	-2.86	-2.27	-5.04	-10.50	-8.38	-7.33	-8.91	-12.01	-15.11	-16.47	-16.63
30	6.08	5.66	5.25	2.05	-.88	-1.06	-4.00	-8.36	-7.22	-6.71	-8.34	-11.15	-13.66	-14.68	-14.82
35	4.96	5.76	5.46	2.68	.68	.05	-2.92	-6.44	-6.00	-5.98	-7.67	-10.21	-12.27	-13.08	-13.21
40	3.78	5.47	5.28	3.10	1.87	.99	-1.88	-4.71	-4.77	-5.18	-6.92	-9.21	-10.93	-11.61	-11.73
45	2.68	4.76	4.72	3.27	2.69	1.71	-.93	-3.19	-3.58	-4.34	-6.10	-8.17	-9.64	-10.24	-10.36

B/LAMBDA = 4.4

FLARE ANGLE	PHI 6	12	18	24	30	36	42	48	54	60	66	72	78	84	90
0	9.19	-8.27	-1.03	-6.78	-8.95	-6.06	-22.03	-10.28	-8.67	-14.13	-33.78	-15.14	-11.93	-10.98	-10.79
5	9.09	-3.99	-.31	-6.30	-8.41	-5.91	-20.14	-10.13	-8.60	-13.99	-28.40	-15.01	-11.87	-10.94	-10.75
10	8.81	.37	1.22	-5.03	-6.95	-5.47	-16.82	-9.70	-8.40	-13.60	-23.35	-14.62	-11.70	-10.82	-10.64

15	8.35	3.13	2.75	-3.34	-5.02	-4.76	-13.74	-9.00	-8.06	-12.97	-19.90	-14.02	-11.42	-10.61	-10.45
20	7.69	4.87	3.97	-1.58	-2.98	-3.83	-11.03	-8.06	-7.59	-12.15	-17.25	-13.25	-11.04	-10.33	-10.19
25	6.87	5.90	4.79	.06	-1.10	-2.76	-8.60	-6.92	-6.97	-11.17	-15.04	-12.35	-10.55	-9.96	-9.85
30	5.90	6.35	5.23	1.45	.52	-1.65	-6.41	-5.66	-6.22	-10.07	-13.11	-11.36	-9.98	-9.51	-9.43
35	4.83	6.30	5.29	2.55	1.82	-.59	-4.44	-4.34	-5.37	-8.89	-11.34	-10.29	-9.31	-8.59	-8.94
40	3.76	5.74	4.97	3.31	2.78	.35	-2.70	-3.05	-4.44	-7.64	-9.70	-9.18	-8.57	-8.39	-8.38
45	2.78	4.67	4.28	3.71	3.37	1.13	-1.22	-1.83	-3.47	-6.37	-8.14	-8.04	-7.76	-7.72	-7.75

B/LAMBDA = 4.8

FLARE ANGLE	PHI														
	6	12	18	24	30	36	42	48	54	60	66	72	78	84	90
0	8.88	-41.02	-.55	-19.44	-5.15	-11.60	-11.43	-8.35	-17.80	-15.98	-10.53	-10.48	-12.29	-14.39	-15.35
5	8.79	-4.77	.01	-14.64	-4.89	-11.26	-11.17	-8.26	-17.43	-15.76	-10.47	-10.44	-12.23	-14.32	-15.26
10	8.54	.94	1.25	-9.33	-4.15	-10.32	-10.43	-8.01	-16.44	-15.14	-10.31	-10.32	-12.09	-14.10	-15.00
15	8.11	3.94	2.58	-5.36	-3.01	-8.92	-9.28	-7.58	-15.07	-14.21	-10.04	-10.11	-11.84	-13.75	-14.58
20	7.51	5.68	3.67	-2.28	-1.64	-7.23	-7.83	-6.97	-13.51	-13.07	-9.65	-9.83	-11.50	-13.28	-14.03
25	6.76	6.61	4.44	.12	-.25	-5.42	-6.20	-6.18	-11.86	-11.78	-9.16	-9.45	-11.07	-12.70	-13.36
30	5.86	6.88	4.85	1.95	1.02	-3.62	-4.52	-5.25	-10.18	-10.40	-8.55	-8.98	-10.54	-12.02	-12.60
35	4.87	6.57	4.92	3.26	2.07	-1.94	-2.89	-4.21	-8.50	-8.97	-7.82	-8.42	-9.92	-11.26	-11.77
40	3.85	5.68	4.64	4.08	2.83	-.45	-1.39	-3.12	-6.84	-7.52	-7.00	-7.77	-9.21	-10.42	-10.87
45	2.89	4.21	4.01	4.42	3.27	.77	-.10	-2.05	-5.25	-6.09	-6.09	-7.04	-8.43	-9.52	-9.91

B/LAMBDA = 5.2

FLARE ANGLE	PHI														
	6	12	18	24	30	36	42	48	54	60	66	72	78	84	90
0	8.45	-9.40	-1.38	-12.30	-5.50	-21.53	-7.61	-16.17	-13.60	-9.83	-13.32	-26.01	-22.32	-16.83	-15.69
5	8.39	-2.83	-.87	-10.55	-5.28	-19.01	-7.49	-15.84	-13.43	-9.77	-13.23	-24.92	-21.85	-16.69	-15.59
10	8.20	2.07	.33	-7.13	-4.64	-15.06	-7.15	-14.91	-12.95	-9.61	-13.00	-22.66	-20.65	-16.31	-15.30
15	7.88	4.83	1.68	-3.79	-3.63	-11.57	-6.56	-13.59	-12.18	-9.33	-12.61	-20.33	-19.13	-15.72	-14.83
20	7.41	6.40	2.89	-.98	-2.37	-8.53	-5.74	-12.01	-11.17	-8.93	-12.08	-18.21	-17.54	-14.97	-14.23
25	6.77	7.12	3.83	1.26	-1.03	-5.84	-4.71	-10.30	-9.97	-8.41	-11.42	-16.31	-15.99	-14.10	-13.50
30	5.96	7.16	4.45	2.94	.25	-3.48	-3.54	-8.51	-8.62	-7.75	-10.62	-14.57	-14.49	-13.14	-12.69
35	5.00	6.55	4.73	4.08	1.37	-1.44	-2.30	-6.72	-7.17	-6.96	-9.71	-12.94	-13.05	-12.13	-11.80
40	3.94	5.30	4.65	4.70	2.25	.25	-1.10	-4.97	-5.68	-6.06	-8.69	-11.38	-11.65	-11.08	-10.85
45	2.88	3.46	4.17	4.78	2.84	1.56	-.02	-3.32	-4.21	-5.07	-7.59	-9.88	-10.28	-9.99	-9.86

SINE-SQUARED PHI VS. PHI

6	12	18	24	30	36	42	48	54	60	66	72	78	84	90
-19.61	-13.64	-10.20	-7.81	-6.02	-4.61	-3.49	-2.58	-1.84	-1.25	-.79	-.44	-.19	-.05	-.00

B/LAMBDA = 5.6

FLARE ANGLE	PHI 6	12	18	24	30	36	42	48	54	60	66	72	78	84	90
0	7.85	-3.89	-3.71	-5.91	-10.00	-8.60	-10.84	-15.09	-9.60	-17.00	-19.59	-12.34	-11.23	-11.56	-11.84
5	7.89	-.62	-3.09	-5.34	-9.60	-8.56	-10.68	-14.79	-9.53	-16.79	-19.26	-12.28	-11.19	-11.53	-11.80
10	7.84	3.17	-1.56	-3.80	-8.48	-7.87	-10.19	-13.96	-9.33	-16.20	-18.37	-12.11	-11.09	-11.42	-11.70
15	7.71	5.56	.26	-1.74	-6.82	-6.74	-9.39	-12.72	-8.99	-15.32	-17.17	-11.83	-10.90	-11.25	-11.52
20	7.42	6.89	1.99	.35	-4.85	-5.26	-8.30	-11.20	-8.49	-14.21	-15.79	-11.44	-10.64	-11.01	-11.27
25	6.91	7.46	3.41	2.14	-2.83	-3.58	-6.97	-9.51	-7.84	-12.96	-14.33	-10.94	-10.30	-10.69	-10.95
30	6.15	7.19	4.42	3.51	-.92	-1.87	-5.47	-7.71	-7.02	-11.60	-12.85	-10.33	-9.88	-10.29	-10.55
35	5.11	6.28	4.98	4.41	.74	-.28	-3.90	-5.89	-6.05	-10.16	-11.35	-9.61	-9.37	-9.81	-10.07
40	3.90	4.72	5.04	4.79	2.06	1.05	-2.36	-4.12	-4.97	-8.66	-9.64	-8.78	-8.76	-9.25	-9.51
45	2.70	2.70	4.56	4.64	2.98	2.14	-.94	-2.47	-3.81	-7.13	-8.33	-7.86	-8.07	-8.61	-8.86

B/LAMBDA = 6.0

FLARE ANGLE	PHI 6	12	18	24	30	36	42	48	54	60	66	72	78	84	90
0	7.20	-1.14	-8.58	-4.04	-132.58	-7.12	-34.87	-9.20	-16.94	-15.21	-10.93	-13.23	-19.46	-31.39	-135.19
5	7.29	.97	-7.17	-3.67	-20.65	-6.96	-25.25	-9.11	-16.69	-15.06	-10.88	-13.18	-19.25	-29.03	-32.86
10	7.49	3.98	-4.13	-2.59	-14.07	-6.50	-19.32	-8.84	-15.98	-14.62	-10.74	-13.00	-18.68	-25.45	-26.78
15	7.63	6.03	-1.00	-1.03	-9.68	-5.70	-15.37	-8.38	-14.92	-13.93	-10.51	-12.72	-17.84	-22.49	-23.15
20	7.56	7.14	1.61	.66	-6.16	-4.61	-12.21	-7.72	-13.62	-13.02	-10.17	-12.32	-16.82	-20.10	-20.50
25	7.15	7.43	3.58	2.19	-3.19	-3.29	-9.43	-6.84	-12.16	-11.94	-9.72	-11.81	-15.69	-18.08	-18.36
30	6.33	7.00	4.89	3.38	-.71	-1.86	-6.89	-5.78	-10.57	-10.71	-9.16	-11.19	-14.51	-16.31	-16.52
35	5.13	5.86	5.55	4.16	1.27	-.46	-4.57	-4.55	-8.91	-9.36	-8.47	-10.46	-13.30	-14.70	-14.88
40	3.69	4.13	5.52	4.47	2.74	.79	-2.49	-3.24	-7.19	-7.92	-7.66	-9.62	-12.06	-13.19	-13.36
45	2.41	2.25	4.79	4.27	3.67	1.79	-.70	-1.94	-5.48	-6.43	-6.73	-8.67	-10.79	-11.75	-11.91

B/LAMBDA = 6.4

FLARE ANGLE	PHI 6	12	18	24	30	36	42	48	54	60	66	72	78	84	90
0	6.34	.37	-24.88	-4.63	-10.58	-10.71	-10.70	-12.58	-15.66	-10.81	-17.88	-22.94	-14.53	-12.74	-12.42
5	6.61	1.94	-12.27	-4.29	-10.05	-10.47	-10.53	-12.45	-15.45	-10.75	-17.70	-22.44	-14.46	-12.70	-12.38
10	7.19	4.43	-5.49	-3.29	-8.58	-9.77	-10.00	-12.03	-14.85	-10.59	-17.19	-21.20	-14.25	-12.57	-12.27
15	7.68	6.21	-1.04	-1.81	-6.46	-8.64	-9.12	-11.36	-13.93	-10.31	-16.41	-19.62	-13.92	-12.36	-12.08
20	7.80	7.14	2.10	-.14	-4.05	-7.14	-7.92	-10.42	-12.75	-9.90	-15.43	-17.97	-13.46	-12.07	-11.81
25	7.42	7.28	4.25	1.45	-1.68	-5.38	-6.43	-9.25	-11.38	-9.36	-14.31	-16.35	-12.88	-11.69	-11.47
30	6.46	6.69	5.55	2.77	.43	-3.50	-4.75	-7.87	-9.85	-8.68	-13.09	-14.78	-12.20	-11.22	-11.05
35	5.00	5.44	6.06	3.71	2.15	-1.66	-3.00	-6.33	-8.20	-7.84	-11.78	-13.24	-11.41	-10.67	-10.54
40	3.33	3.76	5.77	4.21	3.38	.00	-1.32	-4.71	-6.49	-6.86	-10.39	-11.73	-10.54	-10.02	-9.95
45	2.16	2.26	4.65	4.21	4.07	1.37	.17	-3.09	-4.77	-5.75	-8.94	-10.22	-9.57	-9.29	-9.27

B/LAMBDA = 6.8

FLARE ANGLE	PHI 6	12	18	24	30	36	42	48	54	60	66	72	78	84	90
0	5.30	1.07	-12.14	-7.90	-6.66	-47.96	-8.86	-25.21	-10.40	-20.32	-15.64	-11.86	-13.07	-15.57	-16.86

5	5.87	2.35	-8.86	-7.40	-6.41	-24.05	-8.75	-23.38	-10.34	-19.96	-15.52	-11.81	-13.03	-15.50	-16.77
10	6.98	4.52	-3.94	-5.99	-5.63	-17.63	-8.41	-20.15	-10.13	-19.00	-15.18	-11.69	-12.90	-15.29	-16.50
15	7.85	6.13	.06	-3.95	-4.35	13.42	-7.81	-17.14	-9.78	-17.67	-14.64	-11.48	-12.68	-14.96	-16.07
20	8.11	6.94	2.99	-1.67	-2.68	-9.97	-6.95	-14.45	-9.27	-16.16	-13.92	-11.19	-12.38	-14.50	-15.51
25	7.67	7.01	4.96	.49	-.86	-6.91	-5.83	-11.96	-8.59	-14.57	-13.04	-10.80	-11.98	-13.94	-14.83
30	6.48	6.39	6.06	2.32	.86	-4.16	-4.49	-9.59	-7.72	-12.93	-12.02	-10.31	-11.49	-13.27	-14.05
35	4.70	5.19	6.30	3.68	2.31	-1.73	-3.00	-7.30	-6.67	-11.25	-10.87	-9.71	-10.90	-12.52	-13.19
40	2.90	3.71	5.67	4.47	3.34	.31	-1.51	-5.11	-5.45	-9.52	-9.62	-9.00	-10.21	-11.67	-12.25
45	2.13	2.52	4.16	4.60	3.87	1.90	-.12	-3.08	-4.13	-7.77	-8.26	-8.16	-9.42	-10.74	-11.25

B/LAMBDA = 7.2

FLARE ANGLE	PHI 6	12	18	24	30	36	42	48	54	60	66	72	78	84	90
0	4.04	1.15	-6.05	-17.72	-6.91	-11.41	-14.33	-10.91	-16.29	-14.67	-11.97	-18.79	-29.78	-18.76	-17.11
5	5.10	2.27	-4.80	-14.84	-6.68	-11.11	-14.06	-10.80	-16.10	-14.56	-11.92	-18.62	-28.15	-18.61	-17.01
10	6.91	4.26	-1.88	-10.28	-5.99	-10.22	-13.30	-10.48	-15.55	-14.22	-11.78	-18.15	-25.24	-18.19	-16.72
15	8.12	5.80	1.22	-6.14	-4.82	-8.81	-12.11	-9.93	-14.71	-13.67	-11.53	-17.42	-22.56	-17.54	-16.26
20	8.45	6.63	3.71	-2.56	-3.28	-6.97	-10.57	-9.13	-13.61	-12.93	-11.19	-16.51	-20.28	-16.73	-15.65
25	7.86	6.76	5.39	.39	-1.53	-4.85	-8.76	-8.09	-12.31	-12.00	-10.73	-15.47	-18.30	-15.80	-14.93
30	6.37	6.25	6.23	2.66	.20	-2.67	-6.77	-6.80	-10.83	-10.90	-10.14	-14.34	-16.53	-14.79	-14.11
35	4.24	5.20	6.21	4.22	1.72	-.61	-4.69	-5.31	-9.21	-9.64	-9.43	-13.13	-14.89	-13.72	-13.21
40	2.55	3.87	5.30	5.02	2.87	1.15	-2.67	-3.71	-7.47	-8.23	-8.57	-11.85	-13.33	-12.60	-12.24
45	2.42	2.70	3.57	5.01	3.56	2.50	-.82	-2.10	-5.67	-6.72	-7.56	-10.50	-11.82	-11.44	-11.21

B/LAMBDA = 7.6

FLARE ANGLE	PHI 6	12	18	24	30	36	42	48	54	60	66	72	78	84	90
0	2.47	.63	-3.55	-15.89	-11.32	-8.16	-20.77	-11.12	-17.82	-11.77	-26.92	-15.94	-12.72	-12.83	-13.16
5	4.37	1.70	-2.76	-13.53	-10.90	-8.00	-19.73	-11.03	-17.55	-11.71	-25.83	-15.85	-12.68	-12.79	-13.13
10	6.98	3.67	-.66	-9.33	-9.70	-7.50	-17.43	-10.73	-16.78	-11.54	-23.56	-15.58	-12.57	-12.69	-13.02
15	8.47	5.31	1.85	-5.25	-7.85	-6.65	-14.82	-10.23	-15.64	-11.25	-21.19	-15.14	-12.38	-12.51	-12.84
20	8.77	6.32	3.98	-1.68	-5.58	-5.43	-12.20	-9.51	-14.25	-10.83	-19.02	-14.55	-12.10	-12.27	-12.59
25	7.95	6.65	5.43	1.24	-3.13	-3.88	-9.59	-8.55	-12.67	-10.27	-17.04	-13.82	-11.74	-11.94	-12.26
30	6.10	6.33	6.08	3.42	-.79	-2.14	-7.03	-7.35	-10.96	-9.55	-15.19	-12.97	-11.29	-11.54	-11.85
35	3.70	5.39	5.90	4.82	1.25	-.41	-4.55	-5.93	-9.13	-8.66	-13.42	-12.01	-10.75	-11.05	-11.35
40	2.47	4.00	4.90	5.39	2.81	1.13	-2.26	-4.35	-7.22	-7.60	-11.67	-10.93	-10.10	-10.47	-10.77
45	2.95	2.63	3.25	5.05	3.79	2.33	-.26	-2.73	-5.28	-6.38	-9.92	-9.74	-9.34	-9.80	-10.09

B/LAMBDA = 8.0

FLARE ANGLE	PHI 6	12	18	24	30	36	42	48	54	60	66	72	78	84	90
0	.50	-.51	-2.79	-8.04	-131.29	-10.22	-10.42	-25.69	-11.14	-24.71	-13.84	-13.03	-18.40	-30.15	-135.66
5	3.77	.61	-2.14	-7.43	-21.88	-10.03	-10.28	-24.01	-11.07	-23.91	-13.77	-12.98	-18.28	-28.67	-34.12
10	7.20	2.80	-.39	-5.68	-15.24	-9.44	-9.86	-20.95	-10.86	-22.08	-13.57	-12.85	-17.92	-25.92	-28.03
15	8.86	4.78	1.81	-3.14	-10.70	-8.45	-9.13	-18.01	-10.51	-19.98	-13.24	-12.63	-17.37	-23.33	-24.40
20	9.05	6.15	3.77	-.40	-6.87	-7.06	-8.08	-15.35	-9.98	-17.92	-12.76	-12.32	-16.65	-21.11	-21.74
25	7.94	6.77	5.13	2.04	-3.51	-5.32	-6.70	-12.85	-9.28	-15.95	-12.15	-11.91	-15.80	-19.17	-19.60
30	5.68	6.59	5.76	3.90	-.61	-3.37	-5.03	-10.43	-8.37	-14.04	-11.39	-11.39	-14.85	-17.44	-17.76
35	3.20	5.59	5.63	5.03	1.72	-1.39	-3.20	-8.04	-7.24	-12.15	-10.49	-10.76	-13.81	-15.84	-16.10
40	2.75	3.92	4.75	5.34	3.40	.42	-1.36	-5.69	-5.92	-10.24	-9.43	-10.00	-12.70	-14.33	-14.56
45	3.53	2.31	3.33	4.73	4.34	1.90	.31	-3.46	-4.44	-8.31	-8.22	-9.11	-11.52	-12.87	-13.08

B/LAMBDA = 8.4

FLARE ANGLE	PHI 6	12	18	24	30	36	42	48	54	60	66	72	78	84	90
0	-2.10	-2.44	-3.36	-5.65	-11.76	-22.73	-10.31	-13.81	-15.78	-14.30	-13.74	-41.85	-17.00	-14.06	-13.60
5	3.37	-1.05	-2.75	-5.26	-11.24	-20.72	-10.19	-13.64	-15.63	-14.21	-13.69	-32.88	-16.90	-14.02	-13.56
10	7.53	1.77	-1.07	-4.06	-9.77	-17.19	-9.82	-13.17	-15.19	-13.93	-13.50	-27.21	-16.63	-13.89	-13.44
15	9.24	4.40	1.13	-2.16	-7.56	-13.78	-9.19	-12.38	-14.49	-13.48	-13.21	-23.62	-16.20	-13.67	-13.26
20	9.25	6.22	3.17	.08	-4.91	-10.58	-8.25	-11.30	-13.54	-12.85	-12.79	-20.94	-15.62	-13.37	-12.99
25	7.91	7.02	4.70	2.18	-2.15	-7.50	-7.01	-9.93	-12.38	-12.04	-12.25	-18.74	-14.92	-12.98	-12.65
30	5.15	6.09	5.54	3.82	.38	-4.57	-5.47	-8.29	-11.00	-11.05	-11.56	-16.80	-14.10	-12.49	-12.22
35	2.90	5.65	5.63	4.80	2.45	-1.88	-3.73	-6.44	-9.43	-9.87	-10.74	-15.02	-13.18	-11.92	-11.71
40	3.30	3.57	4.93	5.02	3.88	.42	-1.92	-4.46	-7.68	-8.50	-9.75	-13.32	-12.17	-11.25	-11.10
45	3.99	1.96	3.52	4.40	4.55	2.20	-.22	-2.49	-5.82	-6.98	-8.60	-11.65	-11.07	-10.48	-10.40

B/LAMBDA = 8.8

FLARE ANGLE	PHI 6	12	18	24	30	36	42	48	54	60	66	72	78	84	90
0	-5.82	-5.57	-5.42	-5.82	-7.78	-14.50	-19.15	-10.85	-20.25	-12.76	-30.79	-13.68	-13.68	-16.38	-17.98
5	3.31	-3.30	-4.68	-5.47	-7.53	-14.05	-18.55	-10.77	-19.85	-12.70	-28.70	-13.63	-13.64	-16.31	-17.88
10	7.93	.85	-2.68	-4.37	-6.74	-12.81	-17.02	-10.50	-18.79	-12.51	-25.31	-13.48	-13.52	-16.11	-17.61
15	9.51	4.32	-.04	-2.61	-5.38	-10.96	-14.99	-10.05	-17.34	-12.20	-22.39	-13.24	-13.32	-15.79	-17.18
20	9.38	6.54	2.49	-.47	-3.51	-8.66	-12.73	-9.37	-15.66	-11.76	-19.93	-12.90	-13.04	-15.36	-16.61
25	7.56	7.49	4.46	1.62	-1.35	-6.09	-10.32	-8.46	-13.86	-11.16	-17.79	-12.44	-12.67	-14.82	-15.92
30	4.57	7.13	5.65	3.33	.76	-3.45	-7.81	-7.27	-11.96	-10.40	-15.84	-11.88	-12.20	-14.18	-15.14
35	2.64	5.49	5.93	4.46	2.65	-.95	-5.26	-5.83	-9.96	-9.46	-13.99	-11.19	-11.64	-13.43	-14.26
40	3.93	3.02	5.20	4.86	3.78	1.15	-2.81	-4.19	-7.88	-8.32	-12.16	-10.37	-10.97	-12.60	-13.31
45	4.22	1.88	3.49	4.43	4.30	2.19	-.60	-2.46	-5.75	-6.98	-10.33	-9.41	-10.19	-11.67	-12.28

B/LAMBDA = 9.2

FLARE ANGLE	PHI 6	12	18	24	30	36	42	48	54	60	66	72	78	84	90
0	-12.35	-11.27	-9.85	-8.54	-7.97	-9.31	-16.61	-17.17	-11.86	-32.12	-13.17	-16.12	-63.05	-20.39	-18.17
5	3.53	-5.77	-8.40	-8.06	-7.74	-9.14	-16.22	-16.91	-11.78	-29.17	-13.11	-16.05	-34.34	-20.22	-18.07
10	8.35	.49	-5.00	-6.64	-7.02	-8.61	-15.15	-16.18	-11.57	-25.12	-12.96	-15.83	-28.25	-19.75	-17.78
15	9.89	4.61	-1.16	-4.43	-5.77	-7.68	-13.57	-15.06	-11.20	-21.91	-12.70	-15.47	-24.60	-19.04	-17.33
20	9.42	7.00	2.20	-1.79	-4.02	-6.32	-11.62	-13.63	-10.66	-19.28	-12.32	-14.98	-21.92	-18.15	-16.72
25	7.21	7.94	4.66	.80	-1.94	-4.55	-9.39	-11.94	-9.93	-16.99	-11.83	-14.36	-19.74	-17.16	-16.00
30	4.03	7.20	6.06	2.97	.17	-2.52	-6.97	-10.04	-8.98	-14.88	-11.20	-13.61	-17.85	-16.09	-15.18
35	3.32	5.10	6.30	4.46	2.02	-.45	-4.46	-7.94	-7.79	-12.84	-10.42	-12.74	-16.14	-14.96	-14.28
40	4.49	2.48	5.28	5.11	3.35	1.39	-2.04	-5.72	-6.36	-10.81	-9.47	-11.74	-14.51	-13.79	-13.30
45	4.19	2.24	3.09	4.75	4.08	2.77	.10	-3.50	-4.75	-8.74	-8.35	-10.61	-12.94	-12.58	-12.25

B/LAMBDA = 9.6

FLARE ANGLE	PHI 6	12	18	24	30	36	42	48	54	60	66	72	78	84	90
0	-33.37	-39.01	-23.13	-16.53	-12.34	-10.03	-10.51	-18.92	-15.39	-14.07	-16.55	-21.32	-14.08	-13.79	-14.18
5	3.97	-6.77	-13.61	-14.60	-11.90	-9.86	-10.38	-18.53	-15.26	-13.99	-16.45	-21.08	-14.03	-13.75	-14.14
10	8.77	.76	-6.56	-10.78	-10.65	-9.33	-10.01	-17.47	-14.89	-13.76	-16.18	-20.42	-13.91	-13.65	-14.03

15	10.14	5.13	-1.35	-6.70	-8.69	-8.42	-9.36	-15.97	-14.29	-13.37	-15.73	-19.47	-13.70	-13.47	-13.85
20	9.38	7.46	2.55	-2.80	-6.20	-7.08	-8.39	-14.19	-13.46	-12.82	-15.11	-18.33	-13.40	-13.23	-13.59
25	6.77	7.09	5.17	.58	-3.42	-5.33	-7.07	-12.20	-12.40	-12.09	-14.35	-17.08	-13.01	-12.90	-13.26
30	3.67	7.08	6.51	3.21	-.70	-3.28	-5.41	-10.04	-11.12	-11.18	-13.43	-15.77	-12.53	-12.50	-12.84
35	3.89	4.55	6.51	4.90	1.66	-1.15	-3.49	-7.73	-9.60	-10.07	-12.36	-14.41	-11.95	-12.01	-12.34
40	4.87	2.22	5.06	5.53	3.41	.81	-1.50	-5.34	-7.86	-8.75	-11.14	-12.99	-11.25	-11.42	-11.75
45	3.90	2.87	2.47	4.92	4.36	2.36	.35	-3.00	-5.95	-7.22	-9.76	-11.50	-10.43	-10.73	-11.05

B/LAMBDA = 10.0

FLARE ANGLE	PHI 6	12	18	24	30	36	42	48	54	60	66	72	78	84	90
0	-11.27	-12.46	-14.79	-19.66	-130.34	-17.84	-12.10	-11.54	-23.15	-13.82	-20.82	-13.49	-17.69	-29.20	-133.62
5	4.53	-5.23	-11.06	-16.17	-22.85	-17.17	-11.96	-11.45	-22.51	-13.75	-20.57	-13.44	-17.60	-28.19	-35.10
10	9.15	1.54	-5.42	-11.07	-16.17	-15.45	-11.53	-11.17	-20.94	-13.55	-19.90	-13.32	-17.35	-26.06	-29.01
15	10.33	5.76	-.51	-6.42	-11.53	-13.15	-10.79	-10.69	-19.01	-13.21	-18.92	-13.12	-16.95	-23.83	-25.38
20	9.25	7.82	3.24	-2.25	-7.50	-10.52	-9.72	-9.98	-16.99	-12.73	-17.73	-12.82	-16.41	-21.79	-22.72
25	6.28	8.17	5.69	1.23	-3.80	-7.67	-8.30	-9.00	-14.95	-12.09	-16.42	-12.43	-15.74	-19.95	-20.58
30	3.38	6.78	6.79	3.82	-.54	-4.74	-6.52	-7.73	-12.86	-11.27	-15.01	-11.94	-14.96	-18.28	-18.73
35	4.50	3.98	6.45	5.37	2.09	-1.91	-4.47	-6.15	-10.71	-10.25	-13.53	-11.33	-14.08	-16.72	-17.06
40	5.03	2.42	4.59	5.73	3.93	.57	-2.32	-4.33	-8.47	-9.02	-11.95	-10.58	-13.10	-15.22	-15.51
45	3.39	3.40	2.00	4.73	4.79	2.49	-.28	-2.41	-6.17	-7.58	-10.26	-9.69	-12.01	-13.76	-14.02

B/LAMBDA = 10.4

FLARE ANGLE	PHI 6	12	18	24	30	36	42	48	54	60	66	72	78	84	90
0	-5.84	-6.68	-8.01	-9.87	-12.69	-18.65	-28.41	-13.98	-12.57	-46.42	-13.30	-23.13	-19.64	-15.14	-14.53
5	5.14	3.06	-6.71	-9.19	-12.17	-17.81	-25.31	-13.85	-12.49	-32.55	-13.25	-22.81	-19.50	-15.09	-14.48
10	9.49	2.40	-3.38	-7.25	-10.71	-15.76	-21.03	-13.47	-12.27	-26.54	-13.11	-21.98	-19.11	-14.96	-14.37
15	10.43	6.17	.54	-4.33	-8.45	-13.16	-17.48	-12.83	-11.89	-22.81	-12.87	-20.82	-18.51	-14.73	-14.18
20	9.04	8.03	3.84	-1.03	-5.62	-10.29	-14.37	-11.93	-11.33	-19.99	-12.53	-19.49	-17.74	-14.42	-13.91
25	5.79	8.09	5.99	1.98	-2.55	-7.25	-11.42	-10.74	-10.57	-17.60	-12.07	-18.09	-16.85	-14.02	-13.57
30	3.78	6.38	6.80	4.25	.34	-4.17	-8.50	-9.24	-9.58	-15.43	-11.48	-16.67	-15.85	-13.52	-13.14
35	5.01	3.60	6.16	5.52	2.71	-1.27	-5.59	-7.45	-8.33	-13.33	-10.74	-15.22	-14.77	-12.93	-12.62
40	4.98	2.91	4.11	5.58	4.29	1.21	-2.80	-5.42	-6.80	-11.23	-9.83	-13.74	-13.61	-12.24	-12.01
45	2.78	3.83	2.01	4.31	4.86	3.04	-.31	-3.27	-5.05	-9.08	-8.73	-12.19	-12.37	-11.44	-11.30

TABLE C-2: GROSS APPROXIMATION G-SUB-U(A/L, PHI)

A/L	PHI															
	6	12	18	24	30	36	42	48	54	60	66	72	78	84	90
1.0	-6.69	-6.32	-5.74	-4.98	-4.09	-3.12	-2.13	-1.14	-.22	.62	1.35	1.94	2.37	2.63	2.72
1.4	-12.73	-12.40	-11.84	-11.02	-9.91	-8.46	-6.59	-4.31	-2.22	-.41	1.11	2.30	3.16	3.68	3.85
1.8	-16.62	-16.31	-15.78	-15.01	-13.98	-12.65	-10.96	-8.80	-6.00	-2.61	.13	2.21	3.67	4.54	4.82
2.2	-19.53	-19.23	-18.71	-17.97	-16.98	-15.70	-14.09	-12.05	-9.46	-6.05	-1.70	1.64	3.89	5.20	5.64
2.6	-21.88	-21.58	-21.07	-20.34	-19.37	-18.12	-16.55	-14.58	-12.09	-8.88	-4.48	.57	3.86	5.72	6.33
3.0	-23.85	-23.55	-23.05	-22.33	-21.36	-20.13	-18.59	-16.66	-14.23	-11.13	-6.97	-1.04	3.60	6.12	6.93
3.4	-25.55	-25.25	-24.75	-24.04	-23.08	-21.86	-20.33	-18.43	-16.04	-13.01	-8.99	-3.21	3.11	6.42	7.46
3.8	-27.04	-26.75	-26.25	-25.54	-24.59	-23.38	-21.86	-19.97	-17.62	-14.63	-10.71	-5.16	2.39	6.62	7.93
4.2	-28.38	-28.09	-27.59	-26.88	-25.94	-24.73	-23.22	-21.35	-19.01	-16.06	-12.20	-6.81	1.42	6.76	8.36
4.6	-29.59	-29.30	-28.81	-28.10	-27.16	-25.95	-24.45	-22.58	-20.26	-17.33	-13.53	-8.25	.18	6.81	8.75
5.0	-30.70	-30.41	-29.92	-29.21	-28.27	-27.07	-25.57	-23.71	-21.40	-18.49	-14.72	-9.53	-1.32	6.81	9.11
5.4	-31.72	-31.43	-30.93	-30.23	-29.29	-28.09	-26.60	-24.74	-22.44	-19.55	-15.80	-10.68	-2.69	6.74	9.44
5.8	-32.66	-32.37	-31.88	-31.17	-30.24	-29.04	-27.55	-25.70	-23.40	-20.52	-16.80	-11.72	-3.91	6.61	9.75

PHI

A/L	6	12	18	24	30	36	42	48	54	60	66	72	78	84	90
6.2	-33.54	-33.25	-32.76	-32.05	-31.12	-29.93	-28.43	-26.59	-24.30	-21.43	-17.72	-12.68	-5.00	6.42	10.03
6.6	-34.36	-34.07	-33.58	-32.88	-31.94	-30.75	-29.26	-27.42	-25.13	-22.27	-18.58	-13.57	-5.99	6.18	10.30
7.0	-35.14	-34.85	-34.36	-33.65	-32.72	-31.53	-30.04	-28.20	-25.92	-23.06	-19.38	-14.40	-6.91	5.87	10.56
7.4	-35.87	-35.58	-35.09	-34.38	-33.45	-32.26	-30.77	-28.94	-26.66	-23.80	-20.14	-15.18	-7.75	5.50	10.80
7.8	-36.56	-36.27	-35.78	-35.08	-34.14	-32.95	-31.47	-29.63	-27.36	-24.51	-20.85	-15.91	-8.54	5.08	11.03
8.2	-37.21	-36.92	-36.43	-35.73	-34.80	-33.61	-32.13	-30.29	-28.02	-25.17	-21.52	-16.60	-9.28	4.59	11.24
8.6	-37.84	-37.55	-37.06	-36.36	-35.42	-34.24	-32.75	-30.92	-28.65	-25.81	-22.16	-17.25	-9.98	4.03	11.45
9.0	-38.43	-38.14	-37.65	-36.95	-36.02	-34.83	-33.35	-31.52	-29.25	-26.41	-22.77	-17.87	-10.63	3.40	11.64
9.4	-39.00	-38.71	-38.22	-37.52	-36.59	-35.40	-33.92	-32.09	-29.82	-26.98	-23.35	-18.46	-11.26	2.69	11.83
9.8	-39.55	-39.26	-38.77	-38.07	-37.14	-35.95	-34.47	-32.64	-30.37	-27.54	-23.90	-19.03	-11.85	1.92	12.01
10.2	-40.07	-39.78	-39.29	-38.59	-37.66	-36.47	-34.99	-33.16	-30.90	-28.06	-24.44	-19.57	-12.41	1.19	12.19
10.6	-40.57	-40.28	-39.80	-39.09	-38.16	-36.98	-35.50	-33.67	-31.40	-28.57	-24.95	-20.09	-12.95	.51	12.35
11.0	-41.06	-40.77	-40.28	-39.58	-38.65	-37.46	-35.98	-34.15	-31.89	-29.06	-25.44	-20.59	-13.47	-.13	12.51

G-SUB-V(B/L, PHI)

B/L \ PHI	6	12	18	24	30	36	42	48	54	60	66	72	78	84	90
.4	2.02	1.94	1.82	1.66	1.46	1.24	.99	.74	.49	.25	.04	-.13	-.27	-.35	-.38
.8	4.95	4.65	4.16	3.48	2.63	1.62	.54	-.37	-1.11	-1.70	-2.17	-2.52	-2.76	-2.90	-2.95
1.2	6.59	5.90	4.75	3.09	1.31	-.10	-1.22	-2.14	-2.87	-3.46	-3.93	-4.28	-4.52	-4.67	-4.7[illegible]
1.6	7.66	6.42	4.23	1.85	.06	-1.35	-2.47	-3.38	-4.12	-4.71	-5.18	-5.53	-5.77	-5.91	-5.96
2.0	8.40	6.40	3.27	.88	-.91	-2.32	-3.44	-4.35	-5.09	-5.68	-6.15	-6.50	-6.74	-6.88	-6.93
2.4	8.90	5.92	2.48	.09	-1.70	-3.11	-4.23	-5.14	-5.88	-6.47	-6.94	-7.29	-7.53	-7.68	-7.72
2.8	9.23	5.25	1.81	-.58	-2.37	-3.78	-4.90	-5.81	-6.55	-7.14	-7.61	-7.96	-8.20	-8.34	-8.39
3.2	9.41	4.67	1.23	-1.16	-2.95	-4.36	-5.48	-6.39	-7.13	-7.72	-8.19	-8.54	-8.78	-8.92	-8.97
3.6	9.45	4.16	.71	-1.67	-3.46	-4.87	-5.99	-6.91	-7.64	-8.23	-8.70	-9.05	-9.29	-9.44	-9.48
4.0	9.38	3.70	.26	-2.13	-3.92	-5.33	-6.45	-7.36	-8.10	-8.69	-9.16	-9.51	-9.75	-9.89	-9.94
4.4	9.19	3.28	-.16	-2.54	-4.34	-5.74	-6.87	-7.78	-8.51	-9.11	-9.57	-9.92	-10.16	-10.31	-10.35
4.8	8.88	2.91	-.53	-2.92	-4.71	-6.12	-7.24	-8.15	-8.89	-9.48	-9.95	-10.30	-10.54	-10.68	-10.73
5.2	8.53	2.56	-.88	-3.27	-5.06	-6.47	-7.59	-8.50	-9.24	-9.83	-10.29	-10.64	-10.89	-11.03	-11.08

B/L \ PHI	6	12	18	24	30	36	42	48	54	60	66	72	78	84	90
5.6	8.21	2.24	-1.20	-3.59	-5.38	-6.79	-7.91	-8.82	-9.56	-10.15	-10.62	-10.97	-11.21	-11.35	-11.40
6.0	7.91	1.94	-1.50	-3.89	-5.68	-7.09	-8.21	-9.12	-9.86	-10.45	-10.92	-11.27	-11.51	-11.65	-11.70
6.4	7.63	1.66	-1.78	-4.17	-5.96	-7.37	-8.49	-9.40	-10.14	-10.73	-11.20	-11.55	-11.79	-11.93	-11.98
6.8	7.37	1.39	-2.05	-4.43	-6.23	-7.63	-8.76	-9.67	-10.40	-11.00	-11.46	-11.81	-12.05	-12.20	-12.24
7.2	7.12	1.15	-2.29	-4.68	-6.47	-7.88	-9.00	-9.92	-10.65	-11.24	-11.71	-12.06	-12.30	-12.45	-12.49
7.6	6.88	.91	-2.53	-4.92	-6.71	-8.11	-9.24	-10.15	-10.89	-11.48	-11.94	-12.29	-12.54	-12.68	-12.73
8.0	6.66	.69	-2.75	-5.14	-6.93	-8.34	-9.46	-10.37	-11.11	-11.70	-12.17	-12.51	-12.76	-12.90	-12.95
8.4	6.45	.48	-2.96	-5.35	-7.14	-8.55	-9.67	-10.58	-11.32	-11.91	-12.38	-12.73	-12.97	-13.11	-13.16
8.8	6.25	.28	-3.17	-5.55	-7.35	-8.75	-9.88	-10.79	-11.52	-12.12	-12.58	-12.93	-13.17	-13.32	-13.36
9.2	6.05	.08	-3.36	-5.75	-7.54	-8.94	-10.07	-10.98	-11.72	-12.31	-12.77	-13.12	-13.37	-13.51	-13.56
9.6	5.87	-.10	-3.54	-5.93	-7.72	-9.13	-10.25	-11.16	-11.90	-12.49	-12.96	-13.31	-13.55	-13.69	-13.74
10.0	5.69	-.28	-3.72	-6.11	-7.90	-9.30	-10.43	-11.34	-12.08	-12.67	-13.13	-13.48	-13.73	-13.87	-13.92
10.4	5.52	-.45	-3.89	-6.28	-8.07	-9.48	-10.60	-11.51	-12.25	-12.84	-13.30	-13.65	-13.90	-14.04	-14.09

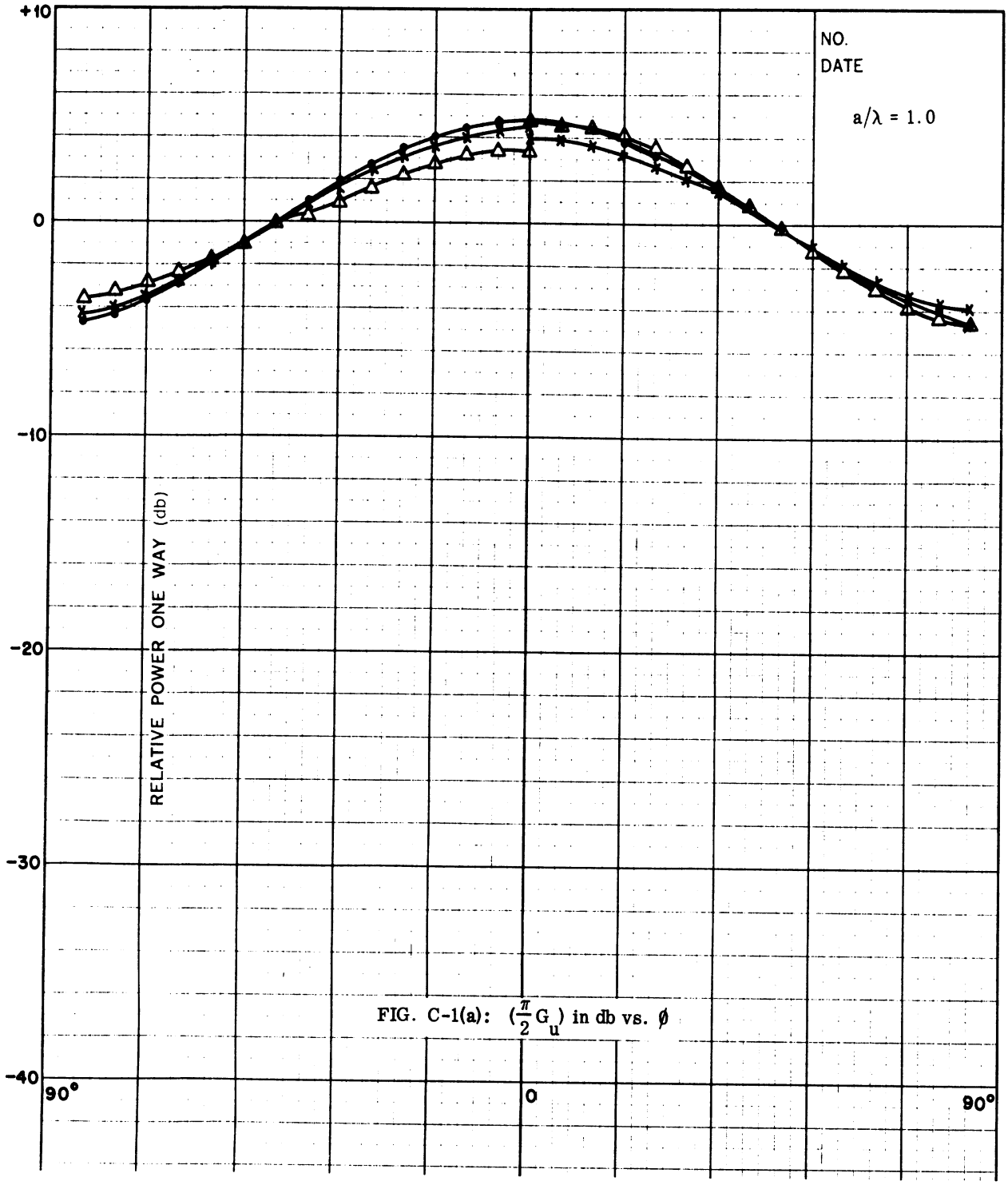

FIG. C-1(a): $(\frac{\pi}{2} G_u)$ in db vs. ϕ

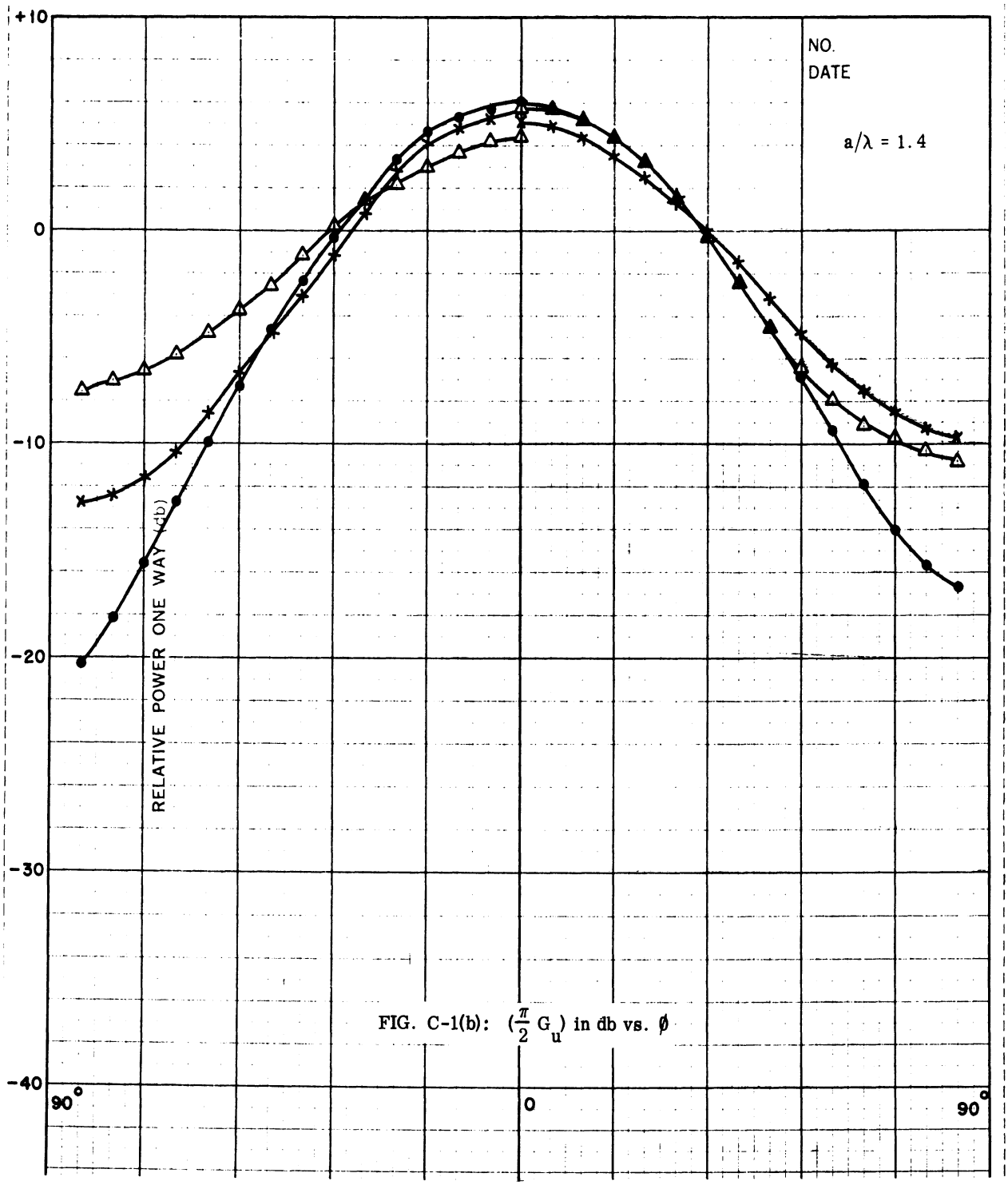

FIG. C-1(b): $(\frac{\pi}{2} G_u)$ in db vs. ϕ

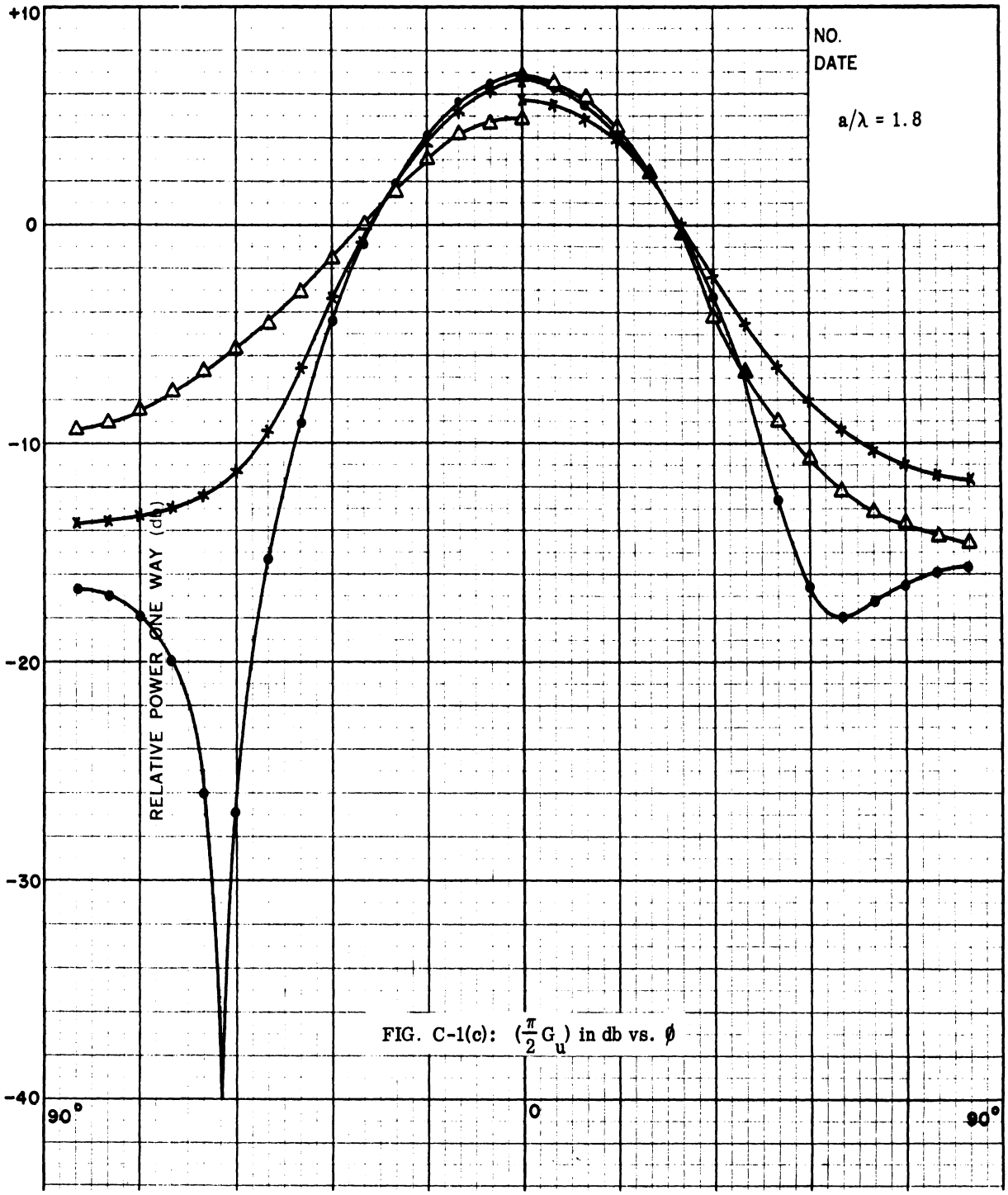

FIG. C-1(c): $(\frac{\pi}{2} G_u)$ in db vs. ϕ

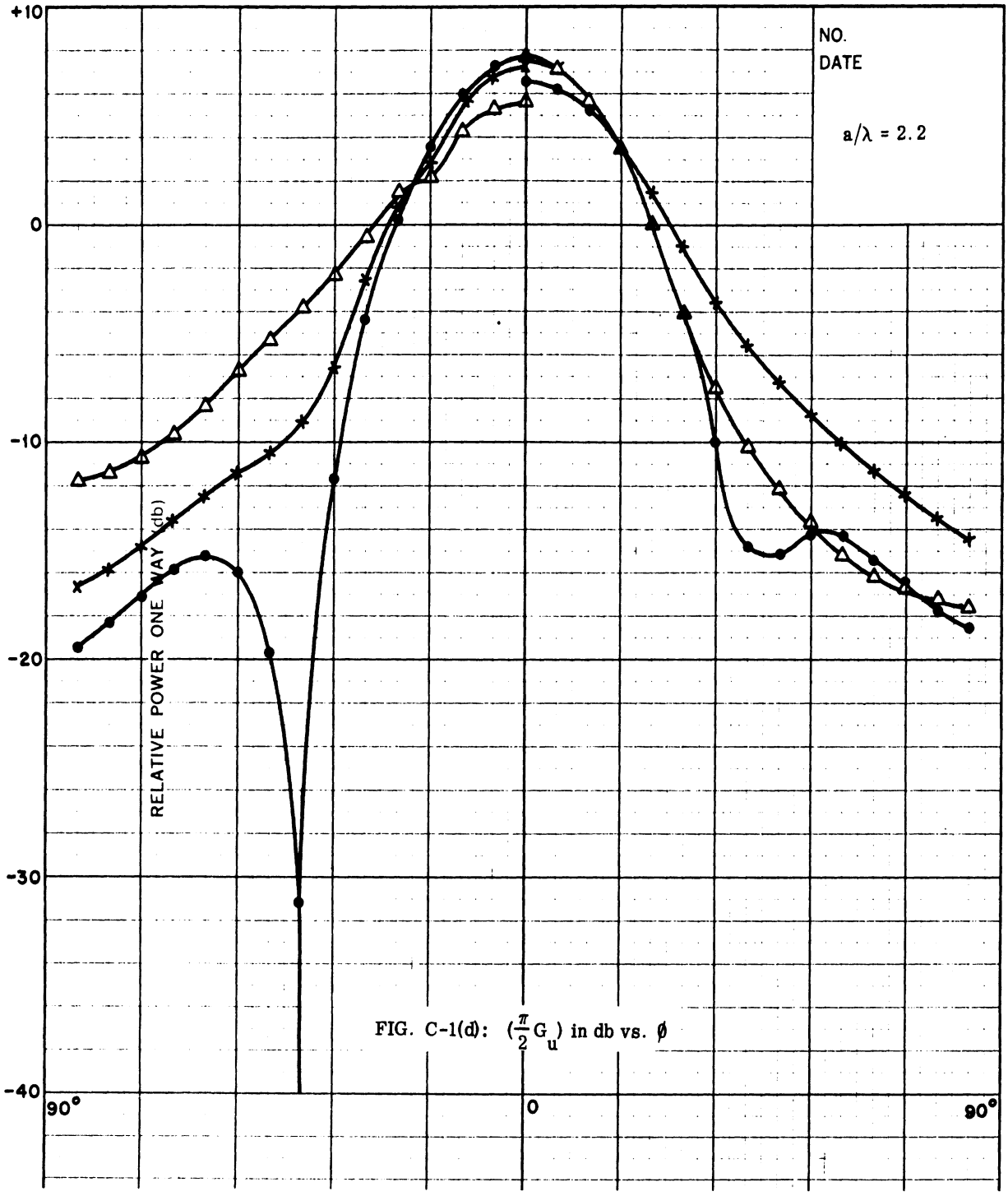

FIG. C-1(d): $(\frac{\pi}{2} G_u)$ in db vs. ϕ

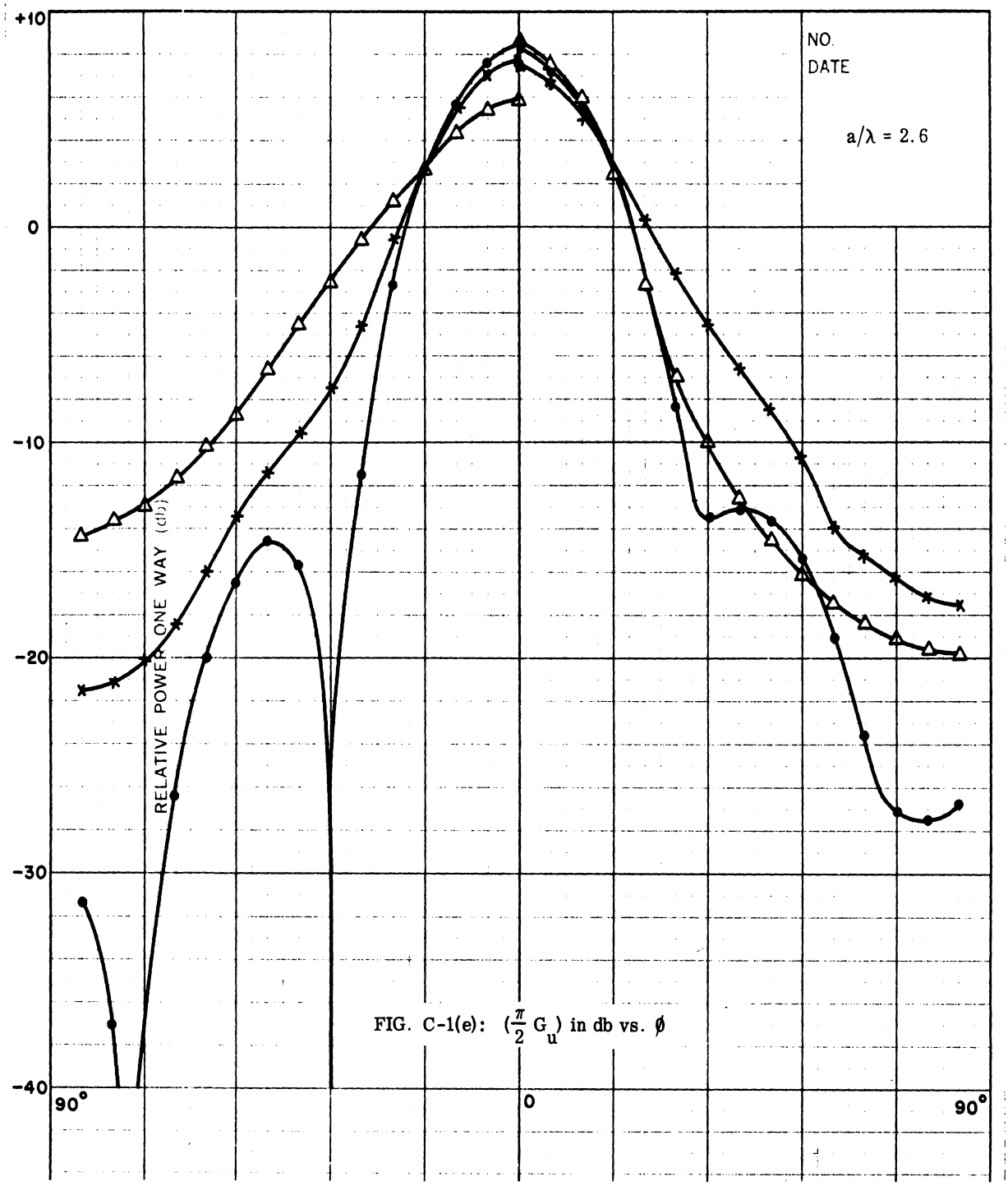

FIG. C-1(e): $(\frac{\pi}{2} G_u)$ in db vs. ϕ

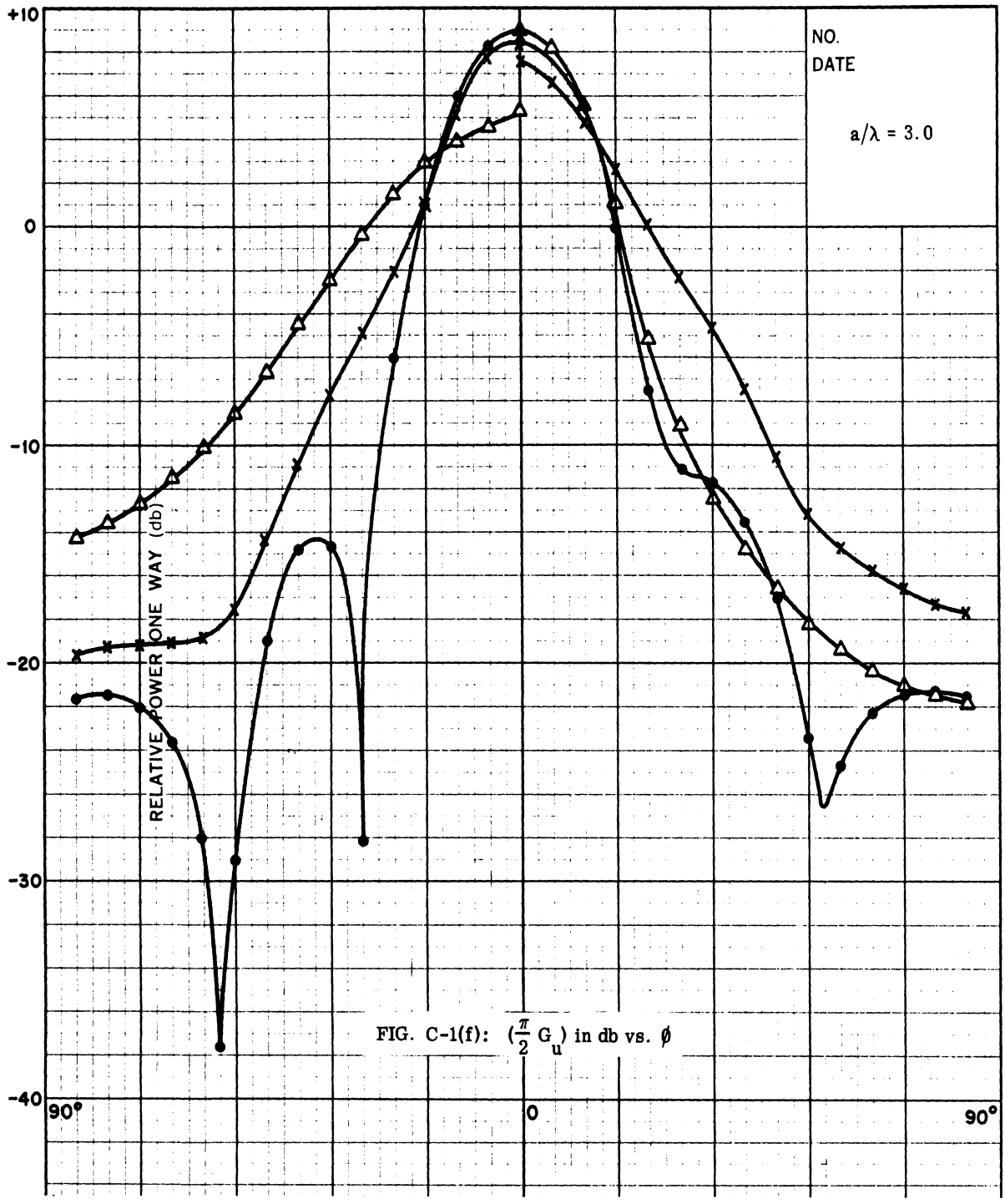

FIG. C-1(f): $(\frac{\pi}{2} G_u)$ in db vs. ϕ

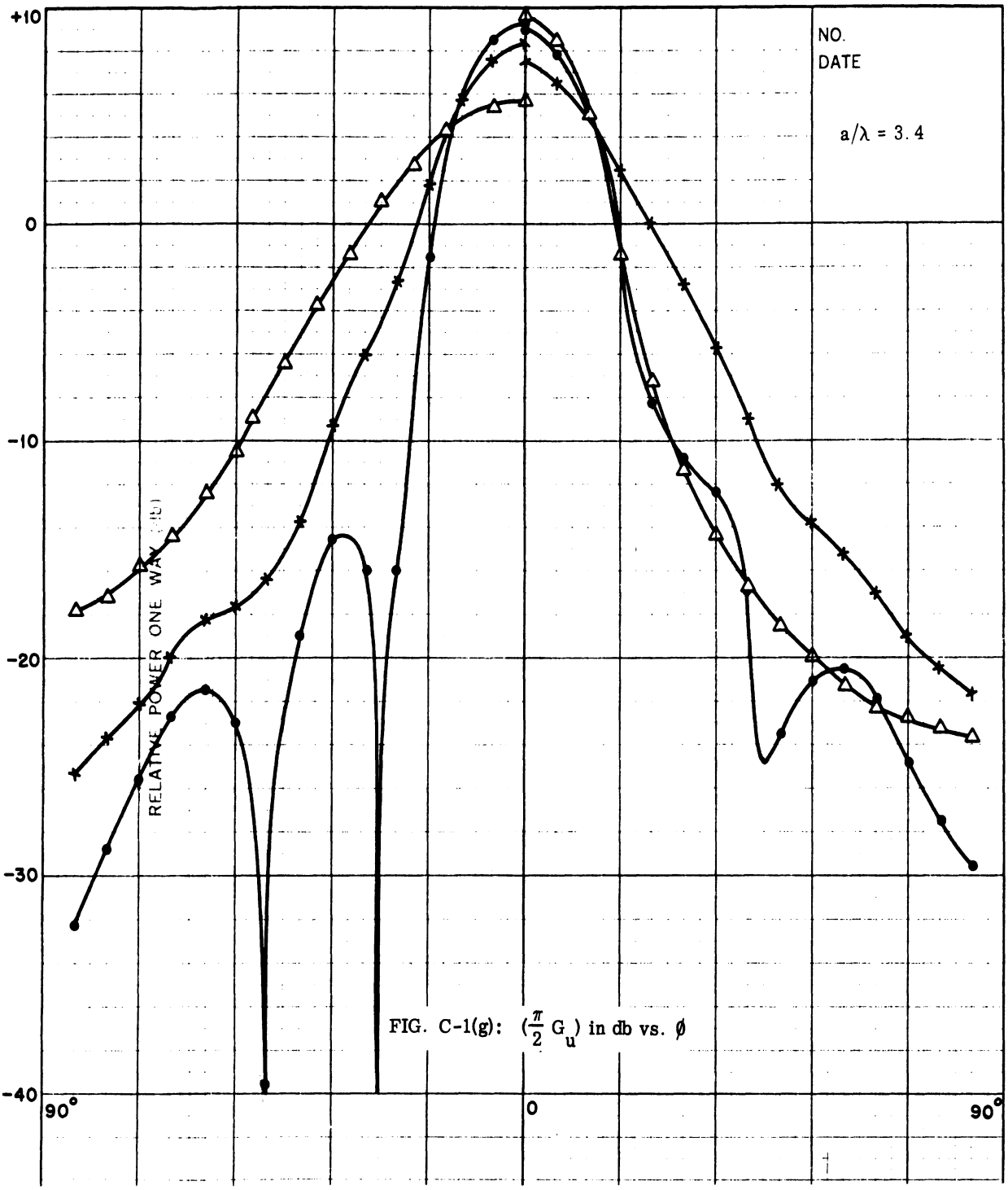

FIG. C-1(g): $(\frac{\pi}{2} G_u)$ in db vs. ϕ

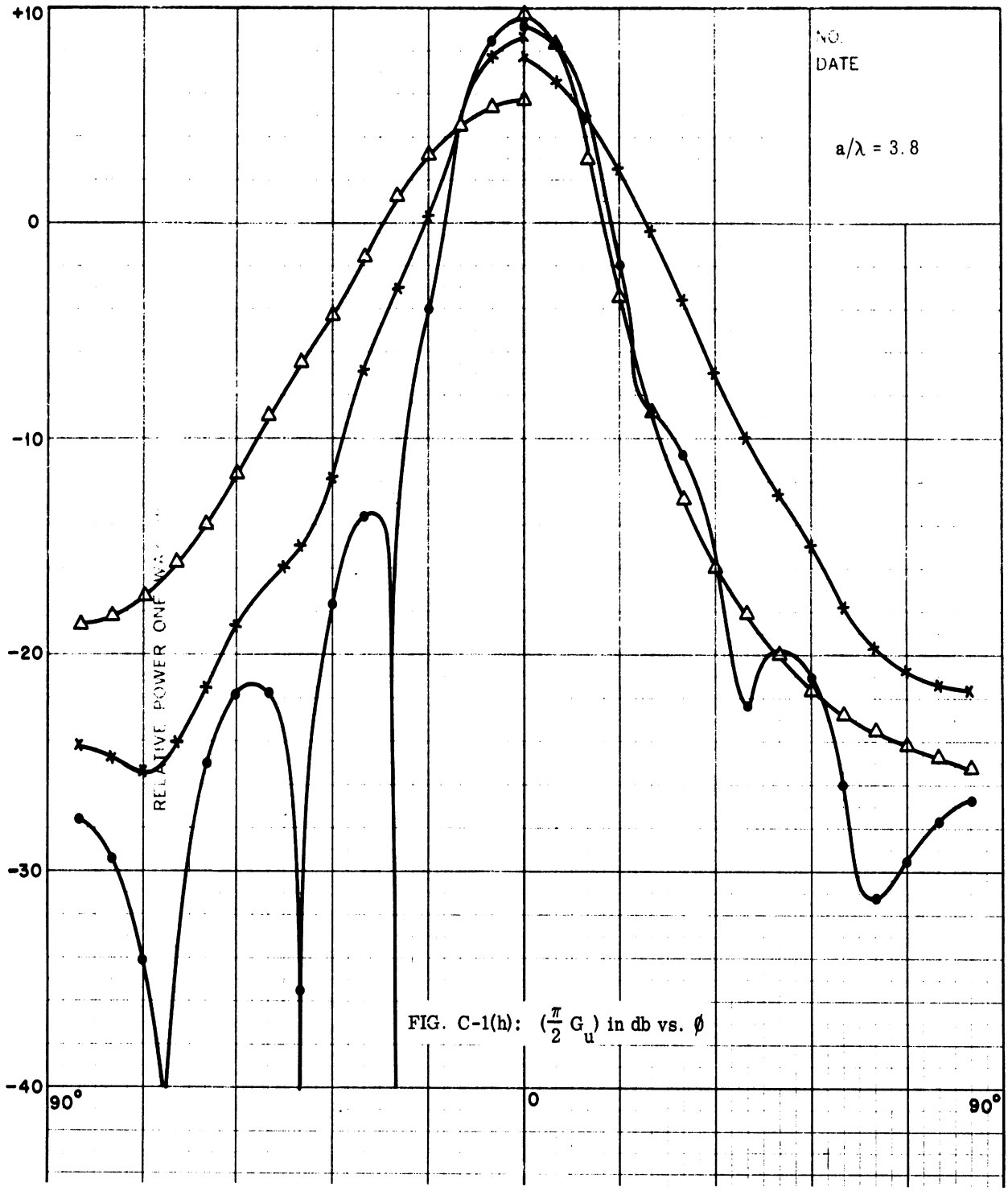

FIG. C-1(h): $(\frac{\pi}{2} G_u)$ in db vs. ϕ

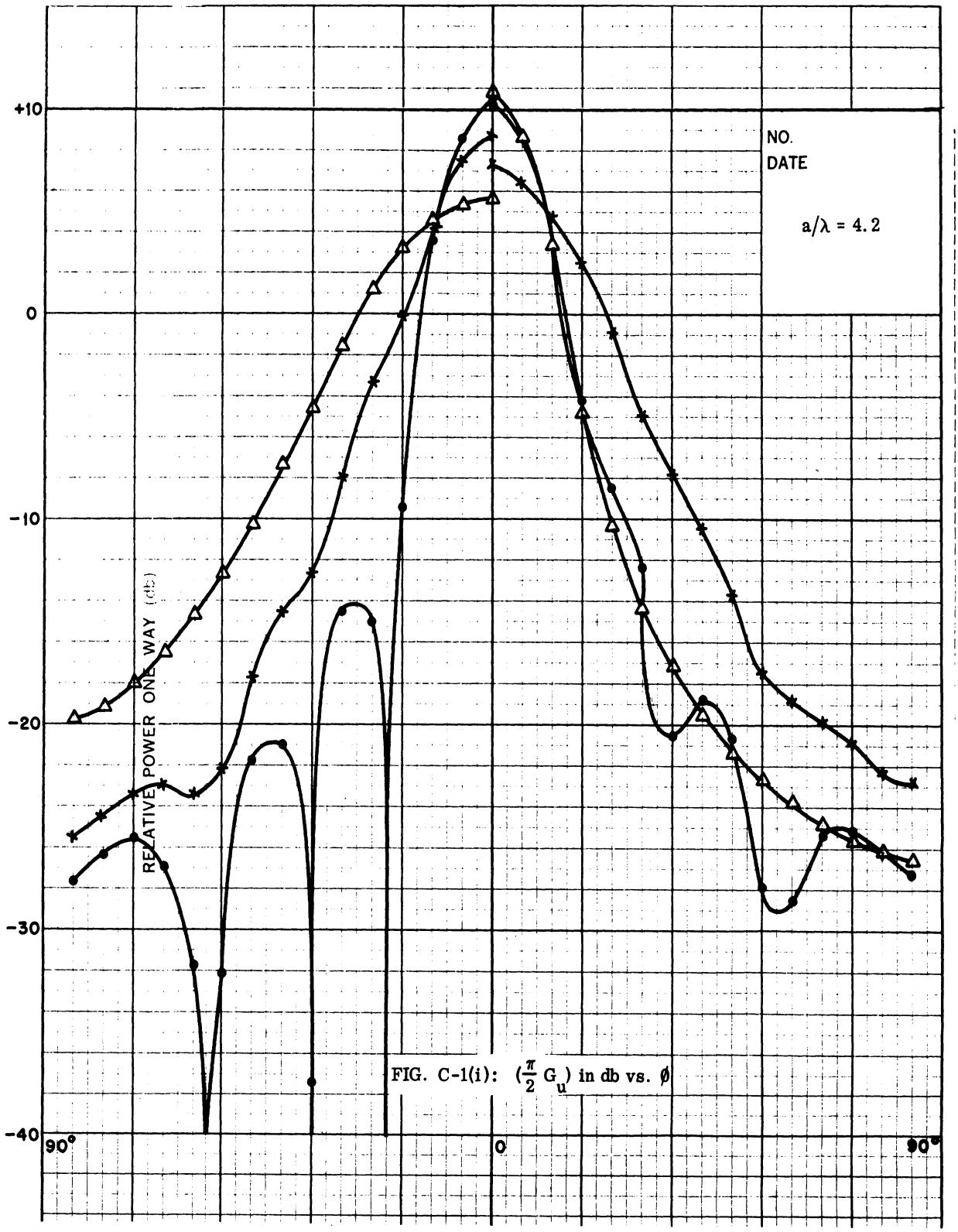

FIG. C-1(i): $(\frac{\pi}{2} G_u)$ in db vs. ϕ

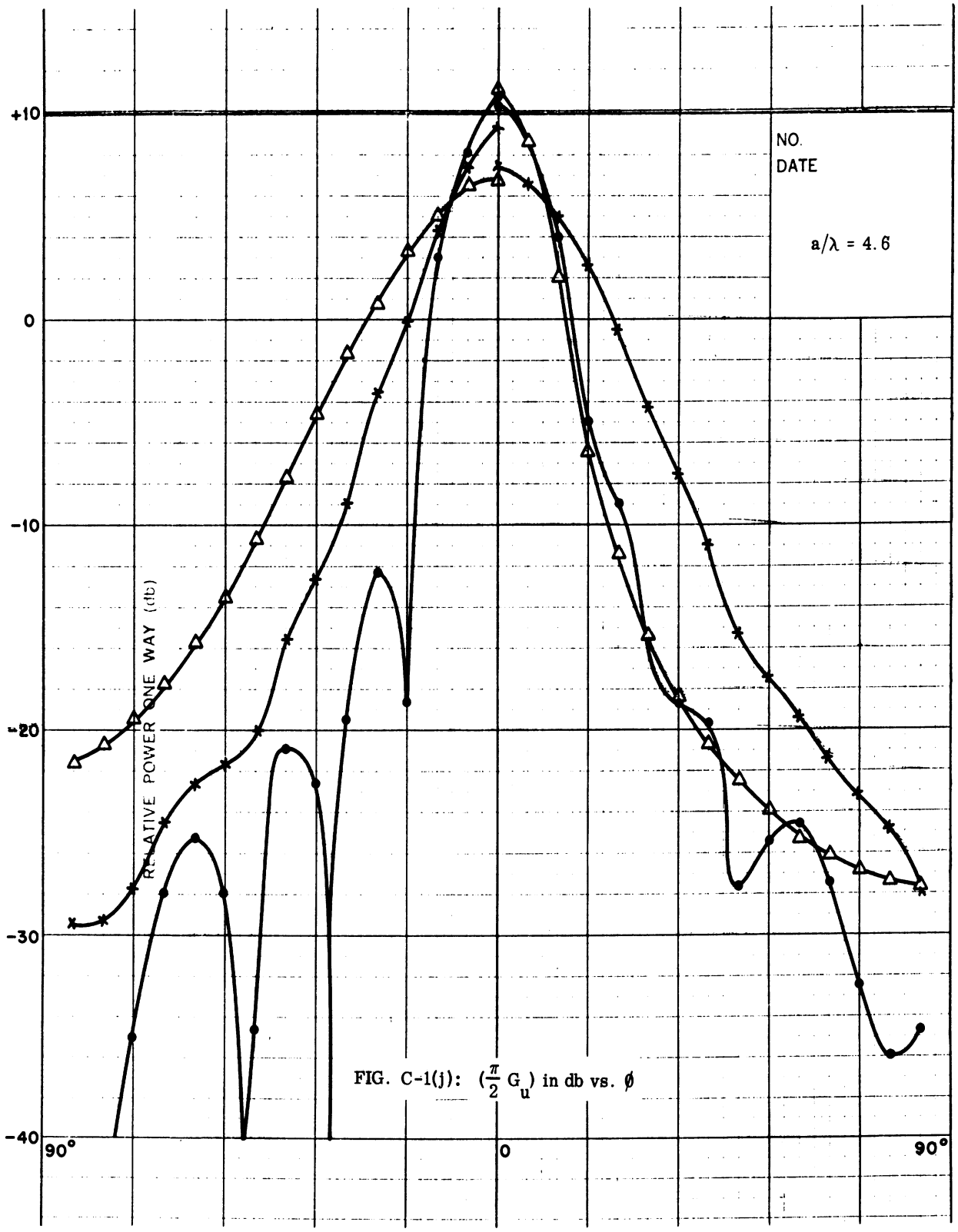

FIG. C-1(j): $(\frac{\pi}{2} G_u)$ in db vs. ϕ

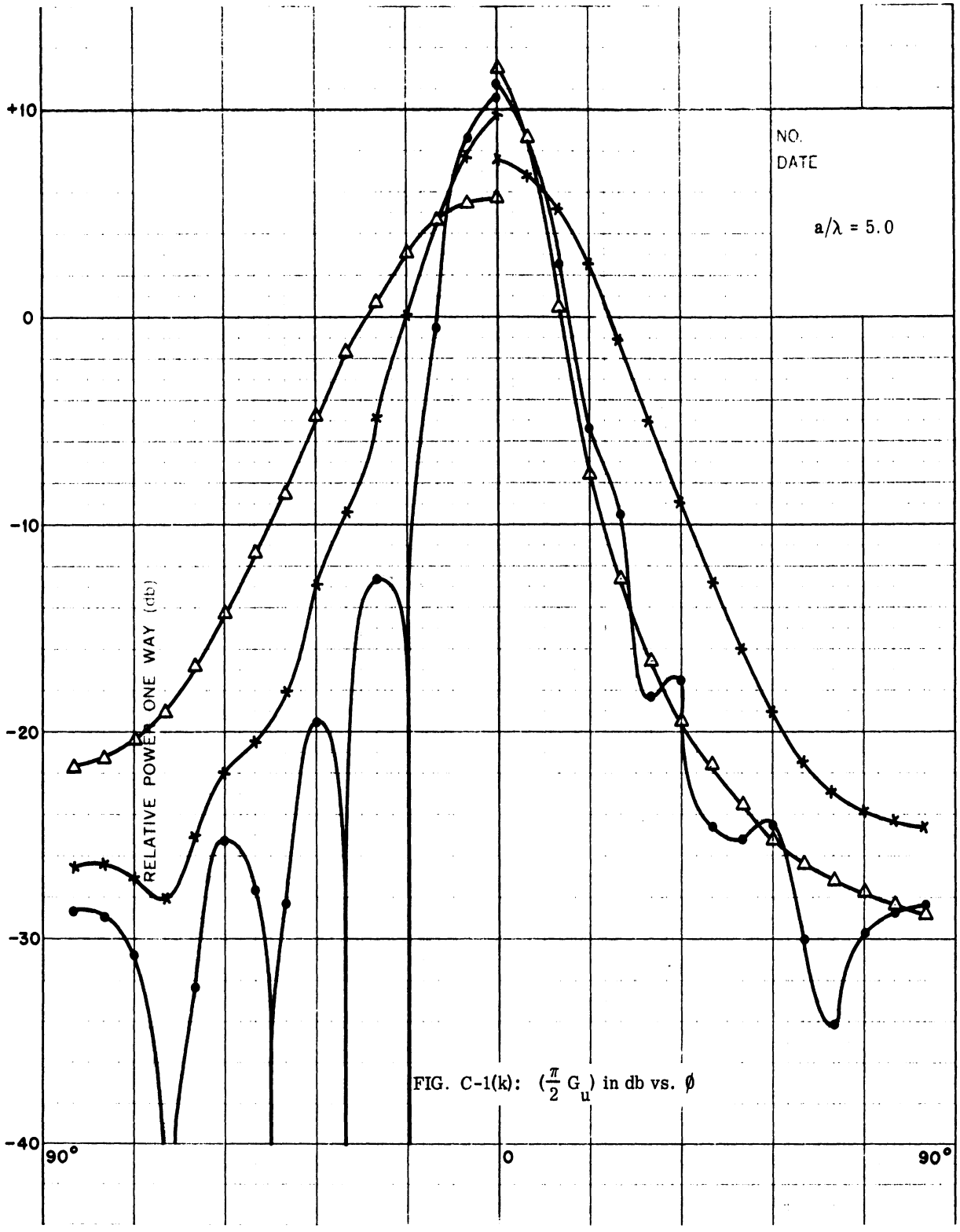

FIG. C-1(k): $(\frac{\pi}{2} G_u)$ in db vs. ϕ

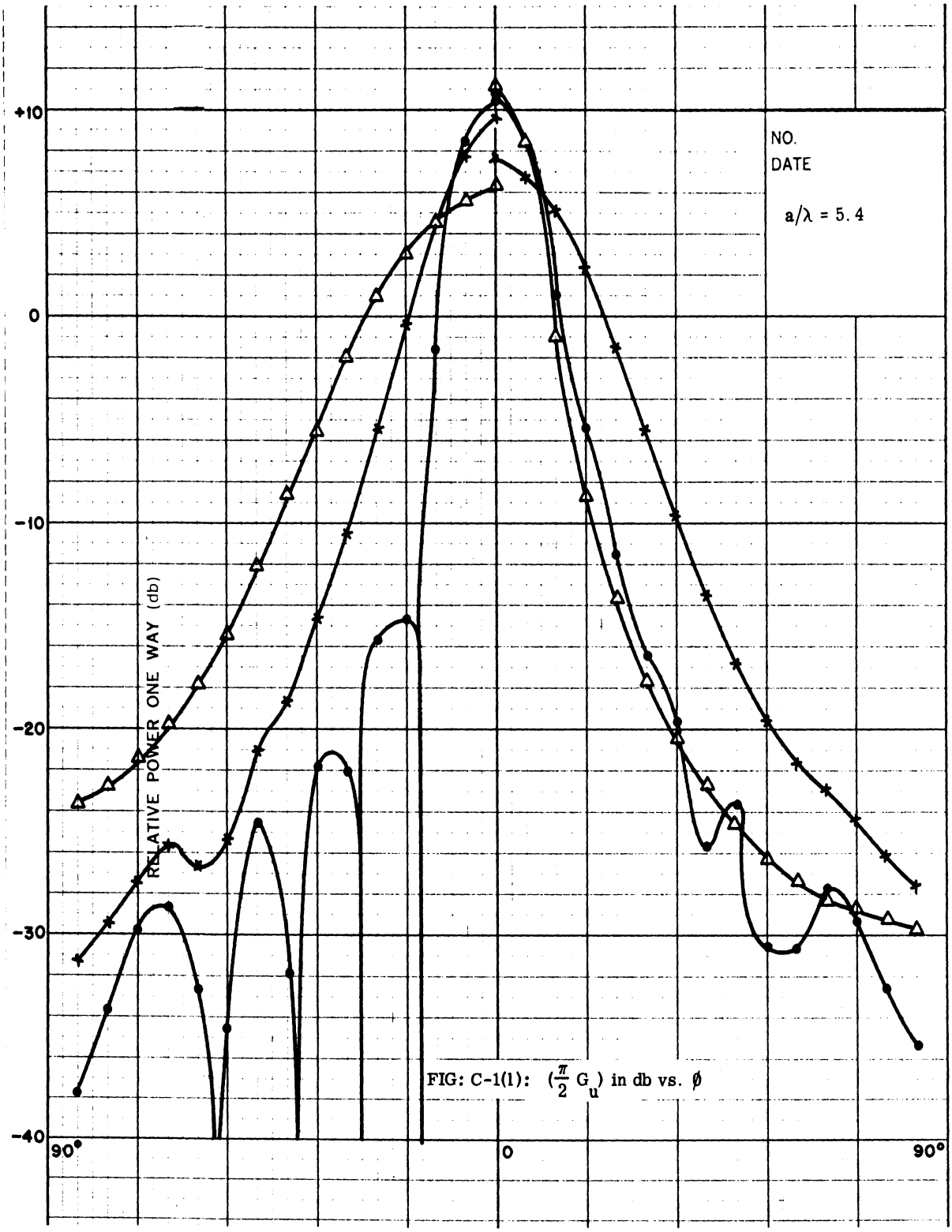

FIG: C-1(1): $(\frac{\pi}{2} G_u)$ in db vs. ϕ

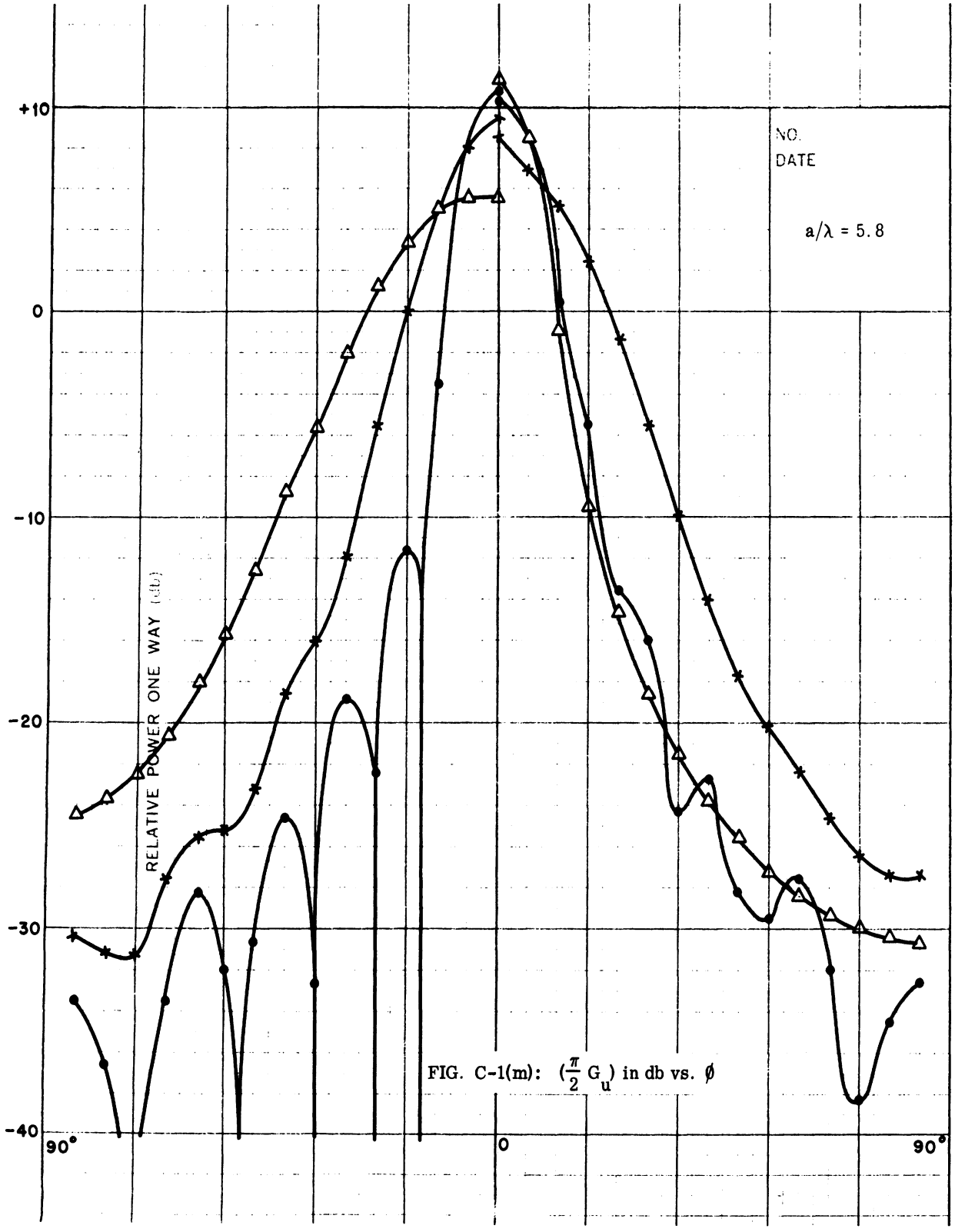

FIG. C-1(m): $(\frac{\pi}{2} G_u)$ in db vs. ϕ

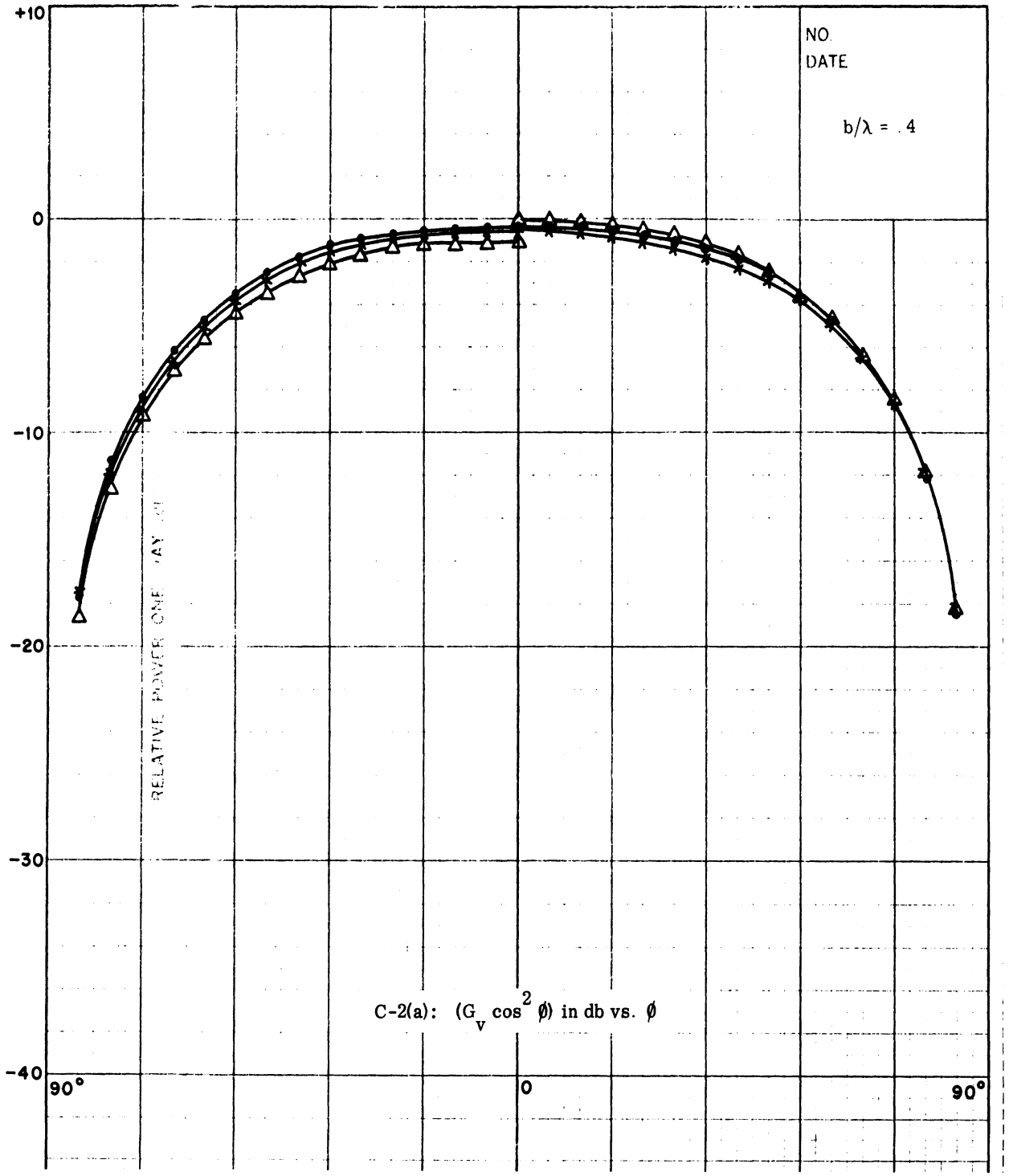

C-2(a): $(G_v \cos^2 \phi)$ in db vs. ϕ

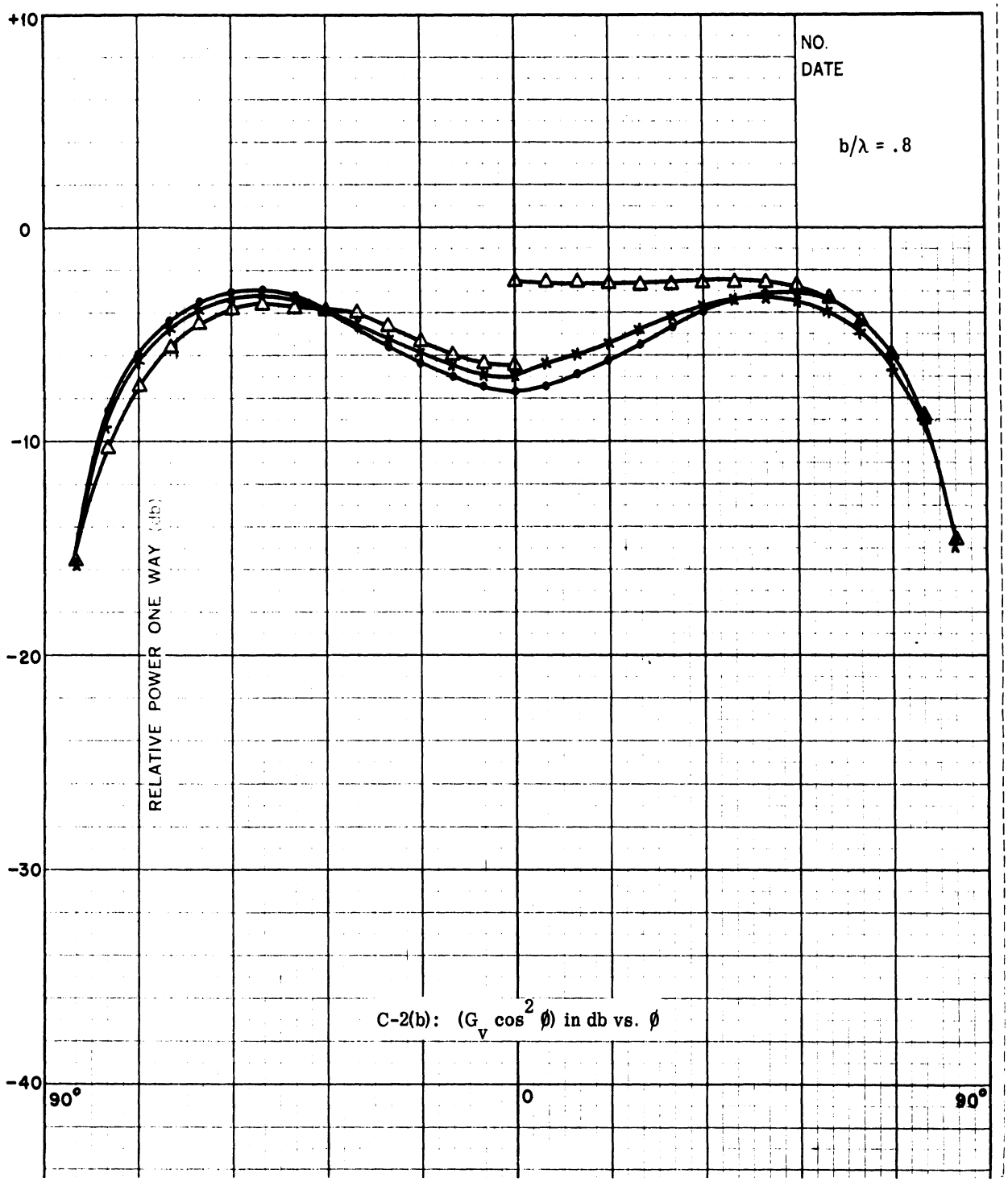
+10
0
-10
-20
-30
-40
NO.
DATE
b/λ = .8
RELATIVE POWER ONE WAY (db)
C-2(b): ($G_v \cos^2 \phi$) in db vs. ϕ
90°
0
90°

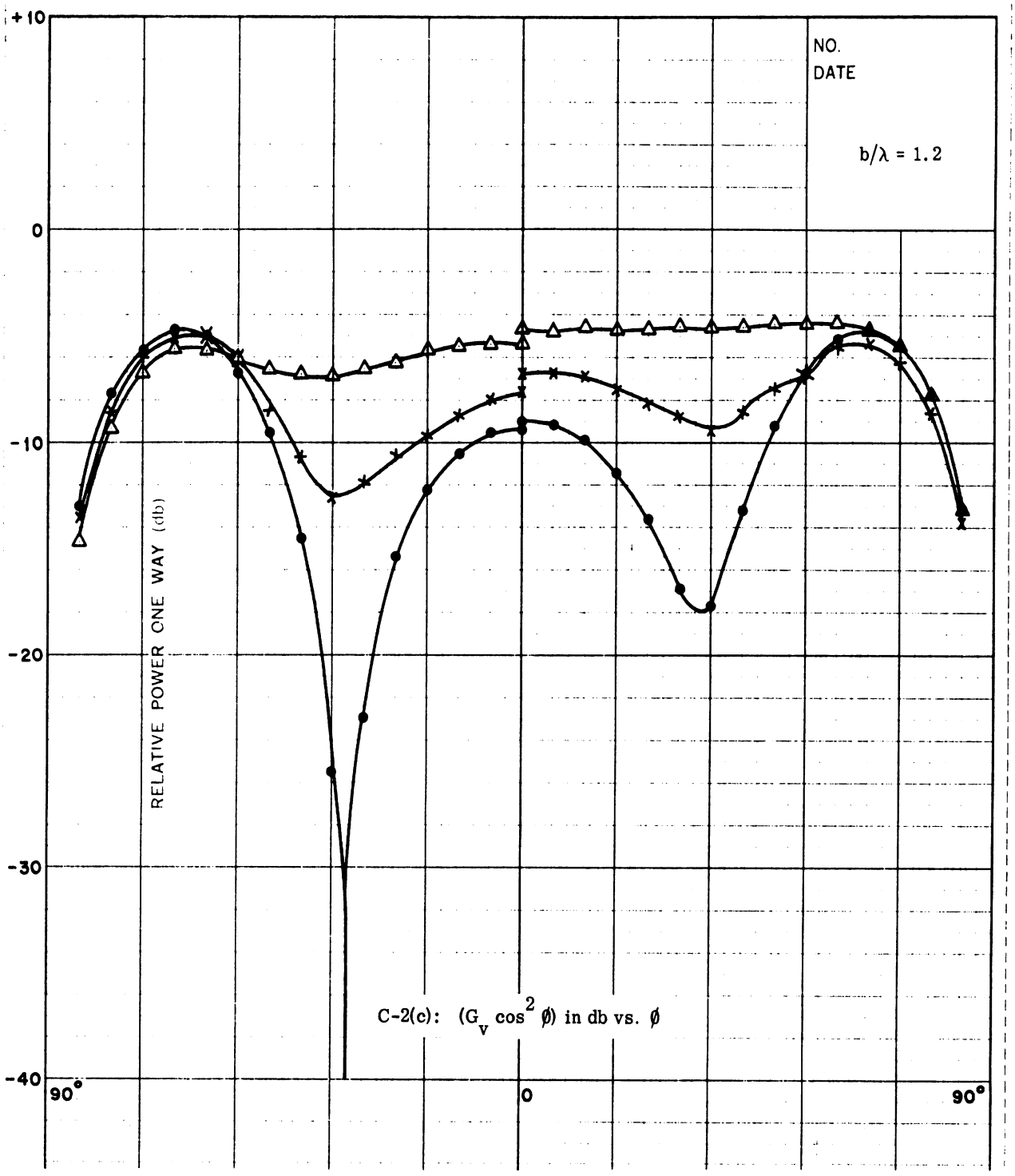
+10
0
-10
-20
-30
-40
90°
0
90°
NO.
DATE
b/λ = 1.2
RELATIVE POWER ONE WAY (db)
C-2(c): (G_v cos^2 ϕ) in db vs. ϕ

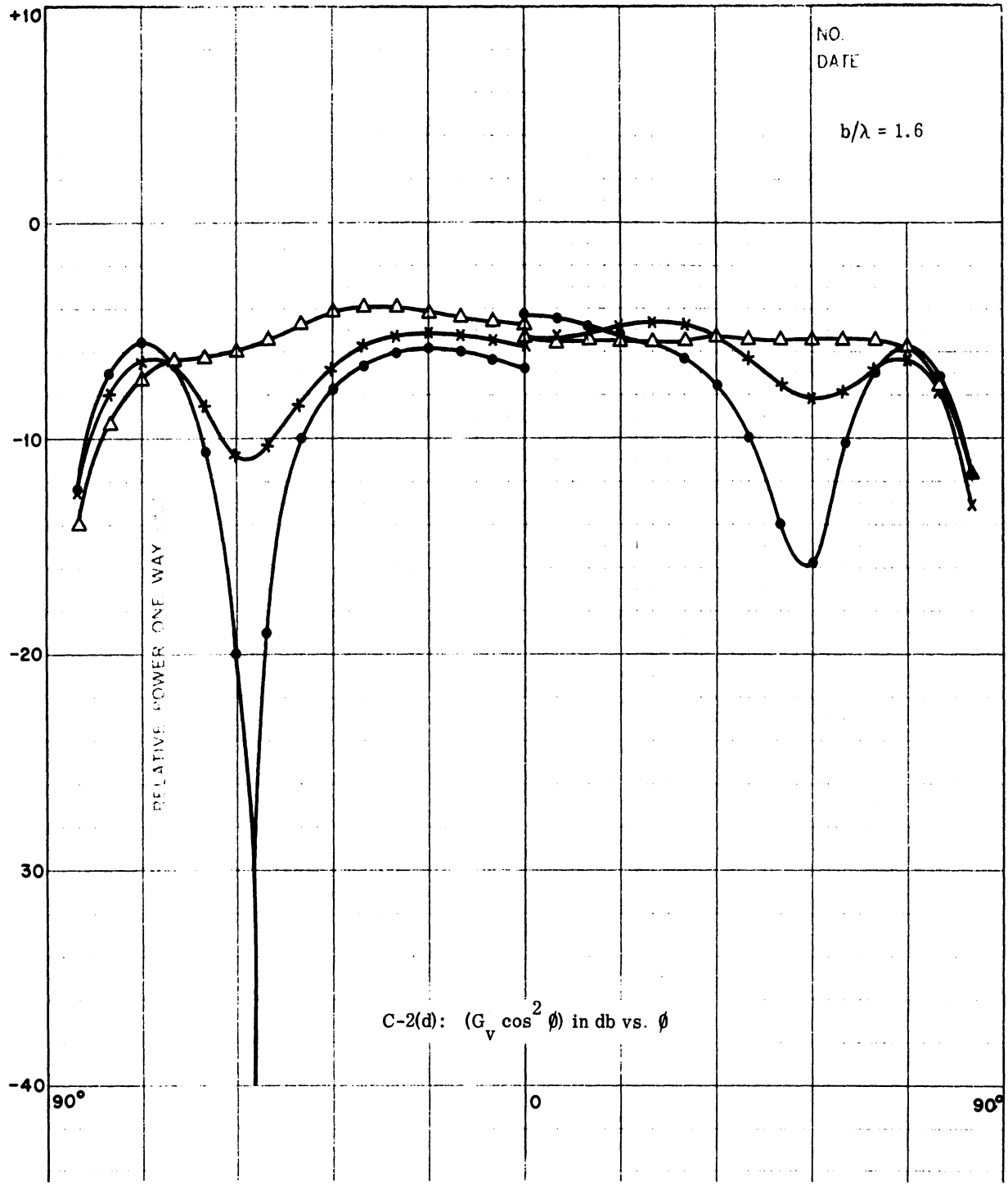
+10
0
-10
-20
30
-40
90°
0
90°
NO.
DATE
b/λ = 1.6
RELATIVE POWER ONE WAY
C-2(d): (G_v cos^2 ∅) in db vs. ∅

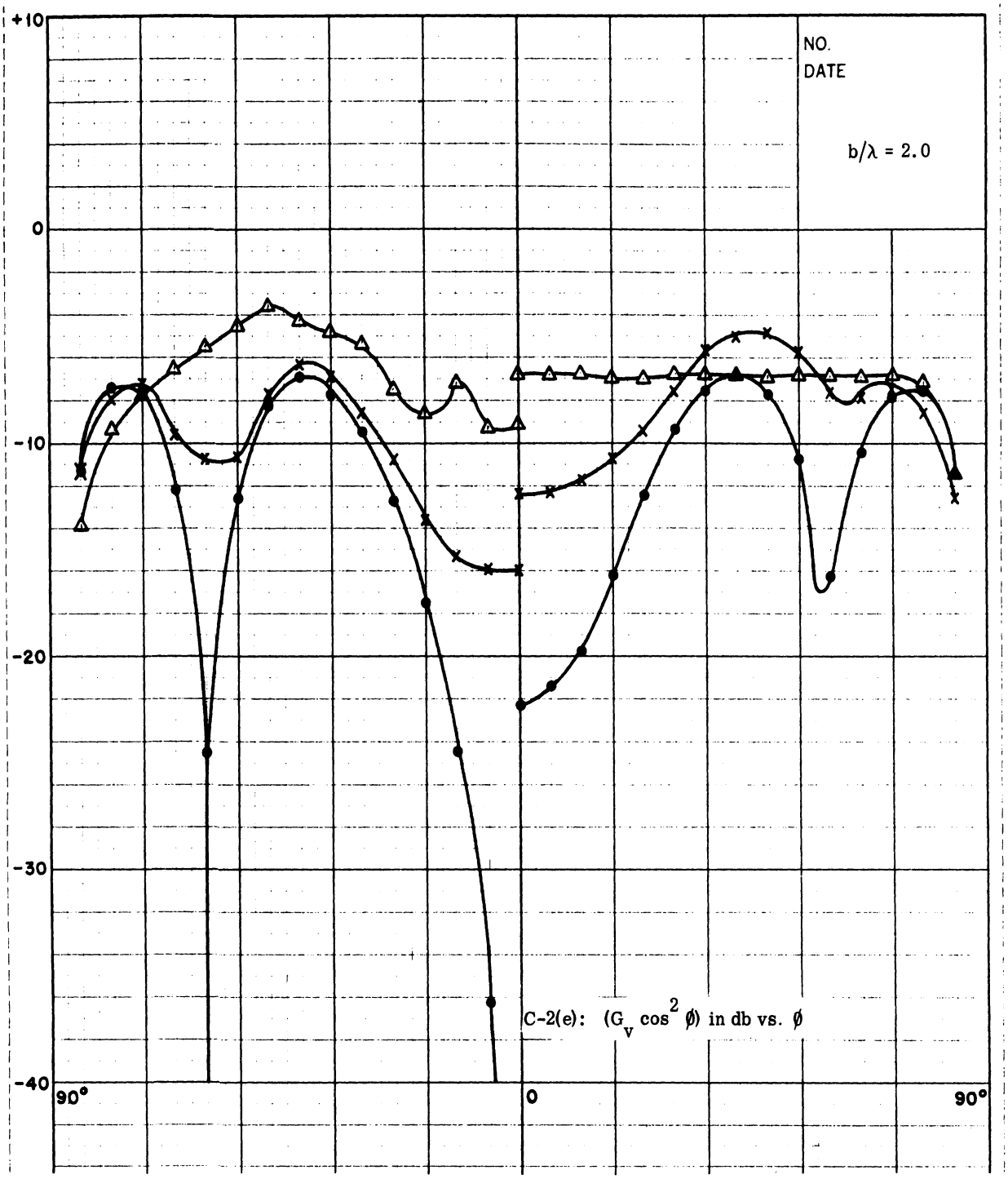
+10
0
-10
-20
-30
-40
90°
0
90°
NO.
DATE
b/λ = 2.0
C-2(e): (G_v cos² ∅) in db vs. ∅

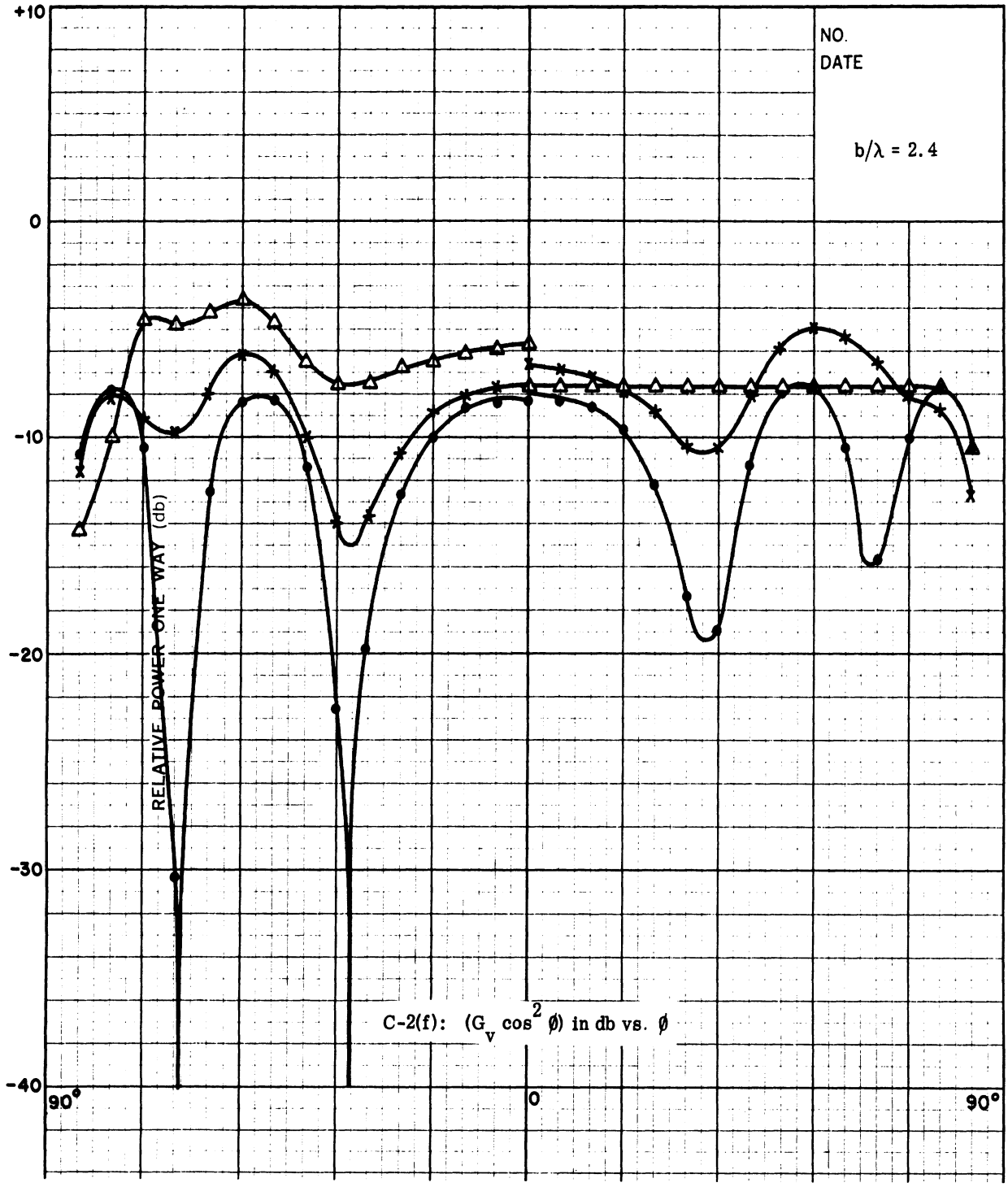
+10
0
-10
-20
-30
-40
NO.
DATE
b/λ = 2.4
RELATIVE POWER ONE WAY (db)
C-2(f): (G_v cos^2 ∅) in db vs. ∅
90°
0
90°

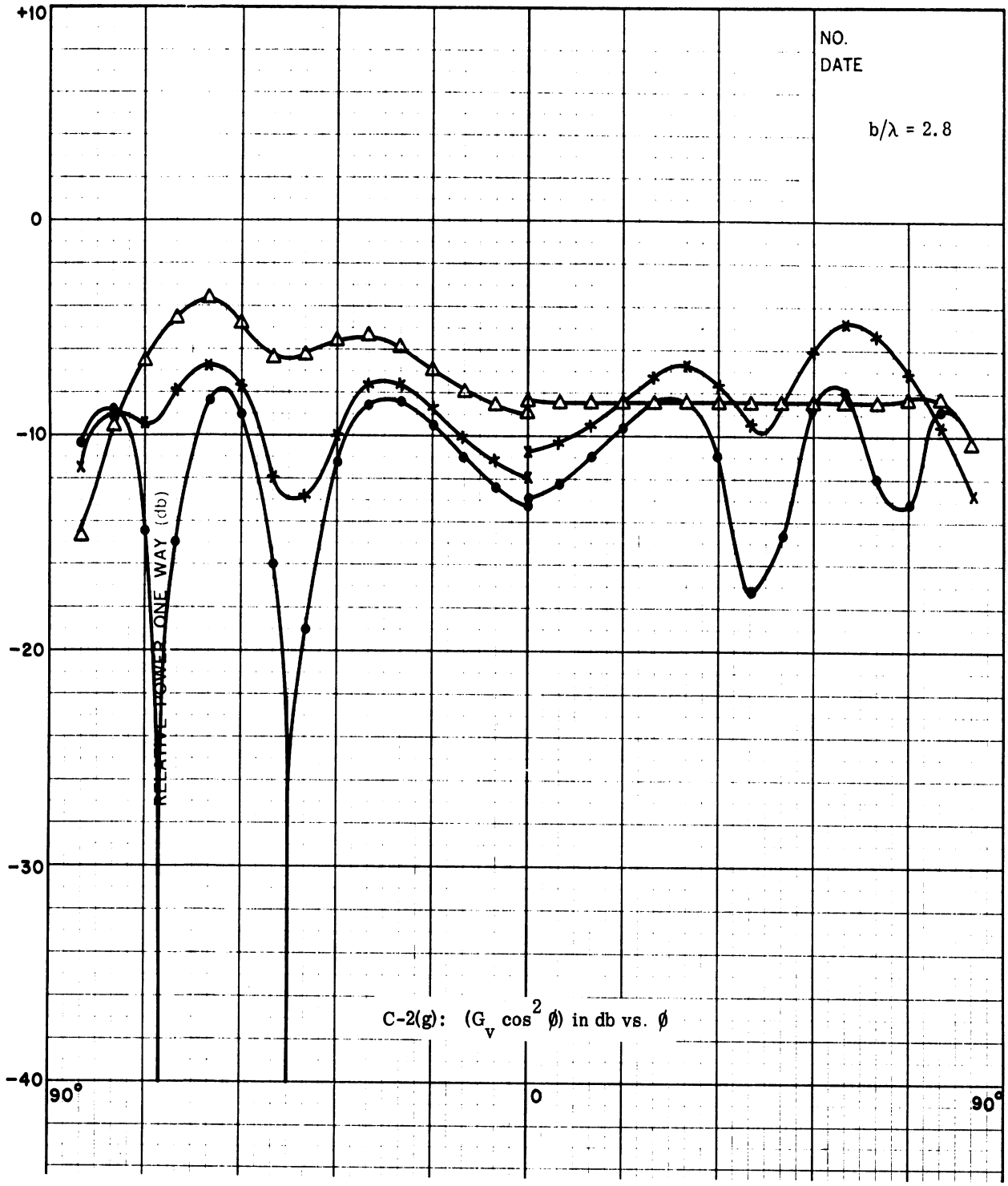
+10
0
-10
-20
-30
-40
NO.
DATE
b/λ = 2.8
RELATIVE POWER ONE WAY (db)
C-2(g): ($G_v \cos^2 \phi$) in db vs. ϕ
90°
0
90°

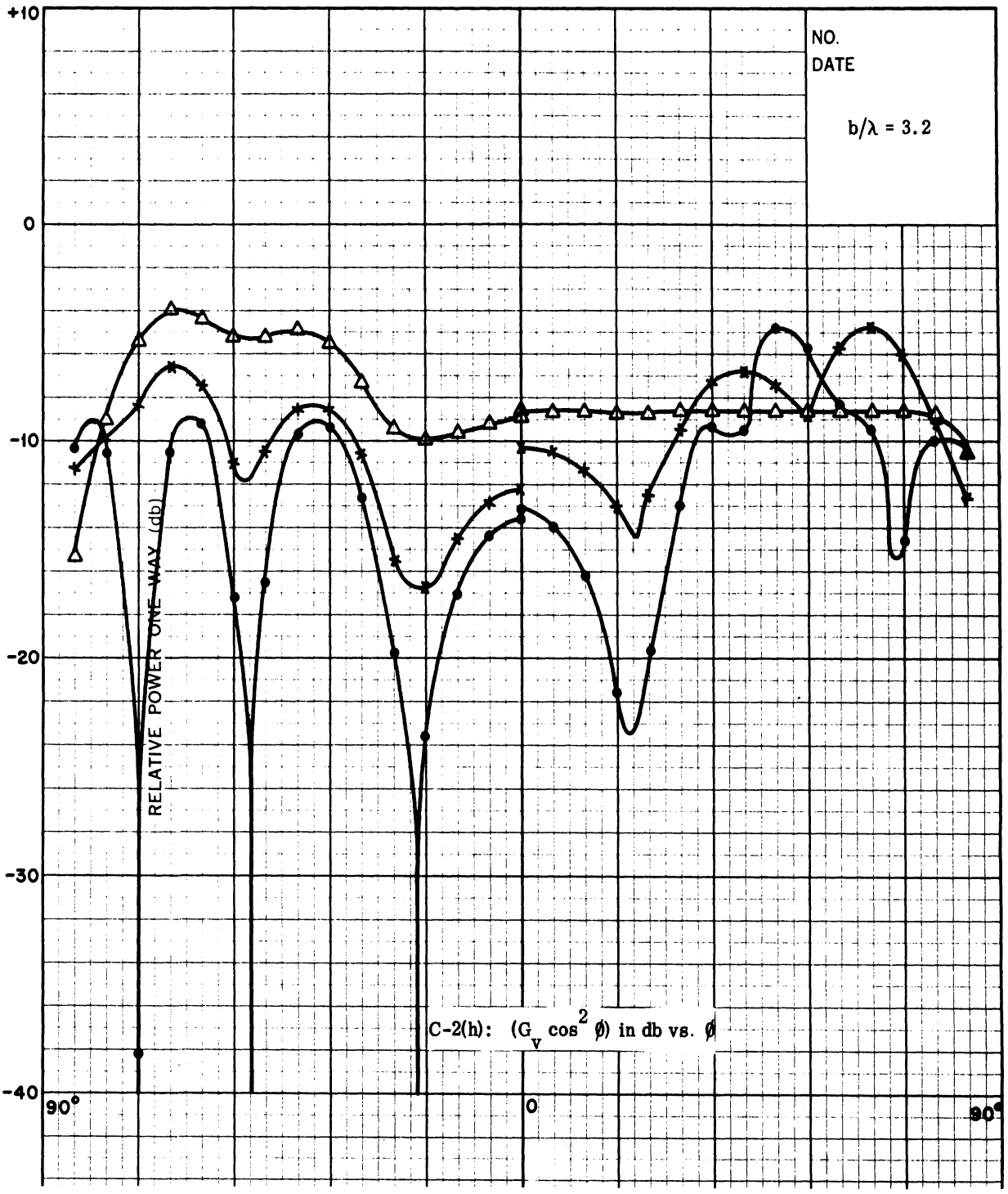
+10
0
-10
-20
-30
-40
NO.
DATE
b/λ = 3.2
RELATIVE POWER ONE WAY (db)
C-2(h): (G_v cos^2 ∅) in db vs. ∅
90°
0
90°

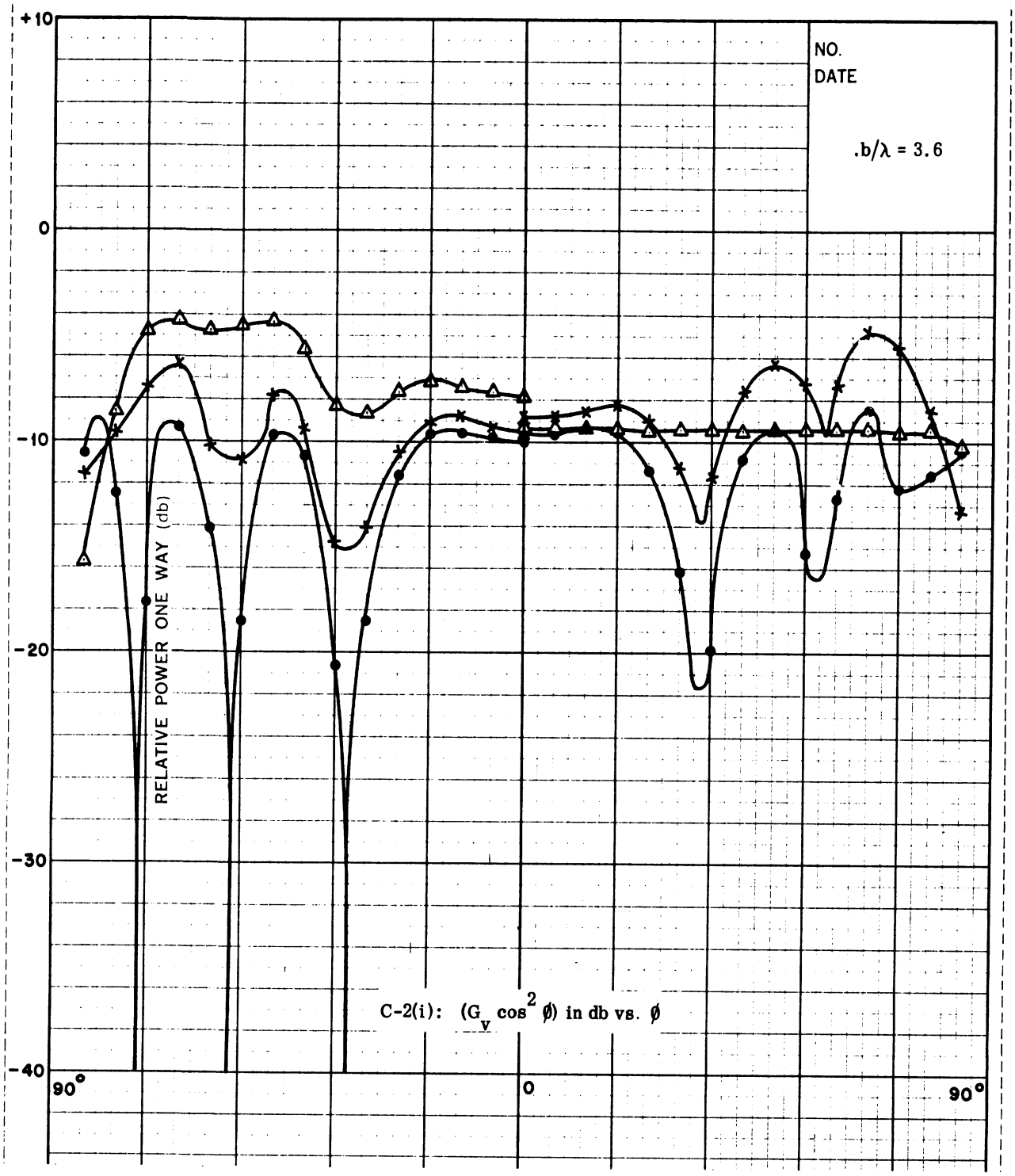
+10
0
-10
-20
-30
-40
RELATIVE POWER ONE WAY (db)
NO.
DATE
.b/λ = 3.6
C-2(i): (G_v cos^2 ∅) in db vs. ∅
90°
0
90°

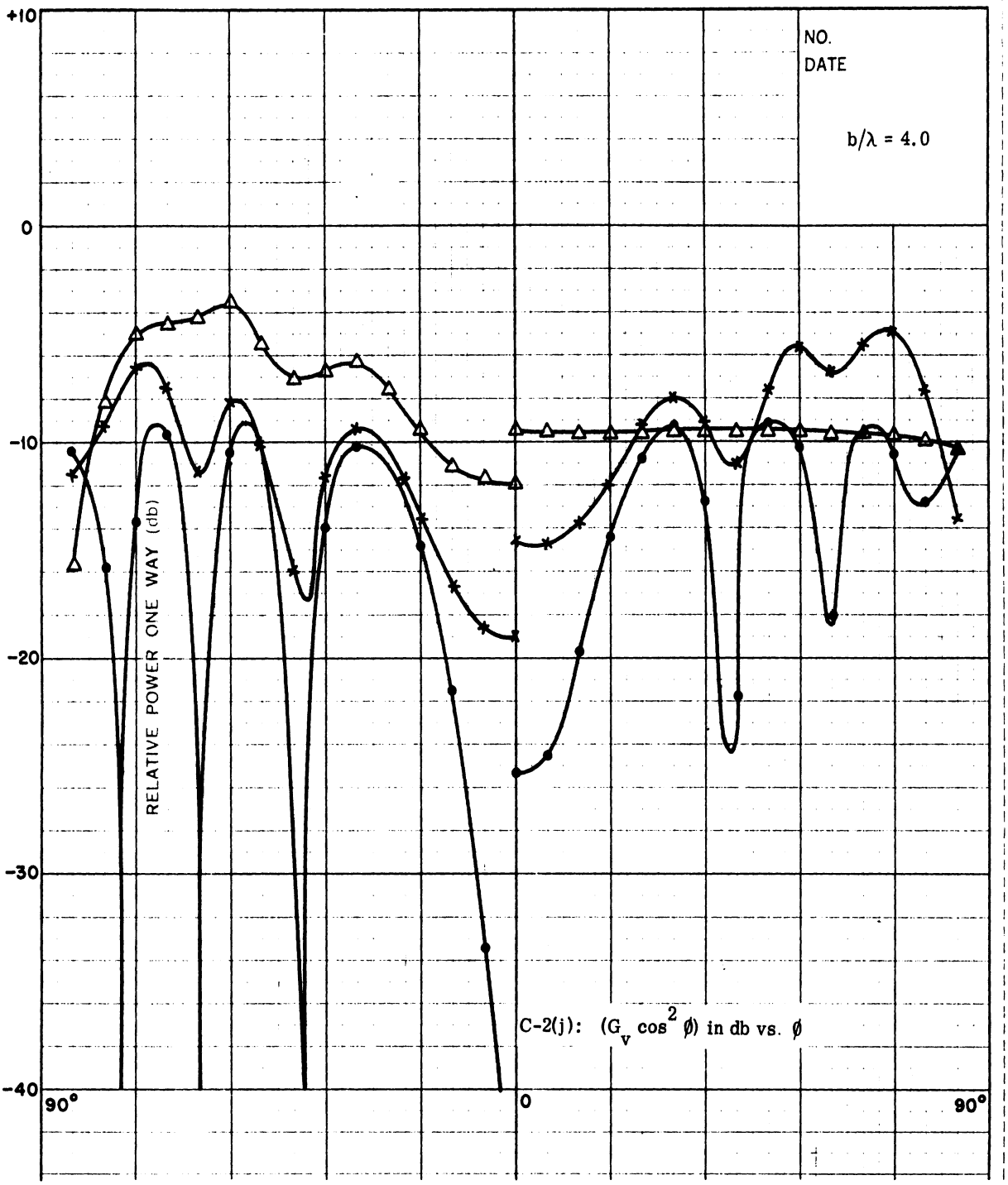
+10
0
-10
-20
-30
-40
NO.
DATE
b/λ = 4.0
RELATIVE POWER ONE WAY (db)
C-2(j): ($G_v \cos^2 \phi$) in db vs. ϕ
90°
0
90°

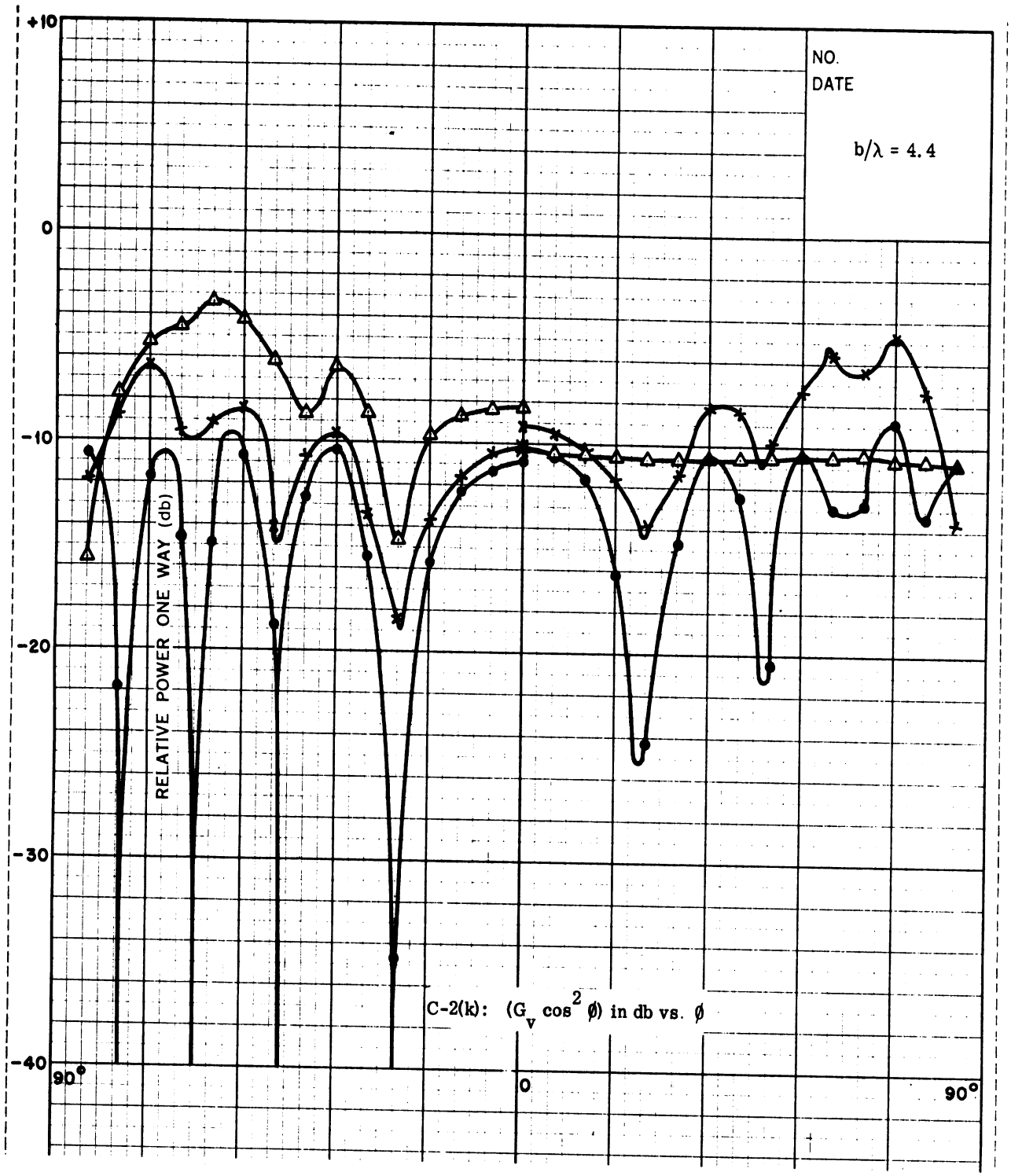
+10
0
-10
-20
-30
-40
RELATIVE POWER ONE WAY (db)
NO.
DATE
b/λ = 4.4
C-2(k): (G_v cos^2 ∅) in db vs. ∅
90°
0
90°

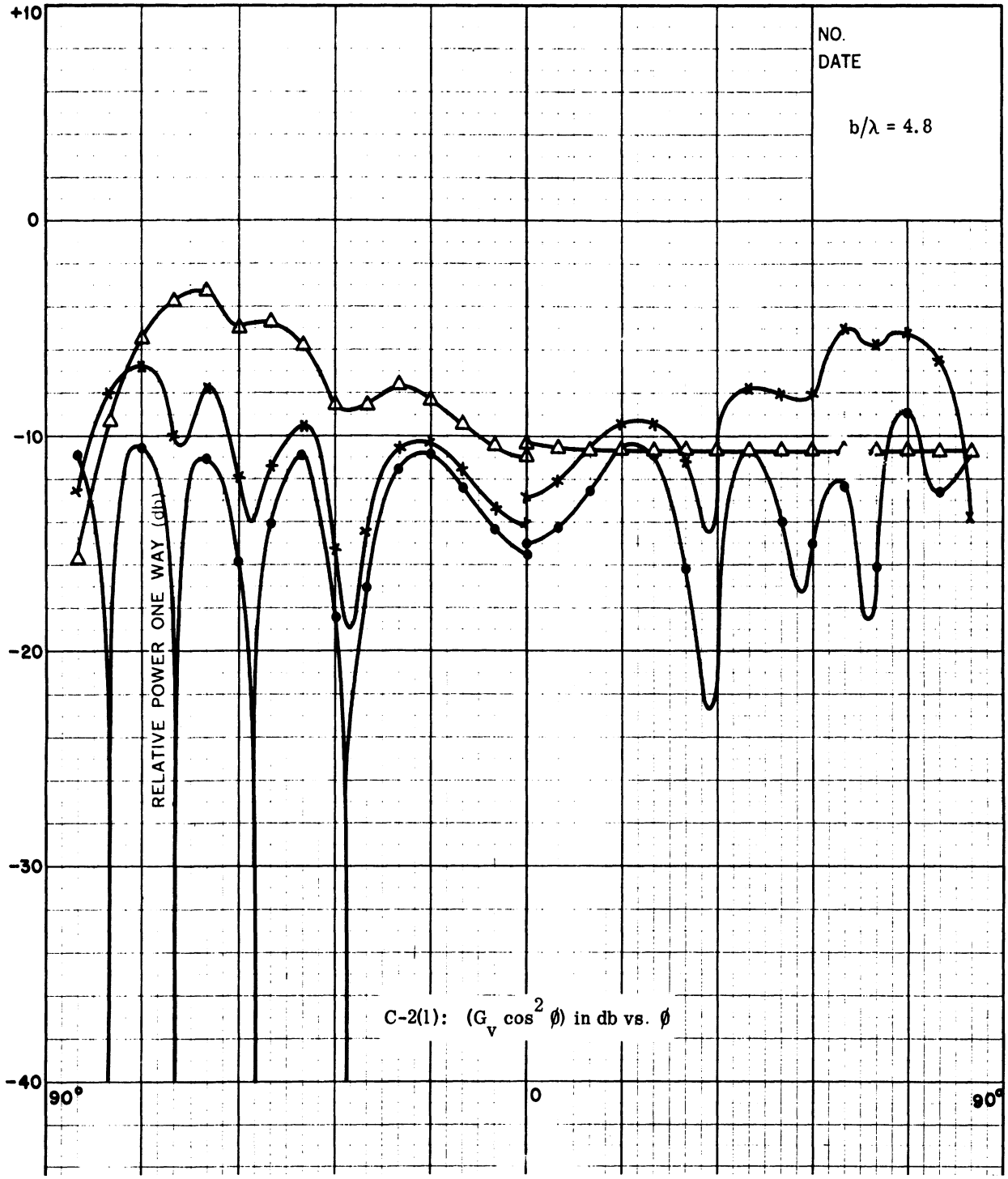
+10
0
-10
-20
-30
-40
90°
0
90°
NO.
DATE
b/λ = 4.8
RELATIVE POWER ONE WAY (db)
C-2(1): (G_v cos^2 ∅) in db vs. ∅

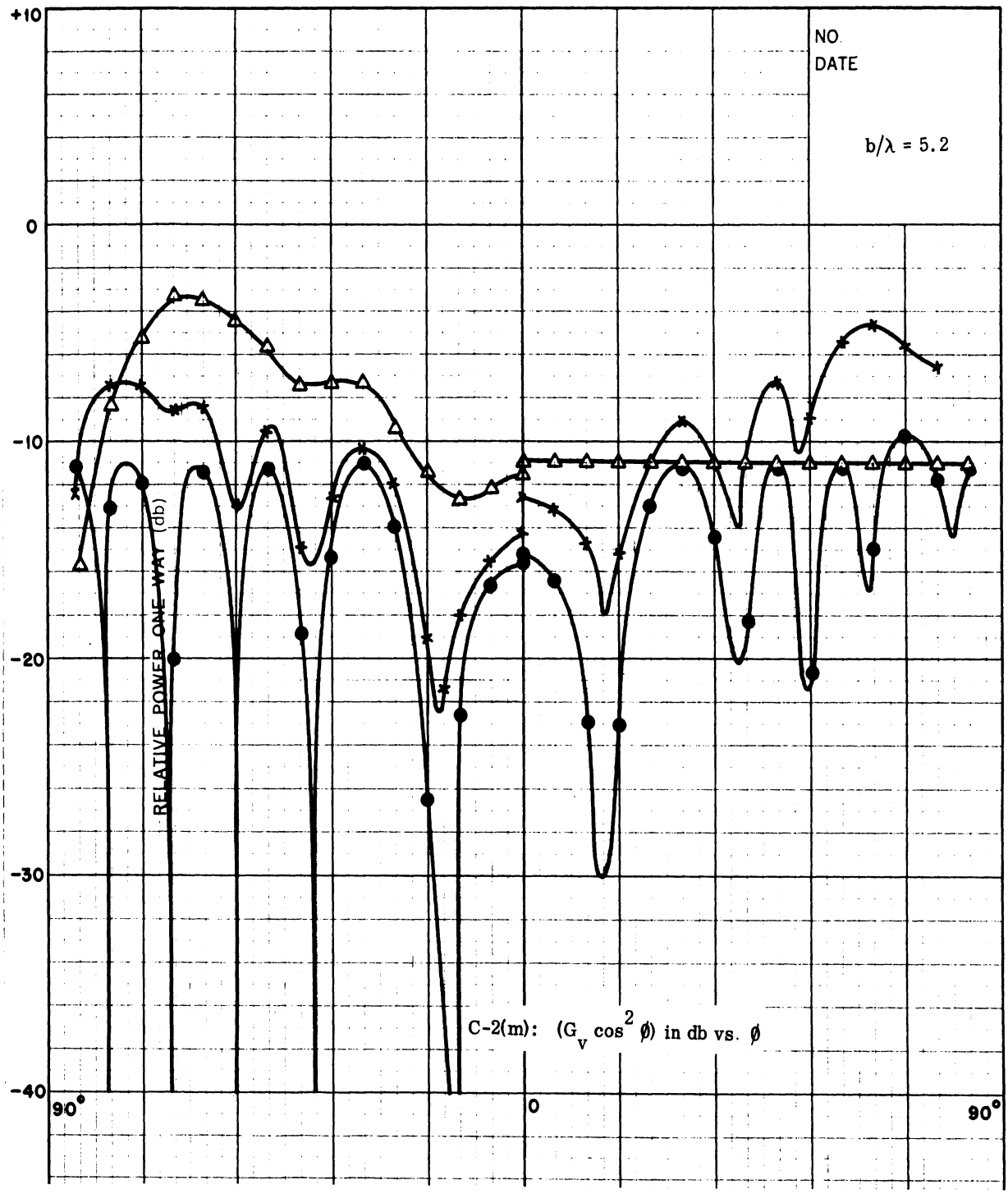
+10
0
-10
-20
-30
-40
90°
0
90°
NO.
DATE
b/λ = 5.2
RELATIVE POWER ONE WAY (db)
C-2(m): (G_V cos² ∅) in db vs. ∅

C.2 Experimental Data: E-plane Coupling

With reference to Fig. 4-24 the E-plane coupling for two identical E-Sectoral horns at a center-to-center spacing R_o of 45.7 cm is given in Figs. C-3a through C-3e, for five frequencies: 8 GHz, 9 GHz, 10 GHz, 11 GHz, and 12 GHz. Wedges were used to obtain several flare angles. These wedges were silver-painted and held in place by adhesion. The coupling patterns for $\theta_b = 10^o$ and 15^o are dropped in the figures for readability. The flare angles and aperture dimensions are listed in Table C-3.

E-plane coupling for H-sectoral horn is indicated in Figs. C-4a through C-4e for the same five frequencies as above. Wedges were used here to obtain several different flare angles. (See Table C-4), The coupling patterns for $\theta_a = 10^o$ and 20^o are dropped by 10 db for readability.

TABLE C-3

θ_b	a	b
10^o	2.3 cm	3.9 cm
15^o	2.3 cm	5.9 cm
23^o	2.3 cm	8.2 cm
30^o	2.3 cm	8.2 cm
40^o	2.3 cm	8.2 cm

TABLE C-4

θ_a	a	b
10^o	3.4 cm	1.0 cm
20^o	5.1 cm	1.0 cm
35^o	8.2 cm	1.0 cm
50^o	8.2 cm	1.0 cm

Figure C-5 demonstrates the variation of coupling with spacing. The spacings of 11.43 cm, 22.86 cm, and 45.72 cm are in the ratio of 1:2:4 and thus are successively a distance octave apart. In the far-field, with no scatterers present, the corresponding couplings should be spaced at 6 db apart. These curves demonstrate the filling-in of the nulls as the spacing is reduced within the Fresnel zone.

In all the figures that follow, ϕ_t and ϕ_r are as indicated in Fig. 5-1 where the base of the horn should be interpreted as "slot".

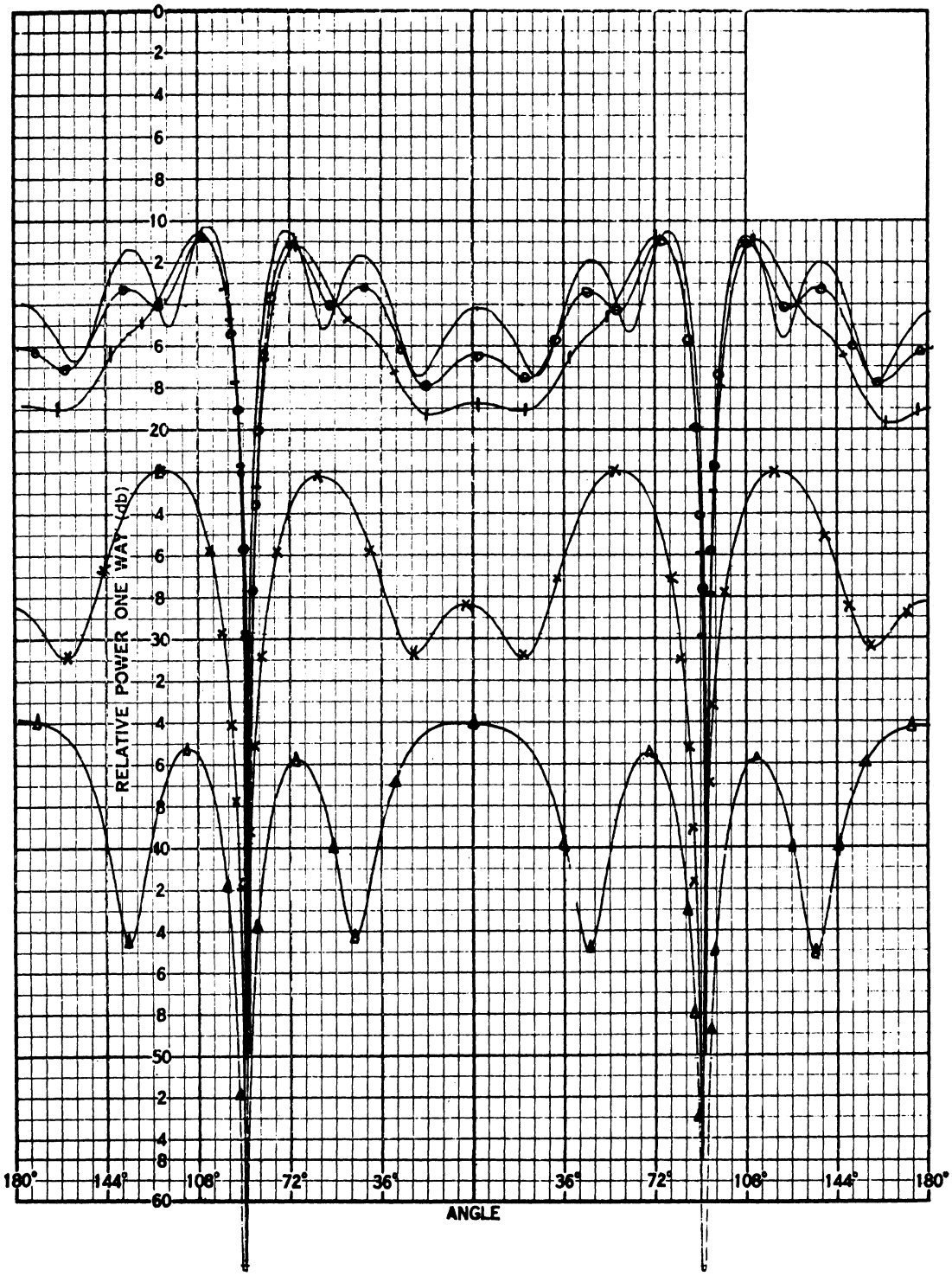

FIG. C-3a: E-PLANE COUPLING FOR E-SECTORAL HORNS
f=8.03 GHz, D=45.72 cm, $\phi_t=0^o$, $-180^o \rightarrow \phi_r \rightarrow 180^o$
(—×—) $\theta_b=10^o$, 0=-40db; (—△—) $\theta_b=15^o$, 0=-20db; (——) $\theta_b=23^o$, 0=-50db;
(—○—) $\theta_b=30^o$, 0=-50db; (—+—) $\theta_b=40^o$, 0=-50db.

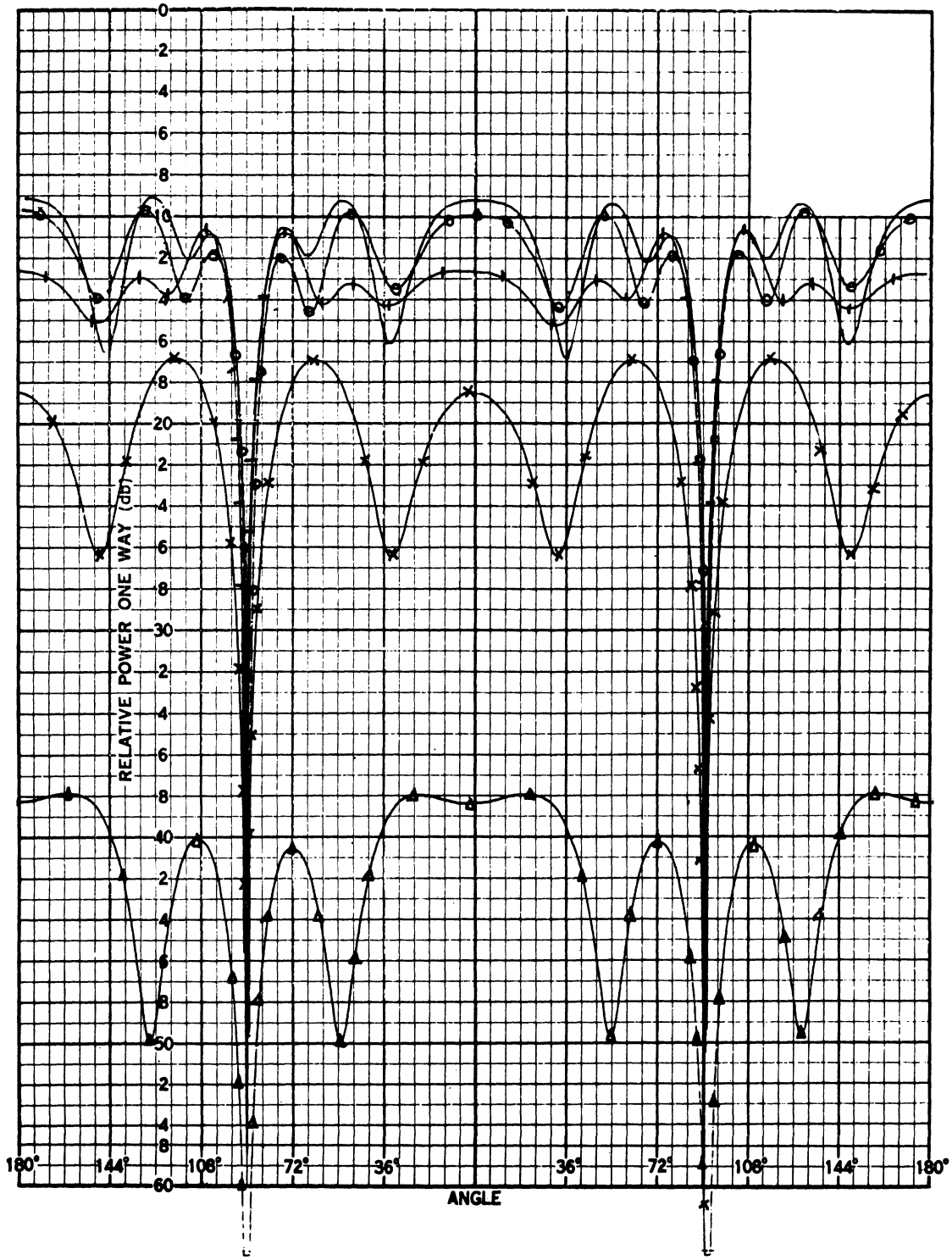

FIG. C-3b: E-PLANE COUPLING FOR E-SECTORAL HORNS

f=9.03 GHz, D=45.72 cm, $\phi_t=0^\circ$, $-180^\circ \rightarrow \phi_r \rightarrow 180^\circ$

(-×-) $\theta_b=10^\circ$, 0=-40db; (-△-) $\theta_b=15^\circ$, 0=-20db; (——) $\theta_b=23^\circ$, 0=-50db;

(-○-) $\theta_b=30^\circ$, 0=-50db; (-|-) $\theta_b=40^\circ$, 0=-50db;

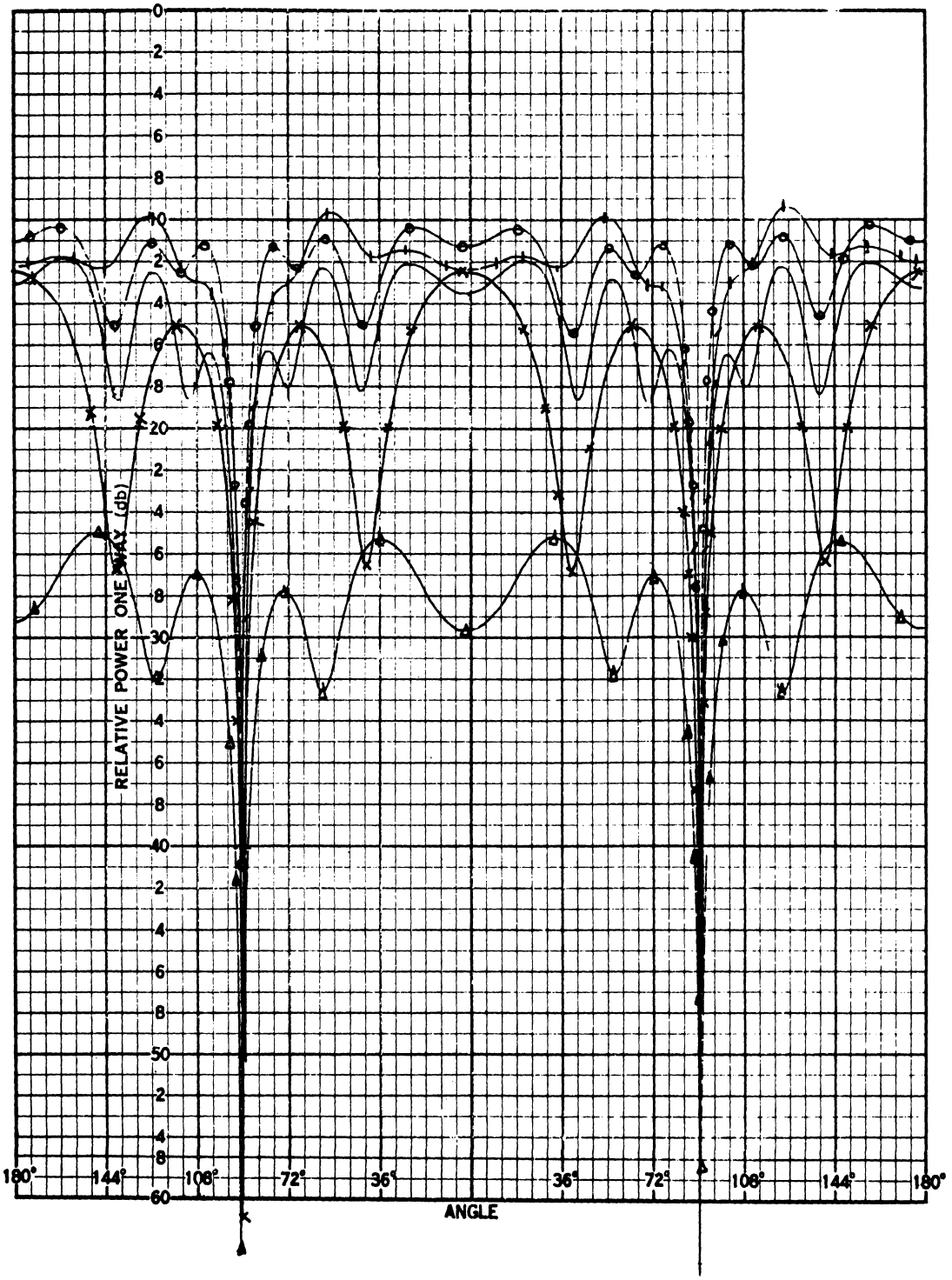

FIG. C-3c: E-PLANE COUPLING FOR E-SECTORAL HORNS
f=10.03 GHz, D=45.72 cm, $\phi_t=0^\circ$, $-180^\circ \rightarrow \phi_r \rightarrow 180^\circ$
(—×—) $\theta_b=10^\circ$, 0=-40db; (—△—) $\theta_b=15^\circ$, 0=-40db; (——) $\theta_b=23^\circ$, 0=-50db;
(—○—) $\theta_b=30^\circ$, 0=-50db; (—|—) $\theta_b=40^\circ$, 0=-50db;

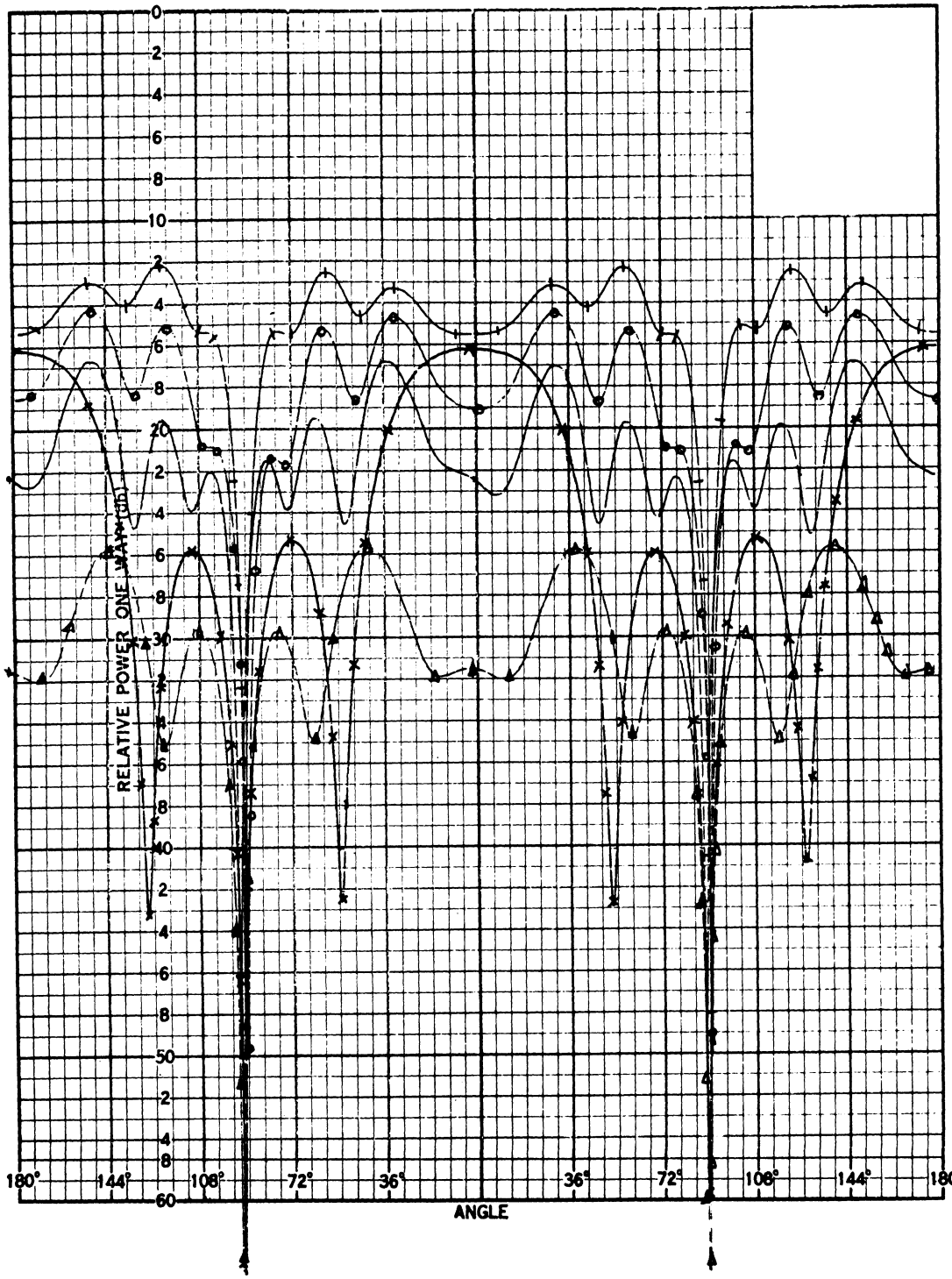

FIG. C-3d: E-PLANE COUPLING FOR E-SECTORAL HORNS

f=11.03 GHz, D=45.72 cm, $\phi_t = 0^\circ$, $-180^\circ \rightarrow \phi_r \rightarrow 180^\circ$

(—×—) $\theta_b=10^\circ$, 0=-40db; (—△—) $\theta_b=15^\circ$, 0=-40db; (——) $\theta_b=23^\circ$, 0=-50db;

(—○—) $\theta_b=30^\circ$, 0=-50db; (—|—) $\theta_b=40^\circ$, 0=-50db;

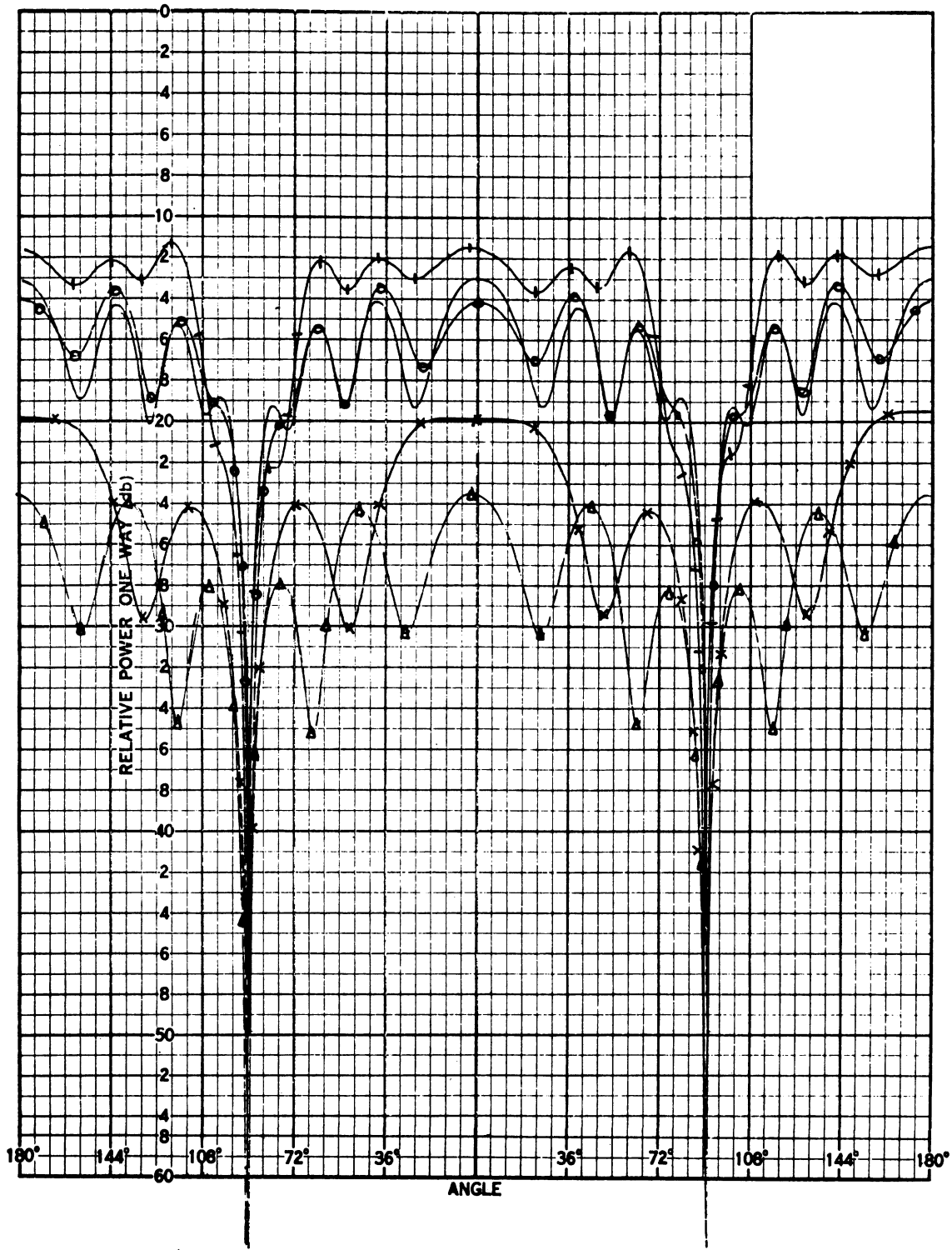

FIG. C-3e: E-PLANE COUPLING FOR E-SECTORAL HORNS

f=12.03 GHz, D=45.72 cm, $\phi_t=0^\circ$, $-180^\circ \rightarrow \phi_r \rightarrow 180^\circ$

(—×—) $\theta_b=10^\circ$, 0=-40 db; (—△—) $\theta_b=15^\circ$, 0=-40db; (——) $\theta_b=23^\circ$, 0=-50db;

(—o—) $\theta_b=30^\circ$, 0=-50db; (—|—) $\theta_b=40^\circ$, 0=-50db;

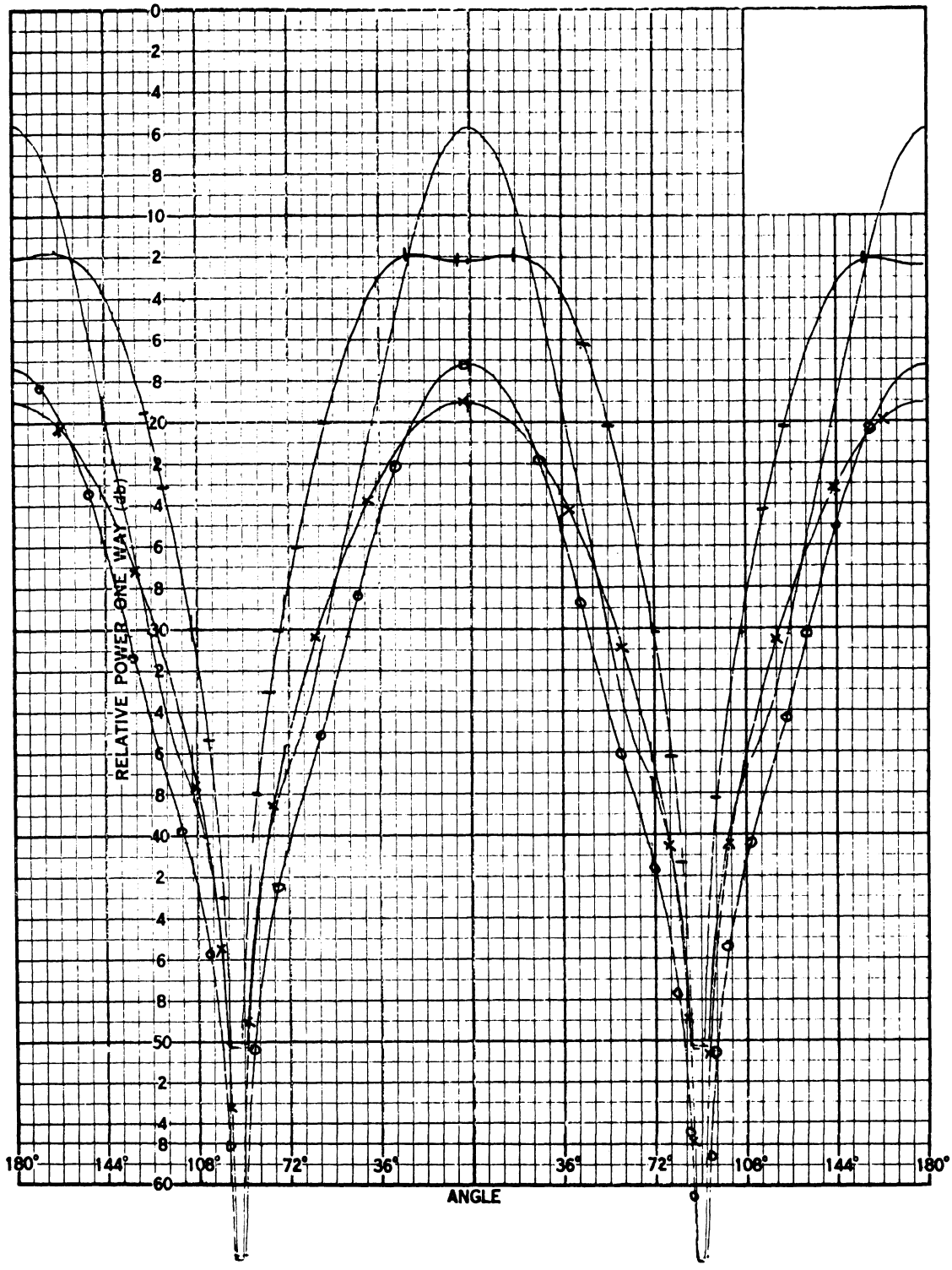

FIG. C-4a: E-PLANE COUPLING FOR H-SECTORAL HORNS
f=8.03 GHz, D=45.72 cm, $\phi_t=0^o$, $-180^o \rightarrow \phi_r \rightarrow 180^o$
(—X—) $\theta_a=10^o$, 0=-20db; (—O—) $\theta_a=20^o$, 0=-20db;
(——)$\theta_a=35^o$, 0=-30db; (—|—) $\theta_a=50^o$, 0=-30db;

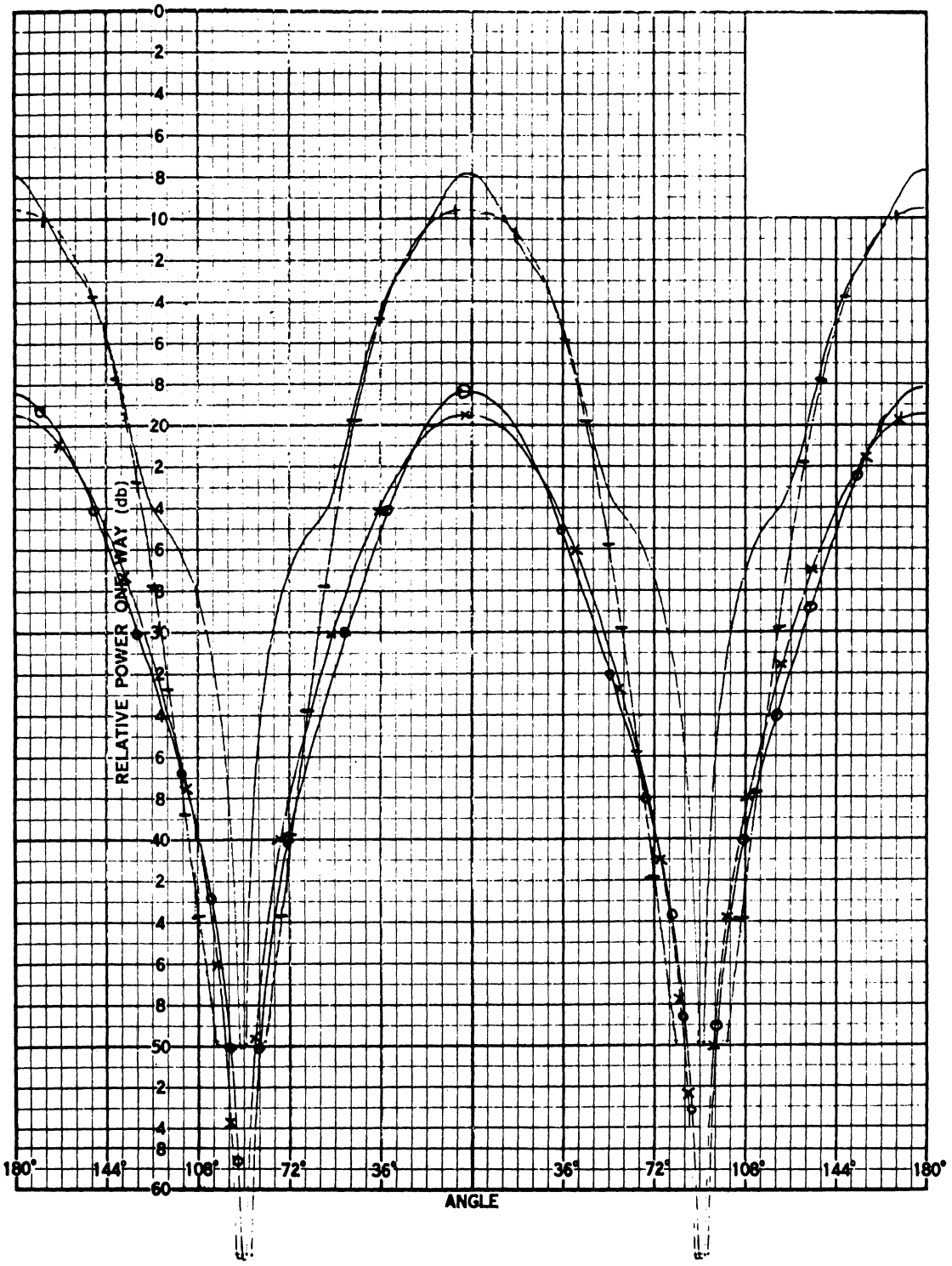

FIG. C-4b: E-PLANE COUPLING FOR H-SECTORAL HORNS

f=9.03 GHz, D=45.72 cm, $\phi_t=0^o$, $-180^o \rightarrow \phi_r \rightarrow 180^o$

(—×—) $\theta_a=10^o$, 0=-20db; (——) $\theta_a=20^o$, 0=-20db;

(——) $\theta_a=35^o$, 0=-30db; (——) $\theta_a=50^o$, 0=-30db;

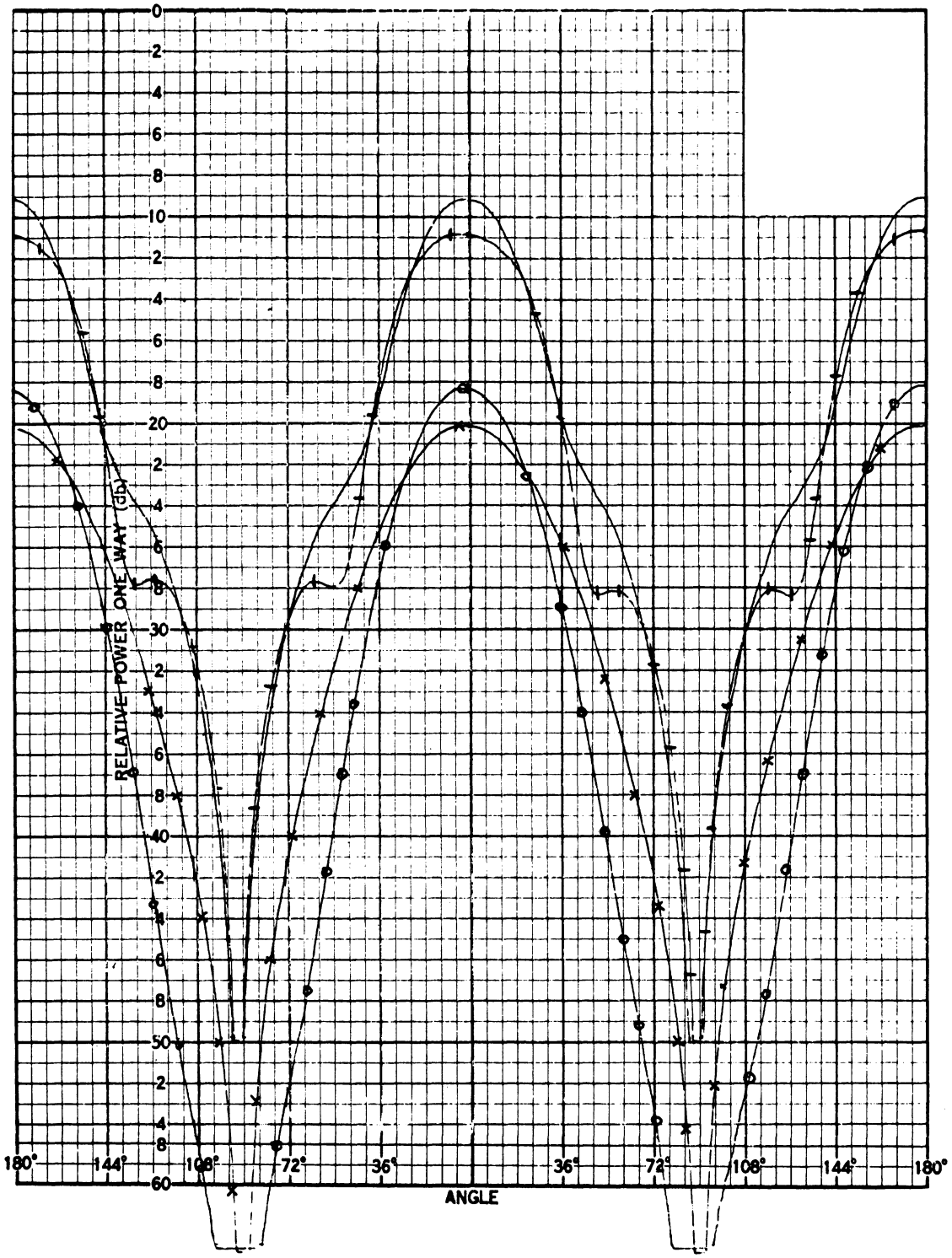

FIG. C-4c: E-PLANE COUPLING FOR H-SECTORAL HORNS

f=10.03 GHz, D=45.72 cm, $\phi_t=0^o$, $-180^o \rightarrow \phi_r \rightarrow 180^o$

(—X—) $\theta_a=10^o$, 0=-20db; (—o—) $\theta_a=20^o$, 0=120db;

(——) $\theta_a=35^o$, 0=-30db; (—|—) $\theta_a=50^o$, 0=-30db.

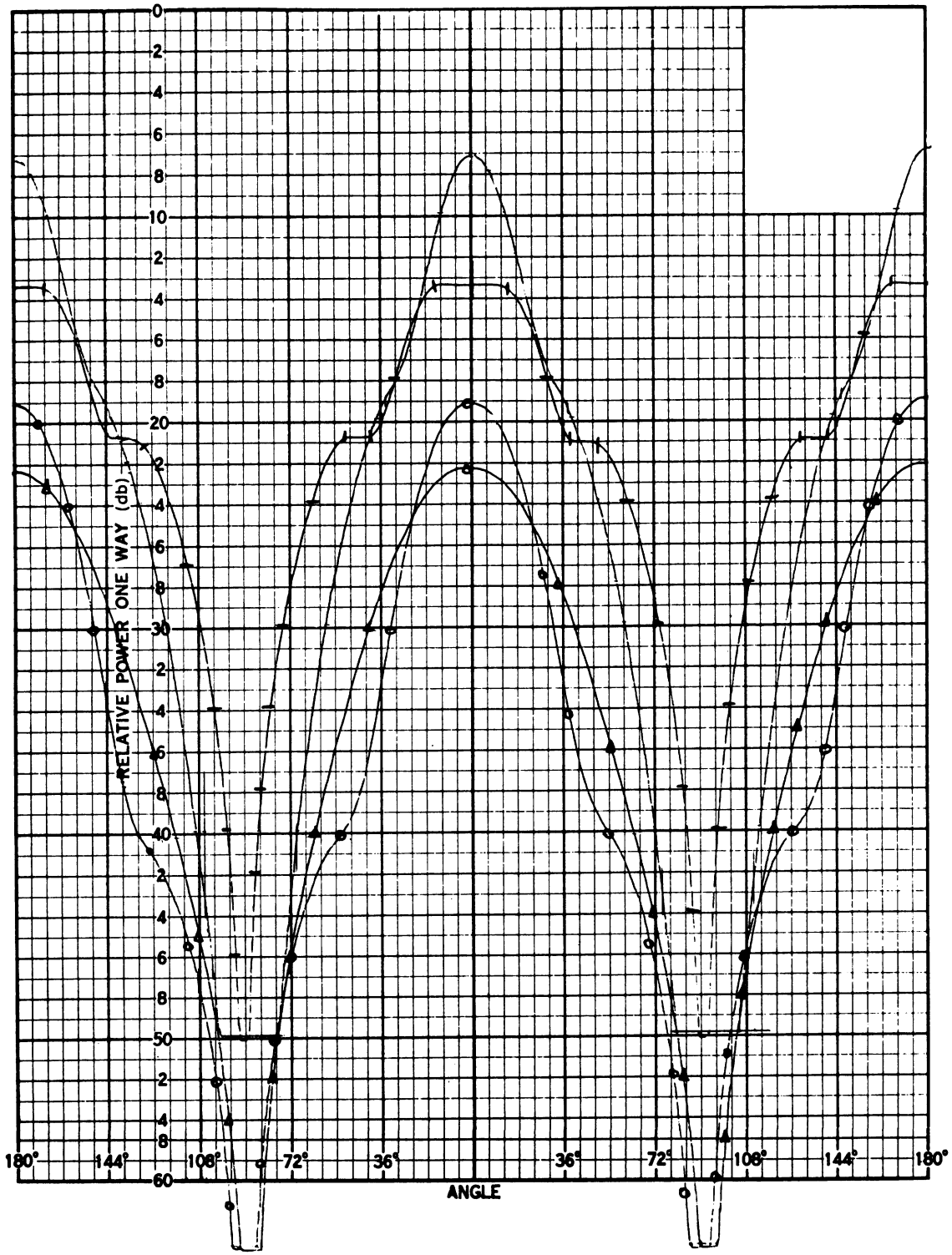

FIG. C-4d: E-PLANE COUPLING FOR H-SECTORAL HORNS

f= 11.03 GHz, D=45.72 cm, $\phi_t=0^\circ$, $-180^\circ \rightarrow \phi_r \rightarrow 180^\circ$

(—×—) $\theta_a=10^\circ$, 0=-20db; (—o—) $\theta_a=20^\circ$, 0=-20db;

(——) $\theta_a=35^\circ$, 0=-30db; (—|—) $\theta_a=50^\circ$, 0=-30db.

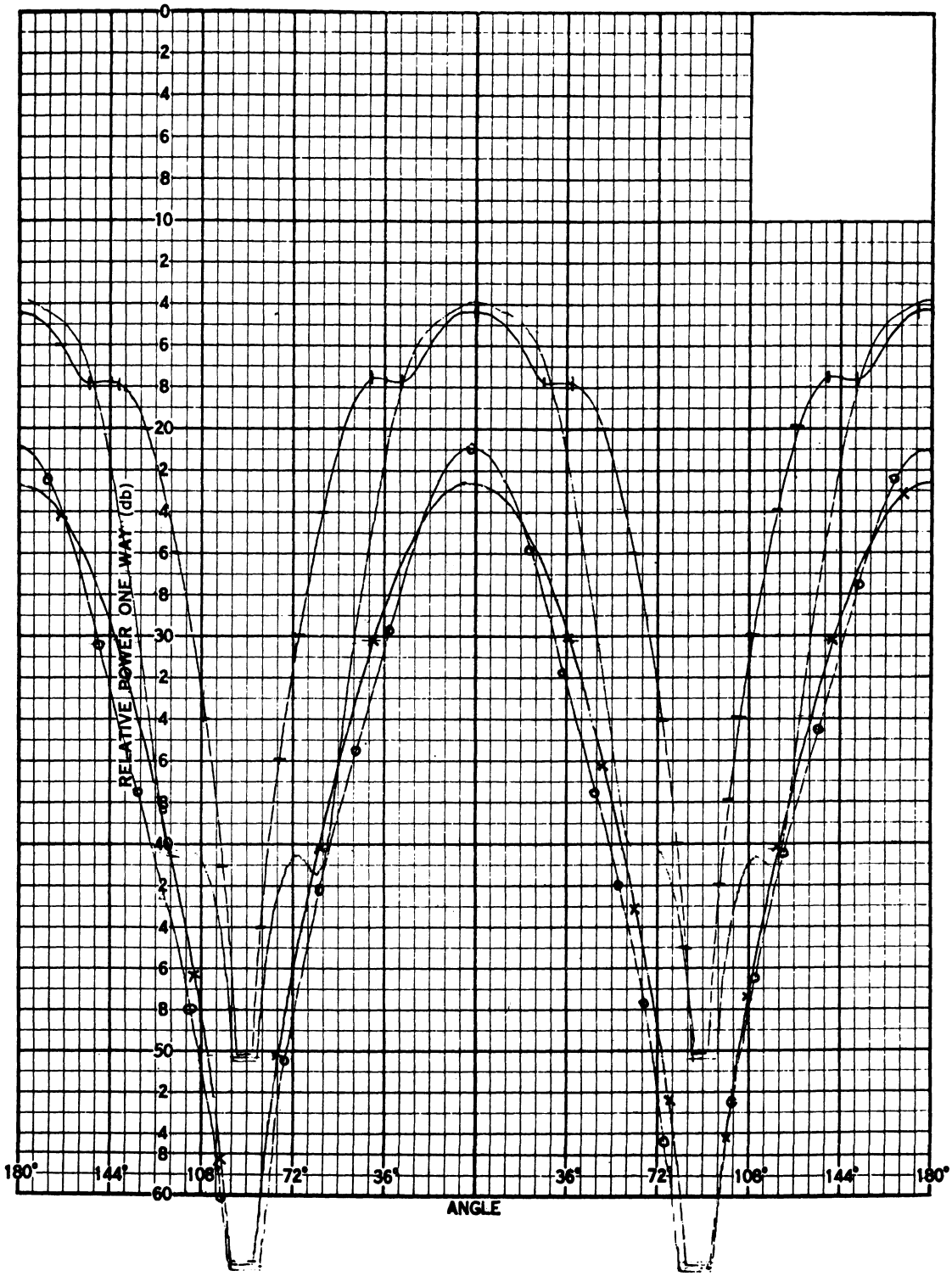

FIG. C-4e: E-PLANE COUPLING FOR H-SECTORAL HORNS

f=12.03 GHz, D=45.72 cm, $\phi_t=0^\circ$, $-180^\circ \rightarrow \phi_r \rightarrow 180^\circ$

(—×—) $\theta_a=10^\circ$, 0=-20db; (—o—) $\theta_a=20^\circ$, 0=-20db;

(——) $\theta_a=35^\circ$, 0=-30db; (—|—) $\theta_a=50^\circ$, 0=-30db.

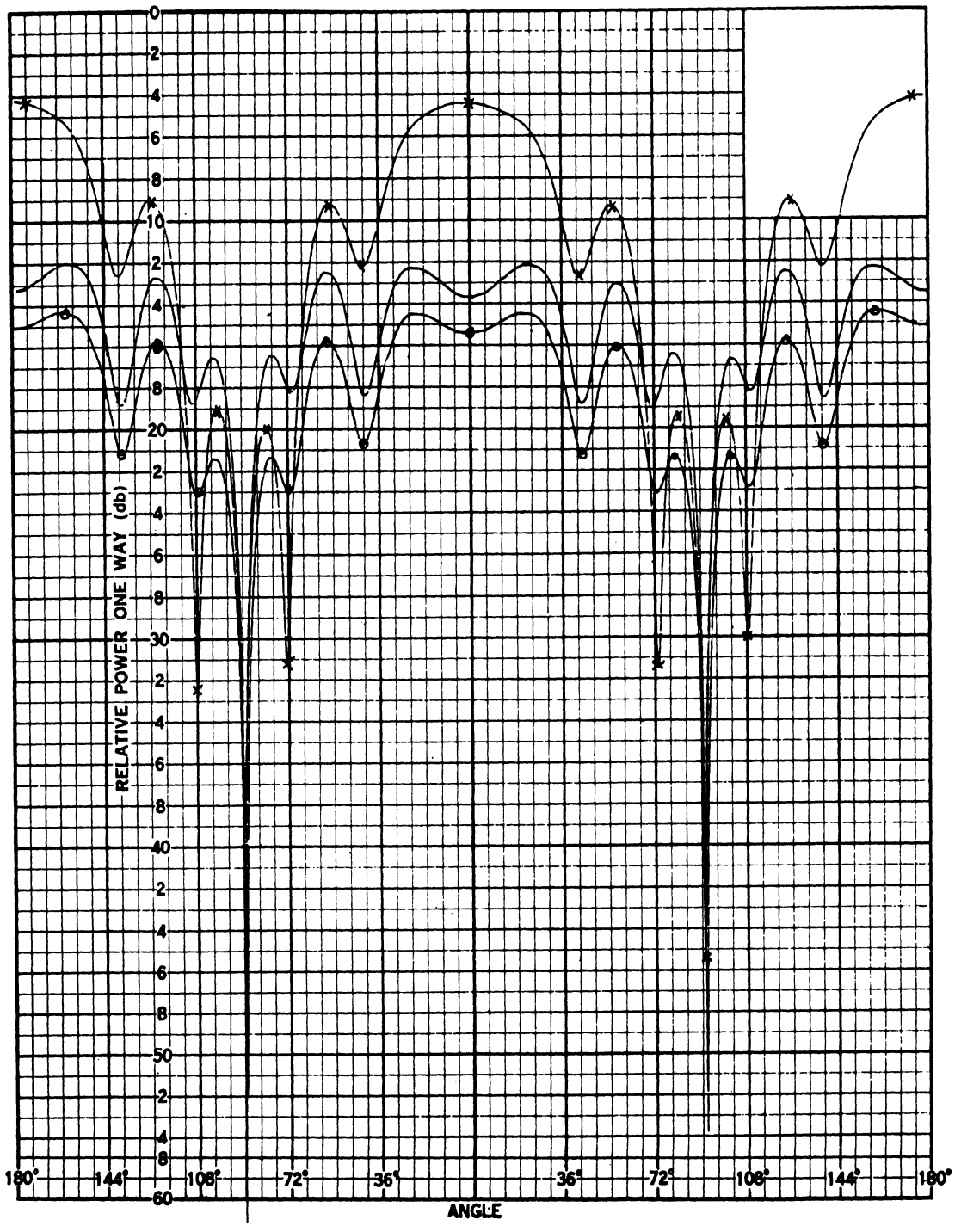

FIG. C-5: VARIATION OF E-PLANE COUPLING WITH SPACING FOR E-SECTORAL HORNS

$\theta_b = 23^\circ$, f=10.03 GHz, $\phi_t = 0^\circ$, $-180^\circ \rightarrow \phi_r \rightarrow 180^\circ$

(—×—) D=11.43 cm, 0=-40 db; (—O—) D=22.86 cm, 0=-40 db;

(——) D=45.72 cm, 0=-50 db.

C.3 Experimental Data: H-plane coupling

Figs. C-6a through C-6e show the H-plane coupling for two identical E-sectoral horns. The coupling is only near-field, in the sense that the receiving antenna is at a null of the transmitting antenna's far-field pattern. Minimum coupling occurs for the T-formation, i.e. when $\phi_t = \pm 90^o$ and $\phi_r = 180^o$ or 0^o, or vice versa. This applies to any rectangular aperture using linear polarization. The center-to-center spacing is 11.43 cm. The designations of table C-3 apply here as well.

For the H-sectoral horns, Table C-4 applies; the coupling patterns are shown in Figs. C-7a through C-7e. These antennas have a fan-shaped beam, and consequently have high energy concentrations in certain regions of the ground plane. Thus the sensitivity to scattering objects is considerable. Since the direct coupling is so low, the interference can dominate.

Fig. 8 shows the variation of coupling with spacing, where, as in section C.2, the spacings are in the ration 1:2:4. Ideally, these curves would be about 12 db apart. The sensitivity of the H-plane coupling to interference is demonstrated quite vividly. The anechoic chamber had been tested and improved (see Section 7.1) far beyond what would be encountered in the field. Thus it would be expected that except for the very close spacings used here, the H-plane coupling will be largely determined by scattering. This is particularly true of H-sectoral horns, or any antenna that radiates a significant amount of its energy along the surface, or in the direction of a reflecting object.

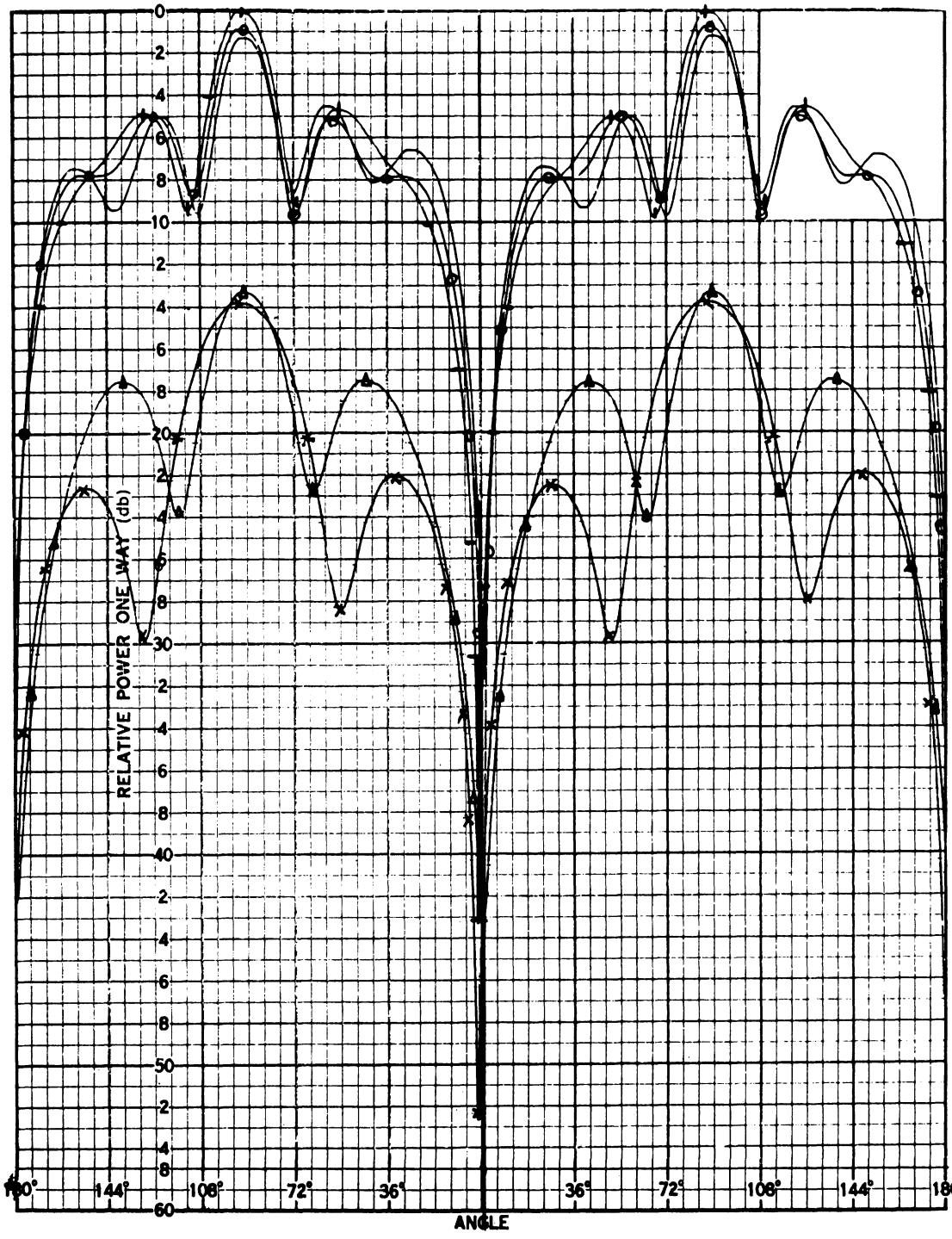

FIG. C-6a: H-PLANE COUPLING FOR E-SECTORAL HORNS

f=8.03 GHz, D=11.43 cm, ϕ_t=90°, -180° → ϕ_r → 180°

(—×—) θ_b=10°, 0=-30db; (—△—) θ_b=15°, 0=-30db; (——) θ_b=23°, 0=-40db;

(—○—) θ_b=30°, 0=-40db; (—+—) θ_b=40°, 0=-40db.

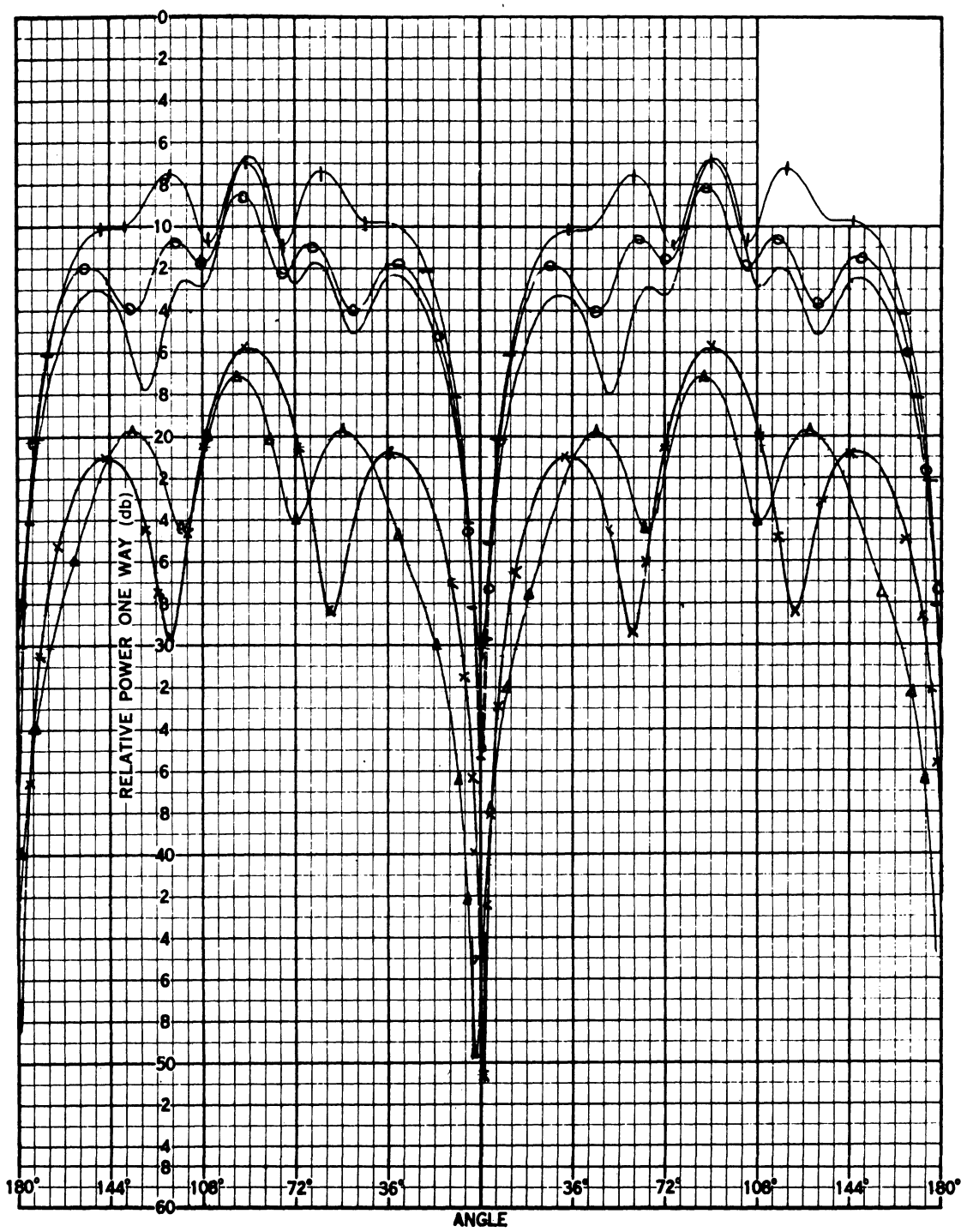

FIG. C-6b: H-PLANE COUPLING FOR E-SECTORAL HORNS

f=9.03 GHz, D=11.43 cm, $\phi_t=90^\circ$, $-180^\circ \rightarrow \phi_r \rightarrow 180^\circ$

(—×—) $\theta_b=10^\circ$, 0=-30db; (—△—) $\theta_b=15^\circ$, 0=-30db;

(——) $\theta_b=23^\circ$, 0=-40db; (—○—) $\theta_b=30^\circ$, 0=-40db;

(—+—) $\theta_b=40^\circ$, 0=-40db.

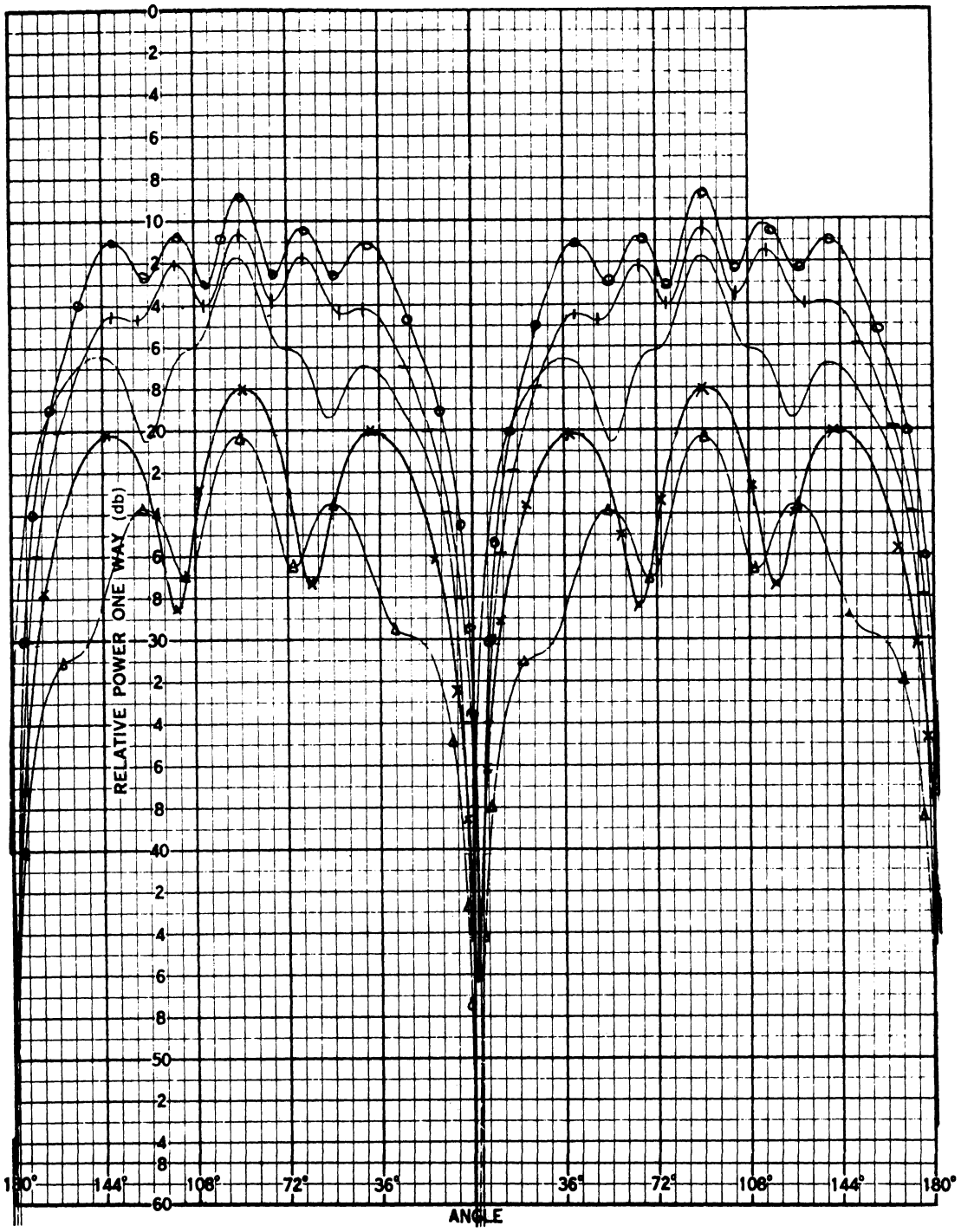

FIG. C-6c: H-PLANE COUPLING FOR E-SECTORAL HORNS

f=10.03 GHz, D=11.43 cm, ϕ_t=90°, -180° → ϕ_r → 180°

(—×—) θ_b=10°, 0=-30db; (—▲—) θ_b=15°, 0=-30db;

(——) θ_b=23°, 0=-40db; (—o—) θ_b=30°, 0=-40db;

(—+—) θ_b=40°, 0=-40db.

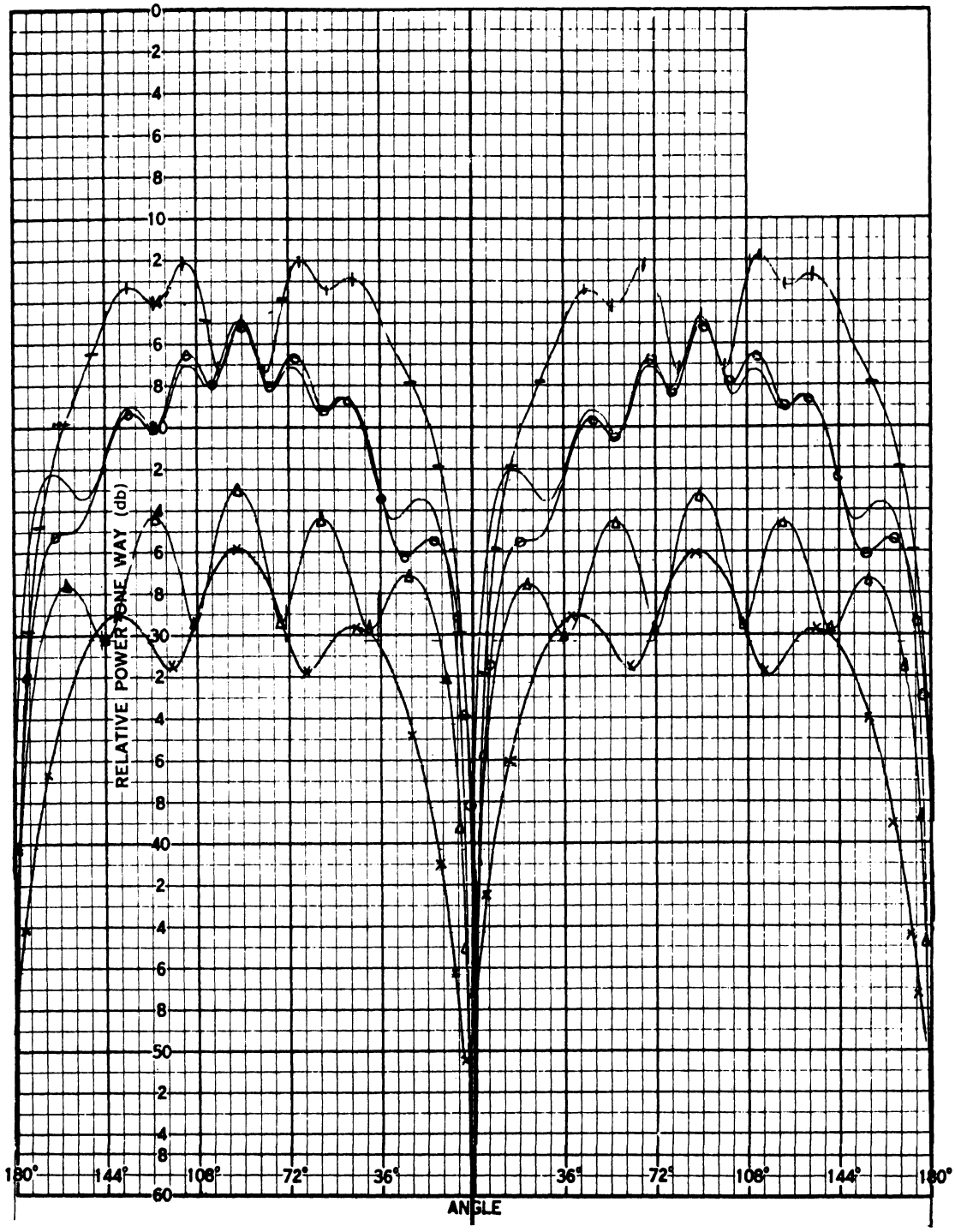

FIG. C-6d: H-PLANE COUPLING FOR E-SECTORAL HORNS

f=11.03 GHz, D=11.43 cm, $\phi_t=90^\circ$, $-180^\circ \rightarrow \phi_r \rightarrow 180^\circ$

(—X—) $\theta_b=10^\circ$, 0=-30db; (—Δ—) $\theta_b=15^\circ$, 0=-30db;

(——) $\theta_b=23^\circ$, 0=-40db; (—O—) $\theta_b=30^\circ$, 0=-40db;

(—|—) $\theta_b=40^\circ$, 0=-40db.

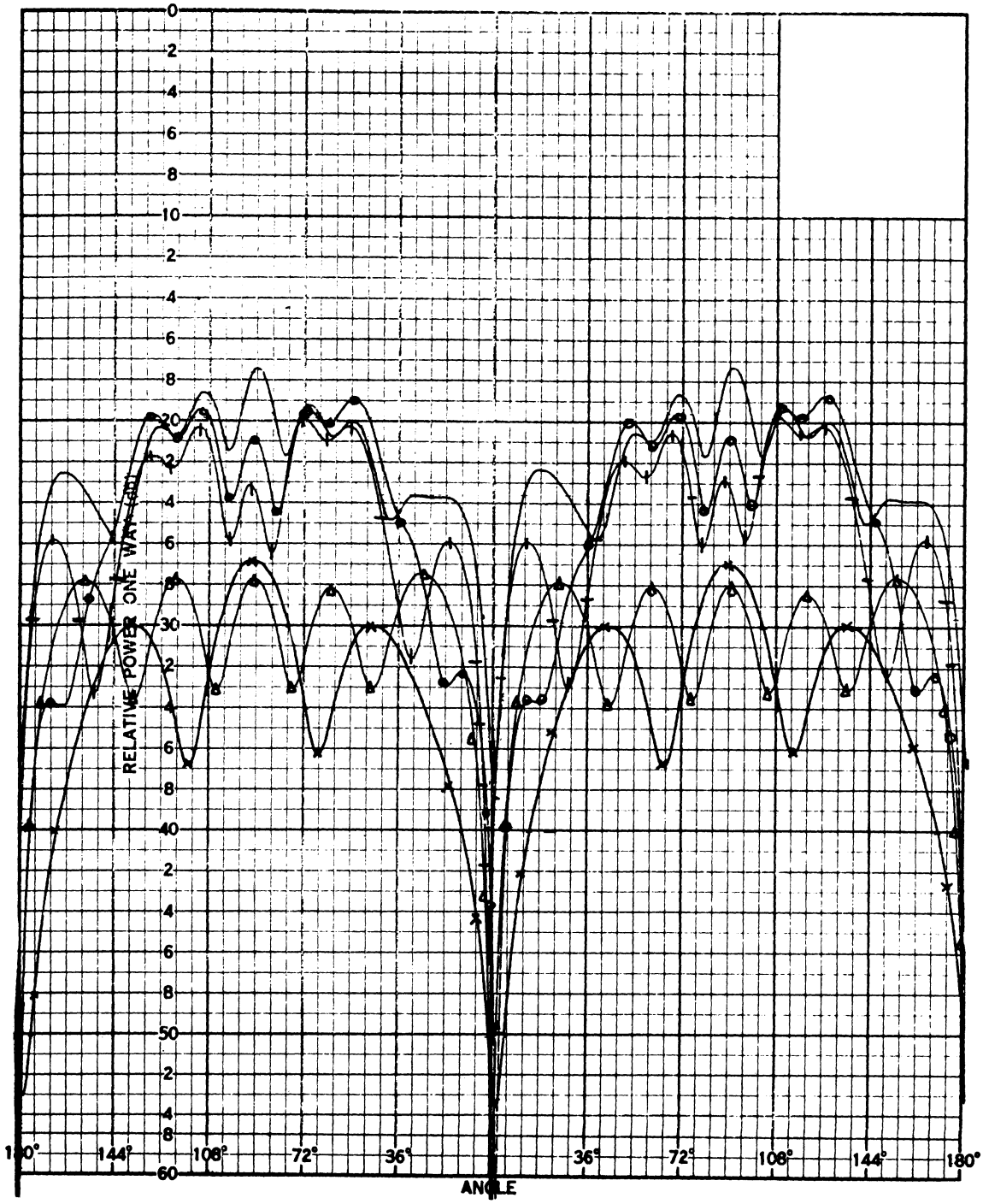

FIG. C-6e: H-PLANE COUPLING FOR E-SECTORAL HORNS

f=12.03 GHz, D=11.43 cm, ϕ_t=90°, -180° → ϕ_r → 180°

(—×—) θ_b=10°, 0=-30db; (—△—) θ_b=15°, 0=-30db;

(——) θ_b=23°, 0=-40db; (—○—) θ_b=30°, 0=-40db;

(—+—) θ_b=40°, 0=-40db.

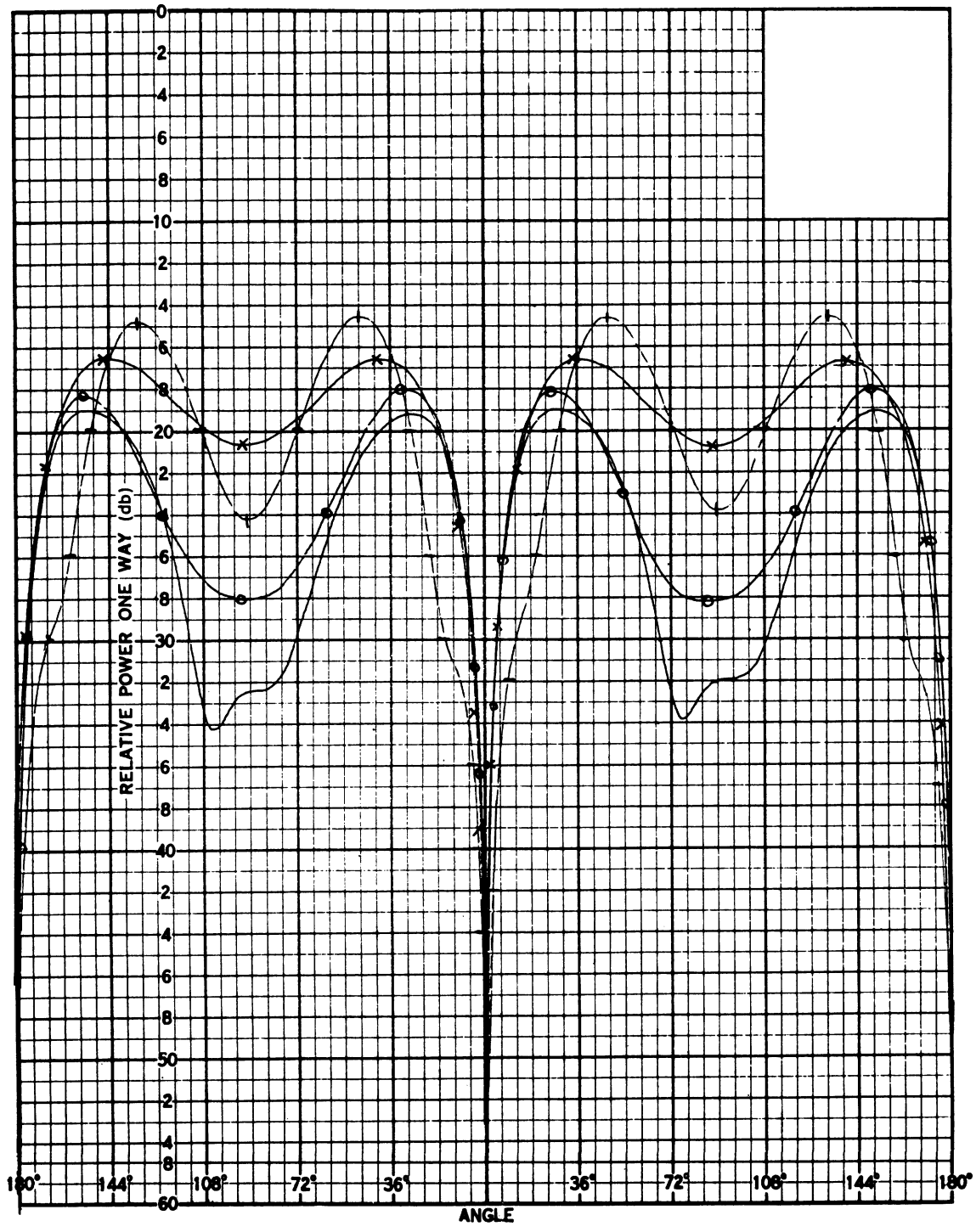

FIG. C-7a: H-PLANE COUPLING FOR H-SECTORAL HORNS

f=8.03 GHz, D=11.43 cm, 0=-40db, $\phi_t=90^\circ$, $-180^\circ \rightarrow \phi_r \rightarrow 180^\circ$

(—×—) $\theta_a=10^\circ$; (—o—)$\theta_a=20^\circ$; (——)$\theta_a=35^\circ$; (—|—)$\theta_a=50^\circ$.

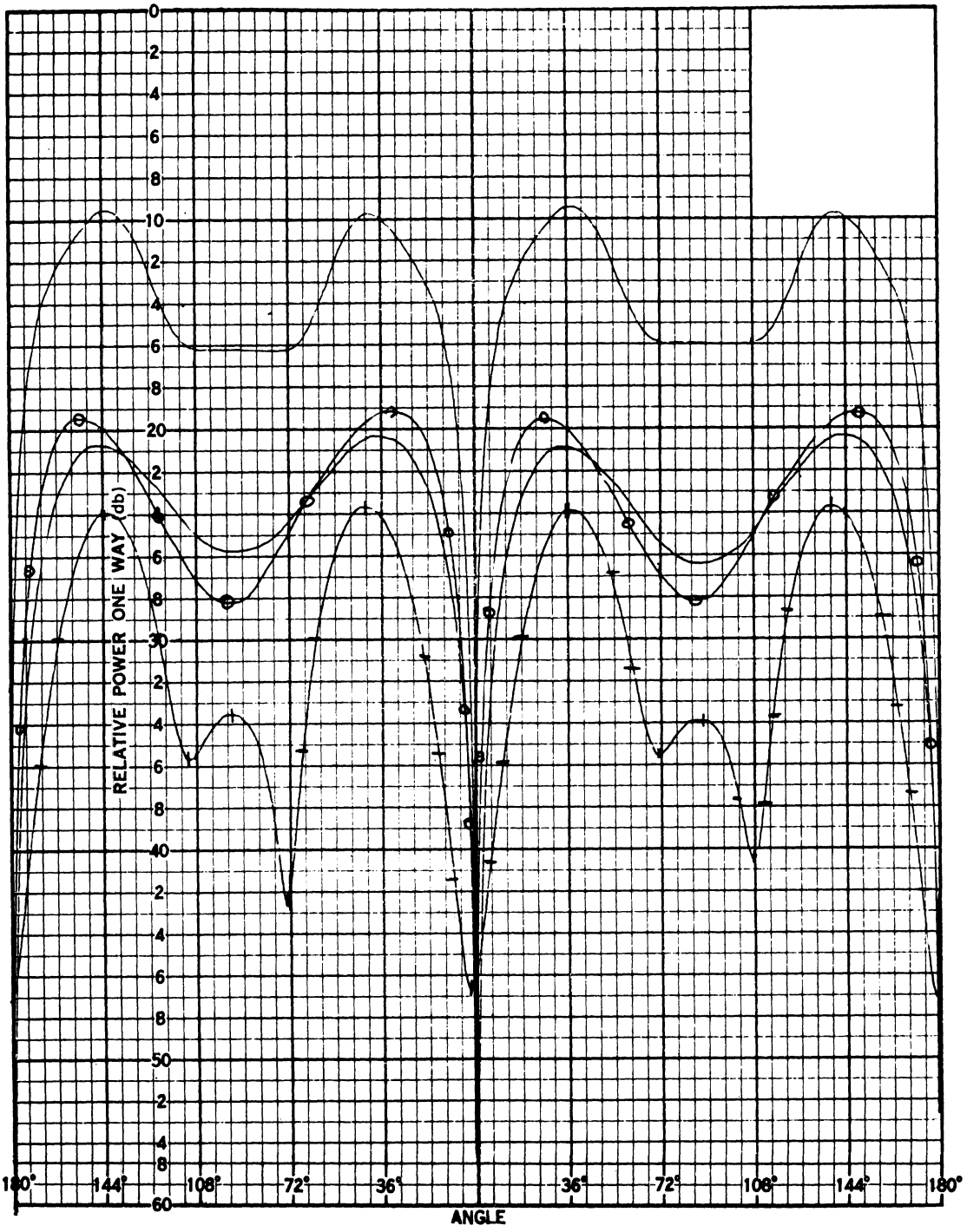

FIG. C-7b: H-PLANE COUPLING FOR H-SECTORAL HORNS
f=9.03 GHz, D=11.43 cm, 0=40db, ϕ_t=90°, -180° → ϕ_r → 180°
(-×-) θ_a=10°, (-o-) θ_a=20°; (——) θ_a=35°; (-+-) θ_a=50°.

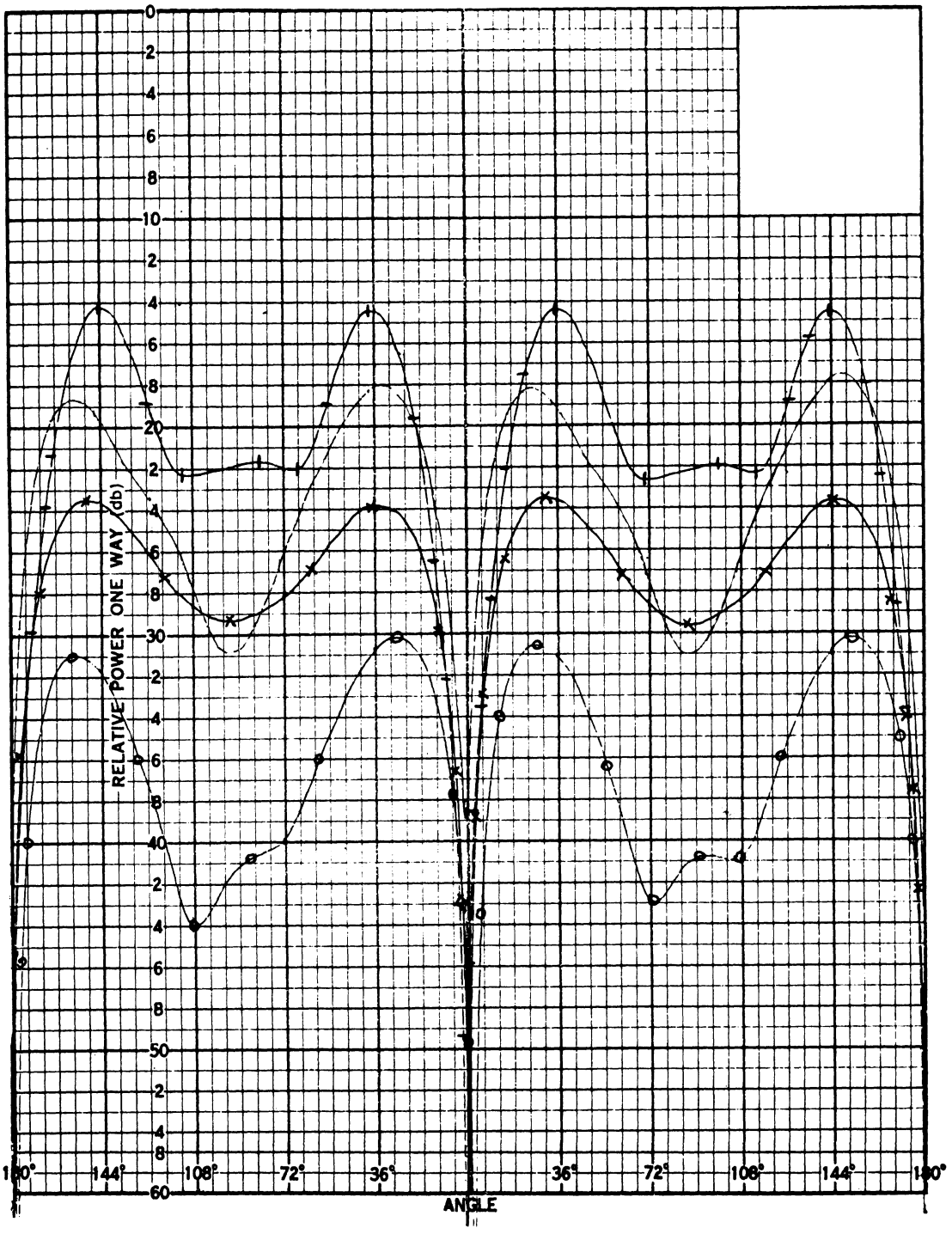

FIG. C-7c: H-PLANE COUPLING FOR H-SECTORAL HORNS

f=10.03 GHz, D=11.43 cm, 0=-40db, $\phi_t = 90^\circ$, $-180^\circ \rightarrow \phi_r \rightarrow 180^\circ$

(—×—) $\theta_a = 10^\circ$; (—o—) $\theta_a = 20^\circ$; (——) $\theta_a = 35^\circ$; (—+—) $\theta_a = 50^\circ$.

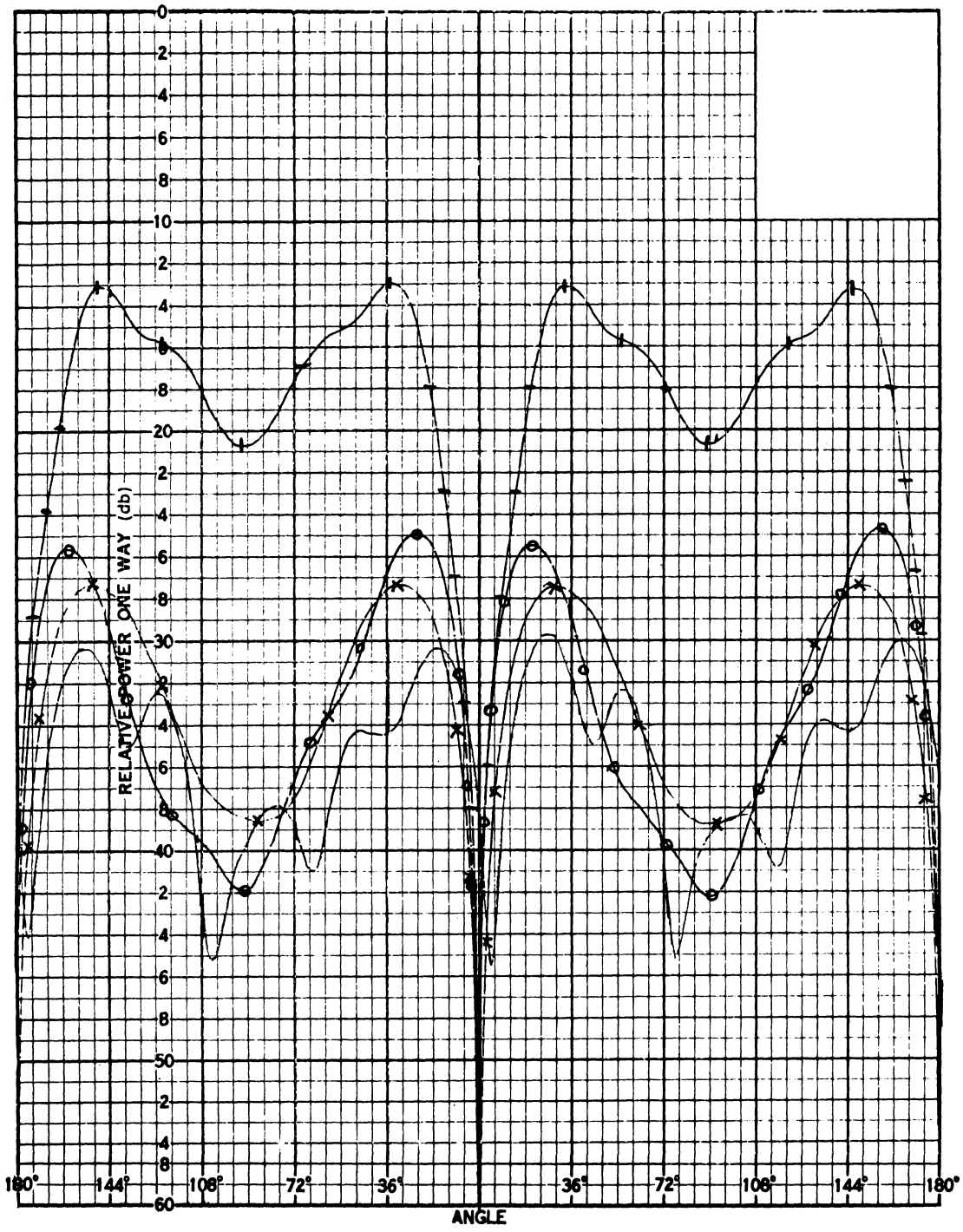

FIG. C-7d: H-PLANE COUPLING FOR H-SECTORAL HORNS
f=11.03 GHz, D=11.43 cm, 0=-40db, ϕ_t=90°, -180° → ϕ_r → 180°
(—×—) θ_a=10°; (—o—) θ_a=20°; (——) θ_a=35°; (—+—) θ_a=50°.

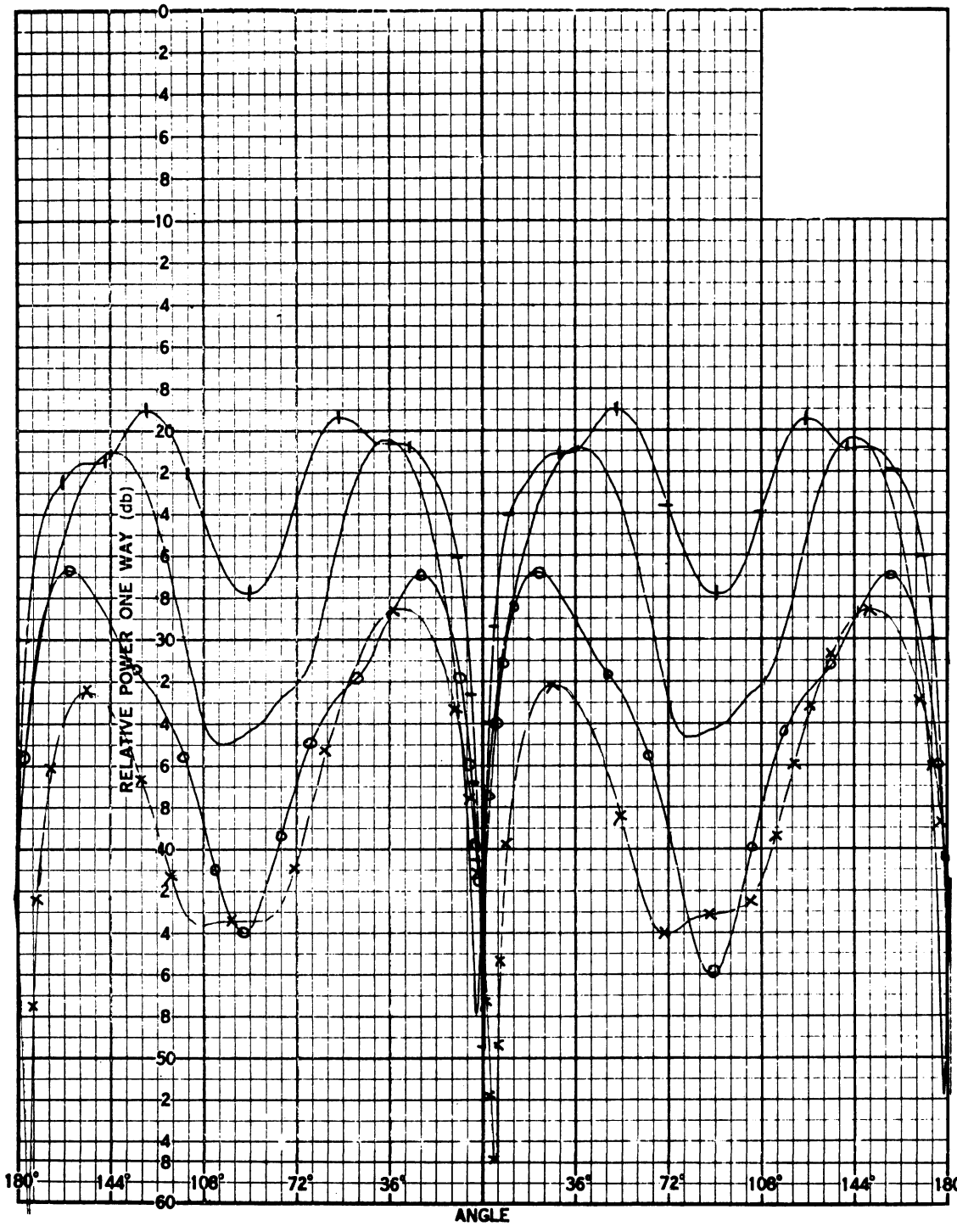

FIG. C-7e: H-PLANE COUPLING FOR H-SECTORAL HORNS
f=12.03 GHz, D=11.43 cm, 0=-40 db, ϕ_t=90°, -180° → ϕ_r → 180°
(—×—) θ_a=10°; (—o—) θ_a=20°; (——) θ_a=35°; (—+—) θ_a=50°.

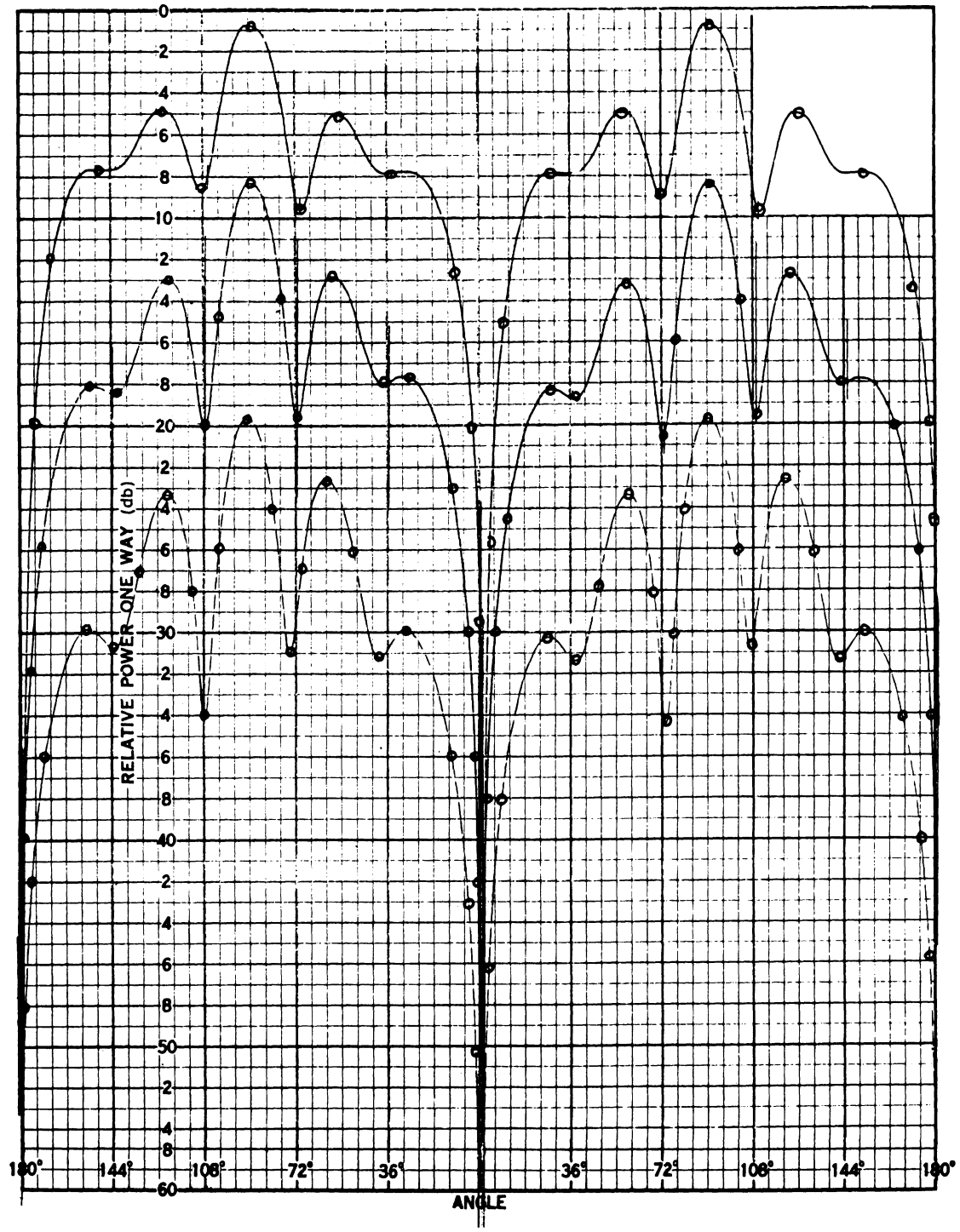

FIG. C-8: VARIATION OF H-PLANE COUPLING WITH SPACING FOR E-SECTORAL HORNS

f=8.03 GHz, θ_b=30°, 0=-40db, ϕ_t=90°, -180° → ϕ_r → 180°

Top, D=11.43 cm; Middle, D=22.86 cm; Bottom, D=45.72 cm .

UNCLASSIFIED

Security Classification

DOCUMENT CONTROL DATA - R&D

(Security classification of title, body of abstract and indexing annotation must be entered when the overall report is classified)

1. ORIGINATING ACTIVITY (Corporate author)	2a. REPORT SECURITY CLASSIFICATION
The University of Michigan Radiation Laboratory Department of Electrical Engineering Ann Arbor, Michigan 48108.	UNCLASSIFIED
	2b GROUP

3. REPORT TITLE

DERIVATION OF AEROSPACE ANTENNA COUPLING-FACTOR INTERFERENCE PREDICTION TECHNIQUES

4. DESCRIPTIVE NOTES (Type of report and inclusive dates)

Final Report, June 1964 through September 1965

5. AUTHOR(S) (Last name, first name, initial)

Lyon, John A.M., Kalafus, Rudolph M., Kwon, Yong-Kuk.
Digenis, Constantine J. Ibrahim, Medhat A.H. Chen, Chao-Chun.

6. REPORT DATE	7a. TOTAL NO. OF PAGES	7b. NO. OF REFS
April 1966	334	21

8a. CONTRACT OR GRANT NO.	9a. ORIGINATOR'S REPORT NUMBER(S)
AF 33(615)-1761	6633-1-F
b. PROJECT NO. 4357, Task 435705	
c.	9b. OTHER REPORT NO(S) (Any other numbers that may be assigned this report) AFAL-TR-66-57
d.	

10. AVAILABILITY/LIMITATION NOTICES

Qualified requesters may obtain copies of this report from DDC

11. SUPPLEMENTARY NOTES	12. SPONSORING MILITARY ACTIVITY
	Air Force Avionics Laboratory, AVWC Research and Technology Division, AFSC Wright-Patterson Air Force Base, Ohio 45433

13. ABSTRACT

This report emphasizes procedures to determine the power interference coupling from one antenna to another. The two antennas need not be similar. Simplified methods including graphs showing the variation of coupling vs angular orientation, frequency or distance are presented for a number of antenna types. Nomographs have been designed to make possible the rapid calculation of the coupling between two antennas. The last chapter of the report (VIII) shows by example the manner of calculation using the nomographs. In the main body of the report, details are given concerning the methods of obtaining the coupling between two antennas by analysis and also by measurements in the laboratory. Some of the more mathematical aspects of the analysis have been introduced as appendices to the report. For a reader interested primarily in the system interference problem, Chapters I and VIII will be helpful. The simplified formulas for coupling in the far region will prove interesting and the numerous experimental data graphs will be helpful for the various types of antennas represented. The presence of a third antenna or acattering object may occasionally influence substantially the coupling between two antennas, especially in the case of very weak coupling. Some discussion of the influence of scattering objects is given.

DD FORM 1 JAN 64 1473

UNCLASSIFIED

Security Classification

14. KEY WORDS	LINK A		LINK B		LINK C	
	ROLE	WT	ROLE	WT	ROLE	WT
INTERFERENCE COUPLING COUPLING NOMOGRAPHS ELECTROMAGNETIC COUPLING ELECTROMAGNETIC INTERFERENCE ARCHIMEDIAN SPIRAL SPIRAL COUPLING RECTANGULAR SLOT COUPLING						

INSTRUCTIONS

1. ORIGINATING ACTIVITY: Enter the name and address of the contractor, subcontractor, grantee, Department of Defense activity or other organization *(corporate author)* issuing the report.

2*a*. REPORT SECURITY CLASSIFICATION: Enter the overall security classification of the report. Indicate whether "Restricted Data" is included. Marking is to be in accordance with appropriate security regulations.

2*b*. GROUP: Automatic downgrading is specified in DoD Directive 5200.10 and Armed Forces Industrial Manual. Enter the group number. Also, when applicable, show that optional markings have been used for Group 3 and Group 4 as authorized.

3. REPORT TITLE: Enter the complete report title in all capital letters. Titles in all cases should be unclassified. If a meaningful title cannot be selected without classification, show title classification in all capitals in parenthesis immediately following the title.

4. DESCRIPTIVE NOTES: If appropriate, enter the type of report, e.g., interim, progress, summary, annual, or final. Give the inclusive dates when a specific reporting period is covered.

5. AUTHOR(S): Enter the name(s) of author(s) as shown on or in the report. Enter last name, first name, middle initial. If military, show rank and branch of service. The name of the principal author is an absolute minimum requirement.

6. REPORT DATE: Enter the date of the report as day, month, year; or month, year. If more than one date appears on the report, use date of publication.

7*a*. TOTAL NUMBER OF PAGES: The total page count should follow normal pagination procedures, i.e., enter the number of pages containing information.

7*b*. NUMBER OF REFERENCES: Enter the total number of references cited in the report.

8*a*. CONTRACT OR GRANT NUMBER: If appropriate, enter the applicable number of the contract or grant under which the report was written.

8*b*, 8*c*, & 8*d*. PROJECT NUMBER: Enter the appropriate military department identification, such as project number, subproject number, system numbers, task number, etc.

9*a*. ORIGINATOR'S REPORT NUMBER(S): Enter the official report number by which the document will be identified and controlled by the originating activity. This number must be unique to this report.

9*b*. OTHER REPORT NUMBER(S): If the report has been assigned any other report numbers *(either by the originator or by the sponsor)*, also enter this number(s).

10. AVAILABILITY/LIMITATION NOTICES: Enter any limitations on further dissemination of the report, other than those imposed by security classification, using standard statements such as:

(1) "Qualified requesters may obtain copies of this report from DDC."

(2) "Foreign announcement and dissemination of this report by DDC is not authorized."

(3) "U. S. Government agencies may obtain copies of this report directly from DDC. Other qualified DDC users shall request through

_____."

(4) "U. S. military agencies may obtain copies of this report directly from DDC. Other qualified users shall request through

_____."

(5) "All distribution of this report is controlled. Qualified DDC users shall request through

_____."

If the report has been furnished to the Office of Technical Services, Department of Commerce, for sale to the public, indicate this fact and enter the price, if known.

11. SUPPLEMENTARY NOTES: Use for additional explanatory notes.

12. SPONSORING MILITARY ACTIVITY: Enter the name of the departmental project office or laboratory sponsoring *(paying for)* the research and development. Include address.

13. ABSTRACT: Enter an abstract giving a brief and factual summary of the document indicative of the report, even though it may also appear elsewhere in the body of the technical report. If additional space is required, a continuation sheet shall be attached.

It is highly desirable that the abstract of classified reports be unclassified. Each paragraph of the abstract shall end with an indication of the military security classification of the information in the paragraph, represented as *(TS), (S), (C), or (U)*.

There is no limitation on the length of the abstract. However, the suggested length is from 150 to 225 words.

14. KEY WORDS: Key words are technically meaningful terms or short phrases that characterize a report and may be used as index entries for cataloging the report. Key words must be selected so that no security classification is required. Identifiers, such as equipment model designation, trade name, military project code name, geographic location, may be used as key words but will be followed by an indication of technical context. The assignment of links, rules, and weights is optional.